Design, Synthese und Optimierung von GSK-3-Inhibitoren und ihre Evaluation in Modellen der Alzheimer-Demenz

TECHNISCHE UNIVERSITÄT DARMSTADT

Vom Fachbereich Chemie
der Technischen Universität Darmstadt

zur Erlangung des akademischen Grades eines
Doctor rerum naturalium (Dr. rer. nat.)

genehmigte
kumulative Dissertation

vorgelegt von

Fabio Lo Monte, Master of Science
aus Hilden

Referent: Prof. Dr. Boris Schmidt
Korreferenten: Prof. Dr. Harald Kolmar
Prof. Dr. Daniel Rauh (TU Dortmund)

Tag der Einreichung: 26. März 2012
Tag der mündlichen Prüfung: 21. Mai 2012

Darmstadt 2012

D17

Die vorliegende Arbeit wurde unter der Leitung von Herrn Prof. Dr. Boris Schmidt am Clemens Schöpf-Institut für Organische Chemie und Biochemie der Technischen Universität Darmstadt von März 2009 bis März 2012 angefertigt.

Teile dieser Arbeit sind bereits veröffentlicht oder zur Veröffentlichung eingereicht

1. Thomas Kramer*, Boris Schmidt, Fabio Lo Monte‡ Small-molecule inhibitors of GSK-3 - Structural insights and their application to Alzheimer's disease models, *International Journal of Alzheimer's Disease* **2012**, im Druck.

2. Fabio Lo Monte*, Thomas Kramer*, Alexander Boländer, Batya Plotkin, Hagit Eldar-Finkelman, Ana Fuertes, Juan Dominguez, Boris Schmidt‡ Synthesis and biological evaluation of glycogen synthase kinase 3 (GSK-3) inhibitors: An fast and atom efficient access to 1-aryl-3-benzylureas, *Bioorganic & Medicinal Chemistry Letters* **2011**, 21, 5610-15. dx.doi.org/10.1016/j.bmcl.2011.06.131

3. Fabio Lo Monte*,‡, Thomas Kramer, Jiamin Gu, Upendra Rao Anumala, Luciana Marinelli, Valeria La Pietra, Ettore Novellino, Ana Fuertes, Juan Manuel Dominguez, Batya Plotkin, Hagit Eldar-Finkelman, Boris Schmidt‡ Identification of Glycogen Synthase Kinase-3 Inhibitors with a Selective Sting for Glycogen Synthase Kinase-3α, *Journal of Medicinal Chemistry* **2012**, 55, 4407-4424. dx.doi.org/10.1021/jm300309a

4. Fabio Lo Monte*,‡, Thomas Kramer, Jiamin Gu, Martin Brodrecht, Johannes Pilakowski, Ana Fuertes, Juan Manuel Dominguez, Batya Plotkin, Hagit Eldar-Finkelman, Boris Schmidt‡ Structure-based optimization of oxadiazole-based GSK-3 inhibitors, *European Journal of Medicinal Chemistry* **2012**, zur Publikation angenommen.

5. Boris Schmidt, Fabio Lo Monte, Thomas Kramer, Hagit Eldar-Finkelman, Fred Van Leuven Verbindungen als Glykogen Synthase Kinase 3 (GSK-3) Inhibitoren für die Behandlung von GSK-3-vermittelten Erkrankungen, *Deutsche Patentanmeldung* **2011**, Nr.: 10 2011 106 990.2.

6. Thomas Kramer*, Fabio Lo Monte*, Stefan Göring, Ghislaine Marlyse Okala Amombo, Boris Schmidt‡ Small molecule kinase inhibitors for LRRK2 and their application to Parkinson´s disease models, *ACS Chemical Neuroscience* **2012**, 3, 151-160. dx.doi.org/10.1021/cn200117j

7. Ghislaine Marlyse Okala Amombo*, Thomas Kramer*, Fabio Lo Monte*, Stefan Göring, Steven Smith, Stephanie Kolb, Robert Schubenel, Karlheinz Baumann, Boris Schmidt‡ Inhibitor modification - An inhibition shift from γ-secretase to FLT-3, *Bioorganic & Medicinal Chemistry Letters*, wird voraussichtlich im Juli 2012 eingereicht.

*Erstautor ; ‡Korrespondenzautor

Danksagung

Meinem Doktorvater Herrn Prof. Dr. Boris Schmidt danke ich für die interessante und spannende Themenstellung, die ständige Gesprächs- und Diskussionsbereitschaft sowie für das mir entgegengebrachte Vertrauen.

Ein weiterer Dank geht an meine Laborkollegen Thomas, Jiamin, Upendra, Stefan, Azadeh, Marlyse, Daniel, Alex, Andrea, Eva, Binia und Nicole für das gute Arbeitsklima und die nette Zusammenarbeit.

Meinen Studenten Steven, Stefan, Martin, Johannes und Matthias danke ich für die lustige Zeit im Labor und deren Mitarbeit am meinen Projekt.

Den „Kicker-Kollegen“ danke ich für die unglaublich lustige Zeit am Tischfußball.

Frau Sahinalp und Frau Rudolf danke ich für die netten Unterhaltungen und das Anfertigen meiner Massenspektren.

Dem *Seventh Framework Programme* (FP7) der europäischen Union danke ich für die finanzielle Unterstützung dieser Arbeit. Ein weiterer Dank geht an das *Neuro.GSK3*-Konsortium für die gute Zusammenarbeit und biologische Testung meiner Verbindungen.

Meiner Lebensgefährtin, meinen Eltern, meinen Freunden und meiner ganzen Familie gilt ein großer Dank für die bedingungslose Unterstützung während meines gesamten Studiums und der Promotion.

Inhaltsverzeichnis

Abkürzungsverzeichnis

Aβ	Amyloid-β-Peptid
Abb.	Abbildung
AD	Alzheimer-Demenz
ADAM	*a disintegrin and metalloprotease*
AICD	*APP intracellular domain*
ALS	amyotrophische Lateralsklerose
APC	*adenomatous polyposis coli*
APH-1	*anterior pharynx defective-1*
APOE	Apoliprotein E
APP	Amyloid-Vorläuferprotein
ATP	Adenosintriphosphat
β-Sekretase	*β-site APP-cleaving enzyme 1*; BACE-1
BSc	Boris Schmidt Substanzdatenbankeintrag
bzw.	beziehungsweise
CDK5	*cyclin dependant kinase 5*
COX	Cyclooxygenase
DVL	*dishevelled*
EOAD	*early onset AD patient*
ERK2	*extracellular signal-regulated kinase-2*
FDA	*Food and Drug Administration*
FLT-3	*FMS-like tyrosine kinase-3*
FRAT	*frequently rearranged during advanced T-cell lymphoma*
GPCRs	*G-protein-coupled receptors*
GSK-3	Glykogen Synthase Kinase 3
HSP 90	*heat shock protein 90*
IC_{50}	mittlere inhibitorische Konzentration
IRS	*insulin-receptor substrate*
LOAD	*late onset AD patient*
LRRK2	*leucine-rich repeat kinase 2*
kDa	Kilodalton
MAP	Mikrotubuli-assoziiertes Protein
MARK 1	*microtubule affinity-regulating kinase 1*

NCSTN	Nicastrin
NFTs	*neurofibrillary tangles*; Neurofibrillenbündel
PDK1	*3-phosphoinositide-dependant protein kinase-1*
PEN-2	*presenilin enhancer-2*
PHFs	*paired helical filaments*; paarige helikale Filamente
PI3K	*phosphatidylinositol 3-kinase*
PIP_2	*phosphatidylinositol(4,5)bisphosphate*
PIP_3	*phosphatidylinositol(3,4,5)bisphosphate*
PK	Proteinkinase
PKA	*cAMP-dependant protein kinase*
PKI	Proteinkinase-Inhibitoren
PP1β.Gm	*protein phosphatase 1*
PS	*Presenilin*
PSA	*polar surface area*; polare Molekülоberfläche
Tab.	Tabelle
TCF	*transcription factor*
z.B.	zum Beispiel
ZNS	Zentralnervensystem

Verzeichnis der Aminosäuren

Ala	Alanin	Leu	Leucin
Arg	Arginin	Lys	Lysin
Asn	Asparagin	Met	Methionin
Asp	Asparaginsäure	Phe	Phenylalanin
Cys	Cystein	Pro	Prolin
Gln	Glutamin	Ser	Serin
Glu	Glutaminsäure	Thr	Threonin
Gly	Glycin	Trp	Tryptophan
His	Histidin	Tyr	Tyrosin
Ile	Isoleucin	Val	Valin

1. Einleitung

1.1 Alzheimer-Demenz (AD)

Vor mehr als hundert Jahren beschrieb Dr. Alois Alzheimer in der städtischen Nervenheilanstalt Frankfurt am Main eine bis dahin unbekannte Krankheit. Seine damalige Patientin Auguste Deter litt mit zunehmender Verschlechterung an Gedächtnisverlust, Desorientiertheit und Verfolgungswahn. Einige Jahre später starb die Patientin und die histologische Untersuchung ihres Gehirns durch Alois Alzheimer führte zur Identifizierung zweier ungewöhnlicher Proteinablagerungen.[1-2] Heute ist diese Erkrankung unter dem Namen Alzheimer-Demenz (AD) bekannt und die Ablagerungen werden als extrazelluläre Amyloid-Plaques und intrazelluläre Neurofibrillenbündel (*neurofibrillary tangles*, NFTs) bezeichnet (Abb. 1).

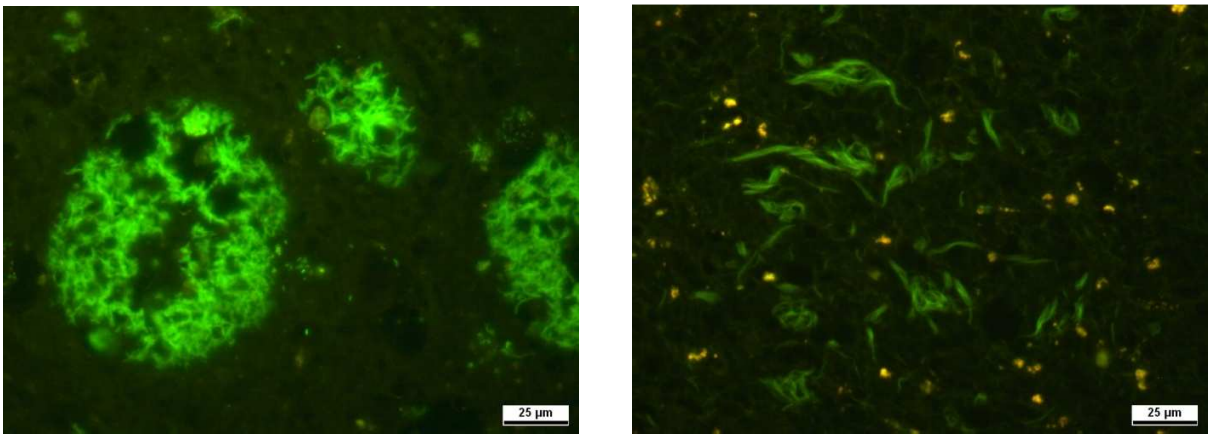

Abb. 1: Histologische Fluoreszenzfärbung der extrazellulären Amyloid-Plaques (links, grün) und der intrazellulären Neurofibrillenbündel (rechts, grün).[3]

Die Amyloid-Plaques, welche aus Polymeren des Amyloid-β-Peptides (Aβ) bestehen, und die NFTs, Ablagerungen des hyperphosphorylierten und Mikrotubuli-assoziierten Tau-Proteins, sind nach wie vor Kennzeichen der AD.[4] Die endgültige AD-Diagnose kann gegenwärtig nur *post mortem* gestellt werden.[5] Infolgedessen wird zurzeit verstärkt an bildgebenden Verfahren und Biomarkern geforscht, um AD frühzeitig zu diagnostizieren und die Wirkung von Therapeutika zu untersuchen.[6] Heutzutage klassifiziert man die Krankheit nach frühem Krankheitsausbruch (*early onset AD patient*, EOAD) und spätem Krankheitsausbruch (*late onset AD patient*, LOAD). EOAD ist eine seltene Form der AD und die heutige hohe Lebenserwartung führt

dazu, dass die Krankheit bei der Mehrzahl der Patienten in höherem Alter ausbricht.[7] Drei Genmutationen, die mit EOAD in Verbindung stehen, konnten bisher identifiziert werden. Diese Gene kodieren für das Amyloid-Vorläuferprotein (APP), *Presenilin 1* (PS1) und *Presenilin 2* (PS2). Die genetische Ursache für LOAD ist derzeit nicht vollständig aufgeklärt, jedoch spielt das Apolipoprotein E (APOE) eine sehr wichtige Rolle bei der Entstehung.[8] Im Jahr 2009 wurden weltweit mehr als 35 Millionen Fälle von AD registriert und Schätzungen zufolge wird sich diese Zahl bis 2050 verdoppeln.[4] Die Kosten, die hierdurch auf das Gesundheitssystem zukommen, sind immens.

Derzeit gibt es fünf Medikamente auf dem Markt, die darauf abzielen die Symptome der AD zu lindern, nicht jedoch die ihr zugrunde liegende Pathologie (Abb. 2).[7,9] Der Verlust an cholinergen Neuronen und Defizite im Acetylcholin-Neurotransmittersystem sind Symptome, die bereits in einem frühen Stadium von AD zu beobachten sind.[7] Donepzil (**1**), Rivastigmin (**2**), Galantamin (**3**) und Huperzin-A (**4**) sind Inhibitoren der Acetylcholinesterase, welche die Defizite im Acetylcholin-Neurotransmittersystem vermindern.[7-9] Verbindung **4** ist derzeit nur in China zugelassen.[9] Tacrin (**5**) ist ebenfalls ein Acetylcholinesterase-Inhibitor und die erste Verbindung, die zur Behandlung der AD-Symptome zugelassen wurde.

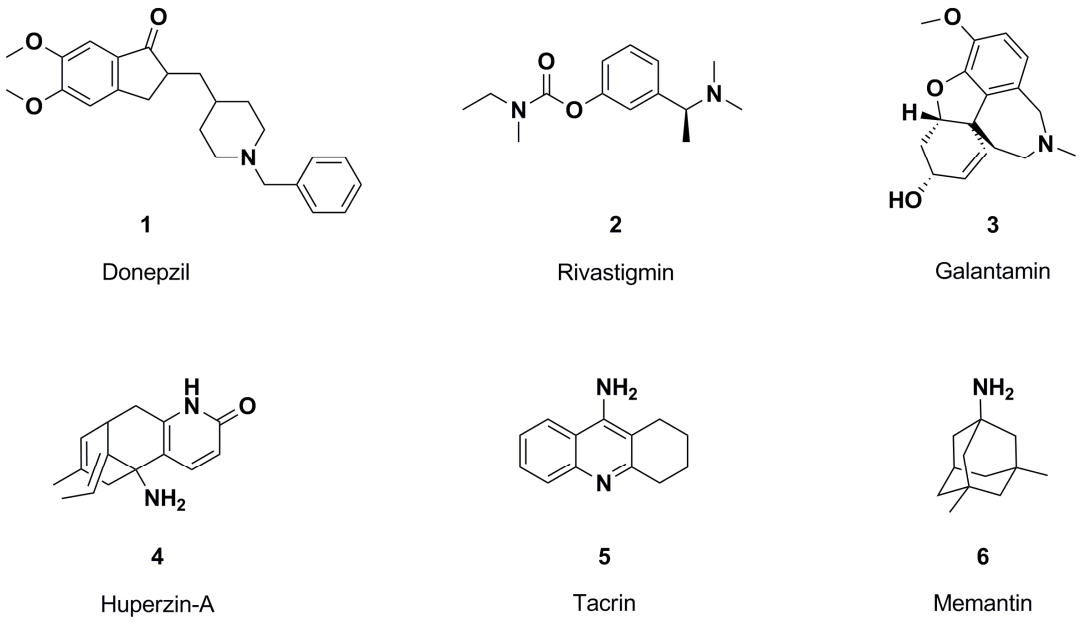

Abb. 2: Zugelassene Medikamente zur symptomatischen Behandlung von AD.

Aufgrund von Nebenwirkungen wurde diese Verbindung jedoch in einigen Ländern vom Markt genommen.[10] Memantin (**6**) ist ein nicht-kompetitiver NMDA (*N*-Methyl-D-Aspartat) Rezeptor-Antagonist und wird bei AD-Patienten mit mittlerem bis schwerem Krankheitsbild eingesetzt. Diese Verbindung kann als Monotherapie oder in Kombination mit einem Acetylcholinesterase-Inhibitor verwendet werden.[9] Desweiteren werden entzündungshemmende Medikamente wie COX-1- (Cyclooxygenase) und COX-2-Inhibitoren untersucht, da häufig Entzündungsvorgänge im Gehirn von AD-Patienten zu beobachten sind.[11-12] Auch an einer Aβ-Immuntherapie wird seit einigen Jahren geforscht. Man erhofft sich durch die Impfung eine Reduktion von Aβ und damit einhergehend eine Verringerung der Amyloid-Plaques. Derzeit befinden sich zehn dieser Impfstoffe in den klinischen Phasen.[8] Substanzen, die gezielt die Bildung von Amyloid-Plaques und NFTs verhindern, befinden sich derzeit in klinischen Studien und könnten in Zukunft eine wichtige Rolle in der Behandlung von AD-Patienten einnehmen.

1.2 APP-Metabolismus und Aβ-Peptide

Die Bildung von Amyloid-Plaques beginnt mit dem Abbau des APP. Beim APP handelt es sich um ein Typ-1-Membranprotein, welches in verschiedenen Geweben des Organismus, in der Peripherie und im Zentralnervensystem (ZNS) hergestellt wird. APP kann auf zwei verschiedenen Wegen abgebaut werden, dem nicht-amyloidogenen Weg und dem amyloidogenen Weg (Abb. 3).[5,7] Drei verschiedene Sekretasen sind für den Abbau von APP verantwortlich, die α-, β- und γ-Sekretase. Beim nicht-amyloidogenen Weg spaltet die α-Sekretase APP in das wasserlösliche sAPPα und das membrangebundene C83. Durch die γ-Sekretase wird das C83 dann weiter zum kürzeren p3-Peptid überführt, welches schnell abgebaut wird und in der Pathologie der AD keine Rolle spielt.[5,7-8] Die α-Sekretase gehört zur Familie der ADAM-Metalloproteasen (*a disintegrin and metalloprotease*) von denen drei (ADAM 9, ADAM 10 und ADAM 17) mit dem nicht-amyloidogenen Weg in Verbindung gebracht werden.[5] Beim pathogenen amyloidogenen Weg wird APP durch die β-Sekretase (*β-site APP-cleaving enzyme 1* oder BACE-1) zum sAPPβ und C99-Fragment abgebaut. Die darauffolgende Spaltung des C99-Fragments durch die γ-Sekretase führt schließlich zur Bildung von Aβ und AICD (*APP intracellular domain*). Die Rolle von AICD in der Entstehung der AD ist derzeit nicht vollständig

geklärt und Bestandteil einer kontroversen Debatte in der Alzheimer-Forschung.[13] Aβ-Peptide können in verschiedenen Längen vorkommen (38-43 Aminosäuren), wobei das dominierende Molekül das $Aβ_{40}$-Peptid ist. Es macht ca. 80-90% aller Aβ-Peptide aus, gefolgt von $Aβ_{42}$ mit einem Anteil von 5-10%.[5,7] $Aβ_{42}$ aggregiert bereitwillig und bildet den Ausgangspunkt für größere Oligomere, Fibrillen und letztlich den Amyloid-Plaques. Die frühen Aggregate und Plaques bestehen hauptsächlich aus $Aβ_{42}$. Sie können jedoch, wenn die Konzentration der Amyloidaggregate einen Schwellenwerte überschreitet, auch $Aβ_{40}$ enthalten.[5,7]

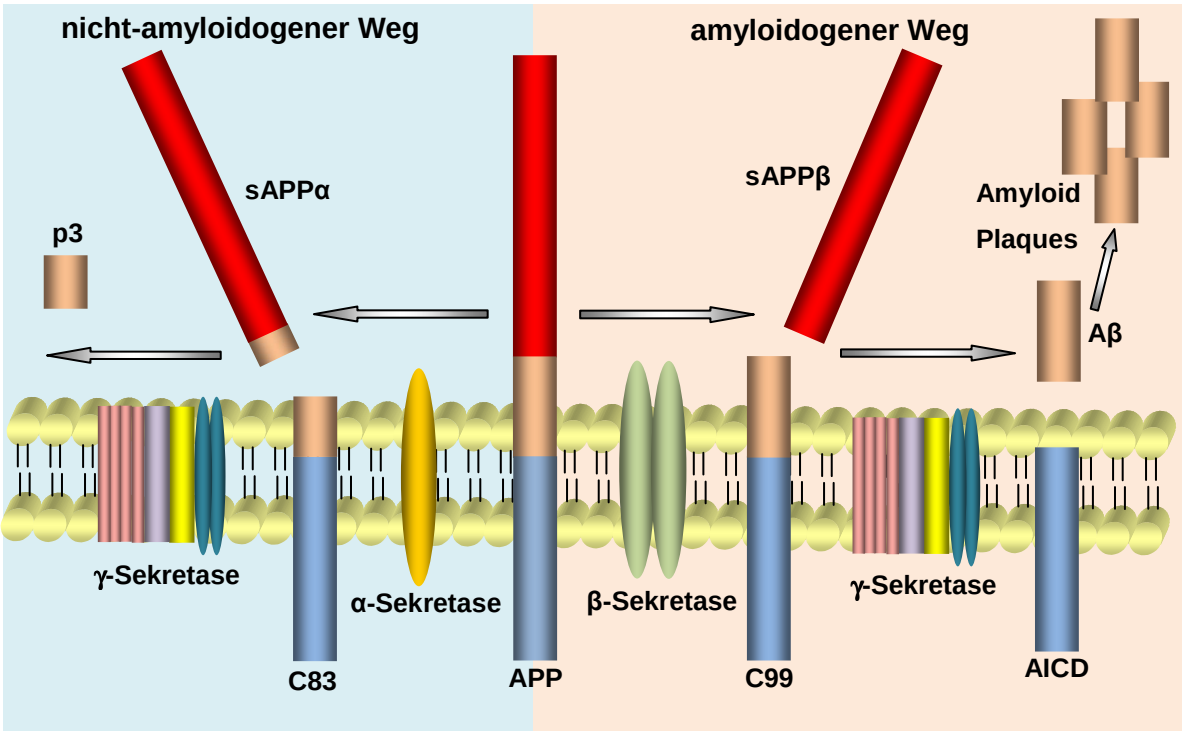

Abb. 3: Prozessierung von APP durch die α-, β- und γ-Sekretase und Bildung der Amyloid-Plaques.

Obwohl Aβ in AD-Gehirnen im Vergleich zu Kontroll-Gehirnen stark erhöht ist, konnte ein direkter Zusammenhang zwischen den Amyloid-Plaques und der Pathologie der AD bisher nicht definitiv geklärt werden. Dennoch bestimmt derzeit die Amyloidhypothese die Modelle zur Entstehung der AD. Die Hypothese besagt, dass die Akkumulation von Aβ im ZNS die Hauptursache von AD darstellt, wodurch eine pathogene Kaskade initiiert wird.[7]

Infolgedessen ergeben sich verschiedene Therapieansätze, die in der pharmazeutischen Industrie und an Hochschulen erforscht werden.[7] Alle Ansätze

richten sich gegen die Bildung von Aβ und somit gegen die Sekretasen. Der Fokus liegt hierbei auf den Inhibitoren und Modulatoren der γ-Sekretase sowie den Inhibitoren der β-Sekretase. Auch der Ansatz von α-Sekretase-Aktivatoren wurde verfolgt, jedoch konnten bisher noch keine aussagekräftigen Hinweise den Nutzen für AD-Patienten belegen.[9]

1.2.1 Modulatoren und Inhibitoren der γ-Sekretase

Die γ-Sekretase ist eine Protease mit vielen potenziellen Substraten und ist in den meisten Geweben des Organismus zu finden. Sie spaltet ihre Substrate in der lipophilen Umgebung der Transmembrandomäne und ist selbst über mehrere Transmembrandomänen in der Zellmembran verankert. Das im APP-Metabolismus durch die Spaltungsreaktion der β-Sekretase entstandene C99-Fragment wird ebenfalls von der γ-Sekretase innerhalb der Transmembrandomäne gespalten, was letztlich zur Bildung der Aβ-Peptide führt.[7,14] Die γ-Sekretase ist ein hochmolekularer Komplex und besteht aus mindestens vier unterschiedlichen Proteinen, dem PS1 oder PS2, NCSTN (Nicastrin), APH-1 (*anterior pharynx defective-1*) und PEN-2 (*presenilin enhancer-2*), die im Verhältnis 1:1:1:1 stehen (Abb. 4).

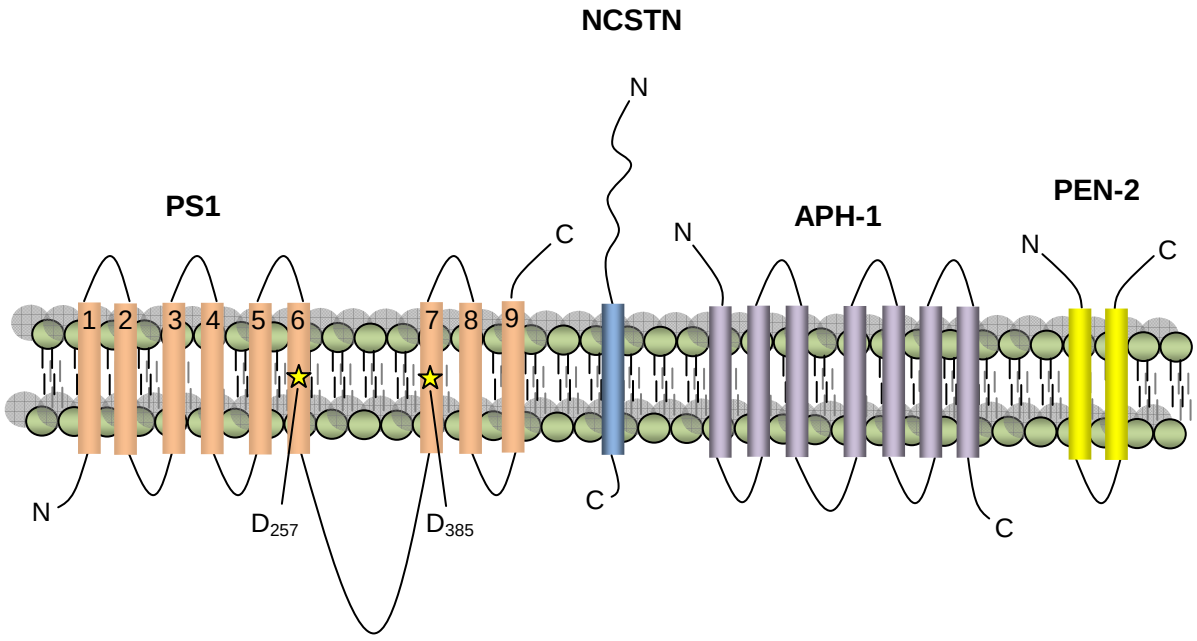

Abb. 4: Schematische Darstellung des γ-Sekretase-Komplexes.

Aufgrund fehlender struktureller Informationen ist bisher wenig über die Rolle der einzelnen Bestandteile bekannt, jedoch sind alle Untereinheiten für die Bildung des aktiven Enzymkomplexes unverzichtbar.[7-8]

Es wird heute davon ausgegangen, dass PS1 und PS2 die katalytische Untereinheit des Komplexes bilden.[7] Humanes PS1 ist ein ~50 kDa großes Transmembranprotein, und das Homolog PS2 ist lediglich vier Aminosäuren kürzer. Im aktiven γ-Sekretase-Komplex wird *Presenilin 1*, bestehend aus neun Transmembrandomänen, wahrscheinlich durch Autoproteolyse in ein N-terminales (~30 kDa, Transmembrandomäne 1-6) und ein C-terminales (~20 kDa, Transmembrandomäne 7-9) Fragment gespalten. Dadurch nimmt *Presenilin 1* seine aktive enzymatische Konformation ein. Zwei Aspartatreste (D257 und D385 beim humanen PS1), die sich zwischen der Transmembrandomäne 6 und 7 befinden, bilden hierbei vermutlich das katalytische Zentrum.[15] Die beiden Aspartatreste könnten eine ähnliche Funktion haben wie bei anderen Aspartatproteasen und die Aufgabe übernehmen, ein Wassermolekül zu aktivieren, das dann die Peptidbindung des Substrats nukleophil angreift. Wird einer dieser Aspartatreste ersetzt, geht die γ-Sekretase-Aktivität und Fähigkeit zur Autoproteolyse vollständig verloren.[7] Mutationen in der PS-Untereinheit stehen in direkter Verbindung zur γ-Sekretase-Aktivität und es wurde gezeigt, dass diese Mutationen zu einer Erhöhung des C99-Fragments führen und infolgedessen vermehrt $A\beta_{42}$ gebildet wird.[16] *Presenilin* interagiert desweiteren mit β-Catenin, weswegen es auch mit der Entstehung von verschiedenen Krebsarten in Verbindung gebracht wird.[15] Bei den drei anderen Untereinheiten wird davon ausgegangen, dass sie in der Bildung und Stabilität des Komplexes involviert sind. Über das NCSTN wurde berichtet, dass die große extrazelluläre Domäne wichtig für die Bindung des Substrats sei und spezifisch die verkürzten Typ-1-Membranproteine nach Abtrennung ihrer extrazellulären Domäne erkennt.[7,15,17] Bis zu 16 Reste des NCSTN können glykosyliert werden, jedoch scheint es, dass die Glykosylierung keinen Einfluss auf die Funktion der γ-Sekretase hat.[15,18] Über die Rolle von APH-1 und PEN-2 ist bisher sehr wenig bekannt.[7] APH-1 kann in zwei Isoformen im Menschen auftreten, APH-1A und APH-1B, jedoch konnte in Zellkulturexperimenten gezeigt werden, dass sich die Menge des gebildeten Aβ nicht unterscheidet. APH-1 besteht aus sieben Transmembrandomänen, und APH-1A kann darüber hinaus in einer langen und einer kurzen Variante

vorkommen.[14-15] Studien zu PEN-2 haben gezeigt, dass diese Untereinheit, welche aus zwei Transmembrandomänen besteht, neben der Stabilität der γ-Sekretase auch Einfluss auf den katalytischen Mechanismus des Enzyms haben könnte.[15,19]

Derzeit befinden sich sieben γ-Sekretase-Inhibitoren in der klinischen Erprobung: LY-450139, MK-0752, E-2012, BMS-708163, PF-3084014, GSI-953 und NIC5-15.[9,20,21] LY-450139 hat gezeigt, dass sie die Aβ-Konzentration im Plasma und die Aβ-Produktion im ZNS verringern kann. Ähnliche Ergebnisse wurden auch für PF-3084014 veröffentlicht.[9] Weitere γ-Sekretase-Inhibitoren wurden in den letzten Jahren in der wissenschaftlichen Literatur und in Patenten dokumentiert (Abb. 5).[7,14]

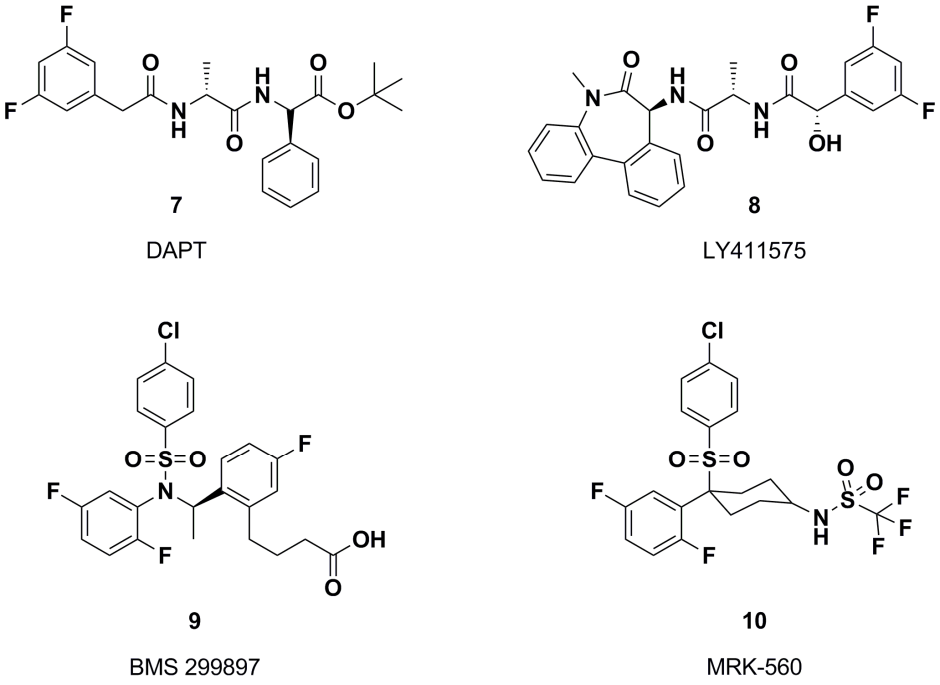

Abb. 5: Beispiele für γ-Sekretase-Inhibitoren.

Bei einer transgenen PDAPP-Maus hat die orale Applikation von DAPT (**7**) innerhalb von drei Stunden eine schnelle Abnahme des Aβ-Gehalts im Gehirn zur Folge.[22] Die Wirksamkeit dieser Verbindung wurde auch in anderen Mausmodellen bestätigt.[7] LY411575 (**8**) konnte denselben Effekt wie Verbindung **7** in der transgenen Maus und im nicht-transgenen Rattenmodell zeigen.[23] Eine häufig auftretende Nebenwirkung von γ-Sekretase-Inhibitoren ist die Inhibition des Notch-Signalwegs, welcher eine wichtige Rolle in der Zelldifferenzierung, embryonalen Entwicklung und Entwicklung von Organen spielt.[9,24] Die Applikation von Verbindung **8** an Mäusen

zeigte Nebenwirkungen, die auf den Notch-Signalweg zurückzuführen sind. BMS-299897 (**9**) hat in zellulären Tests eine 15-fach höhere Affinität für APP gegenüber Notch gezeigt und MRK-560 (**10**) konnte in einer transgenen Maus den Aβ-Gehalt im Gehirn reduzieren, ohne dass Anzeichen einer Notch-Hemmung auftraten.[7,25] Die mechanistische Basis der Selektivität von Verbindung **9** und **10** ist derzeit noch ungeklärt.[7] γ-Sekretase-Modulatoren schaffen eine Alternative zu den klassischen Inhibitoren und können den APP-Metabolismus beeinflussen ohne störende Wirkung auf den Notch-Signalweg zu haben. Manche nichtsteroidale Entzündungshemmer, wie Ibuprofen, Flurbiprofen und Indomethacin agieren als γ-Sekretase-Modulatoren und senken die $A\beta_{40}$- und $A\beta_{42}$-Produktion bei gleichzeitiger Zunahme von $A\beta_{38}$. Tarenflurbil, das R-Enantiomer von Flurbiprofen, wurde in einer Klinischen-Phase-III-Studie an Patienten mit milder AD getestet, konnte jedoch keine positiven Resultate hervorbringen.[7,9] Ein anderer Modulator, CHF-5074, befindet sich derzeit in Phase I einer klinischen Studie und konnte in Tiermodellen gute Ergebnisse aufzeigen.[9]

1.2.2 Inhibitoren der β-Sekretase

Die β-Sekretase ist wie APP ein Typ-1-Transmembranprotein und gehört zur Gruppe der Aspartatproteasen. Sie besitzt eine große extrazelluläre Domäne, welche die katalytischen Asparaginsäurereste enthält, eine kurze intrazelluläre Domäne und eine Transmembrandomäne. Die höchste Expression wurde im ZNS nachgewiesen, doch sie ist auch in peripheren Geweben zu finden.[7-8] BACE-2 (β-Sekretase 2) ist das Homolog von BACE-1 (β-Sekretase 1) und besitzt eine strukturelle Ähnlichkeit von 68%. Es wird vorwiegend in der Peripherie exprimiert und trägt nicht zur Aβ-Generierung bei.[26] Die höchste Aktivität besitzt die β-Sekretase bei pH-Wert ~4-5, was darauf hindeutet, dass sie hauptsächlich in Endosomen aktiv ist.[7,27] Der N-Terminus von Aβ-Peptiden stellt die bevorzugte Spaltstelle von BACE-1 in APP dar.[7] Bei Abwesenheit der β-Sekretase wird kein Aβ gebildet, was in Mäusen durch genetische Inaktivierung des BACE-1-Gens gezeigt werden konnte.[26] Bisher wurden noch keine Mutationen im BACE-1-Gen nachgewiesen, die mit AD in Verbindung gebracht werden können. Nichtsdestotrotz wurde eine erhöhte Aktivität dieser Sekretase in AD-Patienten festgestellt.[8] Neben APP besitzt die β-Sekretase auch andere Substrate, die den Nutzen von Inhibitoren einschränken könnten.[28] Viele

Verbindungen, die in der Literatur beschrieben wurden, sind in zellfreien und zellulären Tests aktiv, doch es fehlen Daten die eine Aktivität nach oraler Gabe in Tiermodellen bestätigen (Abb. 6).[7]

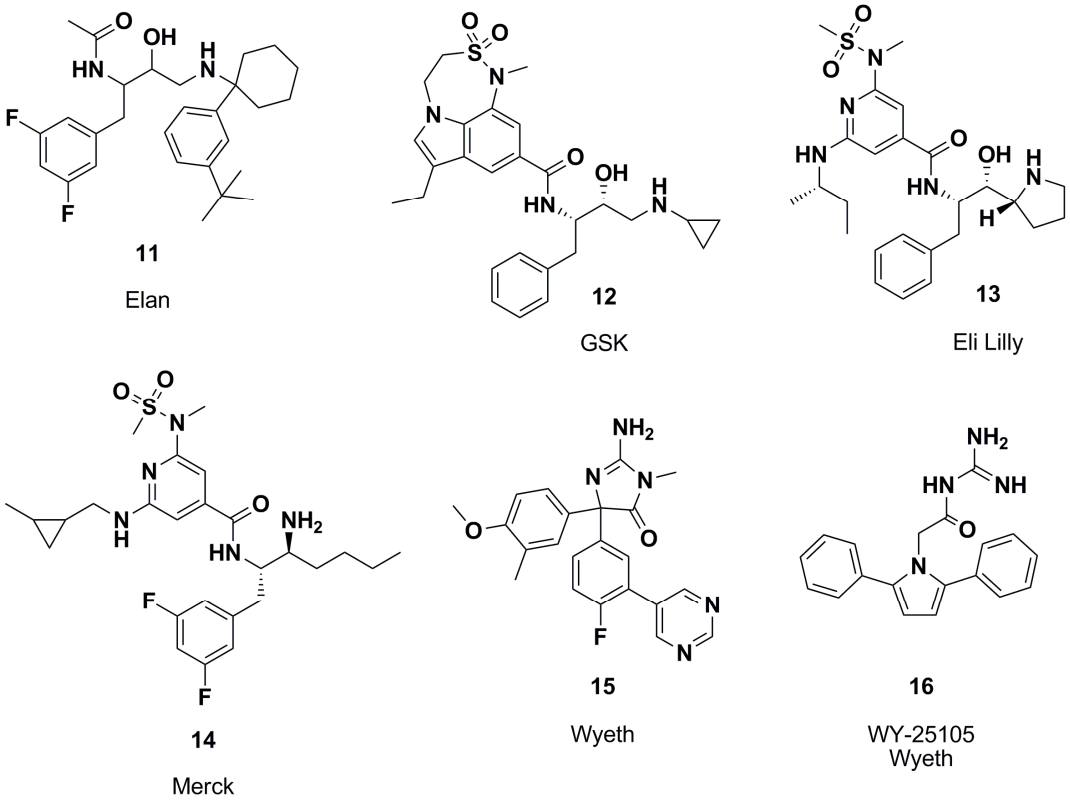

Abb. 6: Beispiele für β-Sekretase-Inhibitoren.

Obwohl schon viele Inhibitoren für Aspartatproteasen entdeckt worden sind, verlief die Suche nach β-Sekretase-Inhibitoren bisher sehr langsam. CTS-21166 ist bisher die einzige Verbindung in der klinischen Erprobung.[7-8] Aufgrund ihrer Aktivität im APP-Metabolismus sollte die β-Sekretase in Zukunft dennoch als Zielprotein (*Target*) für ein AD-Therapeutikum Beachtung finden.

1.3 Entstehung der intrazellulären Neurofibrillenbündel (NFTs)

Axonaler Transport ist eine Voraussetzung für das Funktionieren von Neuronen. Dieser Transport verläuft entlang von Mikrotubuli und wird durch Motorproteine wie Dyneine und Kinesine vermittelt. Die Mikrotubuli sind Bestandteil des Cytoskeletts und binden Mikrotubuli-assoziierte Proteine (MAPs), die verantwortlich für die Regulation ihrer Stabilität sind.[7,29] Das Tau-Protein ist hydrophil, im nativen Zustand ungefaltet und wasserlöslich. Es wird vorwiegend in neuronalen Axonen exprimiert und ist das wichtigste MAP.[7,30] Es gibt sechs Isoformen des humanen Tau-Proteins in den Neuronen, welche durch alternatives Spleißen der Exone 2, 3 und 10 des Chromosoms 17q21.3 entstehen. Sie sind zwischen 352 und 441 Aminosäuren lang und enthalten im C-terminalen Teil drei bis vier sich wiederholende Einheiten zu je 31 Aminosäuren.[7,31] Hierbei handelt es sich um mikrotubulibindende Domänen, die mitverantwortlich für die Bildung von paarigen helikalen Filamenten (*paired helical filaments*, PHFs) sind.[7,30] Das Tau-Protein enthält bis zu 79 Serin/Threonin-Reste, wovon ungefähr 30 unter physiologischen Bedingungen effektiv als Phosphorylierungsstellen agieren können.[30] Partiell phosphoryliertes Tau dient der Stabilisierung von Mikrotubuli, wodurch ein Gleichgewicht zwischen mikrotubuligebundenem und freiem löslichen Tau aufrecht erhalten wird. Dadurch wird der axonale Transport und die Struktur der Neuronen gesichert (Abb. 7).[7,32] Eine Hyperphosphorylierung des Tau-Proteins verringert die Bindung von Tau an Mikrotubuli, wodurch es zur Aggregation und zur Bildung von PHFs kommt.[33] Bisher wurden 25 Phosphorylierungsstellen identifiziert, die in Verbindung zur AD stehen. Besonders die Phosphorylierung von Ser262, Thr231 und Ser235 führt dazu, dass die Bindung von Tau an Mikrotubuli deutlich sinkt.[33] Weiterhin wurde gezeigt, dass die Phosphorylierung von Ser214 und Ser262 die Tau-Aggregation verhindern kann.[34] Die Missfaltung und Aggregation von PHFs führt zu unlöslichen NFTs, wodurch die Menge an Tau und die Stabilisierung von Mikrotubuli verringert wird.[33] Infolgedessen können die Motorproteine den Transport von Organellen, wie Mitochondrien, Peroxisomen und proteingefüllten Vesikeln nicht mehr ausführen, wobei bestimmte Bereiche wie Synapsen und das Ende der Axone Mangelerscheinungen erleiden. Der dadurch entstehende Verlust an Synapsen und Nervenzellen sind charakteristische Kennzeichen bei AD-Patienten.[7] Bislang wurde davon ausgegangen, dass nur NFTs zytotoxisch sind. Untersuchungen an

transgenen Mäusen haben jedoch gezeigt, dass auch PHFs und andere hyperphosphorylierte und lösliche Tau-Aggregate Neurodegeneration induzieren können.[30] Neben den Amyloid-Plaques gehören die NFTs zu den typischen Merkmalen der AD-Pathologie.[8] Tau-Ablagerungen wurden jedoch auch mit anderen neurodegenerativen Erkrankungen wie Morbus Pick und amyotrophe Lateralsklerose in Verbindung gebracht.[7]

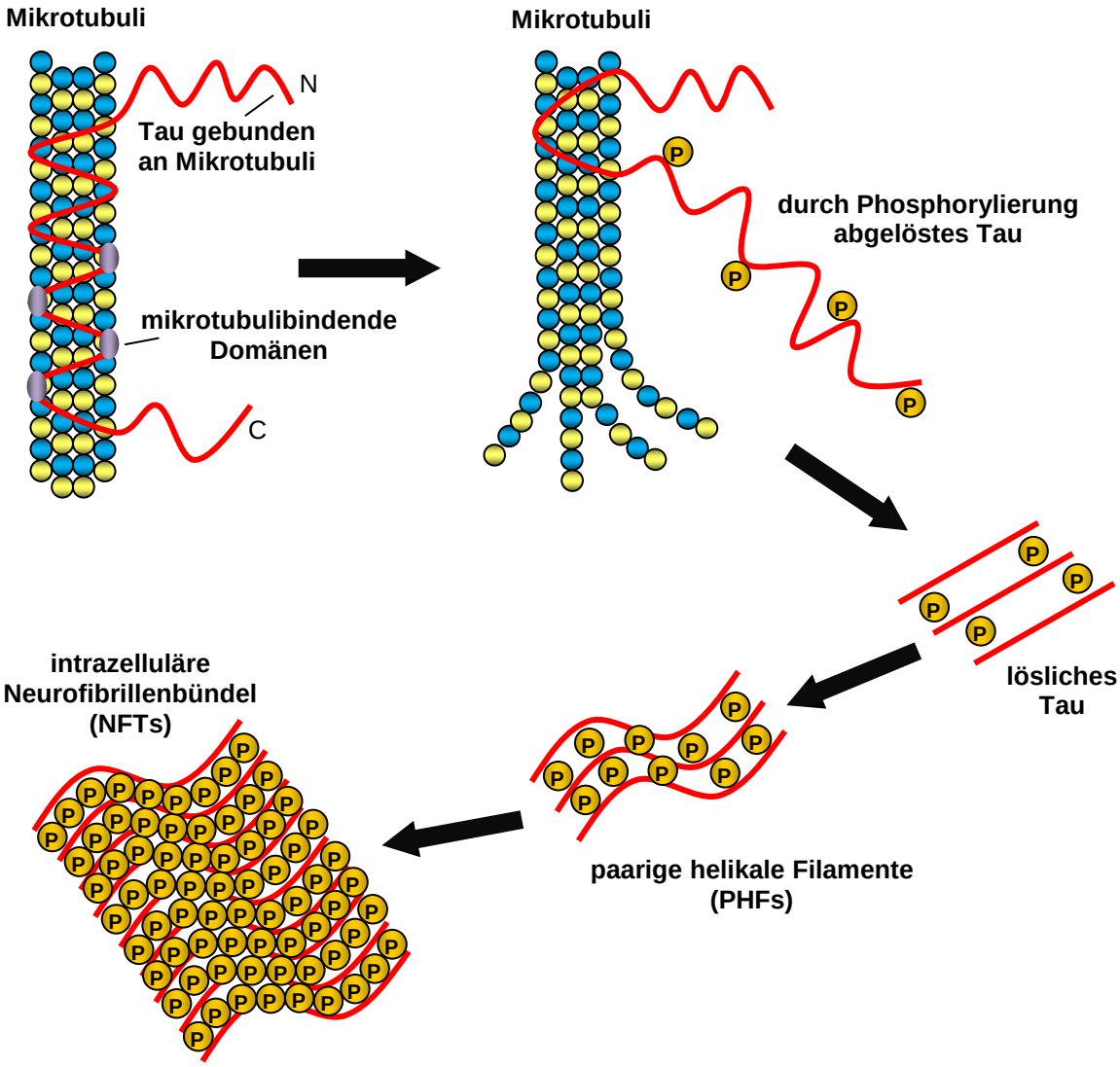

Abb. 7: Schematische Darstellung der Entstehung von NFTs.

Es wird heute davon ausgegangen, dass die Hyperphosphorylierung von Tau durch ein Ungleichgewicht der Aktivitäten von Kinasen und Phosphatasen zustande kommt.[7,33] Mehrere Kinasen haben gezeigt, dass sie Tau *in vitro* phosphorylieren können, wie ERK 2 (*extracellular signal-regulated kinase*-2), MARK 1 (*MAP/microtubule affinity-regulating kinase 1*), PKA (*cAMP-dependent protein*

kinase), CDK 5 (c*yclin dependant kinase* 5) und GSK-3 (Glykogen Synthase Kinase 3). Viele Befunde weisen jedoch darauf hin, dass CDK 5 und GSK-3 die relevanten Kinasen für die Tau-Pathologie sind.[7-8,30,33] Die Inhibition dieser Kinasen ist derzeit eine der Hauptstrategien, um gezielt die Hyperphosphorylierung von Tau und die Entstehung von NFTs zu unterbinden (siehe Kapitel 2.4).[8] Darüber hinaus werden derzeit auch andere Ansätze untersucht. Die Aktivierung von Phosphatasen und damit einhergehend die Dephosphorylierung von Tau ist einer dieser Ansätze. Es wurde berichtet, dass eine Inhibition der Protease PP-2A (*protein phosphatase-2A*) zu einer Hyperphosphorylierung von Tau führt. Demzufolge könnte PP-2A als *Target* für Aktivatoren genutzt werden, die eine Hyperphosphorylierung von Tau vermeiden. Allerdings wurden bisher noch keine pharmakologischen Ansätze hierzu publiziert.[31] Auch Substanzen, die gezielt die Tau-Aggregation und die Fibrillenbildung unterbinden sollen, werden derzeit untersucht (Abb. 8). Hierdurch erhofft man sich, neben dem Abbau der toxischen Spezies auch einen Anstieg von monomeren Tau, welches direkt zur Stabilisierung der Mikrotubuli dienen kann.[31,33]

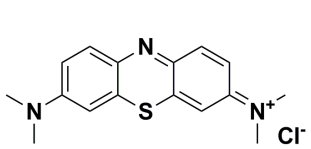

17

Methylenblau

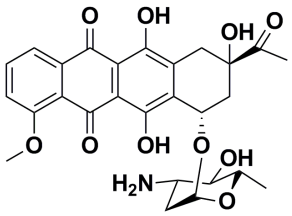

18

Daunorubicin

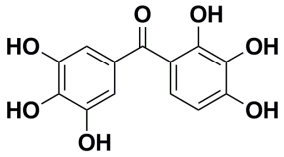

19

Exifon

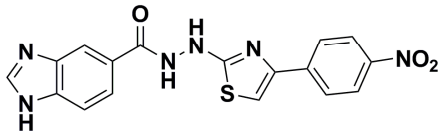

20

Phenylthiazolyl-hydrazid

Abb. 8: Beispiele für Inhibitoren der Tau-Aggregation und Fibrillenbildung.

Den direkten Abbau von Tau-Aggregaten und Fibrillen erhofft man sich momentan durch Inhibitoren von HSP 90 (*heat shock protein 90*). Diese Proteine fungieren als Chaperone, und sind somit wichtig für die korrekte Faltung von Proteinen. Eine

Hemmung von HSP 90 führt zum Abbau der Chaperon-gebundenen Proteine im Proteasom. In transgenen Tau-exprimierenden Mäusen wurde gezeigt, dass HSP 90-Inhibitoren zu einer Reduktion von hyperphosphoryliertem Tau führen.[31,33,35] Darüber hinaus wird derzeit an einer Tau-gerichteten Immuntherapie gearbeitet, und an Substanzen die die Stabilität der Mikrotubuli erhöhen sollen.[31,35]

2. Glykogen Synthase Kinase 3 (GSK-3)

2.1 Struktur und Funktion von Proteinkinasen

Proteinkinasen (PK) sind an der Regulation von fast allen Zellprozessen beteiligt. Sie kontrollieren den Metabolismus, die Transkription, die Apoptose, den Membrantransport und andere grundlegende Abläufe im Körper.[36-37] Sie katalysieren hierbei den Transfer des γ-Phosphats von ATP (Adenosintriphosphat) auf spezifische Aminosäuren des Proteins, bei Eukaryoten üblicherweise Serin-, Threonin- und Tyrosin-Reste. Durch diese Phosphatübertragung werden verschiedene intrazelluläre Signalwege vermittelt. Das menschliche Genom kodiert für 518 PK was einem Anteil von 1.7% aller Gene entspricht.[36,38-39] Durch den hohen Anteil am Genom wird ersichtlich, weshalb Mutationen und Dysregulationen von PK eine entscheidende Rolle bei der Entstehung von Krankheiten einnehmen. Diese Tatsache macht sie zu den zweitwichtigsten *Targets* in der Arzneimittelentwicklung nach den GPCRs (*G-protein-coupled receptors*). Der Hauptteil aller PK ist in zwei Untereinheiten aufgeteilt, einer N-terminalen Untereinheit, geprägt von β-Faltblatt-Strukturen und einer α-Helix, sowie einer C-terminalen Untereinheit, welche überwiegend α-helikal aufgebaut ist (Abb. 9).[37,40-41] Die ATP-Bindungstasche liegt zwischen diesen Untereinheiten und wird als flexible Gelenk-Region (*hinge-region*) bezeichnet. Die Aktivierungsschleife (*activation loop*) der Kinasen beinhaltet ein Serin-, ein Threonin- und ein Tyrosin-Rest, welche alle phosphoryliert werden können. Diese Schleife besetzt, im unphosphorylierten Zustand der Reste, Teile der ATP-Bindungstasche.[40]

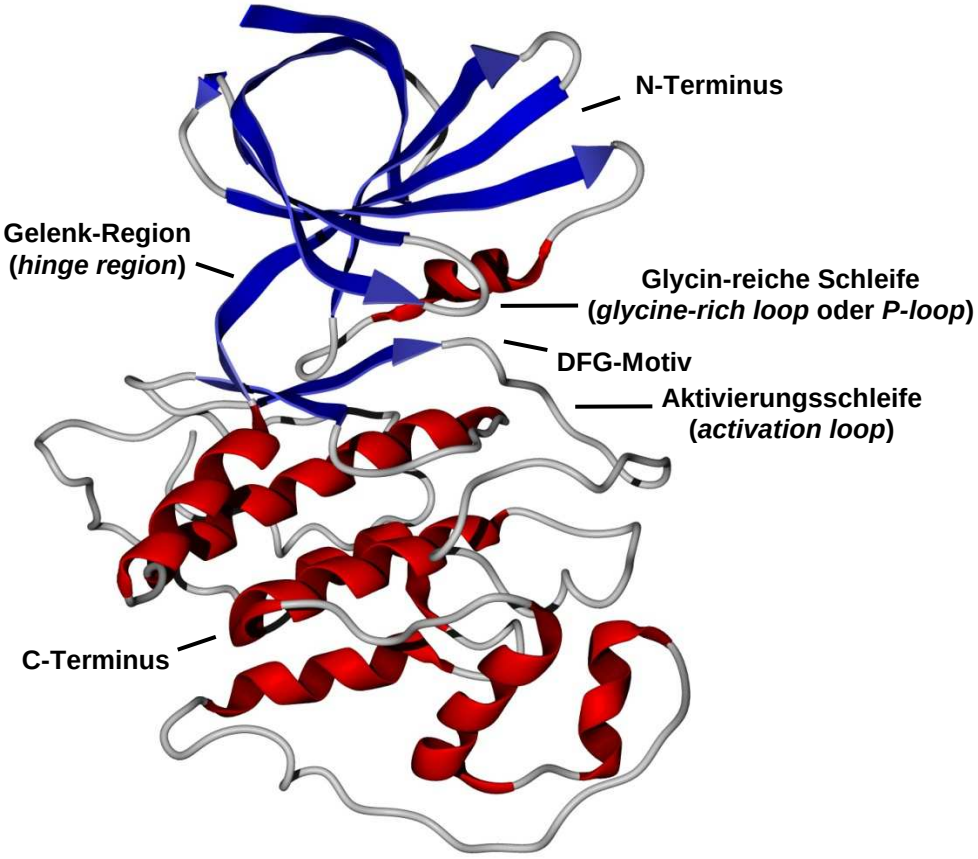

Abb. 9: Allgemeine Struktur einer Kinase dargestellt an GSK-3.

Die Phosphorylierung dieser Aminosäuren bewirkt eine Konformationsänderung, die die Aktivierungsschleife aus der ATP-Bindungstasche entfernt und somit ATP die Bindung und Übertragung eines Phosphatrestes auf das Substrat ermöglicht. Die Glycin-reiche Schleife *(glycine-rich loop* oder *P-loop*) ist ebenfalls Teil der ATP-Bindungstasche und hat eine konservierte GXGXXG-Sequenz.[40] Das DFG-Motiv (D/Asparaginsäure, F/Phenylalanin, G/Glycin) ist ein Abschnitt der Aktivierungsschleife und hochkonserviert. Die Asparaginsäure bzw. das Aspartat-Ion dieses Motivs ist katalytisch im Phosphattransfer involviert und typischerweise Teil einer Salzbrücke (Abb. 9 und Abb. 10). Das DFG-Motiv kann je nach Konformation (DFG-*in* und DFG-*out*) eine weitere hydrophobe Region zugänglich machen. Hierbei kann die DFG-*out* Konformation für die Synthese von Inhibitoren eine entscheidende Rolle spielen (siehe Kapitel 2.2). Eine der wichtigsten Aminosäuren in der ATP-Bindungstasche ist der *Gatekeeper*. Die Größe und das Volumen dieses Restes

bestimmen den Zugang zur hydrophoben Region und können oft zur Selektivität eines Inhibitors beitragen (Abb. 10).[40]

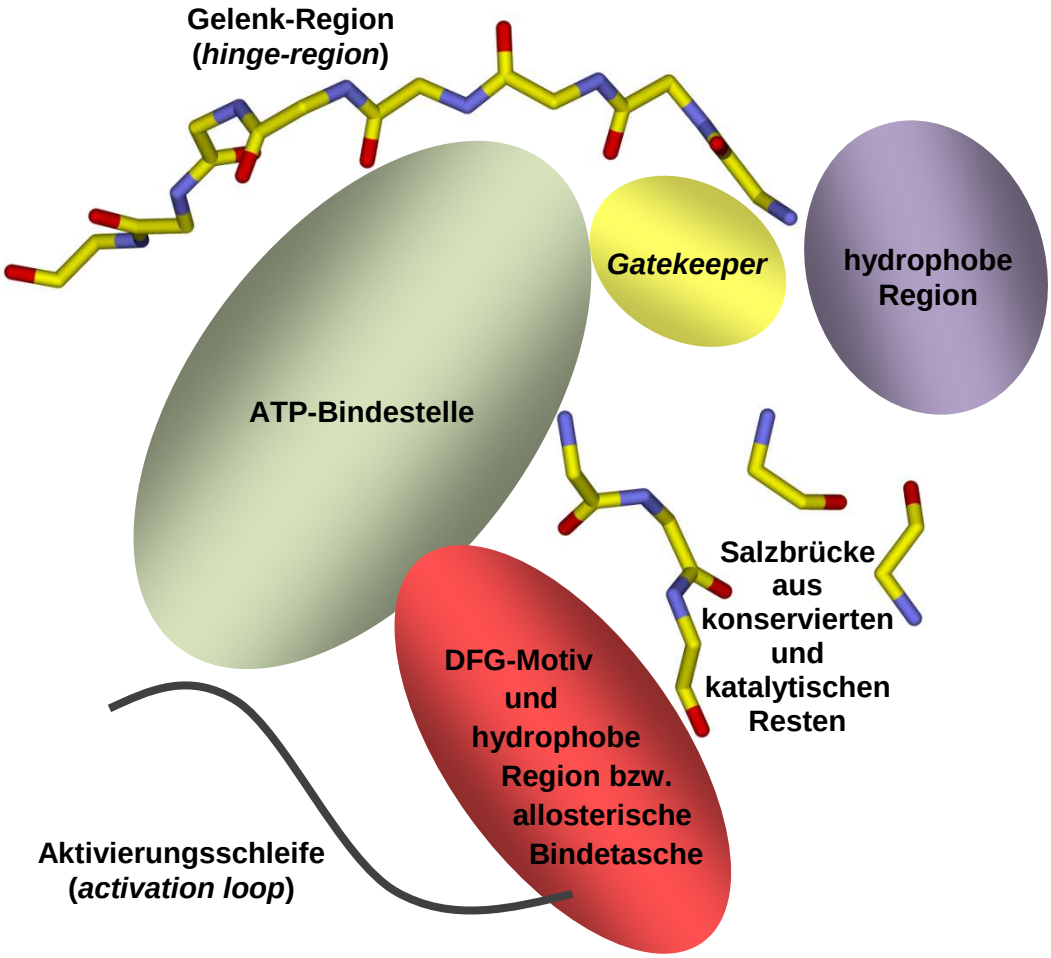

Abb. 10: Schematische Darstellung relevanter Bereiche in der ATP-Bindungstasche.

Mehrere niedermolekulare Proteinkinase-Inhibitoren (PKI) befinden sich derzeit in den klinischen Phasen und acht Verbindungen erhielten bisher die Marktzulassung von der FDA (*Food and Drug Administration*) in den USA (Abb. 11). Gleevec® (**21**) war der erste zugelassene niedermolekulare PKI.[42] Alle bislang zugelassenen PKI haben die Onkologie als Indikationsgebiet, dennoch befinden sich momentan viele PKI mit anderen Indikationsgebieten in den klinischen Phasen. Viele PKI im Bereich der Onkologie scheitern bereits in den klinischen Phasen, bedingt durch eine sich entwickelnde Tumorresistenz. Dieses Problem kann jedoch in Abhängigkeit des Inhibitionstyps unterbunden werden.[43]

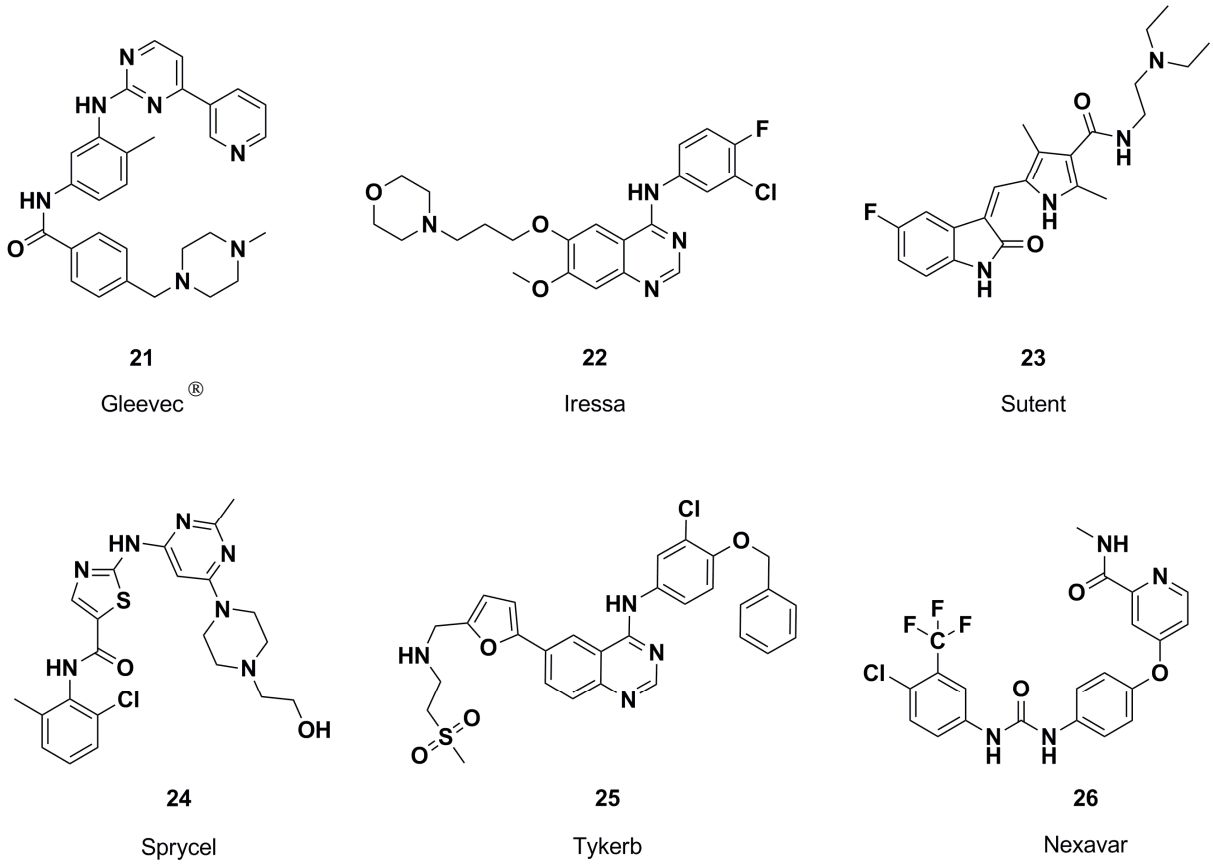

Abb. 11: Beispiele für Kinase-Inhibitoren die von der FDA zugelassen wurden.

2.2 Bindungstypen von Kinaseinhibitoren

In Abhängigkeit ihrer Inhibition lassen sich PKI in verschiedene Gruppen einteilen. Als Typ-I-Inhibitoren werden Verbindungen bezeichnet, die an die ATP-Bindestelle binden und dadurch die Aktivität der Kinase hemmen (Abb. 10). Hierbei konkurrieren die Verbindungen direkt mit ATP um die Bindestelle. Das DFG-Motiv befindet sich in der DFG-*in*-Konformation, wodurch sich die Kinase im enzymatisch aktiven Zustand befindet.[43] Typ-I-Inhibitoren wechselwirken charakteristischerweise über 1-3 Wasserstoffbrückenbindungen mit der Gelenk-Region der Kinase. Darüber hinaus kann die hydrophobe Region, deren Zugang durch den *Gatekeeper* kontrolliert wird, für die Aktivität und Selektivität dieser Inhibitoren ausschlaggebend sein.[43-45] Ein häufig auftretender Nachteil von Typ-I-Inhibitoren ist die Inhibitorresistenz, welche durch eine Mutation am *Gatekeeper* hervorgerufen wird.[43] Dadurch verlieren diese Verbindungen ihre Wirksamkeit und klinische Relevanz für bestimmte Patientengruppen. Durch die strukturelle Ähnlichkeit der PK innerhalb der ATP-

Bindestelle ergeben sich zudem Schwierigkeiten in der Entwicklung von selektiven Inhibitoren.[46] Ein potentieller Vorteil von Typ-I-Inhibitoren ergibt sich aus der Tatsache, dass der enzymatisch aktive Zustand einer Kinase in erkrankten Zellen mit hoher Wahrscheinlichkeit vorzufinden ist.[45]

Durch das Umklappen des DFG-Motivs in die DFG-*out*-Konformation wird eine weitere hydrophobe Region zugänglich, welche auch als allosterische Bindetasche bezeichnet wird. Die PK befindet sich hierdurch im enzymatisch inaktiven Zustand, welcher durch Typ-II-Inhibitoren stabilisiert werden kann.[43-44] Inhibitoren des Typs II binden an die Gelenk-Region der Kinase und in die freigegebene allosterische Bindetasche.[46] Durch die allosterische Bindetasche werden weniger konservierte Proteinseitenketten zur Wechselwirkung für Inhibitoren zugänglich gemacht, wodurch eine höhere Selektivität erzielt werden kann. Interessanterweise können nicht alle Kinasen eine DFG-*out*-Konformation einnehmen, wodurch Typ-II-Inhibitoren keinen Ansatzpunkt für alle Kinasen darstellen.[45-46]

Zu den Typ-III-Inhibitoren werden Verbindungen gezählt, die ausschließlich in die allosterische Tasche der inaktiven Kinase binden. Sie gehen keine Wechselwirkungen mit der Gelenk-Region ein und können Ausgangspunkt für Typ-II-Inhibitoren sein.[43,45] Inhibitoren dieser Klasse weisen üblicherweise eine erhöhte Selektivität auf, da sie mit einzigartigen Bereichen der Kinase interagieren.[47]

Verbindungen, die die enzymatische Aktivität eine Kinase allosterisch modulieren und mit Taschen außerhalb des aktiven Zentrums der Kinase wechselwirken, werden als Typ-IV-Inhibitoren bezeichnet.[43]

Irreversible Kinaseinhibitoren stellen eine weitere Form der Inhibition dar, welche für aktive und inaktive Kinasen Verwendung findet. Der Inhibitor wird hierbei mit einem Michael-Akzeptor versehen, der eine kovalente Bindung mit einer konservierten Cystein-Seitenkette der Kinase eingeht. Es wird vermutet, dass mehr als 200 Kinasen das Potential für solche Inhibitoren aufweisen. Drei kovalente Inhibitoren haben 2009 *Blockbuster*-Status in den USA erreicht, und mehrere Verbindungen dieser Art befinden sich in der klinischen Erprobung.[43,45,47-48]

2.3 Struktur und Substrate von GSK-3

GSK-3 ist eine Serin/Threonin PK und wurde vor mehr als 30 Jahren entdeckt. Lange Zeit galt sie als fest verknüpft mit dem Glykogenstoffwechsel und damit einhergehend mit der Phosphorylierung und Inaktivierung des Enzyms Glykogensynthase.[49-50] Heute jedoch ist bekannt, dass GSK-3 eine wichtige Rolle in einer Vielzahl von Funktionen des menschlichen Organismus einnimmt, wie z.B. in der Zellteilung, der Apoptose, der Proteinsynthese und der Mikrotubuli-Dynamik.[49,51] Diese Tatsache macht GSK-3 zu einem interessanten *Target* für die Entwicklung von Medikamenten.[50] Zwei Isoformen von GSK-3, GSK-3α und GSK-3β, werden in Säugetierzellen ubiquitär exprimiert. GSK-3β hat eine Masse von 47 kDa, während GSK-3α durch eine zusätzliche Glycin-reiche Sequenz am N-Terminus eine Masse von 51 kDa aufweist. Innerhalb ihrer Kinasedomäne sind beide Isoformen zu 98% identisch. Sie weisen jedoch außerhalb dieser Domäne signifikante Unterschiede auf.[49-50,52] Eine untergeordnete Spleißvariante von GSK-3β, GSK-3β2, wurde 2002 entdeckt. Sie enthält eine Insertion von 13 Aminosäuren innerhalb ihrer Kinasedomäne.[50,53] Die Kristallstruktur von GSK-3β wurde 2001 unabhängig voneinander von drei Arbeitsgruppen gelöst und publiziert (Abb. 9).[41,54-55] GSK-3β besitzt den im Kapitel 2.1 beschriebenen typischen Aufbau von PK. Dabei ist die N-terminale Untereinheit von GSK-3β geprägt von β-Faltblatt-Strukturen zwischen den Aminosäureresten 25-138. Die Aminosäurereste 139-343 bilden die C-terminale Untereinheit, welche überwiegend α-helikal aufgebaut ist. Die Aminosäuren Glu97 und Lys85 bilden eine Salzbrücke im aktiven Zentrum aus, welche für die Aktivität von einigen Inhibitoren ausschlaggebend ist.[41] Die Struktur von GSK-3α konnte bisher noch nicht gelöst werden.

Mehr als 40 vermeintliche Substrate sind bisher bekannt, die von GSK-3 phosphoryliert werden können (Tab. 1).[49-50,56] Einige dieser Substrate müssen zunächst durch andere Kinasen an Serin-/Threonin-Resten phosphoryliert werden, damit die Phosphorylierung durch GSK-3 stattfinden kann.[51] Die Konsensussequenz dafür lautet Ser/Thr-X-X-X-pSer/pThr, wobei das erste Serin bzw. Threonin die Aminosäure darstellt, die von GSK-3 phosphoryliert wird.[49] Die Enzymaktivität von GSK-3 kann durch Phosphorylierung eines N-terminalen Serins, Ser21 bei GSK-3α und Ser9 bei GSK-3β, signifikant reduziert werden. In Gegensatz dazu kann die

Phosphorylierung eines Tyrosins, Tyr279 bei GSK-3α und Tyr216 bei GSK-3β, die Aktivität von GSK-3 steigern.[56]

Signalproteine/Stoffwechsel	Transkriptionsfaktoren	Strukturproteine
AcetylCoA carboxylase	AP-1 (Jun family)	DF3/MUC1
Amyloid precursor protein	β-catenin	Dynamin-like protein
APC	C/EBP	Kinesin light chain
ATP-citrate lyase	CREB	MAP1B
Axin	GATA4	MAP2
Cubitus interruptus	Glucocorticoid receptor (rat)	Neural cell-adhesion
Cyclic-AMP-dependent protein kinase	HIF-1	Protein (NCAM)
Cyclin D1	HSF-1	Neurofilaments
Cyclin E	Mash1	Ninein
elF2B	MITF	Tau
Glycogen synthase	c-Myb	Telokin (KRP)
hnRNP	c-Myc	
Insulin receptor subtrate-1	NeuroD	
Myelin basic protein	NFAT	
NGF receptor	NF-κB (p65/p105)	
Nucleoporin p62	Notch	
P21	p53	
Presenilin-1	Timeless	
Protein kinase A (RII subunit)	TCF	
Protein phosphatase 1		
Protein phosphatase inhibitor-2		
Pyruvate dehydrogenase		

Tab. 1: Beispiele für vermeintliche Substrate von GSK-3.

2.4 Die Rolle von GSK-3 in der AD und literaturbekannte Inhibitoren

GSK-3 wird mit einer Vielzahl von Krankheiten in Verbindung gebracht, wie z.B. Typ-2-Diabetes mellitus, Krebs, bipolare affektive Störungen, Schlaganfall, Schizophrenie und AD.[56-59] Infolgedessen wurden bereits viele Inhibitoren für GSK-3 publiziert und patentiert. Lithium (Li^+) war der erste Inhibitor der für GSK-3 entdeckt wurde.[60] Der genaue Mechanismus der Inhibition ist bisher nicht bekannt, aber zwei Hypothesen wurden vorgeschlagen. Die erste Hypothese besagt, dass Lithium (Li^+) ein kompetitiver Inhibitor von GSK-3 ist und in Konkurrenz mit Magnesium (Mg^{2+}) steht, nicht jedoch mit dem Substrat oder ATP. Bei der zweiten Hypothese wird davon ausgegangen, dass Lithium eine inhibierende Wirkung auf den Kaliummangel

hat.[57,61-62] Neben dem Li^+-Ion wurde auch Beryllium (Be^{2+}) als GSK-3-Inhibitor identifiziert.[63]

Die Amyloid-Plaques und die NFTs sind die charakteristischen Merkmale der AD und beide Proteinablagerungen werden mit GSK-3 in Verbindung gebracht.[58] Erhöhte Werte von GSK-3β wurden durch verschiedene Forschungsgruppen im Hirngewebe von verstorbenen AD-Patienten gefunden.[64] Mehrere PK sind in der Lage Tau zu phosphorylieren, jedoch scheint es so, dass GSK-3β die dominanteste dieser Kinasen ist.[65-66] Bis zum heutigen Zeitpunkt sind über 30 Phosphorylierungsstellen an Tau bekannt, die potentiell von GSK-3β phosphoryliert werden können.[65] GSK-3α und GSK-3β haben *in vitro* und *in vivo* gezeigt, dass sie fähig sind eine Hyperphosphorylierung von Tau zu verursachen. Folglich wird angenommen, dass GSK-3 in der Entstehung von NFTs involviert ist. In Neuronen wurde gezeigt, dass eine Inhibition von GSK-3β die Phosphorylierung von Tau reduziert. Dadurch wird die Assoziation von Tau mit den Mikrotubuli verbessert und deren Stabilität erhöht.[64] Auch in GSK-3 transgenen Mäusen konnte eine Tau-Hyperphosphorylierung und Neurodegeneration festgestellt werden, die durch eine Behandlung mit Lithium unterbunden werden konnte.[66-69] In der Fruchtfliege (*Drosophila melanogaster*) führte die Überexpression von Tau in Kombination mit der Phosphorylierung durch das GSK-3-Homolog *Shaggy* zur Bildung von NFTs und zur Neurodegeneration.[66,70] Eine Merkfähigkeitsstörung bei Ratten wurde nach einer temporären Aktivierung von GSK-3 und Tau-Hyperphosphorylierung nachgewiesen.[71] Die Behandlung von neugeborenen Ratten mit Lithiumchlorid führte zu einer Reduktion der Tau-Phosphorylierung in neuronalen und nicht-neuronalen Zellen.[72-75] Ähnliche Ergebnisse wurden auch mit anderen literaturbekannten GSK-3-Inhibitoren beobachtet (Abb. 12). Eine 30-tägige Behandlung von transgenen Mäusen mit dem Inhibitor AR-A014418 (**27**) führte zu einer Reduktion der Phosphorylierung von Tau. Ähnliche Ergebnisse wurden auch mit den TDZDs (Thiadiazolidinone) in transgenen Mäusen erzielt. Diese konnten neben der Reduktion der Tau-Hyperphosphorylierung auch zu einer Verringerung der Amyloid-Plaques im Cortex und im Hippocampus beitragen.[57] Das Aβ-Peptid ist in der Lage, GSK-3 zu aktivieren und die Inhibition dieser Kinase mit dem GSK-3-Inhibitor AR-A014418 (**27**) hat gezeigt, dass die durch Aβ induzierte Neurotoxizität verringert werden kann.[76-78] Zudem wird vermutet, dass GSK-3α, nicht jedoch GSK-3β, in der Lage ist, die Aβ-Produktion zu fördern.[79] Diese

Annahme ist jedoch momentan Bestandteil einer kontroversen Debatte und wird nicht von allen Wissenschaftlern akzeptiert, da bisher nur wenige Daten über GSK-3α publiziert wurden.[80-81] Neben den literaturbekannten GSK-3-Inhibitoren, die zu den Strukturklassen der Indirubine, Maleimide, Paullone, TDZDs und Thiazole zählen, wurden in den letzten Jahren auch andere Strukturklassen, wie Oxadiazole und metallorganische Verbindungen, synthetisiert (Abb. 12).

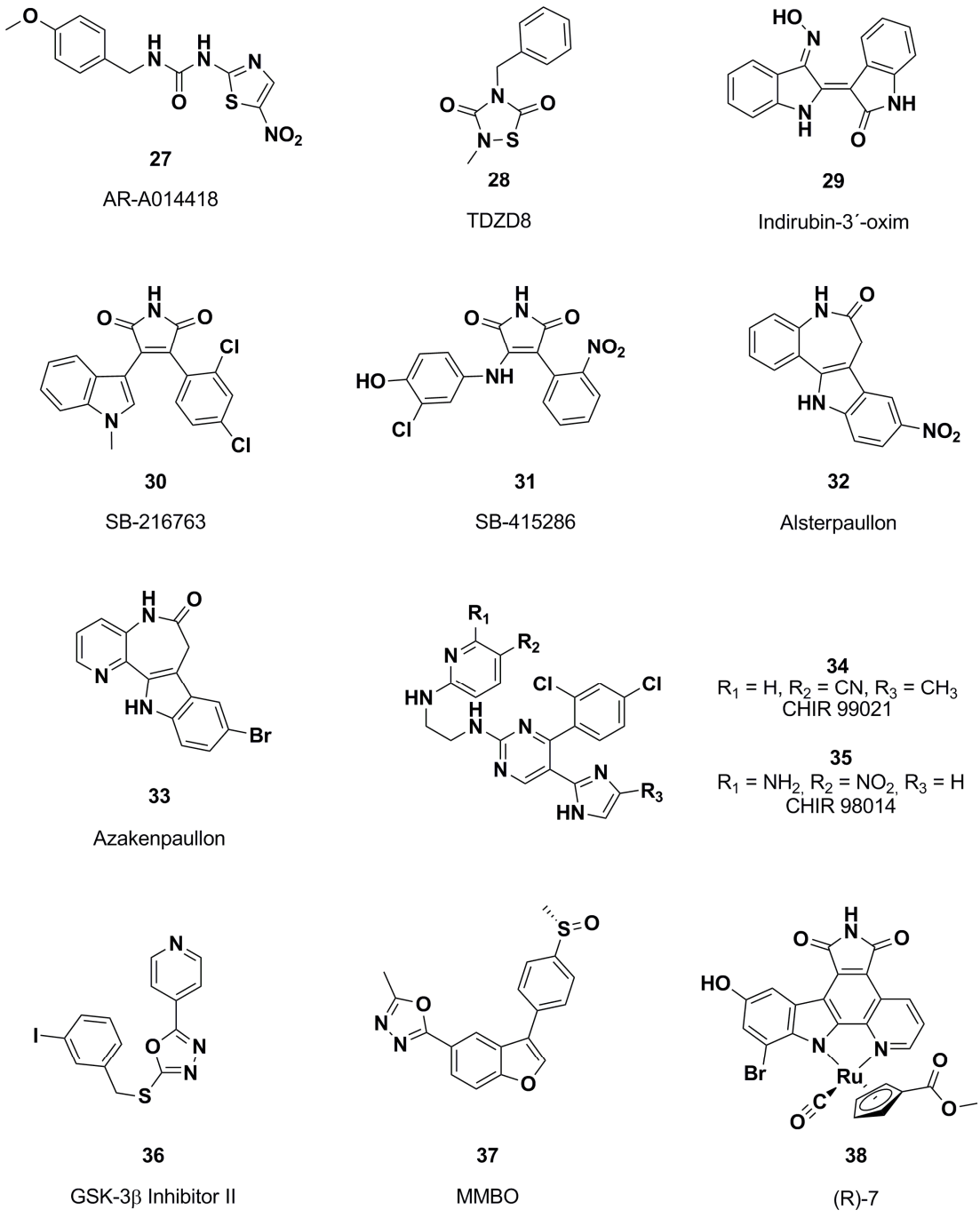

Abb. 12: Beispiele für literaturbekannte GSK-3-Inhibitoren.

Diese Substanzen konnten bisher *in vitro* und *in vivo* sehr gute Ergebnisse im Bereich der AD aufweisen.[82-88] MMBO (**37**) zählt zu diesen Verbindungen und konnte im Hippocampus einer transgenen Maus signifikant die Tau-Phosphorylierung reduzieren und zur Verbesserung der kognitiven Fähigkeiten beitragen.[84] Die genannten Studien und die Menge an Patenten machen deutlich, dass GSK-3 ein vielversprechendes *Target* für die AD-Therapie ist. NP-12 (Tideglusib) gehört zur Klasse der TDZDs und ist derzeit der am weitesten fortgeschrittene GSK-3-Inhibitor in den klinischen Phasen.[89] Die TDZDs gehören zu den nicht-ATP-kompetitiven Inhibitoren und machen nur einen geringen Teil aller bisher publizierten Inhibitoren aus.[90] Der Hauptteil aller publizierten Inhibitoren ist ATP-kompetitiv und konkurriert direkt mit ATP um die ATP-Bindestelle. Alle ATP-kompetitiven Inhibitoren, die im Bereich der AD veröffentlicht wurden, weisen auch eine Aktivität gegenüber anderen Kinasen auf.[57] Dieses Selektivitätsproblem birgt viele Risiken in der Wirkstoffsuche, da ungewünschte Nebenwirkungen auftreten können.[45] Aufgrund der hohen strukturellen Ähnlichkeit der ATP-Bindestelle in GSK-3α und GSK-3β wurde bisher noch kein Inhibitor publiziert, der effizient zwischen diesen zwei Isoformen differenzieren kann.[57,75] Erste Ansätze belegen jedoch, dass die Diskriminierung einer Isoform möglich ist.[91]

Der Wnt-Signalweg hat einen entscheidenden Einfluss auf die Differenzierung, Proliferation und das Schicksal einer Zelle. GSK-3 hat eine Schlüsselfunktion in diesem Signalweg und bildet, bei Abwesenheit des Wnt-Signalproteins, einen Komplex mit APC (*adenomatous polyposis coli*), Axin und β-Catenin (Abb. 13). Hierbei phosphoryliert GSK-3 APC, Axin und β-Catenin, wodurch es zu einem Abbau von β-Catenin kommt. Die Bindung des Wnt-Signalproteins an den Rezeptor Frizzled führt zur Auflösung dieses Komplexes und zur Bindung von GSK-3 an DVL (*dishevelled*) und FRAT (*frequently rearranged during advanced T-cell lymphoma*). Dadurch findet die Phosphorylierung von β-Catenin nicht mehr statt und es kommt zu einer Akkumulation, welche die Translokation von β-Catenin in den Nukleus fördert. β-Catenin und TCF (*transcription factor)* binden anschließend an die DNA und es kommt zur Transkription bestimmter Onkogene.[50,64,66,72,89] Die Beteiligung von GSK-3 an diesem Signalweg hat Bedenken an der Verwendung von GSK-3-Inhibitoren geweckt, da die Vermutung besteht, dass diese zur Entstehung von Krebs beitragen könnten. Diese Annahme hat sich jedoch bis zum heutigen Zeitpunkt nicht *in vivo*

bestätigen lassen. Zudem wird der GSK-3-Inhibitor Lithium bereits seit 60 Jahren als Standardtherapeutikum zur Behandlung von bipolaren affektiven Störungen verwendet, ohne eine erhöhte Krebsentstehung verursacht zu haben.[89] Dennoch sollte angesichts der Beteiligung von GSK-3 an mehreren Signalwegen eine komplette Inhibition vermieden werden.

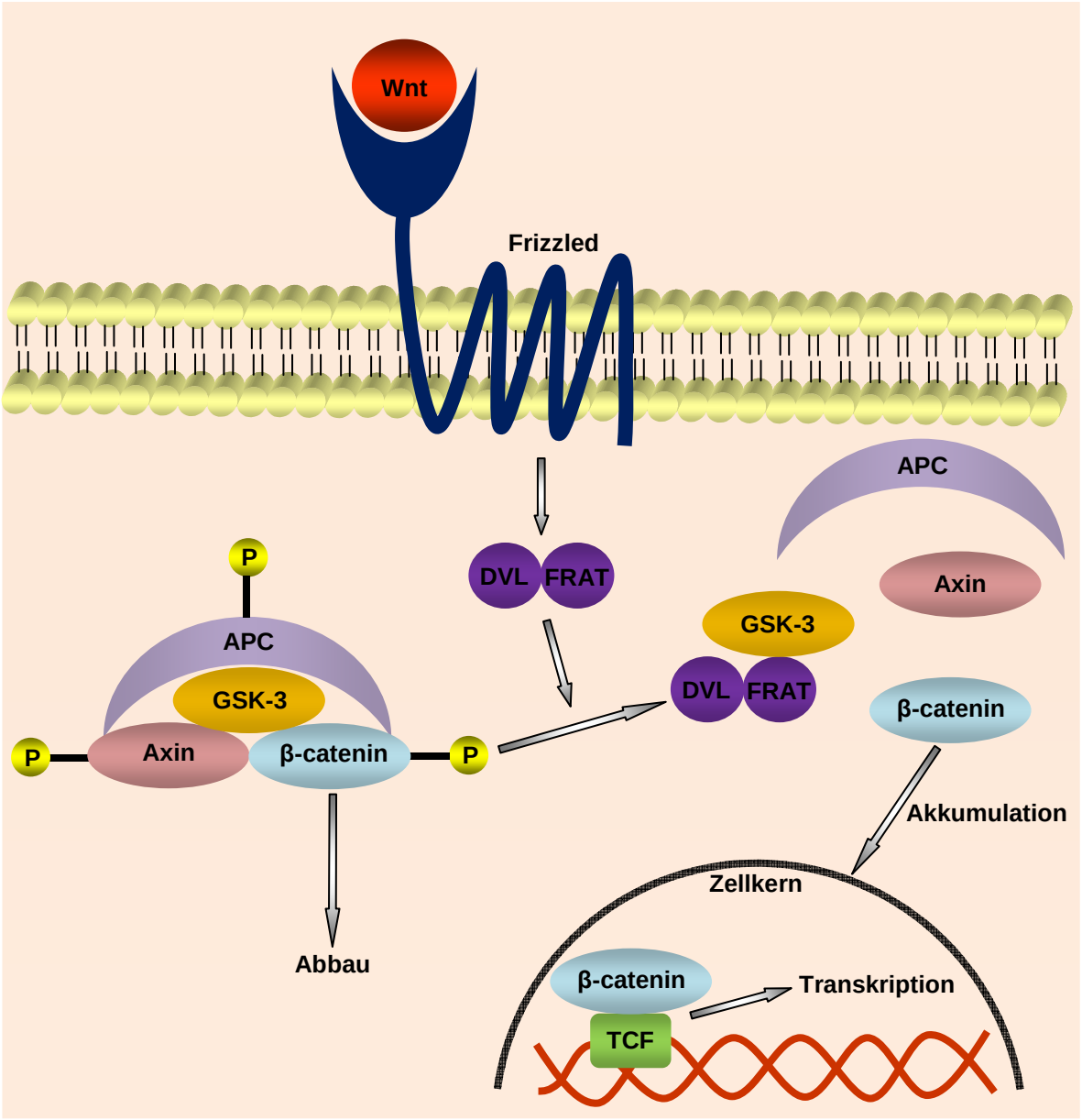

Abb. 13: Schematische Darstellung des Wnt-Signalwegs.

2.5 Weitere Funktionen von GSK-3

Durch die Beteiligung von GSK-3 an verschiedenen Signalwegen werden in diesem Abschnitt weitere Beispiele für die Verwendung von GSK-3-Inhibitoren erläutert.

Diabetes mellitus gehört zu den häufigsten Stoffwechselerkrankungen und es wird zwischen zwei Patientengruppen unterschieden, den Typ-1- und Typ-2-Diabetikern. Typ-1-Diabetiker müssen mehrmals täglich Insulin spritzen, wohingegen Typ-2-Diabetiker das Insulin zwar produzieren können, jedoch eine Resistenz gegenüber diesem Hormon aufweisen. Im Normalfall begünstigt Insulin durch Unterdrückung der GSK-3-Aktivität die Dephosphorylierung und Aktivierung der Glykogensynthase (Abb. 14). In diesem Signalweg kommt es durch die Bindung von Insulin an den Insulinrezeptor zur Phosphorylierung und Aktivierung von IRS1/2 (*insulin-receptor substrate*). Dies wiederrum führt zur Interaktion mit PI3K (*phosphatidylinositol 3-kinase*), wodurch es zur Umsetzung von PIP_2 (*phosphatidylinositol(4,5)bisphosphate*) zu PIP_3 (*phosphatidylinositol(3,4,5)tris-phosphate*) kommt. Durch die Bindung von PIP_3 an PDK1 (*3-phosphoinositide-dependant protein kinase-1*) kommt es zur Phosphorylierung und Aktivierung der Proteinkinase AKT (auch als PKB bekannt). AKT phosphoryliert und inhibiert GSK-3, wodurch es zur Dephosphorylierung und Aktivierung der Glykogensynthase durch PP1β.Gm (*protein phosphatase 1*) kommen kann. Dadurch kann die Glykogensynthase effizienter Glukose in Glykogen umwandeln und den Glukosespiegel im Blut senken. Bei Diabetikern könnten GSK-3-Inhibitoren den Effekt von Insulin nachahmen und dadurch die Umwandlung von Glukose zu Glykogen begünstigen.[56,72,92] Eine Vielzahl von Inhibitoren wurde bereits zu diesem Zweck *in vitro* und *in vivo* evaluiert und einige Beispiele sind in Abbildung 12 gezeigt. Die GSK-3-Inhibitoren SB-216763 (**30**) und SB-415286 (**31**) konnten in humanen Leberzellen zeigen, dass es durch die Inhibition von GSK-3 zu einer Aktivierung der Glykogensynthase kommt und dadurch die Umwandlung von Glukose zu Glykogen beschleunigt wird. Auch in verschiedenen Tiermodellen für Typ-2-Diabetes konnte nachgewiesen werden, dass die Verabreichung von GSK-3-Inhibitoren, wie z.B. Verbindungen **34** und **35**, zu einer Erniedrigung des Glukosespiegels im Blut führt.[72] Durch diese Beispiele wird ersichtlich, dass GSK-3 ein interessantes therapeutisches *Target* für die Insulinresistenz darstellt.

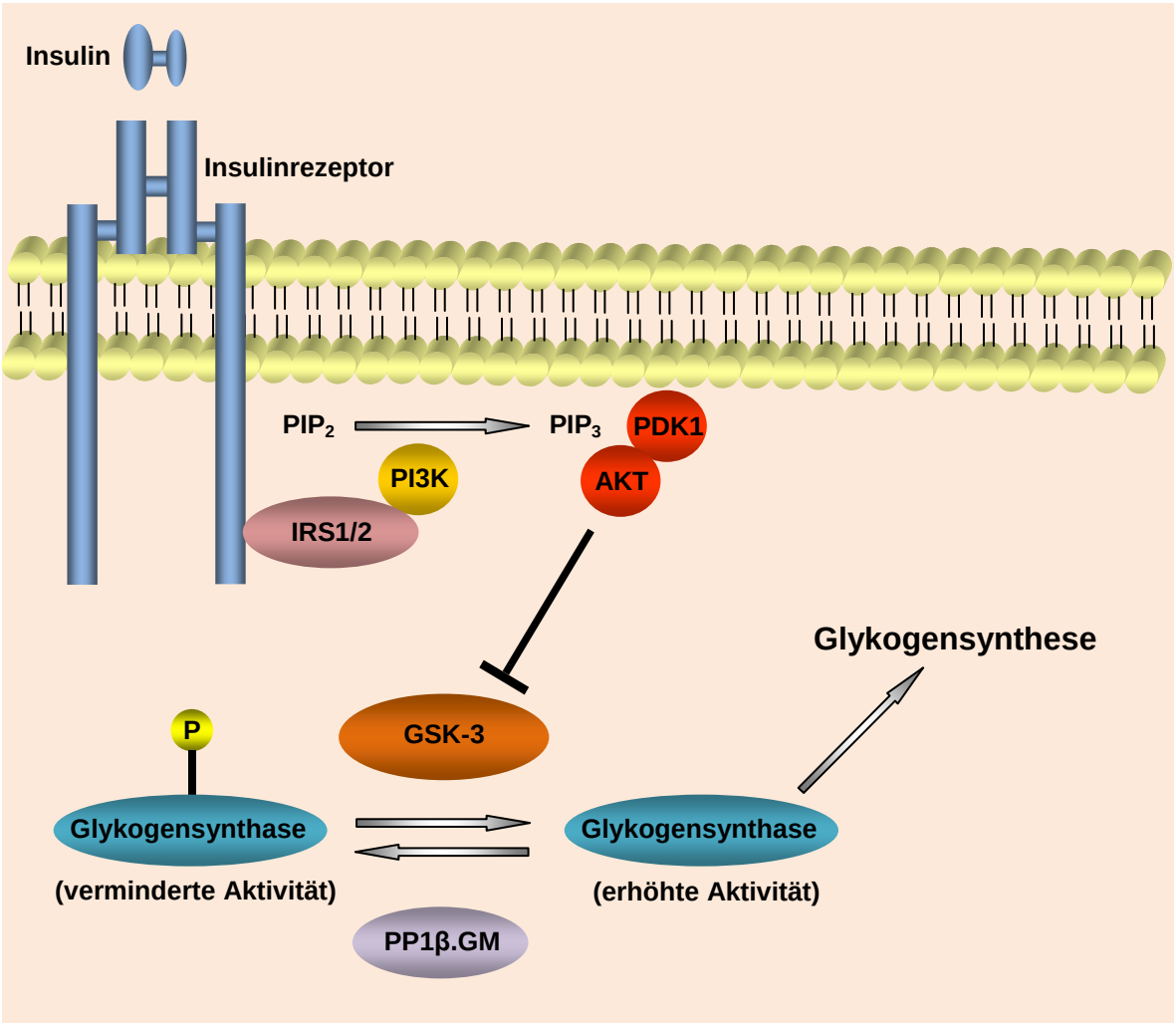

Abb. 14: Einfluss von GSK-3 auf die Glykogensynthese.

Aufgrund der regulatorischen Eigenschaften von GSK-3 in verschiedenen Signalwegen wird diese Kinase auch als *Target* für verschiedene Krebsarten, wie Bauchspeicheldrüsenkrebs und Eierstockkrebs, in Betracht gezogen.[57,93-94] Die Verwendung von Lithiumchlorid konnte bereits in verschiedenen Prostatakrebszellen eine signifikante Reduktion der Zellproliferation hervorrufen. Die akute Inhibition von GSK-3β in Darmkrebszellen durch TDZD-8 (**28**) konnte sogar dem Tumorwachstum entgegenwirken. Desweiteren hat Verbindung **28** auch in anderen Krebszellen positive Ergebnisse erzielt. Auch die Verwendung anderer literaturbekannter GSK-3-Inhibitoren zeigte vielversprechende Resultate.[57,95]

Seit längerer Zeit ist bekannt, dass GSK-3 Entzündungsvorgänge fördern kann, weshalb Inhibitoren dieser Kinase zu einer Linderung dieser Entzündungen

eingesetzt werden könnten. TDZD-8 (**28**), SB-216763 (**30**) und SB-415286 (**31**) wurden zu diesem Zweck getestet und haben gezeigt, dass GSK-3-Inhibitoren die Entwicklung von Entzündungen reduzieren können.[57]

Darüber hinaus wird vermutet, dass die erhöhte Aktivität der Proteinkinase C (α, β und ζ) und GSK-3 das Absterben der Neuronen bei ALS-Patienten (amyotrophische Lateralsklerose) steigert. Die Behandlung von ALS-Tiermodellen mit dem GSK-3-Inhibitor AR-A014418 (**27**) führte zu einer verzögerten Entwicklung der Krankheit und einer Verlängerung der Lebensspanne und bestätigte die Verwendbarkeit dieser Inhibitoren.[57] Auch der Einsatz von GSK-3-Inhibitoren bei affektiven Störungen wurde durch AR-A014418 (**27**) und TDZD-8 (**28**) bestätigt.

Ein neuer und interessanter Einsatz von GSK-3-Inhibitoren in der regenerativen Medizin hat sich durch die Tatsache ergeben, dass GSK-3 eine wichtige Rolle bei der Differenzierung, der Wachstumskontrolle und der Mobilität von Stammzellen zu haben scheint.[96-97]

2.6 Etablierte Tiermodelle für GSK-3

In den letzten Jahren wurden verschiedene Tiermodelle für die Erforschung von neurodegenerativen Erkrankungen und Taupathien entwickelt. Die Überexpression von GSK-3β in einer transgenen Maus resultierte in einer Neurodegeneration und bestätigte, dass diese Mäuse zur Untersuchung von AD-assoziierten Erkrankungen verwendet werden können.[67] Eine doppelt transgene Maus, welche humanes APP und Tau überexprimiert, wurde 2005 entwickelt. Diese Maus konnte bereits die Wirksamkeit von verschiedenen GSK-3-Inhibitoren *in vivo* bestätigen.[98-99] Die APP-V7171xTau-P301L-Maus kombiniert die Amyloid-Plaque- mit der Tau-Pathologie und wird zusammen mit der GSK-3βxTauP301L-Maus, welche nur die Tau-Pathologie entwickelt, zur Untersuchung der molekularen Signale in denen GSK-3 involviert ist, verwendet.[100] Zwei weitere transgene Mäuse, 3xTg-AD und TAPP-Mäuse, wurden entwickelt, um die Interaktionen zwischen APP bzw. Aβ und Tau zu untersuchen.[101-102] Die transgene JNPL3-Maus, welche eine Tau-Pathologie entwickelt, wird sehr häufig zur Untersuchung der Effektivität von GSK-3-Inhibitoren benutzt.[103-104]

Neben den transgenen Mäusen hat sich der transgene Zebrafisch in den letzten Jahren zur Untersuchung der Tau-Pathologie und Neurodegeneration als Tiermodell bewährt. Er ermöglicht eine schnelle und effiziente *in vivo* Evaluierung von GSK-3-Inhibitoren und ist verglichen mit der Maus kostengünstig in der Haltung.[105-106] GSK-3-Inhibitoren können aber auch mittels Wildtyp-Zebrafisch-Embryonen evaluiert werden, wobei die Zugabe des Inhibitors 4-24 Stunden nach der Befruchtung erfolgen muss. Durch die Inhibition von GSK-3 bzw. des Wnt-Signalwegs entstehen spezifische Phänotypen, die eine Aussage über die *in vivo* Effektivität dieser Inhibitoren erlauben.[106] Weitere transgene Zebrafische wurden entwickelt, um die Beteiligung von GSK-3 an der Kardiogenese zu untersuchen. Hierbei wurde festgestellt, dass GSK-3α essentiell für das Überleben von Herzmuskelzellen ist.[107]

Zur Untersuchung von neurodegenerativen Erkrankungen, wie der AD, haben sich auch wirbellose Modellsysteme etabliert. Zu erwähnen sind hierbei die Fruchtfliege (*Drosophila melanogaster*) und der Fadenwurm (*Caenorhabditis elegans*). In beiden Tiermodellen konnte die Bildung von Tau-Filamenten nachgewiesen werden.[108] Dennoch wird die Effektivität von GSK-3-Inhibitoren hauptsächlich in Wirbeltieren untersucht, da diese Modellsysteme dem Menschen evolutionär und morphologisch ähnlicher sind.

2.7 Molekulare Interaktionen

Strukturbasiertes Wirkstoffdesign versucht, molekulare Interaktionen zwischen dem Ligand und dem *Target* zu identifizieren und zu optimieren, um eine Erhöhung der Aktivität und Selektivität zu erreichen. Eine Kristallstruktur des Liganden im Komplex mit dem Zielprotein kann viele Hinweise für mögliche Interaktionen geben. Dennoch gibt eine solche Kristallstruktur nur einen statischen Einblick, da solche Komplexe in der Realität nicht nur durch eine Struktur charakterisiert werden können. Jede Ligandenbindung in der ATP-Bindungstasche des Proteins verdrängt Wassermoleküle aus dieser, welche kristallographisch nur schwer erfasst werden können. Viele dieser Wassermoleküle sind austauschbar, jedoch gibt es auch welche, die als Teil der Proteinstruktur betrachtet werden müssen. Diese können beispielsweise die Flexibilität eines Proteins beeinflussen und direkt oder über ein Wassernetzwerk die Interaktion zwischen dem Ligand und dem Protein vermitteln. Wasserstoffbrückenbindungen sind die wichtigsten Interaktionen in biologischen

Erkennungsprozessen. Hierzu zählen unter anderem die Wechselwirkungen zwischen NH und einer Carbonylgruppe, zwischen einer Hydroxylgruppe und einer Carbonyl-, Ether- oder Estergruppe und Wasserstoffbrückenbindungen zu aromatischen Heterozyklen. Die Bindungsabstände liegen im Normalfall zwischen 2.6-3.2 Å, wobei ungeladene Wasserstoffbrückenbindungen länger sind als geladene.[109] Hydroxylgruppen und NH-Gruppen können auch Wasserstoffbrücken zu aromatischen Systemen ausbilden (Abb. 15). Der Abstand zwischen dem Wasserstoffbrücken-Donoratom und dem Zentroid des aromatischen Ringes beträgt im allgemeinen 3.2-3.8 Å.[110] Auch CH-Gruppen sind fähig Wasserstoffbrückenbindungen auszubilden, und diese Wechselwirkungen sind allgegenwärtig in biologischen Systemen. Hierbei können neben Heteroaromaten auch aromatische Ringe als Wasserstoffbrücken-Akzeptoren agieren. Diese im Vergleich recht schwache Wechselwirkung ist sehr oft bei PKI zu beobachten.[109-110] Kurze Wasserstoffbrückenbindungen weisen meist eine stärkere Interaktion auf und sind bei Salzbrücken zwischen Carboxylat und Ammonium zu finden. Der Hauptteil aller PKI mit direkter Wechselwirkung zur *hinge-region* bildet eine Wasserstoffbrückenbindung mit einem NH dieser Region aus. Besteht diese Interaktion nicht, liegt das NH der *hinge-region* solvatisiert vor.[109] Intramolekulare Wasserstoffbrückenbindungen innerhalb eines Liganden können auch die Wechselwirkung mit dem *Target* beeinflussen.[111]

Die Halogene Chlor, Brom, und Iod sind imstande mit Elektrophilen, Nukleophilen und mit anderen Halogen zu interagieren. Im Gegensatz zu Fluor besitzen die schwereren Halogene einzigartige elektronische Eigenschaften, wenn sie an einer Arylgruppe oder elektronenziehender Alkylgruppe gebunden sind. Durch eine Anisotropie der Elektronendichteverteilung bilden die nichtbindenden Elektronen im äußeren Ring eine negative Ladung aus. Im inneren Ring entsteht dadurch ein positiver Bereich (*σ-hole*), der in der Lage ist mit freien Elektronenpaaren der Carbonylgruppe zu interagieren.[109,112] Die Bindungsabstände liegen zwischen 2.9-3.5 Å und sind im Vergleich zu Wasserstoffbrückenbindungen schwächer. Dennoch kann ein Austausch von Wasserstoff durch Halogene die Bindungsaffinität von Inhibitoren enorm steigern.[109-110,113]

Das Fluor der C-F-Gruppe ist ein schwacher Wasserstoffbrücken-Akzeptor. Dennoch ist die Interaktion C-F•••H-N häufig bei den Wechselwirkungen zwischen Inhibitor und *Target* vorzufinden. Der C-F-Dipol kann desweiteren, wie alle anderen Halogene auch, mit aromatischen Ringen interagieren und orthogonale multipolare Wechselwirkungen eingehen.[109-110,113] Orthogonal multipolare Wechselwirkungen kennzeichnen enge, orthogonale Kontakte zwischen zwei dipolaren funktionellen Gruppen. Solche Interaktionen können beispielsweise zwischen C=O•••C=O, C≡N•••C=O und C-X•••C=O (X = Halogen) auftreten und essentiell für die Stabilität der Proteinkonformation sein. Darüber hinaus können sie die Selektivität einiger Liganden beeinflussen und äußerst gerichtet sein, wodurch enge Wechselwirkungsabstände entstehen. Die Beschaffenheit der $C^1{=}O^1{\bullet\bullet\bullet}C^2{=}O^2$-Wechselwirkung kann am besten als dipolar elektrostatisch beschrieben werden, wobei die auf dem C^2-Atom lokalisierte positive Partialladung ein elektrostatisch anziehendes Zentrum für das partiell negativ geladene O^1-Atom ist. Die Bindungsabstände dieser Interaktionen liegen im Bereich von 2.9-4.0 Å.[109,114-116]

Aren-Aren-Wechselwirkungen sind sehr häufig in biologischen Systemen vorzufinden und für die molekulare Erkennung, die Katalyse und den Transport unentbehrlich. Zudem tragen sie zur Proteinstruktur, der Protein-Ligand-Komplexierung und der Modulation physikalischer Eigenschaften des aktiven Enzyms bei (Abb. 15). Die aromatischen Ringe können hierbei drei verschiedene Geometrien einnehmen, die als parallel verschobene, *Face-to-Face* und T-förmige *Edge-to-Face* Geometrie bezeichnet werden. Elektronenziehende Gruppen wie CN und NO_2 können die Stabilität solcher dimeren Systeme steigern, wohingegen Elektronendonor-Substituenten, wie OH und NH_2, die Wechselwirkung destabilisieren können. Die Bindungsabstände aromatischer π-π-Wechselwirkungen liegen im Bereich von 3.4-3.8 Å.[109-110]

Schwefel-Aren-Wechselwirkungen sind häufig in biologischen Systemen vorzufinden. Insbesondere Methionin- und Cystein-Seitenketten können solche Interaktionen im Bereich von 3.6-4.3 Å eingehen.[109-110]

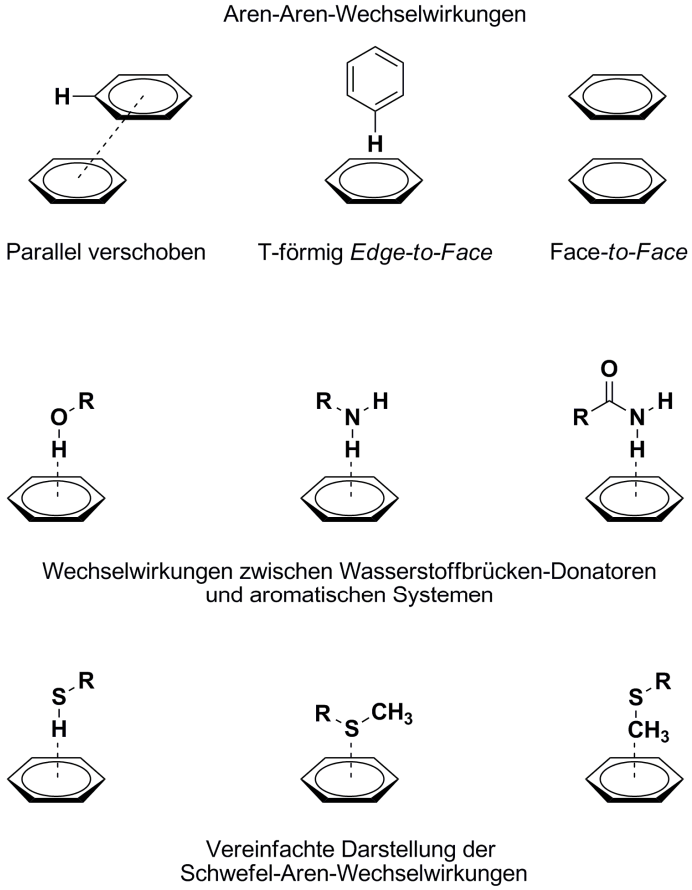

Abb. 15: Molekulare Interaktionen mit aromatischen Systemen.

Arginin- und Lysin-Seitenketten sowie Purine sind imstande Kationen-π-Interaktionen auszubilden. Diese Art von Wechselwirkung ist sehr oft in der Natur anzutreffen und zählt zu den stärksten biologischen Kräften in Komplexierungsprozessen. Ferner sind sie essentiell für viele Erkennungsprozesse in denen Neurorezeptoren involviert sind. Eine eher nebensächliche Bedeutung in biologischen Systemen haben Anionen-π-Interaktionen, da elektronenreiche aromatische Verbindungen negative Ladungen im Bereich ihres π-Systems meiden.[109-110]

2.8 Entwicklung von Wirkstoffen

Das Auffinden und Optimieren von selektiven PKI für die effektive Behandlung verschiedener Krankheiten hat sich im Laufe der letzten Jahre zu einem vielversprechenden Ansatz entwickelt. Jedoch ist die Identifizierung der *Targets*, die für die Anwendung von Kinase-Inhibitoren in Frage kommen, ein vielschichtiger Prozess. Hierbei werden mit Hilfe der Bioinformatik, Zellbiologie, Strukturbiologie

und durch *in vivo* Studien Daten generiert, die letztendlich einen Bezug des Zielproteins zur Krankheit bestätigen. Im Anschluss daran versuchen Pharmafirmen neue Leitstrukturen für spezifische Kinasen aufzufinden. Dies geschieht z.B. mit Hilfe des *High-Throughput-Screenings*, in dem automatisiert riesige Substanzbibliotheken auf ihre Effektivität hin getestet und neue Leitstrukturen für die Entwicklung von Arzneistoffen abgeleitet werden. Bei der Auswahl einer Leitstruktur sollte jedoch nicht nur auf die Aktivität und Selektivität einer Verbindung geachtet werden. Vielmehr sollten potentiell toxische Eigenschaften und physikochemische Parameter der Substanz bei der Entscheidungsfindung mit einbezogen werden. Durch die steigende Anzahl an Kristallstrukturen, die bereits von Kinasen gelöst wurden, hat sich bei der Findung von Leitstrukturen zusätzlich die fragmentbasierte *X-ray crystallography* etabliert.[117-119] Nachdem eine passende Leitstruktur ausgewählt wurde, findet der Optimierungsprozess dieser Verbindung statt. Falls eine Kristallstruktur der Kinase bereits publiziert worden ist, dient molekulares *Docking* dem Chemiker zusätzlich bei der Synthese von Inhibitoren. Mit Hilfe dieser Methodik können Substanzen virtuell auf Bindung an ein Zielprotein getestet und Synthesestrategien entwickelt werden.

Beim Modifizierungs- und Derivatisierung-Prozess von Leitstrukturen versuchen Chemiker bestimmte Kriterien einzuhalten. Zu den wichtigsten Kenngrößen gehören die *Rule of Five*, welche stark mit der Löslichkeit und Permeabilität von Substanzen assoziiert sind. Die *Rule of Five* besagt, dass das Molekulargewicht einer Verbindung < 500 g/mol, die Anzahl der Wasserstoffbrücken-Akzeptoren < 10, die Anzahl der Wasserstoffbrücken-Donoren < 5 und der logP-Wert < 5 sein soll. Eine weitere Kenngröße ist der logD-Wert, welcher die Verteilung einer Substanz zwischen Octanol und Wasser unter verschiedenen pH-Werten beschreibt, wohingegen der logP den pH-Wert nicht berücksichtigt.[120-121] Die polare Moleküloberfläche (*polar surface area*, PSA) ist definiert als die Summe der Oberfläche von polaren Atomen in einem Molekül. Der PSA ist ein guter Parameter zur Vorhersage des molekularen Transports einer Verbindung, wie die intestinale Absorption und die Penetration der Blut-Hirn-Schranke. Die Blut-Hirn-Schranke schützt das ZNS vor Schädigungen und ist entscheidend für die neuronalen Funktionen.[122] Bei Molekülen mit einem PSA > 140 $Å^2$ geht man davon aus, dass die Penetration von Zellmembranen eher schlecht ist, wohingegen ein PSA ≤ 60 $Å^2$ für leicht absorbierbare Moleküle steht. Der

TPSA (*topological polar surface area*) errechnet sich aus der Summe der PSA-Werte einzelner polarer Fragmente des Moleküls und dient ebenfalls der Vorhersage des molekularen Transports.[123-124]

Durch das Einbringen einzelner Substituenten, wie Fluor, oder bestimmter funktioneller Gruppen, wie einer Sulfon- und CN-Gruppe, kann die Basizität einzelner Moleküle gesenkt werden. Hierdurch kann eine verbesserte orale Bioverfügbarkeit erreicht werden. Zudem ist Fluor in der Lage die metabolische Stabilität von Wirkstoffen zu erhöhen und den logD-Wert zu senken. 20% aller der sich auf dem Markt befindenden Arzneimittel beinhalten einen Fluorsubstituenten.[125-127] Nach Optimierung der Leitstruktur und der *in vitro* und *in vivo* Evaluierung werden die Wirkstoffe in klinischen Studien erprobt. Von der Entwicklung bis zur Einführung von Arzneimitteln vergehen 10-12 Jahre. Bei ZNS-Medikamenten erhöht sich die Zeitspanne auf bis zu 16 Jahre, da hier erschwerend die Überwindung der Blut-Hirn-Schranke hinzukommt.[128]

3. Aufgabenstellung und Zielsetzung der Arbeit

Alle bisherigen Maßnahmen zur Behandlung der Alzheimer-Demenz (AD) dienen dem Ziel die Symptome zu lindern, nicht jedoch die ihr zugrunde liegende Pathologie. Aus diesem Grunde werden seit einiger Zeit verschiedene Therapiemöglichkeiten dieser Erkrankung untersucht. Der Fokus wird hierbei auf die Synthese von Wirkstoffen gelegt, die eine Entstehung der Amyloid-Plaques und intrazellulären Neurofibrillenbündel unterbinden sollen. Diese Proteinablagerungen sind die charakteristischen Merkmale der AD, und beide werden mit der Glykogen Synthase Kinase 3 (GSK-3) in Verbindung gebracht. Viele *in vitro* und *in vivo* Studien machen dies deutlich, wodurch GSK-3 ein vielversprechendes *Target* für die AD-Therapie ist. Daraus ergeben sich folgende Aufgabenstellungen, die im Rahmen der vorliegenden Arbeit untersucht und bearbeitet werden sollten:

- Der Einsatz literaturbekannter GSK-3-Inhibitoren hat gezeigt, dass diese Verbindungen imstande sind, die Tau-Hyperphosphorylierung und die Bildung von Amyloid-Plaques zu reduzieren. Aufgrund dessen bestand die erste Aufgabenstellung dieser Arbeit im Design und der Synthese verschiedener ATP-kompetitiver GSK-3-Inhibitoren. Zur Untersuchung der Struktur-Aktivitäts-Beziehung sollten verschiedene Grundgerüste (*scaffolds*) eingesetzt werden.

- Alle bisher publizierten ATP-kompetitiven GSK-3-Inhibitoren, die veröffentlicht oder patentiert wurden, weisen eine Aktivität gegenüber anderen Kinasen auf. Besonders die strukturelle Ähnlichkeit der ATP-Bindetasche in GSK-3α und GSK-3β deuten darauf hin, dass die effiziente Diskriminierung einer Isoform nicht möglich ist. Durch dieses Selektivitätsproblem können Nebenwirkungen auftreten, die den Einsatz dieser Verbindungen zu risikoreich machen würden. Aufgrund dessen sollte mit Hilfe des molekularen *Dockings* und der Struktur-Aktivitäts-Beziehung untersucht werden, ob die Synthese selektiver Inhibitoren möglich ist.

- GSK-3-Inhibitoren können mittels Wildtyp-Zebrafisch-Embryonen *in vivo* evaluiert werden, wobei durch die Inhibition von GSK-3 bzw. des Wnt-Signalwegs spezifische Phänotypen entstehen. Zu diesem Zweck sollten im Anschluss an die *in vitro* Evaluierung, die besten Inhibitoren im Zebrafisch getestet werden, um eine Aussage über die *in vivo* Effektivität bzw. Toxizität dieser Inhibitoren zu treffen.

Zwei weitere Kinasen wurden im Rahmen dieser Arbeit als Teilprojekte untersucht und werden im kumulativen Teil näher beschrieben.

4. Kumulativer Teil der Dissertation

4.1 Untersuchungen zu GSK-3

4.1.1 Das *Target* GSK-3 im Bereich der Alzheimer-Demenz

Der Inhalt dieses Kapitels wurde bereits zur Publikation angenommen:

Thomas Kramer*, Boris Schmidt, Fabio Lo Monte[‡]
Small-molecule inhibitors of GSK-3 – Structural insights and their application to Alzheimer's disease models, *International Journal of Alzheimer's Disease* **2012**, im Druck.

GSK-3 wird mit einer Vielzahl von Krankheiten assoziiert, jedoch steht die Alzheimer-Demenz (AD) momentan im Fokus der Forschung. Hierbei wird diese Kinase mit den charakteristischen Merkmalen der AD, den Amyloid-Plaques und intrazellulären Neurofibrillenbündel, in Verbindung gebracht. Diese Tatsache macht deutlich, weshalb in den letzten Jahren eine Vielzahl von Veröffentlichungen zu GSK-3 publiziert wurden. Lithium war der erste Inhibitor für GSK-3 durch den eine Tau-Hyperphosphorylierung und Neurodegeneration in transgenen Mäusen gestoppt werden konnte.

Seitdem wurden unterschiedlichste ATP-kompetitive GSK-3-Inhibitoren publiziert und patentiert. In diesem Kapitel werden die verschiedenen Strukturklassen diskutiert und tabellarisch zusammengefasst. Die *in vitro* und *in vivo* Daten der einzelnen GSK-3-Inhibitoren sollen das Potential und die Effektivität der Verbindungen im Bereich der AD verdeutlichen. Die wichtigsten Kristallstrukturen der Inhibitoren im Komplex mit dem Zielprotein geben Hinweise auf bereits bekannte sowie mögliche neue Interaktionen und sollen Wissenschaftlern Anregungen für neue Strukturen geben. Die wichtigsten Aminosäuren innerhalb der ATP-Bindestelle, die relevant für die Aktivität bzw. Selektivität eines Inhibitors sein könnten, wurden grafisch dargestellt (Abb. 16).

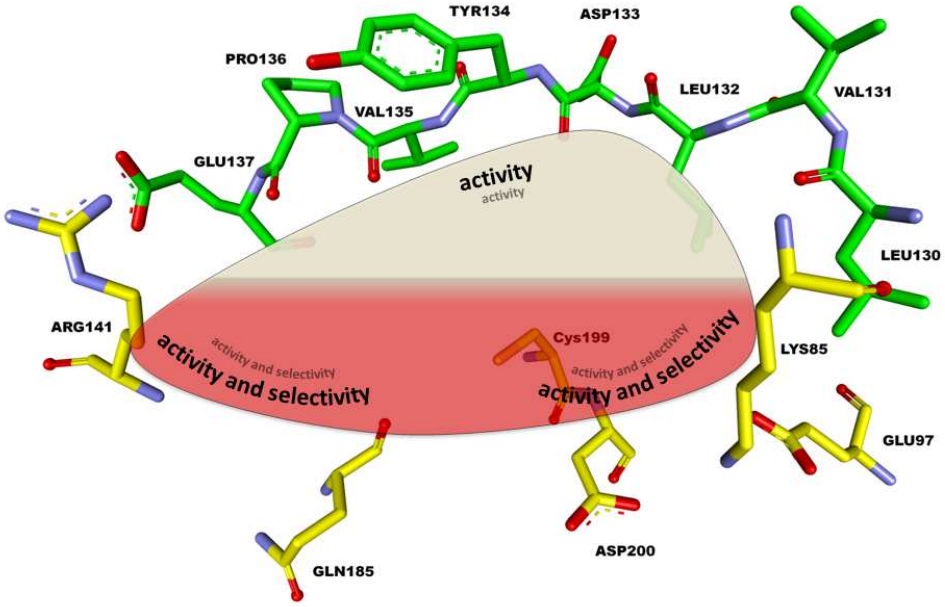

Abb. 16: Schematischer Einblick in die ATP-Bindungstasche von GSK-3β mit Kennzeichnung relevanter Bereiche.

Relevante Tiermodelle im Bereich der AD werden ebenfalls vorgestellt, wobei der Zebrafisch als neueres Modell eine kostengünstigere Alternative zu Mausmodellen darstellt. Verbindungen, die sich gegenwärtig in den präklinischen oder klinischen Phasen befinden, werden separat diskutiert.

Dieses Review soll verdeutlichen, dass GSK-3 ein vielversprechendes *Target* im Bereich der AD-Forschung ist und auch in Zukunft Beachtung finden sollte.

Small-molecule inhibitors of GSK-3 – Structural insights and their application to Alzheimer´s disease models

Thomas Kramer, Boris Schmidt and Fabio Lo Monte

Clemens Schöpf - Institute of Organic Chemistry and Biochemistry, Technische Universität Darmstadt, 64287 Darmstadt, Germany

Fax: +496151-163278; Tel: +496151-164531.

E-mail: schmidt_boris@t-online.de, Fabio.Lo-Monte@gmx.de

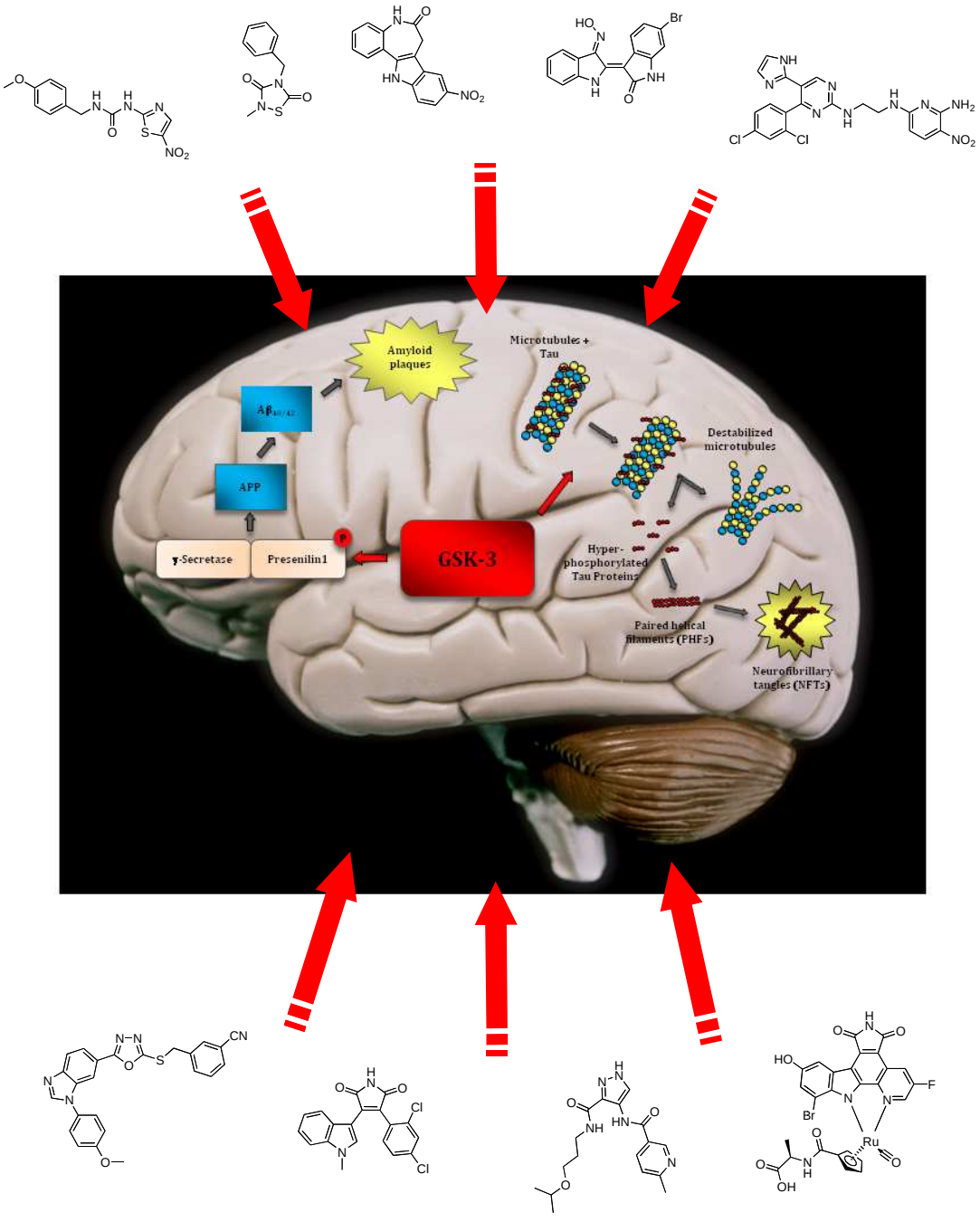

Keywords

Alzheimer´s disease; GSK-3; inhibitors; activity; selectivity; X-ray; pre-/clinical trials

Abstract

The world health organization (WHO) estimated that 18 million people are struck by Alzheimer´s disease (AD). The USA, France, Germany and other countries launched major programmes targeting the identification of risk factors, the improvement of caretaking and fundamental research aiming to postpone the onset of AD. The glycogen synthase kinase 3 (GSK-3) is implicated in multiple cellular processes and has been linked to the pathogenesis of several diseases including diabetes mellitus, cancer and AD. Inhibition of GSK-3 leads to neuroprotective effects, decreased β-amyloid production and a reduction in tau hyperphosphorylation, which are all associated with AD. Various classes of small molecule GSK-3 inhibitors have been published in patents and original publications. Herein we present a comprehensive summary of small molecules reported to interact with GSK-3. We illustrate the interactions of the inhibitors with the active site. Furthermore, we refer to the biological characterisation in terms of activity and selectivity for GSK-3, elucidate *in vivo* studies and pre-/clinical trials.

Introduction

Protein kinases regulate diverse cellular functions and thus are frequently exploited in drug discovery programmes.[1] They regulate signal transduction processes by phosphorylating serine, threonine and tyrosine residues in key proteins. The signalling pathways involved contribute to the pathology in many diseases.[2,3] Glycogen synthase kinase 3 (GSK-3) was identified in the late 1970s and is a constitutively active, ubiquitous expressed serine/threonine kinase, which participates in a number of physiological processes ranging from glycogen metabolism to gene transcription.[4] Initially, the focus of pharmaceutical companies concerning GSK-3 was on diabetes mellitus, but since GSK-3 was linked to Alzheimer's disease (AD), the focus has moved from diabetes to AD. GSK-3 has been linked to all primary abnormalities associated with AD. GSK-3 interacts with different components of the plaque producing amyloid system, participates in phosphorylating the microtubule binding

protein tau that contributes to the formation of neurofibrillary tangles, and has an influence on presenilin and other AD-associated proteins.[4-8] Two related isoforms of GSK-3 are present in mammalians, GSK-3α and β, which share 98% homology in their catalytic domains and have similar biochemical properties.[9] The isoforms are similar in their catalytic domains, yet differ significantly in their N-terminal regions.[10] Alois Alzheimer's first report of the neuropathological hallmarks of AD dates back to 1907.[11,12] The histopathology of the AD brain is characterized by the presence of abnormal filamentous tau-protein inclusions in nerve cells and extracellular amyloid deposits.[13,14] Partially phosphorylated tau contains sequence motifs that support association with tubulin, which entails the stabilization of microtubules in AD-uneffected cells. The pathological hyperphosphorylation of these motifs destabilizes microtubules and consequently interferes with tubulin binding. The misfolding of hyperphosphorylated tau involves the E/Z-isomerisation of a phosphorylated Ser-Pro motive, which leads to the formation of insoluble neurofibrillary tangles (NFTs) and intraneuronal aggregates of paired helical filaments (PHFs).[9,15] GSK-3 phosphorylates multiple sites on tau both *in vitro* and *in vivo*.[9] It exerts a central and crucial role in the pathogenesis of both familial and sporadic forms of AD. Early onset forms of familial Alzheimer´s disease (FAD) have been linked to mutations in amyloid precursor protein (APP), presenilin-1 (PS-1) and presenilin-2 (PS-2). These mutations adversely affect APP processing and result in the increased production of the 40-42 amino acid long β-Amyloid (Aβ) peptides, which are the major component of amyloid deposits. Several risk factors have been associated with sporadic Alzheimer´s disease (SAD). The most prevalent factors are aging and the presence of specific ApoE isoforms, which have been implicated in Aβ clearance. Sporadic Alzheimer´s disease can be caused by the activation of β-secretase, which results in enhanced formation of Aβ. Enhanced Aβ production or deficiency in Aβ clearance will result in the deposition of Aβ aggregates.[4,16] Recent work suggests that enhanced GSK-3 activity increases Aβ production.[17] Several studies support that GSK-3 inhibition leads to decreased Aβ production and a reduction in tau hyperphosphorylation.[1]

A plethora of GSK-3 inhibitors has been described and most of the biological effects were reported for *in vitro* and cellular studies.[17] These studies, the number of patent applications and a successful phase II trial indicate that GSK-3 is a promising drug target for AD therapy, but the ultimate proof of concept has not been presented yet. GSK-3 is highly enriched in the brain and several publications indicate that the GSK-3β isoform is a key kinase required for abnormal hyperphosphorylation of tau.[18,19] Kurt Spittaels *et al.* generated a double transgenic mouse overexpressing human protein tau and constitutively active human GSK-3β and ascertained that this kinase is implicated in aberrant tau phosphorylation and in addition reduced tau binding capacity to microtubules.[15,20] The homology of the ATP-binding pocket in GSK-3α and GSK-3β presents an obstacle for the development of isoform selective

inhibitors. All GSK-3 inhibitors developed until now are able to inhibit the two isoforms with similar potency, except **Λ-OS1** (**36**), which showed a selectivity (up to 7-fold) for GSK-3α.[8,21,22]

The structures of GSK-3β co-crystallized with several inhibitors have been solved by X-ray crystallography recently. These structures provide a remarkable possibility to design both novel and selective GSK-3 inhibitors. There are two fundamental options to inhibit GSK-3: non-ATP competitive inhibition and ATP competitive inhibition.

The non-ATP competitive inhibitors, e.g. substrate competitive inhibitors, usually engage in a weak binding interaction with the enzyme.[23] Non-ATP competitive inhibitors do not compete with the high intracellular ATP-concentration and thus offer a distinct pharmacological advantage. Moreover, the involvement of GSK-3 in several essential signalling pathways imposes a limit on the GSK-3 inhibition, complete inhibition will result in adverse events.

Thus GSK-3 inhibitors suitable for AD therapy have to strike a balance between the different pathways. This delicate balance may be achieved by moderate inhibition in combination with excellent pharmacokinetics. Thiadiazolindiones (TDZDs) are non-ATP competitive GSK-3 inhibitors, which delivered a candidate for phase IIb trials recently.[24] The extended phase II trial (60 days treatment) did not reveal adverse effects.[25] However, the majority of the known GSK-3 inhibitors are ATP competitive and target the ATP binding pocket of GSK-3. Several small-molecule inhibitor/GSK-3 complexes can be extracted from the Protein Data Bank (PDB).[26] A closer view at the interactions of these inhibitors with GSK-3 will be provided in the following chapters.

Small-molecule inhibitors of glycogen synthase kinase 3

Several ATP competitive GSK-3 inhibitors from different structural classes are highlighted in this review. The *in vitro* and *in vivo* data are summarized if available. It should be noted that the IC_{50} values strongly depend on assay conditions and thus may vary 100-fold depending on ATP and enzyme concentration as well as incubation time. The interactions between the inhibitors and the ATP binding pocket are depicted.

Lithiumchloride was the first GSK-3 inhibitor to be discovered. However, there are several other biological targets for lithium resulting in adverse events and a rather small therapeutic window. This effectively rules out the use of LiCl in the therapy of AD. The mechanism by which **lithium** inhibits GSK-3 is unknown, but two hypotheses were proposed: a) **lithium** (**Li^+**) is a competitive inhibitor of GSK-3 with respect to **magnesium** (**Mg^{2+}**), but neither competitive to substrate nor to ATP, b) **lithium** inhibits **potassium** deprivation.[25,27,28]

This review focusses on small organic molecules that target specifically GSK-3, thus the activity of lithium salts will not be reviewed. Also covalent or irreversible inhibitors, like the TDZD **NP-12**, will be noted, but not further discussed as well as the **FRATtide**, a peptide derived from FRAT1, which binds to GSK-3 and blocks GSK-3 from interacting with axin.[29,30]

Maleimide derivatives

Maleimide derivatives have been reported as scaffolds for ATP competitive GSK-3 inhibitors. Researchers at SmithKline Beecham Pharmaceuticals reported that 3-anilino-4-arylmaleimides **1-3** (Table 1) are potent and selective inhibitors of GSK-3.[31] The compounds

Table 1: Examples of maleimide inhibitors with biological activity against GSK-3, selectivity, X-Ray and reference.

No.	R^1	R^2	IC_{50} (nM):	Kinase Panel:	In Vivo	X-Ray	Year/ Lit.
1		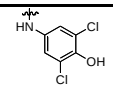	α: 20	-	-	-	2001[31]
2		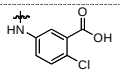	α: 26	β + 24	-	-	2001[31]
3		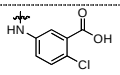	α: 76	-	-	1Q4L	2001, 2003[31,32]

α = GSK-3α; β = GSK-3β.

displayed GSK-3 inhibition (IC_{50}) at low nanomolar concentrations. The selectivity of compound **2** was evaluated using a panel of 25 kinases. The majority of the kinases showed less than 30% inhibition at an inhibitor concentration of 10 µM. The complex of **3** (named **I-5**) with GSK-3β (Figure 1) elucidated the binding mode to the ATP pocket.[32] Herein the maleimide nitrogen interacts with the carbonyl oxygen of Asp133 and the oxygen of compound **3** with the backbone nitrogen of Val135. Two additional interactions are observed between a carboxylate oxygen and Arg141 and with Gln185. Compound **4** (**SB-216763**)

inhibited GSK-3α with an IC_{50} of 34 nM (Table 2). Derivative **4** exhibited little or no

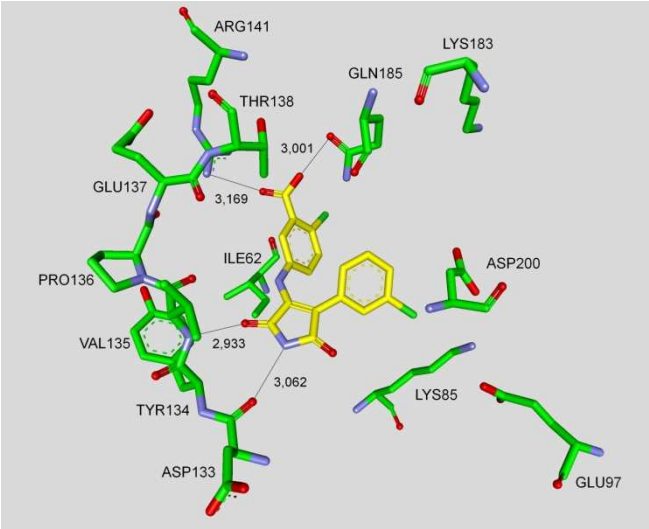

Figure 1. Compound **3** (**I-5**) in the ATP binding pocket of GSK-3β; important protein-inhibitor interactions are shown. The distance is denoted in Å. PDB code 1Q4L.[32]

Table 2: Examples of indolyl-maleimide inhibitors with biological activity against GSK-3, selectivity, X-Ray and reference.

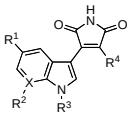

No.	R^1	X	R^2	R^3	R^4	IC_{50}/K_i (nM):	Kinase Panel:	In Vivo	X-Ray	Year/ Lit.
4	H	C	H	Me		α: 34[a]	β + 24	Yes	-	2000, 2001, 2007[33-35]
5	H	N	-			β: 25[b]	β + 79	Yes	-	2004[36]
6	H	N	-			β: 6[b]	β + 79	Yes	-	2004[36]
7	H	N	-			β: 4[a]	-	-	-	2004[37]
8	H	N	-			β: 26[a]	β + 69	Yes	1Q3D[c]	2004[37]
9	H	C	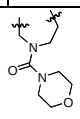			β: 1.3[a]	β + 36	Yes	-	2004[38]

10	H	C	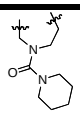		GSK-3: 2.0[a]	GSK-3 + 3	Yes	-	2005[39]
11	H	C	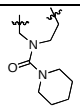		GSK-3: 0.7[a]	GSK-3 + 3	Yes	-	2005[39]
12	Br	C	H	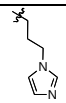		β: 140[a]	β + 5	Yes	1Q3D[c]	2009[40]
13	F	C	H	Me	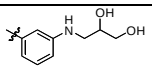	β: 0.6[a]	α & β + 315	Yes	1R0E	2010[41]
14	H	C	H	H		β: 4470[a]	-	-	-	2011[42]
15	H	C	H	Me		β: 890[a]	-	-	-	2011[42]

[a] IC_{50} value; [b] K_i value; [c] Docking studies, PDB code; α = GSK-3α; β = GSK-3β.

inhibition of the 24 kinases tested in the panel.[33] Incubation of cerebrellar granule neurones with this compound reduced the death rate in a concentration dependent manner in response to either stimulus. The maximal neuroprotection was observed with 3 µM of **SB-216763**.[34] A 60% reduction in GSK-3β activity levels was observed in the hippocampus, but not in the cortex of **SB-216763** treated animals versus vehicle treated rats.[35] The compounds **5-11** revealed good potencies against GSK-3. Concerning compounds **7** and **9-11** much higher potencies (IC_{50} < 4 nM) were ascertained in comparison to compound **1** (Table 2).[37-39] The compounds **10** and **11** demonstrated very good GSK-3 inhibition and improved selectivity against PKCβII, CDK2 and CDK4, and inhibit tau phosphorylation in a neuronal cell line.[39] Whereas compound **12** was analyzed by in silico docking the binding mode of **13** (IC_{50} = 0.6 nM) was determined by X-ray crystallographic analysis (Figure 2).[41]

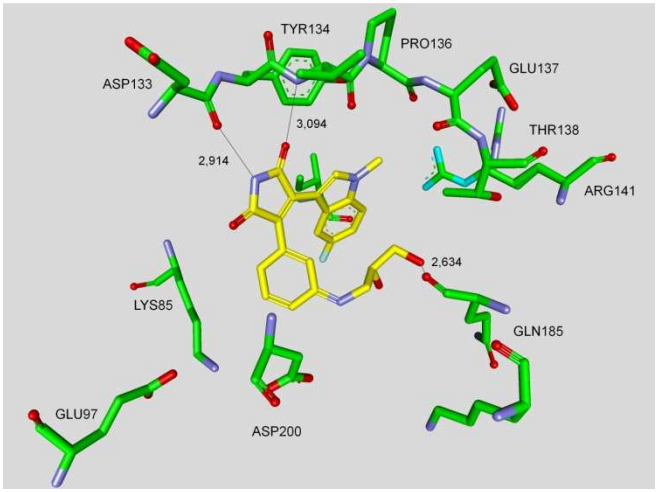

Figure 2. Compound **13** in the ATP binding pocket of GSK-3β; important protein-inhibitor interactions are shown. The distance is denoted in Å. PDB code 1R0E.[41]

Similar to compound **3**, the maleimide nitrogen of **13** interacts with the carbonyl oxygen of Asp133 and its oxygen with the backbone nitrogen of Val135. Furthermore, compound **13** forms a crucial hydrogen bond to Gln185. Maleimide **13** was screened against 315 kinases to provide data on kinase selectivity in order to predict potential safety issues. It was found that compound **13** inhibits only 36 kinases with >90% inhibition at 10 µM.[41] Compound **14** and **15** are reversible GSK-3 inhibitors in the low micromolar or high nanomolar range and can be used as chemical precursors for the corresponding halomethylketones (HMKs). These HMKs are irreversible inhibitors, they alkylate Cys199, which is located in the ATP binding site of GSK-3.[42] Further maleimide derivatives are listed in Table 3.

Table 3: Examples of bisindolyl maleimide and benzofuranyl-indolyl maleimide inhibitors with biological activity against GSK-3, selectivity, X-Ray and reference.

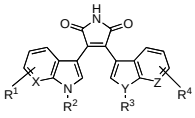

No.	R^1	X	R^2	R^3	Y	Z	R^4	IC_{50}/K_i (nM):	Kinase Panel:	In Vivo	X-Ray	Year/ Lit.
16	H	CH	Me	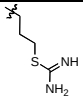	N	CH	H	β: 2.8[a]	-	Yes	-	1999[43]
17	H	N			N	N	H	β: 48[a]	β + 54	Yes	-	2003[44]

18	H	N			N	N	H	β: 34[a]	β + 54	Yes	1H8F[c]	2003[44]
19	H	CH			N	CH	H	β: 25[a]	β + 18	Yes	-	2003[45]
20	H	CH			N	CH	H	β: 4[a]	-	Yes	-	2003[45]
21	H	N	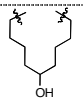		N	N	H	β: 11[b]	β + 65	Yes	-	2004[46]
22	H	N			N	N	H	β: 36[b]	β + 65	Yes	1H8F[c] + 1AQ1[c]	2004[46]
23	H	CH	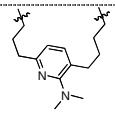		N	CH	H	β: 3[a]	α & β + 98	-	2OW3	2007[47]
24	5-Br	CH	Me	-	O	CH	H	β: 7.0[a] (4.6[b])	β + 22	Yes	1Q3D[c]	2007[48]
25	5-F	CH	Me	-	O	CH	6-CH_2 OH	β: 0.35[a]	β + 1	-	1R0E[c]	2009[49]
26	7-CH_2 OH	CH	Me	-	O	CH	H	β: 5.4[a]	β + 1	-	1R0E[c]	2009[49]
27	7-CH_2 OMe	CH	Me	-	O	CH	H	β: 0.23[a]	β + 1	Yes	-	2009[49]

[a] IC_{50} value; [b] K_i value; [c] Docking studies, PDB code; α = GSK-3α; β = GSK-3β.

All of them, compounds **16-27**, showed IC_{50}/K_i values in the low nanomolar range.[43-49] The majority of these structures was synthesized by Johnson & Johnson Pharmaceutical R & D. The compounds **17** and **18** were evaluated against a broad panel of 55 protein kinases. 10 µM of derivative **17** or **18** inhibited GSK-3β kinase activity by 100% in the presence of 10 µM ATP. Compound **18** exhibited excellent selectivity for GSK-3β except for the moderate selectivity against PKCβII. Meanwhile the bis-7-azaindolylmaleimide **17** exhibited high selectivity at GSK-3β against all kinases tested.[44] The activity of compound **23** was tested in a kinase panel containing 100 diverse protein kinases. An IC_{50} of 3 nM and a 460-fold selectivity for GSK-3β over PKCβII was reported.[47] The X-ray structure analysis of co-crystallized compound **23** and GSK-3β is illustrated in Figure 3.

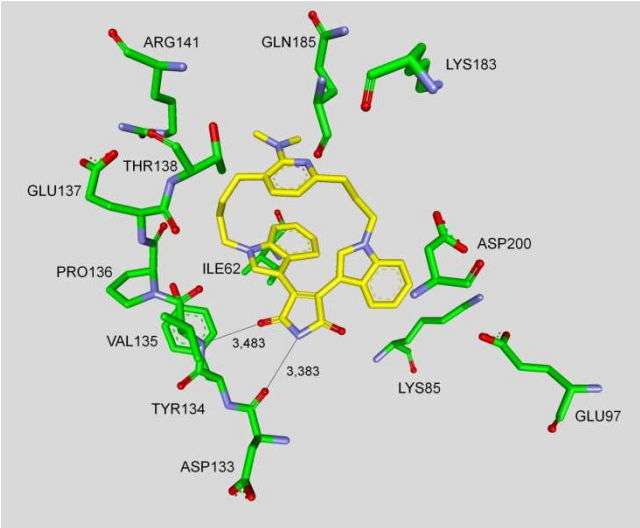

Figure 3. Compound **23** in the ATP binding pocket of GSK-3β; important protein-inhibitor interactions are shown. The distance is denoted in Å. PDB code 2OW3.[47]

The maleimide establishes key hydrogen bond contacts with the residues Asp133 and Val135. The compounds **25** and **26** were docked into the ATP binding site of GSK-3β (PDB code 1R0E). Similar to the other maleimide derivatives, the maleimide nitrogen interacts with the carbonyl oxygen of Asp133 and the oxygen with the backbone NH of Val135. In addition to these main interactions, the hydroxymethyl group of compound **26** interacts with the side chain of Arg141.[49] The benzo[e]isoindole-1,3-dione **28** (Table 4) displays an IC_{50} of 304 nM in the presence of 100 µM ATP.

Table 4: Examples of maleimide inhibitors with biological activity against GSK-3, selectivity, X-Ray and reference.

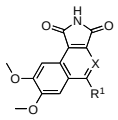

No.	X	R^1	IC_{50} (nM):	Kinase Panel:	In Vivo	X-Ray	Year/ Lit.
28	N	Et	β: 304	β + 21	Yes	1UV5[a]	2009[50]
29	CH	Et	β: 92	β + 2	Yes	1UV5[a]	2010[51]
30	CH	Me	β: 270	β + 2	Yes	1UV5[a]	2010[51]

[a] Docking studies, PDB code; β = GSK-3β.

It was evaluated in a panel of 22 representative kinases. 5 µM of compound **28** inhibited 91% of GSK-3β activity as well as 71% of CDK2/cyclin A and 53% of KDR (VEGFR2).[50] The inhibition of GSK-3 leads to ectopic activation of the Wnt pathway during zebrafish development, resulting in a headless embryo. Thus zebrafish embryos, which were treated with compound **28**, had highly restricted brain defects that ranged from smaller eyes and forebrain to a complete loss of these structures.[50] Compound **29** displayed a lower IC_{50} *in vitro* than **30**, whereas compound **30** displayed better *in vivo* efficacy. 25 µM of derivative **30** resulted in the eyeless phenotype of zebrafish embryos after 3 days of incubation.[51] The synthetic activity dedicated to this structural class has been strong and is ongoing.[52-56]

Staurosporine and organometallic inhibitors

Staurosporine (**31**) is a natural product from the bacterium *Streptomyces staurosporeus*.[57] It exerts antimicrobial, hypotensive and cytotoxic activity.[58] **Staurosporine** (**31**) is also a potent GSK-3β inhibitor with a reported IC_{50} value of 15 nM (Table 5).[59] The co-crystal

Table 5: Staurosporine and organometallic inhibitors with biological activity against GSK-3, selectivity, X-Ray and reference.

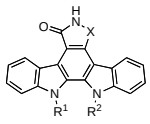

No.	X	R^1	R^2	IC_{50} (nM):	Kinase Panel:	In Vivo	X-Ray	Year/ Lit.
31	CH_2			β: 15	β + 2	-	1Q3D	1977, 1994, 2001, 2003[32,57-59]

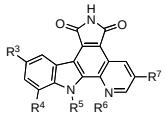

No.	R^3	R^4	R^5	R^6	R^7	IC_{50}/K_i (nM):	Kinase Panel:	In Vivo	X-Ray	Year / Lit.
32	H	H			H	α: 3, β: 10	α & β + 8	Yes	-	2004 [60]

33	OH	Br	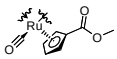	H	α: 0.35[a] β: 0.55[a]	α & β + 55	Yes	-	2006 61
34	OH	H	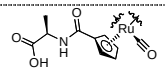	F	β: 0.04[a] (0.005[b])	-	-	2JLD	2008 62
35	OH	H		H	α: 0.5[a] β: 1.00[a]	-	-	3M1S	2011 63
36	H	H		NH_2	α: 0.9[a] β: 6[a]	α & β + 100	-	3PUP	2011 22

[a] IC_{50} value; [b] K_i value; α = GSK-3α; β = GSK-3β.

structure of **Staurosporine** (**31**) with GSK-3β is elucidated in Figure 4. Again, the maleimide **31** interacts with the Asp133 carbonyl oxygen and the backbone nitrogen of Val135. These are the only direct hydrogen bonds observed between GSK-3β and this inhibitor.[32] The other

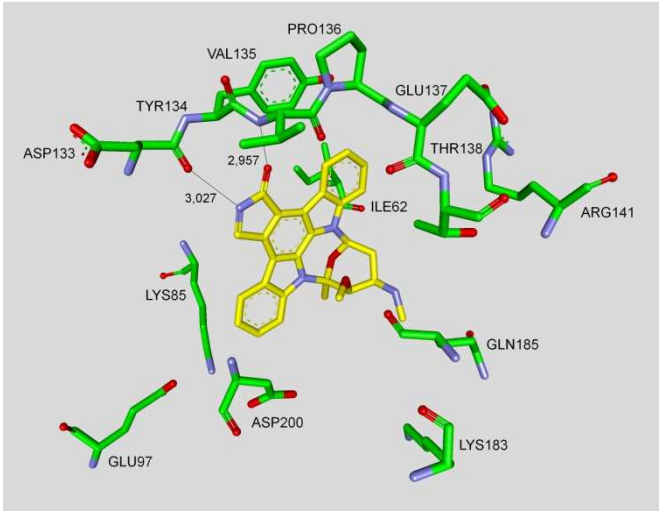

Figure 4. Compound **31** in the ATP binding pocket of GSK-3β; important protein-inhibitor interactions are shown. The distance is denoted in Å. PDB code 1Q3D.[32]

polar interactions, e.g. water-mediated interactions, are not denoted. The organometallic ruthenium complex **32** is a remarkably potent inhibitor of GSK-3 (Table 5). The IC_{50} for GSK-3α is 3 nM and 10 nM for GSK-3β. The compound was evaluated against 10 kinases and displayed activity against GSK-3 and RSK1 (IC_{50} = 100 nM) only. The authors observed a water-mediated contact between the carbonyl ligand and the carbamide of Gln185 and assumed that this contributes to the specificity for GSK-3.[60] Compound **33** showed improved selectivity. A test panel of more than 50 kinases was not significantly inhibited at 100 nM. Compound **33** was reported to activate the Wnt signaling pathway in cell culture experiments

at nanomolar concentrations. The treatment of zebrafish embryos in early development by compound **33** caused malformations, e.g. a head structure lacking the eyes and a stunted tail.[61] The S-diastereomer of compound **34** is a weaker GSK-3β inhibitor than the R-diastereomer: IC_{50} of 0.22 nM at 100 µM. Compound **34** (R-diastereomer, Table 5) exerts the highest reported potency against GSK-3β with an IC_{50} of 40 pM. Unfortunately, the evaluation in a kinase panel was not reported yet.[62] The complex of derivative **34** with GSK-3β (Figure 5) provided insight into the binding mode in the ATP pocket of GSK-3β. The interactions between the imide NH and the carbonyl oxygen of Asp133 and between the imide carbonyl and the NH of Val135 are typical. Another interaction is marked between the carbonyl oxygen of Val135 and the indolyl OH. The compound **34** and the analogues **35** (**(*R*)-DW 12**) & **36** (**Λ-OS1**) contain a carbonyl, which interacts with the flexible glycine-rich loop of GSK-3β (Figure 6 & 7).

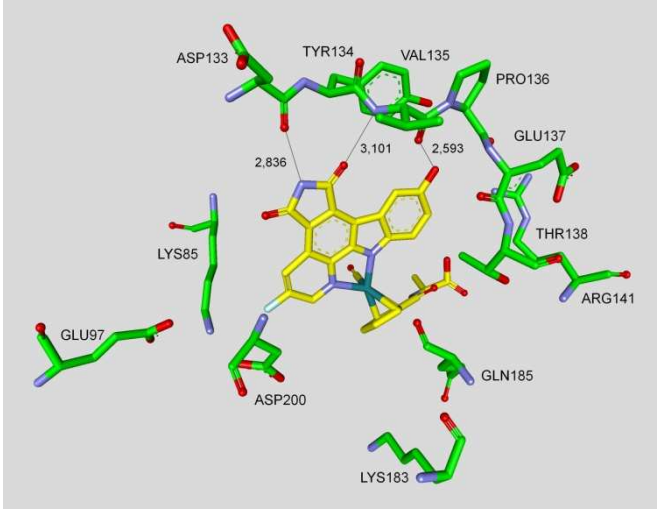

Figure 5. Compound **34** in the ATP binding pocket of GSK-3β; important protein-inhibitor interactions are shown. The distance is denoted in Å. PDB code 2JLD.[62]

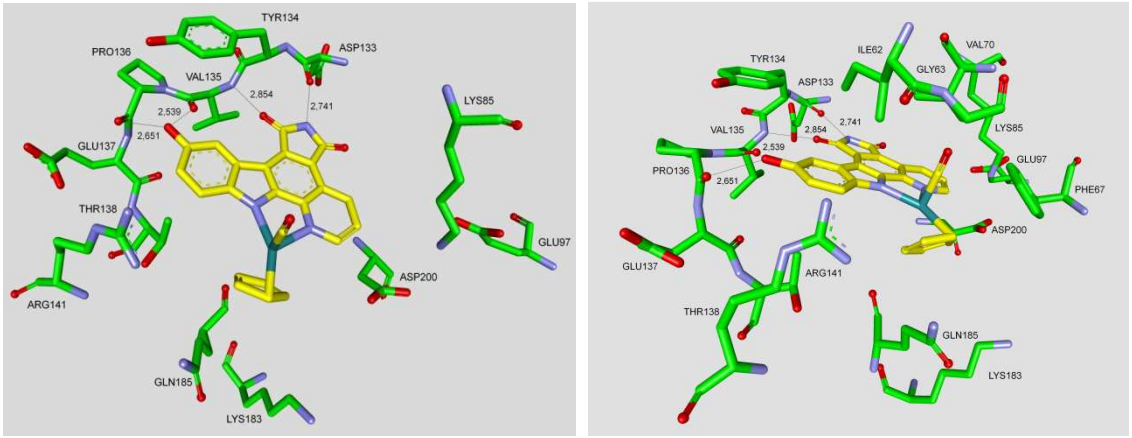

Figure 6. Compound **35** in the ATP binding pocket of GSK-3β; important protein-inhibitor interactions are shown. The distance is denoted in Å. PDB code 3M1S.[63]

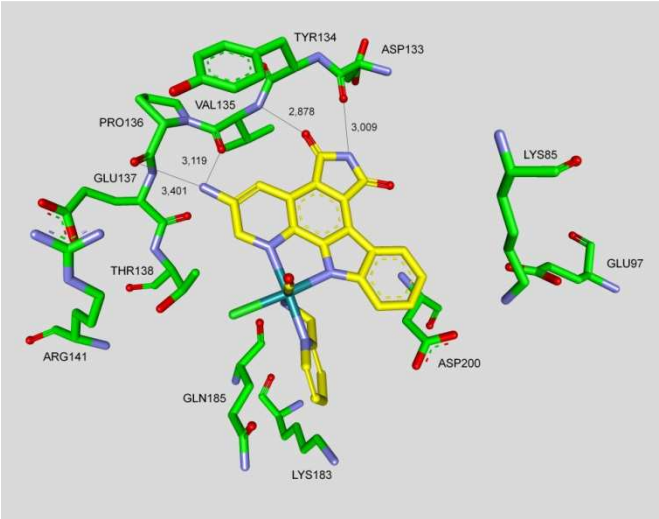

Figure 7. Compound **36** in the ATP binding pocket of GSK-3β; important protein-inhibitor interactions are shown. The distance is denoted in Å. PDB code 3PUP.[22]

Thereby Ile62, Gly63, Phe67 and Val70 form a small hydrophobic pocket (Figure 6 right, compound **35**). The structure activity analysis of ruthenium-based GSK-3 inhibitors lacking the carbonyl revealed the contribution of this carbonyl to potency and selectivity.[22,62,63]

Indole derivatives

Several pharmaceutical companies have reported and patented indole derivatives as GSK-3 inhibitors.[64-71] Indirubins are likewise indole derivatives. They are related to the naturally occurring indigo dyes and their pharmacological properties have long been known in traditional Chinese medicine, for example in the treatment of leukemias.[15] Except for the dye indirubin **38**, all other noted indole derivatives (**37**, **39-50**) revealed an IC_{50} below 100 nM. Compound **37**, the **indirubin-3´-monoxime**, was reported to display an IC_{50} of 22 nM on GSK-3 inhibition (Table 6).

Table 6: Examples of indirubine inhibitors with biological activity against GSK-3, selectivity, X-Ray and reference.

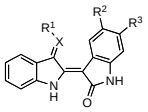

No.	X	R^1	R^2	R^3	IC_{50} (nM):	Kinase-Panel	In Vivo	X-Ray	Year/Lit.

37	N	OH	H	H	β: 22	β + 2	Yes	1Q41	2001, 2003, 2007[32,35,59]
38	O	-	H	H	β: 600	β + 2	-	-	2001[59]
39	N	OH	H	Br	α/β: 5	α/β + 19	Yes	1UV5 + 1Q41[a]	2003, 2004[72,73]
40	N	OAc	H	Br	α/β: 10	α/β + 19	-	-	2003[72]
41	O	-	H	Br	β: 45	β + 2	-	-	2004[73]
42	N	OAc	Cl	Cl	β: 4	β + 2	-	-	2004[73]
43	N	OAc	CH_3	Br	β: 7	β + 2	-	-	2004[73]
44	N	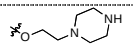	H	Br	α/β: 3.3	α/β + 2	Yes	1UV5[a]	2008[74]
45	N	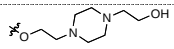	H	Br	α/β: 5.0	α/β + 2	Yes	1UV5[a]	2008[74]
46	N	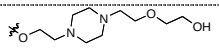	H	Br	α/β: 14	α/β + 2	Yes	-	2008[74]
47	O	-	NH_2	H	α/β: 80	α/β + 4	Yes	-	2009[75]
48	O	-	NHAc	H	α/β: 7.5	α/β + 4	Yes	-	2009[75]
49	N	OH	H	NO_2	α/β: 40	α/β + 4	-	-	2009[75]
50	N	OH	NO_2	H	α/β: 2.1	α/β + 4	-	-	2009[75]

[a] Docking studies; PDB code; β = GSK-3β; α/β = GSK-3α/β.

This unselective compound is a strong inhibitor of the closely related kinases CDK1 and CDK5.[59] Compound **37** did not affect p-tau levels in neither cortex nor hippocampus of P12 rats despite the high concentration of the compound in the brain (13 µM).[35] Three important interactions of compound **37** and GSK-3β are displayed in the X-ray in Figure 8.[32] Maternal Wnt activity is necessary for dorsal axis formation in *Xenopus*

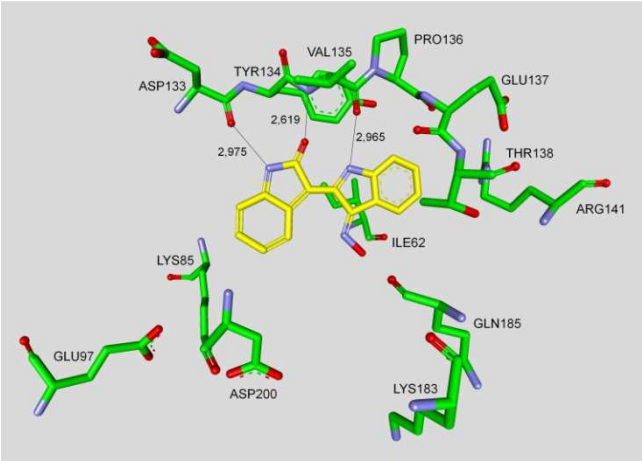

Figure 8. Compound **37** in the ATP binding pocket of GSK-3β; important protein-inhibitor interactions are shown. The distance is denoted in Å. PDB code 1Q41.[32]

laevis embryos, whereas head formation requires the inhibition of zygotic Wnt activity. The *Xenopus laevis* embryos were treated with compound **39** (**BIO**) or **LiCl**, respectively; in order to challenge these two GSK3 regulated events *in vivo*. **LiCl** treatment leads to a hyper dorso-anteriorization at the expense of trunk and tail when applied during early cleavage stage. **39** exerted the same effect on the embryos. Compound **39** inhibited GSK-3 with an IC_{50} of 5 nM, but also CDK1, CDK2 and CDK5 in a nanomolar range.[72,73] The binding mode of **39** in the ATP pocket of GSK-3β has been determined by X-ray crystallographic analysis. The four major interactions between the inhibitor and GSK-3β are shown in Figure 9. The nitrogen

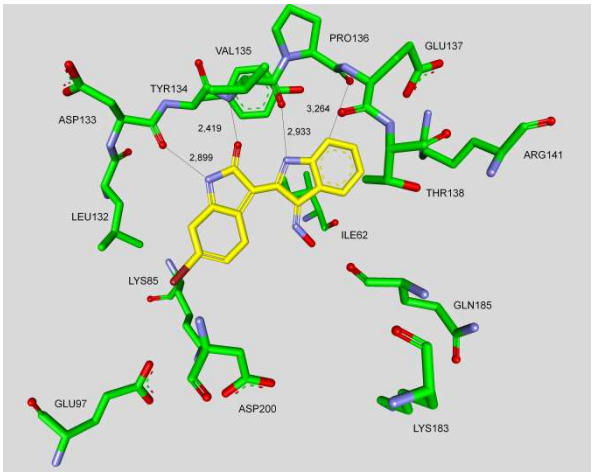

Figure 9. Compound **39** in the ATP binding pocket of GSK-3β; important protein-inhibitor interactions are shown. The distance is denoted in Å. PDB code 1UV5.[72]

interacts with the carbonyl oxygen of Asp133 and the oxygen with the backbone nitrogen of Val135. Moreover, interactions with the oxygens of Val135 and Pro136 as well as the van der Waals contact between the bromine and Leu132 were observed. Compounds **41** and **43** are

potent GSK-3 inhibitors and very selective against CDK1/cyclin B and CDK5/p25.[73] In 2007, this class of indirubine derivatives was patented by Meijer *et al.*[76] This patent lists *in vivo* activity for several compounds. The derivatives **44-46** feature an extended amino side chain at position R^1. They were prepared to enhance selectivity and water solubility versus compound **39**. These compounds were reported to inhibit β-catenin S33/37/T41 phosphorylation by GSK-3. Compounds **44-46** were also less cytotoxic than compound **39** in the MTS reduction assay of SH-SY5Y neuroblastoma cells.[74] The compounds **47-50** are potent, yet unselective GSK-3 inhibitors.[75]

Paullone derivatives

Paullones have been reported as potent ATP competitive inhibitors of CDKs and GSK-3β.[77,78] Compounds **51-55** revealed that a defined derivatisation of one substituent only can increase the GSK-3β inhibition up to 155-fold. Alsterpaullone **55** (**9-nitro-paullone**) is one of the most potent GSK-3β inhibitors and competes with ATP for binding to GSK-3β (Table 7).

Table 7: Examples of paullone inhibitors with biological activity against GSK-3, selectivity, X-Ray and reference.

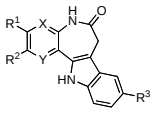

No.	X	Y	R^1	R^2	R^3	IC_{50} (nM):	Kinase Panel:	In Vivo	X-Ray	Year/ Lit.
51	CH	CH	H	H	H	β: 620	α/β + 2	-	-	1999, 2000[77,78]
52	CH	CH	H	H	Cl	β: 24	α/β + 2	-	-	1999, 2000[77,78]
53	CH	CH	H	H	Br	β: 23	α/β + 2	-	-	1999, 2000[77,78]
54	CH	CH	H	H	CN	β: 10	α/β + 2	-	-	1999, 2000[77,78]

55	CH	CH	H	H	NO_2	α: 4 β: 4	α & β + 23	Yes	1Q3W	1999, 2000, 2003, 2007[32,35,77,78]
56	CH	CH	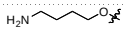	H	Br	β: 30	β + 2	-	-	2002[79]
57	CH	CH	H	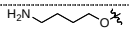	Br	β: 40	β + 2	-	-	2002[79]
58	CH	N	H	H	Br	β: 18	β + 2	-	-	2004[80]
59	N	CH	H	H	Br	β: 6000	β + 2	-	-	2004[80]
60	CH	CH	H	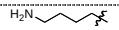	NO_2	β: 6	β + 2	-	-	2005[81]
61	CH	CH	H		NO_2	β: 2.5	β + 2	-	-	2005[81]
62	CH	CH	H		NO_2	β: 6.5	β + 2	-	-	2005[81]
63	CH	CH	H		NO_2	β: 34	β + 2	-	-	2005[81]
64	CH	CH	H		NO_2	β: 0.8	β + 21	-	-	2005[81]

α = GSK-3α; β = GSK-3β.

Compound **55** was evaluated in a kinase panel with 25 kinases and exhibited high selectivity for GSK-3α/β, CDK1/cyclin B, CDK2/cyclin A, CDK2/cyclin E and CDK5/p35. All measured IC_{50} values were in the nanomolar range. Alsterpaullone **55** was reported to inhibit the *in vivo* phosphorylation of tau at AD specific sites by GSK-3β.[77] Paullone **55** formulated in 20% DMSO/25% Tween-80 and injected *s.c.* led to a reduction in 43 kDa tau phosphorylation in cortex after 2 h, though not in the 49 kDa isoform. Furthermore, the phosphorylation levels of the 43 kDa and 49 kDa isoforms in the hippocampus were significantly decreased.[35] Most of the paullone derivatives were patented by Meijer *et al.* in 2001.[82] The binding mode of **55** has been determined by X-ray crystallographic analysis (Figure 10).[32] The interactions of alsterpaullone and GSK-3β include two hydrogen bonds with Val135 and one interaction between the nitro group and the side chain amino group of Lys85. The compounds **56** and **57** inhibited GSK-3 as well as CDK1/cyclin B and CDK5/p25 in the nanomolar range.[79] The exchange of nitrogen and carbon in compound **58** and **59** decreased the inhibitory activity, but provided selectivity to **58,** which is void of CDK-inhibitory effects.[80]

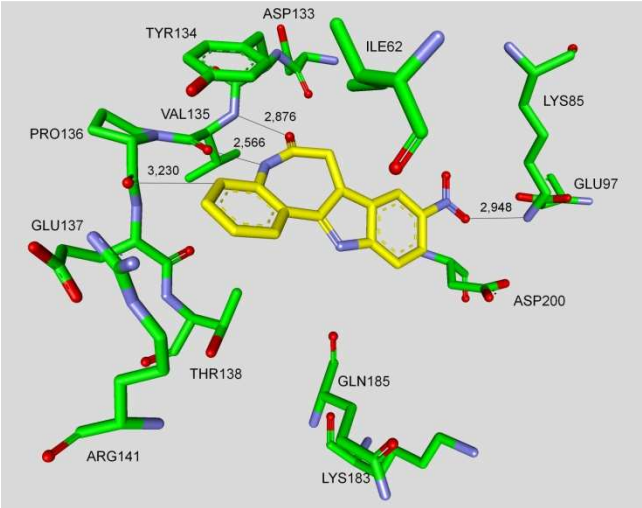

Figure 10. Compound **55** in the ATP binding pocket of GSK-3β; important protein-inhibitor interactions are shown. The distance is denoted in Å. PDB code 1Q3W.[32]

However, compound **58** was testet against three kinases (GSK-3β, CDK1/cyclin B, CDK5/p2) only. The derviatisation of the R^2 motif, see compounds **57** and **60-64** in Table 7, leads to the most potent inhibitor **64**. Compound **64**, with an IC_{50} of 0.8 nM is likewise non-selective for GSK-3. It preferentially inhibited the CDK/GSK-3 family in the nanomolar range and VEGFR-2, VEGFR-3 and Src in the submicromolar range.[81]

Pyrazolamide derivatives

GlaxoSmithKline identified another class of GSK-3 inhibitors in 2003 (Table 8). The precursor was identified by a pharmacophore search of the in house database. The compounds **65-67** were profiled against a panel of 25 kinases including GSK-3β.

Table 8: Examples of pyrazolamide inhibitors with biological activity against GSK-3, selectivity, X-Ray and reference.

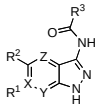

No.	X	Y	Z	R^1	R^2	R^3	IC_{50} (nM):	Kinase Panel:	In Vivo	X-Ray	Year/ Lit.
65	C	N	CH	H	Ph	Propyl	α: 56	β + 24	-	-	2003[83]
66	C	N	CH	H	2-F-Ph	Propyl	α: 18	β + 24	-	-	2003[83]

67	C	N	CH	H	3-Pyridyl	Propyl	α: 11	β + 24	-	-	2003[83]
68	N	N	CH	-	Ph	Propyl	α: 4	β + 24	-	PDB n.p.[a]	2003[84]
69	N	CH	CH	-	Ph	Propyl	α: 7	-	-	-	2003[84]
70	N	N	CH	-	Ph		α: 22	β + 24	-	PDB n.p.[a]	2003[84]
71	C	N	CH	Ph	H		α: 425	-	-	-	2003[85]
72	C	N	CH	Ph-4-OMe	H		α: >5000	-	-	-	2003[85]
73	C	N	CH	Ph-4-OH	H		α: 8	α + 23	-	PDB n.p.[a]	2003[85,86]
74	C	N	CH	Ph-4-OH	Br		α: 0.8	α + 23	-	PDB n.p.[a]	2003[85,86]
75	C	N	CH	Ph	Br		α: 75	α + 23	-	-	2003[86]
76	C	CH	CH	5-Indolyl	H		α: 42	α + 1	-	-	2003[86]
77	C	N	CH	2-Furyl	Br		α: 7	β + 23	-	-	2003[86]

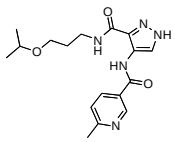

No.	IC_{50}/K_i (nM):	Kinase Panel:	In Vivo	X-Ray	Year/ Lit.
78	α: 2.3 β: 2.0	α & β + 27	Yes	-	2009[87]

[a] Not published as PDB; α = GSK-3α; β = GSK-3β.

An excellent selectivity was obtained against the majority of the kinases. However, a significant inhibition of CDK2/cyclin A was reported.[83] Compounds **68** and **69** displayed improved potency, but nevertheless inhibit CDK2/cyclin A. Only compound **70** showed an excellent GSK-3 potency and improved CDK-2/cyclin A selectivity.[84] The IC_{50} comparison of compounds **71-73** revealed that the Ph-4-OH motif is the best. The most potent inhibitor **74** (IC_{50} = 0.8 nM) was tested against a panel of kinases and showed a reduction in the overall selectivity profile.[85,86] Compounds **75-77** showed an excellent selectivity against CDK-2/cyclin A. In addition, compound **77** demonstrated an excellent overall selectivity profile against all

kinases of the panel.[86] Unfortunately, no further studies were published concerning this series. Takeda Pharmaceutical disclosed compound **78** in 2009. It is a very potent inhibitor of GSK-3 with an IC_{50} of 2.3 nM for GSK-3α and 2.0 nM for GSK-3β. It had no inhibitory effect on 23 kinases, and only a weak inhibition was detected for CDK1/cyclin B, CDK2/ cyclin A, CDK5 and JNK1. The cold-water stress model (CWS) with male C57BL/6Njcl mice was used to evaluate the *in vivo* efficacy of compound **78**. CWS transiently induces *in vivo* tau hyperphosphorylation as reported in previous studies. The compound displayed highly potent inhibition of *in vivo* phosphorylation in CWS mice and reduced sarkosyl insoluble tau in old homozygous JNPL3 mice. Furthermore, compound **78** inhibited tau phosphorylation at GSK-3 directed sites in rat primary neuronal cells and mouse brain tissue.[87] Several structures containing a pyrazole core have shown promising results in animal models of diabetes, for structural information see denoted references. The pyrazolamides developed by Wyeth-Ayerst Research, now Pfizer, showed significant plasma glucose lowering activity (16-42% reduction) in genetically obese, diabetic db/db mice.[88,89] Novartis published a series of compounds with ED_{50} values for glucose reduction in ob/ob mice of 3.0 mg/kg/day.[90] In 2011 the Merck Research Laboratories disclosed a potent human glucagon receptor antagonist with good pharmacokinetic profiles in four preclinical species. One of these compounds showed excellent oral pharmacodynamic efficacy in rhesus monkeys and transgenic mice by blocking glucagon-induced hyperglycemia.[91]

Pyrimidine and furopyrimidine derivatives

GSK-3 inhibitors bearing the pyrimidine moiety are listed in Table 9 and 10. This series is

Table 9: Examples of pyrimidine inhibitors with biological activity against GSK-3, selectivity, X-Ray and reference.

No.	R^1	R^2	R^3	R^4	IC_{50}/K_i (nM):	Kinase Panel:	In Vivo	X-Ray	Year/ Lit.
79	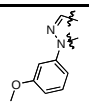		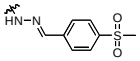	H	β: 2.5[a]	-	Yes	-	2004[92]

80	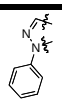	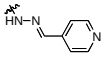	H	β: 100[a]	-	Yes	1GNG[c]	2001, 2004[29,92]
81		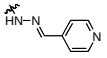	H	β: 4.0[a]	-	Yes	1GNG[c]	2001, 2004[29,92]
82	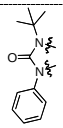	H		β: 2400[a]	-	-	-	2008[93]
83	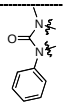	H		β: 1700[a]	-	-	-	2008[93]
84	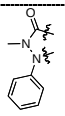	H	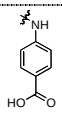	α: 1020[a] β: 960[a]	-	-	-	2008[93]
85	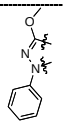	H	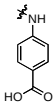	α: 1900[a] β: 760[a]	-	-	-	2008[93]
86	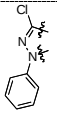	H	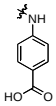	α: 350[a] β: 180[a]	-	-	-	2008[93]

[a] IC_{50} value; [b] K_i value; [c] Docking studies, PDB code (n.d.: not denoted) ; α = GSK-3α; β = GSK-3β.

characterized by a high number of patent applications, particularly by Vertex Pharmaceuticals.[94-119] Compounds **79** and **81** inhibited GSK-3β in the nanomolar range. The *in silico* docking of compound **80** into the ATP-binding pocket of GSK-3β suggested that **80**

Table 9: Continued.

No.	R^1	R^2	R^3	R^4	IC_{50}/K_i (nM):	Kinase Panel:	In Vivo	X-Ray	Year/ Lit.
87	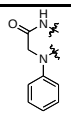		H	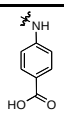	α: 6700[a] β: 3500[a]	-	-	-	2008[93]

88	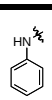	NO_2	H	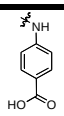	α: 270[a] β: 150[a]	-	-	-	2008[93]
89		CF_3	H	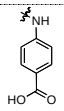	α: 750[a] β: 490[a]	-	-	-	2008[93]
90	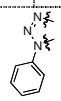		H		α: 330[a] β: 628[a]	α & β + 1	-	1Q5K[c]	2008[93]
91		NO_2	H	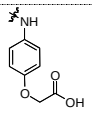	α: 74[a] β: 92[a]	α & β + 1	-	-	2008[93]
92			H	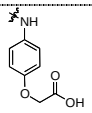	α: 9[a] β: 13[a]	α & β + 1	-	-	2008[93]
93		CF_3	H	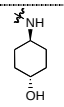	α: 61[a] β: 41[a]	α & β + 1	Yes	-	2008[93]
94	H	Me	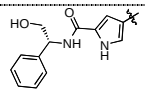		GSK-3: 7[b]	GSK-3 + 4	-	3I4B	2009[120]
95			H	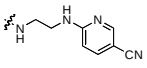	α: 10 β: 6.7[a] (9.8[b])	α & β + 20	Yes	-	2003, 2007[35,121]
96			H	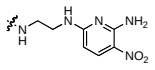	α: 0.65 β: 0.58[a] (0.87[b])	α & β + 20	Yes	-	2003, 2007[35,121]

[a] IC_{50} value; [b] K_i value; [c] Docking studies, PDB code (n.d.: not denoted) ; α = GSK-3α; β = GSK-3β.

makes two hydrogen bonds with the hinge region and one interaction with the positively charged Arg141.[29,92] Unfortunately, the activity of these compounds in a kinase panel was not disclosed. The compounds **82-90** are weak inhibitors of GSK-3 and there are no public data for *in vivo* activity nor selectivity. Docking of **90** into the PDB structure 1Q5K of GSK-3β suggested that one nitrogen and the secondary amine form hydrogen bonds to the hinge region at the Val135 NH and carbonyl, respectively. The following compounds **91-93** showed IC_{50} values below 100 nM, but **91** and **92** inhibit Aurora A in the nanomolar range. Derivative **93** (GSK-3α IC_{50} = 61 nM, GSK-3β IC_{50} = 41 nM) inhibited Aurora A at micromolar

Table 10: Examples of furopyrimidine inhibitors with biological activity against GSK-3, selectivity, X-Ray and reference.

No.	R^1	R^2	R^3	IC_{50} (nM):	Kinase Panel:	In Vivo	X-Ray	Year/ Lit.
97		H		β: 5	β + 2	Yes	-	2004[122]
98		H		β: 32	β + 2	-	-	2004[122]
99		H		β: 23	β + 2	Yes	-	2004[122]
100		H		β: 5	β + 24	Yes	PDB n.d.[a]	2004[122]
101		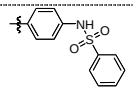	NH_2	β: 30	β□ + 9	Yes	PDB n.d.[a]	2008[123]
102		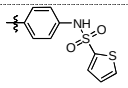	NH_2	β: 23	-	-	-	2008[123]

[a] Docking studies, PDB code (n.d.: not denoted); β = GSK-3β.

concentration only. *In vivo* studies of this compound in rats showed 34% oral bioavailability and good exposure.[93] Compound **94,** a lead compound for ERK2 inhibition, is a non-selective GSK-3 inhibitor and inhibited all 5 kinases in the panel, which included GSK-3.[120] The complex of compound **94** with GSK-3β (Figure 11) provided the binding mode in the

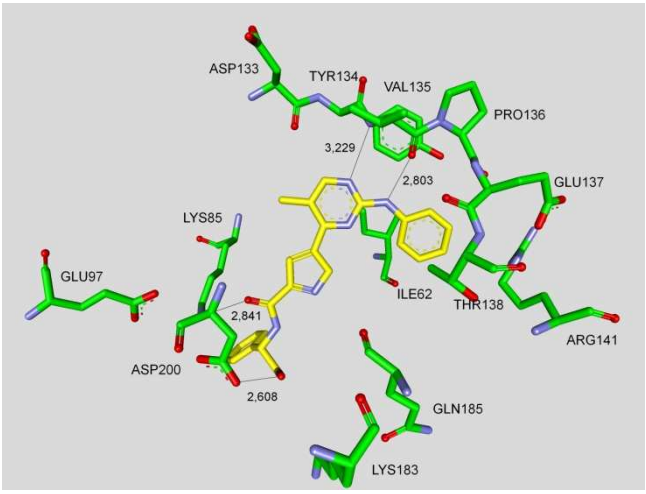

Figure 11. Compound **94** in the ATP binding pocket of GSK-3β; important protein-inhibitor interactions are shown. The distance is denoted in Å. PDB code 3I4B.[120]

ATP pocket of GSK-3. The secondary amine interacts with the carbonyl oxygen of Val135 and the nitrogen of compound **94** with the backbone NH of Val135. Two additional interactions are present between OH and Asp200 and between the carbonyl and the primary amine of Lys85. The arylimidazoles **95** (**CHIR 99021**) and **96** (**CHIR 98014**) are very effective ATP competitive inhibitors of murine and rat GSK-3 (IC_{50} < 10 nM). Both compounds exhibited 500 to 10000-fold selectivity for GSK-3 versus 20 other kinases tested. These GSK-3 inhibitors rapidly lower blood glucose levels in diabetic rodent models and enhance glucose transport as well as GS activation in insulin-resistant oxidative skeletal muscle from type 2 diabetic rats.[121] The nitropyridine **96** exerts a very potent reduction of Ser^{396} tau phosphorylation in a human neuronal cell line. P12 rats were injected *i.v.* with 30 mg/kg of **CHIR 98014** (**96,** dissolved in DMSO) to test the efficacy on tau phosphorylation *in vivo*, resulting in a maximal brain concentration of 7 µM. Tissue analysis by western blotting using a p-tau Ser^{396} antibody showed approximately 40% reduction in the phosphorylation of 43 kDa and 49 kDa tau in the cortex and a significant 3-fold reduction of the 43 kDa isoform in the hippocampus. Moreover, a 50% reduction of GSK-3β activity was observed in compound **96** treated animals versus vehicle.[35] The denoted furopyrimidines **97-102** inhibited GSK-3β with an IC_{50} below 40 nM (Table 10). Compound **100** (GSK-3β IC_{50} = 5 nM) displayed excellent selectivity against 24 kinases, including CDK2/cyclin A, which was inhibited with an IC_{50} of 0.46 µM. Compound **100** was examined in a glycogen accumulation assay in L6 cells and exhibited excellent induction of glycogen accumulation (EC_{50} = 0.39 µM).[122] Compound **101** was also profiled by cross screening against a variety of kinases and showed an excellent overall selectivity against all kinases tested including CDK2. The docking of **101** into the ATP-binding site of GSK-3β provided a likely interaction. One nitrogen and NH_2 of aminopyrimidine are anchored to the carbonyl moiety and NH of Val135 via hydrogen bond interactions. The 3-pyridine moiety is located close to Lys85 of the conserved salt bridge (Lys85/Glu97). The EC_{50} value of compound **101** in the glycogen accumulation assay in L6 cells was 3.2 µM and thus 9-fold higher than for compound **100**.[123]

Oxadiazole derivatives

The Tables 11-13 list GSK-3 inhibitors featuring the oxadiazole moiety. The depicted 1,2,5-oxadiazoles, **103-109**, revealed IC_{50} values from 0.1 µM to more than 1.1 µM. Compounds **104-106** were screened for inhibitory activity against a panel of 32 kinases at

Table 11: Examples of 1,2,5-oxadiazole inhibitors with biological activity against GSK-3, selectivity, X-Ray and reference.

No.	R^1	R^2	IC_{50} (nM):	Kinase Panel:	In Vivo	X-Ray	Year/ Lit.
103	NH_2	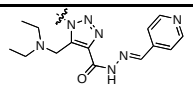	β: 410	-	-	-	2003[124]
104	NH_2	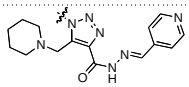	β: 100	β + 31	Yes	-	2003[124]
105	NH_2	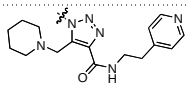	β: 1160	β + 31	Yes	-	2003[124]
106	NH_2	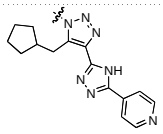	β: 280	β + 31	Yes	-	2003[124]
107	NH_2	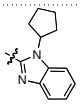	β: 210	β + 3	-	-	2009[125]
108	NH_2	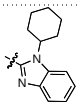	β: 240	β + 3	-	-	2009[125]
109	NH_2		β: 290	β + 3	-	-	2009[125]

β = GSK-3β

100 µM ATP concentration. All compounds gave at least 100-fold selectivity for GSK-3 compared to CDK2. However, 10 µM of compound **104** inhibited other kinases like MSK1 and DYRK1A, the latter activity is of interest for neurodegenerative diseases. The above mentioned compounds **104-106** displayed both sufficient cell penetration and suitable water solubility.[124] The dioxolane **110** was identified as GSK-3β inhibitor (IC_{50} = 65 nM, Table 12) by high throughput screening. The X-ray analysis of the GSK-3β co-crystallized compound

Table 12: Examples of 1,3,4-oxadiazole inhibitors with biological activity against GSK-3, selectivity, X-Ray and reference.

No.	R^1	R^2	IC_{50} (nM):	Kinase Panel:	In Vivo	X-Ray	Year/ Lit.
110	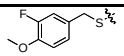		β: 65	-	-	3F7Z	2009[126]
111	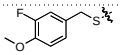		β: 44	-	-	-	2009[126]
112	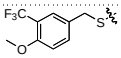		β: 3.1	-	-	-	2009[126]
113	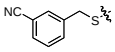	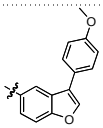	β: 3.5	-	-	-	2009[126]
114	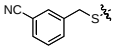	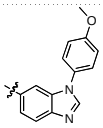	β: 2.3	β + 23	Yes	3F88	2009[126]
115	Me	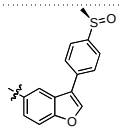	β: 140	-	-	-	2009[127]
116	Me	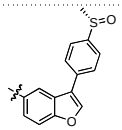	α: 37; β: 34 (53)[a]	β + 22	Yes	3GB2	2009, 2011[127,128]
117	Me	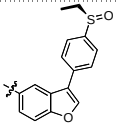	β: 190	-	-	-	2009[127]
118	Me	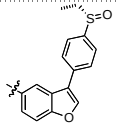	β: 20	β + 22	Yes	-	2009[127]
119			β: 17	β + 1	Yes	1UV5[b]	2010[129]
120	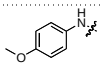		β: 53	-	-	-	2010[129]
121	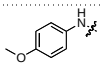		β: 18	-	-	-	2010[129]

122	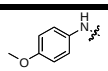		β: 7	-	-	1UV5[b]	2010[129]

[a] Results of different publications; [b] Docking studies, PDB code (n.d.: not denoted); β = GSK-3β.

confirmed the interaction with the ATP-binding site (Figure 12). One oxygen and a neighbouring hydrogen atom of the benzodioxole establish hydrogen bonds with the amide NH hydrogen and carbonyl oxygen of Val135 in the hinge region.

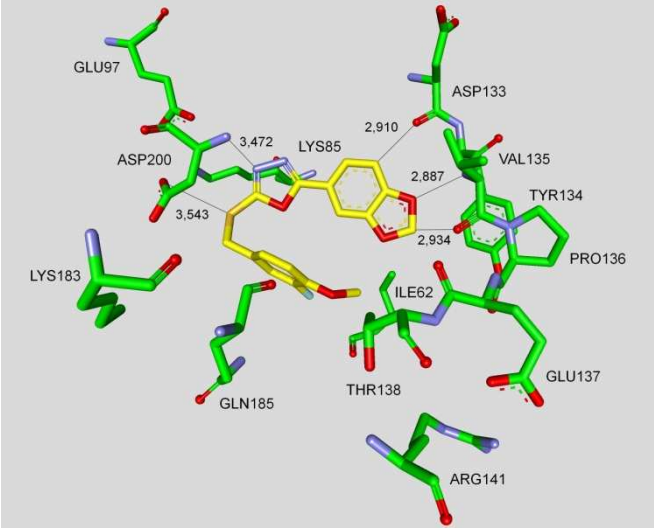

Figure 12. Compound **110** in the ATP binding pocket of GSK-3β; important protein-inhibitor interactions are shown. The distance is denoted in Å. PDB code 3F7Z.[126]

The nitrogen atoms of the oxadiazole engage in an unique hydrogen bond relay network between Lys85-Glu97-Asp200 via two water molecules (Interactions not shown). Further interactions are denoted in Figure 12. After an extensive derivatisation, e.g. **111-114**, compound **114** (Figure 13) exerts a 28-fold increased activity (GSK-3β IC_{50} = 2.3 nM) compared to its homologue **110** (Table 12). The selectivity of **114** was evaluated in a panel of more than 20 kinases to reveal more than 1000-fold selectivity against CDK1, CDK2 and CDK5. In addition, rat cassette dosing experiments of compound **114** were performed, which revealed low oral bioavailability.

Table 13: Examples of 1,2,4-oxadiazole inhibitors with biological activity against GSK-3, selectivity, X-Ray and reference.

No.	R^1	R^2	IC_{50} (nM):	Kinase Panel:	In Vivo	X-Ray	Year/ Lit.
123	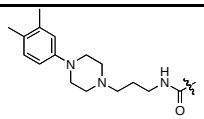		β: 350	β + 8	Yes	-	2008[130]
124	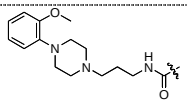		β: 410	β + 8	Yes	-	2008[130]
125	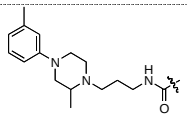		β: 690	β + 8	Yes	-	2008[130]
126	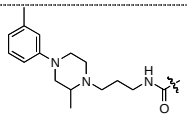		β: 710	-	Yes	-	2008[130]
127	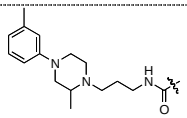		β: 1130	-	Yes	-	2008[130]

β = GSK-3β.

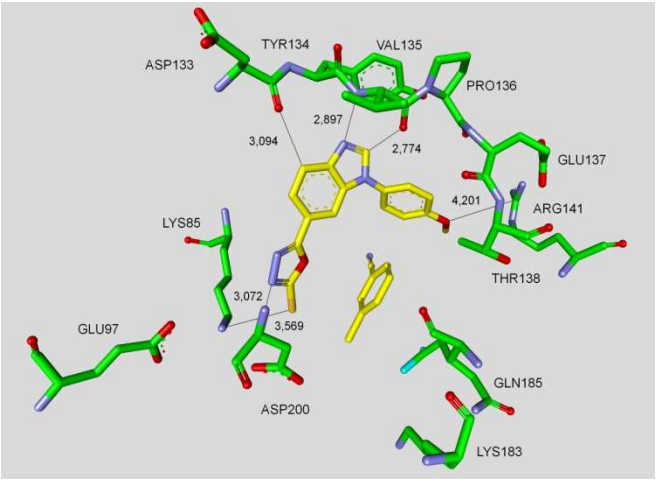

Figure 13. Compound **114** in the ATP binding pocket of GSK-3β; important protein-inhibitor interactions are shown. The distance is denoted in Å. PDB code 3F88.[126]

The co-crystal structure of **114** bound to GSK-3β was not fully characterized due to the cleavage of the S-C bond in the X-ray beam (Figure 13).[126] The co-crystal structure indicated that the nitrogen of the benzimidazole forms a hydrogen bond with the backbone NH of the hinge region at Val135 and one nitrogen of the oxadiazole ring makes a hydrogen bond with the NH of Asp200. The hydrogen atom on the carbon of the benzimidazole made an additional hydrogen bond with the carbonyl oxygen of Val135.[126] The compounds **115** and **116** are enantiomers just as compounds **117** and **118**. The S-isomers **116** and **118** were found to be eutomers. It was reported that the S-isomers possessed good oral absorption in non-fasted Crl:CD(SD)IGS rats with a bioavailability of 72.8% for derivative **116** and 65.5% for derivative **118**. Furthermore, the compounds exhibited favourable blood-brain barrier (BBB) permeability. Compounds **116** and **118** were tested for inhibitory activity against more than 20 kinases and displayed no significant activity. This indicates that these compounds are highly selective GSK-3 inhibitors. The binding mode of **116** in the ATP pocket of GSK-3β has been determined by X-ray crystallographic analysis (Figure 14).[127] One of the nitrogen atoms of the oxadiazole was revealed to interact via a hydrogen bond with the

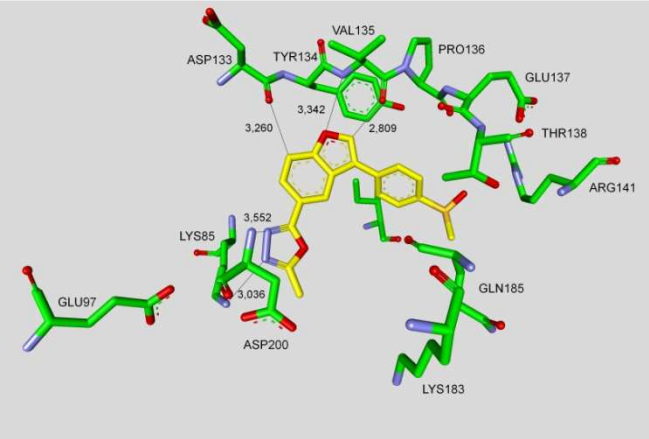

Figure 14. Compound **116** in the ATP binding pocket of GSK-3β; important protein-inhibitor interactions are shown. The distance is denoted in Å. PDB code 3GB2.[127]

side chain of Lys85 and the other with Asp200. The oxygen atom and one carbon hydrogen of the benzofuran ring interact with the main chain of Val135. Another interaction was observed between one carbon hydrogen and the carbonyl of Asp133. Derivatives **116** and **118** were tested *in vivo* using the CWS model in mice. Here, tau phosphorylation was induced at several GSK-3β directed sites such as Ser199, Thr205, Thr231 and Ser396 in mice. As reported, tau phosphorylation was significantly reduced by 35% for compound **116** and 38% for compound **118**.[127] Compound **116** was further investigated and revealed significantly decreased hippocampal tau phosphorylation as well as suppression of tau pathology without affecting amyloid β pathology.[128]

A multistage virtual screening of 289903 molecules resulted in 59 hits of potential GSK-3β inhibitors, e.g. compound **119**. Biological tests confirmed the IC_{50} of 17 nM and good selectivity versus CDK2. It crosses the BBB and has a good hepatic glycogen effect in mice. The derivatisation, e.g. **120-122**, of compound **119** lead to compound **122** with an IC_{50} of 7 nM. Surprisingly, docking experiments of compound **122** revealed a different binding mode in comparison to the co-crystallized oxadiazoles **110**, **114** and **116**. The *in silico* docked oxadiazole motif coordinates to the GSK-3β hinge region, Val135, Tyr134 and Asp133, instead of binding to the polar region, Lys85, Cys199 and Asp200.[129]

The last denoted oxadiazoles are the 1,2,4-oxadiazoles **123-127**, which exert moderate inhibition of GSK-3β only (Table 13). A subset of these oxadiazoles (**123**-**125**) exhibited weak inhibition of Pim-1 and no detectable inhibition towards seven other kinases tested at 10 µM concentration.[130]

Thiazole derivatives

The benzothiazoles **128** and **129** (Table 14) are non-selective GSK-3 inhibitors and showed moderate activity against CDKs.[131] This stands in contrast to the thiazolylurea **130** (**AR-A014418**), which strongly inhibited GSK-3 (IC_{50} = 104 nM) but not any other kinase in the panel.

Table 14: Examples of thiazole inhibitors with biological activity against GSK-3, selectivity, X-Ray and reference.

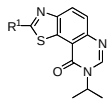

No.	R^1	IC_{50} (nM):	Kinase Panel:	In Vivo	X-Ray	Year/ Lit.
128		α/β: 130	α/β + 2	-	1J1B[b]	2008[131]
129	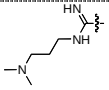	α/β: 560	α/β + 2	-	-	2008[131]

No.	R^2	R^3	IC_{50}/K_i (nM):	Kinase Panel:	In Vivo	X-Ray	Year/Lit.
130	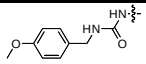	NO_2	β: 104[b] (38[c])	β + 26	Yes	1Q5K	2003, 2005, 2007[35,132,133]

[a] Docking studies, PDB code; [b] IC_{50} value; [c] K_i value; α/β = GSK-3α/β; β = GSK-3β.

AR-A014418 inhibited tau phosphorylation in transfected 3T3-fibroblasts in a dose-dependent fashion exhibiting an IC_{50} of 2.7 µM. The neuronal loss was reduced in the organotypic culture (N2A cells) and compound **130** by itself did not affect neuronal viability. The co-crystal structure analysis of **AR-A014418** and GSK-3β revealed that this compound binds to the hinge region via three hydrogen bond interactions (Figure 15).[132] Furthermore,

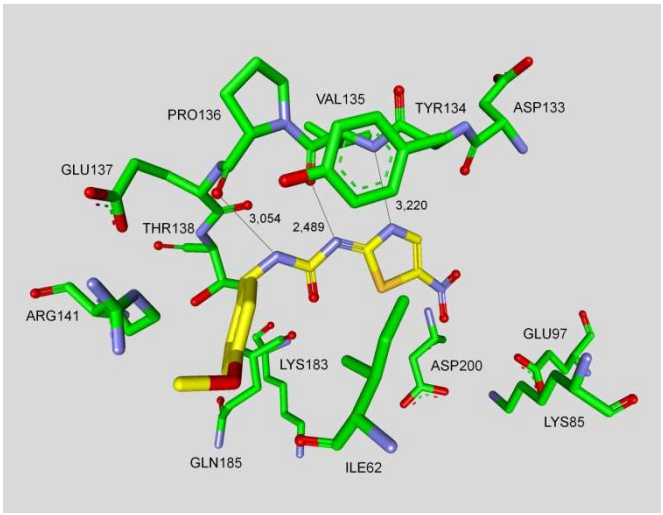

Figure 15. Compound **130** in the ATP binding pocket of GSK-3β; important protein-inhibitor interactions are shown. The distance is denoted in Å. PDB code 1Q5K.[132]

compound **130** significantly reduced insoluble tau levels in the brainstem of JNPL3 mice when compared with vehicle treated animals.[133] Surprisingly, another research group reported that **AR-A014418** showed no effect on the phosphorylation levels of neither 43 kDa nor 49 kDa tau in the cortex or hippocampus of postnatal model rats.[35] Novel compounds based on the scaffold of **AR-A014418** were synthesized recently. They showed improved *in vitro* activity and reduced toxicity in the wild-type zebrafish embryo assay.[134]

Miscellaneous heterocyclic derivatives with GSK-3 activity

Table 15 lists GSK-3 inhibitors featuring a benzimidazole core. There are neither *in vivo* assays nor selectivity data published for these potential metal chelators **131-134**. However, compound **134** (GSK-3β IC_{50} = 15 nM) was co-crystallized with GSK-3β (Figure 16).[135]

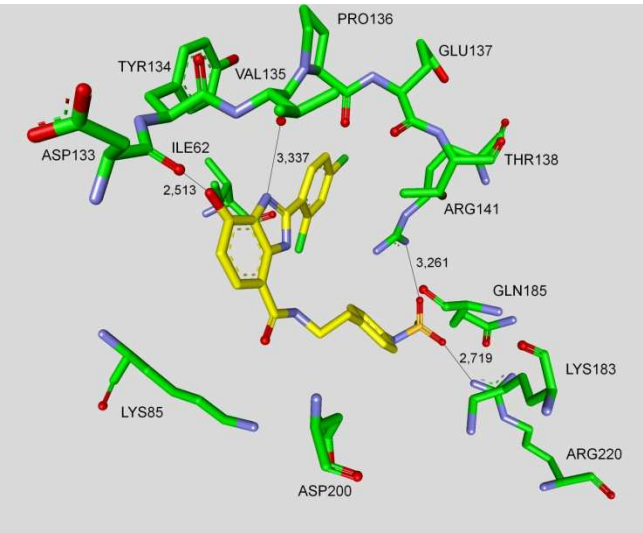

Figure 16. Compound **134** in the ATP binding pocket of GSK-3β; important protein-inhibitor interactions are shown. The distance is denoted in Å. PDB code 2O5K.[135]

Table 15: Examples of miscellaneous heterocyclic inhibitors with biological activity against GSK-3, selectivity, X-Ray and reference.

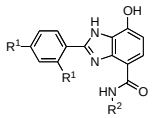

No.	R^1	R^2	IC_{50} (nM):	Kinase Panel:	In Vivo	X-Ray	Year/ Lit.
131	H		-	-	-	1I09[a]	2007[135]
132	H		β: 580	-	-	-	2007[135]
133	H	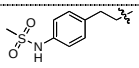	β: 25	-	-	-	2007[135]
134	Cl	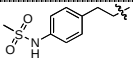	β: 15	-	-	2O5K	2007[135]

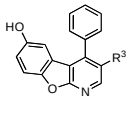

No.	R^3	K_i (nM):	Kinase Panel:	In Vivo	X-Ray	Year/ Lit.
135		β: 5800	β + 4	-	PDB n.d.[a]	2008[136]
136		β: 4100	β + 4	-	PDB n.d.[a]	2008[136]
137		β: 1500	β + 4	-	PDB n.d.[a]	2008[136]

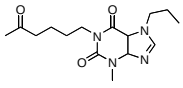

No.	IC_{50} (nM):	Kinase Panel:	In Vivo	X-Ray	Year/ Lit.
138	–	-	Yes	-	2005[137]

[a] Docking studies, PDB code (n.d.: not denoted); β = GSK-3β.

Herein, the secondary amine interacts with the carbonyl oxygen of Val135 and the phenolic OH of **134** with the carbonyl of Asp133. Two more interactions are established between the SO_2 of compound **134** and the arginines Arg141 and Arg220. The 1-aza-9-oxafluorenes **135-137** are moderately active GSK-3β inhibitors, but showed activity for CDKs.[136]

There is no report for an *in vitro* IC_{50} of the synthetic xanthine **propentofylline** (PPF, compound **138**), but studies in the Tg mouse model of AD indicated that PPF exerts a dual effect: reduction of both pathological amyloidogenesis and tau phosphorylation while reducing the ratio of activated versus inactivated GSK-3β.[137]

Table 15: Continued.

No.	R^1	R^2	K_i (nM):	Kinase Panel:	In Vivo	X-Ray	Year/Lit.
139	H		β: 1490	-	-	1Q3D[b]	2010[138]
140			β: 0.8	β + 13	-	-	2010[138]
141			β: 2	β + 13	-	-	2010[138]
142			β: <2	-	-	3L1S	2010[138]
143			β: 4.5	β + 13	-	-	2010[138]

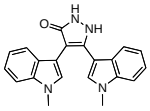

No.	IC_{50} (nM):	Kinase Panel:	In Vivo	X-Ray	Year/Lit.
144	α: 34	β + 39	Yes	1Q3D[b]	2011[139]

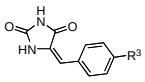

No.	R^3	IC_{50} (nM):	Kinase Panel:	In Vivo	X-Ray	Year/Lit.
145		β: 4200	-	Yes	1Q4I[b]	2009[140]
146		β: 6400	-	-	-	2009[140]
147	SCH_2CH_3	β: 7800	-	-	-	2009[140]

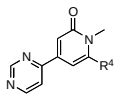

No.	R^4	IC_{50} (nM):	Kinase Panel:	In Vivo	X-Ray	Year/Lit.
148	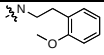	β: 17.4	β + 2[a]	Yes	-	2011[141]

149		β: 8.5	β + 2[a]	Yes	-	2011[141]
150	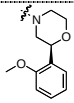	β: 16.1	β + 2[a]	Yes	-	2011[141]

[a] Further it was noted that the compound was screened against a broad panel of kinases; [b] Docking studies, PDB code; β = GSK-3β.

The pyrazolone **139** was identified as potential scaffold in a compound screen for novel GSK-3 inhibitors. Derivatisation has increased the potency of the derivatives (IC_{50}) from 1.49 mM to 0.8 nM.

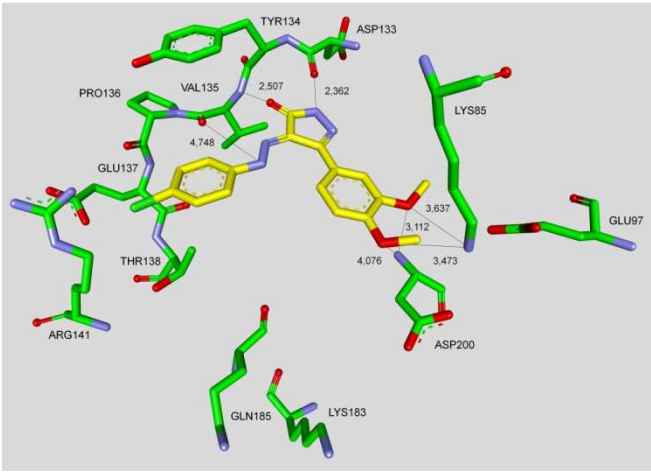

Figure 17. Compound **142** in the ATP binding pocket of GSK-3β; important protein-inhibitor interactions are shown. The distance is denoted in Å. PDB code 3L1S.[138]

The compounds **140**, **141** and **143** showed selectivity in a kinase panel of 14 kinases. A co-crystallisation was realized with compound **142** (Figure 17) and provided the interactions of the pyrazole moiety with the GSK-3 backbone amino acids Asp133 and Val135.

Table 15: Continued.

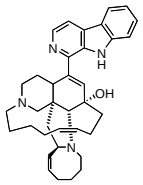

No.	Name	IC_{50} (nM):	Kinase Panel:	In Vivo	X-Ray	Year/Lit.
151	Manzamine A	β: 10200	α & β + 4	Yes	-	2007[142]

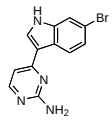

No.	Name	IC_{50} (nM):	Kinase Panel:	In Vivo	X-Ray	Year/Lit.
152	Meridianin D	β: 2500	β + 5	Yes	-	2004[143]

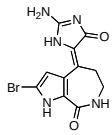

No.	Name	IC_{50} (nM):	Kinase Panel:	In Vivo	X-Ray	Year/Lit.
153	Hymenialdisine	β: 10	β + 31	Yes	-	2000[144]

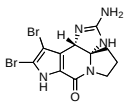

No.	Name	IC_{50} (nM):	Kinase Panel:	In Vivo	X-Ray	Year/Lit.
154	Dibromocantharelline	β: 3000	β + 3	-	1H8F[a]	2010, 2011[144,145]

[a] Docking studies, PDB code; β = GSK-3β.

In addition, the methoxy substituents make hydrogen-bonding contacts with both Asp200 and Lys85. These interactions and the hydrophobic contacts of the phenyl rings are thought to be responsible for the potency and selectivity.[138] A recent docking study of the pyrazolone **144**

confirmed the interactions of compound **142** with GSK-3β. It is an active (IC_{50} of 34 nM) and selective (kinase panel of 40 kinases) structural analogue to the previously described maleimides **9-27** (Table 2 and 3). Furthermore, compound **144** was evaluated in a model of oxidative stress induced by homocysteic acid and displayed full neuroprotective activity at 1 μM. Additionally, it was able to reduce locomotor activity in the chlordiazepoxide/ amphetamine-induced hyperactivity model *in vivo*.[139] The compounds **145-147** are moderate GSK-3 inhibitors and were not tested against other kinases to evaluate their selectivity. Compound **145** increased the glycogen content in the liver of Sprague-Dawley rats in a dose-dependent manner.[140]

Compound 1 is a HTS hit, which was co-crystallized with GSK-3β and solved by X-ray crystallography (Figure 18). The overlap of the inhibitor **Compound 1** with a pyridone derivative revealed interactions with the catalytic triad, especially Lys85, and the protein backbone amino acid Val135 of GSK-3β.[26,141] This leads to the latest ATP competitive GSK-3 inhibitors, the pyridones **148-150**. Compound **150** revealed potent *in vitro* inhibition with an IC_{50} of 16.1 nM against GSK-3β. It was selective in a broad panel of kinases, including CK2 and CLK1. Compared to compound **148**, compound **150** exhibited an improved *in vitro* human liver microsome intrinsic clearance value of 16.3 mL/min/kg. The *in vivo* CNS penetration assay demonstrated a good free brain to free plasma ratio and the assessment of potential genetic toxicology hazards was negative for compound **150**.[141] Last

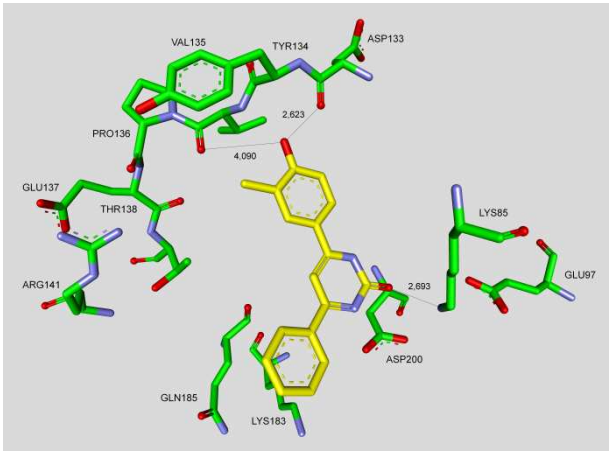

Figure 18. The HTS hit named **Compound 1** in the ATP binding pocket of GSK-3β; important protein-inhibitor interactions are shown. The distance is denoted in Å. PDB code 3Q3B.[141]

but not least, there were several GSK-3 inhibitors isolated from marine organisms. These alkaloids have the potential to provide new scaffolds comparable to the established indirubines. Manzamines, meridianins, **hymenialdisine** and **dibromo-cantharelline** inhibit

GSK-3β in the μM range and display promising selectivity and *in vivo* results (Table 15, compound **151-154**).[142-145]

Activity and selectivity profiling

A plethora of GSK-3 inhibitors was discovered in recent years and most of these displayed good to excellent inhibition of this kinase. However, selectivity and safety against other kinases remains to be a challenge. The structural analysis of the ATP competitive inhibitors may guide the development of more selective GSK-3 inhibitors. All ATP competitive inhibitors establish hydrogen bonds with the backbone atoms of Asp133 and Val135. Contact to these amino acids is a key to enhance affinity to GSK-3 but it does not provide selectivity over other kinases. Moreover, Pro136 appears in several complexes to strengthen the interaction of the inhibitor with the backbone (Figure 19). One region of GSK3 may offer privileged access to enhanced activity and selectivity: it is the region characterized by the amino acids Lys85, Glu97 and Asp200. Lys85 was observed to form a salt-bridge with Glu97 and simultaneously with Asp200, which is expected to be less significant and potent as the one with Glu97.[146]

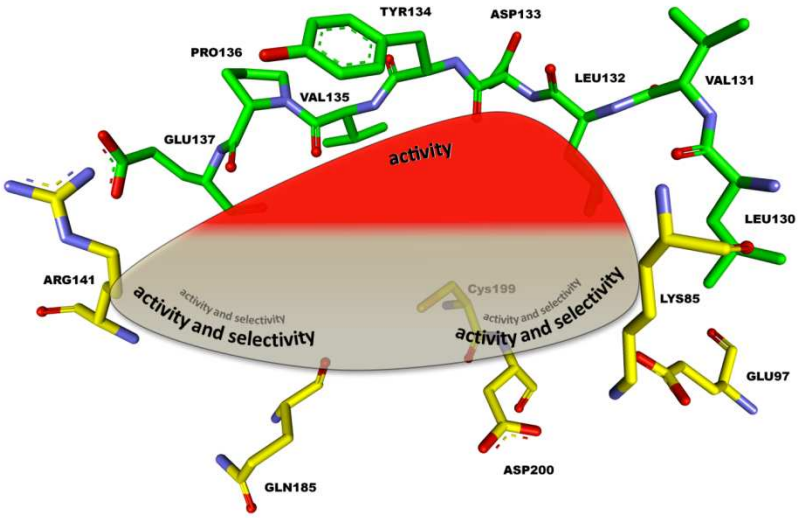

Figure 19. Schematic view in the ATP binding pocket of GSK-3β; Important areas for activity and selectivity are denoted; PDB code 1I09.[147]

The interaction of an inhibitor with this region holds potential to increase activity and selectivity for GSK-3. This interaction can be mediated via water molecules, as observed for **AR-A014418** (**130**), or be established by direct contact. We observed in our dataset that a

direct interaction with this region may cause a loss of selectivity (data not shown). There is a salt-bridge formed by Glu137 and Arg141 in the entrance area of the ATP pocket of GSK-3β. This region seems to contribute to the activity and selectivity of several inhibitors.

Another important interaction between GSK-3 and an organometallic inhibitor was reported by Bregman *et al*. They observed a water-mediated contact between the carbonyl ligand of the inhibitor and the carboxylate of Gln185.[61] This water molecule was also found in other GSK-3β inhibitor complexes and seems to be responsible for an increased activity and especially for an improved selectivity towards GSK-3.

Docking studies with our inhibitors confirmed this interaction and further explain the selectivity of these inhibitors (data not shown). Feng *et al*. observed that the ruthenium-coordinated CO ligand of their inhibitor interacts with the flexible glycine-rich loop formed by Ile62, Gly63, Phe67 and Val70. This pocket, which is not shown in Figure 18, seems to be crucial for potency and selectivity.[22] Figure 19 illustrates in a simple scheme how to enhance activity and selectivity of inhibitors. The interaction with at least two of the three areas deems necessary to provide active and selective inhibitors.

Examples of *in vivo* tests

Over the last decade, several animal models have been developed to study tauopathies and other neurodegenerative disorders *in vivo*. Despite some obvious advantages of the diverse AD invertebrate systems, the vertebrate animal models of AD are generally favoured (for detailed invertebrate reviews, see following ref.[148-150]). Vertebrate models are evolutionary and morphologically closer related to humans, which makes the direct translation of experimental results easier and more reliable. A conditionally GSK-3β overexpressing mouse was reported by Lucas *et al.* in 2001. They demonstrated that GSK-3β overexpression *in vivo* results in neurodegeneration and proposed that these mice can be used to study some aspects of AD.[151] In 2005 Pérez *et al.* and Ribe *et al*. developed and characterized a double transgenic mouse line based on overexpression of human mutant APP and tau.[152,153] They treated this transgenic mouse model with **NP12**, a non-ATP competitive GSK-3β inhibitor, and observed lower levels of tau phosphorylation, decreased amyloid deposition and prevention of memory deficits.[18] The APP-V7171 x Tau-P301L mice with combined amyloid and tau pathology and the GSK-3β x Tau-P301L mice with tauopathy only were reported by Terwel *et al*. in 2008. These models offer the possibility to explore molecular signals that act upstream and downstream of, or in parallel with GSK-3 isozymes.[154] Two transgenic mice models were developed to study the interaction between APP or Aβ and tau: the triple-

transgenic model (3 x Tg-AD) harboring $PS1_{M146V}$, APP_{Swe} and tau_{P301L} transgenes and the TAPP mice.[155,156] The transgenic mice have been the major species used for modelling AD and frontotemporal dementia (FTD). JNPL3 mice are well characterized transgenic mice that express human 4R0N tau with a FTDP-17 (P301L) mutation.[157] In particular, the levels of sarkosyl insoluble tau in JNPL3 mice increase in an age-dependent manner and co-migrate with insoluble tau from AD and FTDP-17 brains. Thus, treatment with GSK-3 inhibitors should result in a significant reduction of sarkosyl insoluble tau, see for example compound **78**.[87,133] Besides JNPL3 mice the transgenic zebrafish larvae have advanced as an AD model system. It combines many of the advantages of invertebrate and vertebrate models. The latest model is a Gal4/UAS-based vector system that efficiently generates transgenic zebrafish overexpressing high levels of human Tau-P301L or other disease-associated proteins. This tau-transgenic fish model could be an effective *in vivo* screening tool to identify quickly promising GSK-3 inhibitors and eliminate compounds without reasonable *in vivo* activity early in the screening process.[158,159]

GSK-3 inhibitors have also specific effects on early wild-type zebrafish development when treatment occurs between 4 and 24 hpf. Thus this animal model can be used to test the efficacy of GSK-3 inhibitors *in vivo*.[134,158] Furthermore, there are two *in vivo* model systems with transiently induced tau hyperphosphorylation that were used to evaluate the activity of GSK-3 inhibitors. One of them is the cold-water stress (CWS) model, which causes a rapid and reversible enhancement of tau phosphorylation in the mouse brain at several GSK-3β directed sites such as pS199, pThr205, pThr231 and pSer396.[126,160] The CWS-model proves the significant reduction of tau phosphorylation in LiCl- or compound **78** treated mice.[87,161] The *in vivo* activities of several other GSK-3 inhibitors (e.g. compound **55** and **96**) were demonstrated in the postnatal rat model.[35] This *in vivo* model takes advantage of the well characterized GSK-3β expression level in the early and later life cycle of rats.[162,163]

Compounds in Preclinical and Clinical Trials

Currently several GSK-3 inhibitors pass through preclinical or clinical trials. Subsequently GSK-3 inhibitors are listed with the therapeutic indication AD. These examples are taken from the database of PharmaProjects by searching for the criteria GSK-3 and Alzheimer (March 2010), the MED-D report of GESENT (May 2009) and ClinicalTrials.gov (August 2011).

The Wayne State University is currently in phase IV with **Lithium carbonate** against bipolar disorder whereas the University of Sao Paulo is in phase II with **Lithium carbonate** against GSK-3 for AD and cognitive impairment. **Lithium** against AD was submitted by the National

Institute of Neurological Disorder and Stroke and is in phase II, but there was no update since March 2008. Two compounds from Noscira, **NP-12** (TDZD) and **NP-103**, are in the pre-/clinical trials. **NP-12** (**NP031112**, **Tideglusib**) is currently in a phase IIb clinical trial for AD. At the moment **NP-103**, **CG-301338** from CrystalGenomics and a GSK-3β inhibitor from Takeda are in preclinical trials. The development status of **XD-4241** from Cambrex, **SB-415286** from GlaxoSmithKline, a GSK-3β inhibitor from Amphora, **SAR-502250** from Sanofi-Aventis, **CEP-16805** from Cephalon and a GSK-3β inhibitor from Lundbeck are not reported. The failure or progress of these compounds into preclinical and clinical trials will stimulate or discourage further research.

Summary

The moderate inhibition of GSK-3 by selective inhibitors with excellent pharmacokinetic properties and excellent blood-brain barrier permeation holds high potential for the treatment of AD. The failure of the first potent GSK-3 inhibitor by Astra-Zeneca indicates the complexity of this target and the therapeutic window of GSK-3 inhibition in adult mammals. Information on the failure is rather limited, it may be due to potential toxicity of the chemical scaffold: P450 mediated metabolism of thiazoles has resulted in hepatotoxicity and thus failure of phase III candidates previously.

Biological characterization has advanced GSK-3 as a potential drug target, and the inhibition of this protein kinase by small molecules resulted in significant inhibition of tau phosphorylation. We have described a wide range of molecules that inhibit GSK-3 and discussed their properties. We focused on several inhibitors interacting with the ATP-binding pocket of GSK-3β. The water molecule interactions are not incorporated in the figures, however they may play a crucial role in the hydrogen bond network between the inhibitor and the amino acids. The amino acids, which are responsible for strong interaction with the enzyme, have been identified. Noteworthy are Asp133, Val135, Glu137, Arg141, Gln185, Asp200 and Arg220, which constitute important amino acids for interactions with the binding pocket of GSK-3. The conserved salt bridge Lys85/Glu97 materializes as an interesting interaction partner. We summarized crucial biological findings and provided an overview on the *in vivo* effects of some inhibitors. Additional *in vivo* assays can be retrieved via the references denoted in the tables next to the structures. We summarized the GSK-3 inhibitors, which are in pre-/clinical trials with the therapeutic indication AD. Yet, a review will be biased and we request your pardon or input, if your favourite inhibitor or *in vivo* studies are not adequately referred to.

Outlook

GSK-3 is an intriguing enzyme, which plays important roles in the pathogenesis of several diseases, e.g. diabetes, cancer and AD. The literature is immense and quite often provides conflicting statements and observations for this kinase. For example, a few studies observed that Pin1 (peptidyl-prolyl cis-trans isomerase) knockout mice display tau hyperphosphorylation and that this enzyme might have an inhibitive role in phosphorylating tau and GSK-3β, thus protecting against AD.[164] Whereas another study ascertained that the GSK-3 inhibitor **BIO** (compound **39**) may be useful in regenerative medicine, by reversibly maintaining human embryonic stem cells in an undifferentiated state.[165] A plethora of GSK-3 inhibitors has been published since it has been linked to AD. Naturally, the vast majority thereof was reported by pharmaceutical companies. Many potent inhibitors with good selectivity have been disclosed so far. The challenge of medicinal chemists will be to develop inhibitors, which translate their potent enzymatic inhibition into cellular settings and finally humans, who will tolerate a moderate GSK-3 inhibition only. A mild GSK-3 inhibition (~35%) is needed, because such an inhibition level provides sufficient insulin sensitization without elevation of β-catenin levels. Thus a moderate inhibition minimizes significant mechanism-based toxicities, ranging from hypoglycemia to tumorigenesis.[166,167] A further indication of a moderate GSK-3 inhibition is the application of lithium for the treatment of bipolar disorder. The GSK-3 inhibitor lithium is estimated to inhibit approximately 25% of total GSK-3 activity. It was used for the treatment of bipolar disorder since the 1950s without association of hypoglycemia, increased levels of tumorigenesis, or deaths from cancer.[168] Nevertheless, the established *in vivo* studies have to be accompanied by the investigation of pleiotropic activity and the determination of a safe therapeutic window for chronic GSK-3 inhibition in humans. The X-ray analysis of co-crystallized structures revealed how the inhibitors interact with the ATP-binding pocket and provide information about essential interaction partners to improve potency and selectivity. The comparison of the IC_{50} values will be much easier, if only one stringent GSK-3 *in vitro* assay would be utilized, which employs a defined final ATP and inhibitor concentration as well as a standardized incubation time. Currently, L. T. Alon *et al.* determined that GSK3β is responsible for the phosphorylation of the embryonic tau isoforms in birds, which harbors the GSK3β gene only. In consideration of their and former studies L. T. Alon *et al.* assume that GSK3α and β have distinct roles in phosphorylating tau in adult and embryonic brain in non-vertebrates. Furthermore, they raise the hypothesis that specific inhibition of GSK3α may be useful for therapeutic intervention in AD.[169] This supposition is enhanced by former siRNA experiments.[170] But all GSK-3 inhibitors developed until now inhibit the two isoforms of GSK-3 equipotently, except **Λ-OS1** (**36**) (~7-fold more selective for

GSK3α). Still most of the GSK-3 inhibitors fail in model animals despite of their good inhibitory activity in cell free assays. This is frequently due to the lack of selectivity, insufficient cell permeation and poor blood-brain barrier permeability. Appropiate animal models were developed in transparent zebrafish to study preclinical efficacy, metabolic stability and toxicity, but their potential is not fully exploited. These *in vivo* tests are fast (3 days), relatively inexpensive and suitable for larger screening efforts in 96 well formats. Furthermore, it has been observed that resistance arises during the therapy. The problem is that most of the kinase inhibitors are ATP competitive type-I-inhibitors. A new generation of type-II-inhibitors, which binds to the ATP site and extends into an allosteric site, may provide a solution.[15,171,172] Such novel type-II-inhibitors must be active, selective and permeate the human blood-brain barrier, which bears further limitations for drug development. However, several pharmaceutical companies continue to develop ATP competitive GSK-3 inhibitors.[173,174] Just a few pharmaceutical companies have started pre-/clinical trials addressing the druggability of GSK-3 inhibition. Noscira launched the phase IIb trial ARGO of **Tideglusib** (**NP-12**) to treat mild-to-moderate AD patients in April 2011. The trial period will be 65 weeks with 2 dosage regimes of **Tideglusib** (500 and 1000 mg/day oral suspension, ClinicalTrials.gov Identifier: NCT01350362). The ongoing clinical trials may lead to a paradigm shift, if the GSK-3 inhibitors display efficacy and safety.

Abbreviations

AD	Alzheimer´s disease
ApoE	Apolipoprotein E
APP	amyloid precursor protein
ATP	adenosine triphosphat
Aβ	β-Amyloid
BBB	blood-brain barrier
CDK	cyclin-dependent kinase
CWS	cold-water stress
DMSO	dimethyl sulfoxide
DYRK1A	dual specificity tyrosine phosphorylation-regulated kinase 1A
EC_{50}	half maximal effective concentration
ERK	Extracellular signal-regulated kinase
FAD	familial Alzheimer´s disease

FTD	frontotemporal dementia
GESENT	Gesellschaft für experimentelle und klinische Neurotherapeutika
GS	glycogen synthase
GSK-3	glycogen synthase kinase 3
HMK	halomethylketon
i.v.	intravenous
IC_{50}	half maximal inhibitory concentration
JNK	c-Jun N-terminal kinase
KDR	kinase insert domain receptor
MED-D	Medikamentenentwicklung für Demenzen in Deutschland
MSK1	mitogen-and stress-activated protein kinase
MTS	(3-(4,5-dimethylthiazol-2-yl)-5-(3-carboxy-methoxyphenyl)-2-(4-sulfophenyl)-2*H*-tetrazolium
NFTs	neurofibrillary tangles
PDB	Protein Data Bank
PHFs	paired helical filaments
Pim-1	proto-oncogene serine/threonine-Protein kinase
Pin1	peptidyl-prolyl cis-trans isomerase
PKCβII	protein kinase C βII
PPF	Propentofylline
PS-1/2	presenilin-1/2
RSK1	also known as RPS6KA1, ribosomal protein S6 kinase alpha-1
SAD	sporadic Alzheimer´s disease
s.c.	subcutane
TDZD	thiadiazolidine
VEGFR	vascular endothelial growth factor receptor
WHO	world health organization
Wnt	signaling pathway
X-ray	X-radiation

References

(1) Chico, L. K.; Van Eldik, L. J.; Watterson, D. M. (2009) Targeting protein kinases in central nervous system disorders. *Nat Rev Drug Discov 8*, 892-909.
(2) Bossemeyer, D. (1995) Protein kinases--structure and function. *FEBS Lett 369*, 57-61.
(3) Peifer, C.; Alessi, D. R. (2008) Small-molecule inhibitors of PDK1. *ChemMedChem 3*, 1810-1838.
(4) Hooper, C.; Killick, R.; Lovestone, S. (2008) The GSK3 hypothesis of Alzheimer's disease. *J Neurochem 104*, 1433-1439.
(5) Ferrer, I.; Gomez-Isla, T.; Puig, B.; Freixes, M.; Ribe, E.; Dalfo, E.; Avila, J. (2005) Current advances on different kinases involved in tau phosphorylation, and implications in Alzheimer's disease and tauopathies. *Curr Alzheimer Res 2*, 3-18.
(6) Hernandez, F.; Gomez de Barreda, E.; Fuster-Matanzo, A.; Lucas, J. J.; Avila, J. (2010) GSK3: a possible link between beta amyloid peptide and tau protein. *Exp Neurol 223*, 322-325.
(7) Leroy, A.; Landrieu, I.; Huvent, I.; Legrand, D.; Codeville, B.; Wieruszeski, J. M.; Lippens, G. (2010) Spectroscopic studies of GSK3{beta} phosphorylation of the neuronal tau protein and its interaction with the N-terminal domain of apolipoprotein E. *J Biol Chem 285*, 33435-33444.
(8) Martinez, A.; Castro, A.; Dorronsoro, I.; Alonso, M. (2002) Glycogen synthase kinase 3 (GSK-3) inhibitors as new promising drugs for diabetes, neurodegeneration, cancer, and inflammation. *Med Res Rev 22*, 373-384.
(9) Eldar-Finkelman, H. (2002) Glycogen synthase kinase 3: an emerging therapeutic target. *Trends Mol Med 8*, 126-132.
(10) Frame, S.; Cohen, P. (2001) GSK3 takes centre stage more than 20 years after its discovery. *Biochem J 359*, 1-16.
(11) Alzheimer, A. (1907) Über eine eigenartige Erkrankung der Hirnrinde. *Allgemeine Zeitschrift für Psychiatrie und psychisch-gerichtiliche Medizin 64*, 146-148.
(12) Alzheimer, A.; Stelzmann, R. A.; Schnitzlein, H. N.; Murtagh, F. R. (1995) An English translation of Alzheimer's 1907 paper, "Über eine eigenartige Erkankung der Hirnrinde". *Clin Anat 8*, 429-431.
(13) Dickson, D.; Weller, R. O. (2011) Neurodegeneration: The Molecular Pathology of Dementia and Movement Disorders. *Wiley-Blackwell 2nd edition*, 62-91.
(14) Duyckaerts, C.; Delatour, B.; Potier, M. C. (2009) Classification and basic pathology of Alzheimer disease. *Acta Neuropathol 118*, 5-36.
(15) Mazanetz, M. P.; Fischer, P. M. (2007) Untangling tau hyperphosphorylation in drug design for neurodegenerative diseases. *Nat Rev Drug Discov 6*, 464-479.
(16) Hernandez, F.; Avila, J. (2008) The role of glycogen synthase kinase 3 in the early stages of Alzheimers' disease. *FEBS Lett 582*, 3848-3854.
(17) Cohen, P.; Goedert, M. (2004) GSK3 inhibitors: development and therapeutic potential. *Nat Rev Drug Discov 3*, 479-487.
(18) Sereno, L.; Coma, M.; Rodriguez, M.; Sanchez-Ferrer, P.; Sanchez, M. B.; Gich, I.; Agullo, J. M.; Perez, M.; Avila, J.; Guardia-Laguarta, C.; Clarimon, J.; Lleo, A.; Gomez-Isla, T. (2009) A novel GSK-3beta inhibitor reduces Alzheimer's pathology and rescues neuronal loss in vivo. *Neurobiol Dis 35*, 359-367.
(19) Takashima, A. (2009) Drug development targeting the glycogen synthase kinase-3beta (GSK-3beta)-mediated signal transduction pathway: role of GSK-3beta in adult brain. *J Pharmacol Sci 109*, 174-178.
(20) Spittaels, K.; Van den Haute, C.; Van Dorpe, J.; Geerts, H.; Mercken, M.; Bruynseels, K.; Lasrado, R.; Vandezande, K.; Laenen, I.; Boon, T.; Van Lint, J.; Vandenheede, J.; Moechars, D.; Loos, R.; Van Leuven, F. (2000) Glycogen synthase kinase-3beta phosphorylates protein tau and rescues the axonopathy in the central nervous system of human four-repeat tau transgenic mice. *J Biol Chem 275*, 41340-41349.
(21) Bhat, R. V.; Budd Haeberlein, S. L.; Avila, J. (2004) Glycogen synthase kinase 3: a drug target for CNS therapies. *J Neurochem 89*, 1313-1317.
(22) Feng, L.; Geisselbrecht, Y.; Blanck, S.; Wilbuer, A.; Atilla-Gokcumen, G. E.; Filippakopoulos, P.; Kraling, K.; Celik, M. A.; Harms, K.; Maksimoska, J.; Marmorstein, R.; Frenking, G.; Knapp, S.; Essen, L. O.; Meggers, E. (2011) Structurally sophisticated octahedral metal complexes as highly selective protein kinase inhibitors. *J Am Chem Soc 133*, 5976-5986.
(23) Eldar-Finkelman, H.; Licht-Murava, A.; Pietrokovski, S.; Eisenstein, M. (2010) Substrate competitive GSK-3 inhibitors - strategy and implications. *Biochim Biophys Acta 1804*, 598-603.
(24) Martinez, A.; Alonso, M.; Castro, A.; Perez, C.; Moreno, F. J. (2002) First non-ATP competitive glycogen synthase kinase 3 beta (GSK-3beta) inhibitors: thiadiazolidinones (TDZD) as potential drugs for the treatment of Alzheimer's disease. *J Med Chem 45*, 1292-1299.
(25) Martinez, A. (2008) Preclinical efficacy on GSK-3 inhibitors: towards a future generation of powerful drugs. *Med Res Rev 28*, 773-796.
(26) PDB codes: 3PUP (15), 1Q4L (25), 1Q3D (25), 1Q41 (25), 1Q3W (25), 1R0E (34), 2OW3 (40), 2JLD (55), 3M1S (56), 1UV5 (65), 3I4B (113), 3F7Z (119), 3F88 (119), 3GB2 (120), 1Q5K (124), 2O5K (127), 3L1S (130), 3Q3B (136), 1I09 (138).
(27) Mora, A.; Sabio, G.; Gonzalez-Polo, R. A.; Cuenda, A.; Alessi, D. R.; Alonso, J. C.; Fuentes, J. M.; Soler, G.; Centeno, F. (2001) Lithium inhibits caspase 3 activation and dephosphorylation of PKB and GSK3 induced by K+ deprivation in cerebellar granule cells. *J Neurochem 78*, 199-206.
(28) Ryves, W. J.; Harwood, A. J. (2001) Lithium inhibits glycogen synthase kinase-3 by competition for magnesium. *Biochem Biophys Res Commun 280*, 720-725.
(29) Bax, B.; Carter, P. S.; Lewis, C.; Guy, A. R.; Bridges, A.; Tanner, R.; Pettman, G.; Mannix, C.; Culbert, A. A.; Brown, M. J.; Smith, D. G.; Reith, A. D. (2001) The structure of phosphorylated GSK-3beta complexed with a peptide, FRATtide, that inhibits beta-catenin phosphorylation. *Structure 9*, 1143-1152.
(30) Domínguez, J. M.; Fuertes, A.; Orozco, L.; del Monte-Millán, M.; Delgado, E.; Medina, M. (2011) Evidence for the irreversible inhibition of glycogen synthase kinas-3beta by tideglusib. *J Biol Chem in Press*.
(31) Smith, D. G.; Buffet, M.; Fenwick, A. E.; Haigh, D.; Ife, R. J.; Saunders, M.; Slingsby, B. P.; Stacey, R.; Ward, R. W. (2001) 3-Anilino-4-arylmaleimides: potent and selective inhibitors of glycogen synthase kinase-3 (GSK-3). *Bioorg Med Chem Lett 11*, 635-639.
(32) Bertrand, J. A.; Thieffine, S.; Vulpetti, A.; Cristiani, C.; Valsasina, B.; Knapp, S.; Kalisz, H. M.; Flocco, M. (2003) Structural characterization of the GSK-3beta active site using selective and non-selective ATP-mimetic inhibitors. *J Mol Biol 333*, 393-407.
(33) Coghlan, M. P.; Culbert, A. A.; Cross, D. A.; Corcoran, S. L.; Yates, J. W.; Pearce, N. J.; Rausch, O. L.; Murphy, G. J.; Carter, P. S.; Roxbee Cox, L.; Mills, D.; Brown, M. J.; Haigh, D.; Ward, R. W.; Smith, D. G.; Murray, K. J.; Reith, A. D.; Holder, J. C. (2000) Selective small molecule inhibitors of glycogen synthase kinase-3 modulate glycogen metabolism and gene transcription. *Chem Biol 7*, 793-803.
(34) Cross, D. A.; Culbert, A. A.; Chalmers, K. A.; Facci, L.; Skaper, S. D.; Reith, A. D. (2001) Selective small-molecule inhibitors of glycogen synthase kinase-3 activity protect primary neurones from death. *J Neurochem 77*, 94-102.
(35) Selenica, M. L.; Jensen, H. S.; Larsen, A. K.; Pedersen, M. L.; Helboe, L.; Leist, M.; Lotharius, J. (2007) Efficacy of small-molecule glycogen synthase kinase-3 inhibitors in the postnatal rat model of tau hyperphosphorylation. *Br J Pharmacol 152*, 959-979.
(36) O'Neill, D. J.; Shen, L.; Prouty, C.; Conway, B. R.; Westover, L.; Xu, J. Z.; Zhang, H. C.; Maryanoff, B. E.; Murray, W. V.; Demarest, K. T.; Kuo, G. H. (2004) Design, synthesis, and biological evaluation of novel 7-azaindolyl-heteroaryl-maleimides as potent and selective glycogen synthase kinase-3beta (GSK-3beta) inhibitors. *Bioorg Med Chem 12*, 3167-3185.
(37) Zhang, H. C.; Ye, H.; Conway, B. R.; Derian, C. K.; Addo, M. F.; Kuo, G. H.; Hecker, L. R.; Croll, D. R.; Li, J.; Westover, L.; Xu, J. Z.; Look, R.; Demarest, K. T.; Andrade-Gordon, P.; Damiano, B. P.; Maryanoff, B. E. (2004) 3-(7-Azaindolyl)-4-arylmaleimides as potent, selective inhibitors of glycogen synthase kinase-3. *Bioorg Med Chem Lett 14*, 3245-3250.
(38) Engler, T. A.; Henry, J. R.; Malhotra, S.; Cunningham, B.; Furness, K.; Brozinick, J.; Burkholder, T. P.; Clay, M. P.; Clayton, J.; Diefenbacher, C.; Hawkins, E.; Iversen, P. W.; Li, Y.; Lindstrom, T. D.; Marquart, A. L.; McLean, J.; Mendel, D.; Misener, E.; Briere, D.; O'Toole, J. C.; Porter, W. J.; Queener, S.; Reel, J. K.; Owens, R. A.; Brier, R. A.; Eessalu, T. E.; Wagner, J. R.; Campbell, R. M.; Vaughn, R. (2004) Substituted 3-imidazo[1,2-a]pyridin-3-yl- 4-(1,2,3,4-tetrahydro-[1,4]diazepino-[6,7,1-hi]indol-7-yl)pyrrole-2,5-dion es as highly selective and potent inhibitors of glycogen synthase kinase-3. *J Med Chem 47*, 3934-3937.

(39) Engler, T. A.; Malhotra, S.; Burkholder, T. P.; Henry, J. R.; Mendel, D.; Porter, W. J.; Furness, K.; Diefenbacher, C.; Marquart, A.; Reel, J. K.; Li, Y.; Clayton, J.; Cunningham, B.; McLean, J.; O'Toole J, C.; Brozinick, J.; Hawkins, E.; Misener, E.; Briere, D.; Brier, R. A.; Wagner, J. R.; Campbell, R. M.; Anderson, B. D.; Vaughn, R.; Bennett, D. B.; Meier, T. I.; Cook, J. A. (2005) The development of potent and selective bisarylmaleimide GSK3 inhibitors. *Bioorg Med Chem Lett 15*, 899-903.
(40) Ye, Q.; Xu, G.; Lv, D.; Cheng, Z.; Li, J.; Hu, Y. (2009) Synthesis and biological evaluation of novel 4-azaindolyl-indolyl-maleimides as glycogen synthase kinase-3beta (GSK-3beta) inhibitors. *Bioorg Med Chem 17*, 4302-4312.
(41) Gong, L.; Hirschfeld, D.; Tan, Y. C.; Heather Hogg, J.; Peltz, G.; Avnur, Z.; Dunten, P. (2010) Discovery of potent and bioavailable GSK-3beta inhibitors. *Bioorg Med Chem Lett 20*, 1693-1696.
(42) Perez, D. I.; Palomo, V.; Perez, C.; Gil, C.; Dans, P. D.; Luque, F. J.; Conde, S.; Martinez, A. (2011) Switching reversibility to irreversibility in glycogen synthase kinase 3 inhibitors: clues for specific design of new compounds. *J Med Chem 54*, 4042-4056.
(43) Hers, I.; Tavare, J. M.; Denton, R. M. (1999) The protein kinase C inhibitors bisindolylmaleimide I (GF 109203x) and IX (Ro 31-8220) are potent inhibitors of glycogen synthase kinase-3 activity. *FEBS Lett 460*, 433-436.
(44) Kuo, G. H.; Prouty, C.; DeAngelis, A.; Shen, L.; O'Neill, D. J.; Shah, C.; Connolly, P. J.; Murray, W. V.; Conway, B. R.; Cheung, P.; Westover, L.; Xu, J. Z.; Look, R. A.; Demarest, K. T.; Emanuel, S.; Middleton, S. A.; Jolliffe, L.; Beavers, M. P.; Chen, X. (2003) Synthesis and discovery of macrocyclic polyoxygenated bis-7-azaindolylmaleimides as a novel series of potent and highly selective glycogen synthase kinase-3beta inhibitors. *J Med Chem 46*, 4021-4031.
(45) Zhang, H. C.; White, K. B.; Ye, H.; McComsey, D. F.; Derian, C. K.; Addo, M. F.; Andrade-Gordon, P.; Eckardt, A. J.; Conway, B. R.; Westover, L.; Xu, J. Z.; Look, R.; Demarest, K. T.; Emanuel, S.; Maryanoff, B. E. (2003) Macrocyclic bisindolylmaleimides as inhibitors of protein kinase C and glycogen synthase kinase-3. *Bioorg Med Chem Lett 13*, 3049-3053.
(46) Shen, L.; Prouty, C.; Conway, B. R.; Westover, L.; Xu, J. Z.; Look, R. A.; Chen, X.; Beavers, M. P.; Roberts, J.; Murray, W. V.; Demarest, K. T.; Kuo, G. H. (2004) Synthesis and biological evaluation of novel macrocyclic bis-7-azaindolylmaleimides as potent and highly selective glycogen synthase kinase-3 beta (GSK-3 beta) inhibitors. *Bioorg Med Chem 12*, 1239-1255.
(47) Zhang, H. C.; Bonaga, L. V.; Ye, H.; Derian, C. K.; Damiano, B. P.; Maryanoff, B. E. (2007) Novel bis(indolyl)maleimide pyridinophanes that are potent, selective inhibitors of glycogen synthase kinase-3. *Bioorg Med Chem Lett 17*, 2863-2868.
(48) Kozikowski, A. P.; Gaisina, I. N.; Yuan, H.; Petukhov, P. A.; Blond, S. Y.; Fedolak, A.; Caldarone, B.; McGonigle, P. (2007) Structure-based design leads to the identification of lithium mimetics that block mania-like effects in rodents. possible new GSK-3beta therapies for bipolar disorders. *J Am Chem Soc 129*, 8328-8332.
(49) Gaisina, I. N.; Gallier, F.; Ougolkov, A. V.; Kim, K. H.; Kurome, T.; Guo, S.; Holzle, D.; Luchini, D. N.; Blond, S. Y.; Billadeau, D. D.; Kozikowski, A. P. (2009) From a natural product lead to the identification of potent and selective benzofuran-3-yl-(indol-3-yl)maleimides as glycogen synthase kinase 3beta inhibitors that suppress proliferation and survival of pancreatic cancer cells. *J Med Chem 52*, 1853-1863.
(50) Zhong, H.; Zou, H.; Semenov, M. V.; Moshinsky, D.; He, X.; Huang, H.; Li, S.; Quan, J.; Yang, Z.; Lin, S. (2009) Characterization and development of novel small-molecules inhibiting GSK3 and activating Wnt signaling. *Mol Biosyst 5*, 1356-1360.
(51) Zou, H.; Zhou, L.; Li, Y.; Cui, Y.; Zhong, H.; Pan, Z.; Yang, Z.; Quan, J. (2010) Benzo[e]isoindole-1,3-diones as potential inhibitors of glycogen synthase kinase-3 (GSK-3). Synthesis, kinase inhibitory activity, zebrafish phenotype, and modeling of binding mode. *J Med Chem 53*, 994-1003.
(52) Kozikowski, A.; Gaysina, I. (2008) *WO 2008/077138 A1*.
(53) Kozikowski, A.; Gaysina, I. (2010) *US 2010/0004308 A1*.
(54) Von Matt, P.; Wagner, J. (2009) Novartis AG. *EP 2075249 A2*.
(55) Zhang, H.; Maryanoff, B.; Ye, H. (2008) Janssen Pharmaceutica N.V. *US 7439363 B2*.
(56) Zhang, H.; Maryanoff, B.; Ye, H. (2008) Janssen Pharmaceutica N.V. *EP 1654255 B1*.
(57) Omura, S.; Iwai, Y.; Hirano, A.; Nakagawa, A.; Awaya, J.; Tsuchya, H.; Takahashi, Y.; Masuma, R. (1977) A new alkaloid AM-2282 OF Streptomyces origin. Taxonomy, fermentation, isolation and preliminary characterization. *J Antibiot (Tokyo) 30*, 275-282.
(58) Funato, N.; Takayanagi, H.; Konda, Y.; Toda, Y.; Harigaya, Y.; Iwai, Y.; Omura, S. (1994) Absolute Configuration of Staurosporine By X-Ray Analysis. *Tetrahedron Lett 35*, 1251-1254.
(59) Leclerc, S.; Garnier, M.; Hoessel, R.; Marko, D.; Bibb, J. A.; Snyder, G. L.; Greengard, P.; Biernat, J.; Wu, Y. Z.; Mandelkow, E. M.; Eisenbrand, G.; Meijer, L. (2001) Indirubins inhibit glycogen synthase kinase-3 beta and CDK5/p25, two protein kinases involved in abnormal tau phosphorylation in Alzheimer's disease. A property common to most cyclin-dependent kinase inhibitors? *J Biol Chem 276*, 251-260.
(60) Bregman, H.; Williams, D. S.; Atilla, G. E.; Carroll, P. J.; Meggers, E. (2004) An organometallic inhibitor for glycogen synthase kinase 3. *J Am Chem Soc 126*, 13594-13595.
(61) Atilla-Gokcumen, G. E.; Williams, D. S.; Bregman, H.; Pagano, N.; Meggers, E. (2006) Organometallic compounds with biological activity: a very selective and highly potent cellular inhibitor for glycogen synthase kinase 3. *Chembiochem 7*, 1443-1450.
(62) Atilla-Gokcumen, G. E.; Pagano, N.; Streu, C.; Maksimoska, J.; Filippakopoulos, P.; Knapp, S.; Meggers, E. (2008) Extremely tight binding of a ruthenium complex to glycogen synthase kinase 3. *Chembiochem 9*, 2933-2936.
(63) Atilla-Gokcumen, G. E.; Di Costanzo, L.; Meggers, E. (2011) Structure of anticancer ruthenium half-sandwich complex bound to glycogen synthase kinase 3beta. *J Biol Inorg Chem 16*, 45-50.
(64) Beher, D.; Bettai, M.; Churcher, I.; Munzo, B.; Prasit, B.; Quddus, A.; Stock, N.; Wrigley, J. (2009) Merck and Co., Inc. *EP 1708997 B1*.
(65) Berg, S.; Hellberg, S.; Nylöf, M.; Xue, Y. (2008) Astra Zeneca AB. *US 7399780 B2*.
(66) Berg, S.; Hellberg, S.; Nylöf, M.; Xue, Y. (2008) Astra Zeneca AB. *EP 1492785 B1*.
(67) Green, J.; Miller, A.; Jimenez, J.; Marhefka, C.; Cao, J.; Court, J.; Bandarage, U.; Gao, H.; Nanthakumar, S. (2009) Vertex Pharmaceuticals Inc. *US 7514448 B2*.
(68) Heckel, A.; Roth, G.; Kley, J.; Hoerer, S.; Uphues, I. (2005) Boehringer Ingelheim Pharma GmbH & Co. KG. *WO 2005/087727 A1*.
(69) Heckel, A.; Roth, G.; Kley, J.; Hoerer, S.; Uphues, I. (2007) Boehringer Ingelheim International GmbH. *US 7262206 B2*.
(70) Heckel, A.; Roth, G.; Kley, J.; Hoerer, S.; Uphues, I. (2007) Boehringer Ingelheim International GmbH. *US 7176231 B2*.
(71) Heckel, A.; Roth, G.; Kley, J.; Hoerer, S.; Uphues, I. (2009) Boehringer Ingelheim International GmbH. *US 7560480 B2*.
(72) Meijer, L.; Skaltsounis, A. L.; Magiatis, P.; Polychronopoulos, P.; Knockaert, M.; Leost, M.; Ryan, X. P.; Vonica, C. A.; Brivanlou, A.; Dajani, R.; Crovace, C.; Tarricone, C.; Musacchio, A.; Roe, S. M.; Pearl, L.; Greengard, P. (2003) GSK-3-selective inhibitors derived from Tyrian purple indirubins. *Chem Biol 10*, 1255-1266.
(73) Polychronopoulos, P.; Magiatis, P.; Skaltsounis, A. L.; Myrianthopoulos, V.; Mikros, E.; Tarricone, A.; Musacchio, A.; Roe, S. M.; Pearl, L.; Leost, M.; Greengard, P.; Meijer, L. (2004) Structural basis for the synthesis of indirubins as potent and selective inhibitors of glycogen synthase kinase-3 and cyclin-dependent kinases. *J Med Chem 47*, 935-946.
(74) Vougogiannopoulou, K.; Ferandin, Y.; Bettayeb, K.; Myrianthopoulos, V.; Lozach, O.; Fan, Y.; Johnson, C. H.; Magiatis, P.; Skaltsounis, A. L.; Mikros, E.; Meijer, L. (2008) Soluble 3',6-substituted indirubins with enhanced selectivity toward glycogen synthase kinase -3 alter circadian period. *J Med Chem 51*, 6421-6431.
(75) Beauchard, A.; Laborie, H.; Rouillard, H.; Lozach, O.; Ferandin, Y.; Le Guevel, R.; Guguen-Guillouzo, C.; Meijer, L.; Besson, T.; Thiery, V. (2009) Synthesis and kinase inhibitory activity of novel substituted indigoids. *Bioorg Med Chem 17*, 6257-6263.
(76) Meijer, L.; Greengard, P.; Knockaert, M.; Skaltsounis, A. (2007) *US 2007/0276025 A1*.
(77) Leost, M.; Schultz, C.; Link, A.; Wu, Y. Z.; Biernat, J.; Mandelkow, E. M.; Bibb, J. A.; Snyder, G. L.; Greengard, P.; Zaharevitz, D. W.; Gussio, R.; Senderowicz, A. M.; Sausville, E. A.; Kunick, C.; Meijer, L. (2000) Paullones are potent inhibitors of glycogen synthase kinase-3beta and cyclin-dependent kinase 5/p25. *Eur J Biochem 267*, 5983-5994.
(78) Schultz, C.; Link, A.; Leost, M.; Zaharevitz, D. W.; Gussio, R.; Sausville, E. A.; Meijer, L.; Kunick, C. (1999) Paullones, a series of cyclin-dependent kinase inhibitors: synthesis, evaluation of CDK1/cyclin B inhibition, and in vitro antitumor activity. *J Med Chem 42*, 2909-2919.
(79) Knockaert, M.; Wieking, K.; Schmitt, S.; Leost, M.; Grant, K. M.; Mottram, J. C.; Kunick, C.; Meijer, L. (2002) Intracellular Targets of Paullones. Identification following affinity purification on immobilized inhibitor. *J Biol Chem 277*, 25493-25501.

(80) Kunick, C.; Lauenroth, K.; Leost, M.; Meijer, L.; Lemcke, T. (2004) 1-Azakenpaullone is a selective inhibitor of glycogen synthase kinase-3 beta. *Bioorg Med Chem Lett 14*, 413-416.
(81) Kunick, C.; Zeng, Z.; Gussio, R.; Zaharevitz, D.; Leost, M.; Totzke, F.; Schachtele, C.; Kubbutat, M. H.; Meijer, L.; Lemcke, T. (2005) Structure-aided optimization of kinase inhibitors derived from alsterpaullone. *Chembiochem 6*, 541-549.
(82) Meijer, L.; Kunick, C. (2001) *WO 2001/60374 A1*.
(83) Witherington, J.; Bordas, V.; Garland, S. L.; Hickey, D. M.; Ife, R. J.; Liddle, J.; Saunders, M.; Smith, D. G.; Ward, R. W. (2003) 5-aryl-pyrazolo[3,4-b]pyridines: potent inhibitors of glycogen synthase kinase-3 (GSK-3). *Bioorg Med Chem Lett 13*, 1577-1580.
(84) Witherington, J.; Bordas, V.; Haigh, D.; Hickey, D. M.; Ife, R. J.; Rawlings, A. D.; Slingsby, B. P.; Smith, D. G.; Ward, R. W. (2003) 5-aryl-pyrazolo[3,4-b]pyridazines: potent inhibitors of glycogen synthase kinase-3 (GSK-3). *Bioorg Med Chem Lett 13*, 1581-1584.
(85) Witherington, J.; Bordas, V.; Gaiba, A.; Garton, N. S.; Naylor, A.; Rawlings, A. D.; Slingsby, B. P.; Smith, D. G.; Takle, A. K.; Ward, R. W. (2003) 6-aryl-pyrazolo[3,4-b]pyridines: potent inhibitors of glycogen synthase kinase-3 (GSK-3). *Bioorg Med Chem Lett 13*, 3055-3057.
(86) Witherington, J.; Bordas, V.; Gaiba, A.; Naylor, A.; Rawlings, A. D.; Slingsby, B. P.; Smith, D. G.; Takle, A. K.; Ward, R. W. (2003) 6-heteroaryl-pyrazolo[3,4-b]pyridines: potent and selective inhibitors of glycogen synthase kinase-3 (GSK-3). *Bioorg Med Chem Lett 13*, 3059-3062.
(87) Uno, Y.; Iwashita, H.; Tsukamoto, T.; Uchiyama, N.; Kawamoto, T.; Kori, M.; Nakanishi, A. (2009) Efficacy of a novel, orally active GSK-3 inhibitor 6-Methyl-N-[3-[[3-(1-methylethoxy)propyl]carbamoyl]-1H-pyrazol-4-yl]pyridi ne-3-carboxamide in tau transgenic mice. *Brain Res 1296*, 148-163.
(88) Kees, K. L.; Caggiano, T. J.; Steiner, K. E.; Fitzgerald, J. J., Jr.; Kates, M. J.; Christos, T. E.; Kulishoff, J. M., Jr.; Moore, R. D.; McCaleb, M. L. (1995) Studies on new acidic azoles as glucose-lowering agents in obese, diabetic db/db mice. *J Med Chem 38*, 617-628.
(89) Kees, K. L.; Fitzgerald, J. J., Jr.; Steiner, K. E.; Mattes, J. F.; Mihan, B.; Tosi, T.; Mondoro, D.; McCaleb, M. L. (1996) New potent antihyperglycemic agents in db/db mice: synthesis and structure-activity relationship studies of (4-substituted benzyl) (trifluoromethyl)pyrazoles and -pyrazolones. *J Med Chem 39*, 3920-3928.
(90) Bebernitz, G. R.; Argentieri, G.; Battle, B.; Brennan, C.; Balkan, B.; Burkey, B. F.; Eckhardt, M.; Gao, J.; Kapa, P.; Strohschein, R. J.; Schuster, H. F.; Wilson, M.; Xu, D. D. (2001) The effect of 1,3-diaryl-[1H]-pyrazole-4-acetamides on glucose utilization in ob/ob mice. *J Med Chem 44*, 2601-2611.
(91) Shen, D. M.; Brady, E. J.; Candelore, M. R.; Dallas-Yang, Q.; Ding, V. D.; Feeney, W. P.; Jiang, G.; McCann, M. E.; Mock, S.; Qureshi, S. A.; Saperstein, R.; Shen, X.; Tong, X.; Tota, L. M.; Wright, M. J.; Yang, X.; Zheng, S.; Chapman, K. T.; Zhang, B. B.; Tata, J. R.; Parmee, E. R. (2011) Discovery of novel, potent, selective, and orally active human glucagon receptor antagonists containing a pyrazole core. *Bioorg Med Chem Lett 21*, 76-81.
(92) Peat, A. J.; Garrido, D.; Boucheron, J. A.; Schweiker, S. L.; Dickerson, S. H.; Wilson, J. R.; Wang, T. Y.; Thomson, S. A. (2004) Novel GSK-3 inhibitors with improved cellular activity. *Bioorg Med Chem Lett 14*, 2127-2130.
(93) Lum, C.; Kahl, J.; Kessler, L.; Kucharski, J.; Lundstrom, J.; Miller, S.; Nakanishi, H.; Pei, Y.; Pryor, K.; Roberts, E.; Sebo, L.; Sullivan, R.; Urban, J.; Wang, Z. (2008) 2,5-Diaminopyrimidines and 3,5-disubstituted azapurines as inhibitors of glycogen synthase kinase-3 (GSK-3). *Bioorg Med Chem Lett 18*, 3578-3581.
(94) Bebbington, D.; Binch, H.; Knegtel, R.; Golec, J.; Patel, S.; Charrier, J.; Kay, D.; davies, R.; Li, P.; Wannamaker, M.; Forster, C.; Pierce, A. (2003) Vertex Pharmaceuticals Inc. *US 6660731 B2*.
(95) Bebbington, D.; Binch, H.; Knegtel, R.; Golec, J.; Patel, S.; Charrier, J.; Kay, D.; Davies, R.; Li, P.; Wannamaker, M.; Forster, C.; Pierce, A. (2006) Vertex Pharmaceuticals Inc. *US 7008948 B2*.
(96) Bebbington, D.; Charrier, J. (2003) Vertex Pharmaceuticals Inc. *US 6656939 B2*.
(97) Bebbington, D.; Charrier, J.; Davies, R.; Everitt, S.; Kay, D.; Knegtel, R.; Patel, S. (2006) Vertex Pharmaceuticals Inc. *US 6989385 B2*.
(98) Bebbington, D.; Charrier, J.; Davies, R.; Golec, J.; Kay, D.; Knegtel, R.; Patel, S. (2002) Vertex Pharmaceuticals Inc. *WO 2002/059111 A2*.
(99) Bebbington, D.; Charrier, J.; Davies, R.; Golec, J.; Kay, D.; Knegtel, R.; Patel, S. (2003) Vertex Pharmaceuticals Inc. *US 6653301 B2*.
(100) Bebbington, D.; Charrier, J.; Golec, J.; Miller, A.; Knegtel, R. (2002) Vertex Pharmaceuticals Inc. *WO 2002/057259 A2*.
(101) Bebbington, D.; Charrier, J.; Golec, J.; Miller, A.; Knegtel, R. (2003) Vertex Pharmaceuticals Inc. *US 6664247 B2*.
(102) Bebbington, D.; Charrier, J.; Golec, J.; Pierard, F. (2004) Vertex Pharmaceuticals Inc. *US 6727251 B2*.
(103) Bebbington, D.; Charrier, J.; Golec, J.; Pierard, F. (2008) Vertex Pharmaceuticals Inc. *US 7427681 B2*.
(104) Davies, R.; Bebbington, D.; Knegtel, R.; Wannamaker, M.; Li, P.; Forster, C.; Pierce, A. (2008) Vertex Pharmaceuticals Inc. *US 739081 B2*.
(105) Davies, R.; Li, P.; Golec, J.; Charrier, J.; Knegtel, R.; Bebbington, D. (2003) Vertex Pharmaceuticals Inc. *US 6610677 B2*.
(106) Freyne, E.; Love, C.; Cooymans, L.; Vandermaessen, N.; Buijnsters, P.; Willems, M.; Embrechts, W. (2008) Janssen Pharmaceutica. *US 7449465 B2*.
(107) Freyne, E.; Love, C.; Cooymans, L.; Vandermaessen, N.; Buijnsters, P.; Willems, M.; Embrechts, W. (2009) Janssen Pharmaceutica. *US 7560458 B2*.
(108) Garcia, A.; Gallet, T.; Taki Li, A.; Lochead, A.; Marguerie, S.; Nedelec, A.; Saady, M.; Yaiche, P. (2009) Sanofi-Aventis Mitsubishi Pharma Corp. *US 7566720 B2*.
(109) George, P.; Lochead, A.; Saady, M.; Slowinski, F.; Yaiche, P. (2009) Sanofi-Aventis Mitsubishi Pharma Corp. *US 7507743 B2*.
(110) Goff, D.; Harrison, S.; Nuss, J.; Ring, D.; Zhou, X. (2002) Chiron Corp. *US 6417185 B1*.
(111) Kataoka, K.; Kosugi, T.; Ishii, T.; Takeuchi, T.; Tsutsumi, T.; Nakano, A.; Knoki, G.; Yamamoto, Y.; Sakai, Y. (2009) Teijin Limited. *US 7528140 B2*.
(112) Kataoka, K.; Kosugi, T.; Ishii, T.; Takeuchi, T.; Tsutsumi, T.; Nakano, A.; Yamamoto, Y.; Yoshioka, N. (2004) Teijin Limited. *EP 1477490 A1*.
(113) Knegtel, R.; Bebbington, D.; Binch, H.; Golec, J.; Patel, S.; Charrier, J.; Kay, D.; Davies, R.; Li, P.; Wannamaker, M.; Forster, C.; Pierce, A. (2003) Vertex Pharmaceuticals Inc. *US 6613776 B2*.
(114) Lochead, A.; Marguerie, S.; Saady, M.; Yaiche, P. (2009) Sanofi-Aventis Mitsubishi Pharma Corp. *US 7608624 B2*.
(115) Nakano, M.; Maeda, Y. (2005) Smithkline Beecham Corp. *WO 2005/061516 A1*.
(116) Nuss, J.; Harrison, S.; Ring, D.; Boyce, R.; Brown, S.; Goff, D.; Johnson, K.; Pfister, K.; Ramurthy, S.; Renhowe, P.; Seely, L.; Subramanian, S.; Wagman, A.; Zhou, X. (2002) Chiron Corp. *US 6489344 B1*.
(117) Nuss, J.; Harrison, S.; Ring, D.; Boyce, R.; Brown, S.; Goff, D.; Johnson, K.; Pfister, K.; Ramurthy, S.; Renhowe, P.; Seely, L.; Subramanian, S.; Wagman, A.; Zhou, X. (2006) Chiron Corp. *US 7037918 B2*.
(118) Nuss, J.; Harrison, S.; Ring, D.; Boyce, R.; Johnson, K.; Pfister, K.; Ramurthy, S.; Seely, L.; Wagman, A.; Desai, M.; Levine, B. (2006) Chiron Corp. *US 7045519 B2*.
(119) Tsutsumi, T.; Sugiura, S.; Koga, M.; Matsumoto, Y.; Ishii, T.; Nakano, A.; Sakai, Y.; Takarada, R.; Ogawa, H. (2009) Teijin Pharma Limited. *US 7557113 B2*.
(120) Aronov, A. M.; Tang, Q.; Martinez-Botella, G.; Bemis, G. W.; Cao, J.; Chen, G.; Ewing, N. P.; Ford, P. J.; Germann, U. A.; Green, J.; Hale, M. R.; Jacobs, M.; Janetka, J. W.; Maltais, F.; Markland, W.; Namchuk, M. N.; Nanthakumar, S.; Poondru, S.; Straub, J.; ter Haar, E.; Xie, X. (2009) Structure-guided design of potent and selective pyrimidylpyrrole inhibitors of extracellular signal-regulated kinase (ERK) using conformational control. *J Med Chem 52*, 6362-6368.
(121) Ring, D. B.; Johnson, K. W.; Henriksen, E. J.; Nuss, J. M.; Goff, D.; Kinnick, T. R.; Ma, S. T.; Reeder, J. W.; Samuels, I.; Slabiak, T.; Wagman, A. S.; Hammond, M. E.; Harrison, S. D. (2003) Selective glycogen synthase kinase 3 inhibitors potentiate insulin activation of glucose transport and utilization in vitro and in vivo. *Diabetes 52*, 588-595.
(122) Maeda, Y.; Nakano, M.; Sato, H.; Miyazaki, Y.; Schweiker, S. L.; Smith, J. L.; Truesdale, A. T. (2004) 4-Acylamino-6-arylfuro[2,3-d]pyrimidines: potent and selective glycogen synthase kinase-3 inhibitors. *Bioorg Med Chem Lett 14*, 3907-3911.

(123) Miyazaki, Y.; Maeda, Y.; Sato, H.; Nakano, M.; Mellor, G. W. (2008) Rational design of 4-amino-5,6-diaryl-furo[2,3-d]pyrimidines as potent glycogen synthase kinase-3 inhibitors. *Bioorg Med Chem Lett 18*, 1967-1971.
(124) Olesen, P. H.; Sorensen, A. R.; Urso, B.; Kurtzhals, P.; Bowler, A. N.; Ehrbar, U.; Hansen, B. F. (2003) Synthesis and in vitro characterization of 1-(4-aminofurazan-3-yl)-5-dialkylaminomethyl-1H-[1,2,3]triazole-4-carboxyl ic acid derivatives. A new class of selective GSK-3 inhibitors. *J Med Chem 46*, 3333-3341.
(125) Bandarage, U.; Hare, B.; Parsons, J.; Pham, L.; Marhefka, C.; Bemis, G.; Tang, Q.; Moody, C. S.; Rodems, S.; Shah, S.; Adams, C.; Bravo, J.; Charonnet, E.; Savic, V.; Come, J. H.; Green, J. (2009) 4-(Benzimidazol-2-yl)-1,2,5-oxadiazol-3-ylamine derivatives: potent and selective p70S6 kinase inhibitors. *Bioorg Med Chem Lett 19*, 5191-5194.
(126) Saitoh, M.; Kunitomo, J.; Kimura, E.; Hayase, Y.; Kobayashi, H.; Uchiyama, N.; Kawamoto, T.; Tanaka, T.; Mol, C. D.; Dougan, D. R.; Textor, G. S.; Snell, G. P.; Itoh, F. (2009) Design, synthesis and structure-activity relationships of 1,3,4-oxadiazole derivatives as novel inhibitors of glycogen synthase kinase-3beta. *Bioorg Med Chem 17*, 2017-2029.
(127) Saitoh, M.; Kunitomo, J.; Kimura, E.; Iwashita, H.; Uno, Y.; Onishi, T.; Uchiyama, N.; Kawamoto, T.; Tanaka, T.; Mol, C. D.; Dougan, D. R.; Textor, G. P.; Snell, G. P.; Takizawa, M.; Itoh, F.; Kori, M. (2009) 2-{3-[4-(Alkylsulfinyl)phenyl]-1-benzofuran-5-yl}-5-methyl-1,3,4-oxadiazol e derivatives as novel inhibitors of glycogen synthase kinase-3beta with good brain permeability. *J Med Chem 52*, 6270-6286.
(128) Onishi, T.; Iwashita, H.; Uno, Y.; Kunitomo, J.; Saitoh, M.; Kimura, E.; Fujita, H.; Uchiyama, N.; Kori, M.; Takizawa, M. (2011) A novel glycogen synthase kinase-3 inhibitor 2-methyl-5-(3-(4-((S)-methylsulfinyl)phenyl)-1-benzofuran-5-yl)-1,3,4-oxadiazole decreases tau phosphorylation and ameliorates cognitive deficits in a transgenic model of Alzheimer´s disease. *J Neurochem early view*.
(129) Khanfar, M. A.; Hill, R. A.; Kaddoumi, A.; El Sayed, K. A. (2010) Discovery of novel GSK-3beta inhibitors with potent in vitro and in vivo activities and excellent brain permeability using combined ligand- and structure-based virtual screening. *J Med Chem 53*, 8534-8545.
(130) Koryakova, A. G.; Ivanenkov, Y. A.; Ryzhova, E. A.; Bulanova, E. A.; Karapetian, R. N.; Mikitas, O. V.; Katrukha, E. A.; Kazey, V. I.; Okun, I.; Kravchenko, D. V.; Lavrovsky, Y. V.; Korzinov, O. M.; Ivachtchenko, A. V. (2008) Novel aryl and heteroaryl substituted N-[3-(4-phenylpiperazin-1-yl)propyl]-1,2,4-oxadiazole-5-carboxamides as selective GSK-3 inhibitors. *Bioorg Med Chem Lett 18*, 3661-3666.
(131) Loge, C.; Testard, A.; Thiery, V.; Lozach, O.; Blairvacq, M.; Robert, J. M.; Meijer, L.; Besson, T. (2008) Novel 9-oxo-thiazolo[5,4-f]quinazoline-2-carbonitrile derivatives as dual cyclin-dependent kinase 1 (CDK1)/glycogen synthase kinase-3 (GSK-3) inhibitors: synthesis, biological evaluation and molecular modeling studies. *Eur J Med Chem 43*, 1469-1477.
(132) Bhat, R.; Xue, Y.; Berg, S.; Hellberg, S.; Ormo, M.; Nilsson, Y.; Radesater, A. C.; Jerning, E.; Markgren, P. O.; Borgegard, T.; Nylof, M.; Gimenez-Cassina, A.; Hernandez, F.; Lucas, J. J.; Diaz-Nido, J.; Avila, J. (2003) Structural insights and biological effects of glycogen synthase kinase 3-specific inhibitor AR-A014418. *J Biol Chem 278*, 45937-45945.
(133) Noble, W.; Planel, E.; Zehr, C.; Olm, V.; Meyerson, J.; Suleman, F.; Gaynor, K.; Wang, L.; LaFrancois, J.; Feinstein, B.; Burns, M.; Krishnamurthy, P.; Wen, Y.; Bhat, R.; Lewis, J.; Dickson, D.; Duff, K. (2005) Inhibition of glycogen synthase kinase-3 by lithium correlates with reduced tauopathy and degeneration in vivo. *Proc Natl Acad Sci U S A 102*, 6990-6995.
(134) Monte, F. L.; Kramer, T.; Bolander, A.; Plotkin, B.; Eldar-Finkelman, H.; Fuertes, A.; Dominguez, J.; Schmidt, B. (2011) Synthesis and biological evaluation of glycogen synthase kinase 3 (GSK-3) inhibitors: an fast and atom efficient access to 1-aryl-3-benzylureas. *Bioorg Med Chem Lett 21*, 5610-5615.
(135) Shin, D.; Lee, S. C.; Heo, Y. S.; Lee, W. Y.; Cho, Y. S.; Kim, Y. E.; Hyun, Y. L.; Cho, J. M.; Lee, Y. S.; Ro, S. (2007) Design and synthesis of 7-hydroxy-1H-benzoimidazole derivatives as novel inhibitors of glycogen synthase kinase-3beta. *Bioorg Med Chem Lett 17*, 5686-5689.
(136) Voigt, B.; Krug, M.; Schachtele, C.; Totzke, F.; Hilgeroth, A. (2008) Probing novel 1-aza-9-oxafluorenes as selective GSK-3beta inhibitors. *ChemMedChem 3*, 120-126.
(137) Chauhan, N. B.; Siegel, G. J.; Feinstein, D. L. (2005) Propentofylline attenuates tau hyperphosphorylation in Alzheimer's Swedish mutant model Tg2576. *Neuropharmacology 48*, 93-104.
(138) Arnost, M.; Pierce, A.; ter Haar, E.; Lauffer, D.; Madden, J.; Tanner, K.; Green, J. (2010) 3-Aryl-4-(arylhydrazono)-1H-pyrazol-5-ones: Highly ligand efficient and potent inhibitors of GSK3beta. *Bioorg Med Chem Lett 20*, 1661-1664.
(139) Chen, W.; Gaisina, I. N.; Gunosewoyo, H.; Malekiani, S. A.; Hanania, T.; Kozikowski, A. P. (2011) Structure-guided design of a highly selective glycogen synthase kinase-3beta inhibitor: a superior neuroprotective pyrazolone showing antimania effects. *ChemMedChem 6*, 1587-1592.
(140) Khanfar, M. A.; Asal, B. A.; Mudit, M.; Kaddoumi, A.; El Sayed, K. A. (2009) The marine natural-derived inhibitors of glycogen synthase kinase-3beta phenylmethylene hydantoins: In vitro and in vivo activities and pharmacophore modeling. *Bioorg Med Chem 17*, 6032-6039.
(141) Coffman, K.; Brodney, M.; Cook, J.; Lanyon, L.; Pandit, J.; Sakya, S.; Schachter, J.; Tseng-Lovering, E.; Wessel, M. (2011) 6-amino-4-(pyrimidin-4-yl)pyridones: novel glycogen synthase kinase-3beta inhibitors. *Bioorg Med Chem Lett 21*, 1429-1433.
(142) Hamann, M.; Alonso, D.; Martin-Aparicio, E.; Fuertes, A.; Perez-Puerto, M. J.; Castro, A.; Morales, S.; Navarro, M. L.; Del Monte-Millan, M.; Medina, M.; Pennaka, H.; Balaiah, A.; Peng, J.; Cook, J.; Wahyuono, S.; Martinez, A. (2007) Glycogen synthase kinase-3 (GSK-3) inhibitory activity and structure-activity relationship (SAR) studies of the manzamine alkaloids. Potential for Alzheimer's disease. *J Nat Prod 70*, 1397-1405.
(143) Gompel, M.; Leost, M.; De Kier Joffe, E. B.; Puricelli, L.; Franco, L. H.; Palermo, J.; Meijer, L. (2004) Meridianins, a new family of protein kinase inhibitors isolated from the ascidian Aplidium meridianum. *Bioorg Med Chem Lett 14*, 1703-1707.
(144) Meijer, L.; Thunnissen, A. M.; White, A. W.; Garnier, M.; Nikolic, M.; Tsai, L. H.; Walter, J.; Cleverley, K. E.; Salinas, P. C.; Wu, Y. Z.; Biernat, J.; Mandelkow, E. M.; Kim, S. H.; Pettit, G. R. (2000) Inhibition of cyclin-dependent kinases, GSK-3beta and CK1 by hymenialdisine, a marine sponge constituent. *Chem Biol 7*, 51-63.
(145) Zhang, N.; Zhong, R.; Yan, H.; Jiang, Y. (2011) Structural features underlying selective inhibition of GSK3beta by dibromocantharelline: implications for rational drug design. *Chem Biol Drug Des 77*, 199-205.
(146) Pande, V.; Ramos, M. J. (2005) Structural basis for the GSK-3beta binding affinity and selectivity against CDK-2 of 1-(4-aminofurazan-3yl)-5-dialkylaminomethyl-1H-[1,2,3] triazole-4-carboxylic acid derivatives. *Bioorg Med Chem Lett 15*, 5129-5135.
(147) ter Haar, E.; Coll, J. T.; Austen, D. A.; Hsiao, H. M.; Swenson, L.; Jain, J. (2001) Structure of GSK3beta reveals a primed phosphorylation mechanism. *Nat Struct Biol 8*, 593-596.
(148) Gotz, J.; Ittner, L. M. (2008) Animal models of Alzheimer's disease and frontotemporal dementia. *Nat Rev Neurosci 9*, 532-544.
(149) Iijima-Ando, K.; Iijima, K. (2010) Transgenic Drosophila models of Alzheimer's disease and tauopathies. *Brain Struct Funct 214*, 245-262.
(150) Wentzell, J.; Kretzschmar, D. (2010) Alzheimer's disease and tauopathy studies in flies and worms. *Neurobiol Dis 40*, 21-28.
(151) Lucas, J. J.; Hernandez, F.; Gomez-Ramos, P.; Moran, M. A.; Hen, R.; Avila, J. (2001) Decreased nuclear beta-catenin, tau hyperphosphorylation and neurodegeneration in GSK-3beta conditional transgenic mice. *EMBO J 20*, 27-39.
(152) Perez, M.; Ribe, E.; Rubio, A.; Lim, F.; Moran, M. A.; Ramos, P. G.; Ferrer, I.; Isla, M. T.; Avila, J. (2005) Characterization of a double (amyloid precursor protein-tau) transgenic: tau phosphorylation and aggregation. *Neuroscience 130*, 339-347.
(153) Ribe, E. M.; Perez, M.; Puig, B.; Gich, I.; Lim, F.; Cuadrado, M.; Sesma, T.; Catena, S.; Sanchez, B.; Nieto, M.; Gomez-Ramos, P.; Moran, M. A.; Cabodevilla, F.; Samaranch, L.; Ortiz, L.; Perez, A.; Ferrer, I.; Avila, J.; Gomez-Isla, T. (2005) Accelerated amyloid deposition, neurofibrillary degeneration and neuronal loss in double mutant APP/tau transgenic mice. *Neurobiol Dis 20*, 814-822.
(154) Terwel, D.; Muyllaert, D.; Dewachter, I.; Borghgraef, P.; Croes, S.; Devijver, H.; Van Leuven, F. (2008) Amyloid activates GSK-3beta to aggravate neuronal tauopathy in bigenic mice. *Am J Pathol 172*, 786-798.
(155) Lewis, J.; Dickson, D. W.; Lin, W. L.; Chisholm, L.; Corral, A.; Jones, G.; Yen, S. H.; Sahara, N.; Skipper, L.; Yager, D.; Eckman, C.; Hardy, J.; Hutton, M.; McGowan, E. (2001) Enhanced neurofibrillary degeneration in transgenic mice expressing mutant tau and APP. *Science 293*, 1487-1491.
(156) Oddo, S.; Caccamo, A.; Shepherd, J. D.; Murphy, M. P.; Golde, T. E.; Kayed, R.; Metherate, R.; Mattson, M. P.; Akbari, Y.; LaFerla, F. M. (2003) Triple-transgenic model of Alzheimer's disease with plaques and tangles: intracellular Abeta and synaptic dysfunction. *Neuron 39*, 409-421.

(157) Lewis, J.; McGowan, E.; Rockwood, J.; Melrose, H.; Nacharaju, P.; Van Slegtenhorst, M.; Gwinn-Hardy, K.; Paul Murphy, M.; Baker, M.; Yu, X.; Duff, K.; Hardy, J.; Corral, A.; Lin, W. L.; Yen, S. H.; Dickson, D. W.; Davies, P.; Hutton, M. (2000) Neurofibrillary tangles, amyotrophy and progressive motor disturbance in mice expressing mutant (P301L) tau protein. *Nat Genet 25*, 402-405.
(158) Paquet, D.; Bhat, R.; Sydow, A.; Mandelkow, E. M.; Berg, S.; Hellberg, S.; Falting, J.; Distel, M.; Koster, R. W.; Schmid, B.; Haass, C. (2009) A zebrafish model of tauopathy allows in vivo imaging of neuronal cell death and drug evaluation. *J Clin Invest 119*, 1382-1395.
(159) Paquet, D.; Schmid, B.; Haass, C. (2010) Transgenic Zebrafish as a Novel Animal Model to Study Tauopathies and Other Neurodegenerative Disorders in vivo. *Neurodegenerative Dis 7*, 99-102.
(160) Okawa, Y.; Ishiguro, K.; Fujita, S. C. (2003) Stress-induced hyperphosphorylation of tau in the mouse brain. *FEBS Lett 535*, 183-189.
(161) Yoshida, S.; Maeda, M.; Kaku, S.; Ikeya, H.; Yamada, K.; Nakaike, S. (2006) Lithium inhibits stress-induced changes in tau phosphorylation in the mouse hippocampus. *J Neural Transm 113*, 1803-1814.
(162) Leroy, K.; Brion, J. P. (1999) Developmental expression and localization of glycogen synthase kinase-3beta in rat brain. *J Chem Neuroanat 16*, 279-293.
(163) Takahashi, M.; Tomizawa, K.; Ishiguro, K. (2000) Distribution of tau protein kinase I/glycogen synthase kinase-3beta, phosphatases 2A and 2B, and phosphorylated tau in the developing rat brain. *Brain Res 857*, 193-206.
(164) Min, S. H.; Cho, J. S.; Oh, J. H.; Shim, S. B.; Hwang, D. Y.; Lee, S. H.; Jee, S. W.; Lim, H. J.; Kim, M. Y.; Sheen, Y. Y.; Kim, Y. K. (2005) Tau and GSK3beta dephosphorylations are required for regulating Pin1 phosphorylation. *Neurochem Res 30*, 955-961.
(165) Sato, N.; Meijer, L.; Skaltsounis, L.; Greengard, P.; Brivanlou, A. H. (2004) Maintenance of pluripotency in human and mouse embryonic stem cells through activation of Wnt signaling by a pharmacological GSK-3-specific inhibitor. *Nat Med 10*, 55-63.
(166) Gould, T. D.; Gray, N. A.; Manji, H. K. (2003) Effects of a glycogen synthase kinase-3 inhibitor, lithium, in adenomatous polyposis coli mutant mice. *Pharmacol Res 48*, 49-53.
(167) Martinez, A.; Castro, A.; Medina, M. (2006) Glycogen Synthase Kinase-3 (GSK-3) and Its Inhibitors. *John Wiley & Sons, Hoboken, NJ, USA*, 3-23.
(168) Martinez, A.; Gil, C.; Perez, D. I. (2011) Glycogen Synthase Kinase 3 Inhibitors in the Next Horizon for Alzheimer's Disease Treatment. *Int J Alzheimers Dis 2011*, 1-7.
(169) Alon, L. T.; Pietrokovski, S.; Barkan, S.; Avrahami, L.; Kaidanovich-Beilin, O.; Woodgett, J. R.; Barnea, A.; Eldar-Finkelman, H. (2011) Selective loss of glycogen synthase kinase-3alpha in birds reveals distinct roles for GSK-3 isozymes in tau phosphorylation. *FEBS Lett 585*, 1158-1162.
(170) Phiel, C. J.; Wilson, C. A.; Lee, V. M.; Klein, P. S. (2003) GSK-3alpha regulates production of Alzheimer's disease amyloid-beta peptides. *Nature 423*, 435-439.
(171) Davis, M. I.; Hunt, J. P.; Herrgard, S.; Ciceri, P.; Wodicka, L. M.; Pallares, G.; Hocker, M.; Treiber, D. K.; Zarrinkar, P. P. (2011) Comprehensive analysis of kinase inhibitor selectivity. *Nat Biotechnol 29*, 1046-1051.
(172) Rauh, D. (2010) Inaktive Kinasekonformationen stabilisieren. *Nachrichten aus der Chemie 58*, 118-121.
(173) Okada, K.; Sato, T.; Kohno, Y.; Nomura, M. (2010) Kyorin Pharmaceutical Co., Ltd. *WO 2010/104205 A1*.
(174) Turner, S. C.; Bakker, M. H. M.; Hornberger, W.; Wolter, F. E. (2010) Abbott GmbH & Co. KG. *WO 2010/109005 A1*.

4.1.2 Effiziente Synthese und Evaluierung von GSK-3-Inhibitoren

Der Inhalt dieses Kapitels wurde bereits veröffentlicht:

Fabio Lo Monte*, Thomas Kramer*, Alexander Boländer, Batya Plotkin, Hagit Eldar-Finkelman, Ana Fuertes, Juan Dominguez, Boris Schmidt‡
Synthesis and biological evaluation of glycogen synthase kinase 3 (GSK-3) inhibitors: An fast and atom efficient access to 1-aryl-3-benzylureas, *Bioorganic & Medicinal Chemistry Letters* **2011**, 21, 5610-5615. dx.doi.org/10.1016/j.bmcl.2011.06.131
Mit freundlicher Genehmigung von Elsevier Ltd.

AR-A014418 (**27**) ist ein potenter und selektiver GSK-3-Inhibitor, der von der Pharmafirma AstraZeneca publiziert und patentiert wurde. Aufgrund toxischer Daten in den klinischen Studien wurde eine analoge Struktur dieses Inhibitors nicht weiter verfolgt. Diese Verbindung wurde, aufgrund des strukturellen Aufbaus, als Leitstruktur für die Inhibition von GSK-3 im Bereich der Alzheimer-Demenz (AD) ausgewählt. Der in unserem *Assay* bestimmte IC_{50}-Wert dieser Verbindung lag bei 330 nM.

Die Synthese des Harnstoffderivats **27** wird bei 100℃ durchgeführt und erfordert im Anschluss eine chromatographische Aufreinigung. Durch verschiedene Untersuchungen konnte eine schnelle und effiziente Synthesemethodik für Harnstoffderivate dieser Art etabliert werden. Die Synthese konnte bei Raumtemperatur durchgeführt werden und erforderte keine chromatographische Aufreinigung. Dadurch war es möglich viele Strukturen in kürzester Zeit herzustellen. Die erhaltenen Strukturen wurden umkristallisiert und konnten anschließend durch eine Suzuki-Kupplung bzw. Mikrowellensynthese weiter modifiziert werden (Abb. 17). Die Endprodukte konnten ebenfalls ohne chromatographische Aufreinigung isoliert werden, indem sie kurz umkristallisiert wurden. Mit Hilfe dieser Methode konnten die hergestellten Derivate für eine intensive Untersuchung der Struktur-Aktivitäts-Beziehung eingesetzt werden. Aufgrund dessen war es möglich, mehrere aktive und selektive GSK-3-Inhibitoren zu synthetisieren.

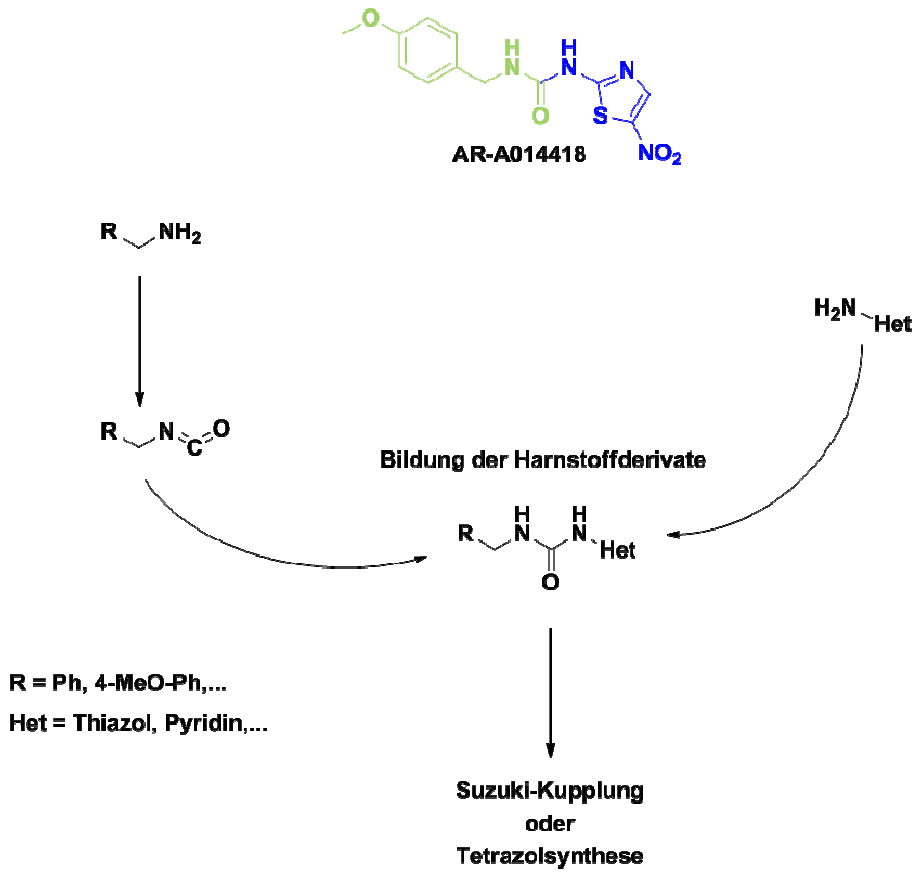

Abb. 17: Schematische Darstellung der Synthesemethodik.

Die aktivste Verbindung, die durch diese Methodik hergestellt werden konnte, hatte einen IC_{50}-Wert von 98 nM für GSK-3β und ist somit dreimal aktiver als AR-A014418 (**27**). Das molekulare *Docking* einer unserer Verbindungen zeigte ein ähnliches Bindungsverhalten wie AR-A014418 (**27**) und bestätigte die Ergebnisse der Struktur-Aktivitäts-Beziehung. Zudem konnte durch eine *in vivo* Evaluation im Zebrafisch-Embryo nachgewiesen werden, dass die synthetisierten Verbindungen im Gegensatz zu Struktur **27** keine Toxizität aufwiesen.

Die im Rahmen dieser Arbeit von Fabio Lo Monte synthetisierten Verbindungen:

BSc4102 (4), BSc4104 (44), BSc4106 (50), BSc4108 (48), BSc4111 (45), BSc4113 (51), BSc4115 (52), BSc4117 (49), BSc4145 (21), BSc4147 (27), BSc4149 (24), BSc4151 (28), BSc4153 (25), BSc4155 (19), BSc4157 (23), BSc4159 (13), BSc4161 (10), BSc4163 (30), BSc4168 (18), BSc4170 (7), BSc4188 (2), BSc4190 (6), BSc4192 (15), BSc4194 (32), BSc4196 (34), BSc4198 (36), BSc4200 (38), BSc4202 (58), BSc4206 (39), BSc4242 (60), BSc4244 (63), BSc4248 (29), BSc4250 (66)

In Klammern die Verbindungsnummer in der Publikation.

Bioorganic & Medicinal Chemistry Letters 21 (2011) 5610–5615

Contents lists available at ScienceDirect

Bioorganic & Medicinal Chemistry Letters

journal homepage: www.elsevier.com/locate/bmcl

Synthesis and biological evaluation of glycogen synthase kinase 3 (GSK-3) inhibitors: An fast and atom efficient access to 1-aryl-3-benzylureas

Fabio Lo Monte [a,†], Thomas Kramer [a,†], Alexander Boländer [a], Batya Plotkin [b], Hagit Eldar-Finkelman [b], Ana Fuertes [c], Juan Dominguez [c], Boris Schmidt [a,*]

[a] Clemens Schöpf—Institute of Organic Chemistry and Biochemistry, Technische Universität Darmstadt, 64287 Darmstadt, Germany
[b] Department of Human Molecular Genetics and Biochemistry, Sackler School of Medicine, Tel Aviv University, Tel Aviv 69978, Israel
[c] Noscira, Tres Cantos, 28760 Madrid, Spain

ARTICLE INFO

Article history:
Received 15 April 2011
Revised 11 June 2011
Accepted 13 June 2011
Available online 18 July 2011

Keywords:
Glycogen synthase kinase 3 (GSK-3)
Alzheimer disease
Structure–activity relationship (SAR)
Suzuki coupling
Microwave irradiation

ABSTRACT

The glycogen synthase kinase 3 (GSK-3) is implicated in multiple cellular processes and has been linked to the pathogenesis of Alzheimer's disease (AD). In the course of our research topic we synthesized a library of potent GSK-3 inhibitors. We utilized the urea scaffold present in the potent and highly selective GSK-3 inhibitor AR-A014418 (AstraZeneca). This moiety suits both (a) a convergent approach utilizing readily accessible building blocks and (b) a divergent approach based on a microwave heating assisted Suzuki coupling. We established a chromatography-free purification method to generate products with sufficient purity for the biological assays. The structure–activity relationship of the library provided the rationale for the synthesis of the benzothiazolylurea **66** (IC_{50} = 140 nM) and the pyridylurea **62** (IC_{50} = 98 nM), which displayed two to threefold enhanced activity versus the reference compound **18** (AR-A014418: IC_{50} = 330 nM) in our assays.

Alzheimer's disease (AD) is a neurodegenerative disorder defined by progressive memory loss and cognitive impairment.[1] The definite diagnosis of AD is possible postmortem only. It is based on the presence of extracellular plaques of β-amyloid (Aβ), and intracellular neurofibrillary tangles (NFTs) consisting of hyperphosphorylated tau protein.[2] Glycogen synthase kinase 3 (GSK-3) interacts with several neuronal proteins that are directly linked to AD.[3] There are two GSK-3 genes, GSK-3α and GSK-3β. Both are ubiquitously expressed and constitutively active proline-directed serine/threonine kinases.[1] Several GSK-3 inhibitors have been studied in kinase assays and cellular test panels. Among these inhibitors are paullones, indirubin, aminomaleimides and other small molecules. The potent and specific GSK-3 inhibitor AR-A014418 (**18**) was reported by AstraZeneca and its interactions with the essential amino acids of GSK-3β are denoted in Figure 1.[4]

AR-A014418 (**18**) is selective against Cdk2, Cdk5 and 26 other kinases tested. It inhibits GSK-3 activity with a strongly assay dependent IC_{50}, the highest activity was reported as IC_{50} = 104 nM.[4] AR-A014418 constitutes a lead compound in our kinase inhibitor programe targeting neurodegenerative diseases.[5]

There is a need of a robust and inexpensive approach to AR-A014418 (**18**), suitable for combinatorial chemistry, which provides straightforward access to related ureas displaying enhanced GSK-3 inhibition. The generation of chemical diversity and the limitation by commercial building blocks stimulated a search for mild reaction conditions, rapid purification strategy and access to the reactive intermediate isocyanates without destillation.[6] The two step protocol utilized the in situ generation of

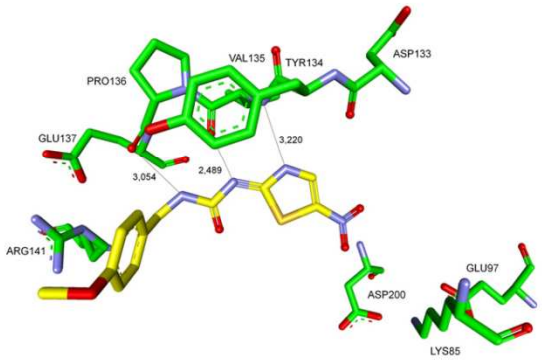

Figure 1. Potent and highly selective GSK-3 inhibitor AR-A014418 (AstraZeneca) in the ATP binding pocket of GSK-3β; important protein–inhibitor interactions are shown. The distance is denoted in Å. PDB code 1Q5K (Accelrys Discovery Studio Visualizer 2.5).

* Corresponding author. Tel.: +49 6151 164531; fax: +49 6151 163278.
E-mail address: schmidt_boris@t-online.de (B. Schmidt).
† These authors contributed equally to this work.

0960-894X/$ - see front matter © 2011 Published by Elsevier Ltd.
doi:10.1016/j.bmcl.2011.06.131

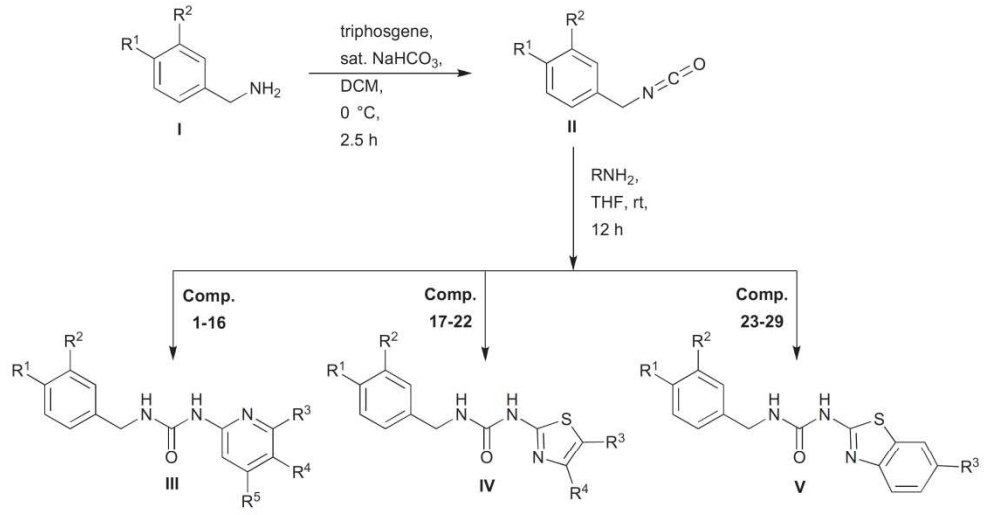

Scheme 1. Mild synthesis and rapidly purified ureas.

Table 1
Mild synthesis provides crystalline ureas free of chromatography

Compd	R^1	R^2	R^3	R^4	R^5	Yield[a] (%)	*c* Log *P*[c]
1	F	H	H	I	H	11	3.74
2	F	H	Br	H	H	52	3.48
3	MeO	H	Br	H	H	41	3.25
4	F	H	H	Br	H	54	3.48
5	MeO	H	H	Br	H	48	3.25
6	MeO	H	H	H	Br	75	3.25
7	F	H	H	H	Cl	31	3.33
8	MeO	H	H	H	Cl	34	3.10
9	MeO	H	H	H	CN	63[b]	2.00
10	F	H	H	NO_2	H	21[b]	2.51
11	MeO	H	H	NO_2	H	13[b]	2.28
12	F	H	H	CN	H	63[b]	2.22
13	MeO	H	H	CN	H	58[b]	2.00
14	Br	H	H	CN	H	34[b]	2.94
15	OCF_3	H	H	CN	H	13[b]	3.10
16	$-OCH_2O-$	H	CN	H	19[b]	2.04	
17	F	H	NO_2	H	—	21[b]	2.34
18	MeO	H	NO_2	H	—	26[b]	2.11
19	F	H	COOEt	Me	—	35[b]	3.02
20	MeO	H	COOEt	Me	—	24[b]	2.80
21	F	H	H	4-Me-Ph	—	29[b]	5.00
22	MeO	H	H	4-Me-Ph	—	46[b]	4.77
23	F	H	Br	—	—	24[b]	4.87
24	MeO	H	F	—	—	52[b]	3.92
25	F	H	CF_3	—	—	31[b]	4.96
26	MeO	H	CF_3	—	—	50[b]	4.74
27	MeO	H	NO_2	—	—	26[b]	3.64
28	F	F	NO_2	—	—	36[b]	3.93
29	MeO	H	CN	—	—	70[b]	3.34

[a] Yields of analytically pure products; products recrystallized from methanol or ethanol.
[b] Amines preactivated with *n*-BuLi.
[c] Determined by CS ChemOffice 2008.

isocyanates from benzylamine and triphosgene. These crude intermediates were dissolved in dry *N*,*N*-dimethylformamide or dry tetrahydrofurane and reacted with nonactivated or *n*-buthyllithium (*n*-BuLi) activated amines (Scheme 1 and Table 1).

Initially, the reaction of aminopyridines was dominated by the dimerization of benzylamines. This resulted in the isolation of known benzylamine adducts **30** and **31** (Scheme 2 and Table 2).[7,8]

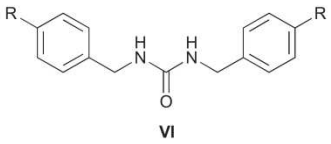

Scheme 2. Commonly observed dimerization product.

Table 2
Dimerization derived products

Compd	R	Yield[a] (%)	*c* Log *P*[b]
30[6,7]	4-F	37	3.17
31[6]	4-MeO	43	2.72

[a] Yields of analytically pure products; products recrystallized from methanol.
[b] Determined by CS ChemOffice 2008.

Using *n*-BuLi for the deprotonation of the heterocyclic amines solved this problem. Furthermore, high-pressure liquid chromatography (HPLC) controls showed that the *n*-BuLi preactivated amines reacted with the isocyanates immediately, but nevertheless the reactions were stirred 12 h at room temperature. Afterward the reaction solution was suspended in vigorously stirred water and precipitation occured promptly. The purification of the crude urea was achieved by filtration and recrystallization. These reaction and purification conditions were standardized for a variety of amines, including benzylamines, aminopyridines and aminothiazoles.

AR-A014418 (**18**) was synthesized without heating and chromatographic purification, which were employed by AstraZeneca 2003.[4] The initial yields of the standard methodology were moderate at best, but they did not require chromatography and the yield of compound **6** obtained by the standard protocol was optimized in scaled up experiments to 75%. Thus the atom efficiency of the total process, which includes the purification, is actually sufficiently high as it produces very little waste material.

The required diversity was introduced by the Suzuki-coupling of arylbromides and boronic acids (Scheme 3 and Table 3).

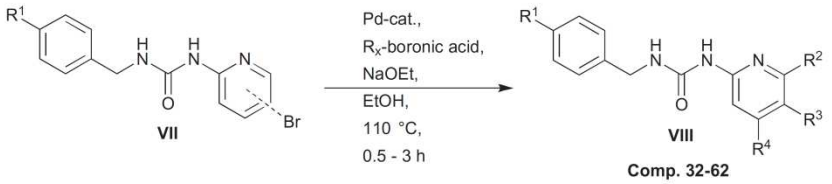

Scheme 3. Suzuki reactions.

Table 3
Urea enlargement supported by Suzuki reaction

Compd	R^1	R^2	R^3	R^4	Yield[a] (%)	*c* Log *P*[d]
32	F	Ph	H	H	40[b]	4.58
33	MeO	Ph	H	H	71[b]	4.36
34	F	3-F-Ph	H	H	29[b]	4.75
35	F	3-MeO-Ph	H	H	31[b]	6.37
36	MeO	3-MeO-Ph	H	H	34[b]	6.13
37	F	3-BnO-Ph	H	H	51[b]	6.37
38	F	4-Py	H	H	67[b]	3.26
39	MeO	4-Py	H	H	50[b]	3.04
40	F	H	Ph	H	70[c]	4.37
41	MeO	H	Ph	H	47[c]	4.15
42	F	H	4-Me-Ph	H	34[c]	4.87
43	MeO	H	4-Me-Ph	H	32[c]	4.65
43	MeO	H	4-Me-Ph	H	32[c]	4.65
44	F	H	3-F-Ph	H	68[c]	4.54
45	MeO	H	3-F-Ph	H	33[c]	4.32
46	F	H	3-MeO-Ph	H	37[c]	4.39
47	MeO	H	3-MeO-Ph	H	34[c]	4.17
48	F	H	3-Isopro-poxy-Ph	H	43[c]	5.23
49	MeO	H	3-Isopro-poxy-Ph	H	61[c]	5.01
50	F	H	3-BnO-Ph	H	26[c]	6.16
51	MeO	H	3-BnO-Ph	H	19[c]	5.94
52	MeO	H	3-CF_3-Ph	H	27[c]	5.07
53	F	H	2,3-di-F-Ph	H	83[c]	4.62
54	MeO	H	2,3-di-F-Ph	H	26[c]	4.40
55	F	H	4-Vinyl-Ph	H	85[c]	5.09
56	MeO	H	4-Vinyl-Ph	H	87[c]	4.87
57	MeO	H	H	Ph	77[b]	4.15
58	MeO	H	H	3-F-Ph	57[b]	4.32
59	MeO	H	H	3-MeO-Ph	62[b]	4.17
60	MeO	H	H	2-MeO-Ph	47[c]	3.61
61	MeO	H	H	2-Thio-phen	33[c]	4.06
62	MeO	H	H	2-F-Py	67	3.03

[a] Yields of analytically pure products; products were recrystallized from methanol.
[b] $Pd(OAc)_2$.
[c] $Pd(PPh_3)_4$.
[d] Determined by CS ChemOffice 2008.

The Suzuki coupling of phenylboronic acids and brominated arylureas was catalyzed by $Pd(OAc)_2$ under standard conditions or subtle modifications thereof.[9,10] Some reactions required catalyst exchange to $Pd(PPh_3)_4$. The boronic acids were activated by sodium ethanolate. The starting materials were suspended in dry ethanol and the reactions were carried out in a sealed, argon flushed vessel. Again, the crude products of the Suzuki reaction were purified by atom efficient recrystallization.

Finally, we obtained four tetrazole derivatives (**63–66**) using microwave radiation in a Biotage Initiator 300. These products were purified by recrystallization and isolated in very good yields requiring no further optimization at this stage (Scheme 4 and Table 4), although the reaction conditions can be improved by using ionic liquids.[11] Be careful while working with azides, they can be explosive and should be handled with great care. During our study we encountered no adverse events.[12]

The arylureas were evaluated for their inhibition of GSK-3 activity. Several compounds were identified to reduce in vitro GSK-3β activity beneath 50% at a concentration of 10 μM (Table 5).[13]

Two derivatives (**66** and **62**) are more potent than our reference compound AR-A014418 (**18**). Five derivatives (**29**, **63**, **11**, **60, and 13**) display comparable inhibitory activity and four of them are not associated with toxicity alerts (Fig. 2). It should be noted that the tetrazoles, for example, compound **63** with a topological polar surface area of 111.83 Å (ChemOffice2008) may not permeate the blood brain barrier.

A docking study of compound **66** and PDB structure 1Q5K of GSK-3β suggested a binding mode along the hinge region of the ATP-binding pocket approximately like AR-A014418 (**18**) (Fig. 3).[4,14] There are two hydrogen bond interactions between **66** and the amino acid Glu137. Furthermore we assume two other interactions, one between the Asp133 carbonyl and a hydrogen of the phenyl group and the other between the tetrazol moiety and the polar pocket consisting of Lys85, Glu97 and Asp200. We hypothesize that the latter interaction is the reason for the enhanced potency of derivative (**66**).

Via the expeditious structure–activity relationship (SAR) we ascertained that the aminothiazole, used by AstraZeneca, can be

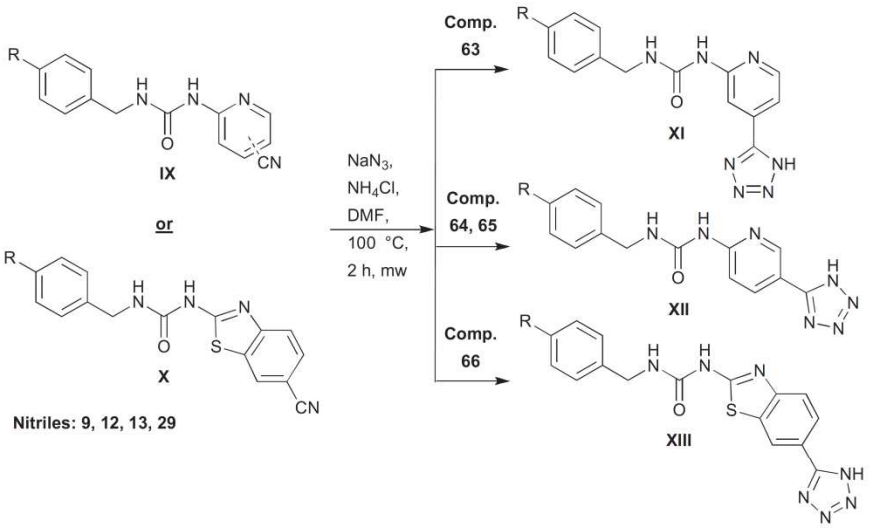

Scheme 4. Microwave reactions.

Table 4
Urea aryl tetrazole formation by microwave reaction

Compd	R	Yield[a] (%)	*c* Log *P*[b]
63	MeO	87	1.75
64	F	81	1.98
65	MeO	88	1.75
66	MeO	91	3.26

[a] Yields of analytically pure products; products recrystallized from methanol.
[b] Determined by CS ChemOffice 2008.

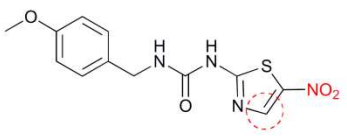

Figure 2. Potential toxic alerts: 1. Nitro group; 2. P450 associated-hepatotoxicity alert.

replaced by aminopyridines and aminobenzothiazoles. We found that an elongation in position R^3 and R^4 of structure **III** entailed reduced activity. However, an acceptor like NO_2 or CN is needed in position R^4 of structure **III** as long as no acceptor is allocated in position R^5. Our future research is focused on structure **V** and position R^5 of structure **III** from which we expect to obtain improved activity.

Table 5
GSK-3β inhibitory activity of selected compounds

Compd	Structure	GSK-3β activity in[a] (%)	
		1 μM of compd	10 μM of compd
62	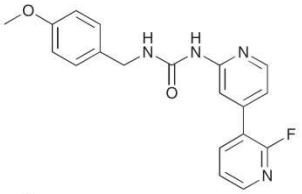	–	12
66	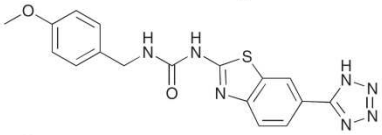	69	18
18	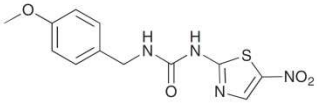	55	20

(*continued on next page*)

Table 5 (*continued*)

Compd	Structure	GSK-3β activity in[a] (%)	
		1 μM of compd	10 μM of compd
29	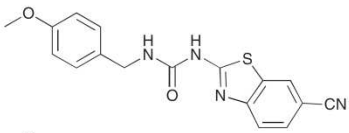	57	24
63	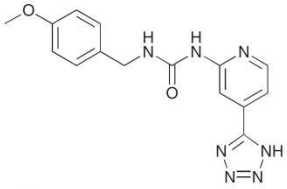	82	24
11	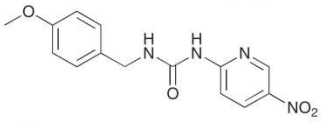	75	31
60	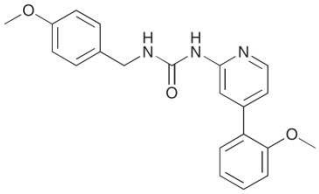	91	32
13	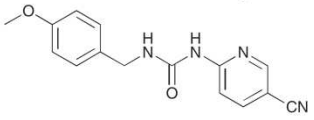	79	40
9	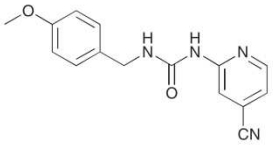	101	42

[a] Conditions for GSK-3β in vitro assay see Supplementary data.[10]

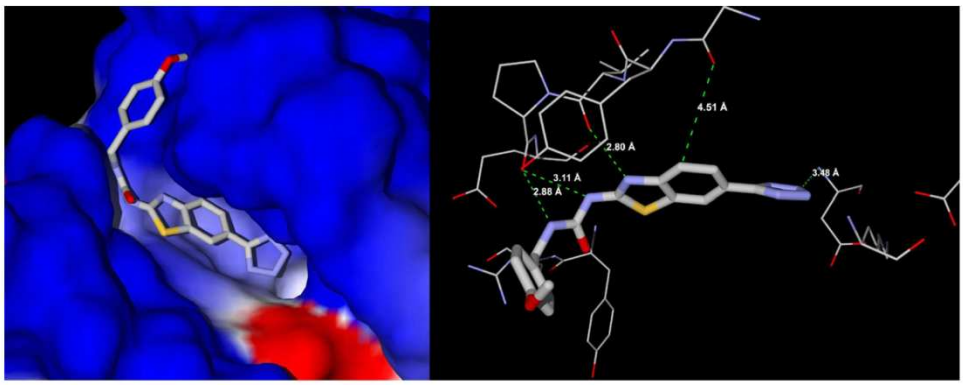

Figure 3. Docking of compound **66** into PDB structure 1Q5K of GSK-3β; Surface illustration of the ATP-binding pocket with **66** (left); Hydrogen bond interactions of **66** with the amino acids of the ATP-binding pocket (right).[4,14]

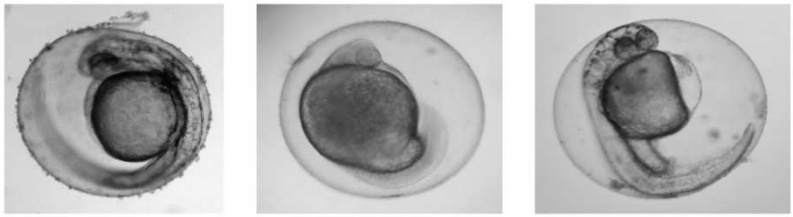

Figure 4. Exposure of zebrafish embryos to 1% DMSO (left), 100 mM **18** (AR-A14418, middle), and 100 mM **66** (right). The embryos were collected and maintained in E2 medium at 30 °C, compounds were added at 8–15 somites, and the phenotypes were compared after 25 h.

Table 6
GSK3 selectivity panel

Compound	IC_{50} values (mM)					
	GSK-3β	GSK-3α	Cdk5/p35	CKIε	AurKA	PKCα
18 (AR-A014418)	0.33	0.07	>100	>100	>100	>100
9	1.43	1.12	>100	>100	>100	>100
27	3.64	0.22	>100	>100	>100	>100
63	0.51	0.37	>100	>100	>100	>100
66	0.14	0.13	26.4	15.3	4.8	24.2

To evaluate the specificity of the family against GSK-3β, four of the synthesized compounds (**9**, **27**, **63** and **66**) were selected and tested against five human protein kinases (GSK-3α, PKCα, AurKA, Cdk5/p35 and CKIε) (Table 6).

Compound **66** with an IC_{50} of 140 nM for GSK3β was the only one able to inhibit all of the kinases tested (PKCα, AurKA, Cdk5/p35 and CKIε) but the IC_{50} values were one or two orders of magnitude above those found for the GSK-3 isoforms, indicating a fair degree of selectivity for this compound towards these latter enzymes. Such selectivity is even larger for the other three compounds tested, which were inactive (or poorly active) against the former kinases when tested up to 100 μM.

In order to demonstrate the utility and nontoxicity of the pyridine and benzothiazole moiety in whole organisms, we performed a zebrafish embryo phenotype assay.[15,16] We exposed the zebrafish embryos to the compounds **66**, **18** (AR-A014418) and **63** at early stages of development (8 till 15 somites, Fig. 4).

Controls after 18 h and 25 h showed that **18** (AR-A014418) is indeed toxic. This toxicity could be diminished by replacement of the thiazole with a benzothiazole (**66**) or pyridine (**63**) moiety (CHIR98014 is not toxic and compound **19** precipitates—data not shown). We observed some deformation in the fishtail at 100 μM (**66**, **63** and at 25 μM of CHIR98014—data not shown) and after eclosion we observed these fishes were swimming in circles only. This correlates with the observation that Wnt signaling, and thus GSK-3β, plays a crucial role in the development of metazoan and that known GSK-3 inhibitors like LiCl and the ruthenium complex (**R**)-**7** perturbe the zebrafish development.[15]

We have established a fast and atom efficient approach to generate kinase targeting urea derivatives. Hereby, it is feasible to diversify the scaffold in a time efficient manner. Thereby we expect to identify novel GSK-3 inhibitors displaying enhanced activity and selectivity. A preview of the biological activity and selectivity of the synthesized compounds is depicted in Tables 5 and 6. They are of comparable potency and selectivity to the reference compound **18** (AR-A014418). The aminothiazole used by AstraZeneca was replaced by other heterocycles. We have also shown that a selection of our compounds compared to **18** (AR-A014418) were less toxic in a zebrafish embryo phenotype assay, albeit some of these are not expected to be brain penetrant. This is subject of ongoing and future research in animal models of Alzheimer's disease.

Acknowledgment

This work was supported by a collaborative project financed by the 7th Framework Program of the European Union.

Supplementary data

Supplementary data associated with this article can be found, in the online version, at doi:10.1016/j.bmcl.2011.06.131.

References and notes

1. Hooper, C.; Killick, R.; Lovestone, S. *J. Neurochem.* **2008**, *104*, 1433.
2. Bhat, R. V.; Haeberlein, S. L. B.; Avila, J. *J. Neurochem.* **2004**, *89*, 1313.
3. Eldar-Finkelman, H. *Trends in Mol. Med.* **2002**, *8*, 126.
4. Bhat, R.; Xue, Y.; Berg, S.; Hellberg, S.; Ormö, M.; Nilsson, Y.; Radesäter, A.; Jerning, E.; Markgren, P.; Borgegard, T.; Nylöf, M.; Giménez-Cassina, A.; Hernández, F.; Lucas, J.; Díaz-Nido, J.; Avila, J. *J. Biol. Chem.* **2003**, *278*, 45937.
5. Hoettecke, N.; Liebeck, M.; Baumann, K.; Schubenel, R.; Winkler, E.; Steiner, H.; Schmidt, B. *Bioorg. Med. Chem. Lett.* **2010**, *20*, 2958.
6. Tsai, J. H.; Takaoka, L. R.; Powell, N. A.; Nowick, J. S. *Org. Synth.* **2002**, *78*, 220.
7. Wiley, R.; Beasley, P.; Knabeschuh, L. *J. Am. Chem. Soc.* **1954**, *76*, 311.
8. Shelton, P.; Zhang, Y.; Nguyen, T.; McElwee-White, L. *Chem. Commun.* **2009**, 947.
9. Miyauro, N.; Suzuki, A. *Chem. Rev.* **1995**, *95*, 2457.
10. Kotha, S.; Lahiri, K.; Kashinath, D. *Tetrahedron* **2002**, *48*, 9633.
11. Schmidt, B.; Meid, D.; Kieser, D. *Tetrahedron* **2007**, *63*, 492.
12. (a) Prudent Practice for Handling Hazardous Chemicals in Laboratories, National Academic: Washington, DC, 1983, 87.; (b) Bräse, S.; Gil, C.; Knepper, K.; Zimmermann, V. *Angew. Chem.* **2005**, *117*, 5320.
13. Liberman, Z.; Eldar-Finkelman, H. *J. Biol.Chem.* **2005**, *280*, 4422.
14. Molegro Virtual Docker, Version 4.2.0 (October 4th, 2010).
15. Atilla-Gokcumen, G. E.; Williams, D. S.; Bregman, H.; Pagano, N.; Meggers, E. *ChemBioChem* **2006**, *7*, 1443.
16. Paquet, D.; Bath, R.; Sydow, A.; Mandelkow, E.; Berg, S.; Hellberg, S.; Fälting, J.; Distel, M.; Köster, R.; Schmid, B.; Haass, C. *J. Clin. Invest.* **2009**, *119*, 1382.

Supporting Information

Synthesis and biological evaluation of glycogen synthase kinase 3 (GSK-3) inhibitors: an fast and atom efficient access to 1-aryl-3-benzylureas

Fabio Lo Monte*[a], Thomas Kramer*[a], Alexander Boländer[a], Batya Plotkin[b], Hagit Eldar-Finkelman[b], Ana Fuertes[c], Juan M. Dominguez[c] and Boris Schmidt†[a]

[a] Clemens Schöpf - Institute of Organic Chemistry and Biochemistry, Technische Universität Darmstadt, 64287 Darmstadt, Hessen, Germany, Fax: +496151-163278; Tel: +496151-164531;
[b] Department of Human Molecular Genetics and Biochemistry, Sackler School of Medicine, Tel Aviv University, Tel Aviv 69978, Israel,
[c] Noscira S. A. Tres Cantos 28760, Madrid, Spain
† E-mail: schmidt_boris@t-online.de
*These authors contributed equally to this work.

Content:

General procedure

1.) Synthesis of the urea derivatives

The amine (0.80 mmol) was added to a stirred mixture of 5 ml saturated sodium bicarbonate solution ($NaHCO_3$) and 5 ml dichloromethane (DCM) at 0 °C. Afterwards triphosgene (0.28 mmol) was added slowly. After 2.5 h at 0 °C 10 ml of DCM were added and the organic layer separated from the aqueous phase. The aqueous phase was washed twice with 10 ml of DCM. The combined organic layers were washed with ammonium chloride (NH_4Cl) and brine and later dried over sodium sulfate, filtered and concentrated to approximately 0.5 ml. To the residue was added dry tetrahydrofuran (THF, 1.5 ml). It was added dropwise to a solution of n-buthyllithium (0.80 mmol, 1.6 M in n-hexane) deprotonated amine (0.80 mmol) in 1.5 ml tetrahydrofuran and stirred at room temperature overnight. The reaction solution was added to a vigorous stirred water to give the solid crude urea. The solid was filtered off and recrystallised from methanol or ethanol.

2.) Suzuki coupling

An urea derivative with a bromo substituent (0.15 mmol), boronic acid (0.19 mmol), sodium ethoxide (0.31 mmol) and 1 mol-% of palladium acetate or 1 mol-% of tetrakis(triphenylphosphine)palladium(0) were suspended in 1 ml dry ethanol and stirred for 0.5 - 3 h at 110 °C. Afterwards the solution was filtered and the solvent evaporated. The residue was added to water and extracted three times with ethyl acetate. The combined organic layers were dried over sodium sulfate, filtered and the solvent was evaporated. The solid was recrystallised from ethanol or methanol.

3.) Microwave synthesis

Entry **9**, 1**2**, **13** or **29** (0.10 mmol), sodium azide (NaN_3, 1.20 mmol) and ammonium chloride (NH_4Cl, 1.20 mmol) were added to 1 ml of *N*,*N*-dimethylformamide (DMF) and stirred for 2 h at 100 °C under microwave irradiation. After cooling to room temperature the reaction solution was added to water, acidified with 2 N HCl and extracted three times with ethyl acetate. The combined organic layers were dried over sodium sulfate, filtered and the solvent evaporated off to provide the product.

Chemical Data

The ^{1}H-NMR spectra were recorded on a Bruker AC 300 spectrometer at 300 MHz and Bruker AC 500 spectrometer at 500 MHz. The ^{13}C-NMR spectra were recorded on a Bruker AC 300 spectrometer at 75 MHz and Bruker AC 500 spectrometer at 125 MHz. Chemical shifts are reported as ppm downfield from Me_4Si. Mass spectrometry was performed on a Bruker-Franzen Esquire LC mass spectrometer and a MAT 95 double focussing sector field MS. Microwave experiments were carried out using a Biotage® Initiator™ microwave apparatus. All microwave experiments were carried out in sealed microwave process vials utilizing the standard absorbance level (300 W maximum power). High performance liquid chromatographies were carried out on an Agilent 1100 (column: reversed phase, Zorbax Eclipse XDB-C8, 4.6 x 150 mm; 254 nm). Melting points were recorded on a SMP 10 Bibby Stuart Scientific apparatus.

1-(4-fluorobenzyl)-3-(5-iodopyridin-2-yl)urea (1)

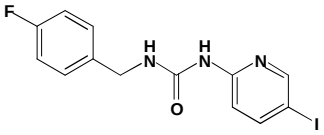

^{1}H-NMR (DMSO-d_6, 500 MHz): δ [ppm] = 4.35 (2H, d, J = 6.0 Hz), 6.91 (2H, m), 7.17 (1H, d, J = 8.8 Hz), 7.28 (2H, m), 7.85 (1H, dd, J = 8.8, J = 2.4); 8.24 (1H, dd, J = 2.2 Hz, J = 0.6 Hz), 8.48 (1H, s), 8.64 (1H, s)
^{13}C-NMR (DMSO-d_6, 125 MHz): δ [ppm] = 43.7, 82.3, 115.4, 116.1, 116.3, 130.5, 130.6, 137.5, 137.6, 147.3, 153.7, 154.3, 156.0, 162.2, 164.1
EI-MS: m/z 371 (M^+)
Melting Point: 169-171 °C
HPLC-Retention Time: 6.7 min

1-(6-bromopyridin-2-yl)-3-(4-fluorobenzyl)urea (2)

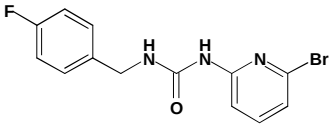

^{1}H-NMR (DMSO-d_6, 500 MHz): δ [ppm] = 4.34 (2H, d, J = 5.9 Hz), 7.16 (3H, m), 7.35 (2H, m), 7.40 (1H, m), 7.62 (1H, m), 7.70 (1H, d, J = 8.2 Hz), 9.56 (1H, s)
^{13}C-NMR (DMSO-d_6, 125 MHz): δ [ppm] = 42.2, 110.8, 115.4, 115.5, 120.8, 129.4, 136.2, 138.5, 141.4, 153.8, 154.5
EI-MS: m/z 323 (M^+)
Melting Point: 170 °C
HPLC-Retention Time: 6.7 min

1-(6-bromopyridin-2-yl)-3-(4-methoxybenzyl)urea (3)

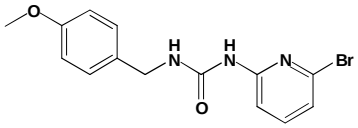

^{1}H-NMR (DMSO-d_6, 500 MHz): δ [ppm] = 3.39 (3H, s), 4.34 (2H, d, J = 5.8 Hz), 6.96 (2H, d, J = 8.6 Hz), 7.20 (1H, dd, J = 7.6 Hz, J = 0.6 Hz), 7.29 (2H, d, J = 8.7 Hz), 7.38 (1H, t, J = 5.7 Hz), 7.68 (1H, m), 7.76 (1H, dd, J = 8.2 Hz, J = 0.5 Hz), 9.51 (1H, s)
^{13}C-NMR (DMSO-d_6, 125 MHz): δ [ppm] = 43.6, 56.5, 111.7, 115.3, 121.7, 129.9, 132.9, 139.6, 142.5, 155.0, 155.5, 159.7
EI-MS: m/z 335 (M^+)
Melting Point: 158 °C
HPLC-Retention Time: 6.2 min

1-(5-bromopyridin-2-yl)-3-(4-fluorobenzyl)urea (4)

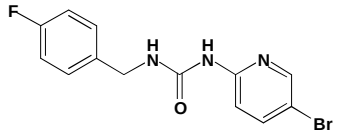

^{1}H-NMR (DMSO-d_6, 500 MHz): δ [ppm] = 4.42 (2H, d, J = 5.8 Hz), 7.22 (2H, m), 7.40 (2H, d, J = 8.6 Hz), 7.59 (1H, d, J = 8.9 Hz), 7.95 (1H, dd, J = 8.9 Hz, J = 2.5 Hz), 8.05 (1H, s), 8.35 (1H, d, J = 2.5 Hz), 9.44 (1H, s)
^{13}C-NMR (DMSO-d_6, 125 MHz): δ [ppm] = 42.2, 111.0, 113.8, 115.4, 129.5, 136.3, 140.9, 147.7, 152.2, 154.4, 154.8
EI-MS: m/z 323 (M^+)
Melting Point: 178-180 °C
HPLC-Retention Time: 6.6 min

1-(5-bromopyridin-2-yl)-3-(4-methoxybenzyl)urea (5)

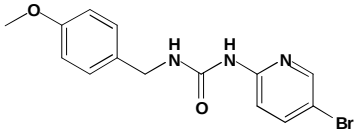

^{1}H-NMR (DMSO-d_6, 500 MHz): δ [ppm] = 3.37 (3H, s), 4.43 (2H, d, J = 5.8 Hz), 6.90 (2H, d, J = 8.6 Hz), 7.22 (2H, d, J = 8.6 Hz), 7.54 (1H, d, J = 8.9 Hz), 7.88 (1H, dd, J = 8.9 Hz, J = 2.5 Hz), 7.91 (1H, s), 8.27 (1H, d, J = 2.2 Hz), 9.32 (1H, s)
^{13}C-NMR (DMSO-d_6, 125 MHz): δ [ppm] = 42.2, 55.5, 111.2, 113.7, 114.1, 128.8, 132.0, 140.8, 147.8, 152.5, 154.7, 158.6
EI-MS: m/z 335 (M^+)
Melting Point: 148-150 °C
HPLC-Retention Time: 6.7 min

1-(4-bromopyridin-2-yl)-3-(4-methoxybenzyl)urea (6)

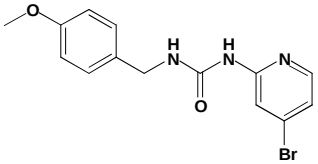

^{1}H-NMR (DMSO-d_6, 500 MHz): δ [ppm] = 3.74 (3H, s), 4.30 (2H, d, J = 5.8 Hz), 6.90 (2H, d, J = 8.6 Hz), 7.17 (1H, dd, J = 5.4 Hz, J = 1.8 Hz), 7.23 (2H, d, J = 8.6 Hz), 7.79 (1H, d, J = 1.6 Hz), 8.00 (1H, s), 8.07 (1H, d, J = 5.5 Hz), 9.36 (1H, s)
^{13}C-NMR (DMSO-d_6, 125 MHz): δ [ppm] = 42.0, 54.8, 113.6, 113.7, 119.6, 128.3, 131.4, 132.8, 148.3, 154.1, 154.2, 158.1
EI-MS: m/z 335 (M^+)
Melting Point: 176 °C
HPLC-Retention Time: 5.3 min

1-(4-chloropyridin-2-yl)-3-(4-fluorobenzyl)urea (7)

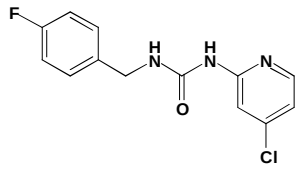

^{1}H-NMR (DMSO-d_6, 500 MHz): δ [ppm] = 4.36 (2H, d, J = 6.0 Hz), 7.05 (1H, dd, J = 5.5 Hz, J = 1.9 Hz), 7.15 (2H, m), 7.35 (2H, m), 7.62 (1H, d, J = 1.8 Hz), 8.11 (1H, s), 8.16 (1H, d, J = 5.7 Hz), 9.44 (1H, s)
^{13}C-NMR (DMSO-d_6, 125 MHz): δ [ppm] = 42.3, 111.2, 115.4, 117.4, 129.4, 136.4, 144.2, 149.0, 154.9, 160.5, 162.5
EI-MS: m/z 279 (M^+)
Melting Point: 195-197 °C
HPLC-Retention Time: 5.2 min

1-(4-chloropyridin-2-yl)-3-(4-methoxybenzyl)urea (8)

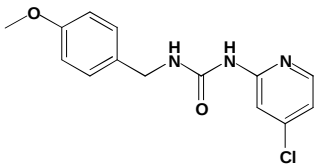

^{1}H-NMR (DMSO-d_6, 500 MHz): δ [ppm] = 3.97 (3H, s), 4.54 (2H, d, J = 5.9 Hz), 7.12 (2H, d, J = 8.7 Hz), 7.29 (1H, dd, J = 5.5 Hz, J = 1.9 Hz), 7.47 (2H, d, J = 8.7 Hz), 7.87 (1H, d, J = 1.8 Hz), 8.23 (1H, s), 8.40 (1H, d, J = 5.7 Hz), 9.62 (1H, s)
^{13}C-NMR (DMSO-d_6, 125 MHz): δ [ppm] = 40.7, 53.6, 109.2, 112.3, 115.6, 127.0, 130.1, 142.3, 147.2, 152.9, 153.0, 156.8
EI-MS: m/z 291 (M^+)
Melting Point: 186-188 °C
HPLC-Retention Time: 4.9 min

1-(4-cyanopyridin-2-yl)-3-(4-methoxybenzyl)urea (9)

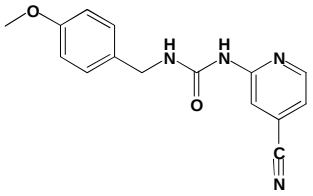

^{1}H-NMR (DMSO-d_6, 500 MHz): δ [ppm] = 3.72 (3H, s), 4.29 (2H, d, J = 5.8 Hz), 6.89 (2H, m), 7.23 (2H, m), 7.34 (1H, dd, J = 1.3 Hz, J = 5.1 Hz), 7.73 (1H, t, J = 5.6 Hz), 7.94 (1H, s), 8.41 (1H, dd, J = 0.6 Hz, J = 5.1 Hz), 9.55 (1H, s)
^{13}C-NMR (DMSO-d_6, 125 MHz): δ [ppm] = 42.1, 55.0, 113.4, 113.8, 116.9, 118.0, 120.7, 128.5, 131.4, 149.0, 153.7, 154.2, 158.3
EI-MS: m/z 282 (M^+)
HRMS: calcd. for $C_{15}H_{14}N_4O_2$ 282.1117, found 282.1099.
HPLC-Retention Time: 6.06 min

1-(4-fluorobenzyl)-3-(5-nitropyridin-2-yl)urea (10)

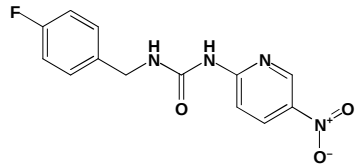

^{1}H-NMR (DMSO-d_6, 500 MHz): δ [ppm] = 4.38 (2H, m), 6.96 (2H, m), 7.30 (2H, m), 7.56 (1H, d, J = 8.0 Hz), 8.35 (2H, m), 8.90 (1H, s), 9.24 (1H, s)
^{13}C-NMR (DMSO-d_6, 125 MHz): δ [ppm] = 43.9, 112.6, 116.2, 116.4, 130.6, 134.8, 137.1, 140.3, 145.5, 155.2, 158.8
EI-MS: m/z 291 (M^+)
Melting Point: 207-209 °C
HPLC-Retention Time: 6.3 min

1-(4-methoxybenzyl)-3-(5-nitropyridin-2-yl)urea (11)

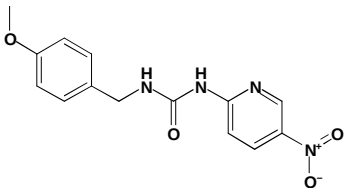

^{1}H-NMR (DMSO-d_6, 500 MHz): δ [ppm] = 3.64 (3H, s), 4.32 (2H, d, J = 5.6 Hz), 6.76 (2H, d, J = 8.4 Hz), 7.18 (2H, d, J = 8.3 Hz), 7.59 (1H, d, J = 9.2 Hz), 8.19 (1H, s), 8.34 (1H, dd, J = 9.2 Hz, J = 2.4 Hz), 8.90 (1H, d, J = 2.2 Hz), 9.15 (1H, s)
^{13}C-NMR (DMSO-d_6, 125 MHz): δ [ppm] = 44.1, 55.9, 112.5, 115.1, 130.0, 132.8, 134.7, 140.2, 145.5, 155.1, 158.9, 160.3
EI-MS: m/z 302 (M^+)
HRMS: calcd. for $C_{14}H_{14}N_4O_4$ 302.1015, found 302.0972.
Melting Point: 189-191 °C
HPLC-Retention Time: 6.1 min

1-(4-fluorobenzyl)-3-(5-cyanopyridin-2-yl)urea (12)

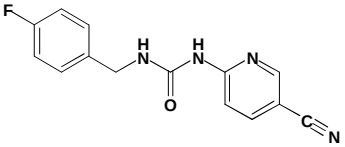

^{1}H-NMR (DMSO-d_6, 500 MHz): δ [ppm] = 4.43 (2H, d, J = 5.6 Hz), 7.21 (2H, m), 7.41 (2H, m), 7.75 (1H, d, J = 8.8 Hz), 8.11 (1H, m), 8.16 (1H, dd, J = 8.8 Hz, J = 2.2 Hz), 8.69 (1H, m), 9.84 (1H, m)
^{13}C-NMR (DMSO-d_6, 125 MHz): δ [ppm] = 42.4, 101.3, 111.7, 114.2, 115.4, 115.6, 117.9, 128.7, 129.4, 129.5, 136.1, 136.1, 141.6, 152.1, 154.4, 156.0, 160.6, 162.5
EI-MS: m/z 270 (M^+)
HRMS: calcd. for $C_{14}H_{11}N_4OF$ 270.0918, found 270.0897.
Melting Point: 221-222 °C
HPLC-Retention Time: 5.7 min

1-(4-methoxybenzyl)-3-(5-cyanopyridin-2-yl)urea (13)

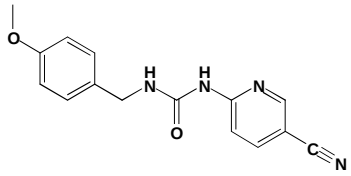

^{1}H-NMR (DMSO-d_6, 500 MHz): δ [ppm] = 3.79 (3H, s), 4.37 (2H, d, J = 5.0 Hz), 6.96 (2H, d, J = 8.7 Hz), 7.29 (2H, d, J = 8.7 Hz), 7.76 (1H, d, J = 8.9 Hz), 8.00 (1H, s), 8.15 (1H, dd, J = 8.8 Hz, J = 2.3 Hz), 8.69 (1H, dd, J = 2.2 Hz, J = 0.6 Hz), 9.79 (1H, s)
^{13}C-NMR (DMSO-d_6, 125 MHz): δ [ppm] = 42.0, 54.8, 100.7, 111.1, 113.6, 117.3, 128.3, 131.1, 141.0, 151.6, 153.7, 155.5, 158.1
EI-MS: m/z 282 (M^+)
HRMS: calcd. for $C_{15}H_{14}N_4O_2$ 282.1117, found 282.1104.
Melting Point: 198-201 °C
HPLC-Retention Time: 5.7 min

1-(4-bromobenzyl)-3-(5-cyanopyridin-2-yl)urea (14)

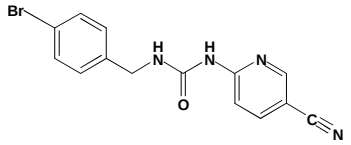

^{1}H-NMR (DMSO-d_6, 500 MHz): δ [ppm] = 4.43 (2H, d, J = 6.0 Hz), 7.34 (2H, d, J = 8.4 Hz), 7.60 (2H, d, J = 8.4 Hz), 7.75 (1H, d, J = 8.9 Hz), 8.15 (1H, d, J = 5.7 Hz), 8.18 (1H, dd, J = 8.8 Hz, J = 2.3 Hz), 8.72 (1H, d, J = 2.2 Hz), 9.89 (1H, s)
^{13}C-NMR (DMSO-d_6, 125 MHz): δ [ppm] = 42.4, 101.2, 111.6, 117.7, 120.1, 129.4, 129.6, 131.3, 131.5, 139.4, 141.5, 152.0, 154.3, 155.9
EI-MS: m/z 331 (M^+)
Melting Point: 224-226 °C
HPLC-Retention Time: 6.5 min

1-(5-cyanopyridin-2-yl)-3-(4-(trifluoromethyl)benzyl)urea (15)

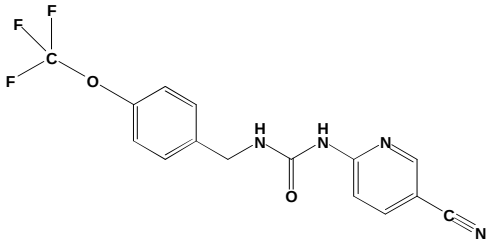

^{1}H-NMR (DMSO-d_6, 500 MHz): δ [ppm] = 4.48 (2H, d, J = 6.0 Hz), 7.39 (2H, d, J = 8.6 Hz), 7.49 (2H, d, J = 8.6 Hz), 7.75 (1H, d, J = 8.9 Hz), 8.17 (1H, dd, J = 8.8 Hz, J = 2.3 Hz), 8.18 (1H, s), 8.71 (1H, dd, J = 2.3 Hz, J = 0.6 Hz), 9.88 (1H, s)
^{13}C-NMR (DMSO-d_6, 125 MHz): δ [ppm] = 42.4, 101.4, 117.9, 121.4, 129.3, 139.6, 141.6, 147.6, 152.2, 154.4, 156.1
EI-MS: m/z 336 (M^+)
Melting Point: 204 °C
HPLC-Retention Time: 6.7 min

1-(benzo[d][1,3]dioxol-5-ylmethyl)-3-(5-cyanopyridin-2-yl)urea (16)

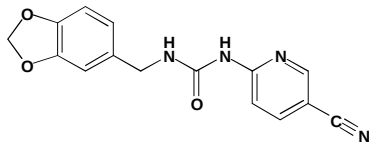

^{1}H-NMR (DMSO-d_6, 500 MHz): δ [ppm] = 4.29 (2H, d, J = 5.9 Hz), 5.99 (2H, s), 6.79 (1H, dd, J = 7.97 Hz, J = 1.6 Hz), 6.86 (1H, d, J = 7.9 Hz), 6.88 (1H, d, J = 1.6 Hz), 7.70 (1H, d, J = 8.9 Hz), 7.96 (1H, t, J = 5.6 Hz), 8.10 (1H, dd, J = 8.8 Hz, J = 2.3 Hz), 8.64 (1H, dd, J = 2.3 Hz, J = 0.6 Hz), 9.74 (1H, s)
^{13}C-NMR (DMSO-d_6, 125 MHz): δ [ppm] = 42.9, 101.2, 101.3, 108.2, 108.5, 111.7, 117.9, 120.7, 133.7, 141.6, 146.5, 147.7, 152.2, 154.3, 156.1
EI-MS: m/z 296 (M^+)
Melting Point: 218 °C
HPLC-Retention Time: 5.6 min

1-(4-fluorobenzyl)-3-(5-nitrothiazol-2-yl)urea (17)

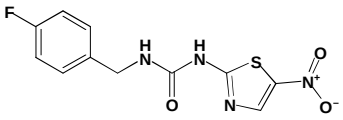

^{1}H-NMR (DMSO-d_6, 500 MHz): δ [ppm] = 4.28 (2H, d, J = 6 Hz), 7.1 (2H, d, J = 8.9 Hz), 7.29 (1H, s), 7.30 (2H, d, J = 8.7 Hz), 8.44 (1H, s), 11.64 (1H, s)
^{13}C-NMR (DMSO-d_6, 125 MHz): δ [ppm] = 42.8, 115.3, 115.5, 129.6, 129.7, 135.5, 143.7, 164.6
EI-MS: m/z 296 (M^+)
Melting Point: 168-170 °C
HPLC-Retention Time: 6.1 min

1-(4-methoxybenzyl)-3-(5-nitrothiazol-2-yl)urea (18)

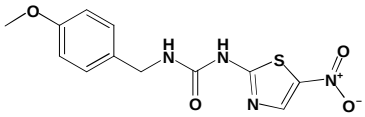

^{1}H-NMR (DMSO-d_6, 500 MHz): δ [ppm] = 3.79 (3H, s), 4.36 (2H, d, J = 5.9 Hz), 6.96 (2H, d, J = 8.7 Hz), 7.29 (1H, s), 7.30 (2H, d, J = 8.7 Hz), 8.56 (1H, s), 11.67 (1H, s)
^{13}C-NMR (DMSO-d_6, 125 MHz): δ [ppm] = 40.7, 53.1, 111.8, 126.7, 128.7, 141.5, 156.5, 162.8
EI-MS: m/z 308 (M^+)
Melting Point: 211-213 °C
HPLC-Retention Time: 6.2 min

Ethyl-2-(3-(4-fluorobenzyl)ureido)-4-methylthiazole-5-carboxylate (19)

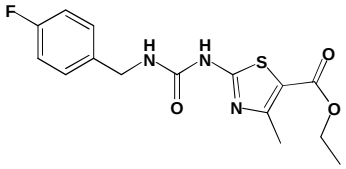

^{1}H-NMR (DMSO-d_6, 500 MHz): δ [ppm] = 1.26 (3H, t, J = 7.1 Hz), 2.48 (3H, s), 4.21 (2H, q, J = 7.1 Hz), 4.33 (2H, d, J = 5.9 Hz), 7.14 (1H, s), 7.17 (2H, d, J = 8.9 Hz), 7.35 (2H, d, J = 8.6 Hz), 10.94 (1H, s)
^{13}C-NMR (DMSO-d_6, 125 MHz): δ [ppm] = 12.7, 15.3, 40.8, 58.7, 111.3, 113.6, 127.8, 134.0, 152.1, 154.9, 158.8, 160.2, 160.7
EI-MS: m/z 337 (M^+)
Melting Point: 293-295 °C
HPLC-Retention Time: 6.4 min

Ethyl-2-(3-(4-methoxybenzyl)ureido)-4-methylthiazole-5-carboxylate (20)

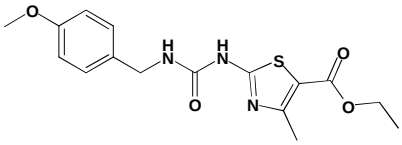

^{1}H-NMR (DMSO-d_6, 500 MHz): δ [ppm] = 1.27 (3H, t, J = 7.1 Hz), 2.48 (3H, s), 3.74 (3H, s), 4.21 (2H, q, J = 7.1 Hz), 4.26 (2H, d, J = 5.8 Hz), 6.90 (2H, d, J = 8.6 Hz), 7.02 (1H, s), 7.23 (2H, d, J = 8.6 Hz), 10.83 (1H, s)
^{13}C-NMR (DMSO-d_6, 125 MHz): δ [ppm] = 14.6, 17.4, 42.8, 55.4, 60.5, 113.1, 114.2, 129.1, 131.5, 153.9, 156.8, 158.8, 162.1, 162.6
EI-MS: m/z 349 (M^+)
Melting Point: 243-247 °C
HPLC-Retention Time: 6.3 min

1-(4-fluorobenzyl)-3-(4-p-tolylthiazol-2-yl)urea (21)

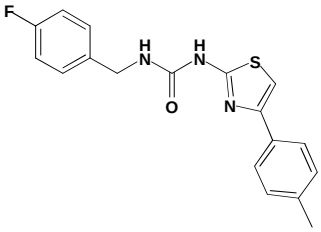

^{1}H-NMR (DMSO-d_6, 500 MHz): δ [ppm] = 2.36 (3H, s), 4.38 (2H, d, J = 6.0 Hz), 7.07 (1H, t, J = 5.7 Hz), 7.21 (1H, m), 7.24 (2H, d, J = 7.9 Hz), 7.40 (3H, m), 7.78 (2H, d, J = 8.1 Hz), 10.73 (1H, s)
^{13}C-NMR (DMSO-d_6, 125 MHz): δ [ppm] = 21.2, 42.6, 106.1, 115.4, 125.8, 129.5, 132.1, 136.2, 137.2, 149.0, 154.4, 160.1, 160.6, 162.6
EI-MS: m/z 341 (M^+)
Melting Point: 179-180 °C
HPLC-Retention Time: 7.5 min

1-(4-methoxybenzyl)-3-(4-p-tolylthiazol-2-yl)urea (22)

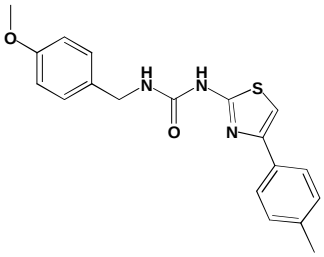

^{1}H-NMR (DMSO-d_6, 500 MHz): δ [ppm] = 2.31 (3H, s), 3.74 (3H, s), 4.28 (2H, d, J = 5.9 Hz), 6.91 (2H, d, J = 8.7 Hz), 6.94 (1H, m), 7.20 (2H, d, J = 8.0 Hz), 7.25 (2H, d, J = 8.7 Hz), 7.36 (1H, s), 7.74 (2H, d, J = 8.1 Hz), 10.60 (1H, s)
^{13}C-NMR (DMSO-d_6, 125 MHz): δ [ppm] = 21.1, 42.7, 55.4, 106.0, 114.2, 125.8, 129.0, 129.6, 131.8, 132.2, 137.2, 149.0, 154.3, 158.7, 160.1
EI-MS: m/z 353 (M^+)
Melting Point: 163 °C
HPLC-Retention Time: 7.4 min

1-(6-bromobenzo[d]thiazol-2-yl)-3-(4-fluorobenzyl)urea (23)

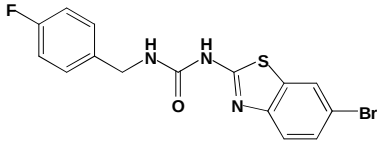

^{1}H-NMR (DMSO-d_6, 500 MHz): δ [ppm] = 4.41 (2H, d, J = 5.8 Hz), 7.22 (2H, d, J = 8.8 Hz), 7.29 (1H, s), 7.42 (2H, d, J = 8.2 Hz), 7.54 (1H, dd, J = 8.5 Hz, J = 1.7 Hz), 7.60 (1H, d, J = 8.5 Hz), 8.16 (1H, d, J = 1.0 Hz), 10.97 (1H, s)
^{13}C-NMR (DMSO-d_6, 125 MHz): δ [ppm] = 42.7, 114.7, 115.5, 121.6, 124.2, 129.1, 129.7, 134.1, 135.9, 154.2, 160.7, 160.9, 162.6
EI-MS: m/z 380 (M^+)
Melting Point: 203-205 °C
HPLC-Retention Time: 7.4 min

1-(6-fluorobenzo[d]thiazol-2-yl)-3-(4-methoxybenzyl)-urea (24)

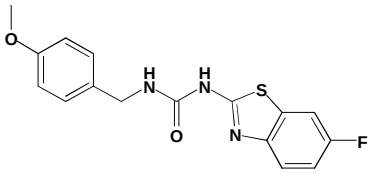

^{1}H-NMR (DMSO-d_6, 500 MHz): δ [ppm] = 3.74 (3H, s), 4.31 (2H, d, J = 5.8 Hz), 6.91 (2H, d, J = 8.6 Hz), 7.12 (1H, s), 7.20 (1H, m), 7.27 (2H, d, J = 8.6 Hz), 7.61 (1H, m), 7.79 (1H, m)
^{13}C-NMR (DMSO-d_6, 125 MHz): δ [ppm] = 42.8, 55.4, 108.2, 113.9, 114.2, 121.0, 129.0, 131.5, 133.0, 154.1, 157.6, 158.7, 159.5, 160.1
EI-MS: m/z 331 (M^+)
Melting Point: 296-299 °C
HPLC-Retention Time: 6.6 min

1-(4-fluorobenzyl)-3-(6-trifluormethyl)benzo[d]thiazol-2-yl)urea (25)

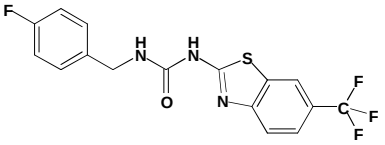

^{1}H-NMR (DMSO-d_6, 500 MHz): δ [ppm] = 4.41 (2H, d, J = 5.9 Hz), 7.22 (2H, d, J = 8.9 Hz), 7.34 (1H, s), 7.42 (2H, d, J = 8.6 Hz), 7.71 (1H, dd, J = 8.5 Hz, J = 1.6 Hz), 7.82 (1H, d, J = 8.4 Hz), 8.43 (1H, s), 11.16 (1H, s)
^{13}C-NMR (DMSO-d_6, 125 MHz): δ [ppm] = 42.7, 115.5, 119.8, 120.3, 123.0, 124.0, 126.1, 129.7, 132.5, 135.8, 154.2, 160.7, 162.6, 163.3
EI-MS: m/z 369 (M^+)
Melting Point: 188-190 °C
HPLC-Retention Time: 7.4 min

1-(4-methoxybenzyl)-3-(6-trifluormethyl)benzo[d]thiazol-2-yl)urea (26)

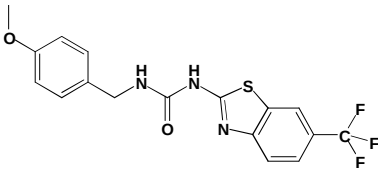

^{1}H-NMR (DMSO-d_6, 500 MHz): δ [ppm] = 3.74 (3H, s), 4.32 (2H, d, J = 5.8 Hz), 6.92 (2H, d, J = 8.6 Hz), 7.18 (1H, s), 7.26 (2H, d, J = 8.6 Hz), 7.66 (1H, dd, J = 8.5 Hz, J = 1.6 Hz), 7.76 (1H, d, J = 8.4 Hz), 8.36 (1H, s), 11.01 (1H, s)
^{13}C-NMR (DMSO-d_6, 125 MHz): δ [ppm] = 43.0, 55.4, 114.3, 119.8, 120.3, 123.0, 123.3, 124.0, 126.1, 129.1, 131.4, 152.4, 154.0, 158.8, 163.3
EI-MS: m/z 381 (M^+)
Melting Point: 225-227 °C
HPLC-Retention Time: 7.3 min

1-(4-methoxybenzyl)-3-(6-nitrobenzo[d]thiazol-2-yl)urea (27)

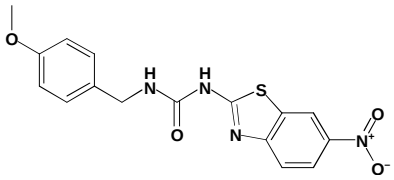

^{1}H-NMR (DMSO-d_6, 500 MHz): δ [ppm] = 3.74 (3H, s), 4.32 (2H, d, J = 5.8 Hz), 6.92 (2H, d, J = 8.6 Hz), 7.23 (1H, s), 7.26 (2H, d, J = 8.6 Hz), 7.75 (1H, d, J = 8.9 Hz), 8.21 (1H, dd, J = 8.9 Hz, J = 2.4 Hz), 8.94 (1H, d, J = 2.3 Hz), 11.23 (1H, s)
^{13}C-NMR (DMSO-d_6, 125 MHz): δ [ppm] = 42.9, 55.4, 114.4, 118.7, 119.8, 122.0, 129.1, 131.3, 132.6, 142.7, 155.8, 155.9, 158.7, 165.7
EI-MS: m/z 358 (M^+)
HRMS: calcd. for $C_{16}H_{14}N_4O_4S$ 358.0736, found 358.0717.
Melting Point: 270 °C
HPLC-Retention Time: 6.8 min

1-(3,4-difluorobenzyl)-3-(6-nitrobenzo[d]thiazol-2-yl)urea (28)

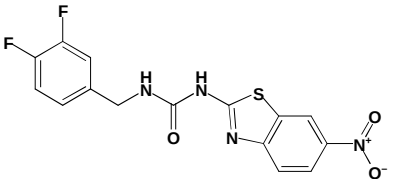

^{1}H-NMR (DMSO-d_6, 500 MHz): δ [ppm] = 4.37 (2H, d, J = 5.9 Hz), 7.18 (1H, m), 7.4 (3H, m), 7.76 (1H, d, J = 8.9 Hz), 8.22 (1H, dd, J = 8.9 Hz, J = 2.5 Hz), 8.94 (1H, d, J = 2.3 Hz), 11.42 (1H, s)
^{13}C-NMR (DMSO-d_6, 125 MHz): δ [ppm] = 43.9, 118.0, 119.2, 120.3, 121.3, 123.4, 125.7, 134.0, 138.9, 144.1, 149.2, 150.1, 151.2, 152.0, 167.1
EI-MS: m/z 364 (M^+)
Melting Point: 210-212 °C
HPLC-Retention Time: 7.1 min

1-(6-cyanobenzo[d]thiazol-2-yl)-3-(4-methoxybenzyl)urea (29)

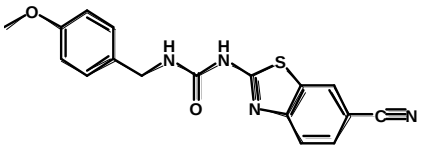

^{1}H-NMR (DMSO-d_6, 300 MHz): δ [ppm] = 3.73 (3H, s), 4.31 (2H, d, J = 5.8 Hz), 6.90 (2H, m), 7.25 (3H, m), 7.75 (2H, d, J = 1.1 Hz), 8.45 (1H, m), 11.34 (1H, s)
^{13}C-NMR (DMSO-d_6, 75 MHz): δ [ppm] = 42.4, 55.0, 104.2, 113.7, 119.3, 120.1, 120.1, 126.3, 128.6, 129.4, 130.9, 132.2, 152.3, 153.6, 158.3, 163.6
EI-MS: m/z 338 (M^+)
HRMS: calcd. for $C_{17}H_{14}N_4O_2S$ 338.0838, found 338.0840.
HPLC-Retention Time: 6.59 min
The precursor of compound **29** (2-aminobenzo[d]thiazole-6-carbonitrile) was synthesized according to following literature: Structural Chemistry, 2003, 14, 6, 587-595.

1,3-bis(4-fluorobenzyl)urea (30)

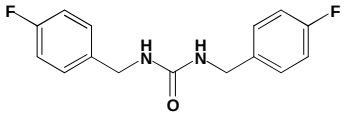

^{1}H-NMR (DMSO-d_6, 500 MHz): δ [ppm] = 4.26 (4H, d, J = 6.0 Hz), 6.51 (2H, t, J = 6.0 Hz), 7.18 (4H, d, J = 8.9 Hz), 7.33 (4H, d, J = 8.7 Hz)
^{13}C-NMR (DMSO-d_6, 125 MHz): δ [ppm] = 42.6, 115.1, 115.3, 129.2, 129.3, 137.4, 137.5, 158.4, 160.4, 162.4
EI-MS: m/z 276 (M^+)
Melting Point: 218-220 °C
HPLC-Retention Time: 5.9 min

1,3-bis(4-methoxybenzyl)urea (31)

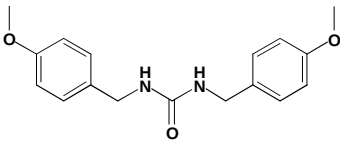

^{1}H-NMR (DMSO-d_6, 500 MHz): δ [ppm] = 3.78 (6H, s), 4.20 (4H, d, J = 6.0 Hz), 6.33 (2H, t, J = 5.9 Hz), 6.92 (4H, d, J = 8.7 Hz), 7.22 (4H, d, J = 8.7 Hz)
^{13}C-NMR (DMSO-d_6, 125 MHz): δ [ppm] = 42.8, 55.4, 114.0, 128.7, 133.1, 158.3, 158.4
EI-MS: m/z 300 (M^+)
Melting Point: 178-180 °C
HPLC-Retention Time: 5.5 min

1-(4-fluorobenzyl)-3-(6-phenylpyridin-2-yl)urea (32)

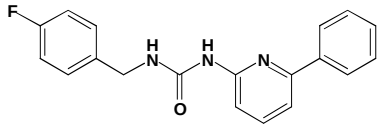

^{1}H-NMR (DMSO-d_6, 300 MHz): δ [ppm] = 4.41 (2H, d, J = 5.5 Hz), 7.18 (2H, m), 7.29 (1H, d, J = 8.1 Hz), 7.40 (5H, m), 7.46 (1H, dd, J = 7.6 Hz, J = 0.6 Hz), 7.77 (3H, m), 8.78 (1H, t, J = 5.5 Hz), 9.45 (1H, s)
^{13}C-NMR (DMSO-d_6, 75 MHz): δ [ppm] = 42.3, 110.5, 113.4, 115.1, 115.4, 126.2, 128.7, 129.0, 129.5, 129.6, 135.6, 135.7, 138.1, 139.3, 153.2, 153.5, 154.4
EI-MS: m/z 321 (M^+)
Melting Point: 204-206 °C
HPLC-Retention Time: 6.8 min

1-(4-methoxybenzyl)-3-(6-phenylpyridin-2-yl)urea (33)

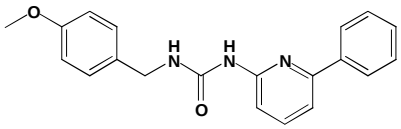

^{1}H-NMR (DMSO-d_6, 300 MHz): δ [ppm] = 3.75 (3H, s), 4.35 (2H, d, J = 5.3 Hz), 6.93 (2H, m), 7.25 (1H, m), 7.30 (2H, m), 7.37 (3H, m), 7.45 (1H, m), 7.75 (3H, m), 8.80 (1H, s), 9.42 (1H, s)
^{13}C-NMR (DMSO-d_6, 75 MHz): δ [ppm] = 42.5, 55.2, 110.5, 113.3, 114.0, 126.2, 128.5, 129.1, 131.2, 138.1, 139.3, 153.2, 153.4, 154.6, 158.4
EI-MS: m/z 333 (M^+)
Melting Point: 202-203 °C
HPLC-Retention Time: 6.7 min

1-(4-fluorobenzyl)-3-(6-(3-fluorophenyl)pyridin-2-yl)urea (34)

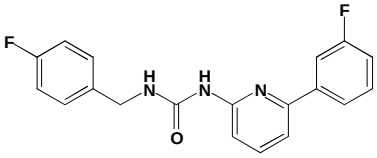

^{1}H-NMR (DMSO-d_6, 500 MHz): δ [ppm] = 4.54 (2H, d, J = 5.6 Hz), 7.31 (2H, m), 7.38 (1H, m), 7.55 (4H, m), 7.67 (1H, d, J = 7.6 Hz), 7.80 (2H, m), 7.93 (1H, m), 8.60 (1H, t, J = 5.1 Hz), 9.57 (1H,s)
^{13}C-NMR (DMSO-d_6, 125 MHz): δ [ppm] = 43.7, 112.6, 114.3, 114.5, 115.3, 116.5, 116.6, 116.8, 117.2, 117.4, 123.7, 130.8, 130.9, 132.1, 132.2, 137.3, 140.9, 154.7, 156.1, 161.7
EI-MS: m/z 339 (M^+)
Melting Point: 158-159 °C
HPLC-Retention Time: 7.3 min

1-(4-fluorobenzyl)-3-(6-(3-methoxyphenyl)pyridin-2-yl)urea (35)

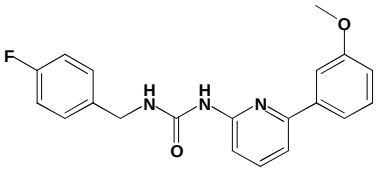

^{1}H-NMR (DMSO-d_6, 300 MHz): δ [ppm] = 3.74 (3H, s), 4.42 (2H, d, J = 5.6 Hz), 6.97 (1H, m), 7.17 (2H, d, J = 8.8 Hz), 7.35 (6H, m), 7.47 (1H, d, J = 7.8 Hz), 7.76 (1H, t, J = 8.3 Hz), 8.74 (1H, t, J = 5.3 Hz), 9.43 (1H, s)
^{13}C-NMR (DMSO-d_6, 75 MHz): δ [ppm] = 42.1, 55.0, 110.6, 111.5, 113.6, 114.8, 115.0, 115.3, 118.6, 129.2, 129.3, 129.8, 135.8, 139.2, 139.7, 153.1, 153.4, 154.8, 159.6
EI-MS: m/z 351 (M^+)
Melting Point: 131 °C
HPLC-Retention Time: 7.0 min

1-(4-methoxybenzyl)-3-(6-(3-methoxyphenyl)pyridin-2-yl)urea (36)

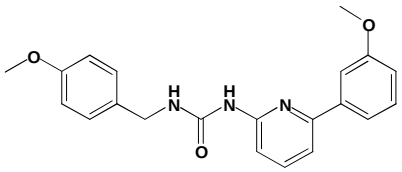

^{1}H-NMR (DMSO-d_6, 300 MHz): δ [ppm] = 3.74 (6H, m), 4.35 (2H, d, J = 5.5 Hz), 6.90 (2H, d, J = 8.2 Hz), 6.97 (1H, m), 7.30 (5H, m), 7.40 (1H, s), 7.47 (1H, d, J = 7.6 Hz), 7.75 (1H, m), 8.71 (1H, s), 9.40 (1H, s)
^{13}C-NMR (DMSO-d_6, 75 MHz): δ [ppm] = 42.3, 55.1, 110.6, 111.5, 113.5, 113.8, 114.7, 118.5, 128.7, 129.6, 131.4, 139.4, 139.7, 153.2, 153.4, 154.7, 158.3, 159.6
EI-MS: m/z 363 (M^+)
Melting Point: 186 °C
HPLC-Retention Time: 6.8 min

1-(6-(3-benzyloxy)phenyl)pyridin-2-yl)-3-(4-fluorobenzyl)urea (37)

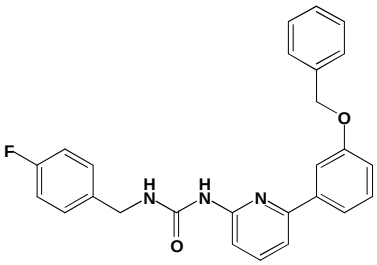

^{1}H-NMR (DMSO-d_6, 300 MHz): δ [ppm] = 4.41 (2H, d, J = 5.7 Hz), 5.11 (2H, s), 7.10 (3H, m), 7.37 (10H, m), 7.47 (1H, d, J = 7.1 Hz), 7.53 (1H, m), 7.76 (1H, m), 8.74 (1H, t, J = 5.1 Hz), 9.43 (1H, s)
^{13}C-NMR (DMSO-d_6, 75 MHz): δ [ppm] = 42.1, 69.2, 110.6, 112.7, 113.6, 115.0, 115.5, 118.7, 127.7, 127.9, 128.4, 129.2, 129.3, 129.8, 135.8, 136.9, 139.2, 139.7, 153.1, 153.3, 154.7, 158.8
EI-MS: m/z 427 (M^+)
Melting Point: 159-160 °C
HPLC-Retention Time: 8.2 min

1-(2,4´-bipyridin-6-yl)-3-(4-fluorobenzyl)urea (38)

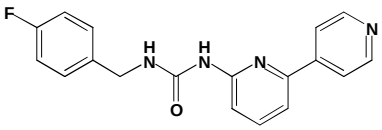

^{1}H-NMR (DMSO-d_6, 500 MHz): δ [ppm] = 4.41 (2H, d, J = 5.5 Hz), 7.20 (2H, m), 7.42 (2H, m), 7.49 (1H, d, J = 8.2 Hz), 7.64 (1H, d, J = 7.4 Hz), 7.77 (2H, d, J = 4.5 Hz), 7.85 (1H, t, J = 7.7 Hz), 8.47 (1H, s), 8.61 (2H, d, J = 4.5 Hz), 9.51 (1H, s)
^{13}C-NMR (DMSO-d_6, 125 MHz): δ [ppm] = 42.7, 112.8, 114.7, 115.5, 115.7, 120.8, 129.9, 130.0, 130.2, 130.3, 139.9, 145.4, 150.6, 151.4, 153.8, 154.9
EI-MS: m/z 322 (M^+)
Melting Point: 206 °C
HPLC-Retention Time: 3.5 min

1-(2,4´-bipyridin-6-yl)-3-(4-methoxybenzyl)urea (39)

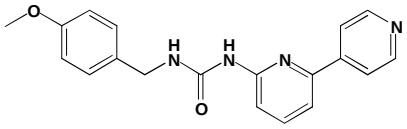

^{1}H-NMR (DMSO-d_6, 500 MHz): δ [ppm] = 3.76 (3H, s), 4.35 (2H, d, J = 5.3 Hz), 6.95 (2H, m), 7.32 (2H, m), 7.44 (1H, d, J = 8.2 Hz), 7.63 (1H, d, J = 7.5 Hz), 7.72 (2H, d, J = 4.5 Hz), 7.84 (1H, m), 8.52 (1H, s), 8.57 (2H, d, J = 4.5 Hz), 9.49 (1H,s)
^{13}C-NMR (DMSO-d_6, 125 MHz): δ [ppm] = 42.3, 54.7, 112.1, 113.6, 113.7, 120.1, 128.7, 130.8, 139.2, 144.7, 149.9, 150.5, 153.2, 154.1, 158.3
EI-MS: m/z 334 (M^+)
Melting Point: 192 °C
HPLC-Retention Time: 2.8 min

1-(4-fluorobenzyl)-3-(5-phenylpyridin-2-yl)urea (40)

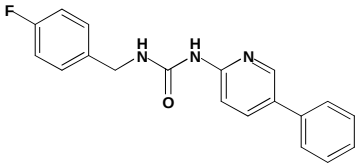

^{1}H-NMR (Acetone-d_6, 500 MHz): δ [ppm] = 4.44 (2H, d, J = 4.9 Hz), 7.00 (2H, d, J = 8.9 Hz), 7.27 (2H, m), 7.35 (4H, m), 7.55 (2H, d, J = 8.0 Hz), 7.90 (1H, dd, J = 8.7 Hz, J = 2.5 Hz), 8.37 (1H, d, J = 2.2 Hz), 8.79 (1H, s), 9.16 (1H, s)
^{13}C-NMR (Acetone-d_6, 125 MHz): δ [ppm] = 45.5, 115.0, 118.1, 129.5, 130.8, 132.2, 132.4, 132.9, 139.6, 139.9, 140.8, 147.6, 156.2, 164.1, 166.0
EI-MS: m/z 321 (M^+)
Melting Point: 168-170 °C
HPLC-Retention Time: 5.8 min

1-(4-methoxybenzyl)-3-(5-phenyl)pyridin-2-yl)urea (41)

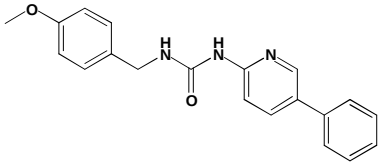

^{1}H-NMR (Acetone-d_6, 500 MHz): δ [ppm] = 3.64 (3H, s), 4.35 (2H, d, J = 5.8 Hz), 6.77 (2H, d, J = 8.6 Hz), 7.18 (2H, d, J = 8.7 Hz), 7.22 (2H, m), 7.32 (2H, t, J = 7.6 Hz), 7.51 (2H, d, J = 8.0 Hz), 7.85 (1H, dd, J = 8.6 Hz, J = 2.5 Hz), 8.31 (1H, d, J = 2.2 Hz), 8.8 (1H, s), 8.98 (1H, s)
^{13}C-NMR (Acetone-d_6, 125 MHz): δ [ppm] = 43.8, 55.9, 113.2, 115.1, 127.6, 128.7, 129.9, 130.2, 130.9, 133.4, 137.9, 138.8, 145.6, 154.4, 156.4, 160.2
EI-MS: m/z 333 (M^+)
Melting Point: 134 °C
HPLC-Retention Time: 5.7 min

1-(4-fluorobenzyl)-3-(5-p-tolylpyridin-2-yl)urea (42)

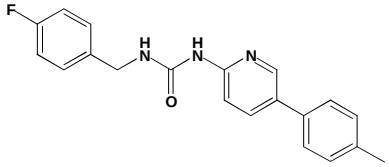

^{1}H-NMR (Acetone-d_6, 500 MHz): δ [ppm] = 2.3 (3H, s), 4.41 (2H, d, J = 5.9 Hz), 6.95 (2H, d, J = 8.8 Hz), 7.14 (2H, d, J = 7.9 Hz), 7.19 (1H, d, J = 8.6), 7.30 (2H, m), 7.38 (2H, d, J = 8.1 Hz), 7.84 (1H, dd, J = 8.6 Hz, J = 2.4 Hz), 8.30 (1H, d, J = 2.2 Hz), 8.8 (1H, s), 9.15 (1H, s)
^{13}C-NMR (Acetone-d_6, 125 MHz): δ [ppm] = 23.8, 46.0, 115.3, 118.4, 118.6, 129.8, 132.8, 133.2, 138.2, 140.1, 140.7, 147.7, 156.4, 158.8, 164.4, 166.4
EI-MS: m/z 335 (M^+)
Melting Point: 182 °C
HPLC-Retention Time: 6.1 min

1-(4-methoxybenzyl)-3-(5-p-tolylpyridin-2-yl)urea (43)

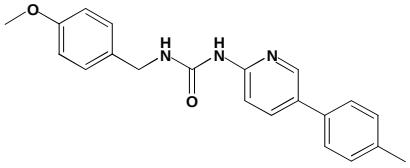

^{1}H-NMR (Acetone-d_6, 500 MHz): δ [ppm] = 2.22 (3H, s), 3.63 (3H, s), 4.34 (2H, d, J = 5.8 Hz), 6.76 (2H, d, J = 8.7 Hz), 7.14 (2H, d, J = 8.0 Hz), 7.19 (3H, m), 7.38 (2H, d, J = 8.1 Hz), 7.82 (1H, dd, J = 8.6 Hz, J = 2.5 Hz), 8.25 (1H, d, J = 2.3 Hz), 8.73 (1H, s), 8.98 (1H, s)
^{13}C-NMR (Acetone-d_6, 125 MHz): δ [ppm] = 22.4, 44.8, 56.8, 113.8, 116.0, 128.4, 130.8, 131.8, 131.9, 134.4, 136.8, 138.7, 139.3, 146.2, 155.1, 157.2, 161.1
EI-MS: m/z 347 (M^+)
Melting Point: 122-124 °C
HPLC-Retention Time: 6.0 min

1-(4-fluorobenzyl)-3-(5-(3-fluorophenyl)pyridin-2-yl)urea (44)

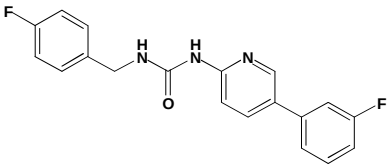

^{1}H-NMR (Acetone-d_6, 500 MHz): δ [ppm] = 4.40 (2H, d, J = 4.5 Hz), 6.97 (3H, m), 7.30 (4H, m), 7.37 (2H, m), 7.90 (1H, dd, J = 8.7 Hz, J = 2.5 Hz), 8.37 (1H, d, J = 2.3 Hz), 8.72 (1H, s), 9.02 (1H, s)
^{13}C-NMR (Acetone-d_6, 125 MHz): δ [ppm] = 44.0, 113.6, 114.8, 115.9, 116.9, 124.1, 130.2, 131.1, 132.8, 138.2, 141.8, 146.5, 155.2, 164.2, 164.8, 166.2
EI-MS: m/z 339 (M^+)
Melting Point: 176 °C
HPLC-Retention Time: 6.2 min

1-(5-(3-fluoroyphenyl)pyridin-2-yl)-3-(4-methoxybenzyl)urea (45)

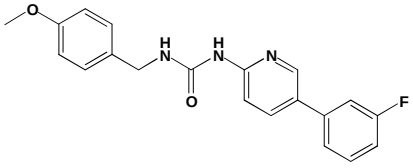

^{1}H-NMR (Acetone-d_6, 500 MHz): δ [ppm] = 3.64 (3H, s), 4.35 (2H, d, J = 5.8 Hz), 6.76 (2H, d, J = 8.7 Hz), 6.98 (1H, m), 7.18 (2H, d, J = 8.5 Hz), 7.25 (1H, d, J = 8.7 Hz), 7.30 (1H, d, J = 10.5 Hz), 7.36 (2H, m), 7.88 (1H, dd, J = 8.7 Hz, J = 2.5 Hz), 8.36 (1H, d, J = 2.4 Hz), 8.80 (1H, s), 8.92 (1H, s)
^{13}C-NMR (Acetone-d_6, 125 MHz): δ [ppm] = 43.8, 55.9, 113.0, 114.1, 114.2, 115.1, 115.3, 123.5, 129.5, 129.9, 132.2, 133.4, 138.0, 141.2, 145.9, 154.8, 156.2, 160.2, 163.6, 165.6
EI-MS: m/z 351 (M^+)
Melting Point: 162 °C
HPLC-Retention Time: 6.0 min

1-(4-fluorobenzyl)-3-(5-(3-methoxyphenyl)pyridin-2-yl)urea (46)

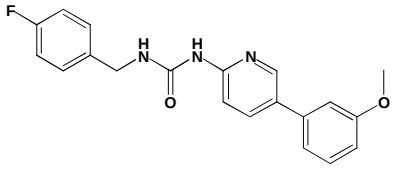

^{1}H-NMR (Acetone-d_6, 500 MHz): δ [ppm] = 3.72 (3H, s), 4.41 (2H, d, J = 5.9 Hz), 6.80 (1H, dd, J = 1.7 Hz, J = 8.3 Hz), 6.96 (2H, m), 7.06 (2H, m), 7.22 (2H, m), 7.31 (2H, m), 7.86 (1H, dd, J = 8.6 Hz, J = 2.5 Hz), 8.33 (1H, d, J = 2.3 Hz), 8.77 (1H, s), 9.12 (1H, s)
^{13}C-NMR (Acetone-d_6, 125 MHz): δ [ppm] = 43.8, 56.0, 113.0, 114.4, 116.4, 119.9, 130.6, 130.9, 131.4, 137.8, 138.1, 140.2, 145.7, 154.4, 156.4, 161.7, 162.2, 164.8
EI-MS: m/z 351 (M^+)
Melting Point: 124 °C
HPLC-Retention Time: 5.9 min

1-(4-methoxybenzyl)-3-(5-(3-methoxyphenyl)pyridin-2-yl)urea (47)

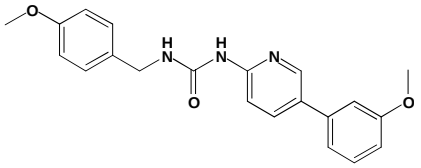

^{1}H-NMR (Acetone-d_6, 500 MHz): δ [ppm] = 3.64 (3H, s), 3.73 (3H, s), 4.34 (2H, d, J = 5.8 Hz), 6.77 (2H, d, J = 8.7 Hz), 6.79 (1H, d, J = 8.4 Hz), 7.06 (2H, d, J = 8.4 Hz), 7.19 (2H, d, J = 8.7 Hz), 7.24 (2H, d, J = 7.8 Hz), 7.85 (1H, dd, J = 8.6 Hz, J = 2.5 Hz), 8.32 (1H, d, J = 2.9 Hz), 8.76 (1H, s), 8.97 (1H, s)
^{13}C-NMR (Acetone-d_6, 125 MHz): δ [ppm] = 43.8, 55.9, 56.0, 112.9, 113.1, 114.3, 115.1, 119.8, 123.5, 129.9, 130.7, 131.4, 133.4, 138.0, 140.2, 145.7, 154.5, 156.4, 160.2, 161.7
EI-MS: m/z 363 (M^+)
Melting Point: 140-142 °C
HPLC-Retention Time: 5.8 min

1-(4-fluorobenzyl)-3-(5-(3-isopropoxyphenyl)pyridin-2-yl)urea (48)

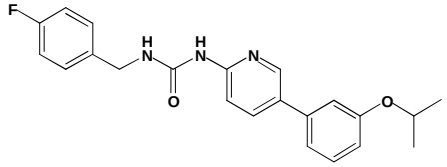

^{1}H-NMR (Acetone-d_6, 500 MHz): δ [ppm] = 1.18 (3H, d, J = 2.2 Hz), 1.19 (3H, d, J = 2.2 Hz), 4.41 (2H, d, J = 5.9 Hz), 4.58 (1H, m), 6.77 (1H, m), 6.95 (2H, m), 7.03 (2H, m), 7.21 (2H, m), 7.30 (2H, m), 7.85 (1H, dd, J = 8.6 Hz, J = 2.5 Hz), 8.32 (1H, d, J = 2.4 Hz), 8.81 (1H, s), 9.14 (1H, s)
^{13}C-NMR (Acetone-d_6, 125 MHz): δ [ppm] = 20.9, 41.8, 68.8, 111.1, 113.2, 114.3, 114.4, 117.8, 128.6, 129.1, 129.5, 136.2, 138.4, 143.8, 152.5, 154.6, 158.1, 160.4, 162.2
EI-MS: m/z 379 (M^+)
Melting Point: 99-100 °C
HPLC-Retention Time: 6.7 min

1-(5-(3-isopropoxyphenyl)pyridin-2-yl)-3-(4-methoxybenzyl)urea (49)

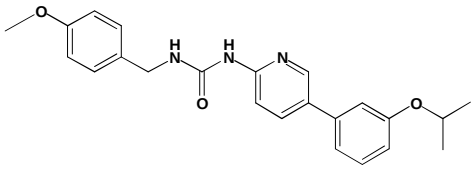

^{1}H-NMR (Acetone-d_6, 500 MHz): δ [ppm] = 1.17 (3H, d, J = 2.0 Hz), 1.19 (3H, d, J = 2.0 Hz), 3.62 (3H, s), 4.35 (2H, d, J = 5.8 Hz), 4.57 (1H, m), 6.75 (2H, d, J = 8.7 Hz), 6.77 (1H, m), 7.02 (2H, m), 7.20 (4H, m), 7.83 (1H, dd, J = 8.6 Hz, J = 2.5 Hz), 8.31 (1H, d, J = 2.5 Hz), 8.98 (1H, s), 9.07 (1H, s)
^{13}C-NMR (Acetone-d_6, 125 MHz): δ [ppm] = 22.7, 43.9, 55.8, 70.7, 113.0, 115.0, 115.1, 116.1, 119.7, 129.8, 130.7, 131.4, 133.4, 138.1, 140.2, 145.6, 154.5, 156.6, 159.9, 160.4
EI-MS: m/z 391 (M^+)
Melting Point: 126-128 °C
HPLC-Retention Time: 6.5 min

1-(5-(3-benzyloxy)phenyl)pyridin-2-yl)-3-(4-fluorobenzyl)urea (50)

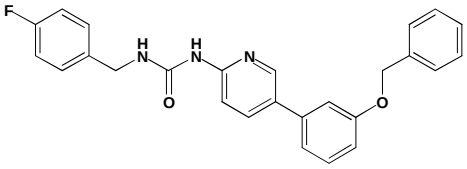

^{1}H-NMR (Acetone-d_6, 500 MHz): δ [ppm] = 4.40 (2H, d, J = 5.8 Hz), 5.07 (2H, s), 6.86 (1H, dd, J = 2.5 Hz, J = 7.5 Hz), 6.95 (2H, d, J = 8.8 Hz), 7.08 (1H, d, J = 7.0 Hz), 7.25 (8H, m), 7.37 (2H, d, J = 7.5 Hz), 7.86 (1H, dd, J = 8.6 Hz, J = 2.5 Hz), 8.34 (1H, d, J = 2.1 Hz), 8.74 (1H, s), 9.09 (1H, s)
^{13}C-NMR (Acetone-d_6, 125 MHz): δ [ppm] = 43.8, 71.0, 113.0, 114.1, 115.3, 116.2, 120.1, 120.7, 129.0, 129.7, 130.5, 130.8, 131.4, 137.8, 138.1, 138.8, 140.3, 145.8, 154.5, 156.4, 160.9, 164.1
EI-MS: m/z 427 (M^+)
Melting Point: 144 °C
HPLC-Retention Time: 7.6 min

1-(5-(3-(benzyloxy)phenyl)pyridin-2-yl)-3-(4-methoxybenzyl)urea (51)

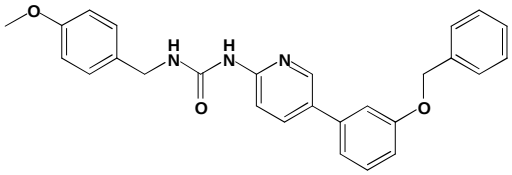

^{1}H-NMR (Acetone-d_6, 500 MHz): δ [ppm] = 3.64 (3H, s), 4.34 (2H, d, J = 5.7 Hz), 5.06 (2H, s), 6.76 (2H, d, J = 8.7 Hz), 6.88 (1H, dd, J = 8.2 Hz, J = 2.4 Hz), 7.08 (1H, d, J = 8.3 Hz), 7.20 (8H, m), 7.37 (2H, d, J = 7.5 Hz), 7.86 (1H, dd, J = 8.6 Hz, J = 2.5 Hz), 8.32 (1H, d, J = 2.2 Hz), 8.55 (1H, s), 8.90 (1H, s)
^{13}C-NMR (Acetone-d_6, 125 MHz): δ [ppm] = 45.2, 57.3, 72.3, 112.9, 114.3, 115.4, 116.4, 121.5, 130.2, 130.4, 131.2, 131.3, 132.1, 132.6, 134.8, 139.4, 140.2, 141.7, 147.2, 155.8, 157.5, 161.6, 162.3
EI-MS: m/z 439 (M^+)
Melting Point: 167 °C
HPLC-Retention Time: 7.3 min

1-(4-methoxybenzyl)-3-(5-(3-trifluoromethyl)phenyl)pyridin-2-yl)urea (52)

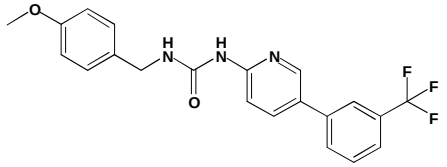

^{1}H-NMR (Acetone-d_6, 500 MHz): δ [ppm] = 3.64 (3H, s), 4.34 (2H, d, J = 5.8 Hz), 6.77 (2H, d, J = 8.6 Hz), 7.18 (2H, d, J = 8.6 Hz), 7.28 (1H, d, J = 8.6 Hz), 7.57 (2H, m), 7.83 (2H, m), 7.95 (1H, dd, J = 8.6 Hz, J = 2.5 Hz), 8.41 (1H, d, J = 2.3 Hz), 8.77 (1H, s), 8.88 (1H, s)
^{13}C-NMR (Acetone-d_6, 125 MHz): δ [ppm] = 43.9, 55.8, 113.0, 115.1, 124.1, 125.2, 128.3, 130.0, 131.2, 131.4, 132.0, 132.2, 133.3, 138.2, 140.0, 146.1, 155.0, 156.2, 160.2
EI-MS: m/z 401 (M^+)
Melting Point: 166 °C
HPLC-Retention Time: 6.8 min

1-(5-(2,3-difluorophenyl)pyridin-2-yl)-3-(4-fluorobenzyl)urea (53)

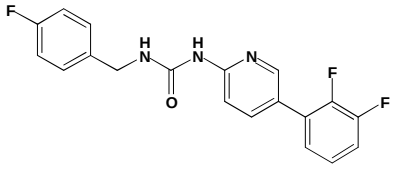

^{1}H-NMR (Acetone-d6, 500 MHz): δ [ppm] 4.59 (2H, d, J = 5.9 Hz), 7.12 (2H, m), 7.36 (3H, m), 7.45 (1H, d, J = 8.7 Hz), 7.48 (2H, m), 7.97 (1H, d, J = 8.6 Hz), 8.44 (1H, s), 9.18 (1H, s), 9.23 (1H, s)
^{13}C-NMR (Acetone-d6, 125 MHz): δ [ppm] = 43.6, 112.8, 116.3, 117.7, 124.7, 126.2, 126.5, 130.4, 137.6, 139.8, 147.5, 154.8, 156.4, 162.1, 164.1
EI-MS: m/z 357 (M^+)
Melting Point: 153 °C
HPLC-Retention Time: 6.7 min

1-(5-(2,3-difluorophenyl)pyridin-2-yl)-3-(4-methoxybenzyl)urea (54)

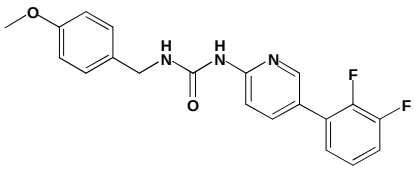

^{1}H-NMR (Acetone-d_6, 500 MHz): δ [ppm] = 3.64 (3H, s), 4.34 (2H, d, J = 5.9 Hz), 6.76 (2H, d, J = 8.7 Hz), 7.20 (5H, m), 7.30 (1H, d, J = 8.6 Hz), 7.85 (1H, m), 8.32 (1H, s), 8.74 (1H, s), 8.82 (1H, s)
^{13}C-NMR (Acetone-d_6, 125 MHz): δ [ppm] = 45.1, 57.1, 114.0, 116.2, 118.8, 118.9, 125.8, 127.4, 127.7, 130.3, 130.4, 131.2, 134.5, 141.0, 148.7, 156.3, 157.3, 161.4
EI-MS: m/z 369 (M^+)
Melting Point: 160-162 °C
HPLC-Retention Time: 6.5 min

1-(4-fluorobenzyl)-3-(5-vinylpyridin-2-yl)urea (55)

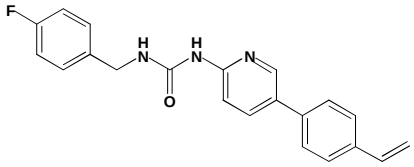

^{1}H-NMR (Acetone-d6, 500 MHz): δ [ppm] = 4.58 (2H, d, J = 6.0 Hz), 5.30 (1H, d, J = 10.9 Hz), 5.90 (1H, d, J = 17.7 Hz), 6.83 (1H, dd, J = 10.9 Hz, J = 17.7 Hz), 7.13 (2H, m), 7.40 (1H, d, J = 8.6 Hz), 7.48 (2H, m), 7.60 (2H, d, J = 8.3 Hz), 7.67 (2H, d, J = 8.3 Hz), 8.05 (1H, d, J = 8.6 Hz), 8.52 (1H, s), 8.90 (1H, s), 9.25 (1H, s)
^{13}C-NMR (Acetone-d6, 125 MHz): δ [ppm] = 43.6, 113.0, 114.7, 116.1, 116.3, 127.7, 128.1, 130.4, 137.6, 137.8, 138.1, 138.2, 145.5, 154.3, 156.3, 164.0
EI-MS: m/z 347 (M^+)
Melting Point: 172 °C
HPLC-Retention Time: 6.5 min

1-(4-methoxybenzyl)-3-(5-vinylpyridin-2-yl)urea (56)

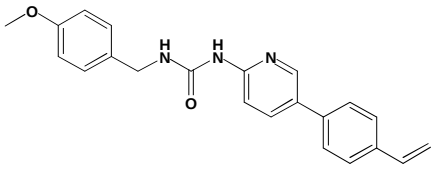

^{1}H-NMR (Acetone-d6, 500 MHz): δ [ppm] = 3.81 (3H, s), 4.53 (2H, d, J = 5.9 Hz), 5.30 (1H, d, J = 10.7 Hz), 5.89 (1H, d, J = 17.7 Hz), 6.83 (1H, dd, J = 10.7, J = 17.7 Hz), 6.93 (2H, d, J = 8.6 Hz), 7.37 (2H, d, J = 8.6 Hz), 7.39 (1H, d, J = 8.7 Hz), 7.59 (2H, d, J = 8.3 Hz), 7.67 (2H, d, J = 8.3 Hz), 8.04 (1H, d, J = 8.7 Hz), 8.51 (1H, s), 8.96 (1H, s), 9.16 (1H, s)
^{13}C-NMR (Acetone-d6, 125 MHz): δ [ppm] = 43.9, 55.8, 113.0 114.7, 115.0, 127.6, 128.1, 129.9, 130.3, 133.4, 137.6, 137.7, 138.0, 138.2, 145.5, 154.4, 156.2, 160.1
EI-MS: m/z 359 (M^+)
Melting Point: 159 °C
HPLC-Retention Time: 6.4 min

1-(4-methoxybenzyl)-3-(4-phenylpyridin-2-yl)urea (57)

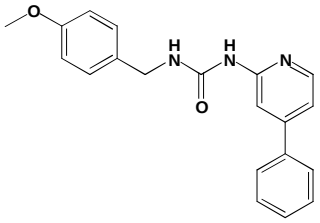

^{1}H-NMR (DMSO-d_6, 500 MHz): δ [ppm] = 3.74 (3H, s), 4.33 (2H, d, J = 5.8 Hz), 6.90 (2H, d, J = 8.7 Hz), 7.25 (3H, m), 7.50 (3H, m), 7.68 (2H, m), 7.75 (1H, s), 8.23 (1H, d, J = 5.4 Hz), 8.60 (1H, s), 9.45 (1H, s)
^{13}C-NMR (DMSO-d_6, 125 MHz): δ [ppm] = 42.4, 55.4, 109.1, 114.1, 115.1, 127.0, 128.8, 129.5, 129.6, 132.3, 137.9, 147.8, 149.5, 154.6, 155.3, 158.6
EI-MS: m/z 333 (M^+)
Melting Point: 202 °C
HPLC-Retention Time: 5.9 min

1-(4-(3-fluorophenyl)pyridin-2-yl)-3-(4-methoxybenzyl)urea (58)

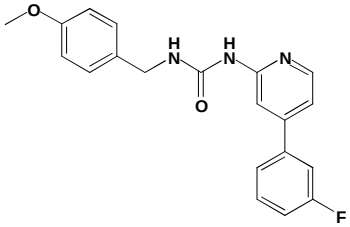

^{1}H-NMR (DMSO-d_6, 300 MHz): δ [ppm] = 3.72 (3H, s), 4.33 (2H, d, J = 5.8 Hz), 6.90 (2H, m), 7.30 (4H, m), 7.55 (3H, m), 7.72 (1H, d, J = 0.9 Hz), 8.24 (1H, dd, J = 5.4 Hz, J = 0.5 Hz), 8.4 (1H, t, J = 5.7 Hz), 9.31 (1H, s)
^{13}C-NMR (DMSO-d_6, 75 MHz): δ [ppm] = 42.1, 55.0, 108.8, 113.3, 113.6, 113.8, 114.8, 115.8, 116.1, 122.8, 128.4, 131.2, 131.3, 131.8, 139.9, 140.1, 147.6, 147.8, 154.1, 154.7, 158.2
EI-MS: m/z 351 (M^+)
Melting Point: 166-168 °C
HPLC-Retention Time: 5.6 min

1-(4-methoxybenzyl)-3-(4-(3-methoxyphenyl)pyridin-2-yl)urea (59)

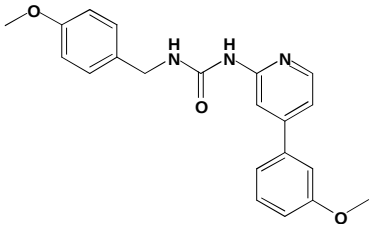

^{1}H-NMR (DMSO-d_6, 500 MHz): δ [ppm] = 3.74 (3H, s), 3.84 (3H, s), 4.35 (2H, d, J = 5.8 Hz), 6.91 (2H, m), 7.06 (1H, dd, J = 8.2 Hz, J = 2.5 Hz), 7.20 (1H, m), 7.26 (4H, m), 7.44 (1H, m), 7.67 (1H, s), 8.23 (1H, d, J = 5.3 Hz), 8.51 (1H, s), 9.30 (1H, s)
^{13}C-NMR (DMSO-d_6, 125 MHz): δ [ppm] = 44.6, 57.5, 57.4, 111.3, 114.7, 116.6, 117.2, 117.4, 121.4, 130.9, 132.8, 134.3, 141.5, 149.8, 151.6, 156.6, 157.3, 160.7, 162.3
EI-MS: m/z 363 (M^+)
Melting Point: 158 °C
HPLC-Retention Time: 5.6 min

1-(4-methoxybenzyl)-3-(4-(2-methoxyphenyl)pyridin-2-yl)urea (60)

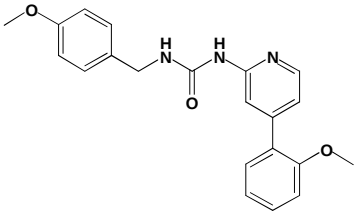

^{1}H-NMR (DMSO-d_6, 500 MHz): δ [ppm] = 3.71 (3H, s), 3.74 (3H, s), 4.46 (2H, d, J = 5.8 Hz), 6.77 (2H, m), 6.91 (1H, dd, J = 0.5 Hz, J = 8.2 Hz), 6.97-7.00 (3H, m), 7.22-7.25 (3H, m), 7.28-7.32 (1H, m), 8.03 (1H, d, J = 5.9 Hz), 8.50 (1H, s), 9.51 (1H, s)
^{13}C-NMR (DMSO-d_6, 125 MHz): δ [ppm] = 42.2, 54.3, 54.6, 110.4, 111.0, 111.3, 112.9, 115.6, 117.0, 120.0, 126.3, 127.6, 129.4, 130.5, 137.2, 152.1, 155.2, 155.6, 157.7
ESI-MS: m/z 364 (M+H)
HRMS: calcd. for $C_{21}H_{21}N_3O_3$ 363.1583, found 363.1542.
HPLC-Retention Time: 5.71 min

1-(4-methoxybenzyl)-3-(4-(thiophen2-yl)pyridin-2-yl)urea (61)

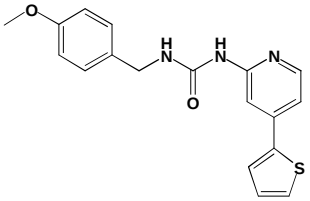

^{1}H-NMR (DMSO-d_6, 500 MHz): δ [ppm] = 3.71 (3H, s), 4.44 (2H, d, J = 5.7 Hz), 6.78 (2H, m), 7.05 (1H, dd, J = 1.2 Hz, J = 5.6 Hz), 7.07 (1H, dd, J = 3.7 Hz, J = 5.0 Hz), 7.15 (1H, s), 7.18 (1H, s), 7.23 (2H, m), 7.39 (1H, d, J = 4.8 Hz), 7.46 (1H, d, J = 2.9 Hz), 7.95 (1H, m), 9.2 (1H, s)
^{13}C-NMR (DMSO-d_6, 125 MHz): δ [ppm] = 42.3, 54.2, 106.9, 112.8, 113.0, 125.2, 127.7, 130.1, 154.9, 157.8
ESI-MS: m/z 340 (M+H)
HRMS: calcd. for $C_{18}H_{17}N_3O_2S$ 339.1042, found 339.1006.
HPLC-Retention Time: 5.29 min

1-(2-fluoro-3,4'-bipyridin-2'-yl)-3-(4-methoxybenzyl)urea (62)

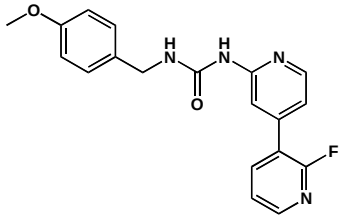

^{1}H-NMR (DMSO-d_6, 500 MHz): δ [ppm] = 3.74 (3H, s), 4.34 (2H, d, J = 5.9 Hz), 6.91 (2H, d, J = 8.7 Hz), 7.17 (1H, m), 7.25 (2H, d, J = 8.6 Hz), 7.54 (1H, m), 7.72 (1H, s), 8.17 (1H, m), 8.29 (1H, d, J = 5.7 Hz), 8.30 (1H, s, br), 8.34 (1H, m), 9.37 (1H, s)
^{13}C-NMR (DMSO-d_6, 125 MHz): δ [ppm] = 42.1, 55.0, 111.0, 113.5, 113.7, 116.5, 122.8, 128.2, 128.4, 131.7, 141.3, 147.4, 147.8, 148.1, 153.9, 154.6, 158.3
EI-MS: m/z 352
HPLC-Retention Time: 4.23 min

1-(4-(1H-tetrazol-5-yl)pyridin-2-yl)-3-(4-methoxybenzyl)urea (63)

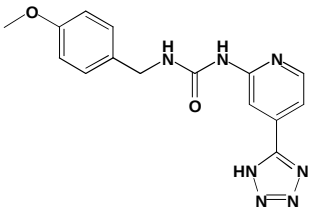

^{1}H-NMR (DMSO-d_6, 500 MHz): δ [ppm] = 3.66 (3H, s), 4.26 (2H, d, J = 5.7 Hz), 6.83 (2H, m), 7.18 (2H, m), 7.43 (1H, d, J = 4.7 Hz), 8.00 (1H, s), 8.18 (1H, s), 8.31 (1H, d, J = 5.0 Hz), 9.40 (1H, s)
^{13}C-NMR (DMSO-d_6, 125 MHz): δ [ppm] = 42.1, 55.0, 108.6, 113.7, 114.1, 128.4, 131.6, 148.4, 154.2, 154.5, 158.2
EI-MS: m/z 325 (M^+)
HPLC-Retention Time: 3.34 min

1-(5-(2H-tetrazol-5-yl)pyridin-2-yl)-3-(4-fluorobenzyl)urea (64)

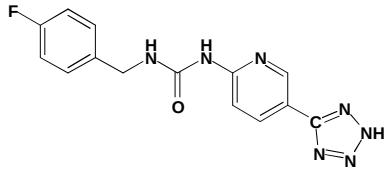

^{1}H-NMR (DMSO-d_6, 500 MHz): δ [ppm] = 4.44 (2H, d, J = 5.7 Hz), 7.21 (2H, d, J = 8.9 Hz), 7.42 (2H, d, J = 8.3 Hz), 7.75 (1H, d, J = 8.8 Hz), 8.31 (1H, s), 8.32 (1H, dd, J = 8.8 Hz, J = 2.2 Hz), 8.87 (1H, d, J = 1.8 Hz), 9.69 (1H, s)
^{13}C-NMR (DMSO-d_6, 125 MHz): δ [ppm] = 42.4, 112.0, 114.4, 115.5, 129.5, 136.4, 137.0, 146.2, 154.5, 155.4, 160.6, 162.5
EI-MS: m/z 313 (M^+)
Melting Point: 148-150 °C
HPLC-Retention Time: 4.2 min

1-(5-(2H-tetrazol-5-yl)pyridin-2-yl)-3-(4-methoxybenzyl)urea (65)

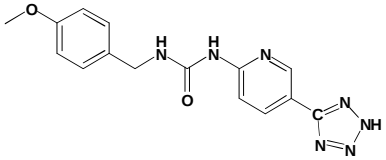

^{1}H-NMR (DMSO-d_6, 500 MHz): δ [ppm] = 3.64 (3H, s), 4.33 (2H, d, J = 5.8 Hz), 6.76 (2H, d, J = 8.7 Hz), 7.19 (2H, d, J = 8.7 Hz), 7.45 (1H, d, J = 8.8 Hz), 8.25 (1H, dd, J = 8.7 Hz, J = 2.3 Hz), 8.60 (1H, s), 8.77 (1H, d, J = 2.0 Hz), 9.08 (1H, s)
^{13}C-NMR (DMSO-d_6, 125 MHz): δ [ppm] = 44.0, 55.8, 113.5, 115.0, 115.2, 129.9, 130.1, 133.0, 138.3, 146.5, 155.9, 156.6, 160.2
EI-MS: m/z 325 (M^+)
Melting Point: 168-170 °C
HPLC-Retention Time: 3.9 min

1-(6-(1H-tetrazol-5-yl)benzo[d]thiazol-2-yl)-3-(4-methoxybenzyl)urea (66)

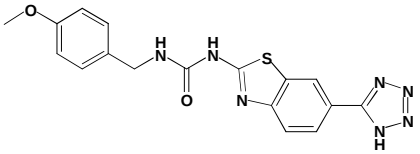

^{1}H-NMR (DMSO-d_6, 500 MHz): δ [ppm] = 3.67 (3H, s), 4.24 (2H, d, J = 5.8 Hz), 6.80 (1H, m), 6.85 (2H, m), 7.10 (1H, m), 7.19 (2H, m), 7.72 (1H, d, J = 8.3 Hz), 7.94 (1H, dd, J = 8.4 Hz, J = 1.8 Hz), 8.49 (1H, m), 10.90 (1H, s)
^{13}C-NMR (DMSO-d_6, 125 MHz): δ [ppm] = 44.4, 56.9, 115.5, 115.6, 115.7, 122.2, 126.6, 130.5, 130.6, 149.1, 150.8, 160.3
EI-MS: m/z Fragmente - 353, 338, 218, 175, 121
HPLC-Retention Time: 5.08 min

GSK-3β *in vitro* assay

Purified GSK-3β (0.5 µg) was incubated in a reaction mixture of 50 mM Tris pH 7.3, 10 mM MgAc, 0.01% β-mercaptoethanol, ^{32}P[γ-ATP](100µM, 0.5 µci/assay), and 100 µM of peptide substrate, pIRS-1 (RREGGMSRPAS(p)VDG (1). **New molecules** were added at various concentrations (1, 10 and 100 µM), and the reaction mixture was incubated for 15 min at 30°C. The reactions were stopped, spotted on p81 paper (Whathman), washed with 10 mM phosphoric acid, and counted for radioactivity as described (1). GSK-3β activity was calculated as the percentage of GSK-3β activity in the absence of inhibitors that was designated to 100%.

Kinase Panel:

Compounds are serially diluted 1/3 in neat DMSO (10 serial dilutions) and these dilutions are further diluted 1/25 with reaction buffer. 2.5µl of these solutions are added to the reaction mixture described below so that final compound concentration in the assay ranges from 100 µM to 5 nM in 1% (v/v) DMSO. The enzymatic activity of the kinases is determined with a commercial system based on the Z'-LYTE® technology, available from Invitrogen Life Technologies (Carlsbad, CA, USA), using human recombinant kinases as the enzyme source. This technology utilizes the fluorescence resonance energy transfer ("FRET") process between fluorescein and coumarin. The assay principle is based on the differential sensitivity of phosphorylated and non-phosphorylated peptide to proteolytic cleavage, which precludes the energy transfer process between the two fluorophores attached to both sides of the cleavage site. Hence, enzymatic phosphorylation will yield a phosphopeptide, which cannot be

hydrolyzed by a suitable protease and energy transfer between the two fluorophores will occur. Opposingly, lack of phosphorylation will cause peptide hydrolysis hence lack of energy transfer as.

The assay is performed in 96-well black plates, in a final volume of 10 µl, with components as detailed in Table 1.

Table 1

Kinase	Enzyme conc. (nM)	ATP conc. (µM)	Peptide used	Peptide conc. (µM)	Buffer
GSK3β	0.54	26	Ser/Thr 9 peptide	2	50 mM Hepes pH 7.5, 10 mM $MgCl_2$, 1 mM EGTA, 0.01% (w/v) Brij-35
CKIε	18.84	32	Ser/Thr 11 peptide	2	50 mM Hepes pH 7.5, 10 mM $MgCl_2$, 1 mM EGTA, 0.01% (w/v) Brij-35
Cdk5	15.9	12.5	Ser/Thr 12 peptide	2	50 mM Hepes pH 7.5, 10 mM $MgCl_2$, 1 mM EGTA, 0.01% (w/v) Brij-35
AurKA	20	10	Ser/Thr 1 peptide	2	50 mM Hepes pH 7.5, 20 mM $MgCl_2$, 1 mM EGTA, 0.01% (w/v) Brij-35
PKCα	1.04	1	Ser/Thr 7 peptide	2	50 mM Hepes pH 7.5, 10 mM $MgCl_2$, 1 mM EGTA, 0.01% (w/v) Brij-35

4.1.3 Synthese selektiver GSK-3α-Inhibitoren mittels biphenylischer Systeme

Der Inhalt dieses Kapitels wurde bereits veröffentlicht:

Fabio Lo Monte*,‡, Thomas Kramer, Jiamin Gu, Upendra Rao Anumala, Luciana Marinelli, Valeria La Pietra, Ettore Novellino, Bénédicte Franco, David Demedts, Fred Van Leuven, Ana Fuertes, Juan Manuel Dominguez, Batya Plotkin, Hagit Eldar-Finkelman, Boris Schmidt‡

Identification of Glycogen Synthase Kinase-3 Inhibitors with a Selective Sting for Glycogen Synthase Kinase-3α, *Journal of Medicinal Chemistry* **2012**, 55, 4407-4424. dx.doi.org/10.1021/jm300309a

Durch die Untersuchung mehrerer Kristallstrukturen von Inhibitoren im Komplex mit GSK-3β konnte eine vereinfachte Darstelllung der ATP-Bindetasche entworfen werden, in der nur relevante Bereiche gekennzeichnet sind (Abb. 18).

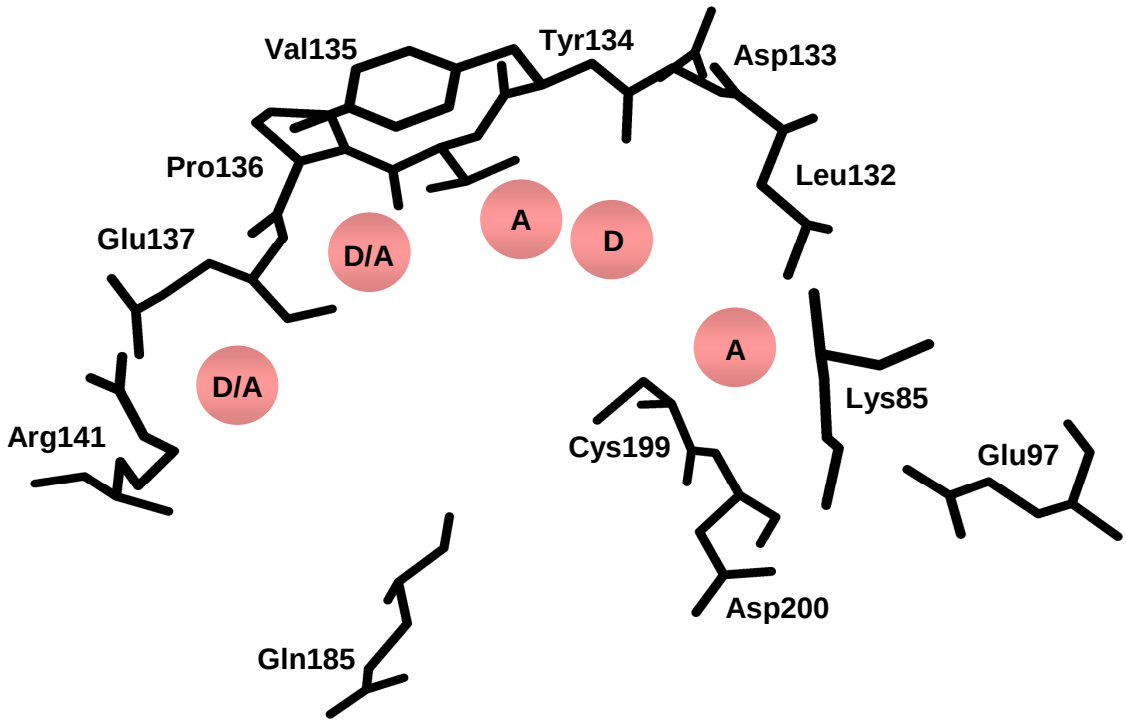

Abb. 18: Relevante Aminosäuren und Bereiche innerhalb der ATP-Bindetasche.

Die Akzeptor (A) und Donor (D) markierten Stellen verweisen auf erforderliche Funktionalitäten bzw. Heteroatome, die nötig sind, um eine Aktivität und Selektivität zu erzielen. Die Mehrzahl aller literaturbekannten GSK-3-Inhibitoren besetzt drei, bestenfalls vier dieser Bereiche. Es wurden mehrere biphenylische Strukturen synthetisiert, die einen großen Teil aller Akzeptor- und Donor-Regionen belegen konnten. Die aktivsten Verbindungen zeigten für GSK-3 IC_{50}-Werte im einstelligen nanomolaren Bereich. Darüber hinaus sind diese Verbindungen in der Lage, gleichzeitig mit der Gelenk-Region und Teilen der Glycin-reichen Schleife zu interagieren. Zur Erhöhung der Löslichkeit wurden verschiedene Linkersysteme eingefügt. Einige Biphenylderivate zeigten eine mehr als 2000-fache Selektivität für GSK-3 gegenüber vier nahe verwandten Kinasen. Durch verschiedene Substitutionsmuster am biphenylischen System konnten Inhibitoren hergestellt werden, die eine Selektivität gegenüber GSK-3α aufwiesen. Die beste Verbindung dieser Serie war sogar 92-fach selektiver für GSK-3α gegenüber GSK-3β. Die bestimmte Selektivität für eine Isoform ist die höchste von der bisher berichtet wurde. Diese Beobachtung kann sehr hilfreich sein, falls die *in vivo* Diskriminierung einer GSK-3-Isoform benötigt wird. Zudem ist es nun möglich, die physiologischen Funktionen und pathologischen Rollen von GSK-3α besser *in vivo* zu untersuchen.

Bei der *in vivo* Evaluation dieser Strukturklasse im Zebrafisch-Embryo konnten die charakteristischen Phänotypen beobachtet werden, welche für eine effektive *in vivo* Inhibition von GSK-3 bekannt sind. Ferner konnte festgestellt werden, dass diese Verbindungen im getesteten Konzentrationsbereich keine Toxizität aufweisen.

Im Rahmen dieser Arbeit wurden alle Verbindungen von Fabio Lo Monte synthetisiert:

BSc4258 (2B), BSc4259 (3B), BSc4260 (4B), BSc4261 (6a), BSc4263 (15a), BSc4392 (4C), BSc4393 (7c), BSc4395 (7b), BSc4396 (7a), BSc4399 (16a), BSc4401 (4A), BSc4404 (5b), BSc4405 (5a), BSc4407 (14c), BSc4408 (8e), BSc4410 (6b), BSc4412 (9f), BSc4414 (9a), BSc4415 (6c), BSc4416 (9e), BSc4603 (22a), BSc4604 (23a), BSc4605 (24a), BSc4606 (22b), BSc4607 (23b), BSc4608 (24b), BSc4609 (25), BSc4615 (14a), BSc4616 (14b), BSc4617 (8c), BSc4618 (8d), BSc4619 (9d), BSc4620 (9c), BSc4624 (8a), BSc4625 (5c), BSc4634 (26), BSc4676 (15b), BSc4681 (14d), BSc4789 (22c), BSc4792 (23c)

In Klammern die Verbindungsnummer in der Publikation.

Journal of Medicinal Chemistry

Article

pubs.acs.org/jmc

Identification of Glycogen Synthase Kinase-3 Inhibitors with a Selective Sting for Glycogen Synthase Kinase-3α

Fabio Lo Monte,*[,†] Thomas Kramer,[†] Jiamin Gu,[†] Upendra Rao Anumala,[†] Luciana Marinelli,[‡] Valeria La Pietra,[‡] Ettore Novellino,[‡] Bénédicte Franco,[§] David Demedts,[§] Fred Van Leuven,[§] Ana Fuertes,[∥] Juan Manuel Dominguez,[∥] Batya Plotkin,[⊥] Hagit Eldar-Finkelman,[⊥] and Boris Schmidt*[,†]

[†]Clemens Schöpf—Institute of Organic Chemistry and Biochemistry, Technische Universität Darmstadt, 64287 Darmstadt, Germany

[‡]Dipartimento di Chimica Farmaceutica e Tossicologica, Università di Napoli "Federico II", 80131 Napoli, Italy

[§]Experimental Genetics Group, Department of Human Genetics, Katholieke Universiteit Leuven, 3000 Leuven, Belgium

[∥]Noscira SA, Drug Discovery, Tres Cantos 28760-Madrid, Spain

[⊥]Department of Human Molecular Genetics and Biochemistry, Sackler School of Medicine, Tel Aviv University, 69978 Tel Aviv, Israel

Supporting Information

ABSTRACT: The glycogen synthase kinase-3 (GSK-3) has been linked to the pathogenesis of colorectal cancer, diabetes, cardiovascular disease, acute myeloid leukemia (AML), and Alzheimer's disease (AD). The debate on the respective contributions of GSK-3α and GSK-3β to AD pathology and AML is ongoing. Thus, the identification of potent GSK-3α-selective inhibitors, endowed with favorable pharmacokinetic properties, may elucidate the effect of GSK-3α inhibition in AD and AML models. The analysis of all available crystallized GSK-3 structures provided a simplified scheme of the relevant hot spots responsible for ligand binding and potency. This resulted in the identification of novel scorpion shaped GSK-3 inhibitors. It is noteworthy, compounds **14d** and **15b** showed the highest GSK-3α selectivity reported so far. In addition, compound **14d** did not display significant inhibition of 48 out of 50 kinases in the test panel. The GSK-3 inhibitors were further profiled for efficacy and toxicity in the wild-type (wt) zebrafish embryo assay.

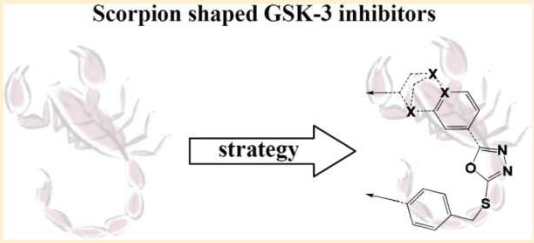

INTRODUCTION

Alzheimer's disease (AD), first described by Alois Alzheimer in 1906, is the most common dementia at old age. AD is characterized by the presence of two abnormal protein deposits: amyloid plaques composed of extracellular deposits of β-amyloid (Aβ) peptides and neurofibrillary tangles (NFTs) are formed by the accumulation of insoluble and hyperphosphorylated tau.[1−3] The 40−42 amino acid β-amyloid peptide is the major component of the amyloid deposits. It is produced from a larger protein, the amyloid precursor protein (APP), by proteolytic cleavage.[4] Tau is a soluble microtubule-binding protein which stabilizes the microtubules in axons.[2] Hyperphosphorylation of tau protein causes destabilization of microtubules and subsequent dissociation of tau, which in turn aggregates to form NFTs.[5] GSK-3 was identified ∼30 years ago and is a serine/threonine protein kinase that participates in a plethora of cellular processes, e.g., cell proliferation, microtubule dynamics, and gene transcription.[6−8] Several studies have linked glycogen synthase kinase-3 (GSK-3) to the primary abnormalities associated with AD, particularly the phosphorylation of tau.[4,9] Two closely related isoforms GSK-3α and GSK-3β are present in mammals.[10] They share 97% sequence similarity within their catalytic kinase domains.[7] GSK-3β has been proposed as the major kinase of tau phosphorylation, suggesting it as a potential, yet risky target for the therapy of AD.[1,5] Dysregulation of GSK-3β has been associated with diseases such as diabetes, Down's syndrome, bipolar disorder, colorectal cancer, and AD.[11] The inhibition of GSK-3α was suggested for the treatment of AD and other CNS diseases.[12−14] Furthermore, GSK-3α inhibition was proposed to modulate β-adrenergic signaling.[15] Recently, it was suggested that GSK-3α is involved in acute myeloid leukemia (AML), supporting a potential role for GSK-3α directed therapy.[16] Yet, the distinct contributions of both GSK-3 isoforms are still unknown. Appropriately, a number of pan-GSK-3α/β inhibitors have been disclosed because of the structure determination of GSK-3β.[17] Lithium chloride is the most thoroughly investigated GSK-3 inhibitor in AD animal models; it results in decreased tau hyperphosphorylation and decreased Aβ levels.[6] However, it is limited by a small therapeutic window. GSK-3 inhibitors were identified from remarkably different classes: organometallic compounds, paullones, indirubins, maleimides, thiadiazolidinones, L803-mts, ureas, and other small organic molecules.[4,10,18−24]

Received: March 5, 2012
Published: April 25, 2012

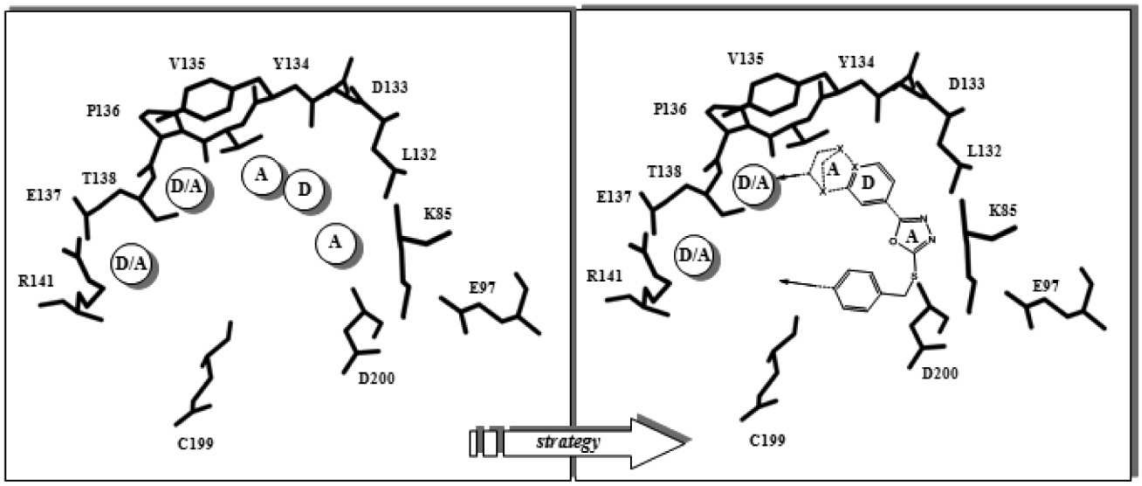

Figure 1. Synthesis strategy based on hot spot analysis of GSK-3 inhibition. The denoted acceptor (A) and donor (D) domains outline the necessary atoms respectively functional groups in the designated areas (left/right). The scaffold **I** used for the synthesis is marked on the right. X stands for heteroatoms.

Scheme 1[a]

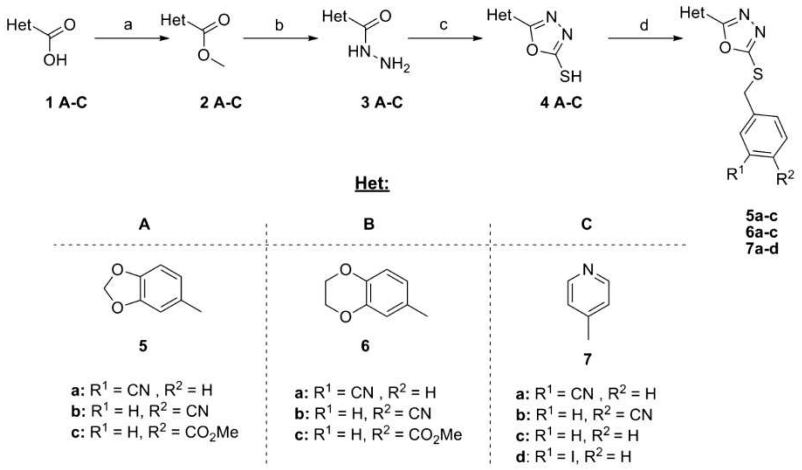

[a]Reagents and conditions: (a) MeOH, $SOCl_2$, 0−50 °C, 83−89%; (b) $NH_2NH_2 \cdot H_2O$, EtOH, reflux, 67−75%; (c) CS_2, Et_3N, EtOH, reflux, 79−89%; (d) benzyl halides, 1N NaOH, DMF, rt, 41−84%.

All GSK-3 inhibitors, except for the thiadiazolidinones and L803-mts, are ATP competitive inhibitors and all of them inhibit the two isoforms, GSK-3α and GSK-3β, with similar potency.[6] The design of selective ligands remains a challenge despite several crystallized GSK-3 inhibitor complexes and substantial differences revealed by GSK-3α/GSK-3β sequence comparison as the major part of the ligand binding site is conserved.[17] Here we report the synthesis and optimization of novel GSK-3 inhibitors, along with their α/β selectivity and the evaluation of their in vivo efficacy in zebrafish embryos, which is an established model system for the validation of GSK-3 inhibitors. The oxadiazole moiety (scaffold **I**; Figure 1) was chosen as lead structure as it provided, if appropriately decorated, high inhibition of GSK-3β.[5,25,26]

The optimization process took advantage of the available cocrystallized GSK-3β inhibitor complexes and the analysis of the relevant hot spots (Figure 1). Most GSK-3 inhibitors occupy three or at most four acceptor/donor domains in the active site. Our main intention was the engagement with as many as possible acceptor/donor areas as depicted in Figure 1. Initially, we investigated the enlargement of **I** to reach R141. Subsequently, different substituents on the heterocyclic scaffold were explored in order to enhance the interaction with the enzyme backbone and to improve solubility at the same time. Most of the resulting compounds were tested for the selective inhibition of GSK-3α/β.

■ CHEMISTRY

The esterification of the carboxylic acids **1A−C** afforded the compounds **2A−C**,[27,28] which were converted to the hydrazides **3A−C**.[28,29] Reaction of the hydrazides **3A−C** with carbon disulfide (CS_2) resulted in the oxadiazoles **4A−C**.[30,31] The heterocyclic derivatives **5a−c**, **6a−c**, and **7a−c**[32] were prepared by benzylation of the mercaptanes **4A−C** (Scheme 1).[26]

dx.doi.org/10.1021/jm300309a | J. Med. Chem. 2012, 55, 4407−4424

Scheme 2[a]

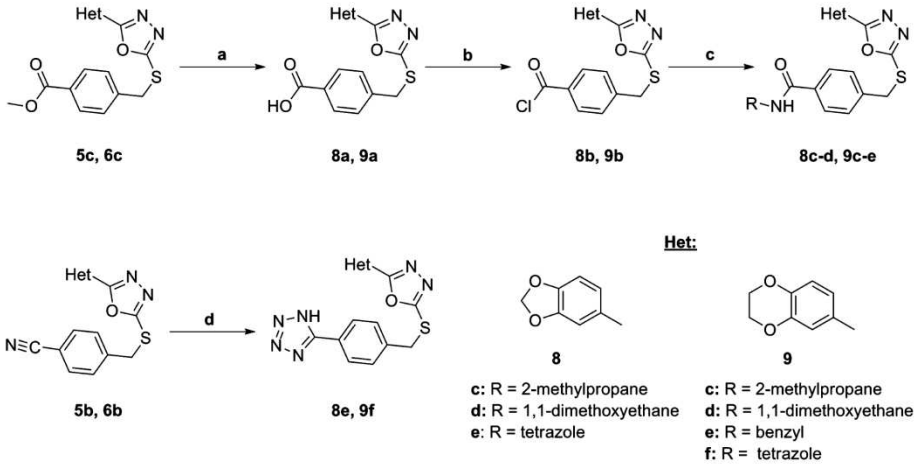

[a]Reagents and conditions: (a) 1N LiOH, THF, 60 °C, 83−91%; (b) $SOCl_2$, toluene, reflux; (c) amine, K_2CO_3, acetone, 0 °C to rt, 79−92%; (d) NaN_3, NH_4Cl, DMF, 100 °C, 67−79%.

Scheme 3[a]

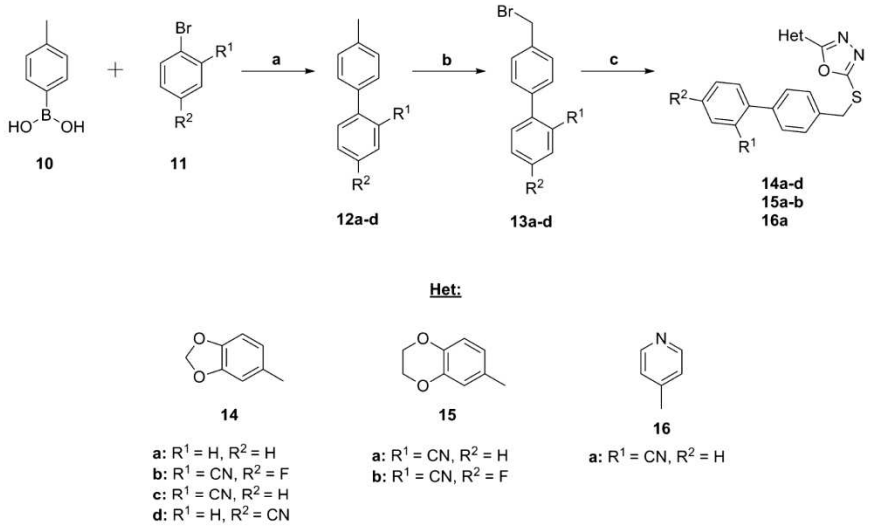

[a]Reagents and conditions: (a) aryl bromide, toluene, EtOH, $Pd(PPh_3)_4$, 2-tolylboronic acid, 2N Na_2CO_3 (aq), 80 °C; (b) NBS, AIBN, CCl_4, reflux; (c) **4**(**A**−**C**), 1N NaOH, DMF, rt, 53−75%.

Compound **7d** is commercially available. The esters **5c** and **6c** were converted to the carboxylic acids **8a** and **9a**, followed by treatment with thionyl chloride ($SOCl_2$) to form the acyl chlorides **8b** and **9b**.[33,34] Coupling of the acyl chlorides with primary amines gave the amides **8c**−**d** and **9c**−**e**.[34] The tetrazoles **8e** and **9f** were prepared from the nitriles **5b** and **6b** using sodium azide under microwave irradiation (Scheme 2).[35]

The biphenylic derivatives **13a**−**d** were prepared in two steps from the commercially available *p*-tolylboronic acid and substituted bromobenzenes. The 4′-(bromomethyl)biphenyl-2-carbonitrile is commercially available. The biphenylmethyl halides were coupled to the mercaptothiadiazoles **4A**−**C** to obtain the thioethers **14a**−**d**, **15a**−**b**, and **16a** (Scheme 3).[26] 3,4-Dihydroxybenzoic acid **17** was esterified to the methyl ester **18**, followed by cyclization with (±)-glycidyl tosylate or epibromohydrin to afford compound **19a**[36] as a mixture of enantiomers.[37−39] The hydrazide **21a** was prepared by methylation of **19a**, followed by the addition of hydrazine.[40] The reaction of the hydrazide **21a** with CS_2 gave the oxadiazole **22a**, which was coupled to 4′-(bromomethyl)biphenyl-2-carbonitrile to afford the thioether **23a**. The methyl ether in **23a** was cleaved by boron tribromide (BBr_3) to result in the alcohol **24a** (Scheme 4).[40] The compounds **23b**−**c** and **24a**−**b** were prepared under similar conditions; see Scheme 4. (*S*)-(+)-Glycidyl tosylate was used to obtain the *R*-enantiomer of compound **19b**.[37] The *S*-enantiomer of compound **19** was synthesized using (*R*)-(−)-glycidyl tosylate.[37] Mesylation of the alcohol **24b** and subsequent displacement of the mesylate by an amine afforded the acetal **26** (Scheme 4).[40]

Scheme 4[a]

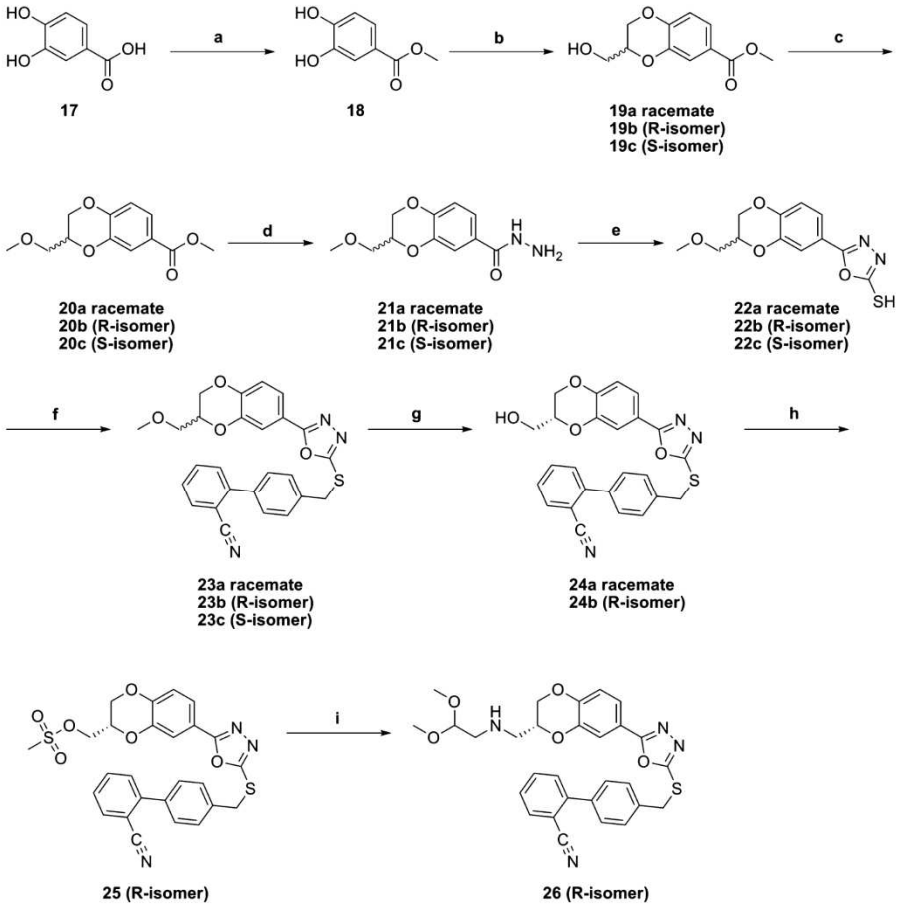

[a]Reagents and conditions: (a) $SOCl_2$, MeOH, 0−50 °C, 97%; (b) (*R*/*S*)-(±)-glycidyl tosylate or epibromohydrin, (*S*)-(+)-glycidyl tosylate or (*R*)-(−)-glycidyl tosylate, K_2CO_3, acetone or DMF, rt or 60 °C, 93−95%; (c) NaH, CH_3I, THF, 0 °C to rt, 68−71%; (d) $NH_2NH_2{\cdot}H_2O$, EtOH, reflux, 78−87%; (e) CS_2, Et_3N, EtOH, reflux, 81−91%; (f) biphenyl halide, 1N NaOH, DMF, rt, 84−88%; (g) BBr_3, DCM, −78 °C to rt; 73−79%; (h) CH_3SO_2Cl, Et_3N, DCM, 0 °C to rt, 98%; (i) amine, THF, Et_3N, 0 °C to reflux, 83%.

■ RESULTS AND DISCUSSION

Molecular Modeling. Compound **15a**, one of the most active inhibitors of the series, was docked, through Glide software, into the GSK-3β active site (PDB code: 3F88) with the aim to assess the ligand−protein interactions and to rationalize the SARs.[26] The docking experiments suggest that the oxadiazole ring positions itself in between the V70 and C199 side chains with one of the two nitrogens establishing an H-bond with the K85 side chain (Figure 2). The biphenyl branch forms a T-shaped interaction with P67 and hydrophobic contacts with the Q185 and Y140 carbons.[41] Furthermore, as shown in Figure 2, the CN substituent forms an H-bond with the T138 hydroxyl group. The latter interaction seems to improve the activity of our ligands, in fact, for example, **14c** is more active against GSK-3β than its analogue **14a**, which lacks the cyano group, and its analogue **14d**, equipped with the cyano group at the R2 site. As regards the **15a** binding mode, the dihydrobenzodioxine moiety establishes several hydrophobic interactions with L132, I62, A83, V110, and L188.

Moreover, one of the two oxygens of the dihydrodioxine ring forms an H-bond with the V135 NH in the hinge region, while

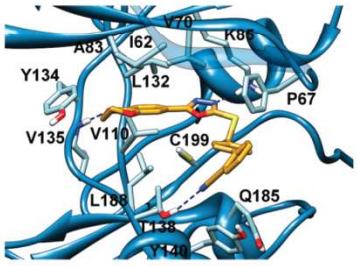

Figure 2. Molecular docking of compound **15a** into the X-ray structure of GSK-3β (PDB code: 3F88). This figure was prepared with Glide software.

the rest of the ring establishes hydrophobic contacts with the Y134. The latter interaction seems to be lost by **14c**, featuring the smaller benzodioxolane ring, while **16a**, a pyridine containing compound, forms a weaker H-bond with the same residue due to the position and the distance of the nitrogen atom of the pyridine ring from the NH of V135. The substitutions on the dihydrobenzodioxine moiety of **23** and **24**,

respectively, do not provide any further interaction with the enzyme, as the groups point out into the solvent. The same holds true for **26**, where the bulky substituent on the dihydrobenzodioxine ring may negatively affect the horseshoe shape (scorpion shape). The proposed binding mode also clarifies the undesirable effect of the substitution of the fluorine atom at the R2 site of the biphenyl branch in **15b**, which is 37-fold less potent for GSK-3β in comparison to **15a**. In fact, the electron-withdrawing atom weakens the H-bond between the cyano substituent and the T138 hydroxyl group; moreover, it comes in proximity of the negative ring density of Y140, providing repulsive edgewise interaction. The good selectivity toward GSK-3α versus GSK-3β which was observed for several compounds and especially for compound **15b**, is far to be trivial to explain. The superposition of the GSK-3β crystallographic structure (PDB code: 3F88) with a homology model built with Prime software (Schrodinger) shows that the differences between the two isoforms are all located out of the binding site and especially in the loop at C-terminus fragment (see the Supporting Information). Thus, it is conceivable that the selectivity of our compounds may be due to subtle enzyme differences, which may affect the ligand entrance/exit processes. This process may include an antechamber site, a step known to play a pivotal role in the inhibitor/enzyme recognition process.[42,43] By analyzing the enzyme surface and the residue mutations, the antechamber site in the GSK-3α or GSK-3β could be represented by the loop at C-terminus fragment as highlighted in Figure S1 in the Supporting Information. Obviously, the latter is a pure speculative hypothesis that has to be confirmed by more advanced theoretical work, mutational analysis, and additional experiments.

Biological Assays and Structure−Activity Relationship (SAR) Studies. The synthesized compounds were tested for their inhibitory activity against GSK-3β in an in house in vitro assay and further profiled in a commercial system based on the Z'-LYTE technology, available from Invitrogen Life Technologies (Carlsbad, CA, USA), using human recombinant GSK-3α or GSK-3β as the enzyme source. Most compounds displayed significant inhibitory activity against GSK-3β at 10 μM, and several compounds exerted more than 50% inhibitory activity against GSK-3β at the initial concentration (10 μM). The potent compounds were selected for IC_{50} determination. We observed differences in the IC_{50} determination between the in-house and the commercial assay and decided to use the results of the commercial system for comparison.

The structure−activity analysis suggested interactions with the GSK-3 backbone, Y134/D133, and the polar binding pocket, K85/E97/D200, to be essential for potent inhibition. These interactions require an acceptor−donor−acceptor motif on the inhibitor. We generated a simplified illustration in which we denoted acceptor (A) and donor (D) domains and drafted scaffold **I** as lead structure (Figure 1). We examined the effect of three heterocycles **5**−**7** as potential hinge binders and different substituents on the *S*-benzyl group (Scheme 1). The oxadiazole derivatives of the heterocycles **5** and **6** provided several GSK-3 inhibitors with an IC_{50} below 100 nM (Table 1) and confirmed previously reported activity.[26] The pyridines **7a**−**c** displayed decreased activity in comparison to the heterocycles **5** and **6**; this may be due to the position of the pyridine moiety in the ATP binding pocket. Thus, they were not pursued further. The compounds **5a** and **6a** indicated that an electron-withdrawing group is required at the 3-position. We introduced the cyano and ester group at the 4-position in order to reach out to R141 and the correlated acceptor/donor domain and thus to engage the ATP binding pocket in its entirety. Our data indicated that the electron-withdrawing group at the 3-position was also tolerated at the 4-position. The oxadiazoles **5b** and **6b**−**c** showed comparable activity to the 3-substituted derivatives and indicated space in the ATP binding pocket. On the basis of these results, we further examined the para-position of our lead structure. The carboxylic acids **8a** and **9a** resulted in a 4-fold less inhibitory activity against GSK-3β at 10 μM concentration compared to their esters **5c** and **6c** (Scheme 2). In the case of **5c**, the percentage of GSK-3β activity increased from 17% of up to 81% (Table 2). In addition, compound **8e**, bearing a hydrophilic tetrazole at the 4-position (IC_{50} value of 107 nM for GSK-3α and 172 nM for GSK-3β), showed decreased inhibitory activity compared to the ester **6c** (Scheme 2). Conversion of the carboxylic acids to the amides **8c**−**d** and **9c**−**e** resulted in an increased activity. Especially, compound **8c** showed good inhibitory property against GSK-3β with a remaining kinase activity of 9% at 10 μM (Table 2). These results and the molecular modeling suggested that compounds containing polar groups at the 4-position were less active than compounds containing hydrophobic groups. Hence, we tried to elongate our compounds with a phenyl ring at the 4-position. Compounds bearing a phenyl group in the para-position showed very good inhibitory activity. The docking analysis of the biphenylic derivatives suggested several hydrophobic contacts, which may be responsible for the enhanced potency. Especially, compound **15a** with an IC_{50} value of <5 nM for GSK-3α and GSK-3β was found to be a potent inhibitor of GSK-3 (Table 3). Slightly decreased activity was observed for compound **14a** with an IC_{50} value of 9 nM for GSK-3α and 176 nM for GSK-3β. We observed an IC_{50} of 2 nM for GSK-3α and 22 nM for GSK-3β for structure **14b**, whereas **14c**, which lacks the fluorine substituent, resulted in slightly decreased IC_{50} values in comparison to **14b**.

The selectivity for the GSK-3α isoform was higher when the substituents were absent in the series **14a**−**c**. The absence of selectivity for GSK-3α in **15a** in comparison with **14c** may be explained by the interaction with Y134 (see Molecular Modeling), which seems to be lost in **14c**. Remarkably, compound **14d** displayed up to 52-fold selectivity in the inhibition of GSK-3α versus GSK-3β. This selectivity was even enhanced with compound **15b**, which is characterized by an IC_{50} of 2 nM for GSK-3α and 185 nM for GSK-3β. Thus, only the interplay respectively of a combination of different substituents was adequate to gain selectivity against one GSK-3 isoform. This observation will be helpful if a discrimination of one GSK-3 isoform is needed. In addition, the physiological functions and pathological roles of GSK-3α can be addressed in vitro and eventually in vivo with these tools. The biphenyl derivative **16a** from the pyridine series showed remarkably increased activity in comparison to the used reference **7d**, 20-fold for GSK-3α, and 19-fold for GSK-3β (Table 1). The effect of the second phenyl suggested an interaction with the glycine-rich loop, such an interaction was reported to have significant effects on binding potency and selectivity recently.[41] Furthermore, the SAR and molecular modeling suggested that an electron-withdrawing group in the ortho position of the second phenyl ring, such as the cyano-group, contributes to the inhibitory activity by interaction with the amino acid T138. We examined different linker systems on the dihydrobenzodioxine moiety with the aim to enhance the interaction with the backbone. Unfortunately, they do not provide any further

Table 1. Inhibitory Activity against GSK-3α and GSK-3β, IC_{50} (μM)

Compound	GSK-3α	GSK-3β	Compound	GSK-3α	GSK-3β
5a	0.015	0.065	**7a**	3.206	3.162
5b	0.015	0.130	**7b**	7.379	10.0
6a	0.095	0.086	**7c**	2.244	1.318
6b	0.045	0.166	**7d**	0.390	0.790
6c	0.012	0.036	**8e**	0.107	0.172

interaction (see Molecular Modeling). The effect of the methoxy group on compound **23a** resulted in an IC_{50} value of 54 nM for GSK-3α and 233 nM for GSK-3β, respectively, 195 nM and 758 nM for compound **23b**. In the case of **23c**, good inhibitory activity was observed against both isoforms of GSK-3, especially for GSK-3α. These results suggest that the *R*-enantiomer **23b** is the distomer of this compound, whereas the *S*-enantiomer **23c** was found to be the eutomer. Despite our expectations that an amine may improve the activity, compound **26** showed markedly reduced potency.

The potent GSK-3 inhibitors **6c**, **14a–d**, **15a–b**, **16a**, and **23a–c** were selected for selectivity profiling and tested against four structurally related protein kinases (Cdk5/p35, CK1ε, AurKA, and PKCα).

Good selectivity was obtained for all compounds tested. Particularly, the biphenyl derivatives **14c**, **15a**, and **16a** showed more than 2000-fold selectivity against these kinases (Table 4). Compound **14d** was not just GSK-3α selective, it was even more selective over the other kinases than compound **15b**. The broader selectivity of compound **14d** was screened at a concentration of 1 μM against 50 human protein kinases (Figure 3); 48 out of the 50 kinases in this panel showed an activity higher than 80%, whereas GSK-3α displayed a residual activity of 5% only. The only kinase which was also significantly inhibited by this compound was GSK-3β with a remaining activity of 27.2%. Therefore, it can be concluded that, within the test panel, compound **14d** is a selective inhibitor of GSK-3α. A bioavailability profile of compound **14d** was evaluated,

Table 2. Inhibitory Activity against GSK-3β at 10 μM

Compound	GSK-3β activity in %	Compound	GSK-3β activity in %	Compound	GSK-3β activity in %
5c	17	**8c**	9	**9c**	37
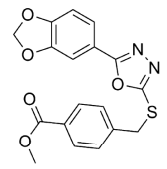		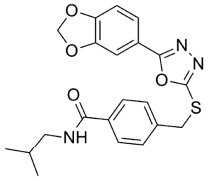		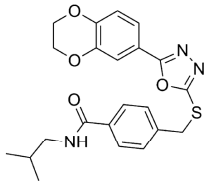	
6c	21	**8d**	31	**9d**	65
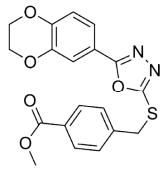		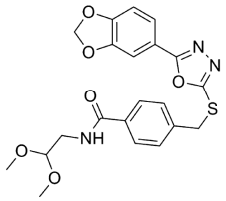		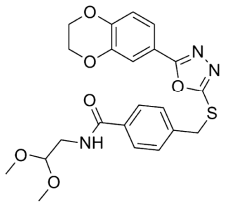	
8a	81	**9a**	102	**9e**	71
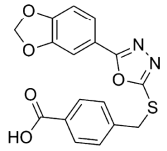		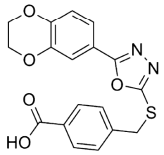		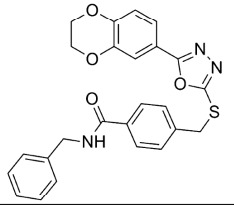	

and the results are shown in the Supporting Information. **14d** possesses a log *D* value of 3.58 and moderate metabolic stability. Nevertheless, the poor aqueous solubility and permeability are adverse properties which limit the potential use of the compound.

The biphenyl derivatives **14c−d**, **15a−b**, and **16a** were further tested for their in vivo activity on wild-type zebrafish embryos. We exposed the embryos to these compounds at early stages of development. The embryos were collected and maintained in E2 medium at ∼28 °C. The compounds were added 5 h post fertilization (hpf), and the phenotypes compared at 44−48 hpf. Compound **14c** causes the eyeless phenotype at 0.5 μM and a stunted and crooked tail at 1 μM. Similar phenotypes were obtained for compound **15a** at 2.5 μM and for compound **16a** at 20 μM (Figure 4). This correlates with the observation that Wnt signaling, and thus GSK-3β plays a crucial role in the development of metazoan and that known GSK-3 inhibitors like LiCl and the ruthenium complex (*R*)-**7** perturb the zebrafish development.[44,45] The zebrafish embryo assay provides evidence of exposure and cell penetration of the biphenyl derivatives, especially for compound **14c**. Interestingly, compounds **14d** and **15b** showed no effect on wild-type zebrafish embryos, suggesting that GSK-3α plays a minor role in the zebrafish Wnt signaling pathway. The lack of response in the zebrafish assay by compounds **14d** and **15b** may be explained by poor cell permeability. However, the structurally analogues compounds **14c** and **15a**, which are characterized by comparable solubility, did result in a GSK-3β-phenotype. Thus, the comparison of these compounds **14c**/**15a** and **14d**/**15b** does not support poor exposure and cell penetration as the dominant factors on the in vivo assay of the α-selective inhibitors. The inhibition of GSK-3α was proposed to regulate β-adrenergic signaling in mice, thus we monitored the heart development of the zebrafish embryo after administration of compound **14d** until day 5 (see the Supporting Information).[15,46] However, no effect was observed until the fifth day of development. All compounds displayed no lethality in our concentration range (<30 μM).

SH-SY5Y neuroblastoma cells stably transfected with Tau.P301L were incubated with increasing concentrations of compounds **14c** and **15a** (0, 30, and 100 μM) for 6 and 24 h. Cells were analyzed for total protein tau by Western blotting with antibody Tau5, directed against nonphosphorylated protein tau. In addition, the same samples were probed with a selection of phospho-specific antibodies that recognize typical GSK-3 dependent epitopes on protein tau. Moreover, the electrophoretic mobility of protein tau is a reliable index of the degree of phosphorylation of protein Tau.P301L: the lesser mobile isoforms carry the most phosphate groups (Figure 5).

Both compounds dose- and time-dependently decreased the phosphorylation of protein tau, expressed relatively to total tau, as demonstrated by the decreased immunoreaction with antibodies pS199, pT231, pS396, and pS404 in Western blotting (Figure 5). Moreover, the marked increase in electrophoretic mobility of the various phospho-isoforms of protein tau induced by treatment of the stably transfected SH-SY5Y cells corroborates their effectiveness in preventing phosphorylation on typical GSK-3 dependent epitopes. The comparison of the biphenyl derivatives indicated that compound **14c** is more effective in preventing phosphorylation than compound **15a**.

Table 3. Inhibitory Activity of the Biphenyls against GSK-3α and GSK-3β, IC_{50} (μM)

Compound	GSK-3α	GSK-3β	Compound	GSK-3α	GSK-3β
14a	0.009	0.176	**15b**	0.002	0.185
14b	0.002	0.022	**16a**	0.019	0.041
14c	< 0.005	0.039	**23a**	0.054	0.233
14d	0.006	0.316	**23b**	0.195	0.758
15a	< 0.005	< 0.005	**23c**	0.015	0.129

This correlates with the observations made in the zebrafish embryo assay in which **14c** showed the best results.

CONCLUSION

On the basis of a simplified scheme of known and important interactions of GSK-3 inhibitors with the ATP binding pocket, we generated hypotheses for improved interaction of with this site. These hypotheses were challenged by three series of structurally closely related inhibitors which are all based on a central oxadiazole moiety. An appropriate decoration resulted in a more extended occupation of the ATP binding site. The most potent inhibitors displayed IC_{50} values in the low nanomolar range and good kinase selectivity versus four closely related kinases. Several inhibitors showed reported phenotypes in the zebrafish embryo assay without lethality at 30 μM. In addition, two inhibitors decreased the phosphorylation of tau protein in SH-SY5Y cells. The docking analysis of the potent inhibitors suggested an interaction with the glycine-rich loop, which was reported to have significant effects on the binding potency and selectivity by Li Feng et al.[41] To our knowledge, the selective inhibition of GSK-3α versus GSK-3β by the compounds **14d** and **15b** is the highest reported so far. In addition, compound **14d** did not show any strong inhibition for 48 out of 50 kinases. The contribution of GSK-3α and GSK-3β to the pathology of Alzheimer's disease is still subject of an ongoing debate.[47,48] Thus, these compounds may be useful tools and starting points for the synthesis of GSK-3α selective inhibitors with enhanced pharmacokinetic properties.

Table 4. Kinase Selectivity of Several Derivatives

	IC_{50} (μM)					
compd	GSK-3α	GSK-3β	Cdk5/p35	CK1ε	AurKA	PKCα
6c	0.012	0.036	>100	>100	>100	>100
14a	0.009	0.176	>100	>100	>100	>100
14b	0.003	0.022	>100	20	30	>100
14c	<0.005	0.039	>100	>100	>100	>100
14d	0.006	0.316	>100	60	30	>100
15a	<0.005	<0.005	>100	>100	>100	>100
15b	0.002	0.185	>100	>100	5	>100
16a	0.019	0.041	>100	>100	>100	>100
23a	0.054	0.233	>100	>100	30	>100
23b	0.195	0.758	>100	>100	>100	>100
23c	0.015	0.129	>100	>100	>100	>100

EXPERIMENTAL SECTION

General Information. All reactions using anhydrous conditions were carried out under argon atmosphere with dry solvents unless otherwise noted. All commercial chemicals were used without further purification. The ^{1}H NMR spectra were recorded on a Bruker AC 300 spectrometer at 300 MHz and Bruker AC 500 spectrometer at 500 MHz. The ^{13}C NMR spectra were recorded on a Bruker AC 300 spectrometer at 75 MHz and Bruker AC 500 spectrometer at 125 MHz. Chemical shifts are reported as ppm downfield from Me_4Si. Abbreviations used to explain the multiplicities: s = singlet, d = doublet, t = triplet, q = quartet, n = nonett, m = multiplet, br = broad. Coupling constants (J values) are given in hertz (Hz). Mass spectrometry was performed on a Bruker−Franzen Esquire LC mass spectrometer and a MAT 95 double focusing sector field MS. Microwave experiments were carried out using a Biotage Initiator microwave apparatus. All microwave experiments were carried out in sealed microwave process vials utilizing the standard absorbance level (300 W maximum power). High performance liquid chromatographies (HPLC) were carried out on an Agilent 1100 (column: reversed phase, Zorbax Eclipse XDB-C18, 4.6 mm × 150 mm; 254 nm). Solvent gradient = 90% A at 0 min, 30% A at 2 min, 10% A at 5 min; solvent A = 0.1% trifluoroacetic acid in water; solvent B = acetonitrile; flow rate 1.0 mL/min; temperature 35 °C. Flash column chromatography was carried out using Merck silica gel 60 (40−63 and 15−40 μm) and 60G (5−40 μm). Thin-layer chromatography (TLC) was carried out using aluminum sheets precoated with silica gel 60 F254 (0.2 mm; E. Merck). All compounds that were evaluated in biological assays had >95% purity using the HPLC method described above.

General Procedure A: Coupling of Aromatic Rings by a Suzuki Reaction (12a−d).[49] To a solution of the aryl bromide **11** (5 mmol) in 15 mL of toluene/EtOH (1/1) was added 0.17 g (0.14 mmol) of $Pd(PPh_3)_4$, and the mixture was stirred under argon atmosphere. Then 2 N aqueous Na_2CO_3 (7.5 mL) and 0.80 g (6 mmol) of 2-tolylboronic acid **10** were added. The mixture was refluxed at 80 °C for 1−2 days until reaction was completed (TLC). After cooling to room temperature, the product was diluted with water and extracted with EtOAc. The organic layers were dried with $MgSO_4$, filtered, and concentrated. Purification was performed by column chromatography using a mixture of cyclohexane/EtOAc.

General Procedure B: Bromination at the Benzylic Position (13a−d).[49] To a stirred solution of the appropriately substituted toluene in CCl_4 (10 mL per mmol) were added 0.95 equiv of NBS and AIBN (5 mg per mmol). The reaction mixture was refluxed at 80 °C for about 40 h and then cooled to room temperature. The product was diluted with water and extracted with EtOAc. The organic layers were dried with $MgSO_4$, filtered, and concentrated. Purification was performed by column chromatography using a mixture of cyclohexane/EtOAc.

Methyl Benzo[*d*][1,3]dioxole-5-carboxylate (2A). To a stirred solution of benzo[*d*][1,3]dioxole-5-carboxylic acid (1.66 g, 10 mmol) in MeOH (20 mL) was added $SOCl_2$ (1.45 mL, 20 mmol) dropwise over 1 h at 0 °C. The mixture solution was further stirred 12 h at 50 °C. The mixture was cooled to room temperature and diluted with water (25 mL). MeOH was evaporated and the pH adjusted to ~6 with aqueous $NaHCO_3$. The mixture was extracted three times

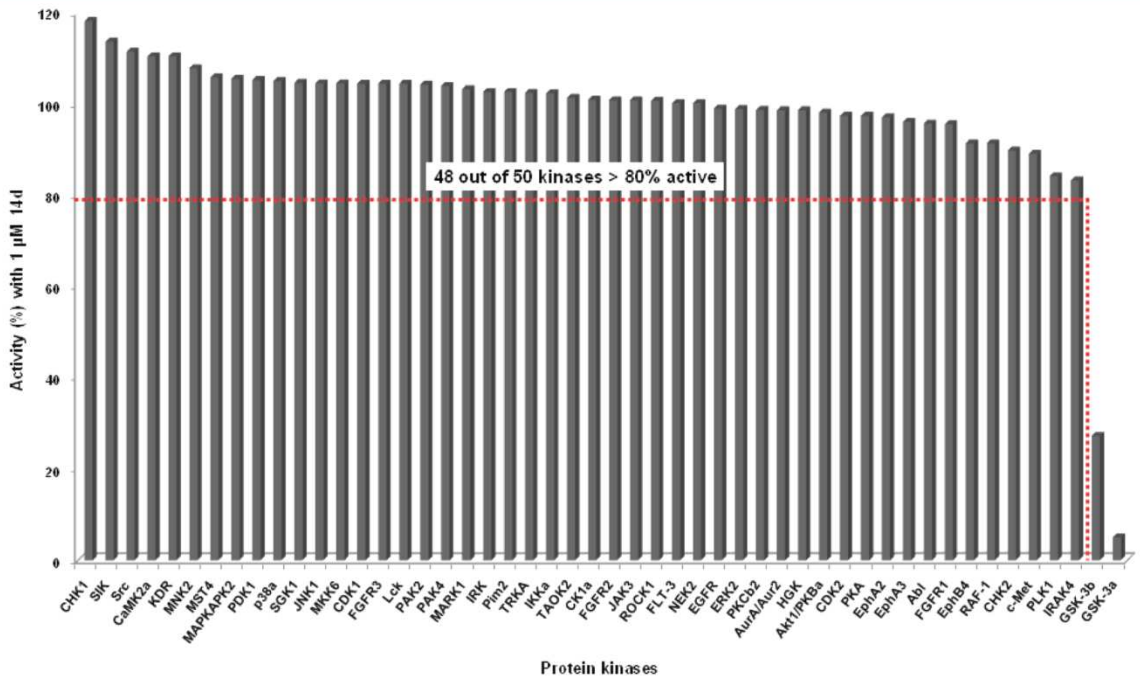

Figure 3. Screening of compound **14d** against a panel of human protein kinases. Each bar represents the activity of one individual protein kinase. Compound **14d** was tested at a concentration of 1 μM against 50 protein kinases. See Supporting Information for more details.

dx.doi.org/10.1021/jm300309a | J. Med. Chem. 2012, 55, 4407−4424

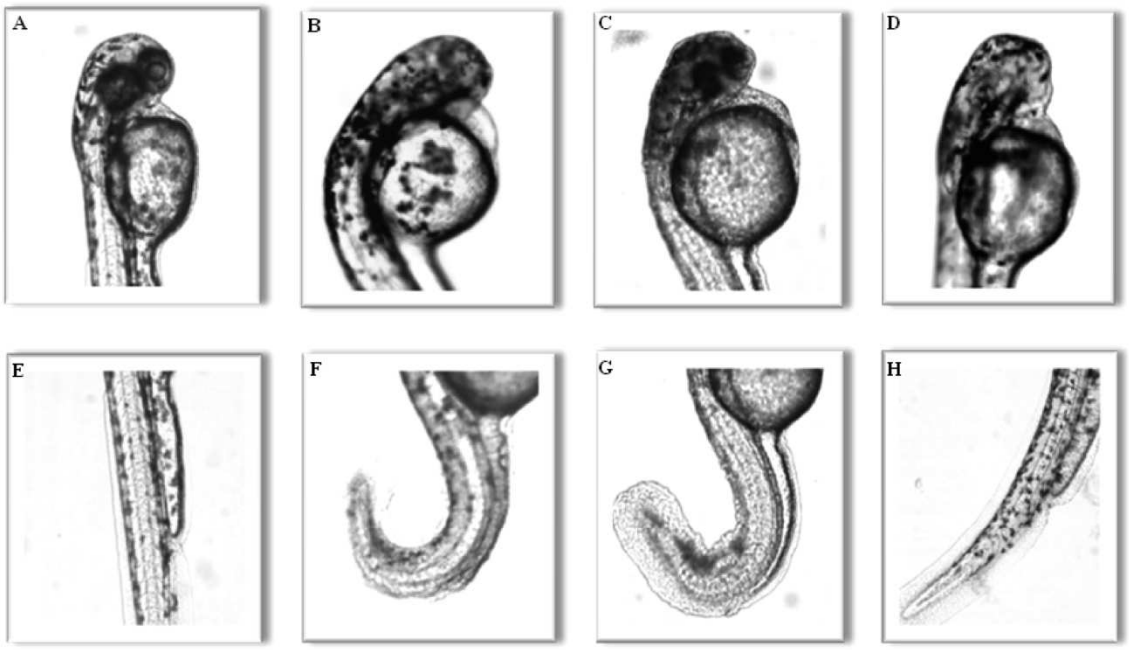

Figure 4. Effects on wild-type zebrafish embryos by compounds **14c**, **15a**, and **16a**. The embryos were collected and maintained in E2 medium at ~28 °C, compounds were added 5 hpf, and the phenotypes were compared at 44−48 hpf. (A,E) Head and tail of control embryos: DMSO (2%). (B,F) Head and tail of embryos treated with **14c**. This compound causes the eyeless phenotype at 0.5 μM and a stunted and crooked tail at 1.0 μM. (C,G) Head and tail of embryos treated with **15a**. A fluffy eye pigmentation and a stunted and crooked tail were observed at 2.5 μM. (D,H) Head and tail of embryos treated with **16a**. This compound causes the eyeless phenotype and a crooked tail at 20 μM.

with EtOAc and successively washed with brine. The organic layer was dried over $MgSO_4$ and concentrated under reduced pressure to give **2A** (1.6 g, 89%) as a colorless solid. ^{1}H NMR (DMSO-d_6, 500 MHz): δ [ppm] = 3.81 (3H, s), 6.14 (2H, s), 7.03 (1H, d, J = 8.1 Hz), 7.38 (1H, d, J = 1.7 Hz), 7.57 (1H, dd, J = 8.1 Hz, J = 1.7 Hz). ^{13}C NMR (DMSO-d_6, 125 MHz): δ [ppm] = 52.0, 102.1, 108.2, 108.5, 123.4, 125.0, 147.6, 151.4, 165.6. EI-MS: m/z = 180 (M^+).

The following compound **2B** was prepared in a similar manner to that described for **2A**.

Methyl 2,3-Dihydrobenzo[*b*][1,4]dioxine-6-carboxylate (2B). Yield 83%, colorless solid. ^{1}H NMR (DMSO-d_6, 500 MHz): δ [ppm] = 3.80 (3H, s), 4.19 (2H, m), 4.23 (2H, m), 6.80 (1H, m), 7.47 (2H, m). ^{13}C NMR (DMSO-d_6, 125 MHz): δ [ppm] = 50.5, 62.7, 63.2, 115.7, 117.6, 122.0, 141.7, 146.4, 165.2. EI-MS: m/z 194 (M^+).

Benzo[*d*][1,3]dioxole-5-carbohydrazide (3A). To a solution of **2A** (1.08 g, 6.0 mmol) in EtOH (30 mL) was added hydrazine hydrate (2.91 mL, 60 mmol), and the mixture was heated at reflux for 2 days. After cooling to room temperature, pure crystals are formed, collected by filtration, and washed several times with EtOH to give compound **3A** (0.72 g, 67%) as a colorless solid. ^{1}H NMR (DMSO-d_6, 500 MHz): δ [ppm] = 4.42 (2H, s), 6.07 (2H, s), 6.96 (1H, d, J = 8.1 Hz), 7.35 (1H, d, J = 1.7 Hz), 7.42 (1H, dd, J = 8.1 Hz, J = 1.7 Hz), 9.59 (1H, s). ^{13}C NMR (DMSO-d_6, 125 MHz): δ [ppm] = 101.5, 106.9, 107.8, 121.8, 127.2, 147.2, 149.5, 165.2. EI-MS: m/z = 180 (M^+).

Compound **3B** was prepared in a similar manner to that described for **3A**.

2,3-Dihydrobenzo[*b*][1,4]dioxine-6-carbohydrazide (3B). Yield 75%, light-yellow solid. ^{1}H NMR (methanol-d_4, 500 MHz): δ [ppm] = 4.28 (2H, m), 4.30 (2H, m), 6.89 (1H, d, J = 8.3 Hz), 7.30 (1H, dd, J = 8.3 Hz, J = 2.1 Hz), 7.33 (1H, d, J = 2.1 Hz), NH signals were not observed. ^{13}C NMR (methanol-d_4, 125 MHz): δ [ppm] = 65.9, 66.3, 117.9, 118.6, 121.9, 127.5, 145.2, 148.6, 169.6. EI-MS: m/z 194 (M^+).

5-(Benzo[*d*][1,3]dioxol-5-yl)-1,3,4-oxadiazole-2-thiol (4A). To a solution of **3A** (535 mg, 3.00 mmol) in EtOH (5 mL) were added carbon disulfide (397 μL, 6.60 mmol) and NEt_3 (469 μL, 3.30 mmol), and the mixture was heated at reflux overnight. The reaction mixture was diluted with EtOAc, and the organic layer was washed with 0.1 N HCl and brine and dried over Na_2SO_4. The solvent was evaporated under reduced pressure, and the obtained residue was recrystallized from cyclohexane/EtOAc to give **4A** (521 mg, 79%) as a pale-yellow solid. ^{1}H NMR (DMSO-d_6, 500 MHz): δ [ppm] = 6.14 (2H, s), 7.10 (1H, d, J = 8.1 Hz), 7.33 (1H, d, J = 1.6 Hz), 7.42 (1H, dd, J = 8.1 Hz, J = 1.6 Hz), SH signal was not observed. ^{13}C NMR (DMSO-d_6, 125 MHz): δ [ppm] = 102.1, 105.6, 109.1, 116.1, 121.5, 148.1, 150.6, 160.3, 177.2. EI-MS: m/z = 222 (M^+).

The compounds **4B−C** were prepared in a similar manner to that described for **4A**.

5-(2,3-Dihydrobenzo[*b*][1,4]dioxin-6-yl)-1,3,4-oxadiazole-2-thiol (4B). Yield 89%, light-brown solid. ^{1}H NMR (DMSO-d_6, 500 MHz): δ [ppm] = 4.32 (2H, m), 4.34 (2H, m), 7.05 (1H, d, J = 8.4 Hz), 7.30 (1H, d, J = 2.0 Hz), 7.36 (1H, dd, J = 8.4 Hz, J = 2.0 Hz), SH signal was not observed. ^{13}C NMR (DMSO-d_6, 125 MHz): δ [ppm] = 64.4, 64.8, 115.0, 115.7, 118.6, 120.0, 144.2, 147.3, 160.6, 177.6. EI-MS: m/z = 236 (M^+).

5-(Pyridin-4-yl)-1,3,4-oxadiazole-2-thiol (4C). Yield 83%, yellow solid. ^{1}H NMR (DMSO-d_6, 500 MHz): δ [ppm] = 7.81 (2H, dd, J = 4.4 Hz, J = 1.6 Hz), 8.81 (2H, dd, J = 4.4 Hz, J = 1.6 Hz), SH signal was not observed. ^{13}C NMR (DMSO-d_6, 125 MHz): δ [ppm] = 119.6, 129.7, 150.8, 158.7, 177.8. EI-MS: m/z = 179 (M^+).

3-((5-Benzo[*d*][1,3]dioxol-5-yl)-1,3,4-oxadiazol-2-ylthio)-methyl)benzonitrile (5a). To a solution of **4A** (55 mg, 0.25 mmol) and 1 N NaOH (0.25 mL, 0.25 mmol) in DMF (1 mL) was added 1-(bromomethyl)-3-methoxybenzene (75 mg, 0.38 mmol) at room temperature, and the mixture was stirred for 5 h. The precipitate formed was collected by filtration and washed once with less DMF (~1 mL) and thereafter several times with EtOH to give compound **5a** (55 mg, 64%) as a brown solid. ^{1}H NMR (DMSO-d_6, 500 MHz): δ [ppm] = 4.61 (2H, s), 6.16 (2H, s), 7.10 (1H, d, J = 8.1 Hz), 7.41 (1H, d, J = 1.4 Hz), 7.47 (1H, dd, J = 8.1 Hz, J = 1.5 Hz), 7.57 (1H, t,

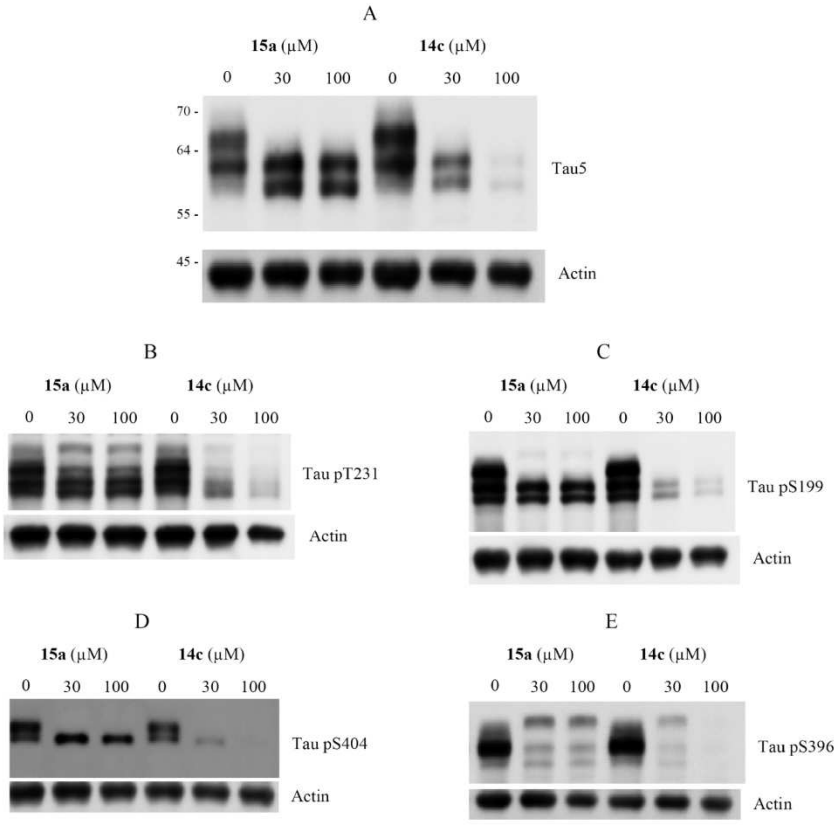

Figure 5. Western blotting for protein Tau.P301L expressed in stably transfected SH-SY5Y neuorblastoma cells, untreated (lanes marked 0) or treated for 6 h with compounds **14c** or **15a** (lanes marked 30 and 100 μM). Total protein tau was detected with antibody Tau5 (A). Phospho-epitopes on protein tau were detected with specific antibodies (B–E). Experiments were performed in triplicate, and representative blots are shown. Similar observations were obtained after 24 h of incubation. Note that compound **14c** specifically decreases the total concentration of protein tau, while levels of the internal marker (actin) remain unchanged.

J = 7.7 Hz), 7.76 (1H, d, J = 7.7 Hz), 7.84 (1H, d, J = 7.8 Hz), 7.96 (1H, s). ^{13}C NMR (DMSO-d_6, 125 MHz): δ [ppm] = 34.7, 102.1, 106.1, 109.1, 111.4, 116.6, 118.5, 121.7, 129.8, 131.4, 132.6, 133.9, 138.8, 148.1, 150.4, 162.2, 165.2. HPLC: 98%; t_R 7.21 min. EI-MS: m/z = 337 (M^+).

The compounds **5b–c**, **6a–c**, and **7a–c** were prepared in a similar manner to that described for **5a**. Note: Compounds which did not precipitate in solution were purified as follows. The reaction mixture was diluted with EtOAc and the organic layer was washed with water and brine, dried over $MgSO_4$, and concentrated in vacuo. The residue was purified by silica gel column chromatography (cyclohexane/EtOAc).

4-((5-Benzo[*d*][1,3]dioxol-5-yl)-1,3,4-oxadiazol-2-ylthio)-methyl)benzonitrile (5b). Yield 67%, brown solid. ^{1}H NMR (DMSO-d_6, 500 MHz): δ [ppm] = 4.64 (2H, s), 6.16 (2H, s), 7.11 (1H, d, J = 8.1 Hz), 7.42 (1H, d, J = 1.6 Hz), 7.48 (1H, dd, J = 8.1 Hz, J = 1.7 Hz) 7.68 (2H, d, J = 8.3 Hz), 7.82 (2H, d, J = 8.3 Hz). ^{13}C NMR (DMSO-d_6, 125 MHz): δ [ppm] = 35.2, 102.1, 106.1, 109.1, 110.4, 116.5, 118.6, 121.7, 130.0, 132.4, 142.8, 148.1, 150.5, 162.2, 165.2. HPLC: 95%; t_R 7.09 min. EI-MS: m/z = 337 (M^+).

Methyl 4-((5-(Benzo[*d*][1,3]dioxol-5-yl)-1,3,4-oxadiazol-2-ylthio)methyl Benzoate (5c). Yield 71%, pale-brown solid. ^{1}H NMR (DMSO-d_6, 500 MHz): δ [ppm] = 3.82 (3H, s), 4.63 (2H, s), 6.15 (2H, s), 7.10 (1H, d, J = 8.1 Hz), 7.41 (1H, d, J = 1.7 Hz), 7.48 (1H, dd, J = 8.1 Hz, J = 1.7 Hz), 7.62 (2H, d, J = 8.4 Hz), 7.92 (2H, d, J = 8.4 Hz). ^{13}C NMR (DMSO-d_6, 125 MHz): δ [ppm] = 35.4, 52.2, 102.2, 106.1, 109.2, 116.6, 121.7, 128.8, 129.4, 142.4, 148.1, 150.4, 162.3, 165.1, 165.9. HPLC: 96%; t_R 7.61 min. EI-MS: m/z = 370 (M^+).

3-((5-(2,3-Dihydrobenzo[*b*][1,4]dioxin-6-yl)-1,3,4-oxadiazol-2ylthio)methyl)benzonitrile (6a). Yield 73%, light-brown solid. ^{1}H NMR (DMSO-d_6, 500 MHz): δ [ppm] = 4.31 (2H, m), 4.34 (2H, m), 4.61 (2H, s), 7.05 (1H, d, J = 8.4 Hz), 7.39 (1H, d, J = 2.0 Hz), 7.42 (1H, dd, J = 8.4 Hz, J = 2.1 Hz), 7.57 (1H, t, J = 7.8 Hz), 7.77 (1H, dt, J = 7.8 Hz, J = 1.3 Hz), 7.84 (1H, dt, J = 7.8 Hz, J = 1.1 Hz), 7.96 (1H, t, J = 1.3 Hz). ^{13}C NMR (DMSO-d_6, 125 MHz): δ [ppm] = 35.2, 64.5, 64.7, 111.8, 115.5, 116.3, 118.5, 118.9, 120.4, 130.1, 131.8, 133.0, 134.4, 139.3, 144.2, 147.1, 162.7, 165.5. HPLC: 99%; t_R 7.53 min. EI-MS: m/z = 351 (M^+).

4-((5-(2,3-Dihydrobenzo[*b*][1,4]dioxin-6-yl)-1,3,4-oxadiazol-2-ylthio)methyl)benzonitrile (6b). Yield 56%, brown solid. ^{1}H NMR (DMSO-d_6, 500 MHz): δ [ppm] = 4.31 (2H, m), 4.34 (2H, m), 4.63 (2H, s), 7.05 (1H, d, J = 8.4 Hz), 7.37 (1H, d, J = 2.0 Hz), 7.41 (1H, dd, J = 8.4 Hz, J = 2.0 Hz), 7.67 (2H, d, J = 8.3 Hz), 7.81 (2H, d, J = 8.3 Hz). ^{13}C NMR (DMSO-d_6, 125 MHz): δ [ppm] = 35.3, 64.0, 64.4, 110.4, 115.0, 115.8, 118.2, 118.6, 119.9, 130.0, 132.4, 142.8, 143.8, 146.7, 162.2, 165.0. HPLC: 95%; t_R 7.49 min. EI-MS: m/z = 351 (M^+).

Methyl 4-((5-(2,3-Dihydrobenzo[*b*][1,4]dioxin-6-yl)-1,3,4-oxadiazol-2-ylthio)methyl) Benzoate (6c). Yield 49%, purple solid. ^{1}H NMR (DMSO-d_6, 500 MHz): δ [ppm] = 3.89 (3H, s), 4.36 (2H, m), 4.39 (2H, m), 4.67 (2H, s), 7.10 (1H, d, J = 8.4 Hz), 7.42 (1H, d, J = 2.0 Hz), 7.47 (1H, dd, J = 8.4 Hz, J = 2.0 Hz), 7.67 (2H, d, J = 8.3 Hz), 7.97 (2H, d, J = 8.3 Hz). ^{13}C NMR (DMSO-d_6, 125 MHz): δ [ppm] = 35.4, 52.1, 64.0, 64.4, 115.0, 115.8, 118.1, 120.0, 128.9, 129.4, 142.4, 143.8, 146.7, 162.3, 165.0, 165.8. HPLC: 99%; t_R 7.66 min.

dx.doi.org/10.1021/jm300309a | J. Med. Chem. 2012, 55, 4407–4424

EI-MS: m/z = 384 (M^+). HRMS (EI): m/z calcd for $C_{19}H_{16}N_2O_5S$ 384.0780, found 384.0809.

3-((5-(Pyridin-4-yl)-1,3,4-oxadiazol-2-ylthio)methyl)-benzonitrile (7a). Yield 41%, yellow solid. ^{1}H NMR (DMSO-d_6, 500 MHz): δ [ppm] = 4.66 (2H, s), 7.58 (1H, t, J = 7.8 Hz), 7.78 (1H, dt, J = 7.7 Hz, J = 1.3 Hz), 7.86 (1H, t, J = 1.2 Hz), 7.88 (2H, dd, J = 4.4 Hz, J = 1.6 Hz), 7.99 (1H, t, J = 1.4 Hz), 8.82 (2H, dd, J = 4.4 Hz, J = 1.6 Hz). ^{13}C NMR (DMSO-d_6, 125 MHz): δ [ppm] = 34.8, 111.4, 118.5, 120.0, 129.8, 130.0, 131.5, 132.7, 134.0, 138.6, 150.9, 163.8, 164.4. HPLC: 96%; t_R 4.51 min. EI-MS: m/z = 294 (M^+).

4-((5-(Pyridin-4-yl)-1,3,4-oxadiazol-2-ylthio)methyl)-benzonitrile (7b). Yield 77%, pale-yellow solid. ^{1}H NMR (DMSO-d_6, 500 MHz): δ [ppm] = 4.69 (2H, s), 7.71 (2H, d, J = 8.2 Hz), 7.83 (2H, d, J = 8.2 Hz), 7.88 (2H, dd, J = 4.4 Hz, J = 1.6 Hz), 8.82 (2H, dd, J = 4.5 Hz, J = 1.5 Hz). ^{13}C NMR (DMSO-d_6, 125 MHz): δ [ppm] = 35.2, 110.5, 118.6, 120.0, 130.0, 130.1, 132.4, 142.6, 150.8, 163.9, 164.4. HPLC: 95%; t_R 4.51 min. EI-MS: m/z = 294 (M^+).

2-(Benzylthio)-5-(pyridin-4-yl)-1,3,4-oxadiazole (7c). Yield 79%, light-yellow solid. ^{1}H NMR (DMSO-d_6, 500 MHz): δ [ppm] = 4.62 (2H, s), 7.30 (1H, m), 7.36 (2H, m), 7.50 (2H, m), 7.90 (2H, dd, J = 4.4 Hz, J = 1.6 Hz), 8.82 (2H, dd, J = 4.4 Hz, 1.6 Hz). ^{13}C NMR (DMSO-d_6, 125 MHz): δ [ppm] = 35.8, 120.0, 127.8, 128.6, 129.1, 130.0, 136.4, 150.8, 163.6, 164.7. HPLC: 100%; t_R 4.89 min. EI-MS: m/z = 269 (M^+).

2-(3-Iodobenzylthio)-5-(pyridin-4-yl)-1,3,4-oxadiazole (7d). **7d** was used as reference. It is commercially available from Calbiochem (361541 GSK-3β Inhibitor II; CAS number, 478482-75-6).

4-((5-(Benzo[*d*][1,3]dioxol-5-yl)-1,3,4-oxadiazol-2-ylthio)-methyl)benzoic Acid (8a). Methyl 4-((5-(benzo[*d*][1,3]dioxol-5-yl)-1,3,4-oxadiazol-2-ylthio)methyl benzoate **5c** (300 mg, 0.81 mmol) was added in 5 mL of a 2 N lithium hydroxide−tetrahydrofuran solution. The reaction mixture was stirred overnight at 60 °C under an argon atmosphere. The reaction mixture was diluted with water and neutralized with 1 N HCl. Afterward, EtOAc was added and the organic layer was washed with water and brine, dried over $MgSO_4$, and concentrated in vacuo to give **8a** (239 mg, 83%) as a rose solid. ^{1}H NMR (DMSO-d_6, 500 MHz): δ [ppm] = 4.56 (2H, s), 6.08 (2H, s), 7.04 (1H, d, J = 8.1 Hz), 7.35 (1H, d, J = 1.6 Hz), 7.43 (1H, dd, J = 8.1 Hz, J = 1.7 Hz), 7.53 (2H, d, J = 8.2 Hz), 7.84 (2H, d, J = 8.2 Hz), 12.8 (1H, s, br). ^{13}C NMR (DMSO-d_6, 125 MHz): δ [ppm] = 35.4, 102.1, 106.1, 109.1, 116.6, 121.7, 129.1, 129.5, 130.4, 141.7, 148.1, 150.4, 162.4, 165.1, 166.9. HPLC: 99%; t_R 6.15 min. EI-MS: m/z = 356 (M^+).

Compound **9a** was prepared in a similar manner to that described for **8a**.

Methyl 4-((5-(2,3-Dihydrobenzo[*b*][1,4]dioxin-6-yl)-1,3,4-oxadiazol-2-ylthio)methyl)benzoic Acid (9a). Yield 91%, colorless solid. ^{1}H NMR (DMSO-d_6, 500 MHz): δ [ppm] = 4.31 (2H, m), 4.34 (2H, m), 4.62 (2H, s), 7.05 (1H, d, J = 8.4 Hz), 7.38 (1H, d, J = 2.0 Hz), 7.43 (1H, dd, J = 8.4 Hz, J = 2.1 Hz), 7.59 (2H, d, J = 8.3 Hz), 7.91 (2H, d, J = 8.3 Hz), 12.95 (1H, s). ^{13}C NMR (DMSO-d_6, 125 MHz): δ [ppm] = 35.4, 64.1, 64.4, 115.1, 115.7, 118.2, 119.8, 129.3, 129.5, 130.1, 141.9, 143.8, 146.7, 162.4, 165.0, 166.8. HPLC: 96%; t_R 6.22 min. EI-MS: m/z = 370 (M^+).

4-((5-(Benzo[*d*][1,3]dioxol-5-yl)-1,3,4-oxadiazol-2-ylthio)-methyl)-*N*-isobutylbenzamide (8c). A mixture of 4-((5-(benzo-[*d*][1,3]dioxol-5-yl)-1,3,4-oxadiazol-2-ylthio)methyl)benzoic acid **8a** (100 mg, 0.28 mmol) and thionyl chloride (30.5 μL, 0.42 mmol) was refluxed in dry toluene (1 mL) for about 2 h. Excess thionyl chloride was removed by repeated evaporation in vacuo with fresh dry toluene (3 × 1 mL). 2-Methylpropan-1-amine (27.8 μL, 0.28 mmol) and K_2CO_3 (38 mg, 0.28 mmol) were added in dry acetone (1 mL) cooled to 0 °C and stirred for 30 min. The crude acyl chloride was dissolved in dry acetone (0.5 mL) and added dropwise to the solution. After the addition was complete, stirring continued for 2 h. The reaction mixture was then diluted with water, extracted three times with EtOAc, and successively washed with brine. The organic layer was dried over $MgSO_4$ and concentrated under reduced pressure. The obtained residue was recrystallized from EtOH to give **8c** (90 mg, 81%) as a beige solid. ^{1}H NMR (DMSO-d_6, 500 MHz): δ [ppm] = 0.86 (6H, d, J = 6.7 Hz), 1.81 (1H, n, J = 6.7 Hz), 3.05 (2H, t, J = 6.7 Hz), 4.60 (2H, s), 6.16 (2H, s), 7.10 (1H, d, J = 8.1 Hz), 7.43 (1H, d, J = 1.6 Hz), 7.50 (1H, dd, J = 8.1 Hz, J = 1.7 Hz), 7.54 (2H, d, J = 8.2 Hz), 7.78 (2H, d, J = 8.3 Hz), 8.42 (1H, t, J = 5.7 Hz). ^{13}C NMR (DMSO-d_6, 125 MHz): δ [ppm] = 20.2, 28.0, 35.4, 46.6, 102.1, 106.1, 109.2, 116.6, 121.8, 127.5, 128.8, 134.1, 139.8, 148.1, 150.5, 162.4, 165.1, 165.8. HPLC: 95%; t_R 7.11 min. EI-MS: m/z = 411 (M^+).

The following compounds **8d** and **9c−e** were prepared in a similar manner to that described for **8c**.

4-((5-(Benzo[*d*][1,3]dioxol-5-yl)-1,3,4-oxadiazol-2-ylthio)-methyl)-*N*-(2,2-dimethoxyethyl)benzamide (8d). Yield 79%, light-yellow solid. ^{1}H NMR (DMSO-d_6, 500 MHz): δ [ppm] = 3.27 (6H, s), 3.33 (2H, br), 4.48 (1H, t, J = 5.6 Hz), 4.61 (2H, s), 6.16 (2H, s), 7.11 (1H, d, J = 8.1 Hz), 7.44 (1H, d, J = 1.7 Hz), 7.50 (1H, dd, J = 8.1 Hz, J = 1.7 Hz), 7.55 (2H, d, J = 8.1 Hz), 7.80 (2H, d, J = 8.1 Hz), 8.52 (1H, t, J = 5.7 Hz). ^{13}C NMR (DMSO-d_6, 125 MHz): δ [ppm] = 35.4, 41.1, 53.2, 101.8, 102.2, 106.2, 109.2, 116.6, 121.7, 127.5, 128.9, 133.5, 140.1, 148.1, 150.4, 162.4, 165.1, 166.0. HPLC: 95%; t_R 6.07 min. EI-MS: m/z = 443 (M^+).

4-((5-(2,3-Dihydrobenzo[*b*][1,4]dioxin-6-yl)-1,3,4-oxadiazol-2-ylthio)methyl)-*N*-isobutyl Benzamide (9c). Yield 92%, light-brown solid. ^{1}H NMR (DMSO-d_6, 500 MHz): δ [ppm] = 0.93 (6H, d, J = 6.7 Hz), 1.88 (1H, n, J = 6.7 Hz), 3.12 (2H, t, J = 6.6 Hz), 4.37 (2H, m), 4.39 (2H, m), 4.66 (2H, s), 7.10 (1H, d, J = 8.4 Hz), 7.45 (1H, d, J = 2.0 Hz), 7.48 (1H, dd, J = 8.4 Hz, J = 2.0 Hz), 7.60 (2H, d, J = 8.2 Hz), 7.85 (2H, d, J = 8.2 Hz), 8.46 (1H, t, J = 5.7 Hz). ^{13}C NMR (DMSO-d_6, 125 MHz): δ [ppm] = 20.2, 28.1, 35.4, 46.6, 64.1, 64.4, 115.0, 115.8, 118.1, 119.9, 127.4, 128.8, 134.1, 139.7, 143.8, 146.7, 162.4, 164.9, 165.8. HPLC: 96%; t_R 7.16 min. EI-MS: m/z = 425 (M^+).

4-((5-(2,3-Dihydrobenzo[*b*][1,4]dioxin-6-yl)-1,3,4-oxadiazol-2-ylthio)methyl)-*N*-(2,2-dimethoxy ethyl)benzamide (9d). Yield 84%, beige solid. ^{1}H NMR (DMSO-d_6, 500 MHz): δ [ppm] = 3.28 (6H, s), 3.35 (2H, d, J = 5.7 Hz), 4.31 (2H, m), 4.34 (2H, m), 4.50 (1H, t, J = 5.6 Hz), 4.61 (2H, s), 7.05 (1H, d, J = 8.3 Hz), 7.40 (1H, d, J = 2.0 Hz), 7.43 (1H, dd, J = 8.3 Hz, J = 2.0 Hz), 7.55 (2H, d, J = 8.2 Hz), 7.81 (2H, d, J = 8.2 Hz), 8.52 (1H, t, J = 5.8 Hz). ^{13}C NMR (DMSO-d_6, 125 MHz): δ [ppm] = 35.4, 41.1, 53.2, 64.0, 64.4, 101.8, 115.0, 105.8, 108.2, 119.9, 127.4, 128.8, 133.5, 140.0, 143.8, 146.7, 162.4, 164.9, 165.9. HPLC: 95%; t_R 6.13 min. EI-MS: m/z = 457 (M^+).

***N*-Benzyl-4-((5-(2,3-dihydrobenzo[*b*][1,4]dioxin-6-yl)-1,3,4-oxadiazol-2-ylthio)methyl)benzamide (9e).** Yield 89%, beige solid. ^{1}H NMR (DMSO-d_6, 500 MHz): δ [ppm] = 4.31 (2H, m), 4.34 (2H, m), 4.47 (2H, d, J = 5.9 Hz), 4.62 (2H, s), 7.05 (1H, d, J = 8.4 Hz), 7.23 (1H, m), 7.32 (4H, m), 7.40 (1H, d, J = 2.0 Hz), 7.43 (1H, dd, J = 8.3 Hz, J = 2.0 Hz), 7.56 (2H, d, J = 8.2 Hz), 7.86 (2H, d, J = 8.2 Hz), 9.01 (1H, t, J = 5.9 Hz). ^{13}C NMR (DMSO-d_6, 125 MHz): δ [ppm] = 35.4, 42.6, 64.1, 64.4, 115.1, 115.8, 118.3, 119.8, 126.7, 127.3, 127.5, 128.4, 128.8, 133.7, 139.6, 140.1, 143.8, 146.7, 162.4, 165.0, 165.8. HPLC: 95%; t_R 7.66 min. EI-MS: m/z = 459 (M^+).

2-(4-(1*H*-Tetrazol-5-yl)benzylthio)-5-(benzo[*d*][1,3]dioxol-5-yl)-1,3,4-oxadiazole (8e). 4-((5-Benzo[*d*][1,3]dioxol-5-yl)-1,3,4-oxadiazol-2-ylthio)methyl)benzonitrile **5b** (34 mg, 0.10 mmol), NaN_3 (78 mg, 1.20 mmol), and NH_4Cl (64 mg, 1.20 mmol) were added to 1 mL of DMF and stirred for 5 h at 100 °C under microwave irradiation. After cooling to room temperature, the reaction solution was added to water (2−3 mL), acidified with 2 N HCl, and extracted three times with ethyl acetate. The combined organic layers were dried over Na_2SO_4, filtered, and the solvent evaporated off to provide **8e** (25 mg, 67%) as a beige solid. ^{1}H NMR (DMSO-d_6, 500 MHz): δ [ppm] = 4.65 (2H, s), 6.15 (2H, s), 7.11 (1H, d, J = 8.1 Hz), 7.43 (1H, d, J = 1.6 Hz), 7.50 (1H, dd, J = 8.1 Hz, J = 1.7 Hz), 7.71 (2H, d, J = 8.3 Hz), 8.00 (2H, d, J = 8.3 Hz), NH signal was not observed. ^{13}C NMR (DMSO-d_6, 125 MHz): δ [ppm] = 35.4, 102.1, 105.0, 106.2, 108.9, 109.1, 116.6, 119.7, 121.7, 127.1, 130.0, 148.1, 150.4, 162.4, 165.1. HPLC: 96%; t_R 5.92 min. EI-MS: m/z = 380 (M^+).

Compound **9f** was prepared in a similar manner to that described for **8e**.

2-(4-(1*H*-Tetrazol-5-yl)benzylthio)-5-(2,3-dihydrobenzo[*d*]-[1,4]dioxin-5-yl)-1,3,4-oxadiazole (9f). Yield 79%, puce solid. ^{1}H NMR (DMSO-d_6, 500 MHz): δ [ppm] = 4.35 (2H, m), 4.38 (2H, m), 4.70 (2H, s), 7.10 (1H, d, J = 8.4 Hz), 7.43 (1H, d, J = 2.0 Hz),

7.47 (1H, dd, J = 8.4 Hz, J = 2.1 Hz), 7.75 (2H, d, J = 8.3 Hz), 8.05 (2H, d, J = 8.3 Hz), NH signal was not observed. ^{13}C NMR (DMSO-d_6, 125 MHz): δ [ppm] = 35.5, 64.0, 64.4, 115.0, 115.8, 118.2, 119.9, 123.6, 127.1, 130.0, 140.1, 143.8, 146.7, 162.4, 165.1. HPLC: 95%; t_R 6.01 min. EI-MS: m/z = 394 (M^+).

The following compounds **14a−d**, **15a−b**, and **16a** were prepared in a similar manner to that described for **5a**.

2-(Benzo[*d*][1,3]dioxol-5-yl)-5-(biphenyl-4-ylmethylthio)-1,3,4-oxadiazole (14a). Yield 75%, beige solid. ^{1}H NMR (DMSO-d_6, 500 MHz): δ [ppm] = 4.55 (2H, s), 6.08 (2H, s), 7.04 (1H, d, J = 8.1 Hz), 7.28 (1H, m), 7.38 (3H, m), 7.45 (1H, dd, J = 8.1 Hz, J = 1.7 Hz), 7.48 (2H, d, J = 8.3 Hz), 7.58 (4H, m). ^{13}C NMR (DMSO-d_6, 125 MHz): δ [ppm] = 35.6, 102.1, 106.2, 109.1, 116.6, 121.7, 126.6, 126.8, 127.6, 128.9, 129.7, 135.8, 139.6, 148.1, 150.5, 162.6, 165.1. HPLC: 95%; t_R 9.12 min. EI-MS: m/z = 388 (M^+).

4′-((5-(Benzo[*d*][1,3]dioxol-5-yl)-1,3,4-oxadiazol-2-ylthio)-methyl)biphenyl-2-carbonitrile (14b). Yield 71%, brown solid. ^{1}H NMR (DMSO-d_6, 500 MHz): δ [ppm] = 4.66 (2H, s), 6.15 (2H, s), 7.11 (1H, d, J = 8.1 Hz), 7.45 (1H, d, J = 1.7 Hz), 7.51 (1H, dd, J = 8.1 Hz, J = 1.7 Hz), 7.57 (2H, d, J = 8.2 Hz), 7.65 (4H, m), 7.96 (1H, dd, J = 8.5 Hz, J = 2.3 Hz). ^{13}C NMR (DMSO-d_6, 125 MHz): δ [ppm] = 35.5, 102.1, 106.1, 109.1, 111.5, 111.6, 116.6, 117.3, 117.4, 120.3, 120.5, 121.0, 121.2, 121.7, 129.0, 129.4, 132.3, 132.4, 136.2, 137.5, 140.8, 140.9, 148.1, 150.4, 159.9, 161.9, 162.6, 165.1. HPLC: 95%; t_R 8.77 min. EI-MS: m/z = 431 (M^+). HRMS (EI): m/z calcd for $C_{23}H_{14}N_3O_3FS$ 431.0740, found 431.0728.

4-((5-(Benzo[*d*][1,3]dioxol-5-yl)-1,3,4-oxadiazol-2-ylthio)-methyl)-4-fluorobiphenyl-2-carbonitrile (14c). Yield 69%, gray solid. ^{1}H NMR (DMSO-d_6, 500 MHz): δ [ppm] = 4.66 (2H, s), 6.16 (2H, s), 7.11 (1H, d, J = 8.1 Hz), 7.45 (1H, d, J = 1.7 Hz), 7.51 (1H, dd, J = 8.1 Hz, J = 1.7 Hz), 7.56 (2H, d, J = 8.2 Hz), 7.65 (4H, m), 7.78 (1H, td, J = 7.7 Hz, J = 1.3 Hz), 7.95 (1H, dd, J = 7.7 Hz, J = 0.9 Hz). ^{13}C NMR (DMSO-d_6, 125 MHz): δ [ppm] = 35.5, 102.1, 106.1, 109.1, 110.1, 116.6, 118.5, 121.7, 128.3, 128.9, 129.4, 130.1, 133.5, 133.8, 137.2, 137.4, 140.0, 148.1, 150.4, 162.6, 165.1. HPLC: 96%; t_R 8.36 min. EI-MS: m/z = 413 (M^+). HRMS (EI): m/z calcd for $C_{23}H_{15}N_3O_3S$ 413.0835, found 413.0804.

4′-((5-(Benzo[*d*][1,3]dioxol-5-yl)-1,3,4-oxadiazol-2-ylthio)-methyl)biphenyl-4-carbonitrile (14d). Yield 51%, gray−brown solid. ^{1}H NMR (DMSO-d_6, 500 MHz): δ [ppm] = 4.63 (2H, s), 6.15 (2H, s), 7.10 (1H, d, J = 8.1 Hz), 7.43 (1H, d, J = 1.7 Hz), 7.51 (1H, dd, J = 8.1 Hz, J = 1.7 Hz), 7.61 (2H, d, J = 8.3 Hz), 7.73 (2H, d, J = 8.3 Hz), 7.87 (2H, d, J = 8.6 Hz), 7.91 (2H, d, J = 8.6 Hz). ^{13}C NMR (DMSO-d_6, 125 MHz): δ [ppm] = 35.9, 102.6, 106.6, 109.6, 110.6, 117.1, 119.3, 122.2, 127.7, 128.0, 130.3, 133.3, 138.0, 138.1, 144.5, 148.6, 150.9, 163.0, 165.5. HPLC: 97%; t_R 8.77 min. EI-MS: m/z = 413 (M^+). HRMS (EI): m/z calcd for $C_{23}H_{15}N_3O_3S$ 413.0835, found 413.0825.

4′-((5-(2,3-Dihydrobenzo[*b*][1,4]dioxin-6-yl)-[1,3,4]oxadiazol-2-ylthio)methyl)biphenyl-2-carbonitrile (15a). Yield 74%, colorless solid. ^{1}H NMR (DMSO-d_6, 500 MHz): δ [ppm] = 4.31 (2H, m), 4.34 (2H, m), 4.65 (2H, s), 7.05 (1H, d, J = 8.4 Hz), 7.41 (1H, d, J = 2.0 Hz), 7.44 (1H, dd, J = 8.4 Hz, J = 2.0 Hz), 7.60 (6H, m), 7.79 (1H, td, J = 7.7 Hz, J = 1.2 Hz), 7.95 (1H, dd, J = 7.7 Hz, J = 0.9 Hz). ^{13}C NMR (DMSO-d_6, 125 MHz): δ [ppm] = 35.9, 64.4, 64.8, 110.5, 115.4, 116.3, 118.5, 118.8, 120.3, 128.6, 129.3, 129.7, 130.5, 133.8, 134.2, 137.5, 137.8, 144.1, 144.3, 147.1, 163.0, 165.3. HPLC: 100%; t_R 8.39 min. EI-MS: m/z 427 (M^+). HRMS (EI): m/z calcd for $C_{24}H_{17}N_3O_3S$ 427.0991, found 427.0962.

4′-((5-(2,3-Dihydrobenzo[*b*][1,4]dioxin-6-yl)-1,3,4-oxadiazol-2-ylthio)methyl)-4-fluorobiphenyl-2-carbonitrile (15b). Yield 29%, light-yellow solid. ^{1}H NMR (DMSO-d_6, 500 MHz): δ [ppm] = 4.32 (2H, m), 4.34 (2H, m) 4.65 (2H, s), 7.05 (1H, d, J = 8.4 Hz), 7.40 (1H, d, J = 2.1 Hz), 7.45 (1H, dd, J = 8.4 Hz, J = 2.1 Hz), 7.56 (2H, d, J = 8.2 Hz), 7.63 (2H, d, J = 8.2 Hz), 7.68 (2H, m), 7.97 (1H, dd, J = 9.0 Hz, J = 1.9 Hz). HPLC: 95%; t_R 8.76 min. EI-MS: m/z = 445 (M^+). HRMS (EI): m/z calcd for $C_{24}H_{16}N_3O_3FS$ 445.0897, found 445.0890.

4-((5-(Pyridine-4-yl)-1,3,4-oxadiazol-2-ylthio)methyl)-biphenyl-2-carbonitrile (16a). Yield 53%, colorless solid. ^{1}H NMR (DMSO-d_6, 500 MHz): δ [ppm] = 4.71 (2H, s), 7.58 (3H, m), 7.62 (1H, d, J = 7.7 Hz), 7.68 (2H, d, J = 8.1 Hz), 7.78 (1H, t, J = 7.7 Hz), 7.91 (2H, d, J = 4.1 Hz), 7.95 (1H, d, J = 7.7 Hz), 8.85 (2H, s, br). ^{13}C NMR (DMSO-d_6, 125 MHz): δ [ppm] = 35.4, 110.1, 118.5, 120.1, 128.2, 128.9, 129.4, 130.0, 130.1, 133.5, 133.7, 137.2, 137.3, 143.9, 150.8, 163.8, 164.8. HPLC: 99%; t_R 6.63 min. EI-MS: m/z = 370 (M^+). HRMS (EI): m/z calcd for $C_{21}H_{14}N_4OS$ 370.0889, found 370.0926.

Methyl 3,4-Dihydroxybenzoate (18). To a stirred solution of 3,4-dihydroxybenzoic acid (2.0 g, 13 mmol) in MeOH (25 mL) was added $SOCl_2$ (1.88 mL, 26 mmol) dropwise over 1 h at 0 °C. The solution was further stirred 12 h at 50 °C. The mixture was cooled to room temperature and diluted with water (30 mL). MeOH was evaporated and the pH adjusted to ∼6 with aqueous $NaHCO_3$. The mixture was extracted three times with EtOAc and successively washed with brine. The organic layer was dried over $MgSO_4$ and concentrated under reduced pressure to give **18** (2.1 g, 97%) as a colorless solid. ^{1}H NMR (DMSO-d_6, 500 MHz): δ [ppm] = 3.75 (3H, s), 6.80 (1H, d, J = 8.2 Hz), 7.31 (1H, dd, J = 8.2 Hz, J = 2.1 Hz), 7.35 (1H, d, J = 2.1 Hz), 9.35 (1H, s), 9.75 (1H, s). ^{13}C NMR (DMSO-d_6, 125 MHz): δ [ppm] = 51.5, 115.3, 116.2, 120.4, 121.7, 145.0, 150.4, 166.1. EI-MS: m/z = 168 (M^+).

Methyl 3-(Hydroxymethyl)-2,3-dihydrobenzo[*b*][1,4]-dioxine-6-carboxylate (19a). Methyl 3,4-dihydroxybenzoate **18** (0.8 g, 4.75 mmol) and K_2CO_3 (0.65 g, 4.75 mmol) were taken in dry acetone (10 mL) and stirred for 15 min at room temperature. Afterward, the solution was treated with epibromohydrin (0.40 mL, 4.75 mmol) and stirred overnight at 70 °C. The reaction mixture was diluted with water and extracted with EtOAc. The organic layer was washed with brine and dried over Na_2SO_4. The solvent was evaporated under reduced pressure and the crude product purified by silica gel column chromatography (DCM/EtOAc, 4:1) to give **19a** (1.01 g, 95%) as a colorless oil. ^{1}H NMR (DMSO-d_6, 500 MHz): δ [ppm] = 3.64 (2H, m), 3.80 (3H, s), 4.10 (1H, m), 4.20 (1H, m), 4.41 (1H, dd, J = 11.4 Hz, J = 2.3 Hz), 5.10 (1H, t, J = 5.7 Hz), 6.98 (1H, d, J = 8.4 Hz), 7.41 (1H, d, J = 2.0 Hz), 7.46 (1H, dd, J = 8.4 Hz, J = 2.0 Hz). ^{13}C NMR (DMSO-d_6, 125 MHz): δ [ppm] = 51.9, 59.7, 65.4, 73.6, 117.0, 117.9, 122.6, 122.7, 142.8, 147.4, 165.6. EI-MS: m/z = 224 (M^+).

Note: Alternatively (*R*/*S*)-(±)-glycidyl tosylate can be used to obtain compound **19a**. For more details see the synthesis of compound **19b−c**.

Methyl 3-(Methoxymethyl)-2,3-dihydrobenzo[*b*][1,4]-dioxine-6-carboxylate (20a). To a suspension of NaH (115 mg, 4.81 mmol) in 5 mL of anhydrous THF was added methyl 3-(hydroxymethyl)-2,3-dihydrobenzo[*b*][1,4]dioxine-6-carboxylate **19a** (900 mg, 4.01 mmol) at 0 °C. The mixture was stirred at room temperature for 30 min, followed by addition of methyl iodide (374 μL, 6.01 mmol). The reaction mixture was stirred at room temperature for 48 h, quenched with 10 mL of water, and extracted with ethyl acetate. The combined organic layer was dried over $MgSO_4$, the solvent was evaporated under reduced pressure, and the crude product purified by silica gel column chromatography (DCM/EtOAc, 20:1) to give **20a** (678 mg, 71%) as a colorless oil. ^{1}H NMR (DMSO-d_6, 500 MHz): δ [ppm] = 3.33 (3H, s), 3.60 (2H, m), 3.80 (3H, s), 4.09 (1H, m), 4.40 (2H, m), 6.99 (1H, m), 7.41 (1H, m), 7.47 (1H, m). ^{13}C NMR (DMSO-d_6, 125 MHz): δ [ppm] = 51.8, 58.7, 65.3, 70.3, 71.8, 117.0, 118.0, 122.7, 122.8, 142.6, 147.2, 165.5. EI-MS: m/z = 238 (M^+).

3-(Methoxymethyl)-2,3-dihydrobenzo[*b*][1,4]dioxine-6-carbohydrazide (21a). To a solution of **20a** (600 mg, 2.51 mmol) in EtOH (15 mL) was added hydrazine hydrate (731 μL, 15.06 mmol). and the mixture was heated at reflux for 2 days. After cooling to room temperature, the reaction mixture was diluted with water and extracted with EtOAc. The organic layer was washed with brine and dried over $MgSO_4$. The solvent was evaporated under reduced pressure and the crude product purified by silica gel column chromatography (MeOH/EtOAc, 1:10) to give **21a** (466 mg, 78%) as a colorless solid. ^{1}H NMR (DMSO-d_6, 500 MHz): δ [ppm] = 3.32 (3H, s), 3.59 (2H, m), 4.04 (1H, m), 4.36 (2H, m), 4.41 (2H, s), 6.92 (1H, d, J = 8.2 Hz), 7.35 (1H, dd, J = 8.2 Hz, J = 2.0 Hz), 7.37 (1H, d, J = 2.0 Hz), 9.52 (1H, s). ^{13}C NMR (DMSO-d_6, 125 MHz): δ [ppm] = 58.7, 65.1, 70.4, 71.8,

115.8, 116.6, 120.3, 126.5, 142.3, 145.3, 165.1. EI-MS: m/z = 238 (M^+).

Compound **22a** was prepared in a similar manner to that described for **4A**.

5-(3-(Methoxymethyl)-2,3-dihydrobenzo[*b*][1,4]dioxin-6-yl)-1,3,4-oxadiazole-2-thiol (22a). Yield 81%, orange solid. ^{1}H NMR (DMSO-d_6, 500 MHz): δ [ppm] = 3.32 (3H, s), 3.61 (2H, m), 4.10 (1H, m), 4.43 (2H, m), 7.07 (1H, m), 7.32 (1H, m), 7.37 (1H, m), 14.60 (1H, s). ^{13}C NMR (DMSO-d_6, 125 MHz): δ [ppm] = 58.7, 65.3, 70.3, 72.1, 114.6, 115.6, 118.0, 119.7, 143.4, 146.4, 160.1, 177.4. EI-MS: m/z = 280 (M^+).

Compound **23a** was prepared in a similar manner to that described for **5a**.

4′-((5-(3-(Methoxymethyl)-2,3-dihydrobenzo[*b*][1,4]dioxin-6-yl)-1,3,4-oxadiazol-2ylthio)methyl)biphenyl-2-carbonitrile (23a). Yield 88%, colorless solid. ^{1}H NMR (DMSO-d_6, 500 MHz): δ [ppm] = 3.33 (3H, s), 3.61 (2H, m), 4.10 (1H, m), 4.44 (2H, m), 4.66 (2H, s), 7.07 (1H, m), 7.45 (2H, m), 7.57 (3H, m), 7.63 (3H, m), 7.78 (1H, td, J = 7.6 Hz, J = 1.2 Hz), 7.95 (1H, dd, J = 7.7 Hz, J = 1.1 Hz). ^{13}C NMR (DMSO-d_6, 125 MHz): δ [ppm] = 35.4, 58.7, 65.2, 70.3, 72.0, 110.1, 115.1, 116.2, 118.0, 118.5, 119.9, 128.2, 128.8, 129.4, 130.1, 133.5, 133.8, 137.1, 137.4, 143.3, 143.9, 146.2, 162.6, 164.9. HPLC: 100%; t_R 8.59 min. EI-MS: m/z = 471 (M^+). HRMS (EI): m/z calcd for $C_{26}H_{21}N_3O_4S$ 471.1253, found 471.1264.

4′-((5-(3-(Hydroxymethyl)-2,3-dihydrobenzo[*b*][1,4]dioxin-6-yl)-1,3,4-oxadiazol-2-ylthio) methyl)biphenyl-2-carbonitrile (24a). To a solution of 4′-((5-(3-(methoxymethyl)-2,3-dihydrobenzo-[*b*][1,4]dioxin-6-yl)-1,3,4-oxadiazol-2ylthio)methyl)biphenyl-2-carbonitrile **23a** (400 mg, 0.85 mmol) in 10 mL of DCM was added 1 N solution of BBr_3 in hexane (850 μL, 0.85 mmol) under argon atmosphere at −78 °C. The reaction mixture was stirred at the same temperature for 1 h and allowed to warm to room temperature and further stirred for 24 h. After treatment with saturated $NaHCO_3$ solution, the reaction mixture was extracted with ethyl acetate. The combined organic layers were dried over $MgSO_4$ and concentrated under reduced pressure. The crude product was purified by silica gel column chromatography (cyclohexane/EtOAc, 1:2) to give compound **24a** (283 mg, 73%) as a light-yellow solid. ^{1}H NMR (DMSO-d_6, 500 MHz): δ [ppm] = 3.59 (1H, s, br), 3.64 (2H, m), 4.10 (1H, m), 4.24 (1H, m), 4.42 (1H, dd, J = 11.5 Hz, J = 2.2 Hz), 4.65 (2H, s) 7.06 (1H, d, J = 8.3 Hz), 7.43 (2H, m), 7.60 (6H, m), 7.78 (1H, td, J = 7.7 Hz, J = 1.2 Hz), 7.94 (1H, dd, J = 7.7 Hz, J = 1.0 Hz). ^{13}C NMR (DMSO-d_6, 125 MHz): δ [ppm] = 35.4, 59.6, 65.4, 73.7, 110.1, 115.1, 116.1, 117.9, 118.5, 119.8, 128.2, 128.8, 129.4, 130.1, 133.4, 133.8, 137.1, 137.4, 143.5, 144.0, 146.2, 162.6, 165.0. HPLC: 96%; t_R 7.39 min. EI-MS: m/z = 457(M^+).

(*R*)-Methyl 3-(Hydroxymethyl)-2,3-dihydrobenzo[*b*][1,4]-dioxine-6-carboxylate (19b). To a round-bottom flask equipped with magnetic stirring and a nitrogen inlet was added methyl-3,4-dihydroxybenzoate **18** (1.0 g, 6 mmol), (2*S*)-(+)-glycidyl tosylate (1.37 g, 6 mmol), K_2CO_3(0.99 g, 7.2 mmol), and DMF (15 mL). This mixture was heated to 60 °C for 5 h. The mixture was cooled to room temperature, diluted with water, and extracted with EtOAc. The organic layer was washed with brine and dried over Na_2SO_4. The solvent was evaporated under reduced pressure and the crude product purified by silica gel column chromatography (DCM/EtOAc, 4:1) to give **19b** (1.25 g, 93%) as a colorless oil. ^{1}H NMR (DMSO-d_6, 500 MHz): δ [ppm] = 3.64 (2H, m), 3.80 (3H, s), 4.10 (1H, m), 4.20 (1H, m), 4.41 (1H, dd, J = 11.4 Hz, J = 2.3 Hz), 5.08 (1H, t, J = 5.7 Hz), 6.98 (1H, d, J = 8.4 Hz), 7.41 (1H, d, J = 2.0 Hz), 7.46 (1H, dd, J = 8.4 Hz, J = 2.0 Hz). ^{13}C NMR (DMSO-d_6, 125 MHz): δ [ppm] = 51.9, 59.7, 65.5, 73.6, 117.0, 117.9, 122.6, 122.7, 142.8, 147.4, 165.6. HPLC: 96%; t_R 2.44 min. EI-MS: m/z = 224 (M^+).

Compound **19c** was prepared in a similar manner to that described for **19b**. (2*R*)-(−)-glycidyl tosylate was used instead of (2*S*)-(+)-glycidyl tosylate to obtain the *S*-isomer.

(*S*)-Methyl 3-(Hydroxymethyl)-2,3-dihydrobenzo[*b*][1,4]-dioxine-6-carboxylate (19c). Yield 89%, as a colorless oil. ^{1}H NMR (DMSO-d_6, 500 MHz): δ [ppm] = 3.64 (2H, m), 3.80 (3H, s), 4.10 (1H, m), 4.20 (1H, m), 4.41 (1H, dd, J = 11.4 Hz, J = 2.3 Hz), 5.10 (1H, s, br), 6.98 (1H, d, J = 8.4 Hz), 7.41 (1H, d, J = 2.0 Hz), 7.46 (1H, dd, J = 8.4 Hz, J = 2.0 Hz). ^{13}C NMR (DMSO-d_6, 125 MHz): δ [ppm] = 51.9, 59.7, 65.5, 73.6, 117.0, 117.9, 122.6, 122.7, 142.8, 147.4, 165.6. EI-MS: m/z = 224 (M^+).

Compounds **20b−c** were prepared in a similar manner to that described for **20a**.

(*R*)-Methyl 3-(Methoxymethyl)-2,3-dihydrobenzo[*b*][1,4]-dioxine-6-carboxylate (20b). Yield 68%, as a colorless oil. ^{1}H NMR (DMSO-d_6, 500 MHz): δ [ppm] = 3.33 (3H, s), 3.60 (2H, m), 3.81 (3H, s), 4.09 (1H, m), 4.40 (2H, m), 6.99 (1H, d, J = 8.4 Hz), 7.42 (1H, d, J = 2.0 Hz), 7.47 (1H, dd, J = 8.4 Hz, J = 2.0 Hz). ^{13}C NMR (DMSO-d_6, 125 MHz): δ [ppm] = 51.9, 58.7, 65.3, 70.3, 71.8, 117.1, 117.9, 122.8, 122.9, 142.6, 147.3, 165.6. EI-MS: m/z = 238 (M^+).

(*S*)-Methyl 3-(Methoxymethyl)-2,3-dihydrobenzo[*b*][1,4]-dioxine-6-carboxylate (20c). After extraction and evaporation of the solvent, compound **20c** was used without further purification.

Compounds **21b−c** were prepared in a similar manner to that described for **21a**.

(*R*)-3-(Methoxymethyl)-2,3-dihydrobenzo[*b*][1,4]dioxine-6-carbohydrazide (21b). Yield 87%, as a colorless solid. ^{1}H NMR (DMSO-d_6, 500 MHz): δ [ppm] = 3.32 (3H, s), 3.59 (2H, m), 4.04 (1H, m), 4.36 (2H, m), 4.41 (2H, s), 6.92 (1H, d, J = 8.3 Hz), 7.35 (1H, dd, J = 8.3 Hz, J = 2.0 Hz), 7.37 (1H, d, J = 2.0 Hz), 9.57 (1H, s). ^{13}C NMR (DMSO-d_6, 125 MHz): δ [ppm] = 58.7, 65.1, 70.4, 71.7, 115.8, 116.6, 120.4, 126.6, 142.3, 145.3, 165.1. EI-MS: m/z = 238 (M^+).

(*S*)-3-(Methoxymethyl)-2,3-dihydrobenzo[*b*][1,4]dioxine-6-carbohydrazide (21c). Yield 92%, as a colorless solid. ^{1}H NMR (DMSO-d_6, 500 MHz): δ [ppm] = 3.32 (3H, s), 3.59 (2H, m), 4.04 (1H, m), 4.36 (2H, m), 4.41 (2H, s), 6.92 (1H, d, J = 8.3 Hz), 7.36 (1H, dd, J = 8.3 Hz, J = 2.0 Hz), 7.37 (1H, d, J = 2.0 Hz), 9.57 (1H, s). ^{13}C NMR (DMSO-d_6, 125 MHz): δ [ppm] = 58.7, 65.1, 70.4, 71.8, 115.8, 116.6, 120.4, 126.6, 142.3, 145.3, 165.2. EI-MS: m/z = 238 (M^+).

Compounds **22b−c** were prepared in a similar manner to that described for **4A**.

(*R*)-5-(3-(Methoxymethyl)-2,3-dihydrobenzo[*b*][1,4]dioxin-6-yl)-1,3,4-oxadiazole-2-thiol (22b). Yield 91%, orange solid. ^{1}H NMR (DMSO-d_6, 500 MHz): δ [ppm] = 3.33 (3H, s), 3.61 (2H, m), 4.10 (1H, m), 4.42 (2H, m), 7.07 (1H, m), 7.31 (1H, m), 7.37 (1H, m), 14.62 (1H, s). ^{13}C NMR (DMSO-d_6, 125 MHz): δ [ppm] = 58.8, 65.3, 70.2, 72.1, 114.6, 115.6, 118.0, 119.7, 143.3, 146.4, 160.1, 177.2. EI-MS: m/z = 280 (M^+).

(*S*)-5-(3-(Methoxymethyl)-2,3-dihydrobenzo[*b*][1,4]dioxin-6-yl)-1,3,4-oxadiazole-2-thiol (22c). Yield 91%, orange solid. ^{1}H NMR (DMSO-d_6, 500 MHz): δ [ppm] = 3.33 (3H, s), 3.61 (2H, m), 4.09 (1H, m), 4.39 (2H, m), 7.02 (1H, m), 7.24 (1H, m), 7.30 (1H, m), SH signal was not observed. ^{13}C NMR (DMSO-d_6, 125 MHz): δ [ppm] = 58.6, 65.3, 70.0, 72.1, 114.6, 115.6, 117.7, 119.7, 143.3, 146.4, 160.1, 177.2. EI-MS: m/z = 280 (M^+).

Compounds **23b−c** were prepared in a similar manner to that described for **5a**.

(*R*)-4′-((5-(3-(Methoxymethyl)-2,3-dihydrobenzo[*b*][1,4]-dioxin-6-yl)-1,3,4-oxadiazol-2-ylthio) methyl)biphenyl-2-carbonitrile (23b). Yield 84%, colorless solid. ^{1}H NMR (DMSO-d_6, 500 MHz): δ [ppm] = 3.38 (3H, s), 3.66 (2H, m), 4.15 (1H, m), 4.47 (2H, m), 4.71 (2H, s), 7.13 (1H, m), 7.50 (2H, m), 7.65 (6H, m), 7.82 (1H, td, J = 7.7 Hz, J = 1.3 Hz), 8.00 (1H, dd, J = 7.7 Hz, J = 0.9 Hz). ^{13}C NMR (DMSO-d_6, 125 MHz): δ [ppm] = 35.4, 58.7, 65.2, 70.4, 72.0, 110.1, 115.1, 116.2, 118.0, 118.4, 119.9, 128.2, 128.8, 129.4, 130.1, 133.5, 133.8, 137.2, 137.4, 143.2, 143.9, 146.2, 162.6, 164.9. HPLC: 99%; t_R 8.70 min. EI-MS: m/z = 471 (M^+).

(*S*)-4′-((5-(3-(Methoxymethyl)-2,3-dihydrobenzo[*b*][1,4]-dioxin-6-yl)-1,3,4-oxadiazol-2-ylthio) methyl)biphenyl-2-carbonitrile (23c). Yield 84%, colorless solid. ^{1}H NMR (DMSO-d_6, 500 MHz): δ [ppm] = 3.33 (3H, s), 3.61 (2H, m), 4.10 (1H, m), 4.42 (2H, m), 4.66 (2H, s), 7.07 (1H, m), 7.44 (2H, m), 7.60 (6H, m), 7.78 (1H, td, J = 7.6 Hz, J = 1.3 Hz), 7.94 (1H, dd, J = 7.7 Hz, J = 0.9 Hz). ^{13}C NMR (DMSO-d_6, 125 MHz): δ [ppm] = 35.2, 58.7, 65.2, 70.1, 71.9, 110.1, 115.1, 116.2, 117.9, 118.4, 119.9, 128.2, 128.6, 129.4, 130.1, 133.5, 133.8, 137.2, 137.4, 143.2, 143.9, 146.2, 162.6, 164.9.

Table 5. Small Kinase Panel Values

kinase	enzyme conc (nM)	ATP conc (μM)	peptide used	peptide conc (μM)	buffer
GSK-3β	2	12.5	Ser/Thr 9 peptide	2	50 mM Hepes pH 7.5, 10 mM $MgCl_2$, 1 mM EGTA, 0.01% (w/v) Brij-35
GSK-3α	0.5	12.5	Ser/Thr 9 peptide	2	50 mM Hepes pH 7.5, 10 mM $MgCl_2$, 1 mM EGTA, 0.01% (w/v) Brij-35
CKIε	12	32	Ser/Thr 11 peptide	2	50 mM Hepes pH 7.5, 10 mM $MgCl_2$, 1 mM EGTA, 0.01% (w/v) Brij-35
Cdk5	10	12.5	Ser/Thr 12 peptide	2	50 mM Hepes pH 7.5, 10 mM $MgCl_2$, 1 mM EGTA, 0.01% (w/v) Brij-35
AurKA	20	10	Ser/Thr 1 peptide	2	50 mM Hepes pH 7.5, 10 mM $MgCl_2$, 1 mM EGTA, 0.01% (w/v) Brij-35
PKCα	0.15	10	Ser/Thr 7 peptide	2	50 mM Hepes pH 7.5, 10 mM $MgCl_2$, 1 mM EGTA, 0.01% (w/v) Brij-35

HPLC: 100%; t_R 8.65 min. EI-MS: m/z = 471 (M^+). HRMS (EI): m/z calcd for $C_{26}H_{21}N_3O_4S$ 471.1253, found 471.1269.

Compound **24b** was prepared in a similar manner to that described for **24a**.

(*R*)-4′-((5-(3-(Hydroxymethyl)-2,3-dihydrobenzo[*b*][1,4]-dioxin-6-yl)-1,3,4-oxadiazol-2-ylthio) methyl)biphenyl-2-carbonitrile (24b). Yield 79%, light-yellow solid. ^{1}H NMR (DMSO-d_6, 500 MHz): δ [ppm] = 3.40 (1H, s, br), 3.59 (2H, m), 4.04 (1H, m), 4.15 (1H, m), 4.34 (1H, dd, J = 11.5 Hz, J = 2.3 Hz), 4.57 (2H, s), 6.98 (1H, d, J = 8.3 Hz), 7.35 (2H, m), 7.53 (6H, m), 7.70 (1H, td, J = 7.7 Hz, J = 1.3 Hz), 7.85 (1H, dd, J = 7.7 Hz, J = 0.9 Hz). ^{13}C NMR (DMSO-d_6, 125 MHz): δ [ppm] = 35.4, 59.6, 65.4, 73.7, 110.1, 115.0, 116.1, 117.9, 118.5, 119.8, 128.2, 128.8, 129.3, 130.1, 133.4, 133.8, 137.1, 137.4, 143.5, 144.0, 146.2, 162.5, 164.9. HPLC: 95%; t_R 7.48 min. EI-MS: m/z = 457 (M^+).

(*S*)-((7-(5-(2′-Cyanobiphenyl-4-yl)methylthio)-1,3,4-oxadiazol-2-yl)-2,3-dihydrobenzo[*b*][1,4] dioxin-2-yl)-methylmethanesulfonate (25). To a solution of **24b** (238 mg, 0.52 mmol) in 10 mL of DCM was added Et_3N (0.72 mL, 5.2 mmol) followed by addition of methanesulfonyl chloride (402 μL, 5.2 mmol) at 0 °C. The reaction mixture was stirred at the same temperature for 1 h and further stirred at room temperature for 4 h. After treating with saturated $NaHCO_3$ solution, the reaction mixture was extracted with DCM. The combined organic layer was dried over $MgSO_4$, concentrated, and purified by column chromatography (EtOAc/cyclohexane, 1:1) to provide **25** (273 mg, 98%) yellow oil. ^{1}H NMR (DMSO-d_6, 500 MHz): δ [ppm] = 3.26 (3H, s), 4.17 (1H, m), 4.45 (1H, m), 4.50 (1H, dd, J = 11.6 Hz, J = 2.4 Hz), 4.55 (1H, dd, J = 11.6 Hz, J = 3.3 Hz), 4.62 (1H, m), 4.67 (2H, s), 7.11 (1H, d, J = 8.1 Hz), 7.48 (2H, m), 7.61 (6H, m), 7.77 (1H, td, J = 7.6 Hz, J = 1.3 Hz), 7.95 (1H, dd, J = 7.7 Hz, J = 0.8 Hz). ^{13}C NMR (DMSO-d_6, 125 MHz): δ [ppm] = 35.4, 36.8, 64.3, 67.8, 70.9, 110.1, 115.2, 116.4, 118.2, 118.5, 120.3, 128.2, 128.8, 129.4, 130.1, 133.5, 133.8, 137.1, 137.4, 142.7, 143.9, 145.9, 162.7, 164.9. HPLC: 96%; t_R 8.46 min. EI-MS: m/z = 535 (M^+).

(*R*)-4′-((5-(3-((2,2-Dimethoxyethylamino)methyl)-2,3-dihydrobenzo[*b*][1,4]dioxin-6-yl)-1,3,4-oxadiazol-2-ylthio)-methyl)biphenyl-2-carbonitrile (26). To a stirred solution of **25** (69 mg, 0.13 mmol) in 2 mL of THF was added 2,2-dimethoxyethylamine (140 μL, 1.3 mmol) and NEt_3 (180 μL, 1.3 mmol) at 0 °C, and the reaction mixture was stirred at room temperature for 5 days. The mixture was diluted with water and extracted with EtOAc. The organic layer was washed with brine and dried over $MgSO_4$. The solvent was evaporated under reduced pressure and the crude product purified by silica gel column chromatography (MeOH/EtOAc, 1:10) to give **26** (58 mg, 83%) as a dark-yellow oil. ^{1}H NMR (DMSO-d_6, 500 MHz): δ [ppm] = 1.91 (1H, m), 2.61 (2H, dd, J = 5.4 Hz, J = 0.7 Hz), 2.80 (2H, m), 3.18 (3H, s), 3.19 (3H, s), 4.00 (1H, m), 4.17 (1H, m), 4.30 (2H, m), 4.54 (2H, s), 6.87 (1H, m), 7.32 (2H, m), 7.44 (1H, dd, J = 7.6 Hz, J = 1.2 Hz), 7.46 (3H, m), 7.52 (2H, m), 7.64 (1H, td, J = 7.8 Hz, J = 1.3 Hz), 7.74 (1H, m). ^{13}C NMR (DMSO-d_6, 125 MHz): δ [ppm] = 36.7, 50.2, 52.1, 53.8, 53.9, 67.7, 74.1, 104.9, 111.8, 116.5, 117.8, 118.7, 119.1, 120.8, 129.0, 130.0, 130.4, 131.1, 134.1, 134.7, 138.4, 138.8, 144.7, 145.4, 147.6, 163.7, 166.3. HPLC: 95%; t_R 6.34 min. EI-MS: m/z = 544 (M^+).

GSK-3β in Vitro Assay. Purified GSK-3β (0.5 μg) was incubated in a reaction mixture of 50 mM Tris pH 7.3, 10 mM $MgAc_2$, 0.01% β-mercaptoethanol, ^{32}P[γ-ATP](100 μM, 0.5 μci/assay), and 100 μM of peptide substrate, pIRS-1 (RREGGMSRPAS(p)VDG (1). New molecules were added at various concentrations (1, 10, and 100 μM), and the reaction mixture was incubated for 15 min at 30 °C. The reactions were stopped, spotted on p81 paper (Whatman), washed with 10 mM phosphoric acid, and counted for radioactivity.[50] GSK-3β activity was calculated as the percentage of GSK-3β activity in the absence of inhibitor that was designated to 100%.

Small Kinase Panel. Compounds were serially diluted 1/3 in neat DMSO (10 serial dilutions), and these dilutions were further diluted 1/25 with reaction buffer. Then 2.5 μL of these solutions were added to the reaction mixture described below so that final compound concentration in the assay ranges from 100 μM to 5 nM in 1% (v/v) DMSO. When compounds showed high inhibition at 5 nM and therefore the data could not be fitted to the corresponding equation, they were re-evaluated in a new range from 400 nM to 20 pM (Table 5).

The enzymatic activity of the kinases was determined with a commercial system based on the Z′-LYTE technology, available from Invitrogen Life Technologies (Carlsbad, CA, USA), using human recombinant kinases as the enzyme source. This technology utilizes the fluorescence resonance energy transfer ("FRET") process between fluorescein and coumarin. The assay principle is based on the differential sensitivity of phosphorylated and nonphosphorylated peptide to proteolytic cleavage, which precludes the energy transfer process between the two fluorophores attached to both sides of the cleavage site. Hence, enzymatic phosphorylation will yield a phosphopeptide, which cannot be hydrolyzed by a suitable protease and energy transfer between the two fluorophores will occur. Opposingly, lack of phosphorylation will cause peptide hydrolysis hence lack of energy transfer as. The assay was performed in 96-well black plates, in a final volume of 10 μL, with components as detailed in Tables 1, 3, and 4.

In Vivo Activity on Zebrafish Embryos. The wt zebrafish was used in this study. The embryos were collected and placed into 24-well plates, 10 embryos per well, and maintained in E2 medium at ~28 °C. Compounds were added 5 hpf (50% epiboly) and the embryos allowed to grow in chemical compound solution up to 2 days. The phenotypes were compared using the Axio Scope.A1 microscope system from Carl Zeiss at 44−48 hpf.[36,37,S1]

Animal Husbandry. All animal experiment were conducted and documented according to the federal and local regulation. All embryo testing was stopped at day 5 of embryonic development.

SH-SY5Y Neuroblastoma Cells. SH-SY5Y neuroblastoma cells stably transfected with Tau.P301L in the pcDNA3 vector were grown to confluency in 6-well cluster plates (~800000 cells/well) in DMEM-F12 medium supplemented with Glutamax and 15% fetal calf serum. The medium contained gentamycin (50 μg/mL) as general antibiotic and Geneticin (250 μg/mL) to maintain selection pressure on transfected cells. Cells were grown at 37 °C in a humidified incubator in an atmosphere of 5.0% CO_2 in air. Stock solutions of the

compounds in DMSO were added to serum-free culture medium to the specified concentrations, using DMSO in the same final concentrations as control. Cells were incubated with the compounds at 37 °C for the indicated periods of time. After incubation, spent medium was removed and cells washed once with PBS containing Ca^{2+} and Mg^{2+}. The cells were rapidly harvested by mechanical scraping after addition of hot 62.5 mM Tris pH 6.8 buffer, containing 1% SDS (180 μL per well). Protein extracts were collected by aspiration and reduced and denatured by addition of 1% β-mercaptoethanol and boiling for 10 min. After separation by SDS-PAGE on 10% Tris-glycine SDS-PAGE, proteins were analyzed by Western blotting using the ECL-system.[52] In brief, after SDS-PAGE, the separated proteins were transferred to nitrocellulose filter-sheets, which were treated against nonspecific binding by incubation in 5% nonfat milk in Tris buffered saline (TBS: 10 mM Tris.HCl, pH 7.2, 0.9% sodium chloride, 0.1% Tween). Blots were subsequently incubated with primary antibodies specifically directed against total protein tau or against its selected phosphorylated epitopes, as specified in Results and Discussion and in the figure legends. After incubation with suitably labeled secondary antibodies, the resulting immune reactions were recorded and analyzed digitally with dedicated apparatus and software (LAS4000, Image-QuantTL, GE Healthcare, Brussels, Belgium). Data for tau and phospho-tau were normalized against actin, revealed by Western blotting of the same samples on the same blots.

Docking Simulations. Molecular docking of **15a** into the X-ray structure of GSK-3β (PDB code: 3F88) was carried out using the Glide 5.5 program.[53] Maestro 9.0.211 was employed as the graphical user interface, and Figure 2 was rendered by the Chimera software package.[54,55]

Ligand and Protein Setup. The inhibitor structure was first generated through the Dundee PRODRG2 server.[56] Then geometry optimized ligand was prepared using Lig-Prep 2.3 as implemented in Maestro. The target protein was prepared through the Protein Preparation Wizard of the graphical user interface Maestro and the OPLS-2001 force field. Water molecules were removed. Hydrogen atoms were added, and minimization was performed until the rmsd of all heavy atoms was within 0.3 Å of the crystallographically determined positions. The binding pocket was identified by placing a 20 Å cube centered on the mass center of the cocrystallized inhibitor. Molecular docking calculations were performed with the aid of Glide 5.5 in extra-precision (XP) mode, using Glidescore for ligand ranking.[57,58] For multiple ligand docking experiments, an output maximum of 5000 ligand poses per docking run with a limit of 100 poses for each ligand was adopted.

Homology Modeling. The homology model was built using the crystal structure of GSK-3β (PDB code: 3F88). The sequence identity between GSK-3α and GSK-3β is 61%. The alignment was performed by Prime, which calculates alignments using a combination of sequence and secondary structure information. The sequence of the human GSK-3α was obtained from the Universal Protein Resource (http://www.uniprot.org/) (code: P49840) and aligned using Prime. The homology model was inspected to ensure that the side chains of the conserved residues were aligned to the template.

■ ASSOCIATED CONTENT

Ⓢ Supporting Information

Homology modeling, in vitro pharmacology, bioavailability profile of compound **14d** and NMR data of compounds **5b**, **5c**, **6b**, **6c**, **14b**, **14c**, **14d**, **15a**, **15b**, **16a**, **23a**, **23b**, and **23c**. This material is available free of charge via the Internet at http://pubs.acs.org.

■ AUTHOR INFORMATION

Corresponding Author

*Phone: +496151-164531. Fax: +496151-163278. E-mail: schmidt_boris@t-online.de (B.S.); Fabio.Lo-Monte@gmx.de (F.L.).

Notes

The authors declare no competing financial interest.

■ ACKNOWLEDGMENTS

This work was supported by a collaborative project financed by the 7th Framework Program of the European Union (neuro.GSK3).

■ ABBREVIATIONS USED

ATP, adenosine triphosphate; AD, Alzheimer's disease; BBB, blood−brain barrier; Cdk, cyclin-dependent kinase; GSK-3, glycogen synthase kinase-3; DMF, dimethylformamide; DMSO, dimethyl sulfoxide; EtOAc, ethyl acetate; EtOH, ethanol; hpf, hours post fertilization; HPLC, high performance liquid chromatography; MeOH, methanol; SAR, structure−activity relationship

■ REFERENCES

(1) Engel, T.; Goni-Oliver, P.; Gómez de Barreda, E.; Lucas, J. J; Hernandez, F.; Avila, J. Lithium, a Potential Protective Drug in Alzheimeŕs Disease. *Neurodegenerative Dis.* **2008**, *5*, 247−249.

(2) Citron, M. Alzheimer's disease: strategies for disease modification. *Nature Rev. Drug Discovery* **2010**, *9*, 387−397.

(3) Mazanetz, M. P.; Fischer, P. M. Untangling tau hyperphosphorylation in drug design for neurodegenerative diseases. *Nature Rev. Drug Discovery* **2007**, *6*, 464−479.

(4) Cohen, P.; Goedert, M. GSK3 Inhibitors: Development and Therapeutic Potential. *Nature Rev. Drug Discovery* **2004**, *3*, 479−487.

(5) Saitoh, M.; Kunitomo, J.; Kimura, E.; Iwashita, H.; Uno, Y.; Onishi, T.; Uchiyama, N.; Kawamoto, T.; Tanaka, T.; Mol, C. D.; Dougan, D. R.; Textor, G. P.; Snell, G. P.; Takizawa, M.; Itoh, F.; Kori, M. 2-[3-[4-(Alkylsulfinyl)phenyl]-1-benzofuran-5-yl]-5-methyl-1,3,4-oxadiazole Derivatives as Novel Inhibitors of Glycogen Synthase Kinase-3β with Good Brain Permeability. *J. Med. Chem.* **2009**, *52*, 6270−6286.

(6) Martinez, A. Preclinical Efficacy on GSK-3 Inhibitors: Towards a Future Generation of Powerful Drugs. *Med. Res. Rev.* **2008**, *28*, 773−796.

(7) Frame, S.; Cohen, P. GSK3 takes centre stage more than 20 years after its discovery. *Biochem. J.* **2001**, *359*, 1−16.

(8) Cohen, P.; Frame, S. The renaissance of GSK3. *Nature Rev. Mol. Cell Biol.* **2001**, *2*, 769−775.

(9) Martinez, A.; Castro, A.; Dorronsoro, I.; Alonso, M. Glycogen Synthase Kinase 3 (GSK-3)—Inhibitors as New Promising Drugs for Diabetes, Neurodegeneration, Cancer and Inflammation. *Med. Res. Rev.* **2002**, *22*, 373−384.

(10) Bhat, R. V.; Budd Haeberlein, S. L.; Avila, J. Glycogen synthase kinase 3: a drug target for CNS therapies. *J. Neurochem.* **2004**, *89*, 1313−1317.

(11) Zou, H.; Zhou, L.; Li, Y.; Cui, Y.; Zhong, H.; Pan, Z.; Yan, Z.; Quan, J. Benzo[*e*]isoindole-1,3-diones as potential Inhibitors of Glycogen Synthase Kinase-3 (GSK-3). Synthesis, Kinase Inhibitory Activity, Zebrafish Phenotype, and Modeling of Binding Mode. *J. Med. Chem.* **2010**, *53*, 994−1003.

(12) Kaidanovich-Beilin, O.; Lipina, T. V.; Takao, K.; van Eede, M.; Hattori, S.; Laliberté, C.; Khan, M.; Pkamoto, K.; Chambers, J. W.; Fletcher, P. J.; MacAulay, K.; Doble, B. W.; Henkelman, M.; Miyakawa, T.; Roder, J.; Woodgett, J. R. Abnormalities in brain structure and behavior in GSK-3alpha mutant mice. *Mol. Brain* **2009**, *2*, 1−23.

(13) Alon, L. T.; Pietrokovski, S.; Barkan, S.; Avrahami, L.; Kaidanovich-Beilin, O.; Woodgett, J. R.; Barnea, A.; Eldar-Finkelman, H. Selective loss of glycogen synthase kinase-3α in birds reveals distinct roles for GSK-3 isozymes in tau phosphorylation. *FEBS Lett.* **2011**, *585*, 1158−1162.

(14) Phiel, C. J.; Wislon, C. A.; Lee, V. M.-Y.; Klein, P. S. GSK-3α regulates production of Alzheimer's disease amyloid-β peptides. *Nature* **2003**, *423*, 435−439.
(15) Zhou, J.; Lal, H.; Chen, X.; Shang, X.; Song, J.; Li, Y.; Kerkela, R.; Doble, B. W.; MacAulay, K.; DeCaul, M.; Koch, W. J.; Farber, J.; Woodgett, J.; Gao, E.; Force, T. GSK-3α directly regulates β-adrenergic signaling and the response of the heart to hemodynamic stress in mice. *J. Clin. Invest.* **2010**, *120*, 2280−2291.
(16) Banerji, V.; Frumm, S. M.; Ross, K. N.; Li, L. S.; Schinzel, A. C.; Hahn, C. K.; Kakoza, R. M.; Chow, K. T.; Ross, L.; Alexe, G.; Tolliday, N.; Inguilizian, H.; Galinsky, I.; Stone, R. M.; DeAngelo, D. J.; Roti, G.; Aster, J. C.; Hahn, W. C.; Kung, A. L.; Stegmaier, K. The intersection of genetic and chemical genomic screens identifies GSK-3α as a target in human acute myeloid leukemia. *J. Clin. Invest.* **2012**, *122*, 935−947.
(17) Dajani, R.; Fraser, E.; Roe, S. M.; Young, N.; Good, V.; Dale, T. C.; Pearl, L. H. Crystal Structure of Glycogen Synthase Kinase 3β: Structural Basis for Phosphate-Primed Substrate Specificity and Autoinhibition. *Cell* **2001**, *105*, 721−732.
(18) Leclerc, S.; Garnier, M.; Hoessel, R.; Marko, D.; Bibb, J. A.; Snyder, G. L.; Greengard, P.; Biernat, J.; Wu, Y. Z.; Mandelkow, E. M.; Eisenbrand, G.; Meijer, L. Indirubins inhibit glycogen synthase kinase-3 beta and CDK5/p25, two protein kinases involved in abnormal tau phosphorylation in Alzheimer's disease. A property common to most cyclin-dependent kinase inhibitors? *J. Biol. Chem.* **2001**, *276*, 251−260.
(19) Leost, M.; Schultz, C.; Link, A.; Wu, Y. Z.; Biernat, J.; Mandelkow, E. M.; Bibb, J. A.; Snyder, G. L.; Greengard, P.; Zaharevitz, D. W.; Gussio, R.; Senderowicz, A. M.; Sausville, E. A.; Kunick, C.; Meijer, L. Paullones are potent inhibitors of glycogen synthase kinase-3beta and cyclin-dependent kinase 5/p25. *Eur. J. Biochem.* **2000**, *267*, 5983−5994.
(20) Martinez, A.; Alonso, M.; Castro, A.; Perez, C.; Moreno, F. J. First non-ATP competitive glycogen synthase kinase 3 beta (GSK-3beta) inhibitors: thiadiazolidinones (TDZD) as potential drugs for the treatment of Alzheimer's disease. *J. Med. Chem.* **2002**, *45*, 1292−1299.
(21) Smith, D. G.; Buffet, M.; Fenwick, A. E.; Haigh, D.; Ife, R. J.; Saunders, M.; Slingsby, B. P.; Stacey, R.; Ward, R. W. 3-Anilino-4-arylmaleimides: potent and selective inhibitors of glycogen synthase kinase-3 (GSK-3). *Bioorg. Med. Chem. Lett.* **2001**, *11*, 635−639.
(22) Lo Monte, F.; Kramer, T.; Boländer, A.; Plotkin, B.; Eldar-Finkelman, H.; Fuertes, A.; Dominguez, J. M.; Schmidt, B. Synthesis and biological evaluation of glycogen synthase kinase 3 (GSK-3) inhibitors: a fast and atom efficient access to 1-aryl-3-benzylureas. *Bioorg. Med. Chem. Lett.* **2011**, *21*, 5610−5615.
(23) Eldar-Finkelman, H.; Martinez, A. GSK-3 inhibitors: preclinical and clinical focus on CNS. *Front. Mol. Neurosci.* **2011**, *4*, 1−18.
(24) Kramer, T.; Schmidt, B.; Lo Monte, F. Small-molecule inhibitors of GSK-3—Structural insights and their application to Alzheimer's disease models. *Int. J. Alzheimer's Dis.* **2012**, in press.
(25) Naerum, L.; Norskov-Lauritsen, L.; Olesen, P. H. Scaffold hopping and optimization towards libraries of glycogen synthase kinase-3 inhibitors. *Bioorg. Med. Chem. Lett.* **2002**, *12*, 1525−1528.
(26) Saitoh, M.; Kunitomo, J.; Kimura, E.; Hayase, Y.; Kobayashi, H.; Uchiyama, N.; Kawamoto, T.; Tanaka, T.; Mol, C. D.; Dougan, D. R.; Textor, G. S.; Snell, G. P.; Itoh, F. Design, synthesis and structure−activity relationships of 1,3,4-oxadiazole derivatives as novel inhibitors of glycogen synthase kinase-3beta. *Bioorg. Med. Chem.* **2009**, *17*, 2017−2029.
(27) Oertby, E.; Pictet, A. Derivatives of Piperonylic Acid. *Ber. Dtsch. Chem. Ges.* **1910**, *43*, 1336−1340.
(28) Yu, T.; Hsu, L.; Wu, S. *Huaxue Xuebao* **1958**, *24*, 170−173.
(29) Mc Fayden, J. S.; Stevens, T. S. New method for the conversion of acids into aldehydes. *J. Chem. Soc.* **1936**, 584−587.
(30) Konig, H. B.; Seifken, W.; Offe, H. A. Sulfur-containing derivatives of pyridine carboxylic acids and compounds derived therefrom. *Chem. Ber.* **1954**, *87*, 825−834.
(31) Mazzone, G.; Bonina, F.; Arrigo-Reina, R. Synthesis and pharmacological activities of some 2-(alkylaminoalkyl)mercapto-5-aryl-(1,3,4-oxadiazoles). *Farmaco, Ed. Sci.* **1977**, *32*, 414−429.
(32) Omar, R. H.; El-Fattah, B. A. Synthesis of certain pyridyl 1,3,4-oxadiazoles of biological interest and study of the cleavage of certain substituted oxadiazole rings with primary amines. *Egypt. J. Pharm. Sci.* **1985**, *24*, 49−56.
(33) Akwabi-Ameyaw, A.; Bass, J. Y.; Caldwell, R. D.; Caravella, J. A.; Chen, L.; Creech, K. L.; Deaton, D. N.; Madauss, K. P.; Marr, H. B.; McFadyen, R. B.; Miller, A. B.; Navas, F., III; Parks, D. J.; Spearing, P. K.; Todd, D.; Williams, S. P.; Wisely, G. B. FXR agonist activity of conformationally constrained analogs of GW 4064. *Bioorg. Med. Chem.* **2009**, *19*, 4733−4739.
(34) Dolezal, M.; Palek, L.; Vinsova, J.; Buchta, V.; Jampilek, J.; Kralova, K. Substituted Pyrazinecarboxamides: Synthesis and Biological Evaluation. *Molecules* **2006**, *11*, 242−256.
(35) Schmidt, B.; Meid, D.; Kieser, D. Safe and fast tetrazole formation in ionic liquids. *Tetrahedron* **2007**, *63*, 492−496.
(36) Funke, A.; Paulsen, A.; Cibrario, N. Chloromethyl- and aminomethyl(acetyl)benzodioxan isomers and derivatives resulting from oxidation of the acetyl group. *Bull. Soc. Chim. Fr.* **1958**, 470−473.
(37) Hormann, R. E.; Tice, C. M.; Chortyk, O.; Smith, H.; Meteyer, T. Diacylhydrazine ligands for modulating the expression of exogenous genes in mammalian systems via an ecdysone receptor complex. PCT-WO 2004/072254 2004, pp 1−120.
(38) Alksnis, A. F.; Surna, J. A. Preparation of Benzodioxane Derivatives. GB Patent 1109275 1965, pp 1−2.
(39) Satoh, Y.; Powers, C.; Toledo, L. M.; Kowalski, T. J.; Peters, P. A.; Kimble, E. F. Derivatives of 2-[[*N*-(Aminocarbonyl)-*N*-hydroxyamino]methyl]-1,4-benzodioxan as Orally Active 5-Lipoxygenase Inhibitors. *J. Med. Chem.* **1995**, *38*, 68−75.
(40) Lee, J. Y.; Park, Y. K.; Seo, S. H.; Yang, B.; Park, H.; Lee, Y. S. 7-Substituted-[1,4]dioxano[2,3-g]quinazolines as Inhibitors of Epidermal Growth Factor Receptor Kinase. *Arch. Pharm. Pharm. Med. Chem.* **2002**, *10*, 487−494.
(41) Feng, L.; Geisselbrecht, Y.; Black, S.; Wilbuer, A.; Atilla-Gokcumen, G. E.; Filippakopoulos, P.; Kräling, K.; Celik, M. A.; Harms, K.; Maksimoska, J.; Marmorstein, R.; Frenking, G.; Knapp, S.; Essen, L.; Meggers, E. Structurally Sophisticated Octahedral Metal Complexes as Highly Selective Protein Kinase Inhibitors. *J. Am. Chem. Soc.* **2011**, *133*, 5976−5986.
(42) Limongelli, V.; Marinelli, L.; Cosconati, S.; La Motta, C.; Sartini, S.; Mugnaini, L.; Da Settimo, F.; Novellino, E.; Parrinello, M. Sampling protein motion and solvent effect during ligand binding. *Proc. Natl. Acad. Sci. U.S.A.* **2012**, *109*, 1467−1472.
(43) Limongelli, V.; Bonomi, M.; Marinelli, L.; Gervasio, F. L.; Cavalli, A.; Novellino, E.; Parrinello, M. Molecular basis of cyclooxygenase enzymes (COXs) selective inhibition. *Proc. Natl. Acad. Sci. U.S.A.* **2010**, *107*, 5411−5416.
(44) Atilla-Gokcumen, G. E.; Williams, D. S.; Bregman, H.; Pagano, N.; Meggers, E. Organometallic Compounds with Biological Activity: A Very Selective and Highly Potent Cellular Inhibitor for Glycogen Synthase Kinase 3. *ChemBioChem* **2006**, *7*, 1443−1450.
(45) Paquet, D.; Bhat, R.; Sydow, A.; Mandelkow, E.; Berg, S.; Hellberg, S.; Fälting, J.; Distel, M.; Köster, R. W.; Schmid, B.; Haass, C. A zebrafish model of tauopathy allows in vivo imaging of neuronal cell death and drug evaluation. *J. Clin. Invest.* **2009**, *119*, 1382−1395.
(46) Azoulay-Alfaguter, I.; Yaffe, Y.; Licht-Murava, A.; Urbanska, M.; Jaworski, J.; Pietrokovski, S.; Hirschberg, K.; Eldar-Finkelman, H. Distinct molecular regulation of glycogen synthase kinase-3alpha isozyme controlled by its N-terminal region: functional role in calcium/calpain signaling. *J. Biol. Chem.* **2011**, *286*, 13470−13480.
(47) Jaworski, T.; Dewachter, I.; Lechat, B.; Gees, M.; Kremer, A.; Demedts, D.; Borghgreaf, P.; Devijver, H.; Kügler, S.; Patel, S.; Woodgett, J. R.; Van Leuven, F. GSK-3α/β kinases and amyloid production in vivo. *Nature* **2011**, *480*, E4−E5.
(48) Phiel, C. J.; Wislon, C. A.; Lee, V. M.-Y.; Klein, P. S. Phiel et al. reply. *Nature* **2011**, *480*, E6.

(49) Tromp, R. A.; van Ameijde, S.; Pütz, C.; Sundermann, C.; Sundermann, B; von Frijtag Drabbe Künzel, J. K.; IJzerman, P. Inhibition of Nucleoside Transport by New Analogues of 4-Nitrobenzylthioinosine: Replacement of the Ribose Moiety by Substituted Benzyl Groups. *J. Med. Chem.* **2004**, *47*, 5441−5450.
(50) Liberman, Z.; Eldar-Finkelman, H. Serine 332 phosphorylation of insulin receptor substrate-1 by glycogen synthase kinase-3 attenuates insulin signaling. *J. Biol. Chem.* **2005**, *280*, 4422−4428.
(51) Kimmel, C. B.; Ballard, W. W.; Kimmel, S. R.; Ullmann, B.; Schilling, T. F. Stages of Embryonic Development of the Zebrafish. *Dev. Dyn.* **1995**, *203*, 253−310.
(52) Dutschmann, M.; Menuet, C.; Stettner, G. M.; Gertreau, C.; Borghgraef, P.; Devijver, H.; Gielis, L.; Hilaire, G.; Van Leuven, F. Upper airway dysfunction of Tau.P301L mice correlates with tauopathy in midbrain and ponto-medullary brainstem nuclei. *J. Neurosci.* **2010**, *30*, 1810−1821.
(53) *Glide*, version 5.5; Schrödinger, LLC: New York, 2009.
(54) *Maestro*, version 9.0.211; Schrödinger, LLC: New York, 2009.
(55) Pettersen, E. F.; Goddard, T. D.; Huang, C. C.; Couch, G. S.; Greenblatt, D. M.; Meng, E. C.; Ferrin, T. E. UCSF chimera—a visualization system for exploratory research and analysis. *J. Comput. Chem.* **2004**, *25*, 1605−1612.
(56) Schuttelkopf, A. W.; van Aalten, D. M. PRODRG: a tool for high-throughput crystallography of protein−ligand complexes. *Acta Crystallogr., Sect. D: Biol. Crystallogr.* **2004**, *60*, 1355−1363.
(57) Friesner, R. A.; Murphy, R. B.; Repasky, M. P.; Frye, L. L.; Greenwood, J. R.; Halgren, T. A.; Sanschagrin, P. C.; Mainz, D. T. Extra precision glide: docking and scoring incorporating a model of hydrophobic enclosure for protein-ligand complexes. *J. Med. Chem.* **2006**, *49*, 6177−6196.
(58) Friesner, R. A.; Banks, J. L.; Murphy, R. B.; Halgren, T. A.; Klicic, J. J.; Mainz, D. T.; Repasky, M. P.; Knoll, E. H.; Shelley, M.; Perry, J. K.; Shaw, D. E.; Francis, P.; Shenkin, P. S. Glide: a new approach for rapid, accurate docking and scoring. 1. Method and assesment of docking accuracy. *J. Med. Chem.* **2004**, *47*, 1739−1749.

SUPPORTING INFORMATION

Identification of Glycogen Synthase Kinase-3 Inhibitors with a Selective Sting for Glycogen Synthase Kinase-3α

Fabio Lo Monte,[a,] Thomas Kramer,[a] Jiamin Gu,[a] Upendra Rao Anumala,[a] Luciana Marinelli,[b] Valeria La Pietra,[b] Ettore Novellino,[b] Bénédicte Franco,[c] David Demedts,[c] Fred Van Leuven,[c] Ana Fuertes,[d] Juan Manuel Dominguez,[d] Batya Plotkin,[e] Hagit Eldar-Finkelman[e] and Boris Schmidt[a,]**

[a] Clemens Schöpf - Institute of Organic Chemistry and Biochemistry, Technische Universität Darmstadt, 64287 Darmstadt, Germany

[b] Dipartimento di Chimica Farmaceutica e Tossicologica, Università di Napoli "Federico II", 80131 Napoli, Italy

[c] Experimental Genetics Group, Department of Human Genetics, Katholieke Universiteit Leuven, 3000 Leuven, Belgium

[d] Noscira S.A., Drug Discovery, Tres Cantos 28760 - Madrid, Spain

[e] Department of Human Molecular Genetics and Biochemistry, Sackler School of Medicine, Tel Aviv University, 69978 Tel Aviv, Israel

* To whom correspondence should be addressed. Phone: +496151-164531.
Fax: +496151-163278.
E-Mail: schmidt_boris@t-online.de; Fabio.Lo-Monte@gmx.de

Table of contents

Homology Modeling

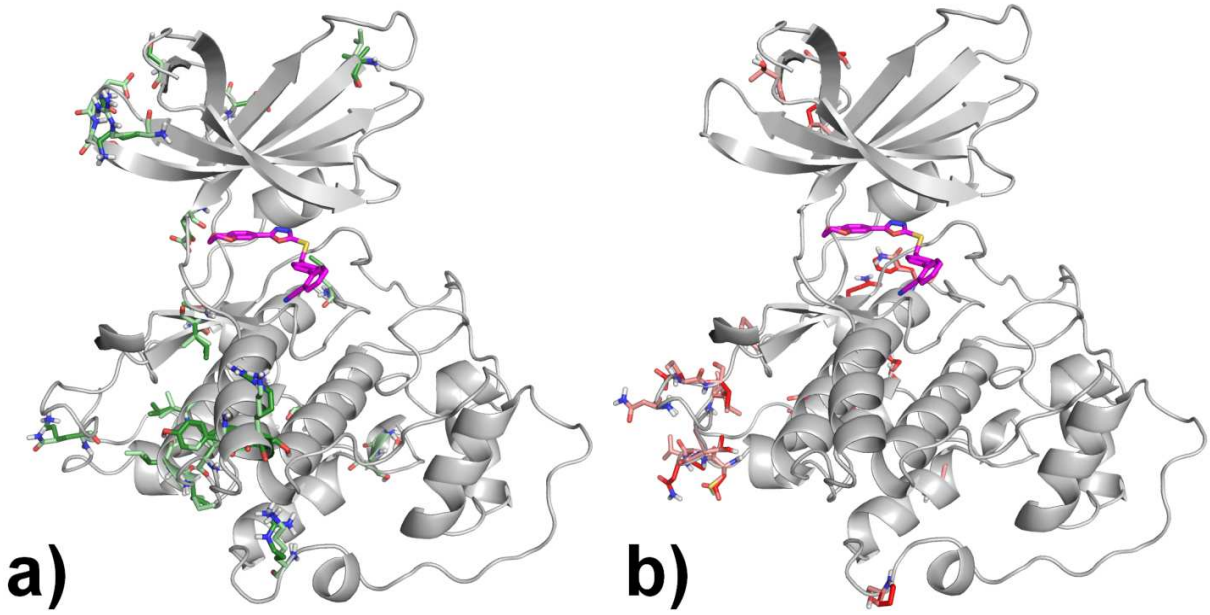

Figure S1. Superposition of 3D structure of GSK-3β (PDB code 3F88) and the homology-based 3D structure of GSK-3α. Both proteins are shown as white cartoons; conservative mutations are displayed as forest and light green stick, for GSK-3β and GSK-3α respectively (**a**), while non-conservative mutations are represented as red and pink sticks, for GSK-3β and GSK-3α respectively (**b**). It is evident that the majority of the mutations are located at the loop at the C-terminus fragment of the proteins (D345-T363 in GSK-3β and R407-A427 in GSK-3α).

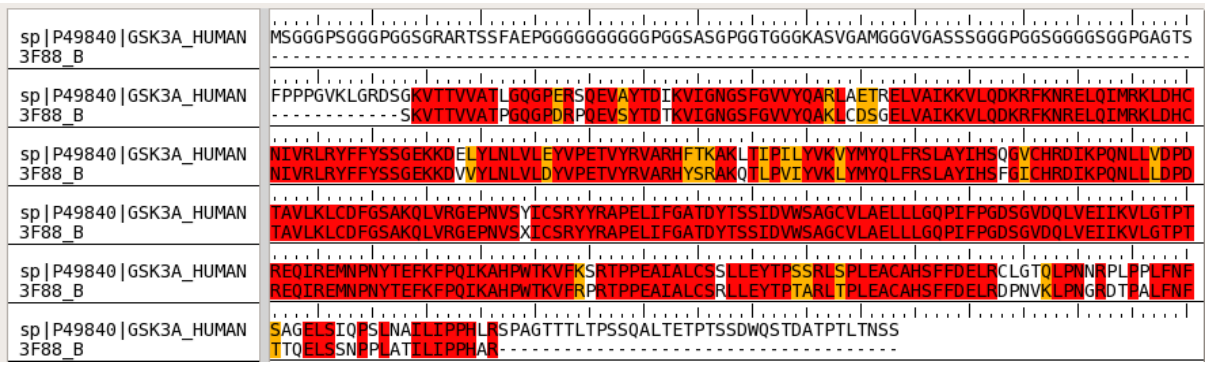

Figure S2. Alignment between GSK-3α (Swiss-Prot code: P49840) and GSK-3β sequences (PDB code: 3F88). Identical residues are colored in red, conservative residues in orange, while non-conservative residues are not painted. Gaps are represented as dashes.

In Vitro Pharmacology: Screening of compound 14d

The ExpresS Diversity kinase profile is a fast turnaround profile conducted by Cerep. Percentage kinase activities of compound **14d** at one concentration (1 μM) in panels of human protein kinases determined by Cerep. Measurements were performed in duplicate and the average was taken.

CHK1	118,1		**FGFR2**	100,8
SIK	113,6		**JAK3**	100,8
Src	111,4		**ROCK1**	100,7
CaMK2a	110,4		**FLT-3**	100,2
KDR	110,4		**NEK2**	100,2
MNK2	107,8		**EGFR**	99
MST4	105,8		**ERK2**	98,9
MAPKAPK2	105,5		**PKCb2**	98,7
PDK1	105,2		**AurA/Aur2**	98,6
p38a	105		**HGK**	98,6
SGK1	104,6		**Akt1/PKBa**	98,1
JNK1	104,5		**CDK2**	97,4
MKK6	104,5		**PKA**	97,4
CDK1	104,4		**EphA2**	97,1
FGFR3	104,4		**EphA3**	96,1
Lck	104,4		**Abl**	95,7
PAK2	104,2		**FGFR1**	95,6
PAK4	103,9		**EphB4**	91,4
MARK1	103,2		**RAF-1**	91,4
IRK	102,6		**CHK2**	89,8
Pim2	102,6		**c-Met**	89,1
TRKA	102,4		**PLK1**	84,2
IKKa	102,3		**IRAK4**	83,3
TAOK2	101,3		**GSK-3b**	27,2
CK1a	100,9		**GSK-3a**	5

Assay Kinases	Source	Substrate/Stimulus/Tracer	Incubation	Measured Component
Abl kinase (h)	human recombinant (insect cells)	ATP + Ulight-TK peptide (100 nM)	60 min RT	phospho-Ulight-TK-peptide
Akt1/PKB α (h)	human recombinant (insect cells)	ATP + CREBtide (CKRREILSRRPSYRK) (25 nM)	60 min RT	phospho-CREBtide (CKRREILSRRPSYRK)
AurA/Aur2 kinase (h)	human recombinant (Sf21 cells)	ATP + Ulight-RRRSLLE (100 nM)	15 min RT	phospho-Ulight-RRRSLLE
CaMK2α *(h)*	human recombinant	ATP + Ulight-CGSGSGRPRTSSFAEG (50 nM)	30 min RT	phospho-Ulight-CGSGSGRPRTSSFAEG
CDC2/CDK1 (h) (cycB)	human recombinant (insect cells)	ATP + Ulight-CFFKNIVTPRTPPPSQGK-amide (100 nM)	15 min RT	phospho-Ulight-CFFKNIVTPRTPPPSQGK-amide
CDK2 *(h)* (cycA)	human recombinant	ATP + Ulight-CFFKNIVTPRTPPPSQGK-amide (50 nM)	30 min RT	phospho-Ulight-CFFKNIVTPRTPPPSQGK-amide
CHK1 *(h)*	human recombinant (insect cells)	ATP + CREBtide (CKRREILSRRPSYRK) (25 nM)	30 min RT	phospho-CREBtide (CKRREILSRRPSYRK)
CHK2 *(h)*	human recombinant (insect cells)	ATP + CREBtide (CKRREILSRRPSYRK) (25 nM)	15 min RT	phospho-CREBtide (CKRREILSRRPSYRK)
CK1α *(h)*	human recombinant	ATP + Ulight-ARTKQTARKSTGGKAPRKQLAGCG (25 nM)	60 min RT	phospho-Ulight-ARTKQTARKSTGGKAPRKQLAGCG
c-Met kinase *(h)*	human recombinant (insect cells)	ATP + Ulight-CAGAGAIETDKEYYTVKD (25 nM)	60 min RT	phospho-Ulight-CAGAGAIETDKEYYTVKD
EGFR kinase *(h)*	human recombinant (insect cells)	ATP + Ulight-CAGAGAIETDKEYYTVKD (100 nM)	15 min RT	phospho-Ulight-CAGAGAIETDKEYYTVKD
EphA2 kinase *(h)*	human recombinant	ATP + Ulight-TK peptide (50 nM)	30 min RT	phospho-Ulight-TK-peptide
EphA3 kinase *(h)*	human recombinant	ATP + Ulight-TK peptide (50 nM)	60 min RT	phospho-Ulight-TK-peptide
EphB4 kinase *(h)*	human recombinant (insect cells)	ATP + Ulight-TK peptide (100 nM)	90 min RT	phospho-Ulight-TK-peptide

ERK2 *(h)* ($P42^{mapk}$)	human recombinant (*E. coli*)	ATP + Ulight-CFFKNIVTPRTPPPSQGK-amide (100 nM)	15 min RT	phospho-Ulight-CFFKNIVTPRTPPPSQGK-amide
FGFR1 kinase *(h)*	human recombinant (insect cells)	ATP + Ulight-CAGAGAIETDKEYYTVKD (100 nM)	60 min RT	phospho-Ulight-CAGAGAIETDKEYYTVKD
FGFR2 kinase *(h)*	human recombinant	ATP + Ulight-CAGAGAIETDKEYYTVKD (25 nM)	15 min RT	phospho-Ulight-CAGAGAIETDKEYYTVKD
FGFR3 kinase *(h)*	human recombinant	ATP + Ulight-CAGAGAIETDKEYYTVKD (100 nM)	90 min RT	phospho-Ulight-CAGAGAIETDKEYYTVKD
FLT-3 kinase *(h)*	human recombinant (insect cells)	ATP + Ulight-CAGAGAIETDKEYYTVKD (100 nM)	90 min RT	phospho-Ulight-CAGAGAIETDKEYYTVKD
GSK3α *(h)*	human recombinant	ATP + Ulight-CFFKNIVTPRTPPPSQGK-amide (100 nM)	60 min RT	phospho-Ulight-CFFKNIVTPRTPPPSQGK-amide
GSK3β *(h)*	human recombinant	ATP + Ulight-CFFKNIVTPRTPPPSQGK-amide (100 nM)	90 min RT	phospho-Ulight-CFFKNIVTPRTPPPSQGK-amide
HGK *(h)* (MAP4K4)	human recombinant	ATP + Ulight-FLGFTYVAP (50 nM)	90 min RT	phospho-Ulight-FLGFTYVAP
IKKα *(h)*	human recombinant (Sf21 cells)	ATP + Ulight-IkappaB-alpha (100 nM)	30 min RT	phospho-Ulight-IkappaB-alpha
IRAK4 *(h)*	human recombinant (insect cells)	ATP + Ulight-FLGFTYVAP (50 nM)	90 min RT	phospho-Ulight-FLGFTYVAP
IRK *(h)* (InsR)	human recombinant	ATP + Ulight-Poly GAT[EAY(1:1:1)]n (50 nM)	10 min RT	phospho-Ulight-Poly GAT[EAY(1:1:1)]n
JAK3 *(h)*	human recombinant	ATP + Ulight-CAGAGAIETDKEYYTVKD (100 nM)	60 min RT	phospho-Ulight-CAGAGAIETDKEYYTVKD
JNK1 *(h)*	human recombinant	ATP + Ulight-CFFKNIVTPRTPPPSQGK-	60 min RT	phospho-Ulight-CFFKNIVTPRTPPPSQ

	(*E. coli*)	amide (100 nM)		GK-amide
KDR kinase *(h)* (VEGFR2)	human recombinant (Sf9 cells)	ATP + Ulight-CAGAGAIETDKEYYTVKD (100 nM)	60 min RT	phospho-Ulight-CAGAGAIETDKEYYTVKD
Lck kinase *(h)*	human recombinant (insect cells)	ATP + Ulight-Poly GAT[EAY(1:1:1)]n (25 nM)	30 min RT	phospho-Ulight-Poly GAT[EAY(1:1:1)]n
MAPKAPK2 *(h)*	human recombinant (*E. coli*)	ATP + CREBtide (CKRREILSRRPSYRK) (25 nM)	15 min RT	phospho-CREBtide (CKRREILSRRPSYK)
MARK1 *(h)*	human recombinant	ATP + Ulight-RRRSLLE (50 nM)	30 min RT	phospho-Ulight-RRRSLLE
MKK6 *(h)*	human recombinant	ATP + inactive p38a (50 nM)	10 min RT	phospho-p38a
MNK2 *(h)*	human recombinant (Sf21 cells)	ATP + CREBtide (CKRREILSRRPSYRK) (25 nM)	90 min RT	phospho-CREBtide (CKRREILSRRPSYR)

MST4 kinase *(h)*	human recombinant	ATP + Ulight TM- PKC (50 nM)	30 min RT	Phospho-Ulight-TM-PKC
NEK2 *(h)*	human recombinant (insect cells)	ATP + Ulight-FLGFTYVAP (50 nM)	60 min RT	phospho-Ulight-FLGFTYVAP
p38α kinase *(h)*	human recombinant (*E. coli*)	ATP + Ulight-CFFKNIVTPRTPPPSQGK-amide (100 nM)	60 min RT	phospho-Ulight-CFFKNIVTPRTPPPSQGKamide
PAK2 *(h)*	human recombinant (Sf9 cells)	ATP + Ulight-RRRSLLE (50 nM)	60 min RT	phospho-Ulight-RRRSLLE
PAK4 *(h)*	human recombinant (insect cells)	ATP + Ulight-RRRSLLE (50 nM)	30 min RT	phospho-Ulight-RRRSLLE
PDK1 *(h)*	human recombinant (insect cells)	ATP + Ulight-FLGFTYVAP (400 nM)	90 min RT	phospho-Ulight-FLGFTYVAP
Pim2 kinase *(h)*	human recombinant (insect cells)	ATP + CREBtide (CKRREILSRRPSYRK) (25 nM)	60 min RT	phospho-CREBtide (CKRREILSRRPSYRK)

PKA *(h)*	human recombinant (*E. coli*)	ATP + Ulight-RRRSLLE (50 nM)	10 min RT	phospho-Ulight-RRRSLLE
PKCβ2 *(h)*	human recombinant	ATP + CREBtide (CKRREILSRRPSYRK) (25 nM)	15 min RT	phospho-CREBtide (CKRREILSRRPSYRK)
PLK1 *(h)*	human recombinant	ATP + Ulight-FLGFTYVAP (40 nM)	60 min RT	phospho-Ulight-FLGFTYVAP
RAF-1 kinase *(h)*	human recombinant	ATP + Ulight-ARTKQTARKSTGGKAPRKQ LAGCG (50 nM)	180 min RT	phospho-Ulight-ARTKQTARKSTGGKA PRKQ LAGCG
ROCK1 *(h)*	human recombinant	ATP + Ulight-RRRSLLE (50 nM)	30 min RT	phospho-Ulight-RRRSLLE
SGK1 *(h)*	human recombinant	ATP + Ulight-RRRSLLE (50 nM)	30 min RT	phospho-Ulight-RRRSLLE
SIK *(h)*	human recombinant (Sf21 cells)	ATP + CREBtide (CKRREILSRRPSYRK) (25 nM)	90 min RT	phospho-CREBtide (CKRREILSRRPSYRK)
Src kinase *(h)*	human recombinant (insect cells)	ATP + Ulight-Poly GAT[EAY(1:1:1)]n (5 nM)	10 min RT	phospho-Ulight-Poly GAT[EAY(1:1:1)]n
TAOK2 (TAO1) *(h)*	human recombinant	ATP + Ulight-FLGFTYVAP (40 nM)	60 min RT	phospho-Ulight-FLGFTYVAP
TRKA *(h)*	human recombinant (insect cells)	ATP + Ulight-Poly GAT[EAY(1:1:1)]n (5 nM)	10 min RT	phospho-Ulight-Poly GAT[EAY(1:1:1)]n

Bioavailability profile of compound 14d (conducted by Cerep).

Assay	Technique	Test concentration	Incubation	Detection mode
Aqueous solubility (PBS, pH 7.4)	shake-flask	200 µM	24hr/RT	HPLC-UV/VIS
Partition coefficient (log D, n-octanol /PBS, pH 7.4)	shake-flask	100 µM	60min/RT	HPLC-UV/VIS
Protein binding (plasma, human)	Equilibrium dialysis	10 µM	Overnight (18 ± 2hr) 37°C	HPLC-MS/MS

Assay	Source	Incubation	Detection mode
A-B permeability (Caco-2, pH 6.5/7.4)	Caco-2 cell line	0 and 60 min 37°C	HPLC-MS/MS

Assay	Source	Subtrate	Incubation	Measured Component	Detection mode
Metabolic stability (liver microsomes, human)	Human liver microsomes (0.3 mg/mL)	Test compound	0 and 60 min 37°C	Test compound	HPLC-MS/MS

Assay	Test Concentration (M)	Result
Partition coefficient (logD, n-octanol/PBS, pH 7.4)	1.0E-04	3.58
Protein binding (plasma, human)	1.0E-05	91% Protein Bound 121% Recovery
A-B permeability (Caco-2, pH 6.5/7.4)	1.0E-05	<0.1 Permeability 68% Recovery
Metabolic stability (liver microsomes, human)	1.0E-06	25% Parent Remaining
Aqueous solubility (PBS, pH 7.4)	2.0E-04	Below the limit of quantitation

Monitoring of the heart development on zebrafish embryos.

The wt zebrafish was used in this study. The embryos were collected and placed into 24-well plates, ten embryos per well and maintained in E2 medium at ~28°C. Compounds were added 5 hpf (50% epiboly) and the embryos allowed to grow in chemical compound solution up to 5 days. The phenotypes were compared using the Axio Scope.A1 microscope system from Carl Zeiss at 48, 72 and 96 hpf. The heart beat was counted for one minute and compared to the control. - **Animal husbandry.** All animal experiments were conducted and documented according to the federal and local regulations. According to the federal law and regulation all embryo testing was stopped at day 5 of embryonic development.

NMR Data of compounds 5b, **5c**, **6b**, **6c**, **14b**, **14c**, **14d**, **15a**, **15b**, **16a**, **23a**, **23b** and **23c**

The ^{1}H-NMR spectra were recorded on a Bruker AC 300 spectrometer at 300 MHz and Bruker AC 500 spectrometer at 500 MHz. The ^{13}C-NMR spectra were recorded on a Bruker AC 300 spectrometer at 75 MHz and Bruker AC 500 spectrometer at 125 MHz.

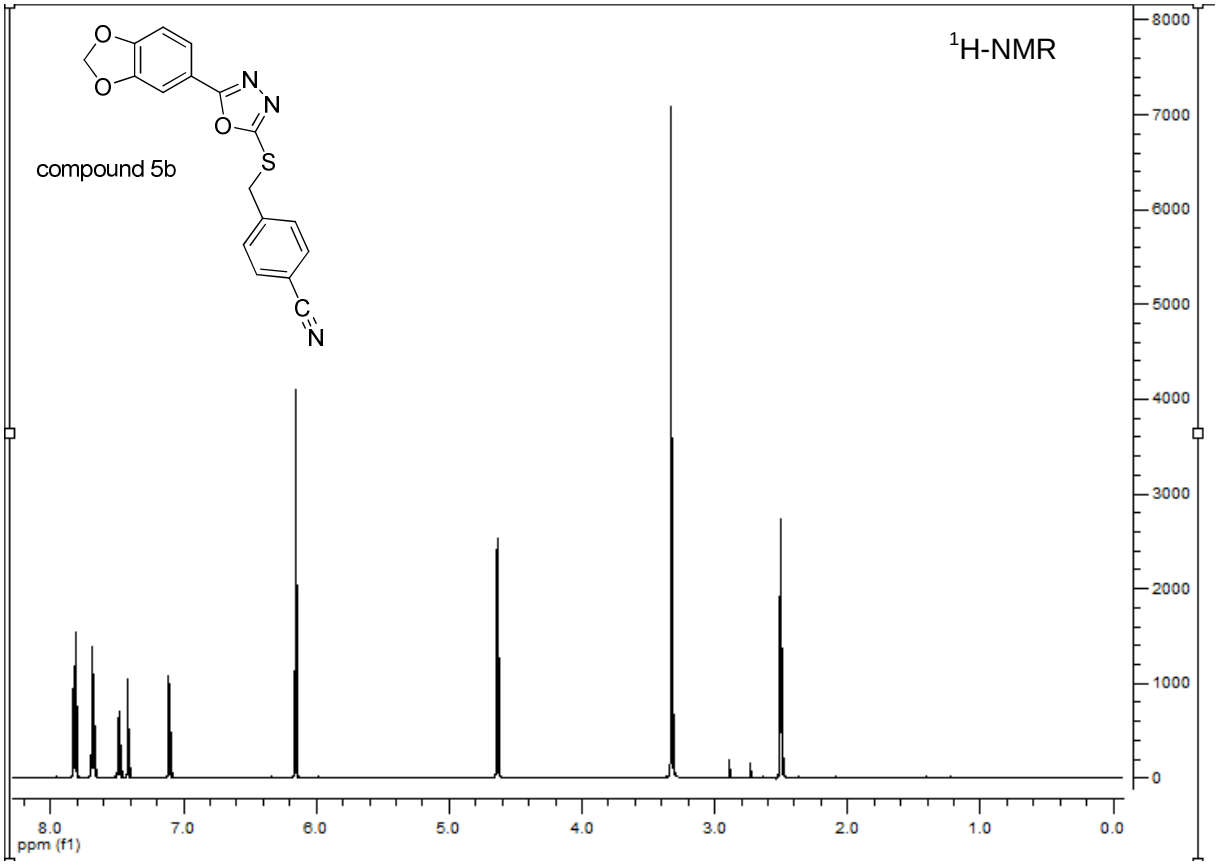
compound 5b
^{1}H-NMR
8000
7000
6000
5000
4000
3000
2000
1000
0
8.0
7.0
6.0
5.0
4.0
3.0
2.0
1.0
0.0
ppm (f1)

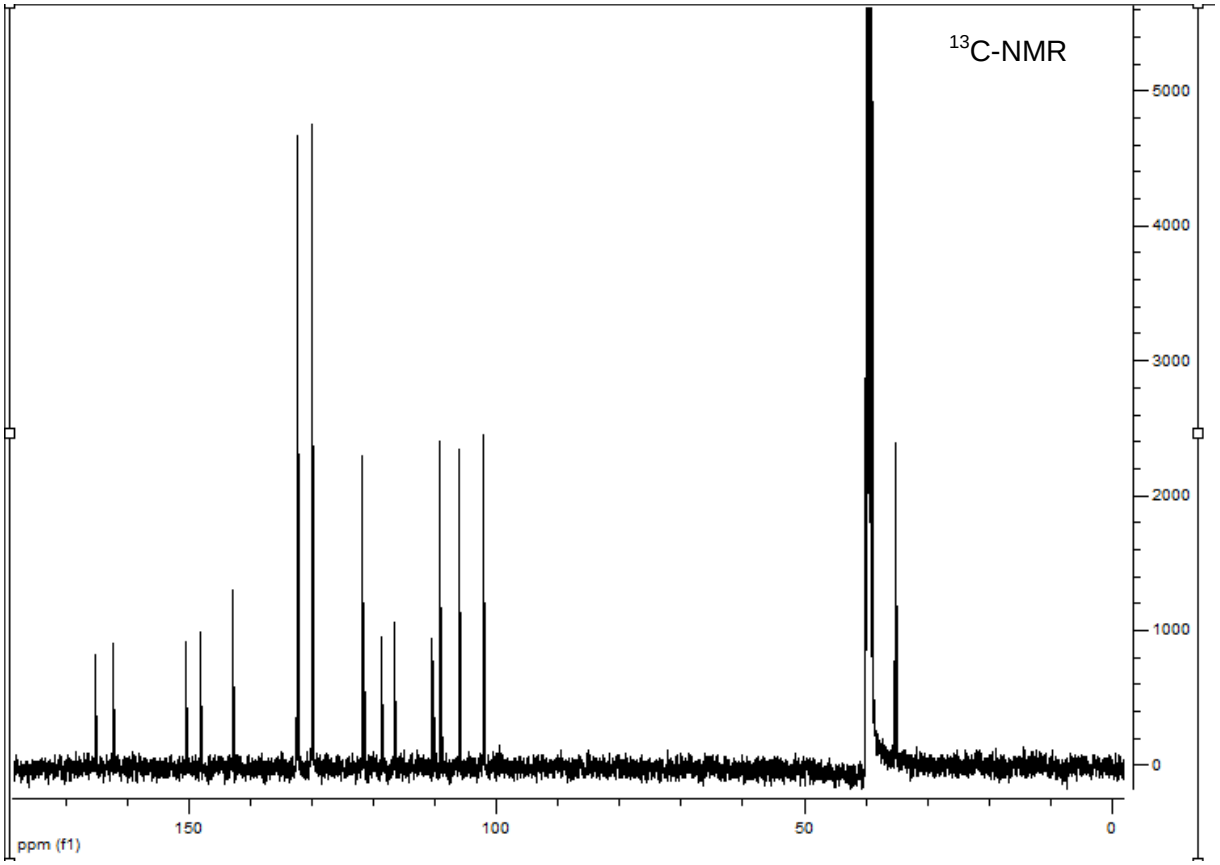
^{13}C-NMR
5000
4000
3000
2000
1000
0
150
100
50
0
ppm (f1)

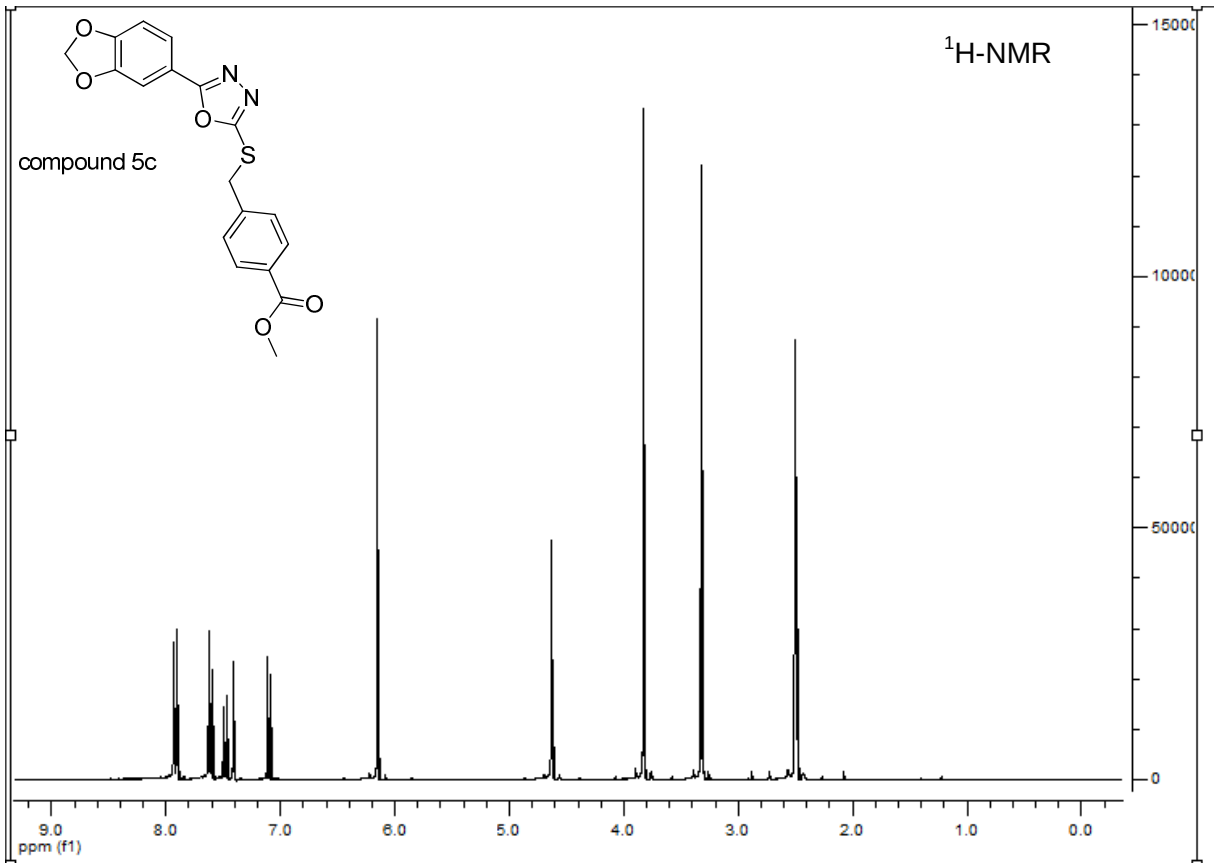
compound 5c
^{1}H-NMR
ppm (f1)

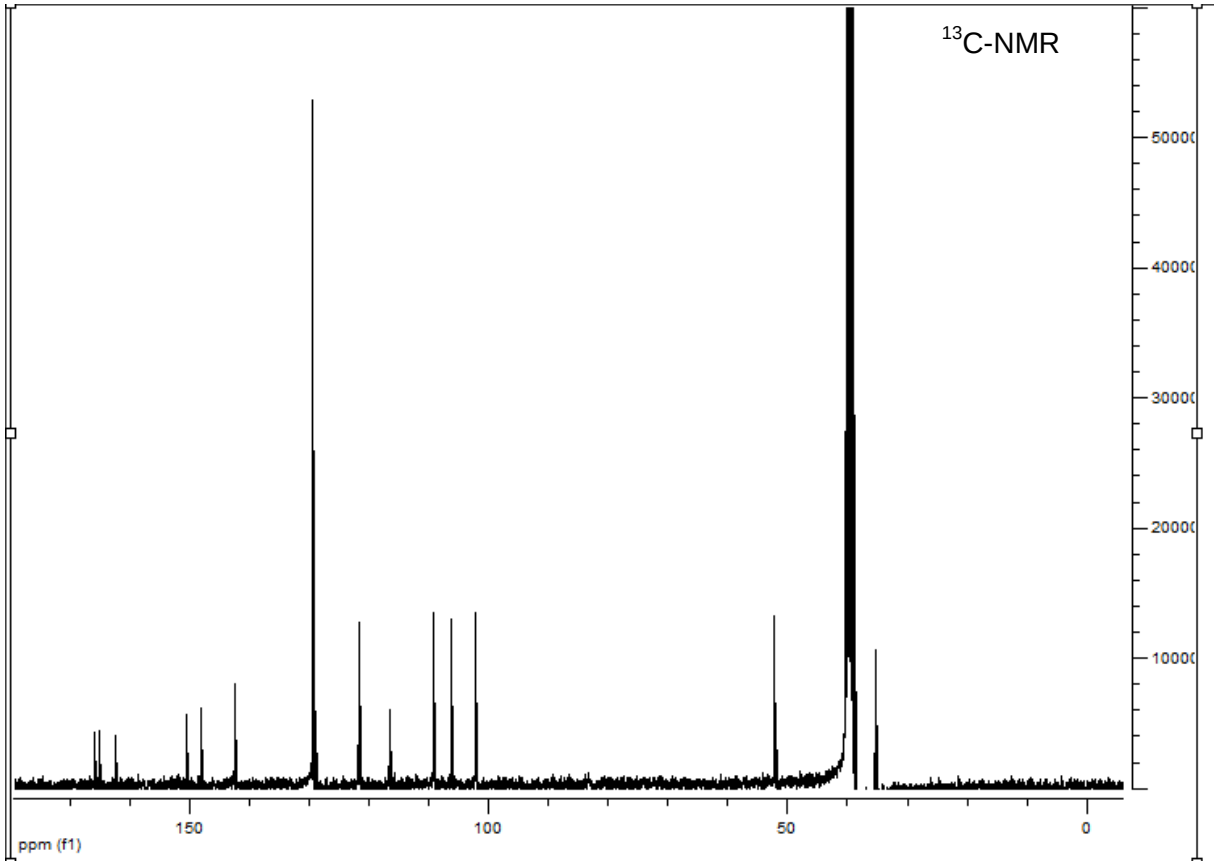
^{13}C-NMR
ppm (f1)

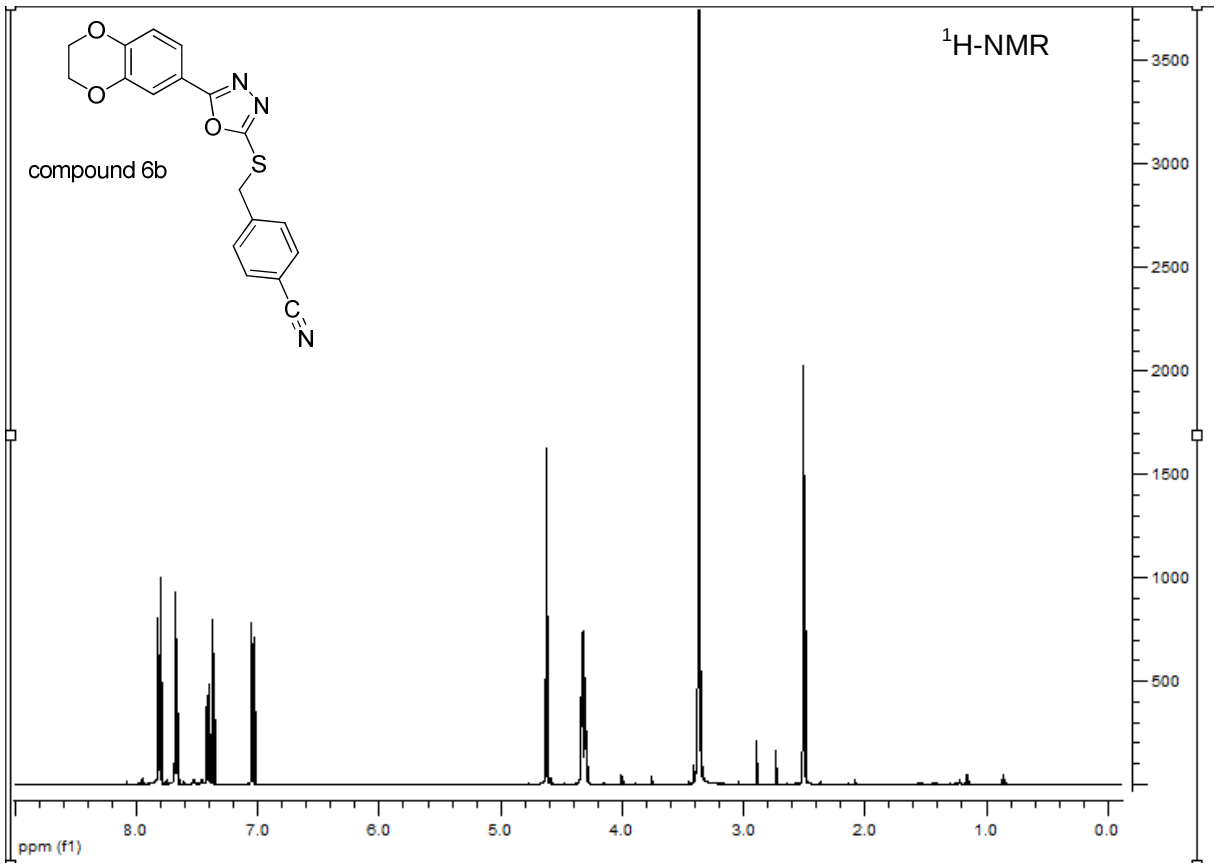
compound 6b
^{1}H-NMR
3500
3000
2500
2000
1500
1000
500
8.0
7.0
6.0
5.0
4.0
3.0
2.0
1.0
0.0
ppm (f1)

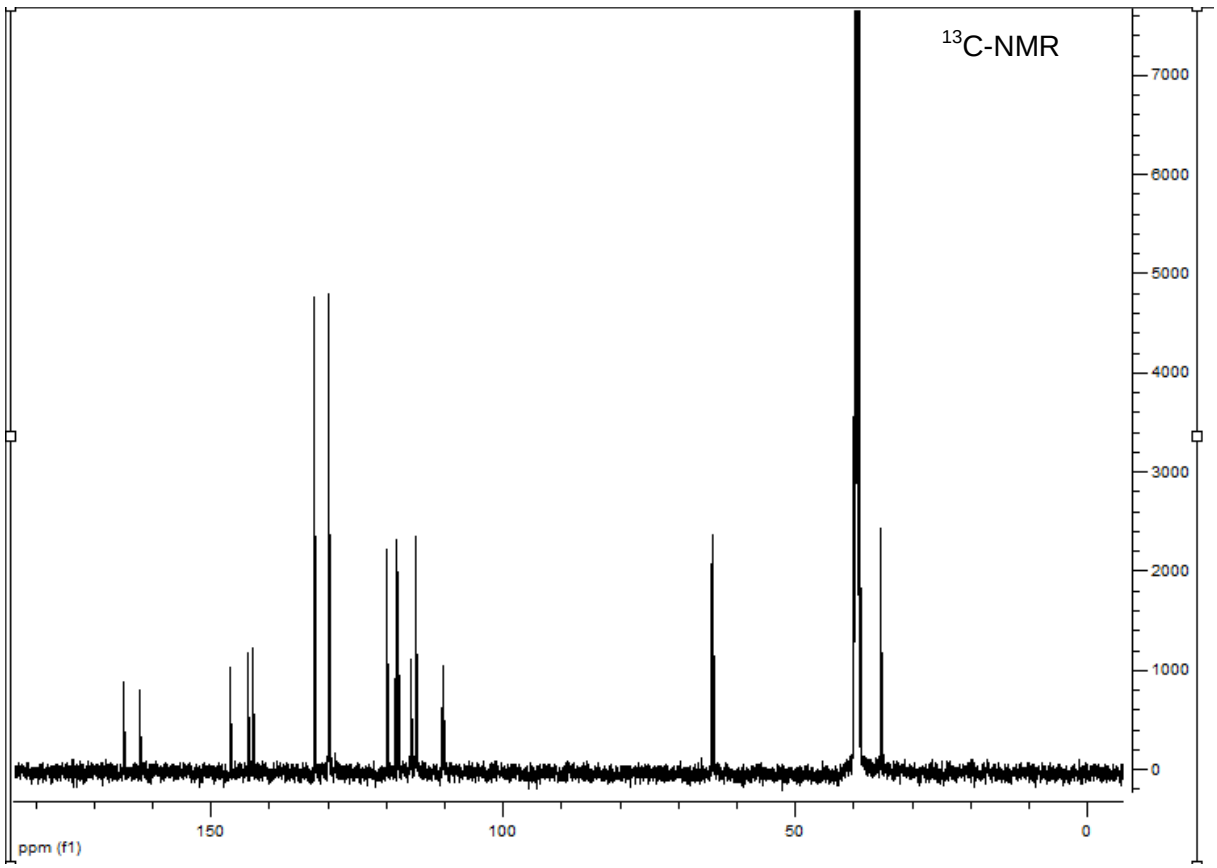
^{13}C-NMR
7000
6000
5000
4000
3000
2000
1000
0
150
100
50
0
ppm (f1)

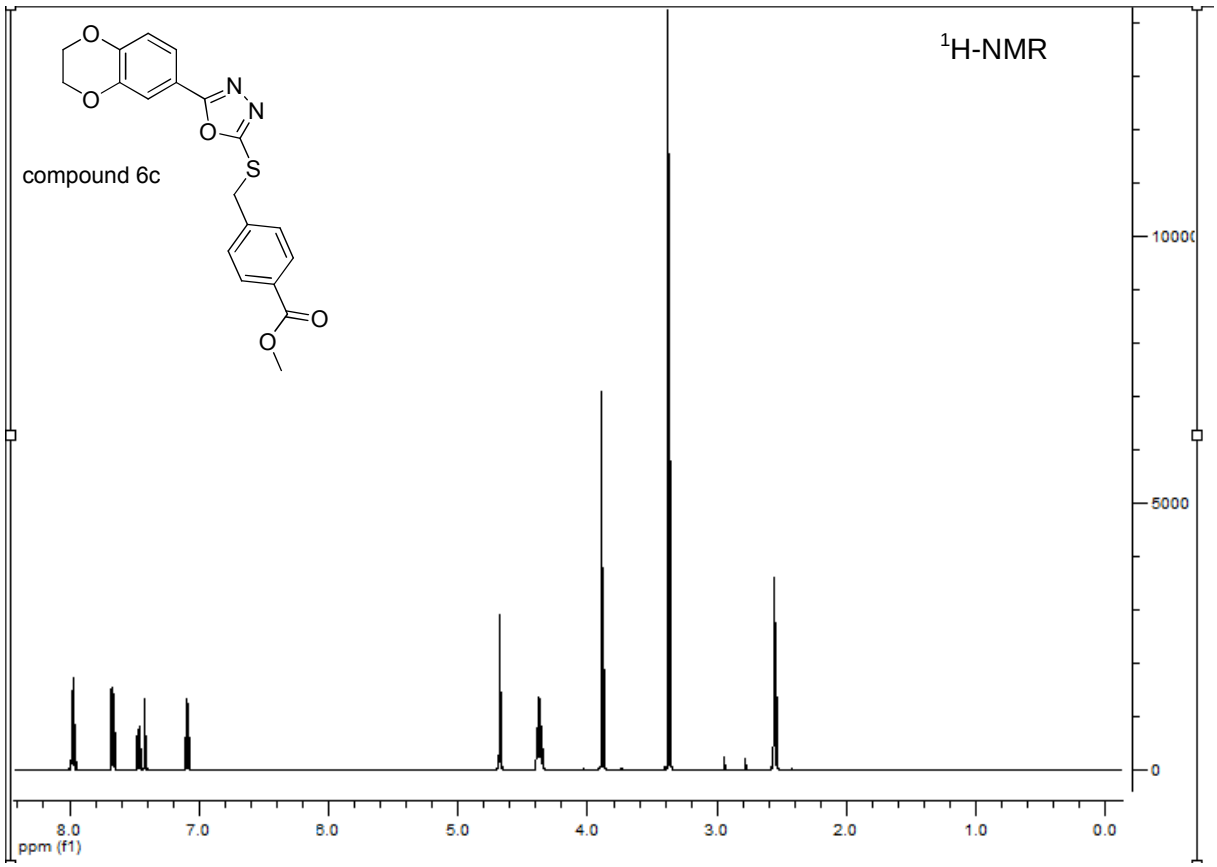
compound 6c
^{1}H-NMR
ppm (f1)

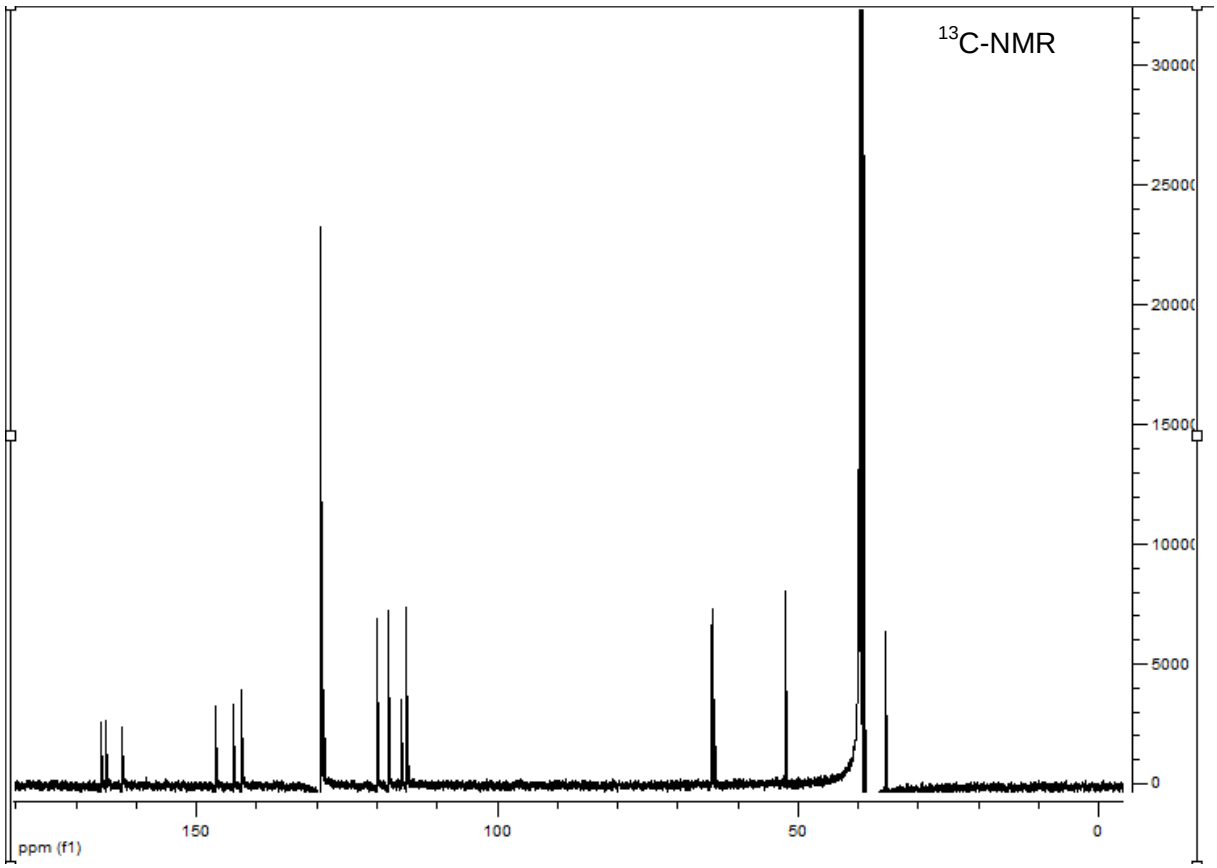
^{13}C-NMR
ppm (f1)

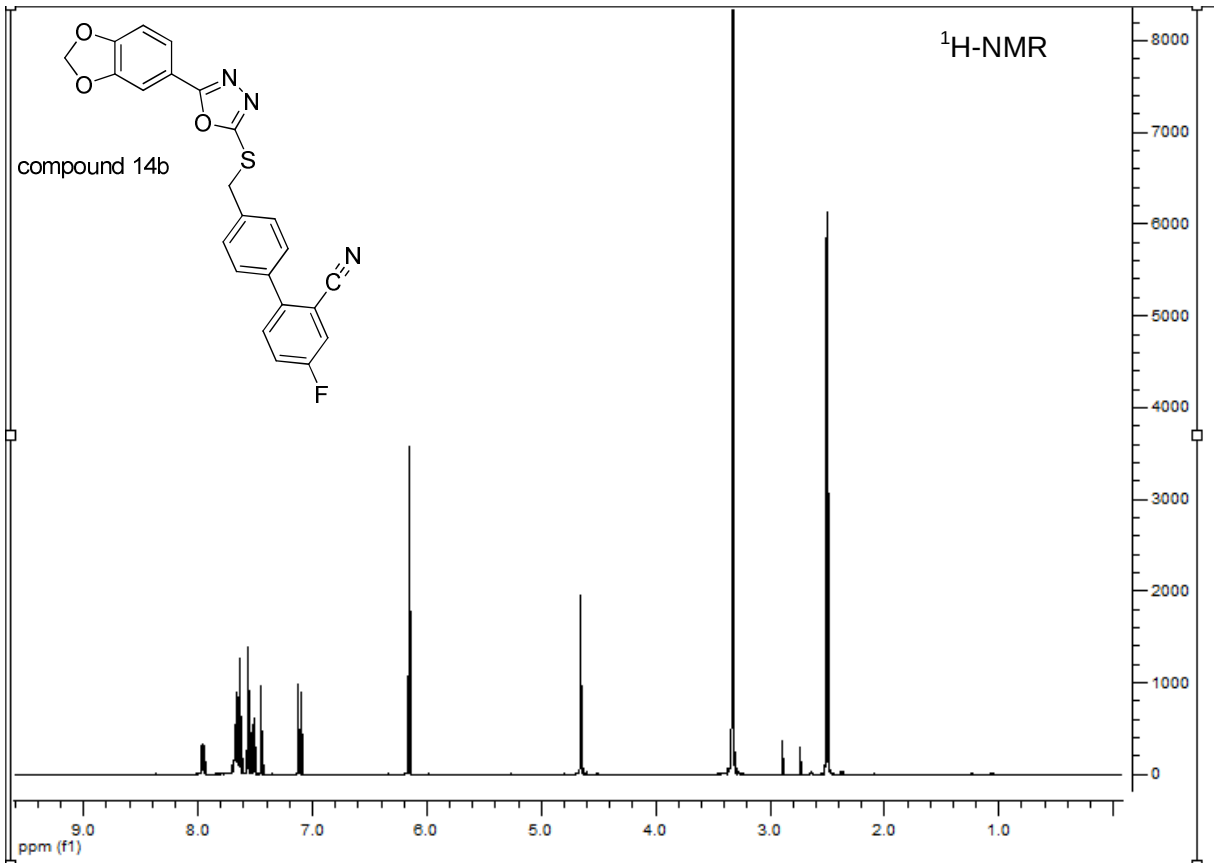
compound 14b
^{1}H-NMR
ppm (f1)

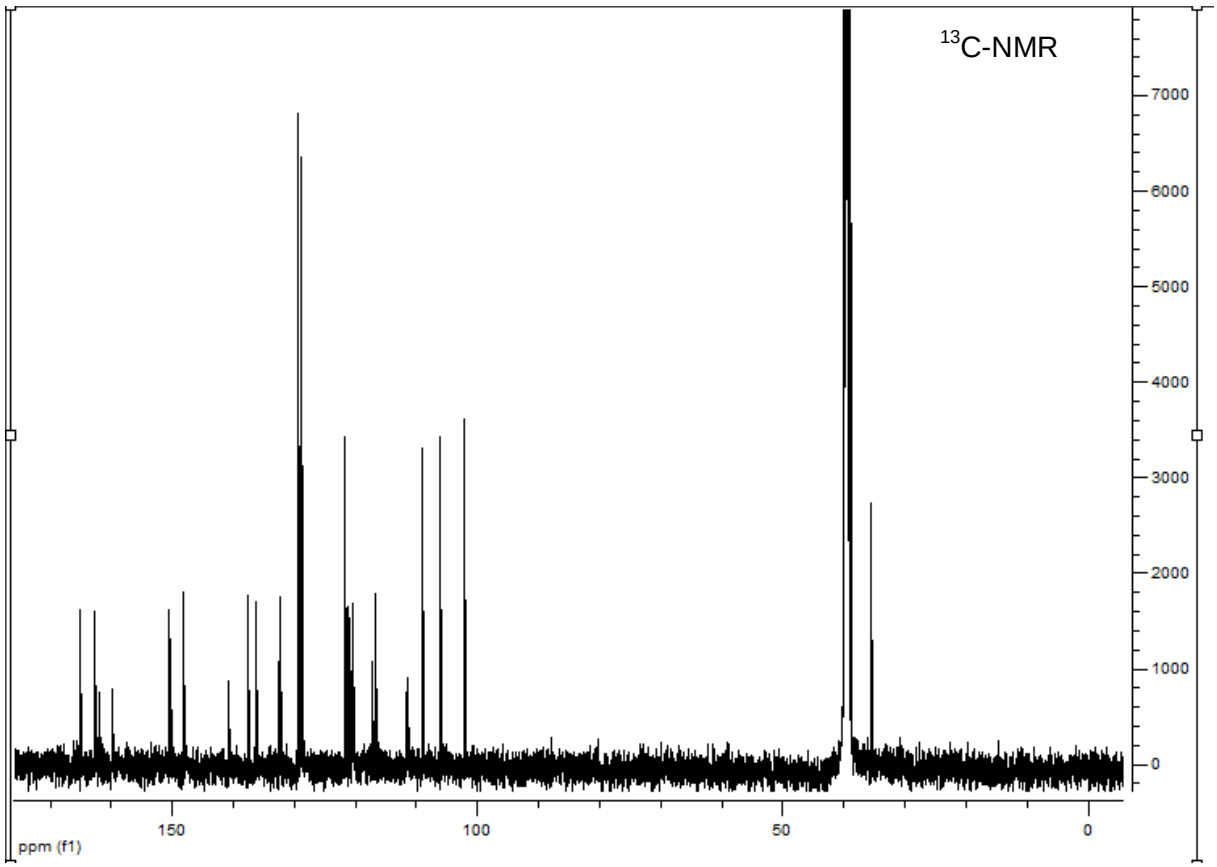
^{13}C-NMR
ppm (f1)

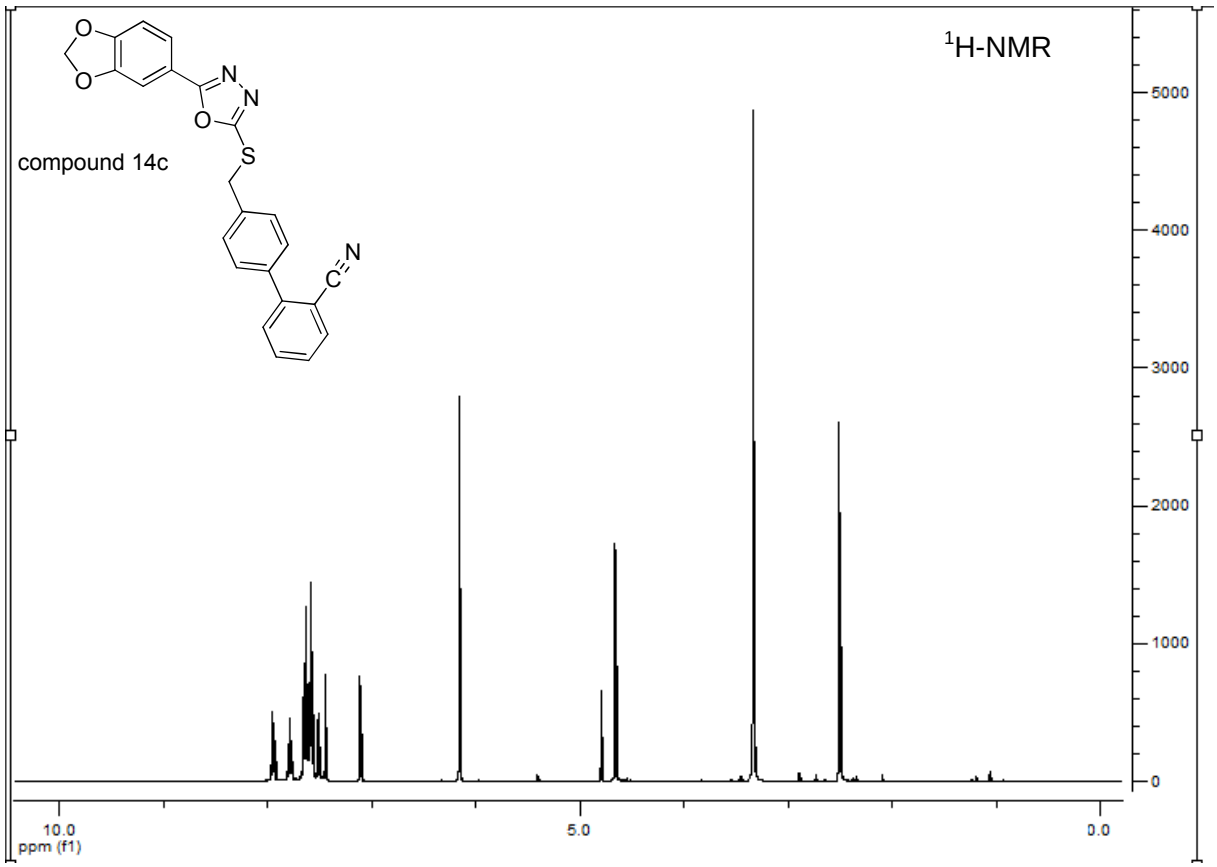
compound 14c
^{1}H-NMR
5000
4000
3000
2000
1000
0
10.0
ppm (f1)
5.0
0.0

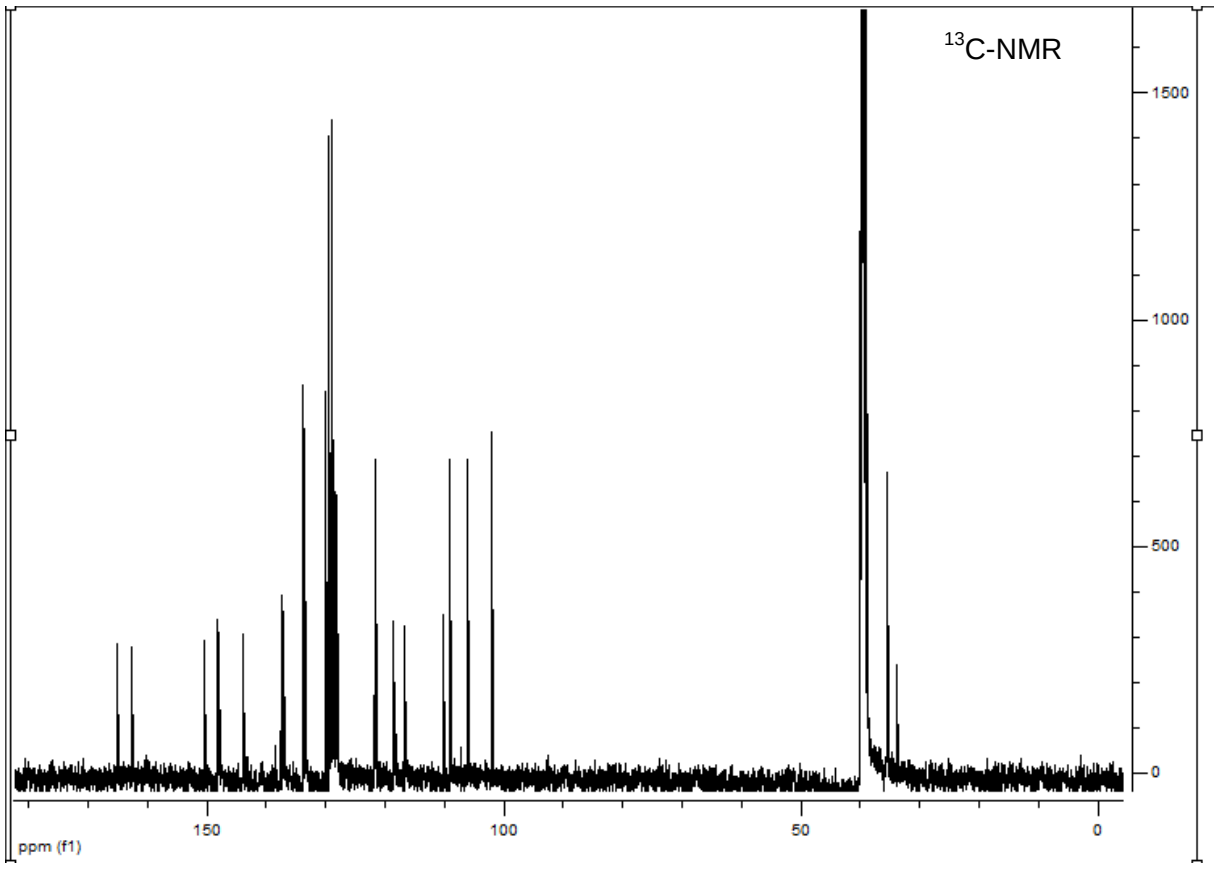
^{13}C-NMR
1500
1000
500
0
150
100
50
0
ppm (f1)

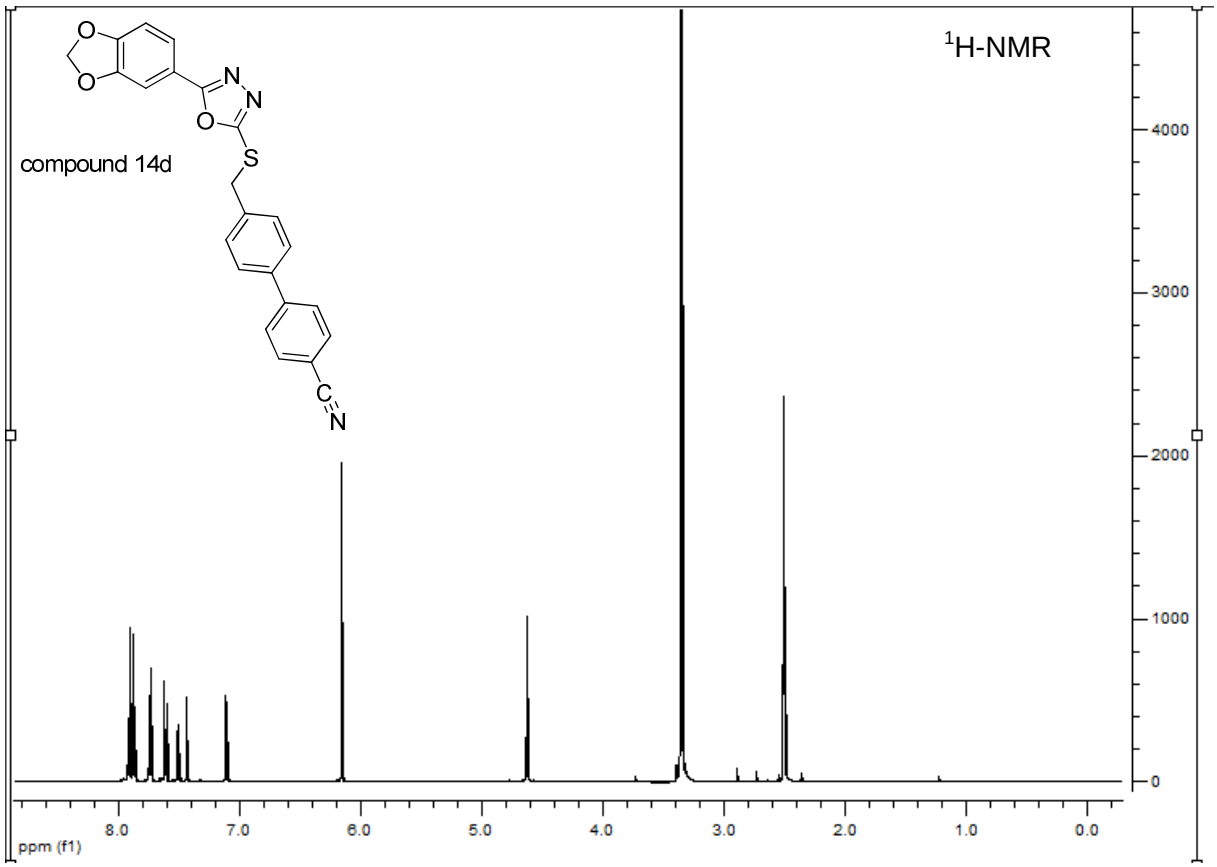
compound 14d
^{1}H-NMR
4000
3000
2000
1000
0
8.0
7.0
6.0
5.0
4.0
3.0
2.0
1.0
0.0
ppm (f1)

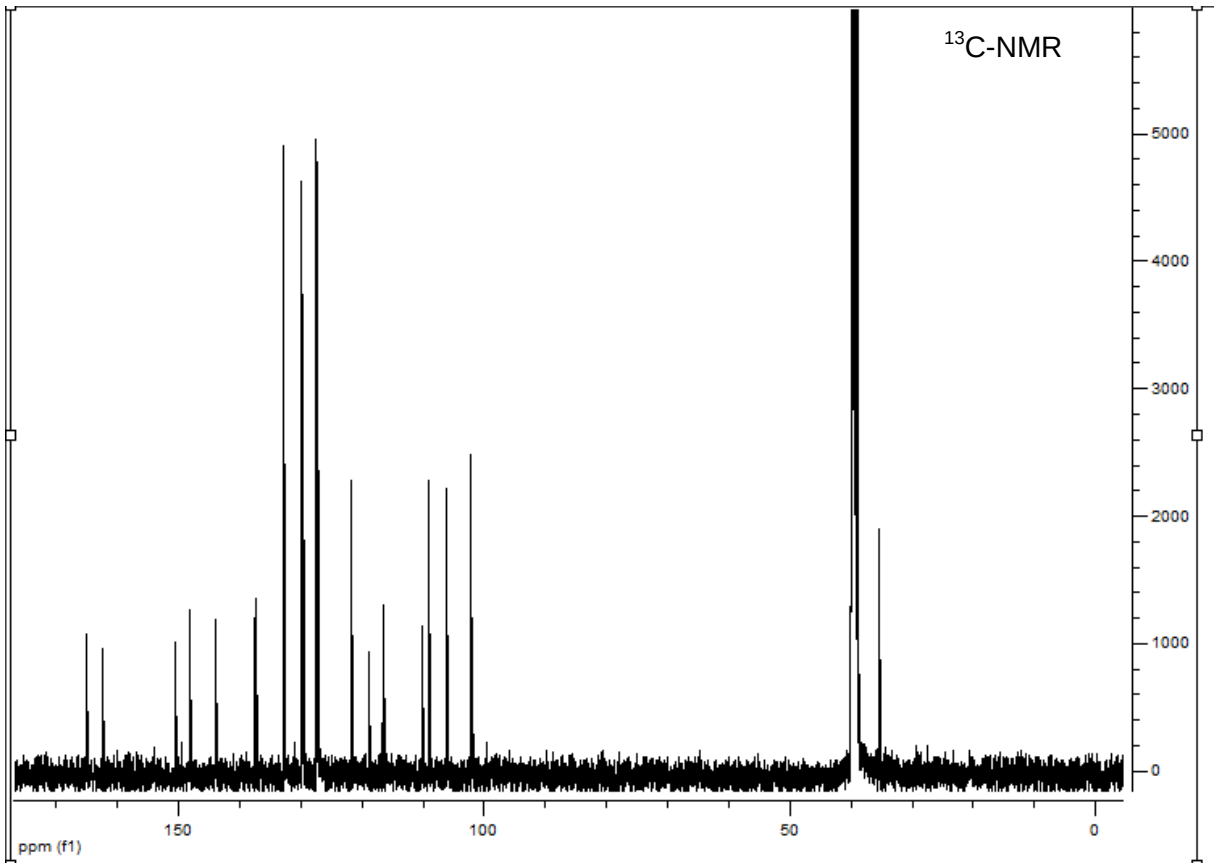
^{13}C-NMR
5000
4000
3000
2000
1000
0
150
100
50
0
ppm (f1)

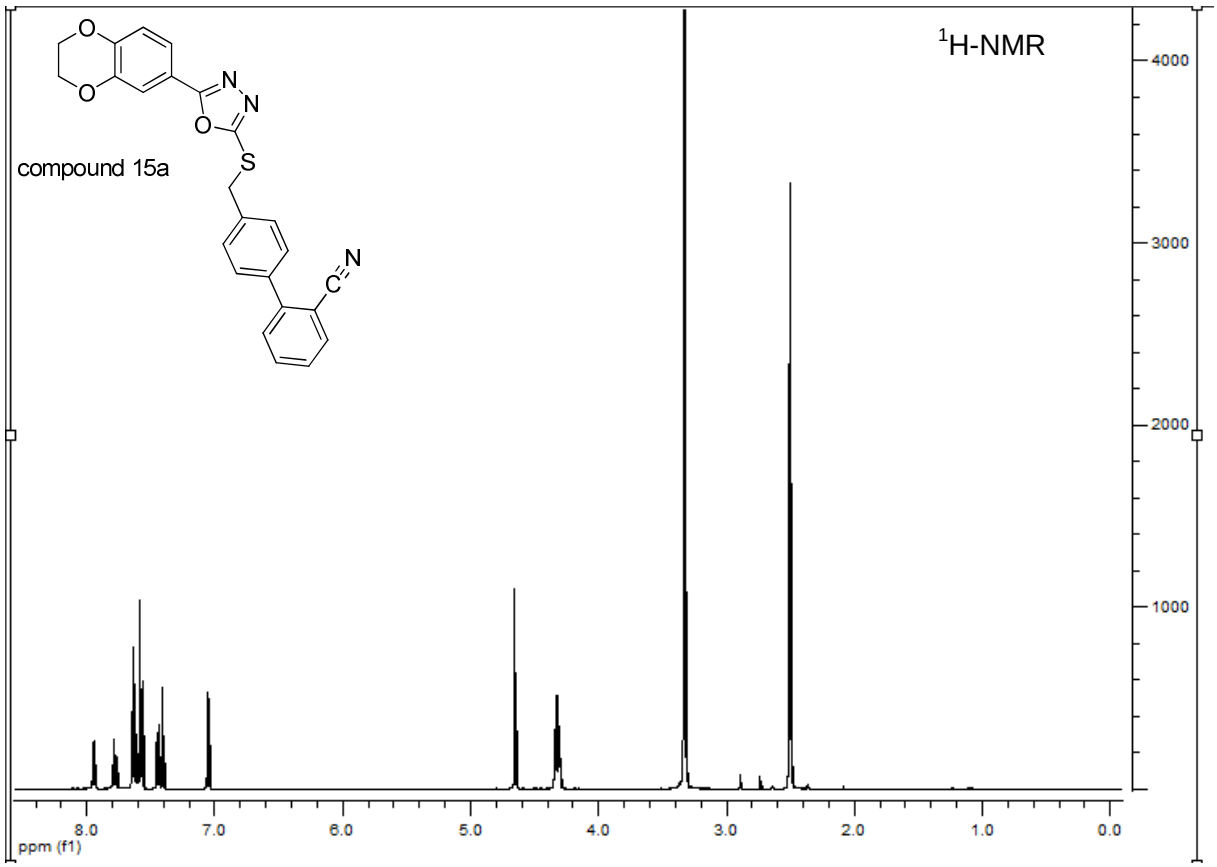
compound 15a
^{1}H-NMR
4000
3000
2000
1000
8.0
7.0
6.0
5.0
4.0
3.0
2.0
1.0
0.0
ppm (f1)

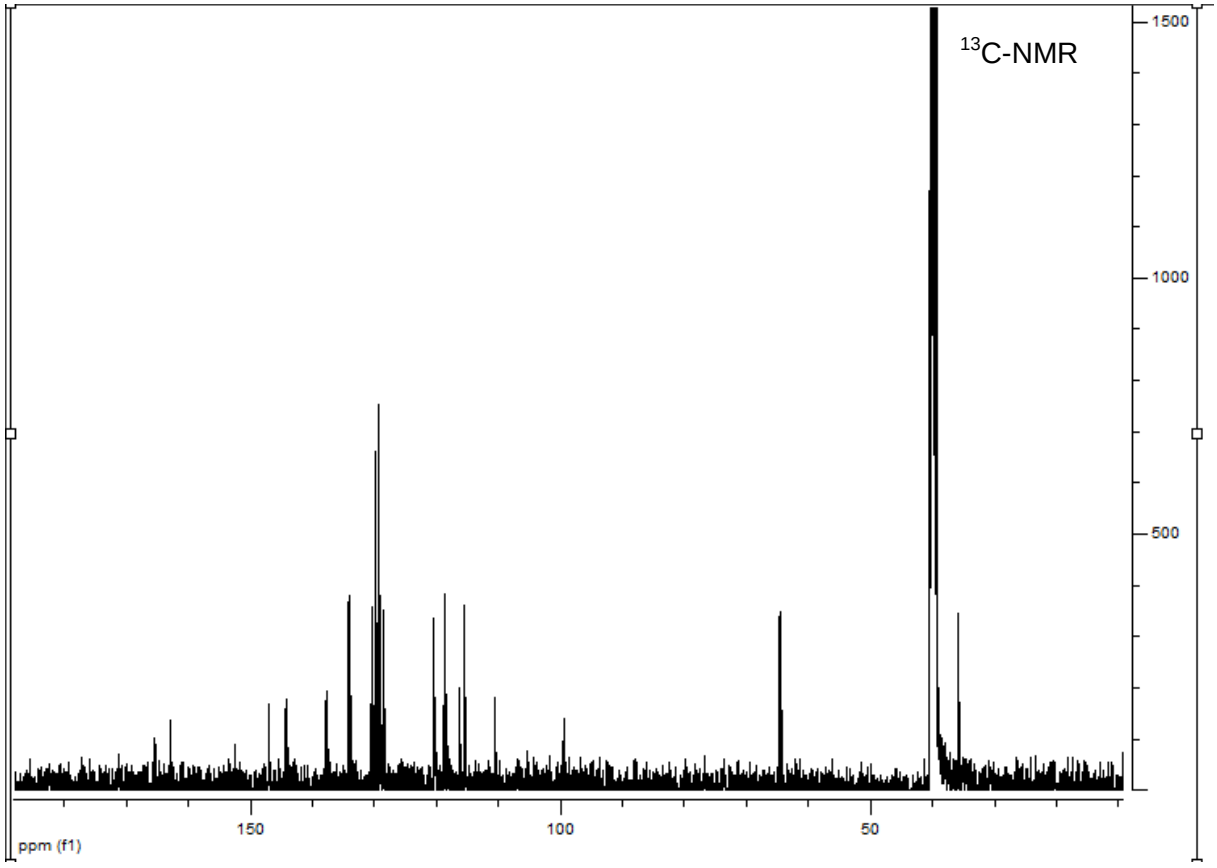
^{13}C-NMR
1500
1000
500
150
100
50
ppm (f1)

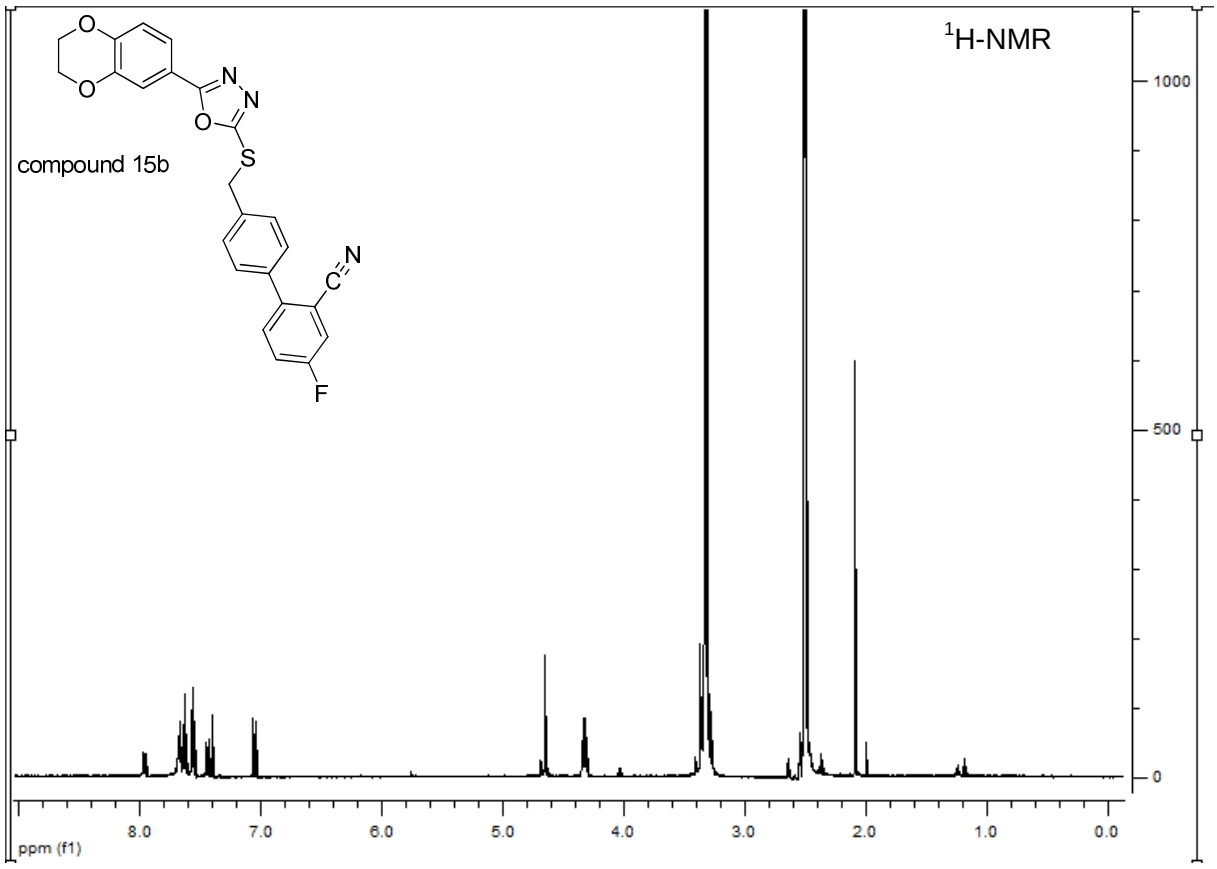

Due to solubility problems it was not possible to measure a ^{13}NMR. Compound **15b** was verified further via High Resolution Mass Spectrometry (HRMS).

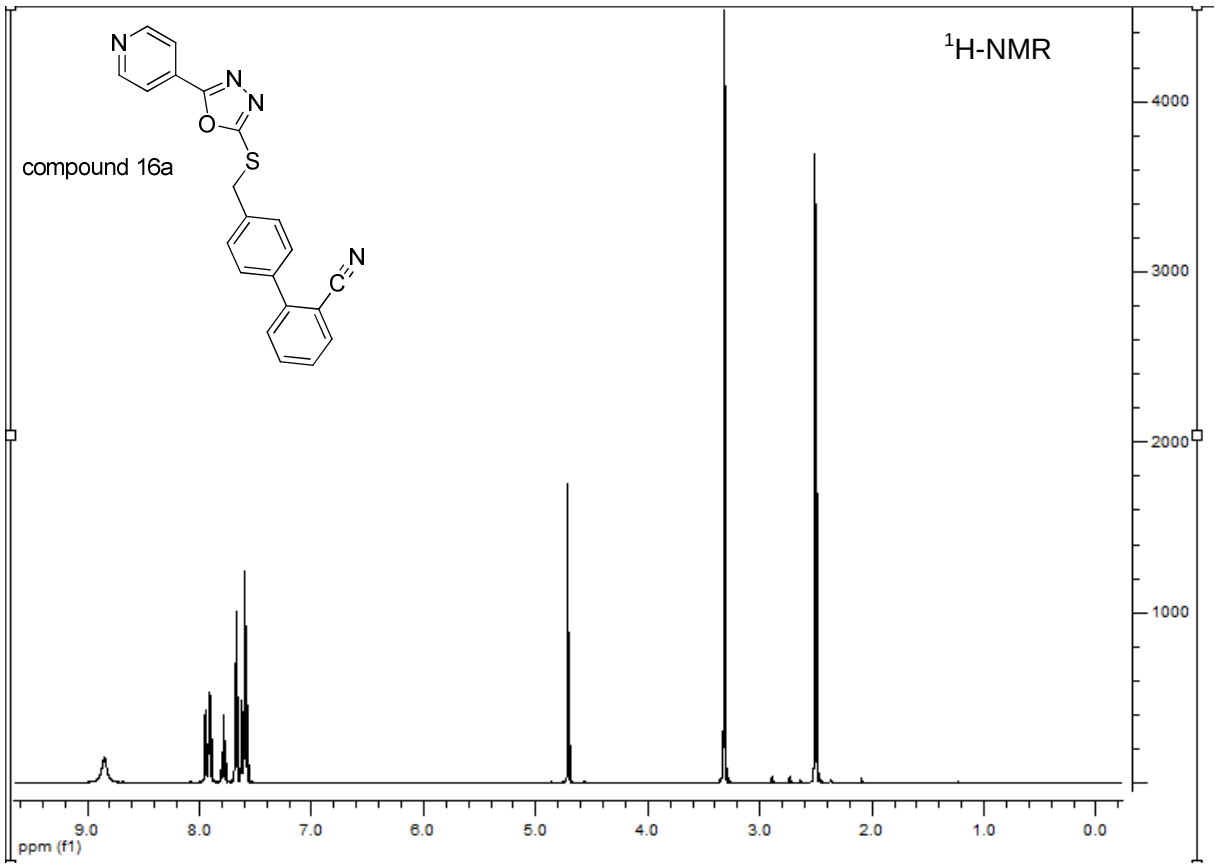
compound 16a
^{1}H-NMR
4000
3000
2000
1000
9.0
8.0
7.0
6.0
5.0
4.0
3.0
2.0
1.0
0.0
ppm (f1)

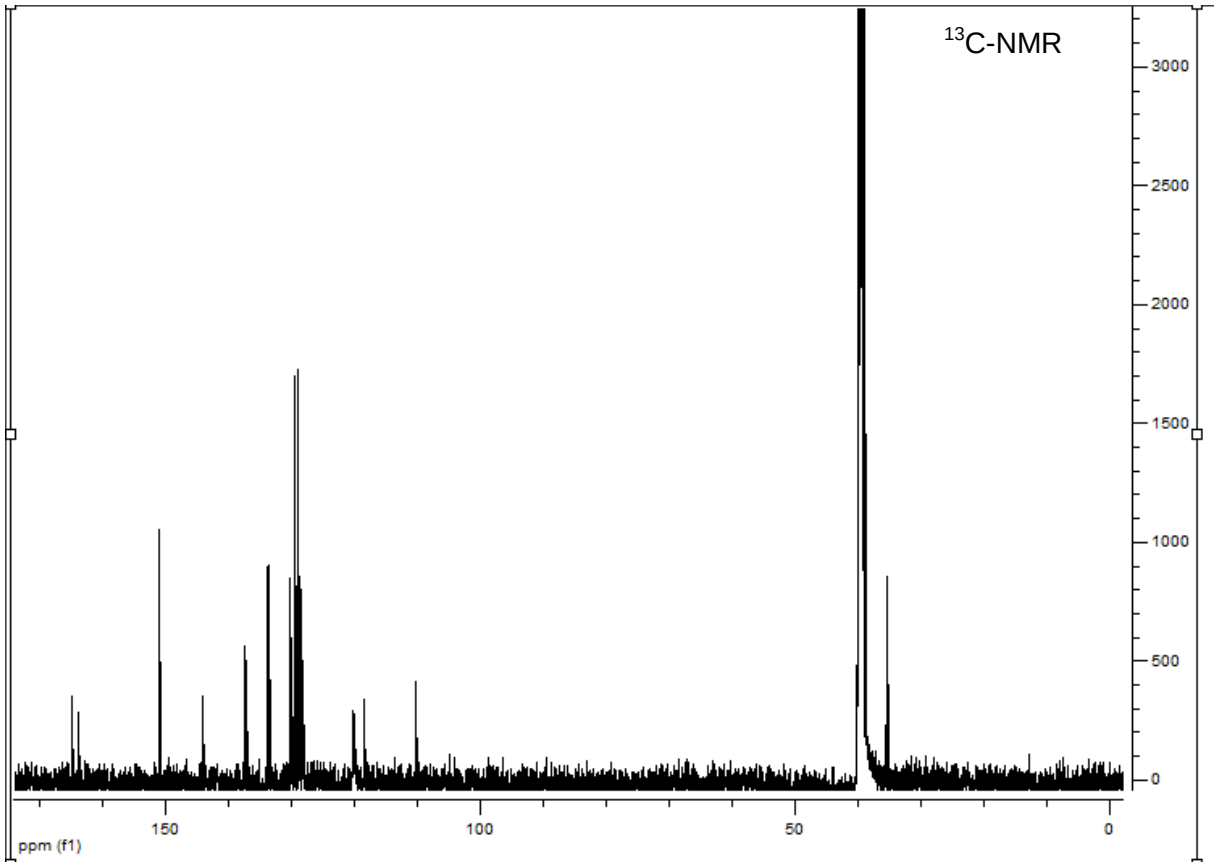
^{13}C-NMR
3000
2500
2000
1500
1000
500
0
150
100
50
0
ppm (f1)

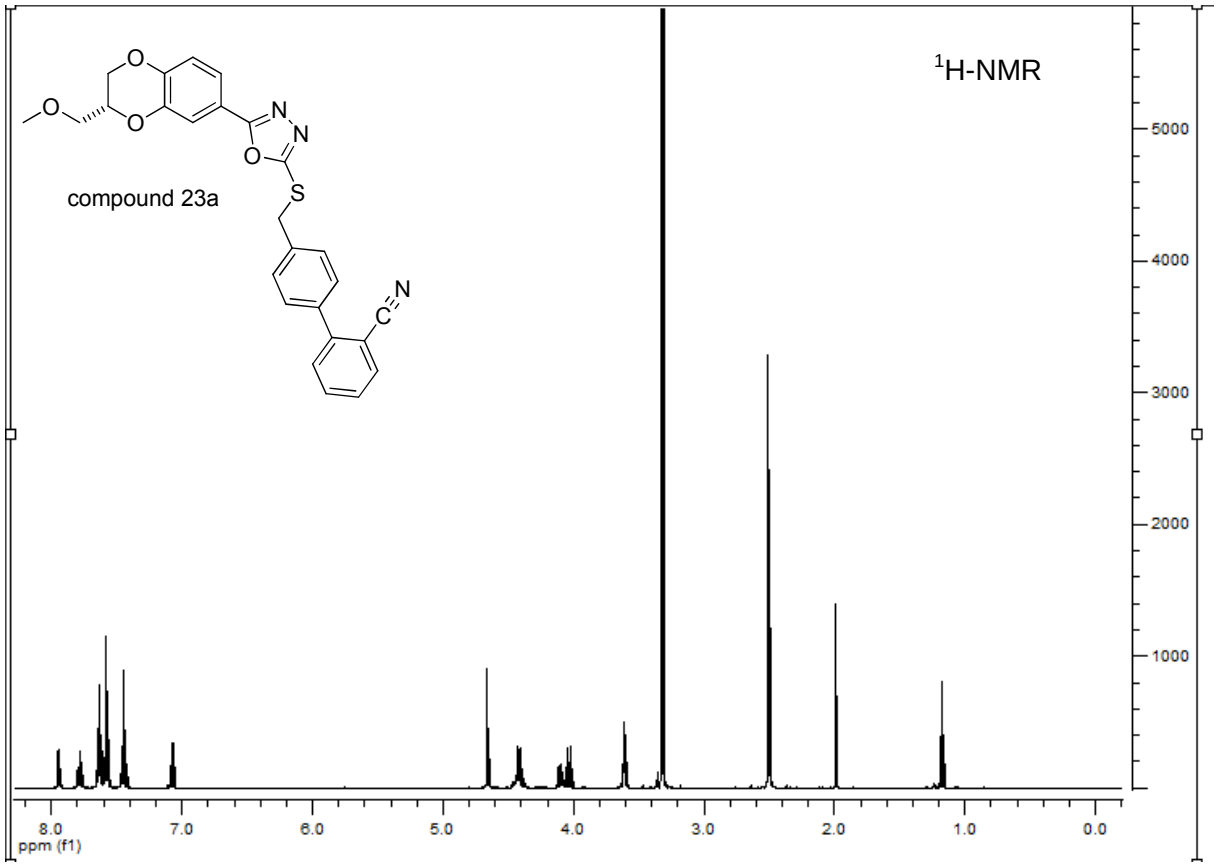
compound 23a
^{1}H-NMR
5000
4000
3000
2000
1000
8.0
7.0
6.0
5.0
4.0
3.0
2.0
1.0
0.0
ppm (f1)

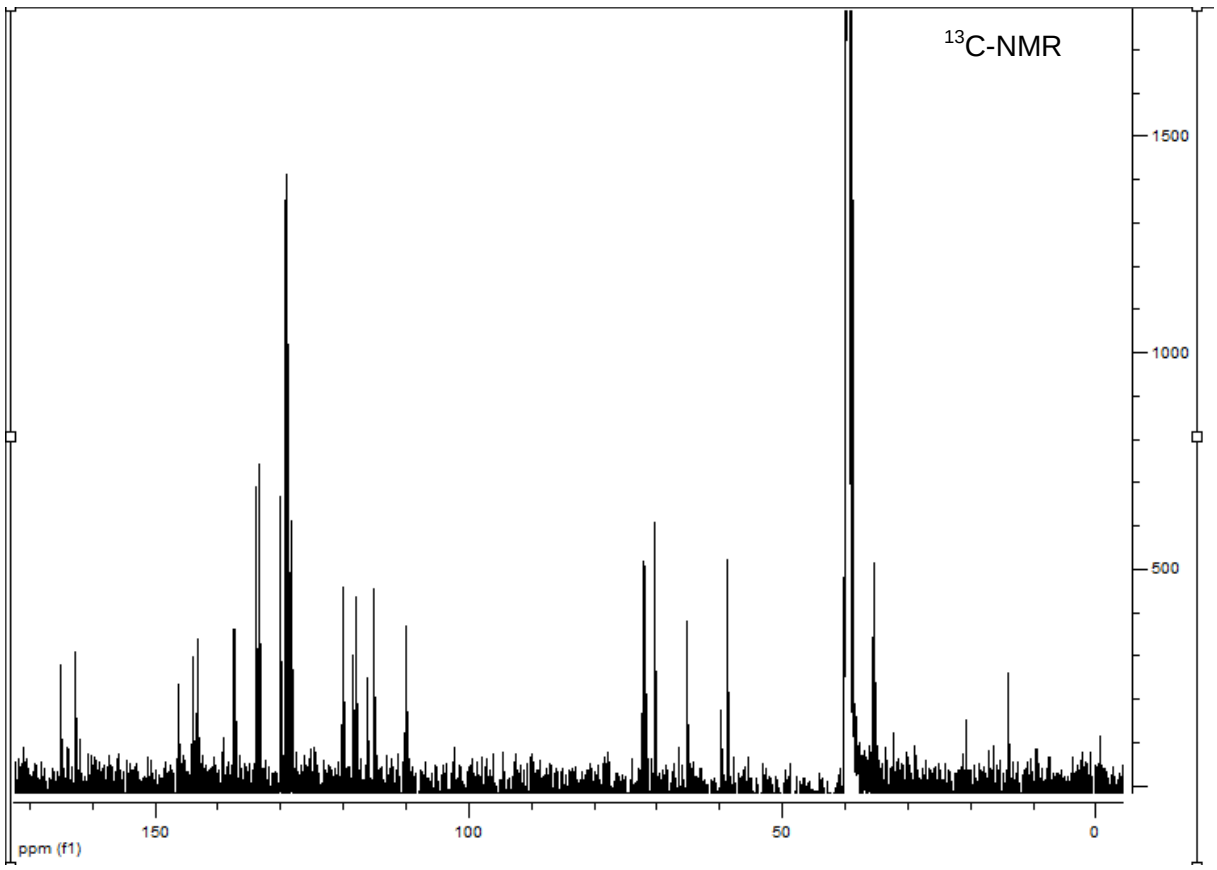
^{13}C-NMR
1500
1000
500
150
100
50
0
ppm (f1)

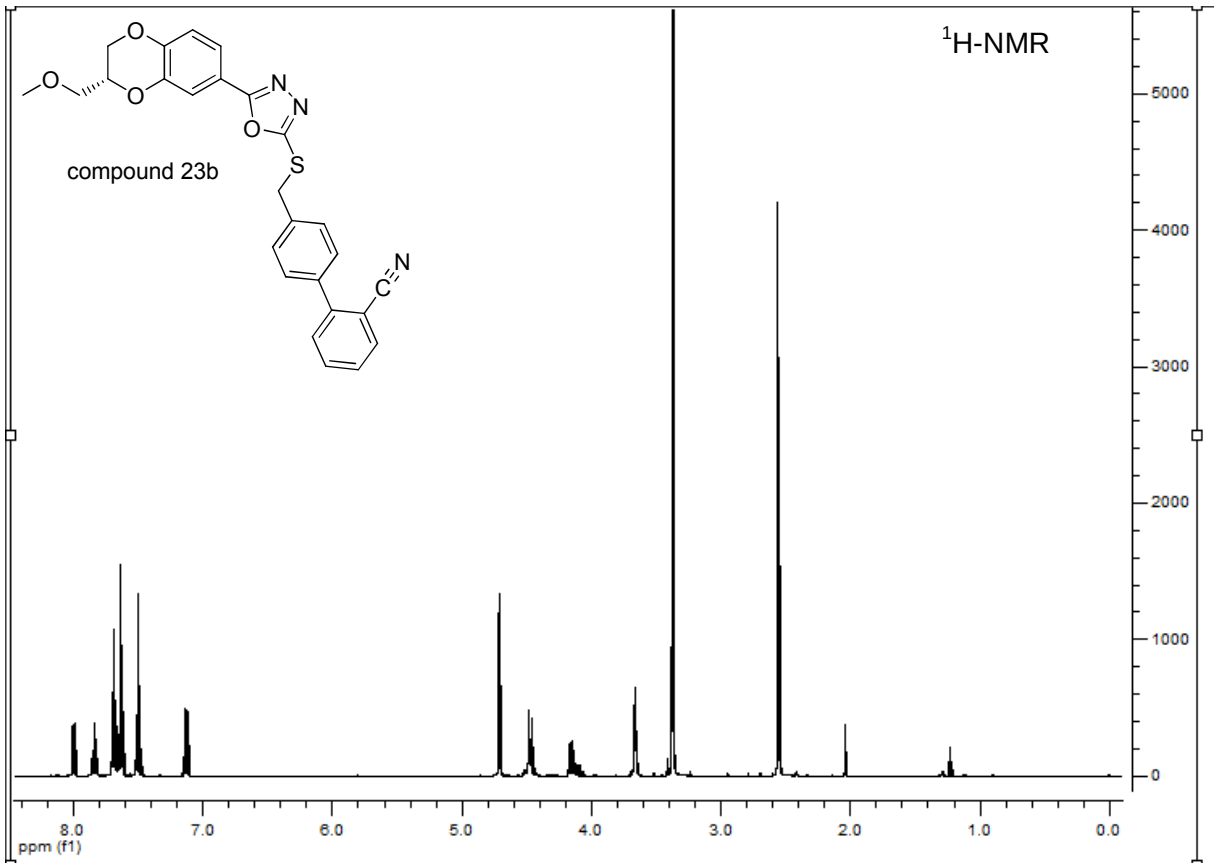
compound 23b
^{1}H-NMR
5000
4000
3000
2000
1000
0
8.0
7.0
6.0
5.0
4.0
3.0
2.0
1.0
0.0
ppm (f1)

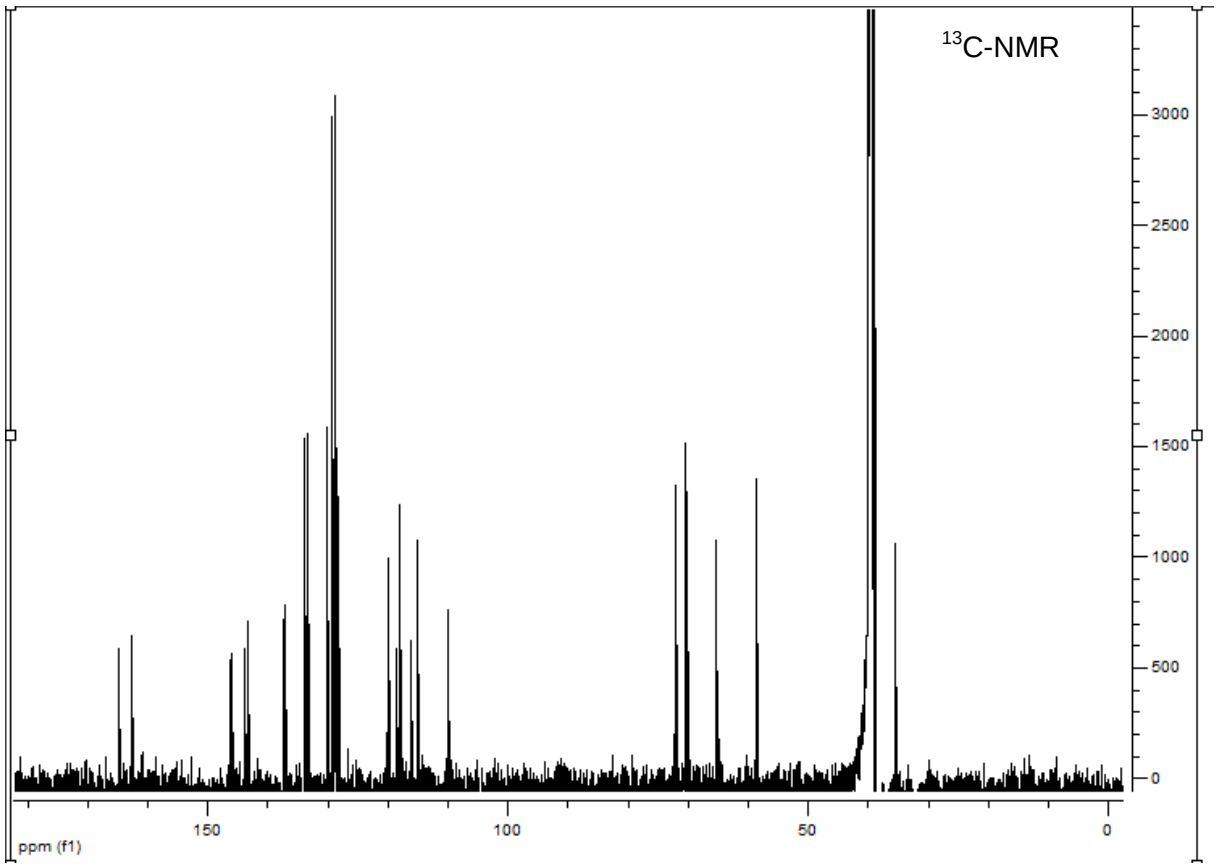
^{13}C-NMR
3000
2500
2000
1500
1000
500
0
150
100
50
0
ppm (f1)

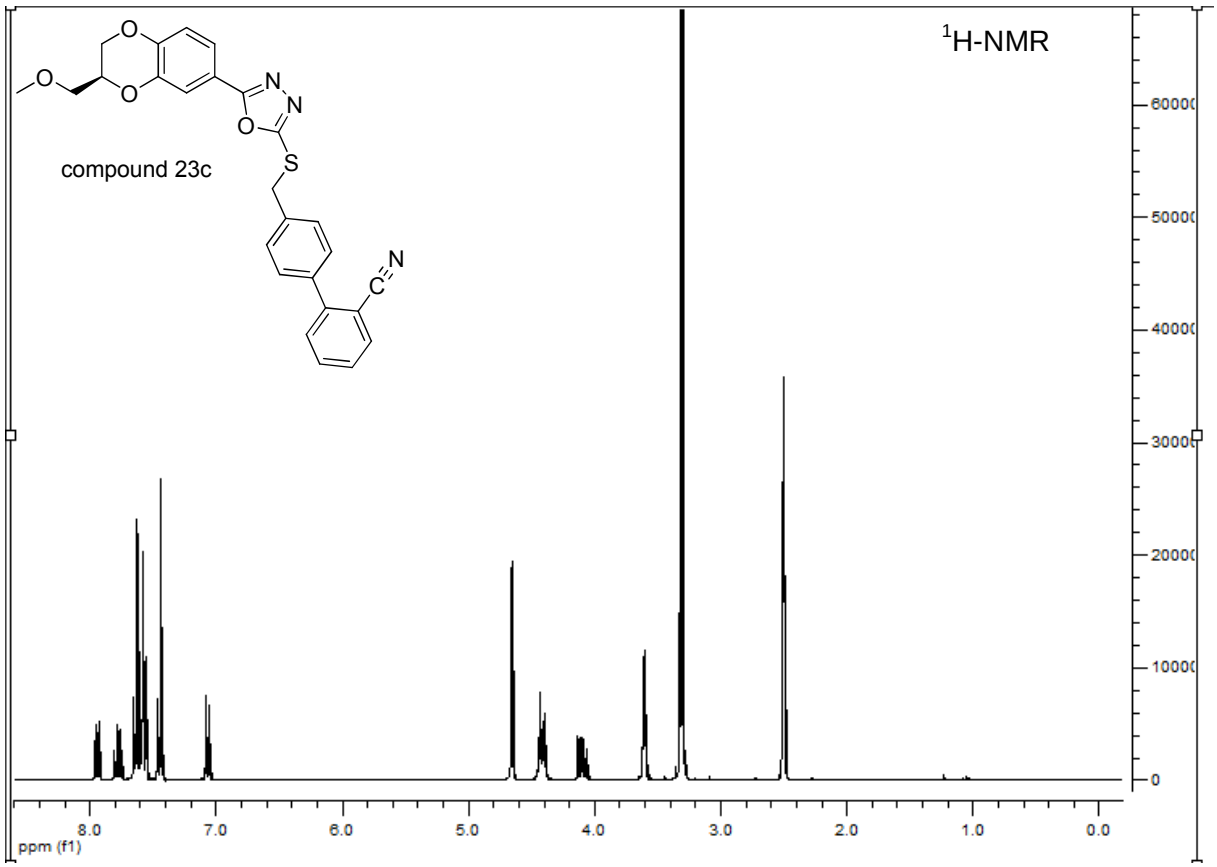
compound 23c
^{1}H-NMR
ppm (f1)

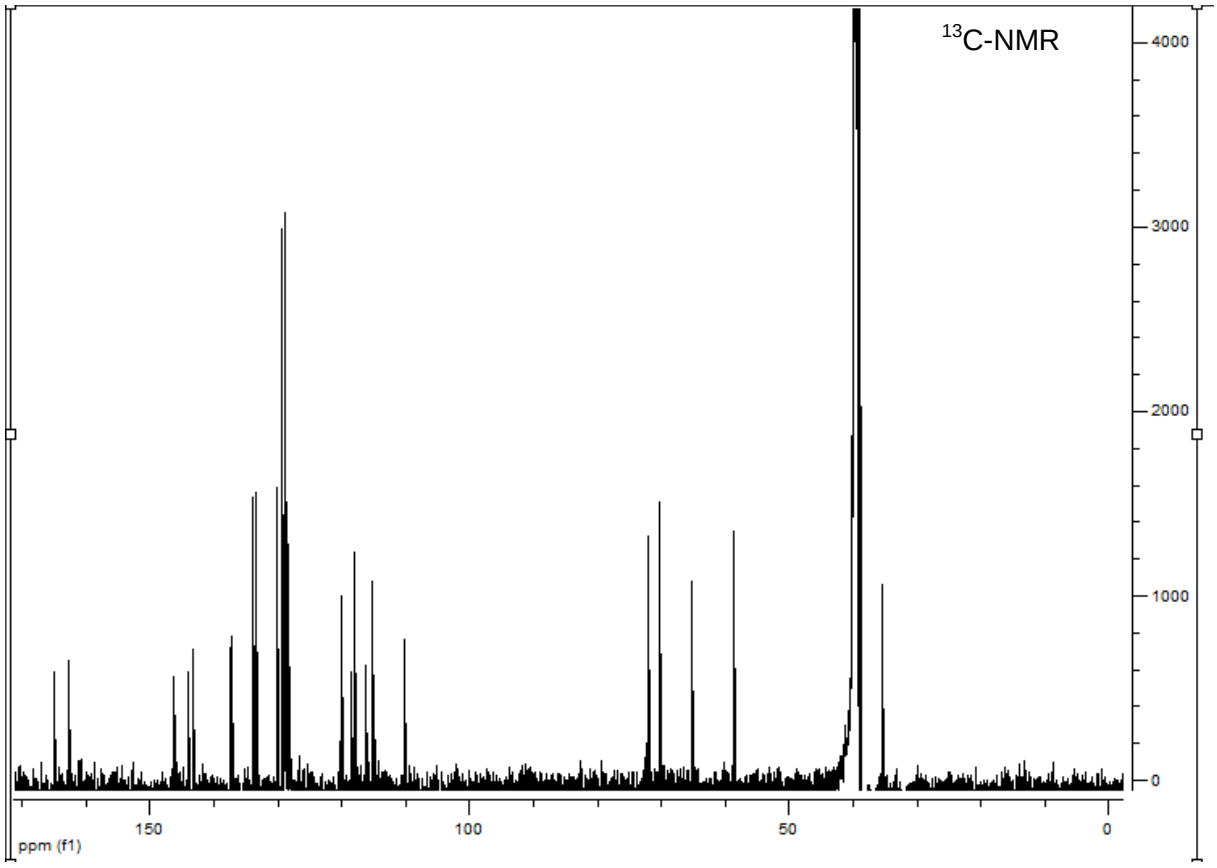
^{13}C-NMR
ppm (f1)

4.1.4 Strukturbasierte Optimierung von Oxadiazolderivaten

Der Inhalt dieses Kapitels wurde bereits zur Publikation angenommen:

Fabio Lo Monte*,‡, Thomas Kramer, Jiamin Gu, Martin Brodrecht, Johannes Pilakowski, Ana Fuertes, Juan Manuel Dominguez, Batya Plotkin, Hagit Eldar-Finkelman, Boris Schmidt‡

Structure-based optimization of oxadiazole-based GSK-3 inhibitors, *European Journal of Medicinal Chemistry* **2012**, zur Publikation angenommen.

Basierend auf vorherigen Untersuchungen wurde das Oxadiazol-Grundgerüst als Startpunkt für eine Reihe von Derivaten eingesetzt. Hierbei wurden verschiedene Systeme und funktionelle Gruppen mit dem Oxadiazol gekuppelt und ausgetestet, um einen genaueren Einblick in die ATP-Bindetasche zu erhalten. Neben den heteroaromatischen und aromatischen Strukturen wurde auch ein Trizyklus getestet, der aber keine Aktivität vorweisen konnte. Letztlich führte die Testung dieser und das Wissen über alte Verbindungen zu drei Fragmenten, von denen ausgegangen wurde, dass sie zu aktiven und selektiven GSK-3-Inhibitoren führen können (Abb. 19).

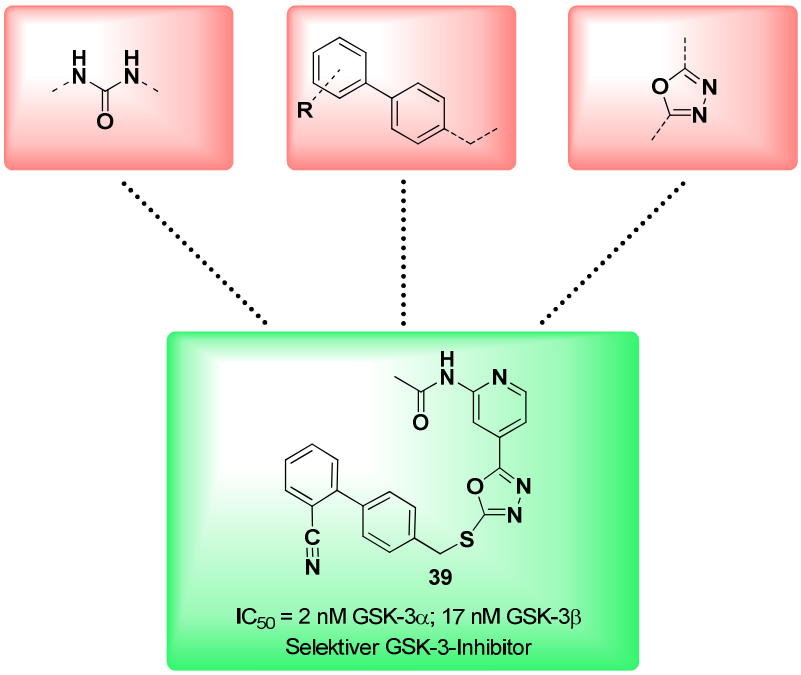

Abb. 19: Schematische Darstellung eines über drei Fragmente erhaltenen GSK-3-Inhibitors.

Die strukturbasierte Strategie mit Hilfe der drei Fragmente konnte zwar nicht auf alle Zyklen übertragen werden, führte jedoch für die Pyridinderivate zu aktiven und selektiven GSK-3-Inhibitoren. Verbindung **39** erwies sich als besonders aktiv und konnte, gegenüber vier anderen getesteten Kinasen, eine mehr als 5000-fache Selektivität für beide Isoformen von GSK-3 aufzeigen. Diese Verbindung verdeutlicht dass die verfolgte Strategie, mit den Kenntnissen über die ATP-Bindetasche und deren Inhibitoren, verwendet werden kann, um gezielt neue Strukturen zu synthetisieren. Das molekulare *Docking* erhärtete unsere Ergebnisse und machte deutlich, dass die Amidfunktion, wie die Harnstofffunktion bei AR-A014418 (**27**), bevorzugt mit der Gelenk-Region wechselwirkt. Bei der *in vivo* Evaluation dieser Strukturklasse im Zebrafisch-Embryo wurde festgestellt, dass diese Verbindungen im getesteten Konzentrationsbereich keine Toxizität aufweisen.

Die im Rahmen dieser Arbeit von Fabio Lo Monte synthetisierten Verbindungen:

BSc4258 (2a), BSc4259 (3a), BSc4260 (4a), BSc4392 (4c), BSc4401 (4b), BSc4611 (26d), BSc4612 (26b), BSc4613 (26c), BSc4614 (26a), BSc4670 (9b), BSc4672 (9a), BSc4674 (8b), BSc4678 (10e), BSc4680 (9d), BSc4682 (9f), BSc4683 (9c), BSc4684 (8e), BSc4685 (8d), BSc4686 (8g), BSc4687 (8c), BSc4688 (10d), BSc4689 (10c), BSc4734 (10a)

In Klammern die Verbindungsnummer in der Publikation.

Structure-based optimization of oxadiazole-based GSK-3 inhibitors

Fabio Lo Monte,[a,*] Thomas Kramer,[a] Jiamin Gu,[a] Martin Brodrecht,[a] Johannes Pilakowski,[a] Ana Fuertes,[b] Juan Manuel Dominguez,[b] Batya Plotkin,[c] Hagit Eldar-Finkelman[c] and Boris Schmidt[a,*]

[a] Clemens Schöpf - Institute of Organic Chemistry and Biochemistry, Technische Universität Darmstadt, 64287 Darmstadt, Germany

[b] Noscira S.A., Drug Discovery, Tres Cantos 28760 - Madrid, Spain

[c] Department of Human Molecular Genetics and Biochemistry, Sackler School of Medicine, Tel Aviv University, 69978 Tel Aviv, Israel

* To whom correspondence should be addressed. Phone: +496151-164531. Fax: +496151-163278. E-Mail: schmidt_boris@t-online.de; Fabio.Lo-Monte@gmx.de

Keywords: Glycogen Synthase Kinase-3 (GSK-3); Alzheimer´s Disease; Structure-Activity Relationship (SAR); Reversible Inhibition; Zebrafish Phenotype

Abstract

Inhibition of glycogen synthase kinase-3 (GSK-3) induces neuroprotective effects, e.g. decreases β-amyloid production and reduces tau hyperphosphorylation, which are both associated with Alzheimer´s disease (AD). The two isoforms of GSK-3 in mammalians are GSK-3α and β, which share 98% homology in their catalytic domains. We investigated GSK-3 inhibitors based on 2 different scaffolds in order to elucidate the demands of the ATP binding pocket [1]. Particularly, the oxadiazole scaffold provided potent and selective GSK-3 inhibitors. For example, the most potent inhibitor of the present series, the acetamide **26d**, is characterized by an IC_{50} of 2 nM for GSK-3α and 17 nM for GSK-3β. In addition, the benzodioxane **8g** showed up to 27-fold selectivity for GSK-3α over GSK-3β, with an IC_{50} of 35 nM for GSK-3α. Two GSK-3 inhibitors were further profiled for efficacy and toxicity in the wild-type (wt) zebrafish embryo assay to evaluate simultaneously permeability and safety.

1. Introduction

Alzheimer´s disease (AD) is a neurodegenerative disorder and characterized by the presence of abnormal filamentous protein inclusions in nerve cells of the brain [2]. The neuropathological hallmarks of AD were first reported by Alois Alzheimer and date back to 1907 [3-4]. These inclusions are formed by extracellular amyloid deposits and intracellular microtubule-associated protein tau [5]. Early onset forms of familial Alzheimer´s disease (FAD) have been linked to mutations in the amyloid precursor protein (APP), presenilin-1 (PS-1) and presenilin-2 (PS-2). These mutations adversely affect APP processing and result in the increased production of the 40-42 amino acid long β-amyloid (Aβ) peptides, which are the major component of amyloid deposits. Several risk factors have been associated with sporadic Alzheimer´s disease (SAD). The most prevalent is aging and the presence of specific ApoE isoforms, which have been implicated in Aβ clearance. The activation of β-secretase may be involved in Aβ generation, which in combination with a deficiency in Aβ clearance will result in the accumulation of Aβ aggregates [2, 6]. Partially phosphorylated tau in the normal adult brain features sequences that support association with tubulin, which entails the stabilization of microtubules. The pathological hyperphosphorylation of tau causes destabilization of microtubules, which in turn interferes with tubulin binding. The misfolding of hyperphosphorylated tau leads to the formation of insoluble neurofibrillary tangles (NFTs) and intraneuronal aggregates of paired helical filaments (PHFs) [7-8]. GSK-3 was shown to phosphorylate tau both *in vitro* and *in vivo* on multiple sites [7]. Several studies demonstrate that inhibition of GSK-3 induces decreased Aβ production and a reduction in tau hyperphosphorylation [9-10]. GSK-3 was identified in the late 1970s and is a constitutively active, ubiquitously expressed serine/threonine kinase, which participates in a number of physiological processes [2, 11]. Two related isoforms of GSK-3 exist in mammals, GSK-3α and β, which share 98% homology in their catalytic domains and have similar biochemical properties [7, 12]. The isoforms differ significantly outside of their catalytic domains at their N-terminal regions [13]. Furthermore, an alternative splice variant of GSK-3β: GSK-3β2, has been reported for rodents and humans [14-15]. The crystal structure of GSK-3β was determined in 2001 [16-17]. GSK-3 is highly enriched in the brain and several publications indicate that the GSK-3β isoform is a key kinase required for abnormal hyperphosphorylation of tau [18-20]. Lithium chloride was the first GSK-3 inhibitor to be discovered. However there are several other biological targets for lithium cations, which impose limits on the therapeutic window. Considering the homology of GSK-3α and β within the ATP-binding

pocket it appears difficult to identify an inhibitor that differentiates the two isoforms. All GSK-3 inhibitors developed until now are able to inhibit the two isoforms with almost similar potency, except compound **Λ-OS1**, which showed up to 7-fold selectivity for GSK-3α and compound **15b**, which showed up to 92-fold selectivity for GSK-3α [21-24]. A plethora of GSK-3 inhibitors has been described and most of the effects were observed *in vitro* and cellular studies (Fig. 1) [5, 25-26]. These studies and the ongoing patent filing indicate that GSK-3 is a potential drug target not just for the treatment of AD. Several research groups and pharmaceutical companies are interested in the discovery of novel GSK-3 inhibitors with good selectivity and bioavailability despite of the Wnt-pathway associated risks, which may result in adverse cell proliferation. In the present study, the 1,3,4-oxadiazole-moiety served as a scaffold for a variety of GSK-3 inhibitors. This particular heterocycle was chosen because it has favourable properties over 1,2,4-oxadiazoles and other five-membered heterocycles [27]. The inhibition potencies of these compounds were compared to those of the previously reported 1,3,4-oxadiazoles and substituted ureas in the attempt to identify additional heterocycles and substituents that enhance GSK-3 inhibition [1, 28-30]. The resulting interactions with the ATP binding pocket of GSK-3α and β were also investigated to generate a hypothesis for isoform discrimination. We employed the wild-type zebrafish embryo in order to validate the utility of these compounds *in vivo*.

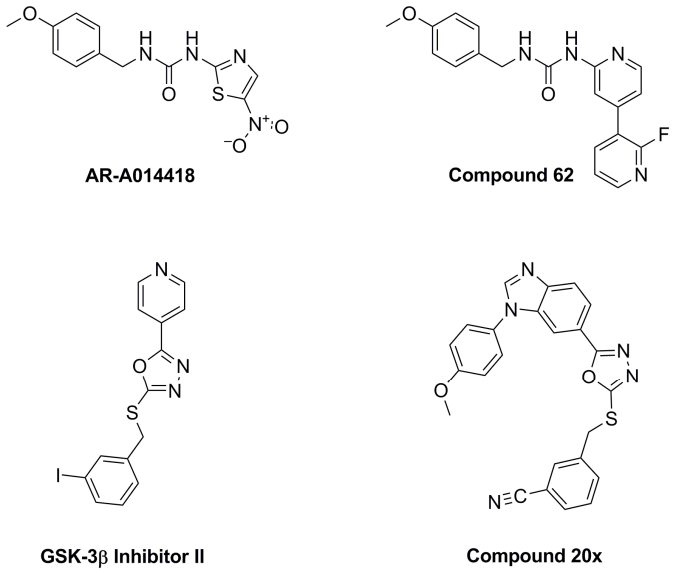

Fig. 1. Structures of previously reported GSK-3 inhibitors.

2. Chemistry

The esterfication of the carboxylic acids **1a, b** afforded compounds **2a, b** which were converted to the hydrazides **3a, b**. The hydrazide **3c** was commercially available. Reaction of the hydrazides **3a-c** with carbon disulfide (CS_2) afforded the oxadiazoles **4a-c** (Scheme 1) [28, 31-32].

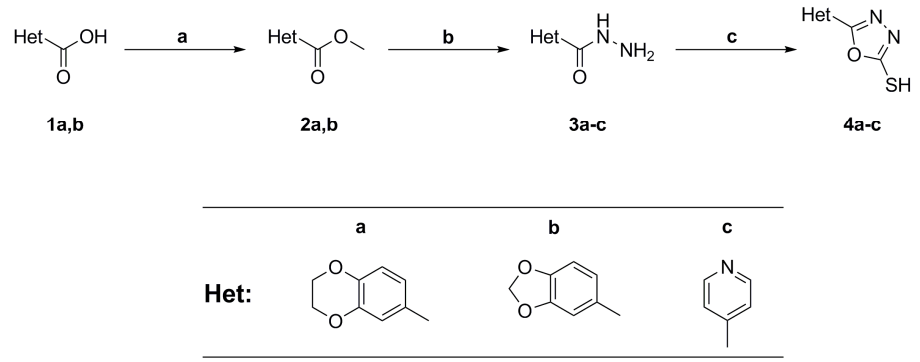

Scheme 1. Reagents and conditions: (a) MeOH, $SOCl_2$, 0°C to 50°C, 83-89%; (b) $NH_2NH_2 \cdot H_2O$, EtOH, reflux, 67-75%; (c) CS_2, Et_3N, EtOH, reflux, 79-89%.

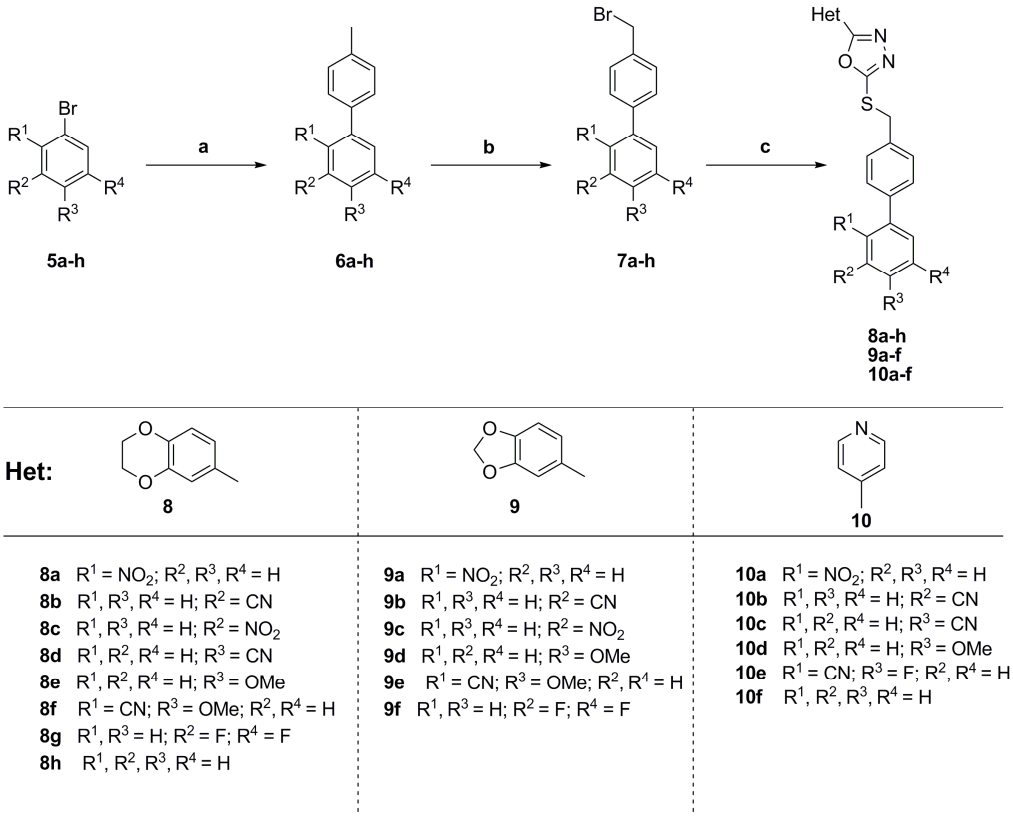

Scheme 2. Reagents and conditions: (a) aryl bomide, toluene, EtOH, $Pd(PPh_3)_4$, 2-tolylboronic acid, 2 N Na_2CO_3(aq.), 80°C; (b) NBS, AIBN, CCl_4, reflux; (c) oxadiazoles (4a-c), 1N NaOH, DMF, rt, 27-79%.

The biphenyls **7a-h** were prepared in two steps from commercial *p*-tolylboronic acid and bromobenzene bearing substituents at the 1- to 4-position [33]. The biphenyl halides **7a-h** were coupled with the heterocycles **4a-c** to obtain the compounds **8a-h**, **9a-f** and **10a-f** (Scheme 2). The thioethers **15-18 (a-d)** (Scheme 3) were synthesized similar to method described in Scheme 1 and 2 [28, 34-35]. The hydrazones **20a-d** were prepared using isoniazid **19** (Scheme 4) and 4 different benzaldehydes [36-38]. The esterification of acid **21** to the ester **22** employed standard conditions, it was followed by reaction with acetic anhydride to provide the amide **23** (Scheme 5) [39-40]. The thioethers **26a-d** were synthesized according to the method described in Scheme 1 and 2. Esterfication of compound **27**, followed by cyclization gave compound **29** (Scheme 6) [41-42].

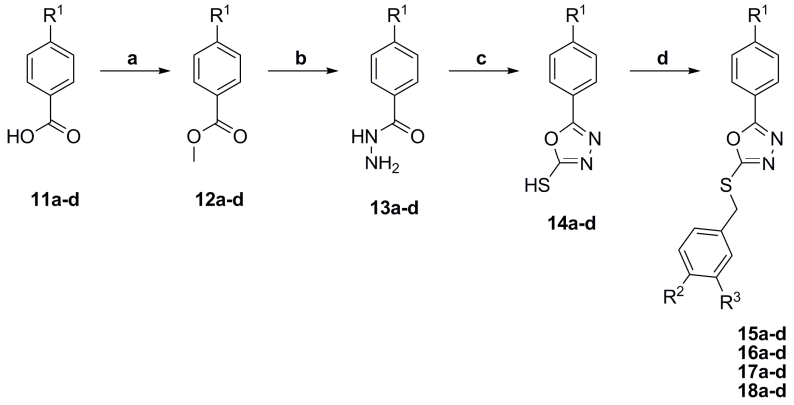

15a	R^1, R^2, R^3 = H	**16a**	R^1 = OMe; R^2, R^3 = H
15b	R^1 = H, R^2 = 2-benzonitrile; R^3 = H	**16b**	R^1 = OMe, R^2 = 2-benzonitrile; R^3 = H
15c	R^1 = H; R^2 = H, R^3 = OMe	**16c**	R^1 = OMe; R^2 = H, R^3 = OMe
15d	R^1 = H; R^2 = H, R^3 = CN	**16d**	R^1 = OMe; R^2 = H, R^3 = CN
17a	R^1 = CN; R^2 = H, R^3 = H	**18a**	R^1 = NO_2; R^2 = H, R^3 = H
17b	R^1 = CN, R^2 = 2-benzonitrile; R^3 = H	**18b**	R^1 = NO_2, R^2 = 2-benzonitrile; R^3 = H
17c	R^1 = CN; R^2 = H, R^3 = OMe	**18c**	R^1 = NO_2; R^2 = H, R^3 = OMe
17d	R^1 = CN; R^2 = H, R^3 = CN	**18d**	R^1 = NO_2; R^2 = H, R^3 = CN

Scheme 3. Reagents and conditions: Reagents and conditions: (a) MeOH, $SOCl_2$, 0°C to 50°C, 68-76%; (b) $NH_2NH_2 \bullet H_2O$, EtOH, reflux, 81-89%; (c) CS_2, Et_3N, EtOH, reflux, 74-88%; (d) Benzyl halides, 1N NaOH, DMF, rt, 32-71%.

Compound **30** was obtained using the conditions described for compound **23** [40]. Saponification of the ester **30**, followed by reaction with *tert*-butyl carbazate, gave compound **32** [28, 43]. Cleavage of the *tert*-butylamine in **32** by TFA and submission to the reaction conditions described in Scheme 1 and 2 provided the final product **35** [28]. Bromination of the 4-hydroxybenzoic acid **36**, gave compound **37** (Scheme 7) [44]. The dibenzofuran **38** was obtained by the combination of two reactions in a one-pot synthesis [45-46]. The final

compound **41** was prepared in relation to the method described in Scheme 1 and 2. The structures of all compounds were verified by mass spectrometry, ^{1}H-NMR and ^{13}C-NMR.

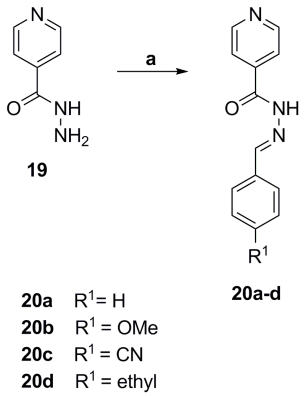

Scheme 4. Reagents and conditions: (a) EtOH/H_2O, Aldehydes, rt, 83-97%.

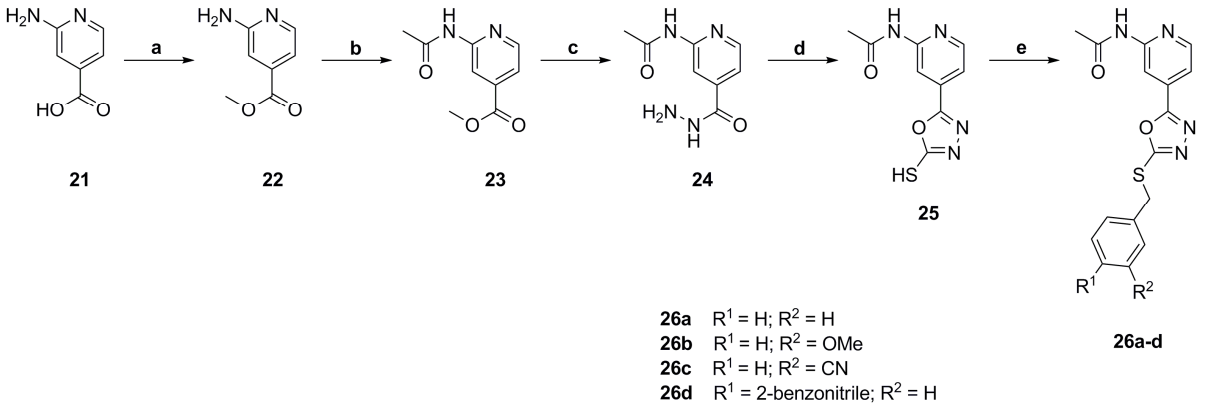

Scheme 5. Reagents and conditions: (a) MeOH, $SOCl_2$, 0°C to 50°C, 89%; (b) acetic anhydride, 105°C, 69%; (c) NH_2NH_2•H_2O, EtOH, reflux, 74%; (d) CS_2, Et_3N, EtOH, reflux, 92%; (e) Benzyl halides, 1N NaOH, DMF, rt, 37-68%.

3. Results and discussion

The synthesized compounds were evaluated for GSK-3 inhibition in a commercial system based on the Z'-LYTE® technology, available from Invitrogen Life Technologies (Carlsbad, CA, USA), using human recombinant GSK-3α or GSK-3β as the enzyme source and further for their inhibitory activity *in vitro* against GSK-3β. Several compounds displayed more than 50% inhibitory activity against GSK-3β at 10 µM concentration. We focussed our interest on inhibitors with potential occupation of the entire ATP-binding pocket, and thereby to enhance potency and selectivity (Fig. 2). Heterocycles featuring the oxadiazole ring typically interact within the green marked area of GSK3 (Fig. 2). Our goal was to extend our compounds to the

area highlighted in blue. Furthermore, we tried to enhance the potential interaction with the backbone by replacing heterocycles with phenyl rings bearing different acceptors and to investigate the contribution deriving from the rigidity of a tricyclic system [26]. The 3 heterocyclic fragments **4a-c** were introduced as potential hinge binders in order to interact with the GSK-3 backbone: Asp133/Tyr134/Val135 (Scheme 1). The oxadiazole moiety is assumed to engage with the polar binding pocket, consisting of three amino acids (Lys85/Glu97/Asp200). Such interactions were previously reported for the GSK-3β inhibitor II and 20x (Fig. 1). We coupled the compounds **4a-c** to biphenyl systems bearing different substituents on the second phenyl ring (Scheme 2). Most of these compounds showed remarkable activities and selectivities (Table 1).

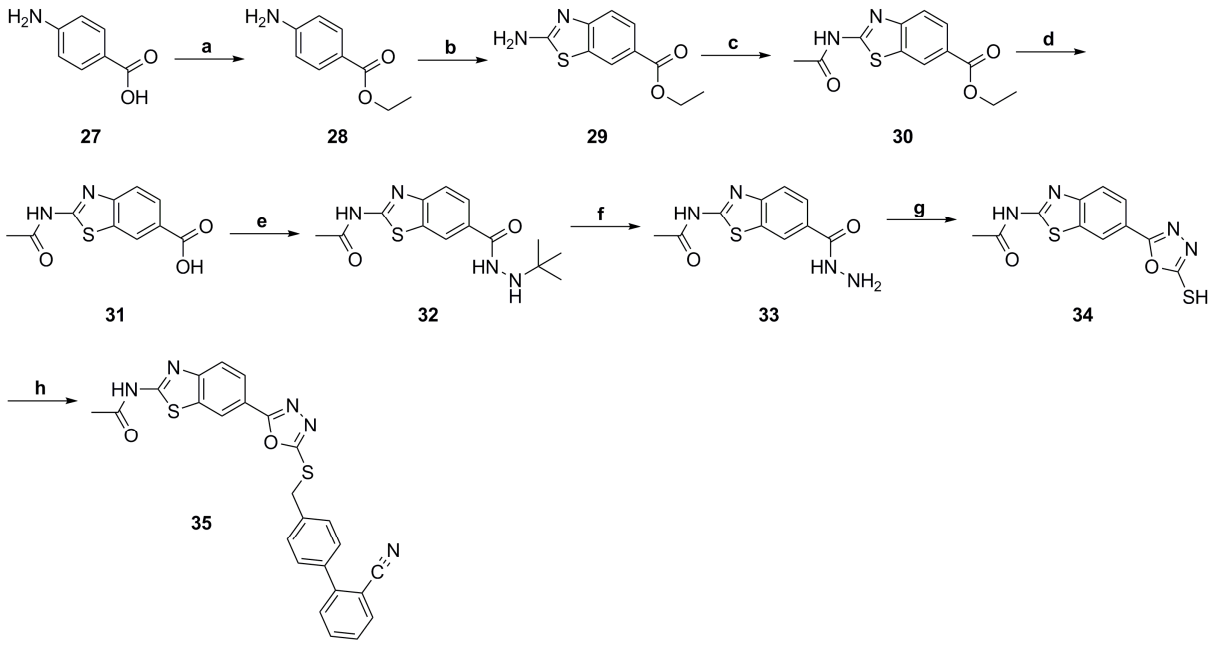

Scheme 6. Reagents and conditions: (a) EtOH, H_2SO_4, reflux, 91%; (b) CH_3COOH, KSCN, Br_2, rt, 67%; (c) acetic anhydride, 105°C, 58%; (d) MeOH, 1N NaOH, rt, 94%; (e) DMF, *tert*-Butyl carbazate, EDCI, HOBt•H_2O, rt, 77%; (f) TFA, rt, 99%; (g) CS_2, Et_3N, EtOH, reflux, 81%; (h) Benzyl halide, 1N NaOH, DMF, rt, 47%.

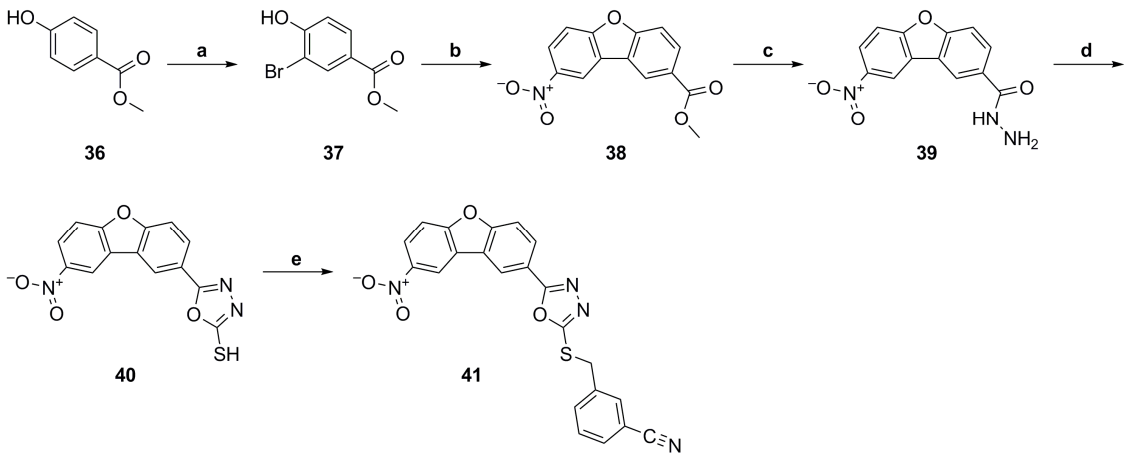

Scheme 7. Reagents and conditions: (a) DCM, Br_2, rt, 65%; (b) DMF, $Pd(OAc)_2$, K_2CO_3, 130°C, 30%; (c) $NH_2NH_2 \bullet H_2O$, rt, 99%; (d) CS_2, Et_3N, EtOH, reflux, 48%; (e) Benzyl halide, 1N NaOH, DMF, rt, 44%.

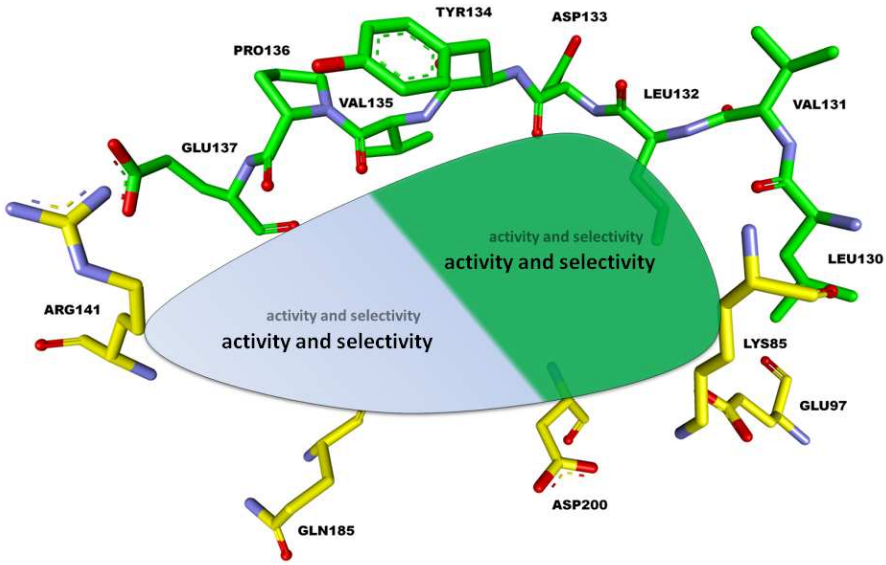

Fig. 2. Schematic overview of the GSK-3 ATP-binding pocket. The green marked area reveals the interaction site of the heterocycle and oxadiazole ring. The area we wanted to occupy with our structures is marked in light blue.

The compounds **8f** and **9a-e** were found to be potent inhibitors of both isoforms of GSK-3 as characterized by IC_{50} values in the low nanomolar range. In addition, all of them showed good selectivities against other kinases. Substituents in the ortho- and para-positions of structure **8** and **9** lead to potent inhibition of both isoforms as indicated for compound **8f** and **9e** with an IC_{50} value of 5 nM for GSK-3α respectively 14 nM and 32 nM for GSK-3β. We reasoned that only the interplay respectively combination of different substituents is adequate to gain selectivity against one GSK-3 isoform. Compounds **8b** and **8g** enhance the selectivity for

GSK-3α up to 27-fold. An inverse effect was observed for pyridine **10e** where a substituent in meta- and para-position leads to slightly increased selectivity for inhibition of GSK-3β. All compounds lacking the heterocycle (Scheme 3) or oxadiazole ring (Scheme 4) completely lost most of their ability to inhibit GSK-3 and resulted in a residual GSK-3β activity of more than 50% at 10 µM. We attempted the combination of different lead structures by the addition of an amide function at the pyridine and benzothiazole (Scheme 4 and 5). A similar moiety serves as an ambident moiety on Sorafenib. It was reported to establish hydrogen bonds with the same amide on the target hinge region either via the pyridyl nitrogen or through the carbonyl of the acetyl amide [47-48].

Table 1

Inhibitory activity against different kinases *in vitro* and *in silico* parameters (calc. with ChemDraw Ultra 9.0.1).

	IC_{50} (µM)						**clogP**	**tPSA ($Å^2$)**
Compound	GSK-3α	GSK-3β	Cdk5/p35	CK1ε	AurKA	PKCα		
8a	0.004	0.090	> 100	> 100	> 100	> 100	4.62	112.2
8b	0.009	0.225	> 100	> 100	> 100	> 100	4.31	84.8
8c	0.015	0.164	> 100	> 100	> 100	> 100	4.62	112.2
8d	0.195	1.995	> 100	> 100	50.0	> 100	4.31	84.8
8e	0.019	0.127	> 100	> 100	> 100	> 100	4.80	79.0
8f	0.005	0.032	> 100	> 100	> 100	> 100	4.56	98.9
8g	0.035	0.966	> 100	> 100	> 100	> 100	5.16	64.9
8h	0.051	0.234	> 100	> 100	> 100	> 100	4.88	64.9
9a	0.003	0.027	> 100	> 100	> 100	> 100	4.66	112.2
9b	0.004	0.029	> 100	> 100	> 100	> 100	4.35	84.8
9c	0.015	0.086	> 100	> 100	> 100	> 100	4.66	112.2
9d	0.007	0.075	> 100	20.0	40.0	> 100	4.84	79.0
9e	0.005	0.014	> 100	50.0	45.0	> 100	4.60	98.9
9f	0.051	0.195	> 100	80.0	> 100	> 100	5.21	64.9
10a	0.027	0.164	> 100	> 100	5.0	> 100	3.28	95.3
10b	0.046	0.084	> 100	> 100	60.0	> 100	2.97	67.9
10c	0.077	0.153	> 100	> 100	> 100	> 100	2.97	67.9
10d	0.240	0.176	> 100	> 100	> 100	> 100	3.45	62.1
10e	0.324	0.056	> 100	> 100	> 100	> 100	3.11	67.9

10f	0.052	0.083	> 100	> 100	> 100	> 100	3.53	48.0
26a	0.020	0.035	> 100	> 100	60.0	> 100	1.58	83.1
26c	0.017	0.019	> 100	> 100	> 100	> 100	1.01	103.0
26d	0.002	0.017	> 100	> 100	> 100	> 100	2.90	103.0

Thus the amide was expected to increase the interaction with the backbone of GSK-3 as observed in the tight binding of **Compound 62** and **AR-A014418** (Fig. 1). We determined promising activities and selectivities for the pyridines **26a**, **26c** and **26d**. Especially compound **26d** with an IC_{50} value of 2 nM for GSK-3α and 17 nM for GSK-3β showed more than 5000-fold selectivity against Cdk5/p35, CK1ε, AurKA and PKCα (Table 1). However, the additional amide on the benzothiazole **35** reduced activity for both isoforms indicating too close proximity to the backbone. Moreover, the acetamide **26d** is characterized by a clogP of 2.90 and a tPSA of 103.0 $Å^2$. The letter value exceeds the limits for likely blood-brain barrier permeation. In addition, the structural rigidity of the dibenzofuran **41** resulted in loss of inhibitory activity against GSK-3.

A docking study of compound **9e** and **26d** into the PDB structure 3F88 of GSK-3β suggested a binding mode that uses the ATP-binding pocket in its entirety. The oxadiazole interacts in both cases with the polar pocket consisting of Lys85 and Asp200. For compound **9e** the amide functions leads to a binding mode along the hinge region of the ATP-binding pocket. The biphenyl system interacts with Ile62, Gly63, Phe67 and Val70, which form part of the flexible glycine-rich loop. The methoxy group of compound **9e** is located in close proximity to the salt bridge formed by Glu137 and Arg141, which may be responsible for the activity of this compound. Nevertheless, this structure does not provide insight into the selective inhibition of the GSK-3β isoforms as all amino acid residues shown in Figure 3 are identical in both isoforms. Hence, only a complex of GSK-3β co-crystallized with one of these inhibitors, solved by X-ray crystallography, may provide the necessary insights.

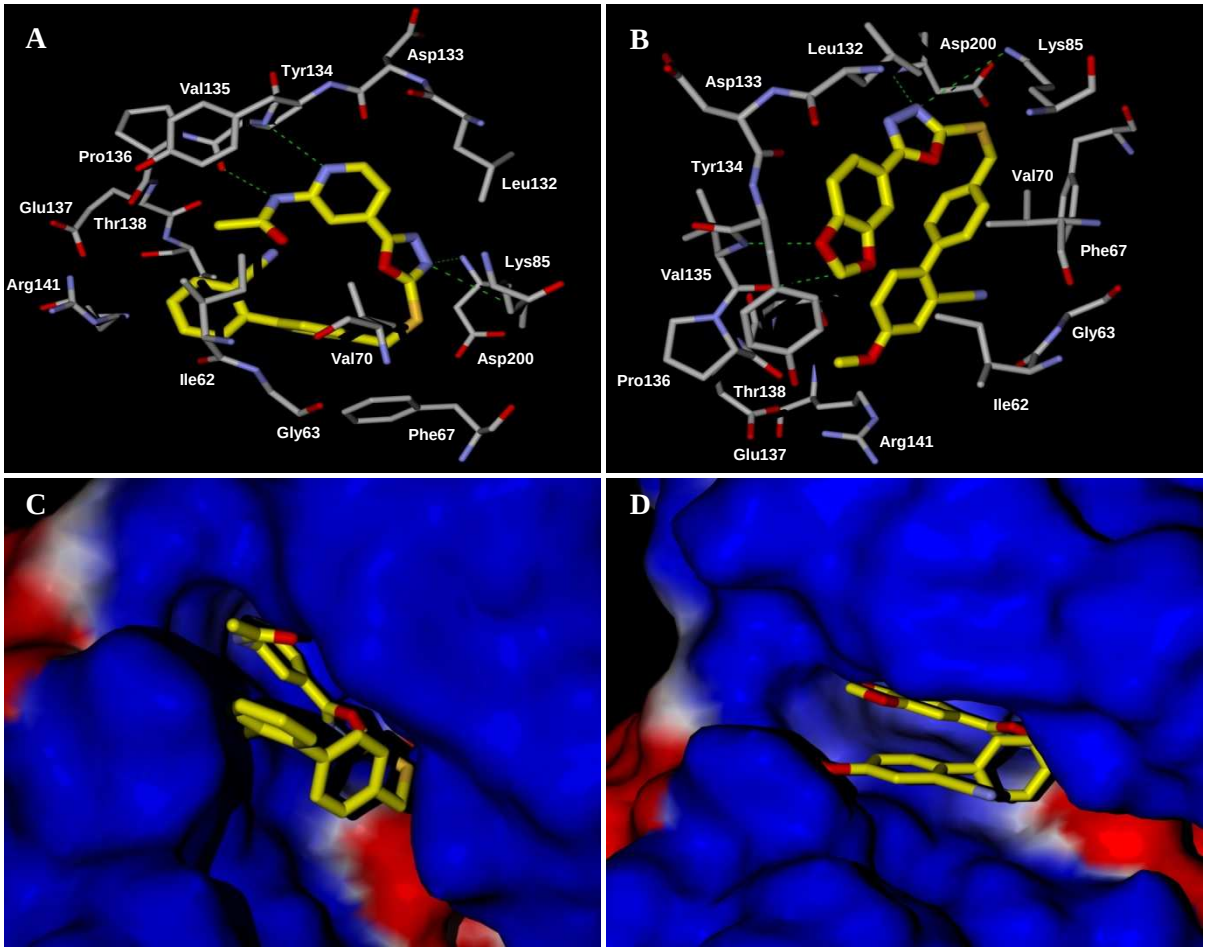

Fig. 3. Docking of compounds **9e** and **26d** into PDB structure 3F88 of GSK-3β; Hydrogen bond interactions of compound **26d** (A) and **9e** (B) with the amino acids of the ATP-binding pocket; Surface illustration of the ATP-binding pocket with compound **26d** (C) and **9e** (D). The inhibitors are shown in yellow. These figures were prepared with Molegro Virtual Docker 5.

After evaluation of the *in vitro* activity and selectivity of these compounds the biphenyl derivatives **9e** and **26d** were further tested for their *in vivo* activity on wt zebrafish embryos. We exposed the embryos to these compounds at early stages of development (Figure 4). The embryos were collected and maintained in E2 medium at ~28°C. The compounds were added 5 hpf (hour post fertilization), and the phenotypes were compared at 44-48 hpf. Compounds **9e** and **26d** cause a stunted and crooked tail at 30 µM. This correlates with the observation that Wnt signaling, and thus GSK-3β activity, plays a crucial role in the development of metazoan. This was demonstrated for the known GSK-3 inhibitors LiCl and the ruthenium complex (**R**)**-7**, which both perturb zebrafish development [49-50]. However, it must be noted that compound **9e** and **26d** were not completely dissolved in the E2-medium at 30 µM. Thus, an exact concentration cannot be stated for these compounds. Nevertheless, both compounds exerted no toxicity in the observation range (< 30 µM).

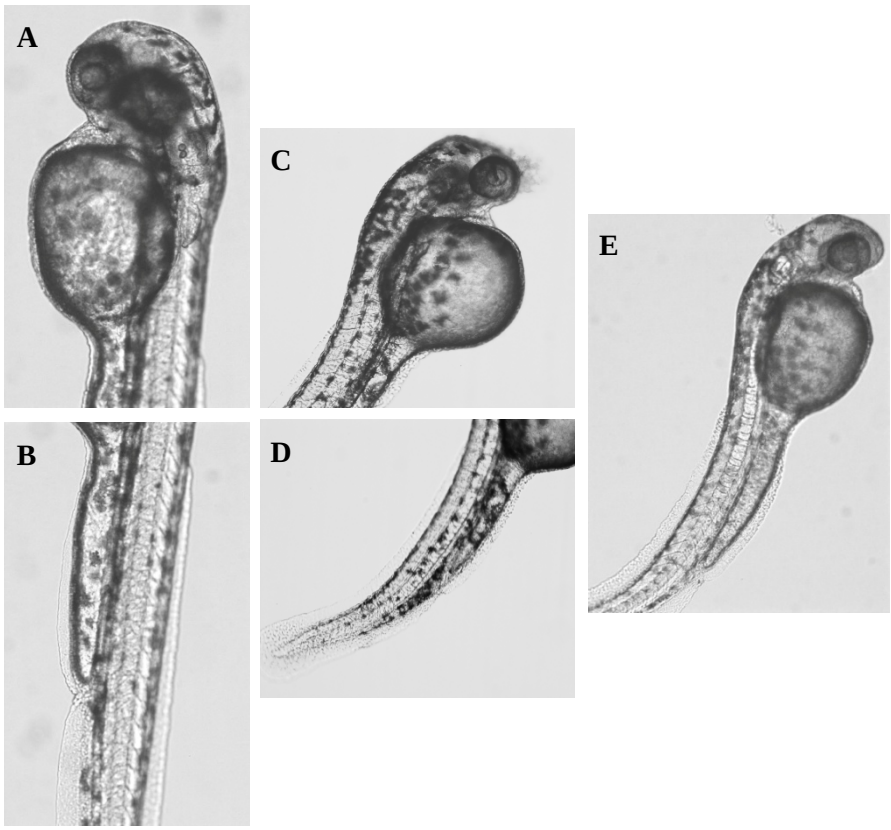

Fig. 4. Effect on the wild-type zebrafish embryo by compounds **9e** and **26d**. The embryos were collected and maintained in E2 medium at ~28°C, compound was added 5 hpf, and the phenotypes were compared at 44-48 hpf. (A, B) Head and tail of control embryos - DMSO (2%). (C, D) Embryo treated with compound **9e**. This compound causes a stunted and crooked tail at 30 µM. (E) Embryo treated with compound **26d**. This compound causes a stunted and crooked tail at 30 µM.

4. Conclusion

In this report, we describe the synthesis and evaluation of oxadiazole based GSK3 inhibitors. Occupation of the ATP binding pocket in its entirety led to the identification of several potent and selective compounds. These compounds are characterized by IC_{50} values in the low nanomolar range and good selectivity versus other kinases. Surprisingly, we ascertained that the addition of different functional groups onto the biphenyl system was adequate to gain selectivity against one GSK-3 isoform. To the best of our knowledge the selectivity of compound **8g** for GSK-3α compared to GSK-3β is among the highest ever reported. These observations will be helpful, if the discrimination of one GSK-3 isoform is needed *in vivo*. The discriminating factor for this isoform selectivity is still unknown as the ATP binding sites are almost identical in the two isoforms (Figure 3). Differences in the amino acid sequence of the channels leading to the binding sites may hold a cue, but the lack of a crystallized GSK-3α makes this hypothesis highly speculative. Furthermore, amino acids in the second-sphere

close to the ATP binding pocket do vary for GSK-3α and thus may contribute to conformational changes. The interaction with the glycine-rich loop might have significant effects on the binding potencies and selectivities of the biphenyl derivatives similar to the compounds reported by Li Feng *et al* [22]. The amide function in compound **26d** indicated a potential interaction with the backbone exploitable for further improvement. However, this moiety causes a significant contribution to the tPSA (103.0 $Å^2$) and thus impairs potential blood-brain barrier permeation. We exposed wt zebrafish embryos to two of these compounds at early stages of development and obtained desirable *in vivo* efficacy for compound **9e** and **26d**. We suppose that GSK-3α inhibition offers a new approach to reduce the formation of both amyloid plaques and neurofibrillary tangles and thus may be valuable in the treatment of AD [51]. On the basis of these results the derivatives **8b**, **8g** and **26d** were selected for further pharmacological and structural evaluations.

5. Experimental

5.1. Chemistry

All reactions under anhydrous conditions were carried out under argon atmosphere with dry solvents, unless otherwise noted. All the commercial chemicals were used without further purification. The ^{1}H-NMR spectra were recorded on a Bruker AC 300 spectrometer at 300 MHz and Bruker AC 500 spectrometer at 500 MHz. The ^{13}C-NMR spectra were recorded on a Bruker AC 300 spectrometer at 75 MHz and Bruker AC 500 spectrometer at 125 MHz. Chemical shifts are reported as ppm downfield from Me_4Si. Abbreviations used to explain the multiplicities: s = singlet, d = doublet, t = triplet, q = quartet, m = multiplet, br = broad. Coupling constants (*J* values) are given in hertz (Hz). Mass spectrometry was performed on a Bruker-Franzen Esquire LC mass spectrometer and a MAT 95 double focusing sector field MS. High performance liquid chromatographies were carried out on an Agilent 1100 (column: reversed phase, Zorbax Eclipse XDB-C8, 4.6 x 150 mm; 254 nm). Flash column chromatography was carried out using Merck silica gel 60 (40-63 and 15-40 μm) and 60G (5-40 μm). Thin-layer chromatography (TLC) was carried out using aluminum sheets precoated with silica gel 60 F254 (0.2 mm; E. Merck).

5.2.1 Methyl 2,3-dihydrobenzo[*b*][1,4]dioxine-6-carboxylate (**2a**)

To a stirred solution of 2,3-dihydrobenzo[*b*][1,4]dioxine-6-carboxylic acid **1a** (1.80 g, 10 mmol) in MeOH (20 mL) was added $SOCl_2$ (1.45 mL, 20 mmol) dropwise at 0°C over 1 h. The mixture was further stirred 12 h at 50°C. The solution was cooled to room temperature and diluted with water (25 mL). MeOH was evaporated and the pH adjusted to ~6 with aqueous $NaHCO_3$. The mixture was extracted three times with EtOAc and successively washed with brine. The organic layer was dried over $MgSO_4$ and concentrated under reduced pressure to give **2a** (1.6 g, 83%) as a colorless solid. ^{1}H-NMR (DMSO-d_6, 500 MHz): δ [ppm] = 3.80 (3H, s), 4.19 (2H, m), 4.23 (2H, m), 6.80 (1H, m), 7.47 (2H, m). ^{13}C-NMR (DMSO-d_6, 125 MHz): δ [ppm] = 50.5, 62.7, 63.2, 115.7, 117.6, 122.0, 141.7, 146.4, 165.2. EI-MS: m/z 194 (M^+).

5.2.2 Compound **2b** was prepared in a similar manner to that described for **2a**

Methyl benzo[*d*][1,3]dioxole-5-carboxylate (**2b**). Yield 89%, colorless solid. ^{1}H-NMR (DMSO-d_6, 500 MHz): δ [ppm] = 3.81 (3H, s), 6.14 (2H, s), 7.03 (1H, d, *J* = 8.1 Hz), 7.38 (1H, d, *J* = 1.6 Hz), 7.57 (1H, dd, *J* = 8.1 Hz, *J* = 1.7 Hz). ^{13}C-NMR (DMSO-d_6, 125 MHz): δ [ppm] = 52.0, 102.1, 108.2, 108.5, 123.4, 125.0, 147.6, 151.4, 165.6. EI-MS: m/z = 180 (M^+).

5.3.1 2,3-Dihydrobenzo[*b*][1,4]dioxine-6-carbohydrazide (**3a**)

To a solution of **2a** (1.16 g, 6.0 mmol) in EtOH (30 mL) was added hydrazine hydrate (2.91 mL, 60 mmol) and the mixture was heated at reflux for 2 days. After cooling to room temperature pure crystals are formed, collected by filtration and washed several times with EtOH to give compound **3a** (0.87 g, 75%) as a light yellow solid. ^{1}H-NMR (DMSO-d_6, 500 MHz): δ [ppm] = 4.28 (2H, m), 4.30 (2H, m), 6.89 (1H, d, *J* = 8.4 Hz), 7.30 (1H, dd, *J* = 8.3 Hz, *J* = 2.1 Hz), 7.33 (1H, d, *J* = 2.1 Hz). ^{13}C-NMR (DMSO-d_6, 125 MHz): δ [ppm] = 65.9, 66.3, 117.9, 118.6, 121.9, 127.5, 145.2, 148.6, 169.6. EI-MS: m/z 194 (M^+).

5.3.2 Compound **3b** was prepared in a similar manner to that described for **3a**

Benzo[*d*][1,3]dioxole-5-carbohydrazide (**3b**). Yield 67%, colorless solid. ^{1}H-NMR (DMSO-d_6, 500 MHz): δ [ppm] = 4.42 (2H, s), 6.07 (2H, s), 6.96 (1H, d, *J* = 8.1 Hz), 7.35 (1H, d, *J* = 1.7 Hz), 7.42 (1H, dd, *J* = 8.1 Hz, *J* = 1.7 Hz), 9.59 (1H, s). ^{13}C-NMR (DMSO-d_6, 125 MHz): δ [ppm] = 101.5, 106.9, 107.8, 121.8, 127.2, 147.2, 149.5, 165.2. EI-MS: m/z = 180 (M^+).

5.4.1 5-(2,3-Dihydrobenzo[*b*][1,4]dioxin-6-yl)-1,3,4-oxadiazole-2-thiol (**4a**)

To a solution of **3a** (582 mg, 3.00 mmol) in EtOH (5 mL) were added carbon disulfide (397 µL, 6.60 mmol) and Et_3N (469 µL, 3.30 mmol) and the mixture was heated at reflux overnight. The reaction mixture was diluted with EtOAc and the organic layer was washed with 0.1 N HCl, brine and dried over Na_2SO_4. The solvent was evaporated under reduced pressure, and the obtained residue was recrystallized from CH/EtOAc (1:2) to give **4a** (630 mg, 89%) as a light brown solid. ^{1}H-NMR (DMSO-d_6, 500 MHz): δ [ppm] = 4.32 (2H, m), 4.34 (2H, m), 7.05 (1H, d, *J* = 8.4 Hz), 7.30 (1H, d, *J* = 2.0 Hz), 7.36 (1H, dd, *J* = 8.4 Hz, *J* = 2.0 Hz), 14.2 (1H, s, br). ^{13}C-NMR (DMSO-d_6, 125 MHz): δ [ppm] = 64.4, 64.8, 115.0, 115.7, 118.6, 120.0, 144.2, 147.3, 160.6, 177.6. EI-MS: m/z = 236 (M^+).

5.4.2 Compound **4b** was prepared in a similar manner to that described for **4a**

5-(Benzo[*d*][1,3]dioxol-5-yl)-1,3,4-oxadiazole-2-thiol (**4b**). Yield 79%, pale yellow solid. ^{1}H-NMR (DMSO-d_6, 500 MHz): δ [ppm] = 6.14 (2H, s), 7.10 (1H, d, *J* = 8.1 Hz), 7.33 (1H, d, *J* = 1.6 Hz), 7.42 (1H, dd, *J* = 8.1 Hz, *J* = 1.6 Hz). ^{13}C-NMR (DMSO-d_6, 125 MHz): δ [ppm] = 102.1, 105.6, 109.1, 116.1, 121.5, 148.1, 150.6, 160.3, 177.2. EI-MS: m/z = 222 (M^+).

5.4.3 Compound **4c** was prepared in a similar manner to that described for **4a**

5-(Pyridin-4-yl)-1,3,4-oxadiazole-2-thiol (**4c**). Yield 83%, yellow solid. ^{1}H-NMR (DMSO-d_6, 500 MHz): δ [ppm] = 7.81 (2H, dd, *J* = 4.4 Hz, *J* = 1.6 Hz), 8.81 (2H, dd, *J* = 4.4 Hz, *J* = 1.6 Hz). ^{13}C-NMR (DMSO-d_6, 125 MHz): δ [ppm] = 119.6, 129.7, 150.8, 158.7, 177.8. EI-MS: m/z = 179 (M^+).

5.5.1. General procedure for synthesis of compounds **6a-h** [33]

To a solution of the aryl bromide (5 mmol) in 15 mL of toluene/EtOH (1/1) was added 0.17 g (0.14 mmol) of $Pd(PPh_3)_4$, and the mixture was stirred under argon atmosphere. Then 2 N aqueous Na_2CO_3 (7.5 mL) and 0.80 g (6 mmol) of 2-tolylboronic acid were added. The mixture was refluxed at 80°C for 1-2 days until reaction was completed (TLC). After cooling to room temperature, the product was diluted with water and extracted with EtOAc. The organic layers were dried with $MgSO_4$, filtered, and concentrated. Purification was performed by column chromatography using a mixture of CH/EtOAc (9:1). The compounds were used, without structure determination, directly for the next step.

5.6.1. General procedure for synthesis of compounds **7a-h** [33]

To a stirred solution of the appropriately substituted toluene in CCl_4 (10 mL per mmol) were added 0.95 eq. of NBS and AIBN (5 mg per mmol). The reaction mixture was refluxed at 80°C and then cooled to room temperature. The product was diluted with water and extracted with EtOAc. The organic layers were dried with $MgSO_4$, filtered, and concentrated. Purification was performed by column chromatography using a mixture of CH/EtOAc (6:1). The compounds were used, without structure determination, directly for the next step.

5.7.1. General procedure for synthesis of compounds **8a-h, 9a-f** and **10a-f**

To a solution of compound **4a-c** (0.25 mmol) and 1 N NaOH (0.25 mmol) in DMF (1 mL) was added the appropriate substituted biphenyl system (0.38 mmol) at room temperature, and the mixture was stirred for 5 h. The precipitate formed was collected by filtration and washed once with less DMF and thereafter several times with EtOH to give compounds **8a-h, 9a-f** and **10a-f**.

Note: The compounds which did not precipitate from the solution were purified as follows. The reaction mixture was diluted with EtOAc and the organic layer was washed with water and brine, dried over $MgSO_4$ and concentrated *in vacuo*. The residue was purified by silica gel column chromatography (DCM/EtOAc – 20:1).

5.7.2. 2,3-Dihydrobenzo[*b*][1,4]dioxin-6-yl-5-((2'-nitrobiphenyl-4-yl)methylthio)-1,3,4-oxadiazole (**8a**). Yield 77%, yellow solid. ^{1}H-NMR (DMSO-d_6, 500 MHz): δ [ppm] = 4.31 (4H, m), 4.63 (2H, s), 7.10 (1H, d, *J* = 8.4 Hz), 7.35 (2H, m), 7.44 (1H, s), 7.41 (1H, d, *J* = 8.4 Hz), 7.53 (3H, m), 7.64 (1H, t, *J* = 7.8 Hz), 7.72 (1H, t, *J* = 7.6 Hz), 8.05 (1H, d, *J* = 8.1 Hz). ^{13}C-NMR (DMSO-d_6, 125 MHz): 36.0, 64.5, 64.9, 115.5, 116.4, 118.6, 120.4, 124.5, 128.5, 129.4, 129.9, 132.3, 133.4, 135.0, 136.8, 137.4, 144.3, 147.2, 149.3, 163.1, 165.4. EI-MS: m/z = 447 (M^+).

5.7.3. 4'-((5-(2,3-Dihydrobenzo[*b*][1,4]dioxin-6-yl)-1,3,4-oxadiazol-2-ylthio)methyl)-biphenyl-3-carbonitrile (**8b**). Yield 36%, colorless solid. ^{1}H-NMR (DMSO-d_6, 500 MHz): δ [ppm] = 4.30 (4H, m), 4.62 (2H, s), 7.05 (1H, d, *J* = 8.5 Hz), 7.39 (1H, d, *J* = 2.1 Hz), 7.44 (1H, dd, *J* = 8.5 Hz, *J* = 2.1 Hz), 7.59 (2H, d, *J* = 8.3 Hz), 7.66 (1H, m), 7.74 (2H, d, *J* = 8.3 Hz), 7.82 (1H, td, *J* = 6.6 Hz, *J* = 1.3 Hz), 8.02 (1H, d, *J* = 8.0 Hz), 8.14 (1H, s). ^{13}C-NMR (DMSO-d_6, 125 MHz): δ [ppm] = 36.0, 64.5, 64.9, 112.6, 115.5, 116.4, 118.6, 119.2, 120.4, 127.6, 130.2, 130.6, 130.7, 131.6, 131.9, 137.6, 137.8, 141.1, 144.3, 147.2,

163.0, 165.4. EI-MS: m/z = 427 (M^+). HRMS (EI): m/z calcd for $C_{24}H_{17}N_3O_3S$ 427.0991, found 427.0976.

5.7.4. 2-(2,3-Dihydrobenzo[*b*][1,4]dioxin-6-yl)-5-((3'-nitrobiphenyl-4-yl)methylthio)-1,3,4-oxadiazole (**8c**). Yield 37%, colorless solid. ^{1}H-NMR (DMSO-d_6, 500 MHz): δ [ppm] = 4.32 (4H, m), 4.63 (2H, s), 7.05 (1H, d, *J* = 8.1 Hz), 7.39 (1H, d, *J* = 2.1 Hz), 7.44 (1H, dd, *J* = 8.4 Hz *J* = 2.1 Hz), 7.62 (2H, d, *J* = 8.5 Hz), 7.77 (3H, m), 8.13 (1H, m), 8.21 (1H, m), 8.42 (1H, m). ^{13}C-NMR (DMSO-d_6, 125 MHz): δ [ppm] = 36.0, 64.5, 64.9, 115.5, 116.4, 118.6, 120.4, 121.5, 122.7, 127.7, 130.3, 130.9, 133.7, 137.6, 137.8, 141.7, 144.3, 147.2, 148.9, 163.0, 165.5. EI-MS: m/z = 447 (M^+).

5.7.5. 4'-((5-(2,3-Dihydrobenzo[*b*][1,4]dioxin-6-yl)-1,3,4-oxadiazol-2-ylthio)methyl)-biphenyl-4-carbonitrile (**8d**). Yield 36%, colorless solid. ^{1}H-NMR (DMSO-d_6, 500 MHz): δ [ppm] = 4.33 (4H, m), 4.62 (2H, s), 7.05 (1H, d, *J* = 8.3 Hz), 7.39 (1H, d, *J* = 2.1 Hz), 7.44 (1H, dd, *J* = 8.5 Hz, *J* = 2.1 Hz), 7.61 (2H, d, *J* = 8.5 Hz), 7.74 (2H, d, *J* = 8.5 Hz), 7.90 (4H, m). ^{13}C-NMR (DMSO-d_6, 125 MHz): δ [ppm] = 36.0, 64.5, 64.9, 110.6, 115.5, 116.4, 118.6, 119.3, 120.4, 127.7, 128.0, 130.3, 133.3, 138.0, 138.1, 144.3, 144.5, 147.2, 163.0, 165.4. EI-MS: m/z = 427 (M^+).

5.7.6. 2-(2,3-Dihydrobenzo[*b*][1,4]dioxin-6-yl)-5-((4'-methoxybiphenyl-4-yl)methylthio)-1,3,4-oxadiazole (**8e**). Yield 39%, colorless solid. ^{1}H-NMR (DMSO-d_6, 500 MHz): δ [ppm] = 3.87 (3H, s), 4.31 (4H, m), 4.58, (2H, s), 7.01 (2H, d, *J* = 8.8 Hz), 7.04 (1H, d, *J* = 8.3 Hz), 7.43 (2H, m), 7.51 (2H, m), 7.58 (4H, m). ^{13}C-NMR (DMSO-d_6, 125 MHz): δ [ppm] = 36.2, 55.6, 64.5, 64.9, 114.8, 115.5, 116.4, 118.6, 120.4, 126.6, 128.2, 130.0, 132.4, 135.5, 139.7, 144.3, 147.1, 159.4, 163.1, 165.4. EI-MS: m/z = 432 (M^+).

5.7.7. 4'-((5-(2,3-Dihydrobenzo[*b*][1,4]dioxin-6-yl)-1,3,4-oxadiazol-2-ylthio)methyl)-4-methoxybiphenyl-2-carbonitrile (**8f**). Yield 50%, colorless solid. ^{1}H-NMR (DMSO-d_6, 500 MHz): δ [ppm] = 3.85 (3H, s), 4.33 (4H, m), 4.64 (2H, s), 7.05 (1H, d, *J* = 8.4 Hz), 7.35 (1H, dd, *J* = 8.7 Hz, *J* = 2.8 Hz), 7.41 (1H, d, *J* = 2.0 Hz), 7.44 (1H, dd, *J* = 8.4 Hz, *J* = 2.1 Hz), 7.53 (4H, m), 7.61 (2H, d, *J* = 8.3 Hz). ^{13}C-NMR (DMSO-d_6, 125 MHz): δ [ppm] = 36.0, 56.4, 64.5, 64.9, 111.3, 115.5, 116.4, 118.5, 118.6, 118.8, 120.4, 120.6, 129.3, 129.8, 131.9, 137.0, 137.4, 144.3, 147.2, 159.0, 163.1, 165.4. EI-MS: m/z = 457 (M^+). HRMS (EI): m/z calcd for $C_{25}H_{19}N_3O_4S$ 457.1097, found 457.1122.

5.7.8. 2-((3',5'-Difluorobiphenyl-4-yl)methylthio)-5-(2,3-dihydrobenzo[*b*][1,4]dioxin-6-yl)-1,3,4-oxadiazole (**8g**). Yield 41%, colorless solid. ^{1}H-NMR (DMSO-d_6, 500 MHz): δ [ppm] = 4.33 (4H, m), 4.61 (2H, s), 7.05 (1H, d, *J* = 8.5 Hz), 7.22 (1H, m), 7.38 (1H, d, *J* = 2.1 Hz), 7.43 (3H, m), 7.57 (2H, d, *J* = 8.2 Hz), 7.73 (2H, d, *J* = 8.2 Hz). ^{13}C-NMR (DMSO-d_6, 125 MHz): δ [ppm] = 36.0, 64.5, 64.9, 103.2, 110.1, 110.3, 115.5, 116.4, 118.6, 120.4, 127.5, 130.2, 137.4, 137.9, 143.7, 144.3, 147.2, 162.4, 163.0, 164.3, 165.4. EI-MS: m/z = 438 (M^+).

5.7.9. 2-(Biphenyl-4-ylmethylthio)-5-(2,3-dihydrobenzo[*b*][1,4]dioxin-6-yl)-1,3,4-oxadiazole **(8h).** Yield 38%, colorless solid. ^{1}H-NMR (DMSO-d_6, 500 MHz): δ [ppm] = 4.31 (4H, m), 4.60 (2H, s), 7.03 (1H, d, *J* = 8.4 Hz), 7.33-7.68 (11H, m). ^{13}C-NMR (DMSO-d_6, 125 MHz): δ [ppm] = 36.1, 64.5, 64.9, 115.5, 116.4, 118.6, 120.4, 127.1, 127.3, 127.5, 128.0, 129.4, 130.1, 136.4, 140.1, 144.3, 147.2, 163.1, 165.4. EI-MS: m/z = 402 (M^+).

5.7.10. 2-(Benzo[*d*][1,3]dioxol-5-yl)-5-((2'-nitrobiphenyl-4-yl)methylthio)-1,3,4-oxadiazole (**9a**). Yield 27%, yellow solid. ^{1}H-NMR (DMSO-d_6, 500 MHz): δ [ppm] = 4.62 (2H, s), 6.15 (2H, s), 7.11 (1H, d, *J* = 8.13 Hz), 7.32 (2H, d, *J* = 6.4 Hz), 7.42-7.66 (6H, m), 7.75 (1H, td, *J* = 7.6 Hz, *J* = 1.3 Hz), 7.97 (1H, dd, *J* = 8.0 Hz, *J* = 1.2 Hz). ^{13}C-NMR (DMSO-d_6, 125 MHz): δ [ppm] = 36.0, 102.6, 106.6, 109.6, 117.1, 122.2, 124.5, 128.5, 129.4, 129.9, 132.3, 133.4, 135.0, 136.8, 137.3, 148.6, 149.3, 150.9, 163.1, 165.6. EI-MS: m/z = 433 (M^+).

5.7.11. 4'-((5-(Benzo[*d*][1,3]dioxol-5-yl)-1,3,4-oxadiazol-2-ylthio)methyl)biphenyl-3-carbonitrile (**9b**). Yield 41%, off-white. ^{1}H-NMR (DMSO-d_6, 500 MHz): δ [ppm] = 4.62 (2H, s), 6.16 (2H, s), 7.11 (1H, d, *J* = 8.1 Hz), 7.43 (1H, d, *J* =1.7 Hz), 7.51 (1H, dd, *J* = 8.2 Hz, *J* = 1.7 Hz), 7.60 (2H, d, *J* = 8.2 Hz), 7.66 (1H, m), 7.73 (2H, d, *J* = 8.2 Hz), 7.82 (1H, d, *J* = 7.7 Hz), 8.01 (1H, d, *J* = 8.0 Hz), 8.14 (2H, m). ^{13}C-NMR (DMSO-d_6, 125 MHz): δ [ppm] = 36.0, 102.5, 106.6, 109.61, 112.5, 117.0, 119.2, 122.1, 127.5, 130.2, 130.5, 130.6, 131.5, 131.8, 137.5, 137.8, 141.1, 148.5, 150.9, 163.0, 165.5. EI-MS: m/z = 413 (M^+). HRMS (EI): m/z calcd for $C_{23}H_{15}N_3O_3S$ 413.0835, found 413.0828.

5.7.12. 2-(Benzo[*d*][1,3]dioxol-5-yl)-5-((3'-nitrobiphenyl-4-yl)methylthio)-1,3,4-oxadiazole (**9c**). Yield 48%, grey/brown solid. ^{1}H-NMR (DMSO-d_6, 500 MHz): δ [ppm] = 4.64 (2H, s), 6.16 (2H, s), 7.11 (1H, d, *J* = 8.6 Hz), 7.44 (1H, d, *J* = 1.7 Hz), 7.52 (1H, dd, *J* = 8.1 Hz, *J* = 1.6 Hz), 7.63 (2H, d, *J* = 8.4 Hz), 7.77 (3H, m), 8.14 (1H, m), 8.22 (1H, m), 8.43 (1H, m).

^{13}C-NMR (DMSO-d_6, 125 MHz): δ [ppm] = 36.0, 102.6, 106.6, 109.6, 117.1, 121.5, 122.2, 122.7, 127.7, 130.4, 131.0, 133.7, 137.6, 137.8, 141.4, 148.6, 148.9, 150.9, 163.0, 165.6. EI-MS: m/z = 433 (M^+).

5.7.13. 2-(Benzo[*d*][1,3]dioxol-5-yl)-5-((4'-methoxybiphenyl-4-yl)methylthio)-1,3,4-oxadiazole (**9d**). Yield 48%, grey/brown solid. ^{1}H-NMR (DMSO-d_6, 500 MHz): δ [ppm] = 3.79 (3H, s), 4.60 (2H, s), 6.16 (2H, s), 7.01 (2H, dd, *J* = 2.1 Hz, *J* = 8.8 Hz), 7.11 (1H, d, *J* = 8.2 Hz), 7.44 (1H, d, *J* = 1.8 Hz), 7.52 (3H, m), 7.59 (4H, m). ^{13}C-NMR (DMSO-d_6, 125 MHz): δ [ppm] = 36.2, 53.6, 102.6, 106.6, 109.6, 114.8, 117.1, 122.2, 126.7, 128.2, 130.0, 132.4, 135.5, 139.7, 148.6, 150.9, 159.4, 163.1, 165.5. EI-MS: m/z = 418 (M^+).

5.7.14. 4'-((5-(Benzo[*d*][1,3]dioxol-5-yl)-1,3,4-oxadiazol-2-ylthio)methyl)-4-methoxybiphenyl-2-carbonitrile (**9e**). Yield 47%, off-white. ^{1}H-NMR (DMSO-d_6, 500 MHz): δ [ppm] = 3.86 (3H, s), 4.64 (2H, s), 6.16 (2H, s), 7.11 (1H, d, *J* = 8.2 Hz), 7.35(1H, dd, *J* = 8.7 Hz, *J* = 2.8 Hz), 7.45 (1H, d, *J* = 1.7 Hz), 7.52 (5H, m), 7.61 (2H, d, *J* = 8.3 Hz). ^{13}C-NMR (DMSO-d_6, 125 MHz): δ [ppm] = 35.9, 56.3, 102.6, 106.6, 109.6, 111.3, 117.1, 118.5, 118.8, 120.6, 122.2, 129.3, 129.8, 131.9, 137.0, 137.3, 137.4, 148.6, 150.9, 159.0, 163.1, 165.6. EI-MS: m/z = 443 (M^+). HRMS (EI): m/z calcd for $C_{24}H_{17}N_3O_4S$ 443.0940, found 443.0902.

5.7.15. 2-(Benzo[*d*][1,3]dioxol-5-yl)-5-((3',5'-difluorobiphenyl-4-yl)methylthio)-1,3,4-oxadiazole (**9f**). Yield 50%, grey/brown solid. ^{1}H-NMR (DMSO-d_6, 500 MHz): δ [ppm] = 4.62 (2H, s), 6.16 (2H, s), 7.11 (1H, d *J* = 8.1 Hz), 7.22 (1H, m), 7.44 (3H, m), 7,52 (1H, dd, *J* = 8.1 Hz, *J* = 1.8 Hz), 7.58 (2H, d, *J* = 8.3 Hz), 7.73 (2H, d, *J* = 8.3 Hz). ^{13}C-NMR (DMSO-d_6, 125 MHz): δ [ppm] = 35.9, 102.6, 103.2, 106.6, 109.6, 110.1, 110.3, 117.1, 122.2, 127.5, 130.2, 137.4, 137.9, 143.7, 148.6, 150.9, 162.3, 163.0, 164.2, 165.6. EI-MS: m/z = 424 (M^+).

5.7.16. 2-((2'-Nitrobiphenyl-4-yl)methylthio)-5-(pyridine-4-yl)-1,3,4-oxadiazole (**10a)**. Yield 79%, yellow solid. ^{1}H-NMR (DMSO-d_6, 500 MHz): δ [ppm] = 4.7 (2H, s), 7.3 (2H, d, *J* = 8.2 Hz), 7.5 (1H, d, *J* = 7.7 Hz), 7.6 (2H, d, *J* = 8.2 Hz), 7.6 (1H, t, *J* = 7.8 Hz), 7.8 (1H, t, *J* = 7.6 Hz), 7.9 (2H, d, *J* = 6.1 Hz), 8.0 (1H, d, *J* = 8.1 Hz), 8.8 (2H, d, *J* = 6.1 Hz). ^{13}C-NMR (DMSO-d_6, 125 MHz): δ [ppm] = 36.0, 120.5, 124.6, 128.5, 129.4, 130.0, 130.5, 132.2, 133.4, 135.0, 136.9, 137.2, 149.3, 151.4, 164.3, 165.3. EI-MS: m/z = 390 (M^+).

5.7.17. 4'-((5-(Pyridine-4-yl)-1,3,4-oxadiazol-2-ylthio)methyl)biphenyl-3-carbonitrile (**10b**). Yield 53%, yellow solid. ^{1}H-NMR (DMSO-d_6, 500 MHz): δ [ppm] = 4.68 (2H, s), 7.64 (3H, m), 7.74 (2H, d), 7.82 (1H, dt, *J* = 7.7 Hz, *J* = 1.3 Hz), 7.90 (2H, dd, *J* = 4.5 Hz, *J* = 1.7 Hz), 8.01 (1H, m), 8.15 (1H, m), 8.82 (2H, dd, *J* = 4.5 Hz, *J* = 1.7 Hz). ^{13}C-NMR (DMSO-d_6, 125 MHz): δ [ppm] = 36.0, 112.6, 119.2, 120.4, 127.6, 130.3, 130.5, 130.6, 130.7, 131.6, 131.9, 137.3, 137.9, 141.1, 151.4, 164.2, 165.2. EI-MS: m/z = 370 (M^+).

5.7.18. 4'-((5-(Pyridine-4-yl)-1,3,4-oxadiazol-2-ylthio)methyl)biphenyl-4-carbonitrile (**10c**). Yield 32%, colorless solid. ^{1}H-NMR (DMSO-d_6, 500 MHz): δ [ppm] = 4.69 (2H, s), 7.64 (2H, d, *J* = 8.1 Hz), 7.75 (2H, d, *J* = 8.1 Hz), 7.86-7.93 (6H, m), 8.82 (2H, m). ^{13}C-NMR (DMSO-d_6, 125 MHz): δ [ppm] = 35.9, 110.6, 119.3, 120.4, 127.8, 128.0, 130.4, 130.5, 133.3, 137.8, 138,1, 144.5, 151.4, 165.2, 164.3. EI-MS: m/z = 370 (M^+).

5.7.19. 2-((4'-Methoxybiphenyl-4-yl)methylthio)-5-(pyridine-4-yl)-1,3,4-oxadiazole (**10d**). Yield 37%, colorless solid. ^{1}H-NMR (DMSO-d_6, 500 MHz): δ [ppm] = 3.79 (3H, s), 4.66 (2H, s), 7.01 (2H, d, *J* = 8.6 Hz), 7.55 (2H, d, *J* = 8.2 Hz), 7.60 (4H, m), 7.90 (2H, d, *J* = 5.8 Hz), 8.82 (2H, d, *J* = 5.8 Hz). ^{13}C-NMR (DMSO-d_6, 125 MHz): δ [ppm] = 36.1, 55.6, 114.8, 120.4, 126.8, 128.2, 130.1, 130.5, 132.4, 135.3, 139.8, 151.4, 159.5, 164.2, 165.3. EI-MS: m/z = 375 (M^+).

5.7.20. 4-Fluoro-4'-((5-(pyridine-4-yl)-1,3,4-oxadiazol-2-ylthio)methyl)biphenyl-2-carbonitrile (**10e**). Yield 31%, yellow solid. ^{1}H-NMR (DMSO-d_6, 500 MHz): δ [ppm] = 4.71 (2H, s), 7.57 (2H, d, *J* = 1.8 Hz), 7.67 (4H, m), 7.90 (2H, dd, *J* = 4.4 Hz, *J* = 1.7 Hz), 7.97 (1H, m), 8.82 (2H, dd, *J* = 4.4 Hz, *J* = 1.7 Hz). ^{13}C-NMR (DMSO-d_6, 125 MHz): δ [ppm] = 35.9, 112.1, 117.9, 120.5, 121.0, 121.5, 129.5, 129.9, 130.5, 132.9, 136.8, 137.8, 141.3, 151.4, 164.3, 165.3. EI-MS: m/z = 388 (M^+). HRMS (EI): m/z calcd for $C_{21}H_{13}N_4OFS$ 388.0795, found 388.0825.

5.7.21. 2-(Biphenyl-4-ylmethylthio)-5-(pyridine-4-yl)-1,3,4-oxadiazole (**10f**). Yield 32%, yellow solid. ^{1}H-NMR (DMSO-d_6, 500 MHz): δ [ppm] = 4.67 (2H, s), 7.36 (1H, m), 7.46 (2H, m), 7.66-7.70 (6H, m), 7.9 (2H, d, *J* = 6.1 Hz), 8.8 (2H, d, *J* = 6.1 Hz). ^{13}C-NMR (DMSO-d_6, 125 MHz): δ [ppm] = 36.1, 120.5, 127.1, 127.3, 128.0, 129.4, 130.2, 130.5, 136.2, 140.0, 140.1, 151.4, 164.1, 165.3. EI-MS: m/z = 345 (M^+).

5.8.1. Compounds 1**2a-d** were prepared in a similar manner to that described for **2a**. The compounds were used, without structure determination, directly for the next step.

5.9.1. Compounds **13a-d** were prepared in a similar manner to that described for **3a**. The compounds were used, without structure determination, directly for the next step.

5.10.1. Compounds **14a-d** were prepared in a similar manner to that described for **4a**. The compounds were used, without structure determination, directly for the next step.

5.11.1. Compounds **15-18** (**a-d**) were prepared in a similar manner to that described for compounds **8a-h, 9a-f** and **10a-f**.

5.11.2. 2-(Benzylthio)-5-phenyl-1,3,4-oxadiazole (**15a**). Yield 67%, colorless solid. ^{1}H-NMR (DMSO-d_6, 500 MHz): δ [ppm] = 4.59 (2H, s), 7.29 (1H, m), 7.35 (2H, m), 7.48 (2H, m), 7.60 (3H, m), 7.95 (2H, m). ^{13}C-NMR (DMSO-d_6, 125 MHz): δ [ppm] = 35.9, 122.9, 126.3, 127.7, 128.5, 129.0, 129.4, 132.0, 136.5, 163.2, 165.2. EI-MS: m/z = 268 (M^+).

5.11.3. 4'-((5-Phenyl-1,3,4-oxadiazol-2-ylthio)methyl)biphenyl-2-carbonitrile (**15b**). Yield 58%, colorless solid. ^{1}H-NMR (DMSO-d_6, 300 MHz): δ [ppm] = 4.68 (2H, s), 7.53-7.69 (9H, m, br), 7.78 (1H, td, *J* = 7.7 Hz, *J* = 1.4 Hz), 7.95 (3H, m). ^{13}C-NMR (DMSO-d_6, 75 MHz): δ [ppm] = 35.4, 110.0, 118.4, 122.9, 126.3, 128.2, 128.8, 129.3, 130.0, 131.9, 133.4, 133.8, 137.1, 137.3, 143.9, 163.2, 165.2. EI-MS: m/z = 369 (M^+).

5.11.4. 2-(3-Methoxybenzylthio)-5-phenyl-1,3,4-oxadiazole (**15c**). Yield 51%, colorless solid. ^{1}H-NMR (DMSO-d_6, 500 MHz): δ [ppm] = 3.72 (3H, s), 4.55 (2H, s), 6.84 (1H, m), 7.05 (2H, m), 7.26 (1H, t, *J* = 7.8 Hz), 7.62 (3H, m), 7.97 (2H, m). ^{13}C-NMR (DMSO-d_6, 125 MHz): δ [ppm] = 35.9, 55.0, 113.2, 114.6, 121.1, 122.9, 126.3, 129.4, 129.6, 132.0, 138.0, 159.2, 163.2, 165.2. EI-MS: m/z = 298 (M^+).

5.11.5. 3-((5-Phenyl-1,3,4-oxadiazol-2-ylthio)methyl)benzonitrile (**15d**). Yield 38%, colorless solid. ^{1}H-NMR (DMSO-d_6, 500 MHz): δ [ppm] = 4.63 (2H, s), 7.60 (4H, m), 7.77 (1H, d, *J* = 7.7 Hz), 7.85 (1H, d, *J* = 7.9 Hz), 7.94 (2H, m), 7.98 (1H, s). ^{13}C-NMR (DMSO-d_6, 125 MHz): δ [ppm] = 34.8, 111.3, 118.4, 122.9, 126.3, 129.3, 129.7, 131.4, 132.0, 132.6, 133.9, 138.8, 162.9, 165.3. EI-MS: m/z = 293 (M^+).

5.11.6. 2-(Benzylthio)-5-(4-methoxyphenyl)-1,3,4-oxadiazole (**16a**). Yield 63%, colorless solid. ^{1}H-NMR (DMSO-d_6, 500 MHz): δ [ppm] = 3.85 (3H, s), 4.56 (2H, s), 7.13 (2H, m), 7.28 (1H, m), 7.33 (2H, m), 7.47 (2H, m), 7.89 (2H, m). ^{13}C-NMR (DMSO-d_6, 125 MHz): δ [ppm] = 35.9, 55.5, 114.8, 115.3, 127.7, 128.2, 128.5, 128.9, 136.6, 162.0, 162.3, 165.1. EI-MS: m/z = 298 (M^+).

5.11.7. 4'-((5-(4-Methoxyphenyl)-1,3,4-oxadiazol-2-ylthio)methyl)biphenyl-2-carbonitrile (**16b**). Yield 71%, orange solid. ^{1}H-NMR (DMSO-d_6, 300 MHz): δ [ppm] = 4.62 (2H, s), 7.22-7.43 (3H, m, br), 7.50 (2H, m), 8.22 (2H, m), 8.41 (2H, m). ^{13}C-NMR (DMSO-d_6, 75 MHz): δ [ppm] = 35.8, 124.5, 127.7, 127.7, 128.4, 128.5, 129.0, 136.3, 149.1, 163.8, 164.7. EI-MS: m/z = 399 (M^+).

5.11.8. 2-(3-Methoxybenzylthio)-5-(4-methoxyphenyl)-1,3,4-oxadiazole (**16c**). Yield 57%, colorless solid. ^{1}H-NMR (DMSO-d_6, 500 MHz): δ [ppm] = 3.72 (3H, s), 3.85 (3H, s), 4.53 (2H, s), 6.84 (1H, m), 7.03 (2H, t, *J* = 5.0 Hz), 7.13 (2H, m), 7.25 (1H, t, *J* = 7.9 Hz), 7.90 (2H, m). ^{13}C-NMR (DMSO-d_6, 125 MHz): δ [ppm] = 35.9, 55.0, 55.5, 113.2, 114.6, 114.8, 115.3, 121.1, 128.2, 129.6, 138.0, 159.2, 162.0, 162.4, 165.1. EI-MS: m/z = 328 (M^+).

5.11.9. 3-((5-(4-Methoxyphenyl)-1,3,4-oxadiazol-2-ylthio)methyl)benzonitrile (**16d**). Yield 41%, colorless solid. ^{1}H-NMR (DMSO-d_6, 500 MHz): δ [ppm] = 3.84 (3H, s), 4.60 (2H, s), 7.13 (1H, m), 7.57 (2H, t, *J* = 7.8 Hz), 7.76 (1H, dt, *J* = 7.7 Hz, *J* = 1.3 Hz), 7.83 (1H, m), 7.88 (2H, m), 7.96 (1H, t, *J* = 1.5 Hz). ^{13}C-NMR (DMSO-d_6, 125 MHz): δ [ppm] = 34.8, 55.5, 111.3, 114.8, 115.2, 118.4, 128.2, 129.7, 131.4, 132.6, 133.9, 138.8, 162.0, 165.3. EI-MS: m/z = 323 (M^+).

5.11.10. 4-(5-(Benzylthio)-1,3,4-oxadiazol-2-yl)benzonitrile (**17a**). Yield 32%, colorless solid. ^{1}H-NMR (DMSO-d_6, 300 MHz): δ [ppm] = 4.61 (2H, s), 7.31 (3H, m), 7.49 (2H, d, *J* = 7.3 Hz), 8.09 (4H, td, *J* = 8.2 Hz, *J* = 0.9 Hz). ^{13}C-NMR (DMSO-d_6, 75 MHz): δ [ppm] = 35.8, 114.0, 118.0, 126.9, 127.0, 127.7, 128.5, 129.0, 133.3, 136.4, 164.0, 164.4. EI-MS: m/z = 293 (M^+).

5.11.11. 4'-((5-Phenyl-1,3,4-oxadiazol-2-ylthio)methyl)biphenyl-2-carbonitrile (**17b**). Yield 53%, orange solid. ^{1}H-NMR (DMSO-d_6, 500 MHz): δ [ppm] = 4.72 (2H, s), 7.48 (1H, m), 7.51 (1H, m), 7.57 (2H, m), 7.62 (2H, m), 7.67 (1H, dt, *J* = 7.7 Hz, *J* = 1.3 Hz), 7.79 (1H, dd,

J = 7.7 Hz, *J* = 0.9 Hz), 7.81 (2H, m), 8.13 (2H, m). ^{13}C-NMR (DMSO-d_6, 125 MHz): δ [ppm] = 36.4, 111.2, 115.1, 117.8, 118.5, 127.1, 127.4, 127.8, 129.2, 129.5, 129.9, 132.8, 132.9, 133.8, 136.0, 138.0, 144.6, 164.3, 165.1. EI-MS: m/z = 394 (M^+).

5.11.12. 4-(5-(3-Methoxybenzylthio)-1,3,4-oxadiazol-2-yl)benzonitrile (**17c**). Yield 47%, colorless solid. ^{1}H-NMR (DMSO-d_6, 500 MHz): δ (ppm) = 3.77 (3H, s), 4.49 (2H, s), 6.82 (1H, dd, *J* = 8.3 Hz, *J* = 2.0 Hz), 6.97 (1H, m), 7.00 (1H, d, *J* = 7.6 Hz), 7.23 (1H, t, *J* = 7.9 Hz), 7.75 (2H, m), 8.08 (2H, m). ^{13}C-NMR (DMSO-d_6, 125 MHz): δ (ppm) = 36.9, 55.3, 113.8, 114.7, 115.1, 117.9, 121.4, 127.1, 127.5, 129.9, 132.9, 136.7, 159.9, 164.3, 165.3. EI-MS: m/z = 323 (M^+).

5.11.13. 3-((5-(4-Cyanophenyl)-1,3,4-oxadiazol-2-ylthio)methyl)benzonitrile (**17d**). Yield 45%, colorless solid. ^{1}H-NMR (DMSO-d_6, 300 MHz): δ [ppm] = 4.47 (2H, s), 7.40 (1H, t, *J* = 7.8 Hz), 7.52 (1H, m), 7.70 (4H, m), 8.03 (2H, dt, *J* = 6.8 Hz, *J* = 0.9 Hz). ^{13}C-NMR (DMSO-d_6, 75 MHz): δ [ppm] = 34.9, 112.2, 114.5, 117.1, 117.6, 126.4, 126.5, 129.0, 131.1, 131.9, 132.2, 133.0, 136.8, 163.8, 163.9. EI-MS: m/z = 318 (M^+).

5.11.14. 2-(Benzylthio)-5-(4-nitrophenyl)-1,3,4-oxadiazole (**18a**). Yield 46%, light yellow solid. ^{1}H-NMR (DMSO-d_6, 300 MHz): δ [ppm] = 4.62 (2H, s), 7.32 (3H, m), 7.49 (2H, m), 8.21 (2H, m), 8.41 (2H, m). ^{13}C-NMR (DMSO-d_6, 75 MHz): δ [ppm] = 35.8, 124.5, 127.7, 127.7, 128.4, 128.5, 129.0, 136.3, 149.1, 163.8, 164.7. EI-MS: m/z = 313 (M^+).

5.11.15. 4'-((5-(4-Nitrophenyl)-1,3,4-oxadiazol-2-ylthio)methyl)biphenyl-2-carbonitrile (**18b**). Yield 58%, orange solid. ^{1}H-NMR (DMSO-d_6, 500 MHz): δ [ppm] = 4.71 (2H, s), 7.60 (4H, m), 7.68 (2H, d, *J* = 8.2 Hz), 7.78 (1H, dt, *J* = 7.7 Hz, *J* = 1.2 Hz), 7.94 (1H, dd, *J* = 7.7 Hz, *J* = 0.9 Hz), 8.22 (2H, m), 8.41 (2H, m). ^{13}C-NMR (DMSO-d_6, 125 MHz): δ [ppm] = 35.9, 110.5, 118.9, 125.0, 128.2, 128.7, 129.0, 129.4, 129.9, 130.5, 134.0, 134.3, 137.7, 137.7, 144.4, 149.6, 164.4, 165.2. EI-MS: m/z = 414 (M^+).

5.11.16. 2-(3-Methoxybenzylthio)-5-(4-nitrophenyl)1,3,4-oxadiazole (**18c**). Yield 33%, yellow solid. ^{1}H-NMR (DMSO-d_6, 500 MHz): δ (ppm) = 3.73 (3H, s), 4.59 (2H, s), 6.86 (1H, m), 7.07 (2H, m), 7.27 (1H, t, *J* = 7.9 Hz), 8.23 (2H, m), 8.40 (2H, m). ^{13}C-NMR (DMSO-d_6, 125 MHz): 35.8, 55.0, 113.3, 114.6, 121.2, 124.5, 127.7, 128.4, 129.7, 137.8, 149.1, 159.2, 163.9, 154.7. EI-MS: m/z = 343 (M^+).

5.11.17. 3-((5-(4-Nitrophenyl)-1,3,4-oxadiazol-2-ylthio)methyl)benzonitrile (**18d**). Yield 47%, orange solid. ^{1}H-NMR (DMSO-d_6, 300 MHz): δ [ppm] = 4.66 (2H, s), 7.58 (1H, t, *J* = 7.8 Hz), 7.76 (1H, m), 7.86 (1H, m), 7.99 (1H, dd, *J* = 2.3 Hz, *J* = 1.1 Hz), 8.20 (2H, m), 8.41 (2H, m). ^{13}C-NMR (DMSO-d_6, 75 MHz): δ [ppm] = 34.7, 111.3, 118.4, 124.5, 127.7, 128.4, 129.7, 131.4, 132.6, 134.0, 138.6, 149.1, 164.0, 164.4. EI-MS: m/z = 338 (M^+).

5.12.1. General procedure for synthesis of compounds **20a-d** [52]

The appropriate benzaldehyde (1.0 eq.) was dissolved in 5 mL EtOH and isoniazid (1.0 eq.) was added slowly to the solution. The reaction mixture was stirred at room temperature for 16 h. The solvent was removed under vacuum and the residue was purified by recrystallization in EtOH.

5.12.2. (E)-N'-Benzylideneisonicotinohydrazide (**20a**). Yield 85%, colorless solid. ^{1}H-NMR (DMSO-d_6, 500 MHz): δ [ppm] = 7.47 (3H, m), 7.76 (2H, m,), 7.83 (2H, dd, *J* = 4.3 Hz, *J* = 1.5 Hz), 8.47 (1H, s), 8.79 (2H, dd, *J* = 4.5 Hz, *J* = 1.5 Hz), 12.09 (1H, s). ^{13}C-NMR (DMSO-d_6, 125 MHz): δ [ppm] = 121.4, 127.1, 128.7, 130.2, 133.9, 140.3, 148.9, 150.2, 161.5. EI-MS: m/z = 225 (M^+).

5.12.3. (E)-N'-(4-Methoxybenzylidene)isonicotinohydrazide (**20b**). Yield 97%, yellow solid. ^{1}H-NMR (DMSO-d_6, 500 MHz): δ [ppm] = 3.83 (3H, s), 7.03 (2H, d, *J* = 9.0 Hz), 7.70 (2H, d, *J* = 9.0 Hz), 7.81 (2H, dd, *J* = 4.5 Hz, *J* = 1.5 Hz), 8.42 (1H, s), 8.78 (2H, dd, *J* = 4.5 Hz, *J* = 1.5 Hz), 11.93 (1H, s). ^{13}C-NMR (DMSO-d_6, 125 MHz): δ [ppm] = 55.24, 114.31, 121.3, 126.4, 128.2, 140.5, 148.8, 150.2, 161.0, 161.3. EI-MS: m/z = 255 (M^+).

5.12.4. (E)-N'-(4-Cyanobenzylidene)isonicotinohydrazide (**20c**). Yield 83%, colorless solid. ^{1}H-NMR (DMSO-d_6, 500 MHz): δ [ppm] = 7.83 (2H, dd, *J* = 4.3 Hz, *J* = 1.5 Hz), 7.94 (4H, s), 8.51 (1H, s), 8.80 (2H, dd, *J* = 4.5 Hz, *J* = 1.5 Hz), 12.27 (1H, s). ^{13}C-NMR (DMSO-d_6, 125 MHz): δ [ppm] = 112.1, 118.4, 121.4, 127.7, 128.3, 132.6, 140.0, 146.9, 150.2, 161.8. EI-MS: m/z = 250 (M^+).

5.12.5. (E)-N'-(4-Ethylbenzylidene)isonicotinohydrazide (**20d**). Yield 96%, colorless solid. ^{1}H-NMR (DMSO-d_6, 500 MHz): δ [ppm] = 1.20 (3H, t, *J* = 7.5 Hz), 2.65 (2H, m), 7.32 (2H, d, *J* = 8.1 Hz), 7.67 (2H, d, *J* = 8.1 Hz), 7.82 (2H, dd, *J* = 4.5 Hz, *J* = 1.8 Hz), 8.44 (1H, s),

8.78 (2H, dd, *J* = 4.5 Hz, *J* = 1.8 Hz), 11.99 (1H, s). ^{13}C-NMR (DMSO-d_6, 125 MHz): δ [ppm] = 15.2, 28.0, 121.4, 127.2, 128.2, 131.4, 140.4, 146.4, 149.0, 150.2, 161.4. EI-MS: m/z = 253 (M^+).

5.13.1. Compound **22** was prepared in a similar manner to that described for **2a**.

Methyl 2-aminoisonicotinate (**22**). Yield 89%, colorless solid. ^{1}H-NMR (DMSO-d_6, 500 MHz): δ [ppm] = 3.84 (3H, s), 6.28 (2H, s), 6.87 (1H, dd, *J* = 5.2 Hz, *J* = 1.5 Hz), 6.96 (1H, m), 8.05 (1H, dd, *J* = 5.2 Hz, *J* = 0.6 Hz). ^{13}C-NMR (DMSO-d_6, 125 MHz): δ [ppm] = 52.4, 107.4, 110.0, 137.8, 148.9, 160.5, 165.7. EI-MS: m/z = 152 (M^+).

5.14.1. Methyl 2-acetamidoisonicotinate (**23**)

A solution of compound **22** (760 mg, 5 mmol) in acetic anhydride (20 mL) was heated at 80°C for 6 h. The reaction was cooled to room temperature and the precipitate formed was filtered off and well washed with water to obtain compound **23** (0.67 g, 69%) as yellow solid. ^{1}H-NMR (DMSO-d_6, 500 MHz): δ [ppm] = 2.12 (3H, s), 3.89 (3H, s), 7.52 (1H, dd, *J* = 5.0 Hz, *J* = 1.4 Hz), 8.48 (1H, d, *J* = 5.0 Hz), 8.57 (1H, s), 10.74 (1H, s). ^{13}C-NMR (DMSO-d_6, 125 MHz): δ [ppm] = 23.8, 52.7, 112.2, 117.9, 138.6, 149.0, 153.0, 165.1, 169.6. EI-MS: m/z = 154 (M^+).

5.15.1. Compound **24** was prepared in a similar manner to that described for **3a**.

N-(4-(Hydrazinecarbonyl)pyridin-2-yl)acetamide (**24**). Yield 74%, light yellow solid. ^{1}H-NMR (DMSO-d_6, 500 MHz): δ [ppm] = 2.11 (3H, s), 4.58 (2H, s), 7.38 (1H, dd, *J* = 5.1 Hz, *J* = 1.5 Hz), 8.38 (1H, dd, *J* = 5.1 Hz, *J* = 0.7 Hz), 8.41 (1H, s), 9.99 (1H, s), 10.59 (1H, s). ^{13}C-NMR (DMSO-d_6, 125 MHz): δ [ppm] = 23.9, 111.3, 116.2, 142.8, 148.2, 152.7, 164.2, 169.3. EI-MS: m/z = 194 (M^+).

5.16.1. Compound **25** was prepared in a similar manner to that described for **4a**.

N-(4-(5-Mercapto-1,3,4-oxadiazol-2-yl)pyridin-2-yl)acetamide (**25**). Yield 92%, yellow solid. ^{1}H-NMR (DMSO-d_6, 500 MHz): δ [ppm] = 2.14 (3H, s), 7.49 (1H, dd, *J* = 5.1 Hz, *J* = 1.5 Hz), 8.53 (1H, dd, *J* = 5.1 Hz, *J* = 0.7 Hz), 8.54 (1H, s), 10.82 (1H, s), 14.90 (1H, s). ^{13}C-NMR (DMSO-d_6, 125 MHz): δ [ppm] = 23.9, 108.8, 114.9, 131.4, 149.4, 153.0, 158.8, 169.8, 177.7. EI-MS: m/z = 236 (M^+).

5.17.1. Compounds **26a-d** were prepared in a similar manner to that described for compounds **8a-h, 9a-f** and **10a-f**.

5.17.2. *N*-(4-(5-(Benzylthio)-1,3,4-oxadiazol-2-yl)pyridin-2-yl)acetamide (**26a**). Yield 68%, colorless solid. ^{1}H-NMR (DMSO-d_6, 500 MHz): δ [ppm] = 2.15 (3H, s), 4.61 (2H, s), 7.30 (1H, m), 7.36 (2H, m), 7.51 (2H, m), 7.58 (1H, dd, *J* = 5.1 Hz, *J* = 1.5 Hz), 8.52 (1H, dd, *J* = 5.1 Hz, *J* = 0.8 Hz), 8.63 (1H, s), 10.80 (1H, s). ^{13}C-NMR (DMSO-d_6, 125 MHz): δ [ppm] = 24.0, 35.9, 109.2, 115.4, 127.8, 128.6, 129.1, 131.7, 136.4, 149.4, 153.0, 163.8, 164.4, 169.8. EI-MS: m/z = 326 (M^+).

5.17.3. ***N***-(4-(5-(3-Methoxybenzylthio)-1,3,4-oxadiazol-2-yl)pyridin-2-yl)acetamide (**26b**). Yield 51%, yellow solid. ^{1}H-NMR (DMSO-d_6, 500 MHz): δ [ppm] = 2.14 (3H, s), 3.73 (3H, s), 4.58 (2H, s), 6.86 (1H, m), 7.07 (2H, m), 7.27 (1H, m), 7.58 (1H, dd, *J* = 5.1 Hz, *J* = 1.5 Hz), 8.52 (1H, dd, *J* = 5.1 Hz, *J* = 0.7 Hz), 8.63 (1H, s), 10.80 (1H, s). ^{13}C-NMR (DMSO-d_6, 125 MHz): δ [ppm] = 24.0, 35.9, 55.0, 109.2, 113.3, 114.6, 115.4, 121.2, 129.7, 131.8, 137.8, 149.4, 153.0, 159.3, 163.8, 164.7, 169.8. EI-MS: m/z = 356 (M^+).

5.17.4. ***N***-(4-(5-(Benzylthio)-1,3,4-oxadiazol-2-yl)pyridin-2-yl)acetamide (**26c**). Yield 37%, colorless solid. ^{1}H-NMR (DMSO-d_6, 500 MHz): δ [ppm] = 2.14 (3H, s), 4.64 (2H, s), 7.57 (2H, m), 7.77 (1H, d, *J* = 7.8 Hz), 7.87 (1H, d, *J* = 7.8 Hz), 7.97 (1H, s), 8.51 (1H, d, *J* = 5.1 Hz), 8.61 (1H, s), 10.81 (1H, s). ^{13}C-NMR (DMSO-d_6, 125 MHz): δ [ppm] = 23.9, 34.8, 109.2, 111.4, 115.4, 118.5, 129.8, 131.5, 131.8, 132.6, 134.1, 138.6, 149.5, 153.0, 163.9, 164.4, 169.8. EI-MS: m/z = 351 (M^+). HRMS (EI): m/z calcd for $C_{17}H_{13}N_5O_2S$ 351.0791, found 351.0787.

5.17.5. *N*-(4-(5-((2'-Cyanobiphenyl-4-yl)methylthio)-1,3,4-oxadiazol-2-yl)pyridin-2-yl)acetamide (**26d)**. Yield 62%, light yellow solid. ^{1}H-NMR (DMSO-d_6, 500 MHz): δ [ppm] = 2.14 (3H, s), 4.70 (2H, s), 7.56-7.61 (5H, m), 7.68 (2H, d, *J* = 8.2 Hz), 7.78 (1H, td, *J* = 7.6 Hz, *J* = 1.3 Hz), 7.94 (1H, dd, *J* = 7.6 Hz, *J* = 1.1 Hz), 8.52 (1H, dd, *J* = 5.1 Hz, *J* = 0.7 Hz), 8.64 (1H, s), 10.80 (1H, s). ^{13}C-NMR (DMSO-d_6, 125 MHz): δ [ppm] = 23.9, 35.5, 109.3, 110.1, 115.4, 118.5, 128.3, 128.9, 129.4, 130.1, 131.8, 133.5, 133.9, 137.2, 144.0, 149.5, 153.1, 163.9, 164.7, 169.8. EI-MS: m/z = 427 (M^+). HRMS (EI): m/z calcd for $C_{23}H_{17}N_5O_2S$ 427.1104, found 427.1104.

5.18.1. Ethyl 4-aminobenzoate (**28**)

To a solution of compound **27** (3.4 g, 25 mmol) in ethanol (30 mL) was added dropwise concentrated sulfuric acid (2.4 mL). The mixture was heated under reflux for 6 h. The resulting solution was diluted with water (200 mL) and made neutral by addition of concentrated ammonia water. The precipitation was collected by filtration and then washed with water and subsequently dried to afford compound **28** (3.68 g, 91%) as colorless solid. The compound was used, without structure determination, directly for the next step.

5.18.2. Ethyl 2-aminobenzo[*d*]thiazole-6-carboxylate (**29**)

Compound **28** (2.0 g, 12 mmol) was dissolved in 16 mL of acetic acid, and to the resulting solution was suspended potassium thiocyanate (4.67 g, 48 mmol). A solution of 0.61 mL of bromine in 8 ml of acetic acid was slowly added, and the reaction mixture was stirred at room temperature overnight. Water was added and the mixture was made neutral by addition of aqueous ammonium hydroxide. The precipitation was collected by filtration and then washed with water and subsequently dried to afford compound **29** (1.80 g, 67%) as light yellow solid. The compound was used, without structure determination, directly for the next step.

5.18.3. Compound **30** was prepared in a similar manner to that described for **23**.
Ethyl 2-acetamidobenzo[*d*]thiazole-6-carboxylate (**30**). Yield 58%, light brown solid. The compound was used, without structure determination, directly for the next step.

5.18.4. 2-Acetamidobenzo[*d*]thiazole-6-carboxylic acid (**31**)

A solution of compound **30** (1.0 g, 3.8 mmol), 1 N NaOH (40 mL), and MeOH (15 mL) was stirred at room temperature for 4 h and then the solvent was evaporated. To the resulting aqueous layer was added water (10 mL) and the solution acidified with 1 N HCl to pH 2. The resulting solid was collected by filtration and washed with water. The solid was dried to afford compound **31** (0.84 g, 94%) as light brown solid. The compound was used, without structure determination, directly for the next step.

5.18.5. *N*-(6-(2-*tert*-Butylhydrazinecarbonyl)benzo[*d*]thiazol-2-yl)acetamide (**32**)

To a solution of **31** (0.80 g, 3.3 mmol), *tert*-butyl carbazate (0.47 g, 3.6 mmol) and 1-(3-dimethylaminopropyl)-3-ethylcarbodiimide hydrochloride (EDCI) (0.74 g, 3.9 mmol) in DMF (10 mL) was added 1-hydroxybenzotriazole hydrate (HOBt•H_2O) (0.59 g, 3.9 mmol)

and the mixture stirred overnight at room temperature. The reaction mixture was diluted with EtOAc and the organic layer was washed with water and brine, dried over Na_2SO_4 and concentrated in vacuo. The residue was recrystallized in EtOAc/CH to give **32** (0.79 g, 77%) as light brown solid. The compound was used, without structure determination, directly for the next step.

5.18.6. *N*-(6-(Hydrazinecarbonyl)benzo[*d*]thiazol-2-yl)acetamide (**33**)

A solution of **32** (0.75 g, 2.4 mmol) in trifluoroacetic acid (5 mL) was stirred at room temperature for 1 h. The solvent was concentrated to give **33** (0.59 g, 99%) as colorless solid. The compound was used, without structure determination, directly for the next step.

5.18.7. Compound **34** was prepared in a similar manner to that described for **4a**. *N*-(6-(5-Mercapto-1,3,4-oxadiazol-2-yl)benzo[*d*]thiazol-2-yl)acetamide (**34**). Yield 81%, light brown solid. The compound was used, without structure determination, directly for the next step.

5.18.8. Compounds **35** was prepared in a similar manner to that described for compounds **8a-h, 9a-f** and **10a-f**. *N*-(6-(5-((2'-Cyanobiphenyl-4-yl)methylthio)-1,3,4-oxadiazol-2-yl)benzo[*d*]thiazol-2-yl)acetamide (**35**). Yield 47%, light brown solid. ^{1}H-NMR (DMSO-d_6, 500 MHz): δ [ppm] = 2.23 (3H, s), 4.69 (2H, s), 7.59 (4H, m), 7.67 (2H, d, *J* = 8.3 Hz), 7.78 (1H, td, *J* = 7.7 Hz, *J* = 1.4 Hz), 7.88 (1H, d, *J* = 8.5 Hz), 7.94 (1H, dd, *J* = 7.8 Hz, *J* = 1.1 Hz), 8.01 (1H, dd, *J* = 8.5 Hz, *J* = 1.8 Hz), 8.64 (1H, d, *J* = 1.5 Hz), 12.56 (1H, s). ^{13}C-NMR (DMSO-d_6, 125 MHz): δ [ppm] = 22.7, 35.5, 110.0, 117.8, 118.4, 120.6, 121.0, 124.3, 128.2, 128.9, 129.4, 130.0, 132.4, 133.5, 133.8, 137.1, 137.3, 143.9, 151.1, 160.7, 162.9, 165.4, 169.7. EI-MS: m/z = 483 (M^+).

5.19.1. Methyl 3-bromo-4-hydroxybenzoate (**37**)

To a solution of **36** (3.15 g, 20.7 mmol) in DCM (230 mL) was added slowly at -5°C a solution of bromine (1.1 mL, 21 mmol) in DCM (50 mL). The mixture was stirred for 4.5 h at room temperature. The reaction mixture was diluted with EtOAc and the organic layer was washed with water and brine, dried over $MgSO_4$ and concentrated *in vacuo*. The residue was purified by silica gel column chromatography (DCM / EtOAc) to give **37** (3.10 g, 65%) as colorless solid. The compound was used, without structure determination, directly for the next step.

5.19.2. Methyl 8-nitrodibenzo[*b*,*d*]furan-2-carboxylate (**38**)

A mixture of compound **37** (0.51 g, 2.2 mmol), 1-fluoro-4-nitrobenzene (0.36 g, 2.2 mmol) and Palladium(II) acetate (0.05 g, 0.22 mmol) in *N*,*N*-dimethylacetamide (2 mL) was stirred overnight at 130°C. The reaction mixture was diluted with EtOAc (20 mL) and filtered over celite. The solvent was removed *in vacuo* and the resulting oil was diluted with water (7 mL). The precipitate formed was collected by filtration and recrystallized in EtOH to give compound **38** (0.18 g, 30%) as colorless solid. The compound was used, without structure determination, directly for the next step.

5.19.3. 8-Nitrodibenzo[*b*,*d*]furan-2-carbohydrazide (**39**)

To compound **38** (160 mg, 0.59 mmol) was added hydrazine hydrate (1.5 mL) and the mixture was heated at reflux for 6 h. After cooling to room temperature pure crystals are formed, collected by filtration and washed several times with EtOH to give compound **39** (158 mg, 99%) as a yellow solid. The compound was used, without structure determination, directly for the next step.

5.19.4. Compound **40** was prepared in a similar manner to that described for **4a**.
5-(8-Nitrodibenzo[*b*,*d*]furan-2-yl)-1,3,4-oxadiazole-2-thiol (**40**). Yield 48%, light brown solid. The compound was used, without structure determination, directly for the next step.

5.19.5. Compound **41** was prepared in a similar manner to that described for compounds **8a-h, 9a-f** and **10a-f**. 3-({[5-(8-Nitrodibenzo[*b*,*d*]furan-2-yl)-1,3,4-oxadiazol-2-yl] sulfanyl}methyl)benzonitril (**41**). Yield 44%, yellow solid. ^{1}H-NMR (DMSO-d_6, 500 MHz): δ [ppm] = 4.71 (2H, s), 7.63 (1H, t, *J* = 7.8 Hz), 7.81 (1H, m), 7.96 (1H, m), 8.03 (3H, m), 8.25 (1H, d, *J* = 8.7 Hz), 8.58 (1H, d, *J* = 9.1 Hz), 9.11 (1H, s), 9.42 (1H, s). ^{13}C-NMR (DMSO-d_6, 125 MHz): δ [ppm] = 35.7, 64.5, 114.0, 119.7, 122.3, 125.0, 128.3, 130.7, 132.4, 133.6, 134.9. EI-MS: m/z = 428 (M^+).

5.20.1. Determination of GSK-3 inhibition

GSK-3β in vitro assay: Purified GSK-3β (0.5 µg) was incubated in a reaction mixture of 50 mM Tris pH 7.3, 10 mM MgAc, 0.01% β-mercaptoethanol, ^{32}P[γ-ATP](100 µM, 0.5 µci/assay), and 100 µM of peptide substrate, pIRS-1 (RREGGMSRPAS(p)VDG). New molecules were added at various concentrations (1, 10 and 100 µM), and the reaction mixture

was incubated for 15 min at 30°C. The reactions were stopped, spotted on p81 paper (Whatman), washed with 10 mM phosphoric acid, and counted for radioactivity [53]. GSK-3β activity was calculated as the percentage of GSK-3β activity in the absence of inhibitors that was designated to 100%.

Kinase Panel: Compounds are serially diluted 1/3 in neat DMSO (10 serial dilutions) and these dilutions are further diluted 1/25 with reaction buffer. 2.5 µL of these solutions are added to the reaction mixture described below so that final compound concentration in the assay ranges from 100 µM to 5 nM in 1 % (v/v) DMSO. The enzymatic activity of the kinases is determined with a commercial system based on the Z'-LYTE® technology, available from Invitrogen Life Technologies (Carlsbad, CA, USA), using human recombinant kinases as the enzyme source.

Kinase	**Enzyme conc. (nM)**	**ATP conc. (µM)**	**Peptide used**	**Peptide conc. (µM)**	**Buffer**
GSK-3β	2	12.5	Ser/Thr 9 peptide	2	50 mM Hepes pH 7.5,10 mM $MgCl_2$,1 mM EGTA, 0.01% (w/v) Brij-35
GSK-3α	0.5	12.5	Ser/Thr 9 peptide	2	"
CKIε	12	32	Ser/Thr 11 peptide	2	"
Cdk5	10	12.5	Ser/Thr 12 peptide	2	"
AurKA	20	10	Ser/Thr 1 peptide	2	"
PKCα	0.15	10	Ser/Thr 7 peptide	2	"

This technology utilizes the fluorescence resonance energy transfer ("FRET") process between fluorescein and coumarin. The assay principle is based on the differential sensitivity of phosphorylated and non-phosphorylated peptide to proteolytic cleavage, which precludes the energy transfer process between the two fluorophores attached to both sides of the cleavage site. Hence, enzymatic phosphorylation will yield a phosphopeptide, which cannot be hydrolyzed by a suitable protease and energy transfer between the two fluorophores will occur. Opposingly, lack of phosphorylation will cause peptide hydrolysis hence lack of energy transfer as. The assay is performed in 96-well black plates, in a final volume of 10 µL.

5.20.2 Determination of the *in vivo* activity on wt Zebrafish Embryos

In Vivo Activity on Zebrafish Embryos: The wt zebrafish was used in this study. The embryos were collected and placed into 24-well plates, ten embryos per well and maintained in E2 medium at ~28°C. Compounds were added 5 hpf (50% epiboly) and the embryos allowed to grow in chemical compound solution up to 2 days. The phenotypes were compared using the Axio Scope.A1 microscope system from Carl Zeiss at 44-48 hpf [49-50, 54].

5.20.3 Docking simulations

Molecular docking of **9e** and **26d** into the X-ray structure of GSK-3β (PDB code: 3F88) was carried out using Molegro Virtual Docker 5.

Acknowledgments

This work was supported by a collaborative project financed by the 7th Framework Program of the European Union: NeuroGSK3.

References

[1] F. Lo Monte, T. Kramer, A. Boländer, B. Plotkin, H. Eldar-Finkelman, A. Fuertes, J. Dominguez, B. Schmidt, Synthesis and biological evaluation of glycogen synthase kinase 3 (GSK-3) inhibitors: An fast and atom efficient access to 1-aryl-3-benzylureas, Bioorg. Med. Chem. Lett. 21 (2011) 5610-5615.

[2] C. Hooper, R. Killick, S. Lovestone, The GSK3 hypothesis of Alzheimer's disease, J. Neurochem. 104 (2008) 1433-1439.

[3] A. Alzheimer, Über eine eigenartige Erkankung der Hirnrinde, Allgemeine Zeitschrift für Psychiatrie und psychisch-gerichtliche Medizin (Berlin) 64 (1907) 146-148.

[4] A. Alzheimer, R.A. Stelzmann, H.N. Schnitzlein, F.R. Murtagh, An English translation of Alzheimer's 1907 paper, "Über eine eigenartige Erkankung der Hirnrinde", Clin. Anat. 8 (1995) 429-431.

[5] P. Cohen, M. Goedert, GSK3 Inhibitors: Development and Therapeutical Potential, Nature Rev. Drug Discov. 3 (2004) 479-487.

[6] F. Hernández, J. Avila, The role of glycogen synthase kinase 3 in the early stages of Alzheimers' disease, FEBS Letters 582 (2008) 3848-3854.

[7] Eldar-Finkelman, Glycogen synthase kinase 3: an emerging therapeutic target, Trends Mol. Med. 8 (2002) 126-132.

[8] M. Mazanetz, P. Fischer, Untangling tau hyperphosphorylation in drug design for neurodegenerative diseases, Nature Rev. Drug Discov. 6 (2007) 464-479.

[9] L. Chico, L. Van Eldik, D. Watterson, Targeting protein kinases in central nervous system disorders, Nature Rev. Drug Discov. 8 (2009) 892-809.

[10] L. Meijer, M. Flajolet, P. Greengard, Pharmacological inhibitors of glycogen synthase kinase 3, TRENDS. Pharmacol. Sci. 25 (2004) 471-480.

[11] A. Martinez, C. Gil, D.I. Perez, Glycogen Synthase Kinase 3 Inhibitors in the Next Horizon for Alzheimer's Disease Treatment, International Journal of Alzheimer´s Disease 2011 (2011) 1-7.
[12] K.F. Lau, C.C.J. Miller, B.H. Anderton, P.C. Shaw, Expression analysis of glycogen synthase kinase-3 in human tissues, J. Peptide Res. 54 (1999) 85-91.
[13] S. Frame, P. Cohen, GSK3 takes centre stage more than 20 years after its discovery, Biochem. J. 359 (2001) 1-16.
[14] E. Hur, F. Zhou, GSK3 signalling in neural development, Nature Rev. Neurosci. 11 (2010) 539-551.
[15] F. Mukai, K. Ishiguro, Y. Sano, S.C. Fujita, Alternative splicing isoform of tau protein kinase I/glycogen synthase kinase 3 beta, J. Neurochem. 81 (2002) 1073-1083.
[16] E. ter Haar, J.T. Coll, D.A. Austen, H. Hsiao, L. Swenson, J. Jain, Structure of GSK3β reveals a primed phosphorylation mechanism, Nature Struct. Biol. 8 (2001) 593-596.
[17] R. Dajani, E. Fraser, S.M. Roe, N. Young, V. Good, T.C. Dale, L.H. Pearl, Crystal Structure of Glycogen Synthase Kinase 3: Structural Basis for Phosphate-Primed Substrate Specificity and Autoinhibition, Cell 105 (2001) 721-732.
[18] Takashima, A., Drug Development Targeting the Glycogen Synthase Kinase-3β (GSK-3β)-Mediated Signal Transduction Pathway: Role of GSK-3β in Adult Brain, J. Pharmacol. Sci. 109 (2009) 174-178.
[19] L. Serenó, M. Coma, M. Rodriguez, P. Sánchez-Ferrer, M.B. Sánchez, I. Gich, J.M. Agulló, ,J. Avila M. Pérez, C. Guardia-Laguarta, J. Clarimón, A. Lleó, T. Gómez-Isla, A novel GSK-3β inhibitor reduces Alzheimer's pathology and rescues neuronalloss in vivo, Neurobiol. Dis. 35 (2009) 359-367.
[20] H. Yamaguchi, K. Ishiguro, T. Uchida, A. Takashima, C.A. Lemere, K. Imahori, Preferential labeling of Alzheimer neurofibrillary tangles with antisera for tau protein kinase (TPK) I/glycogen synthase kinase-3β and cyclin-dependent kinase 5, a component of TPK II, Acta Neuropathol. 92 (1996) 232-241.
[21] A. Martinez, A. Castro, I. Dorronsoro, M. Alonso, Glycogen Synthase Kinase 3 (GSK-3) Inhibitors as New Promising Drugs for Diabetes, Neurodegeneration, Cancer, and Inflammation, Med. Res. Rev. 22 (2002) 373-384.
[22] L. Feng, Y. Geisselbrecht, S. Blanck, A. Wilbuer, G.E. Atilla-Gokcumen, P. Filippakopoulos, K. Krling, M.A. Celik, K. Harms, J. Maksimoska, R. Marmorstein, G. Frenking, S. Knapp, L. Essen, E. Meggers, Structurally sophisticated octahedral metal complexes as highly selective protein kinase inhibitors, J. Am. Chem. Soc. 133 (2011) 5976-5986.
[23] R.V. Bhat, S.L. Budd Haeberlein, J. Avila, Glycogen synthase kinase 3: a drug target for CNS therapies, J. Neurochem. 89 (2004) 1313-1317.
[24] F. Lo Monte, T. Kramer, J. Gu, U. Rao Anumala, L. Marinelli, V. La Pietra, E. Novellino, B. Franco, D. Demedts, F. Van Leuven, A. Fuertes, J.M. Dominguez, B. Plotkin, H. Eldar-Finkelman, B. Schmidt, Identification of Glycogen Synthase Kinase-3 Inhibitors with a Selective Sting for Glycogen Synthase Kinase-3α, J. Med. Chem. 55 (2012) 4407-4424.
[25] T. Kramer, B. Schmidt, F. Lo Monte, Small-molecule inhibitors of GSK-3 - Structural insights and their application to Alzheimer´s disease models, International Journal of Alzheimer´s Disease, accepted (2012) http://www.hindawi.com/journals/ijad/aip/381029/.
[26] B. Voigt, M. Krug, C. Schächtele, F. Totzke, A. Hilgeroth, Probing Novel 1-Aza-9-oxafluorenes as Selective GSK-3β Inhibitors, ChemMedChem 3 (2008) 120-126.
[27] J. Boström, A. Hogner, A. Llinás, E. Wellner, A.T. Plowright, Oxadiazoles in Medicinal Chemistry, J. Med. Chem. 55 (2012) 1817-1830.
[28] M. Saitoh, J. Kunitomo, E. Kimura, Y. Hayase, H. Kobayashi, N. Uchiyama, T. Kawamoto, T. Tanaka, C.D. Mol, D.R. Dougan, G.S. Textor, G.P. Snell, F. Itoh, Design, synthesis and structure–activity relationships of 1,3,4-oxadiazole derivatives as novel inhibitors of glycogen synthase kinase-3β, Bioorg. Med. Chem. 17 (2009) 2017-2029.
[29] L. Naerum, L. Norskov-Lauritsen, P.H. Olesen, Scaffold Hopping and Optimization towards Libraries of Glycogen Synthase Kinase-3 Inhibitors, Bioorg. Med. Chem. Lett. 12 (2002) 1525-1528.
[30] R. Bhat, X. Xue, S. Berg, S. Hellberg, M. Ormö, Y. Nilsson, A. Radesäter, E. Jerning, P. Markgren, M. Nylöf, T. Borgegard, A. Giménez-Cassina, F. Hernández, J.J. Lucas, J. Díaz-

Nido, J. Avila, Structural Insights and Biological Effects of Glycogen Synthase Kinase 3-specific Inhibitor AR-A014418, J. Biol. Chem. 278 (2003) 45937-45945.
[31] H.B. Konig, W. Seifken, H.A. Offe, Sulfur-containing derivatives of pyridine carboxylic acids and compounds derived therefrom, Chem. Berichte 87 (1954) 825-834.
[32] G. Mazzone, F. Bonina, R. Arrigo-Reina, Synthesis and pharmacological activities of some 2-(alkylaminoalkyl)mercapto-5-aryl-(1,3,4-oxadiazoles), Farmaco, Ed. Scient. 32 (1977) 414-429.
[33] R.A. Tromp, S.van Ameijde, C. Pütz, C. Sundermann, B. Sundermann, J.K. von Frijtag Drabbe Künzel, P. IJzerman, Inhibition of Nucleoside Transport by New Analogues of 4-Nitrobenzylthioinosine: Replacement of the Ribose Moiety by Substituted Benzyl Groups, J. Med. Chem. 47 (2004) 5441-5450.
[34] S. Chao, S. Li, X. Hui, P. Xu, L. Dong Synthesis and antibacterial activities of 2-phenyl-5-[[2'-cyano(1,1'-biphenylyl)-4-]methyl]mercapto-1,3,4-oxadiazole, Xinxiang Yixueyuan Xuebao 23 (2006) 5-6.
[35] S. Giri, H. Singh, L.D.S. Yadav, Studies in oxadiazoles. Synthesis of some 2-mercapto-1,3,4-oxadiazoles and related compounds as potential fungicides, Agr. Biol. Chem. 40 (1976) 17-21.
[36] M.C. da Silva Lourenco, M. de Lima Ferreira, M.V.N. de Souza, M.A. Peralta, T.R.A. Vasconcelos, M. das Gracas Henriques, Synthesis and anti-mycobacterial activity of (E)-N'-(monosubstituted-benzylidene)isonicotinohydrazide derivatives, Eur. J. Med. Chem. 43 (2008) 1344-1347.
[37] I. Ninomiya, O. Yamamoto, Photochemistry of isonicotinohydrazide and its analogs in alcohol, Heterocycles 4 (1976) 475-481.
[38] R.R. Shah, R.D. Mehta, A.R. Parikh, Studies on isoniazid derivatives. Preparation and antimicrobial activity of 2-aryl-3-(pyridylcarbomyl)-5-carboxymethyl-4-thiazolidinones, J. Ind. Chem. Soc. 62 (1985) 255-257.
[39] S.K. Boovanahalli, X. Jin, Y. Jin, J.H. Kim, N.T. Dat, Y. Hong, J.H. Lee, S. Jung, K. Lee, J.J. Lee, Synthesis of (aryloxyacetylamino)-isonicotinic/nicotinic acid analogues as potent hypoxia-inducible factor (HIF)-1a inhibitors, Bioorg. Med. Chem. Lett. 17 (2007) 6305-6310.
[40] M.A. Chowdhury, K.R.A. Abdellatif, Y. Dong, M. Rahman, D. Das, M.R. Suresh, E.E. Knaus, Synthesis of 1-(methanesulfonyl- and aminosulfonylphenyl)acetylenes that possess a 2-(N-difluoromethyl-1,2-dihydropyridin-2-one pharmacophore: Evaluation as dual inhibitors of cyclooxygenases and 5-lipoxygenase with anti-inflammatory activity, Bioorg. Med. Chem. Lett. 19 (2009) 584-588.
[41] Q. Zheng, F. Zhang, K. Cheng, Y. Yang, Y. Chen, Y. Qian, H. Zhang, L. Li, C. Zhou, S. An, Q. Jiao, H. Zhu, Synthesis, biological evaluation and molecular docking studies of amide-coupled benzoic nitrogen mustard derivatives as potential antitumor agents, Bioorg. Med. Chem. 18 (2010) 880-886.
[42] A. Molinos-Gómez, X. Vidal, M. Maymó, D. Velasco, J.Martorell, F. López-Calahorra, Tautomeric enhancement of the hyperpolarizability in new acridine-benzothiazolylamine based NLO chromophores, Tetrahedron 61 (2005) 9075-9081.
[43] K. Yamazaki, Y. Kaneko, K. Suwa, S. Ebara, K. Nakazawa, K. Yasuno, Synthesis of potent and selective inhibitors of Candida albicans N-myristoyltransferase based on the benzothiazole structure, Bioorg. Med. Chem. 13 (2005) 2509-2522.
[44] P. Basabe, A. Diego, S. Delgado, D. Díez, I. S. Marcos, J. G. Urones, Short and efficient synthesis of (+)-subersic acids, Tetrahedron 59 (2003) 9173-9177.
[45] M. Ebisawa, M. Ueno, Y. Oshimo, Y. Kondo, Synthesis of dictyomedins using phosphazene base catalyzed diaryl ether formation, Tetrahedron Lett. 48 (2007) 8918-8921.
[46] L. Campeau, M. Parisien, A. Jean, K. Fagnou, Catalytic Direct Arylation with Aryl Chlorides, Bromides, and Iodides: Intramolecular Studies Leading to New Intermolecular Reactions, J. Am. Chem. Soc. 128 (2006) 581-590.
[47] H. V. Namboodiri, M. Bukhtiyarova, J. Ramcharan, M. Karpusas, Y. Lee, E. B. Springman, Analysis of Imatinib and Sorafenib Binding to p38a Compared with c-Abl and b-Raf Provides Structural Insights for Understanding the Selectivity of Inhibitors Targeting the DFG-Out Form of Protein Kinases, Biochemistry 49 (2010) 3611-3618.

[48] J. R. Simard, M. Getlik, C. Grütter, V. Pawar, S. Wulfert, M. Rabiller, D. Rauh, Development of a Fluorescent-Tagged Kinase Assay System for the Detection and Characterization of Allosteric Kinase Inhibitors, J. Am. Chem. Soc. 131 (2009) 13286-13296.
[49] D. Paquet, R. Bhat, A. Sydow, E. Mandelkow, S. Berg, S. Hellberg, J. Fälting, M. Distel, R.W. Köster, B. Schmid, C. Haass, A zebrafish model of tauopathy allows in vivo imaging of neuronal cell death and drug evaluation, J. Clin. Invest. 119 (2009) 1382–1395.
[50] G.E. Atilla-Gokcumen, D.S. Williams, H. Bregman, N. Pagano, E. Meggers, Organometallic Compounds with Biological Activity: A Very Selective and Highly Potent Cellular Inhibitor for Glycogen Synthase Kinase 3, ChemBioChem 7 (2006) 1443-1450.
[51] C.J. Phiel, C.A. Wilson, V.M.Y. Lee, P.S. Klein, GSK-3 alpha regulates production of Alzheimer's disease amyloid-beta peptides, Nature 423 (2003) 435-439.
[52] M. Cristina da Silva Lourenco, M. de Lima Ferreira, M. Vinícius Nora de Souza, M. Amado Peralta, T. Rocha Alves Vasconcelos, M.O. das Gracas, M. Henriques, Synthesis and anti-mycobacterial activity of (E)-N´-(monosubstituted-benzylidene)isonicotinohydrazide derivatives, Eur. J. Med. Chem. 43 (2008) 1344-1347.
[53] Z. Liberman, H. Eldar-Finkelman, Serine 332 phosphorylation of insulin receptor substrate-1 by glycogen synthase kinase-3 attenuates insulin signaling, J. Biol. Chem. 280 (2005) 4422-4428.
[54] C.B. Kimmel, W.W. Ballard, S.R. Kimmel, B. Ullmann, T.F. Schilling, Stages of Embryonic Development of the Zebrafish, Develop. Dynamics 203 (1995) 253-310.

Supporting Information

Structure-based optimization of oxadiazole-based GSK-3 inhibitors

Fabio Lo Monte,[a,*] Thomas Kramer,[a] Jiamin Gu,[a] Martin Brodrecht,[a] Johannes Pilakowski,[a] Ana Fuertes,[b] Juan Manuel Dominguez,[b] Batya Plotkin,[c] Hagit Eldar-Finkelman[c] and Boris Schmidt[a,*]

[a] Clemens Schöpf - Institute of Organic Chemistry and Biochemistry, Technische Universität Darmstadt, 64287 Darmstadt, Germany

[b] Noscira S.A., Drug Discovery, Tres Cantos 28760 - Madrid, Spain

[c] Department of Human Molecular Genetics and Biochemistry, Sackler School of Medicine, Tel Aviv University, 69978 Tel Aviv, Israel

*To whom correspondence should be addressed. Phone: +496151-164531. Fax: +496151-163278. E-Mail: schmidt_boris@t-online.de; Fabio.Lo-Monte@gmx.de

NMR Data of compounds 8a-h, **9a-f**, **10a-f**, **26a** and **26c-d**.

The ^{1}H-NMR spectra were recorded on a Bruker AC 300 spectrometer at 300 MHz and Bruker AC 500 spectrometer at 500 MHz. The ^{13}C-NMR spectra were recorded on a Bruker AC 300 spectrometer at 75 MHz and Bruker AC 500 spectrometer at 125 MHz.

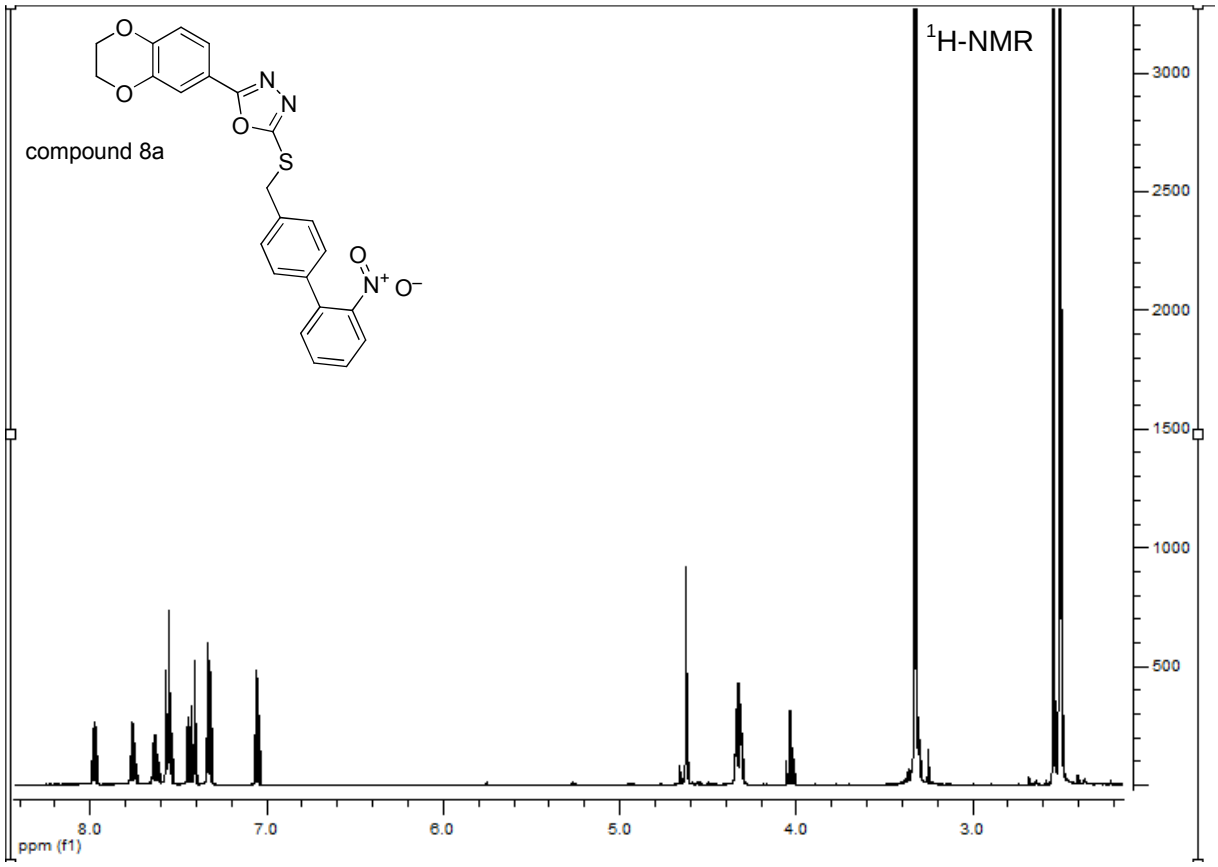
compound 8a
^{1}H-NMR
3000
2500
2000
1500
1000
500
8.0
7.0
6.0
5.0
4.0
3.0
ppm (f1)

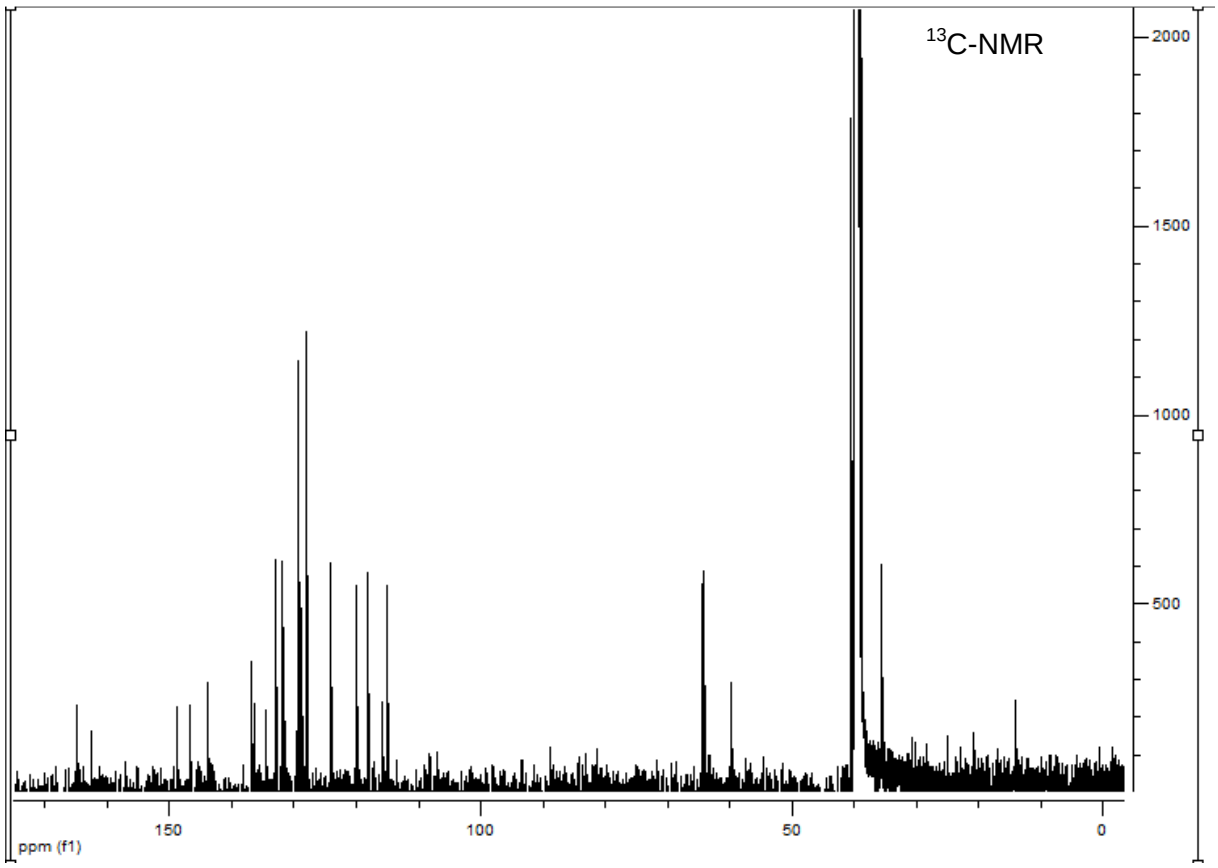
^{13}C-NMR
2000
1500
1000
500
150
100
50
0
ppm (f1)

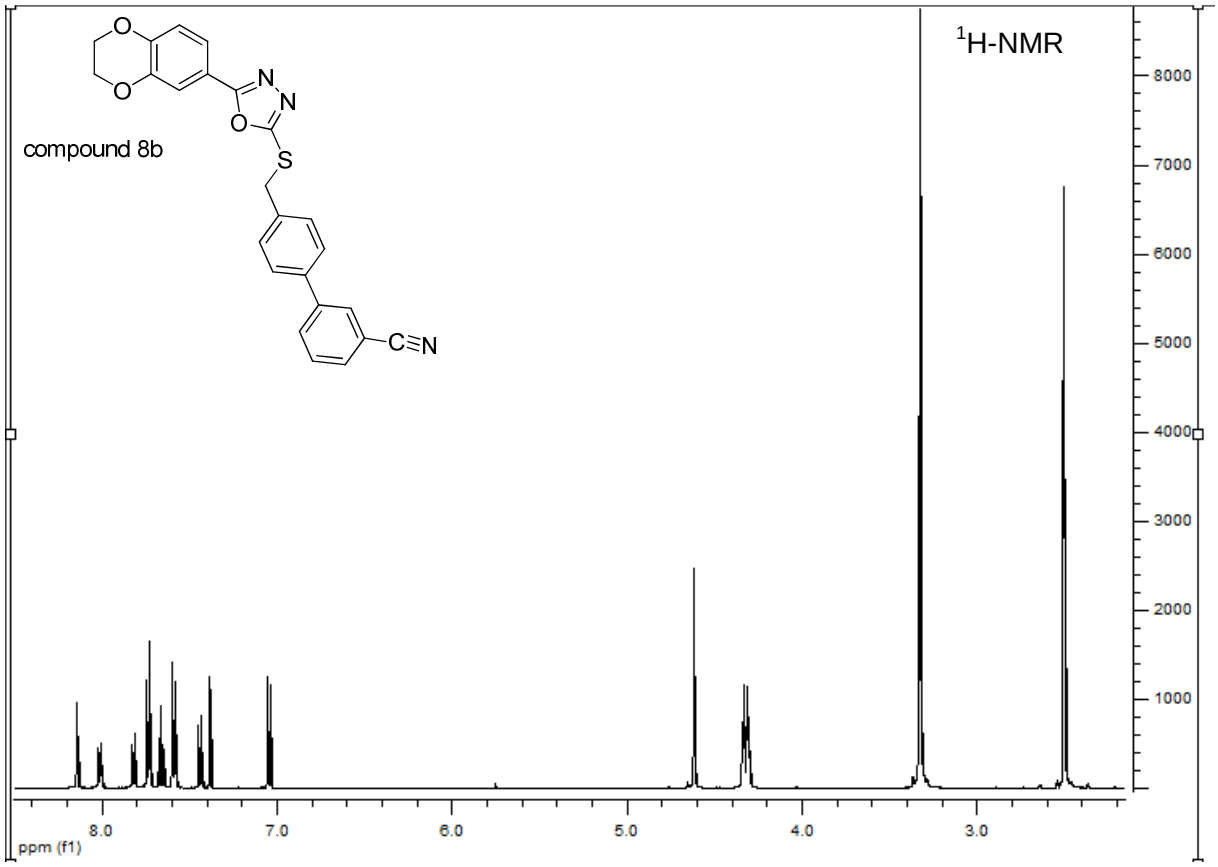
compound 8b
^{1}H-NMR
8000
7000
6000
5000
4000
3000
2000
1000
8.0
7.0
6.0
5.0
4.0
3.0
ppm (f1)

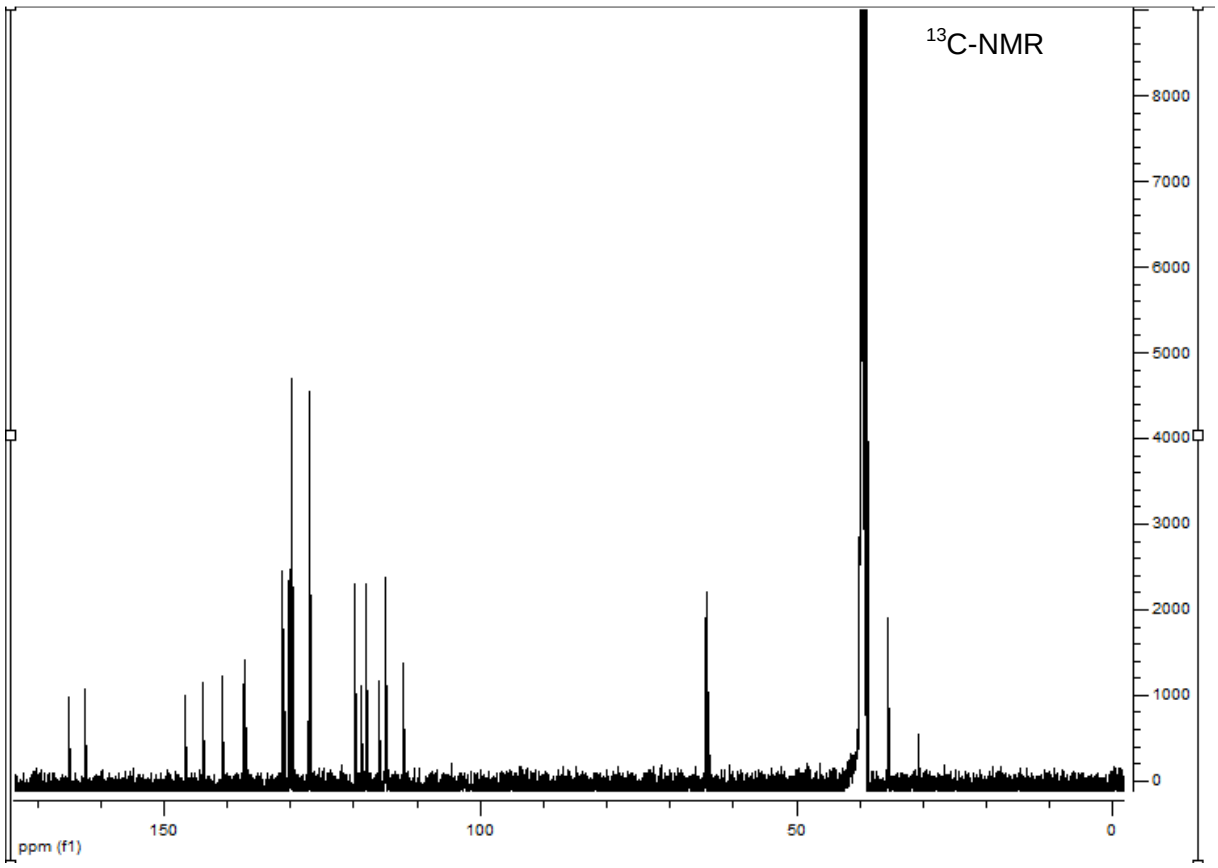
^{13}C-NMR
8000
7000
6000
5000
4000
3000
2000
1000
0
150
100
50
0
ppm (f1)

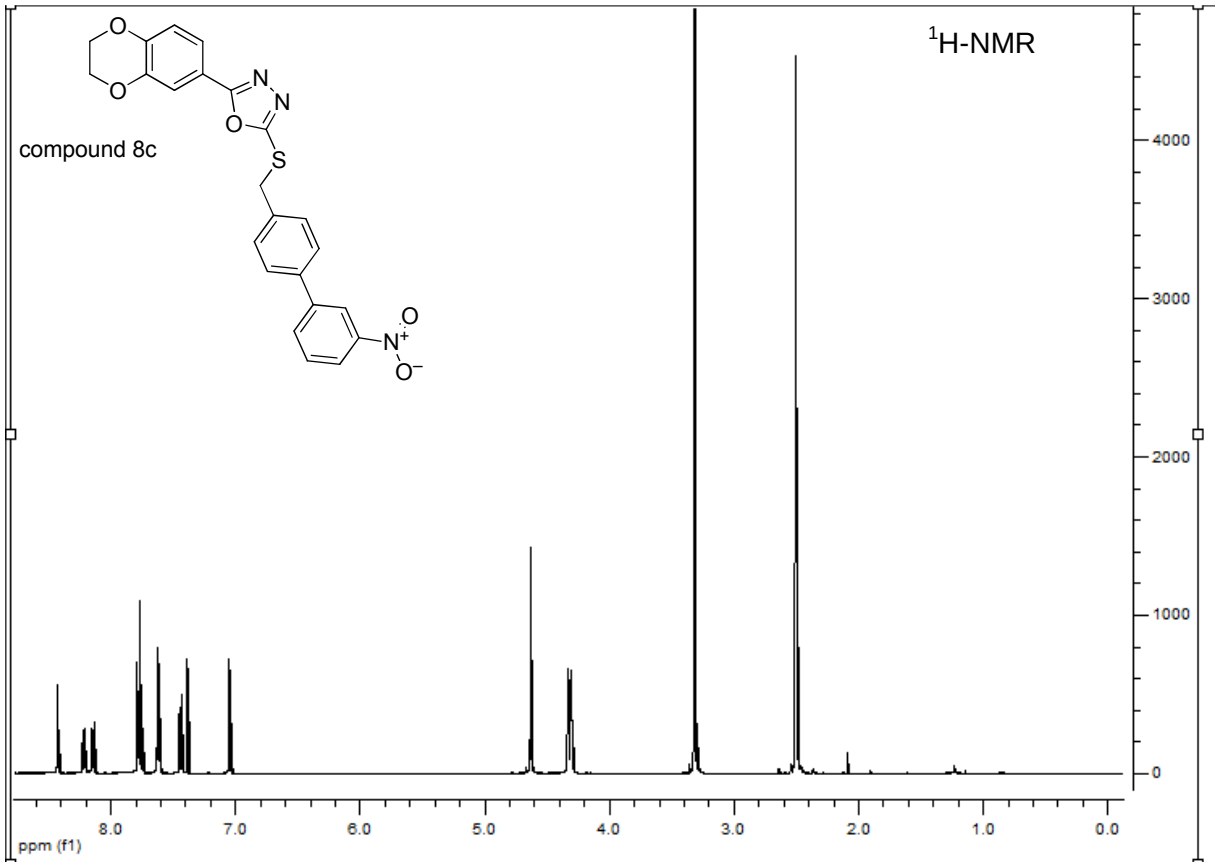
compound 8c
^{1}H-NMR
4000
3000
2000
1000
0
8.0
7.0
6.0
5.0
4.0
3.0
2.0
1.0
0.0
ppm (f1)

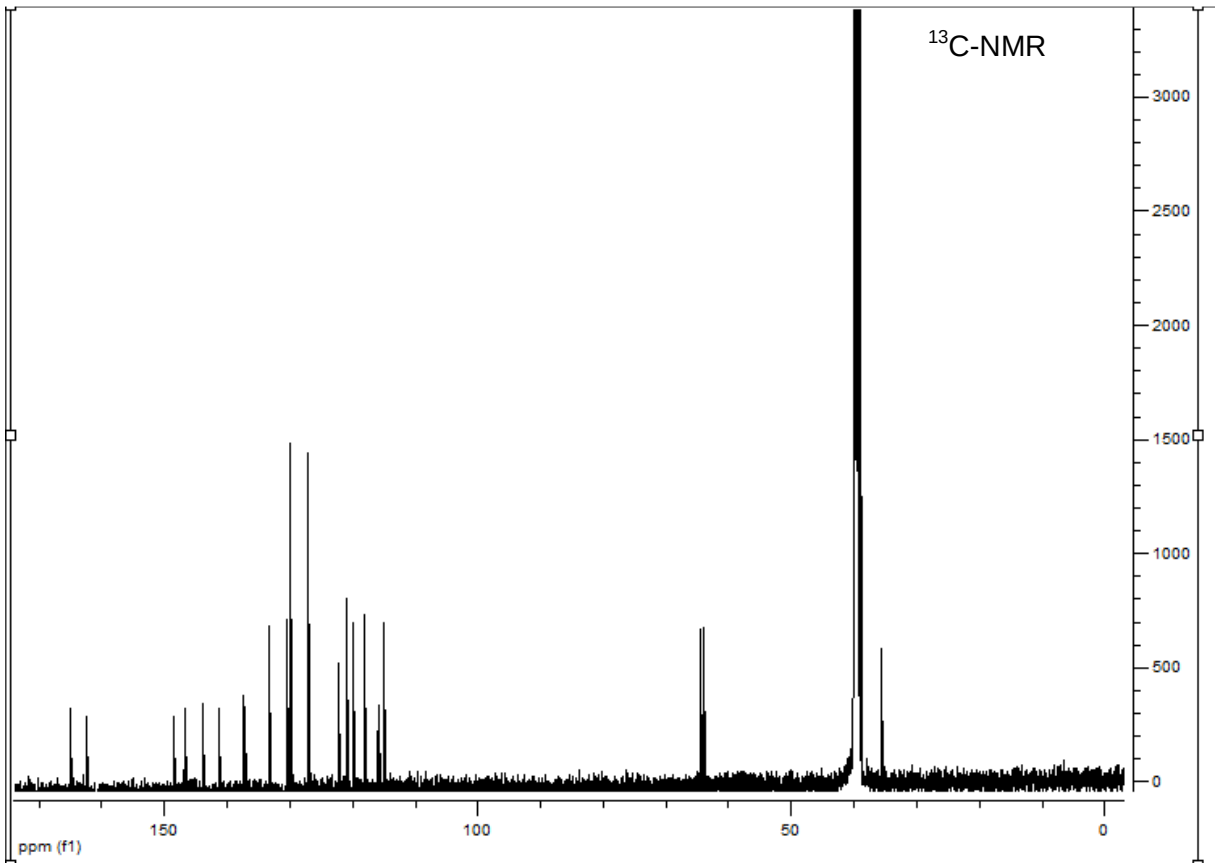
^{13}C-NMR
3000
2500
2000
1500
1000
500
0
150
100
50
0
ppm (f1)

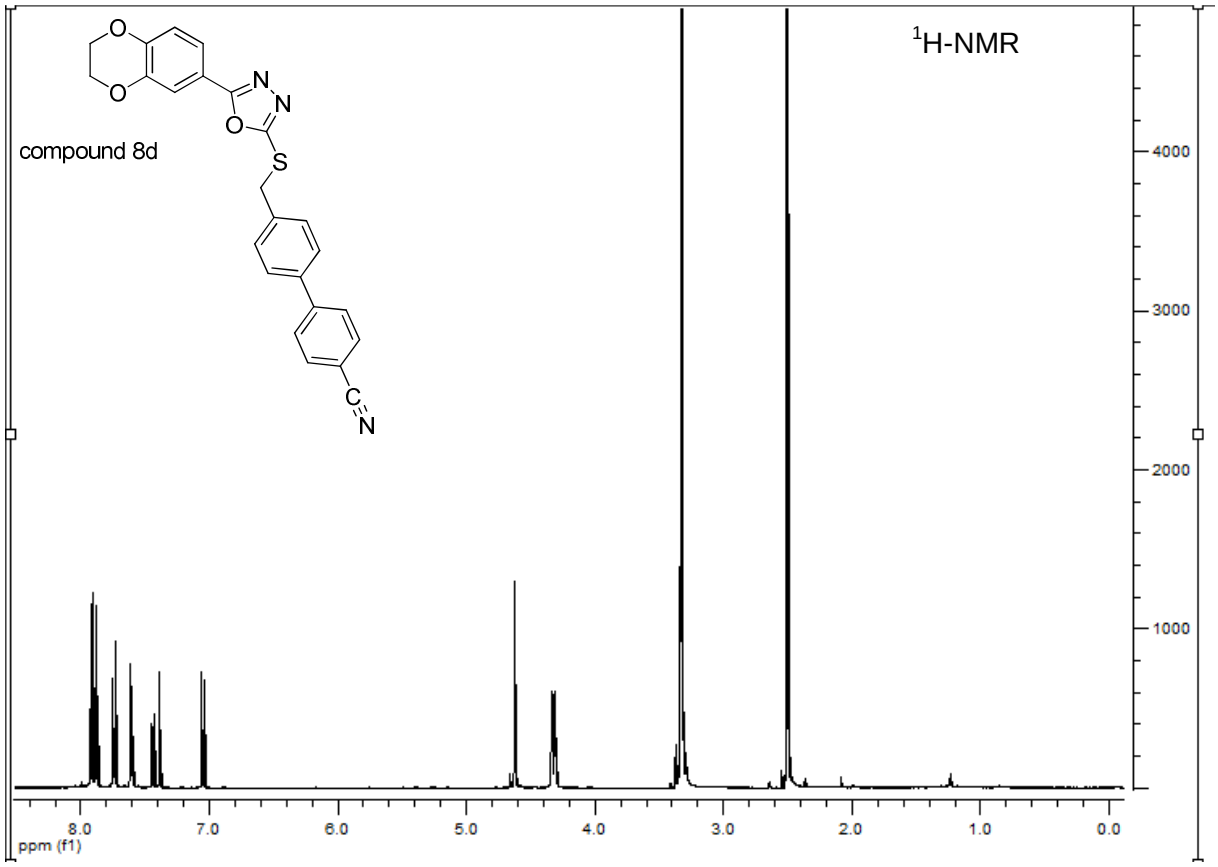
compound 8d
^{1}H-NMR
4000
3000
2000
1000
8.0
7.0
6.0
5.0
4.0
3.0
2.0
1.0
0.0
ppm (f1)

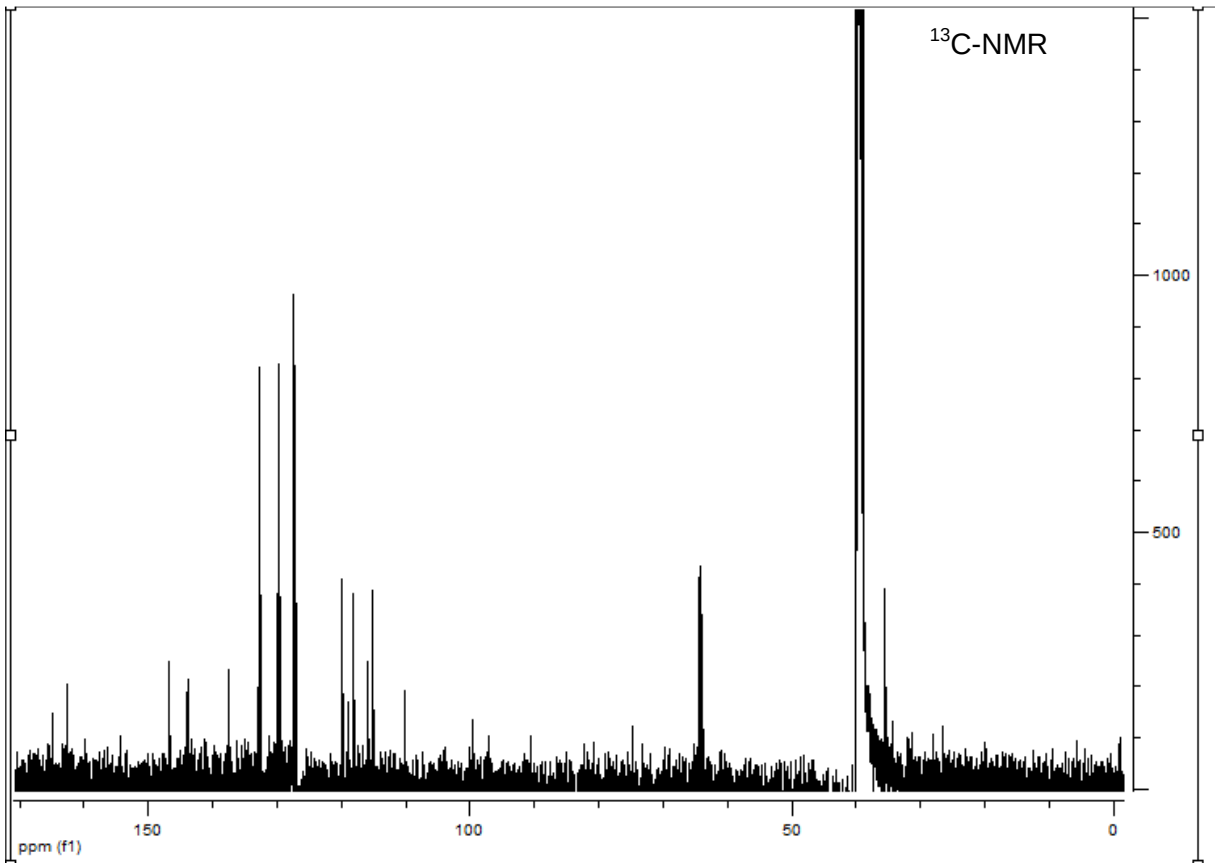
^{13}C-NMR
1000
500
150
100
50
0
ppm (f1)

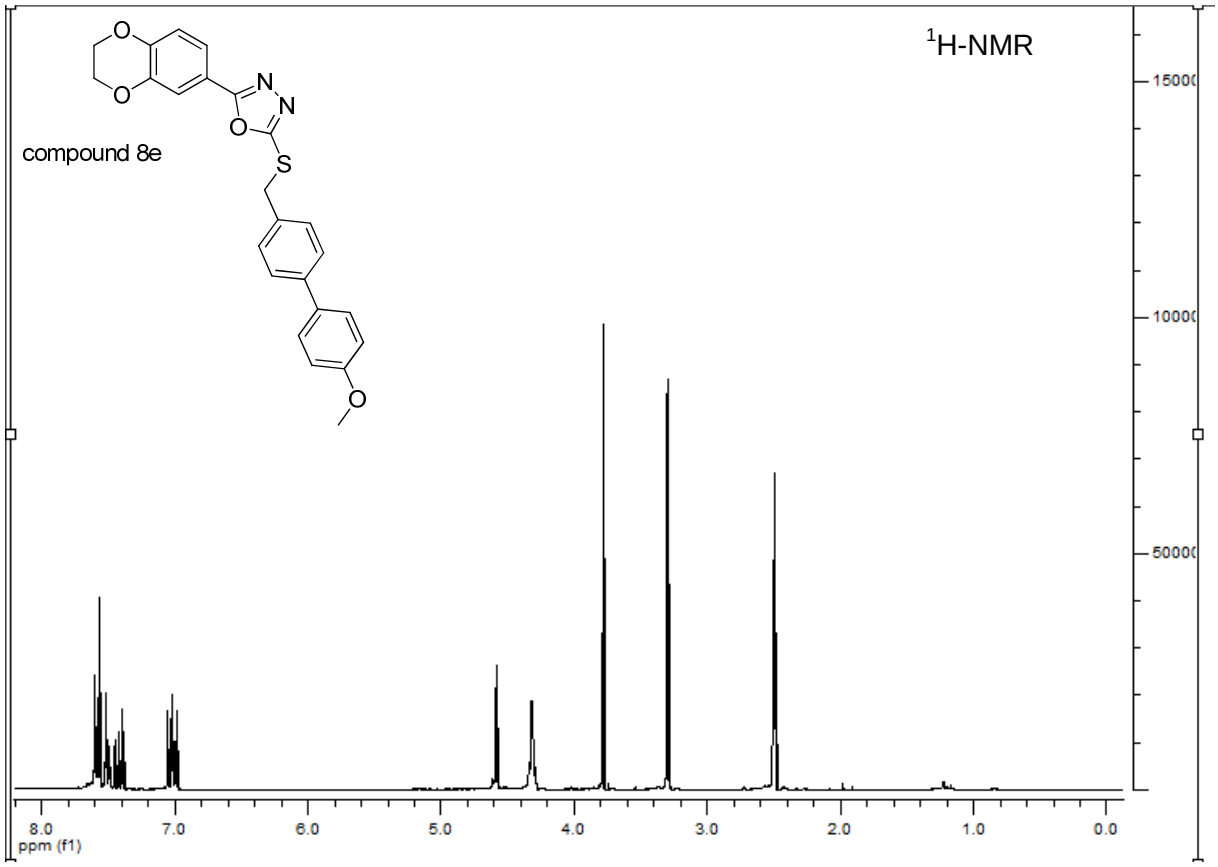
compound 8e
^{1}H-NMR
15000
10000
5000
8.0
7.0
6.0
5.0
4.0
3.0
2.0
1.0
0.0
ppm (f1)

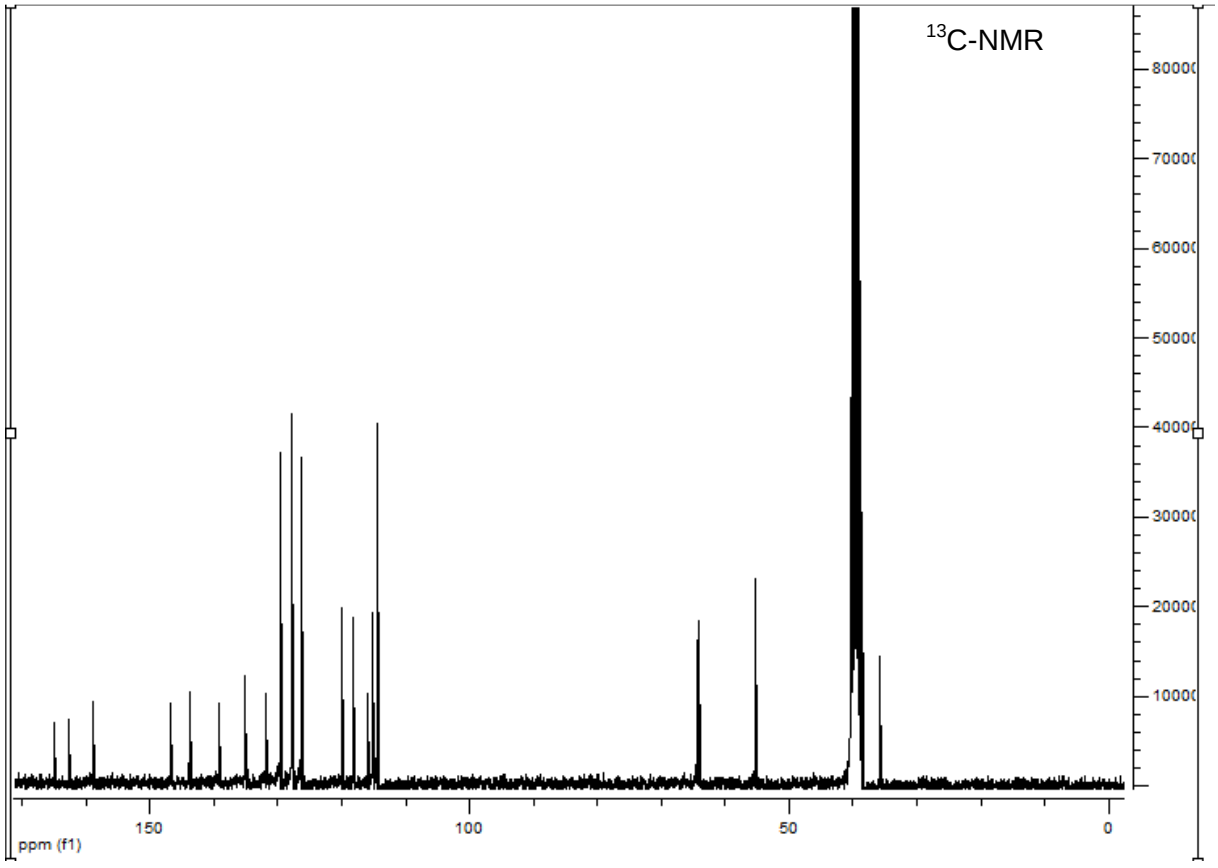
^{13}C-NMR
80000
70000
60000
50000
40000
30000
20000
10000
150
100
50
0
ppm (f1)

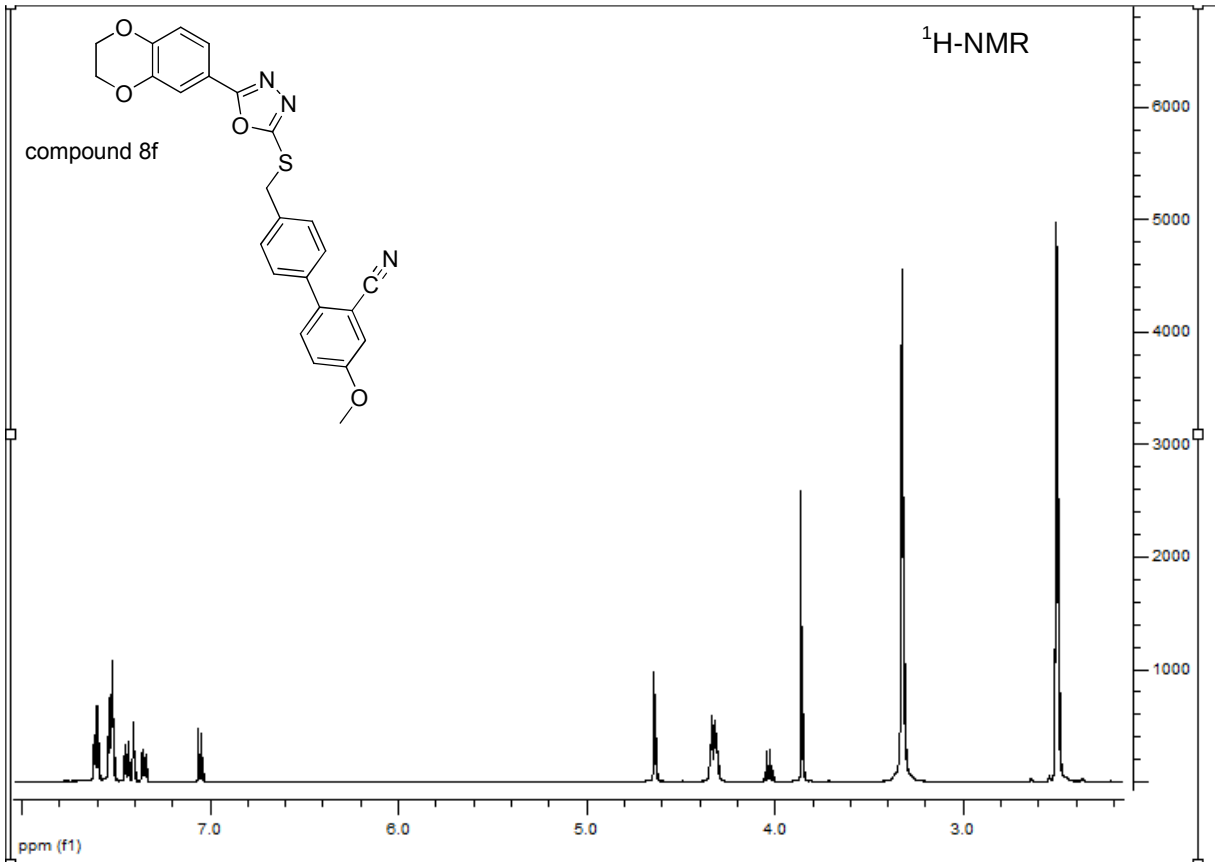
compound 8f
^{1}H-NMR
6000
5000
4000
3000
2000
1000
7.0
6.0
5.0
4.0
3.0
ppm (f1)

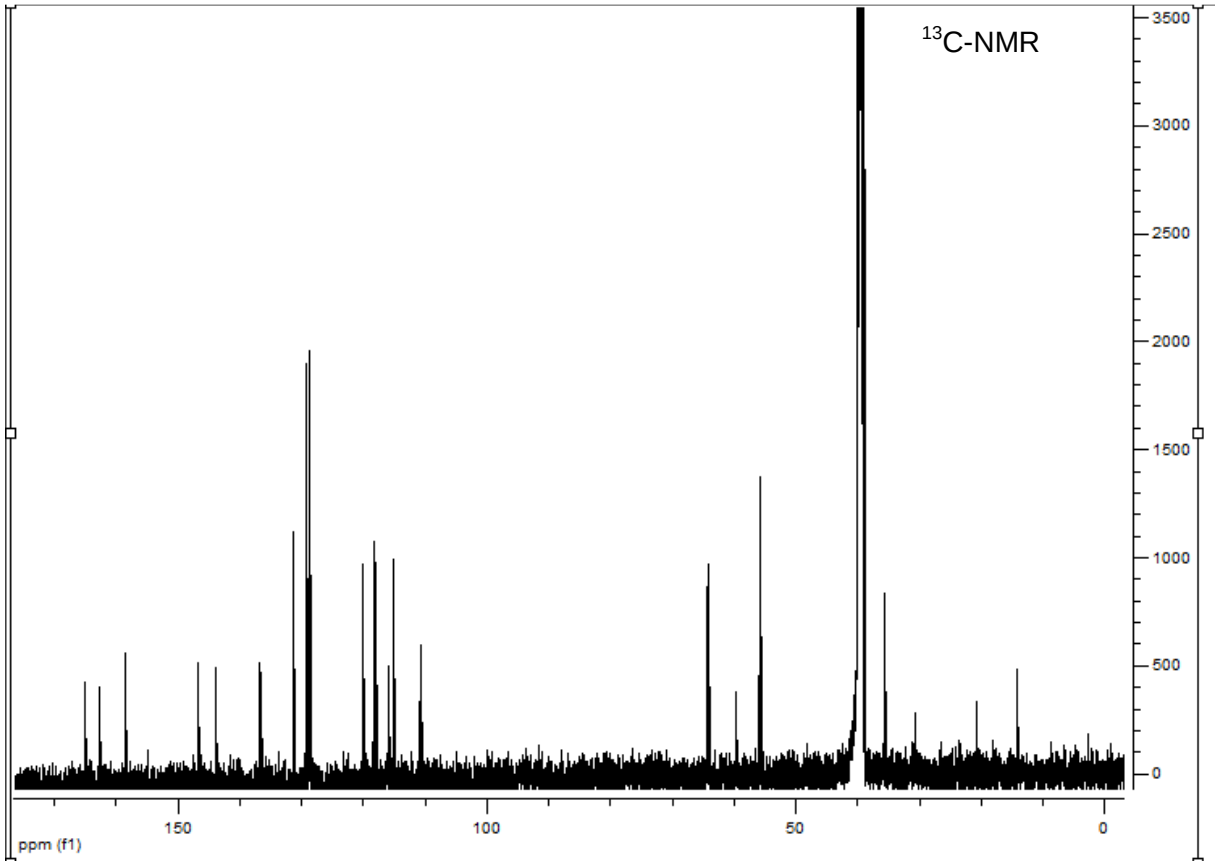
^{13}C-NMR
3500
3000
2500
2000
1500
1000
500
0
150
100
50
0
ppm (f1)

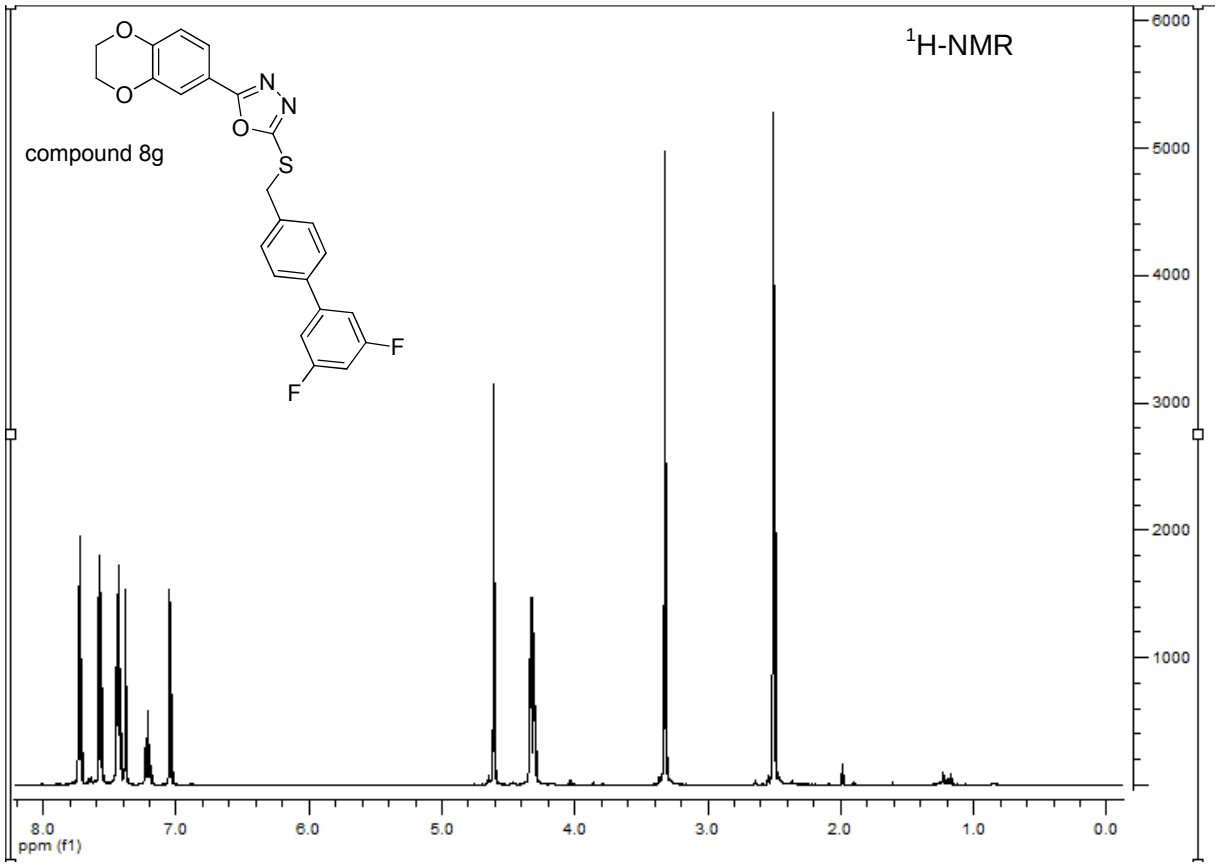
compound 8g
^{1}H-NMR
O
O
N
N
O
S
F
F
6000
5000
4000
3000
2000
1000
8.0
7.0
6.0
5.0
4.0
3.0
2.0
1.0
0.0
ppm (f1)

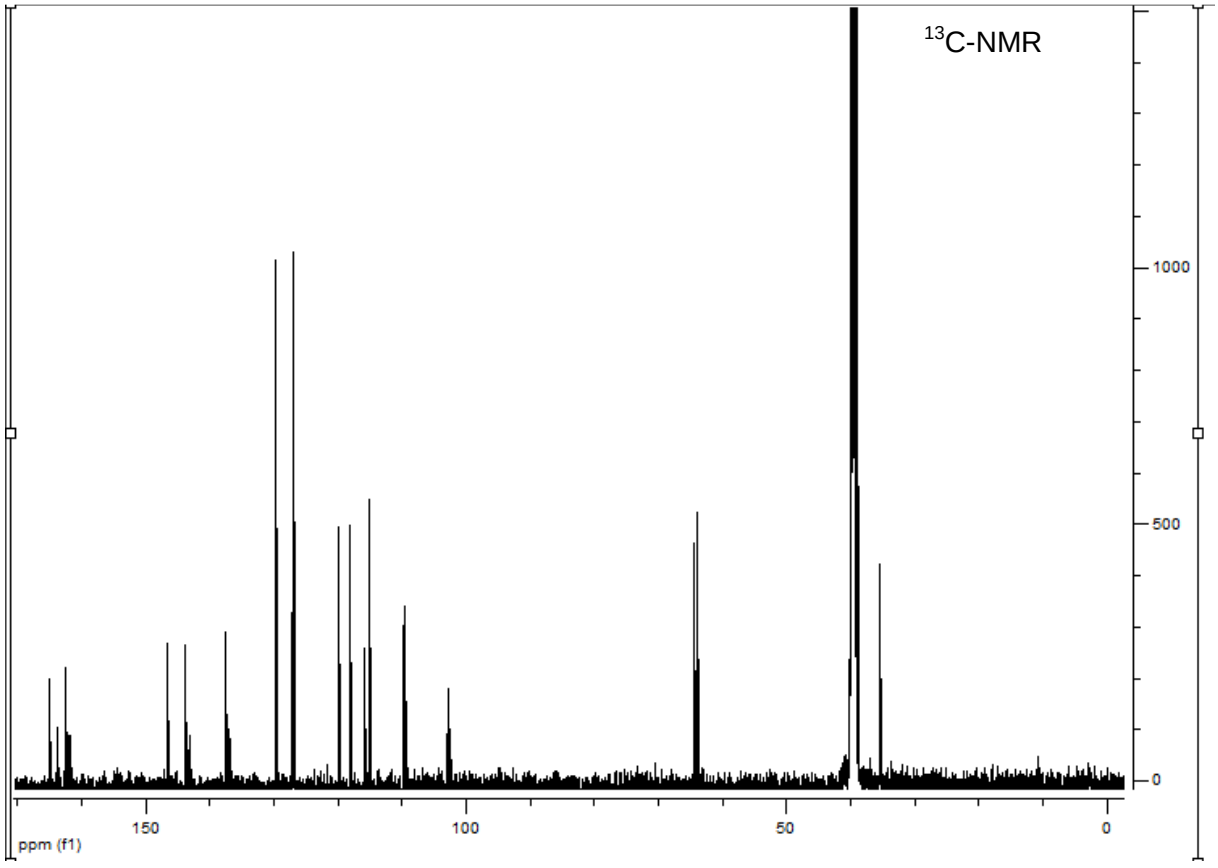
^{13}C-NMR
1000
500
0
150
100
50
0
ppm (f1)

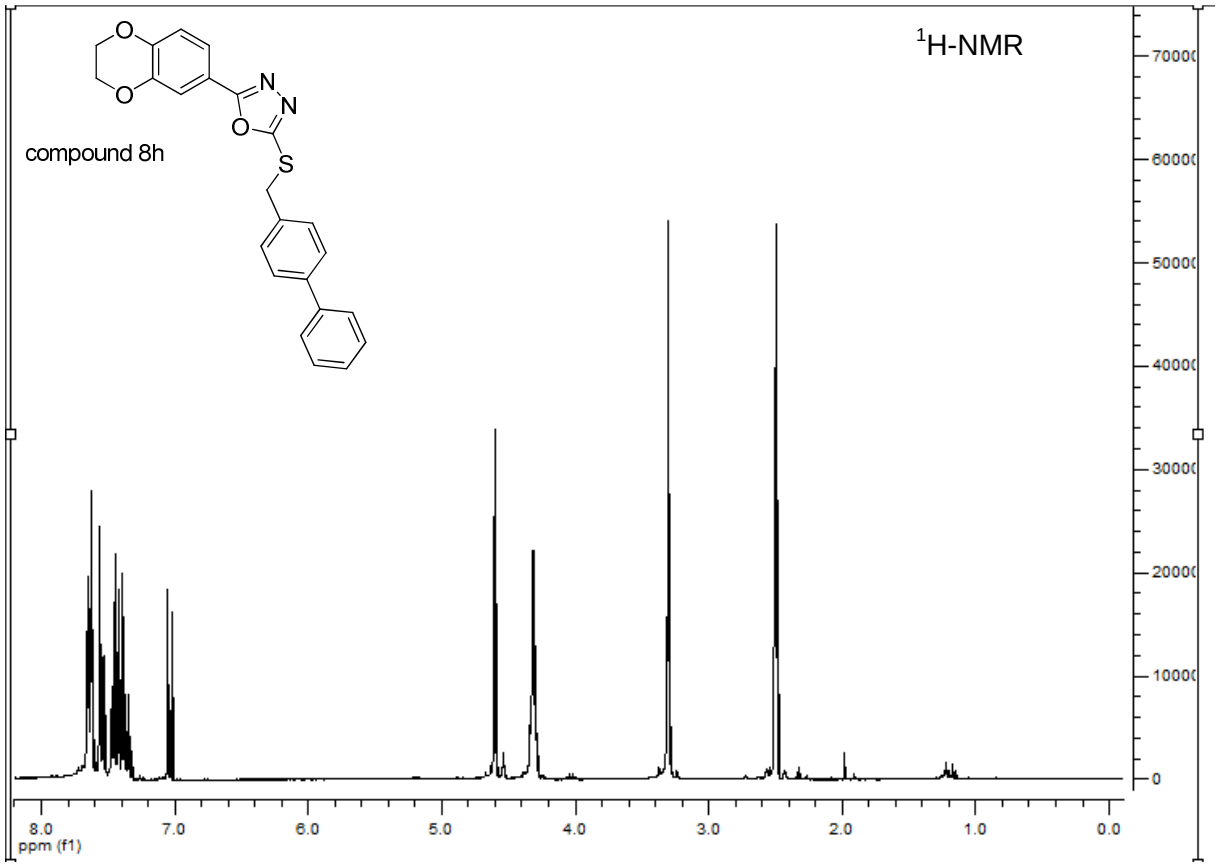
compound 8h
^{1}H-NMR
8.0
7.0
6.0
5.0
4.0
3.0
2.0
1.0
0.0
ppm (f1)

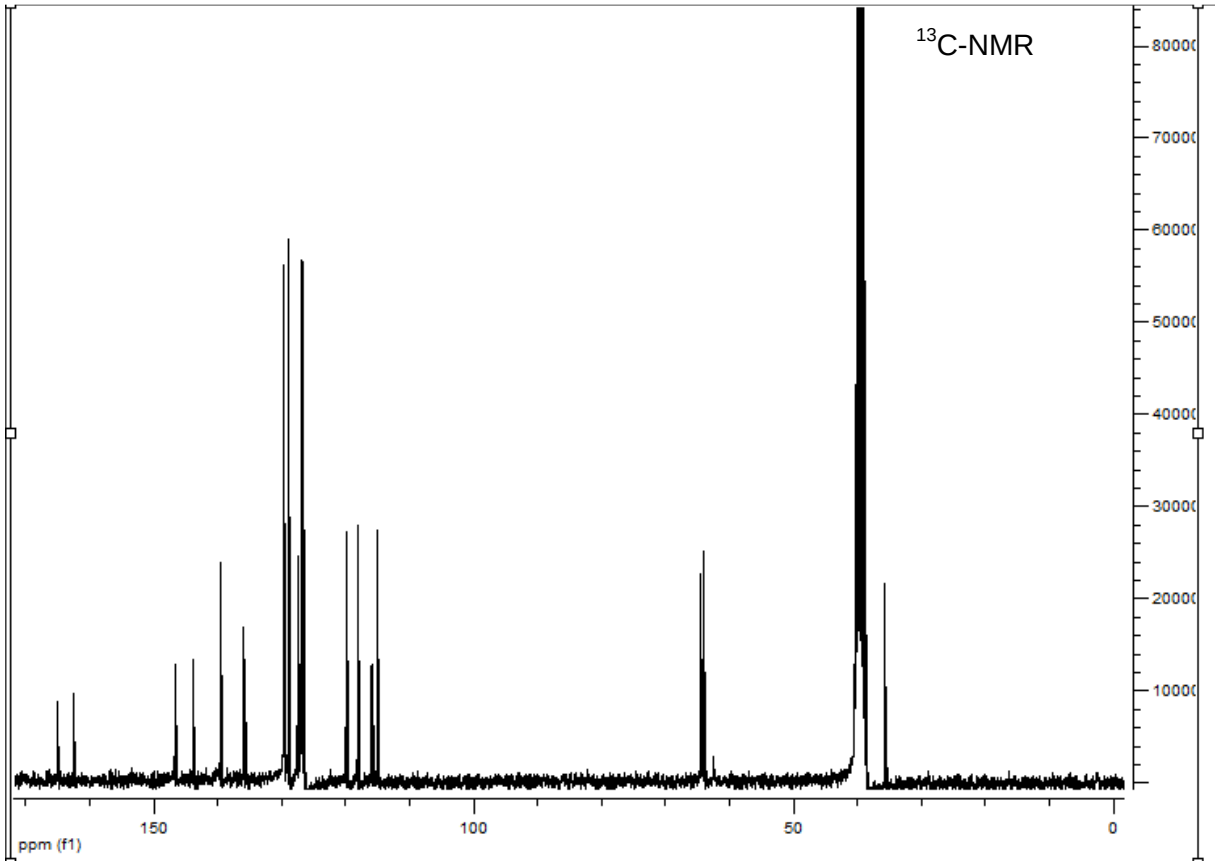
^{13}C-NMR
150
100
50
0
ppm (f1)

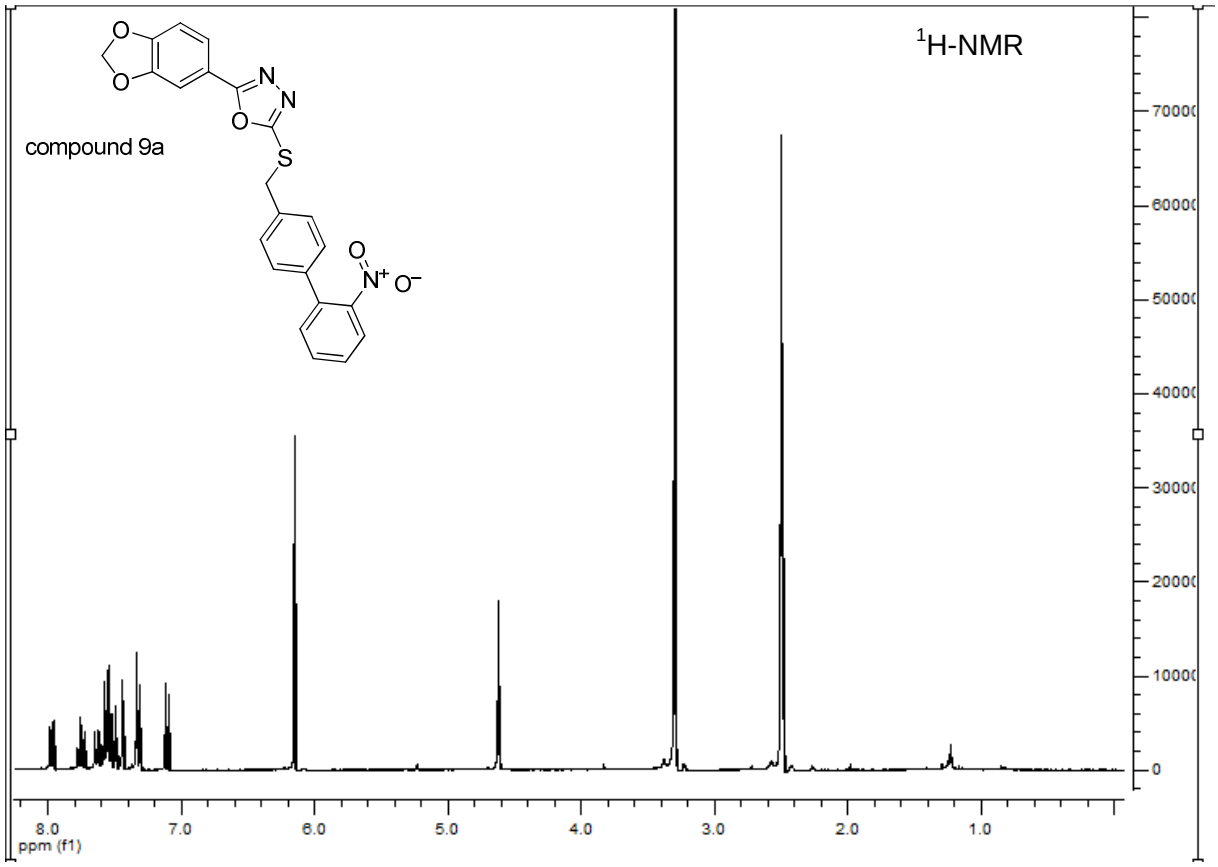
compound 9a
^{1}H-NMR
8.0
7.0
6.0
5.0
4.0
3.0
2.0
1.0
ppm (f1)

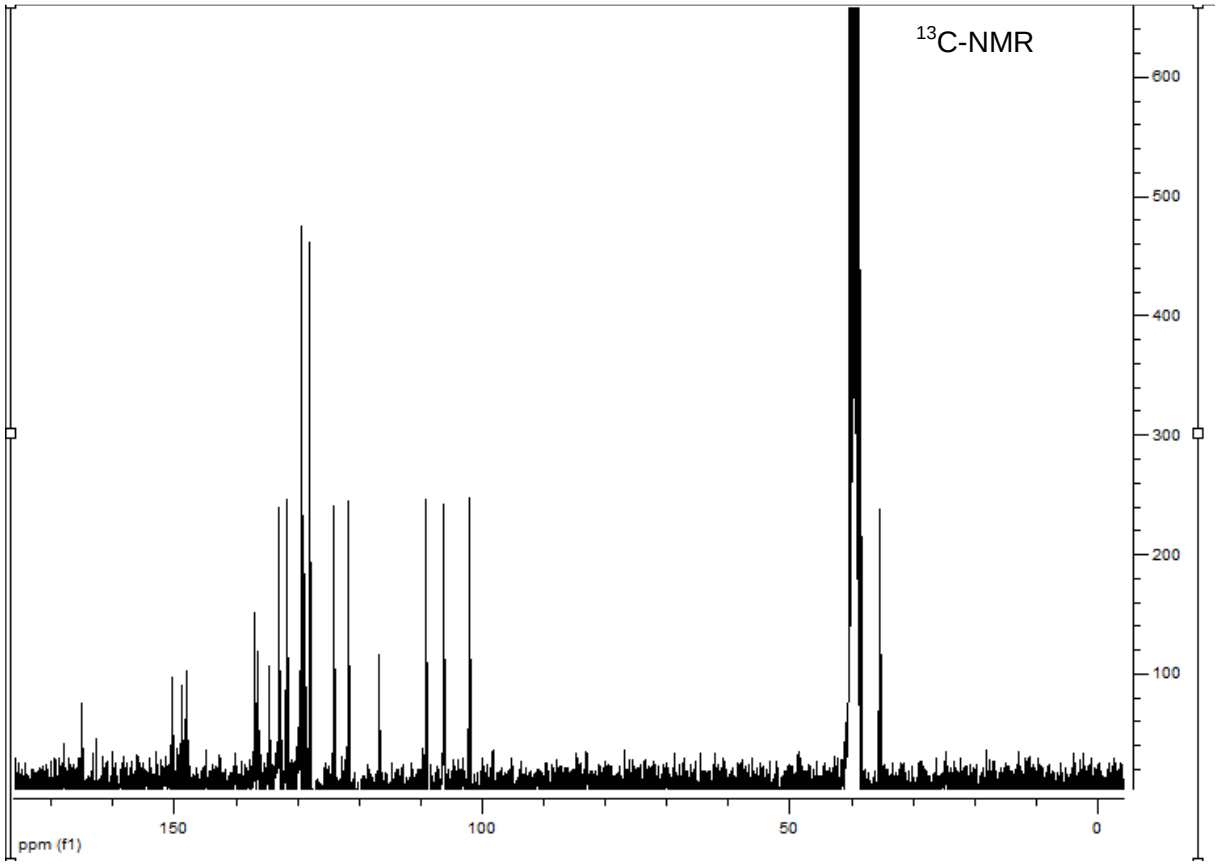
^{13}C-NMR
150
100
50
0
ppm (f1)

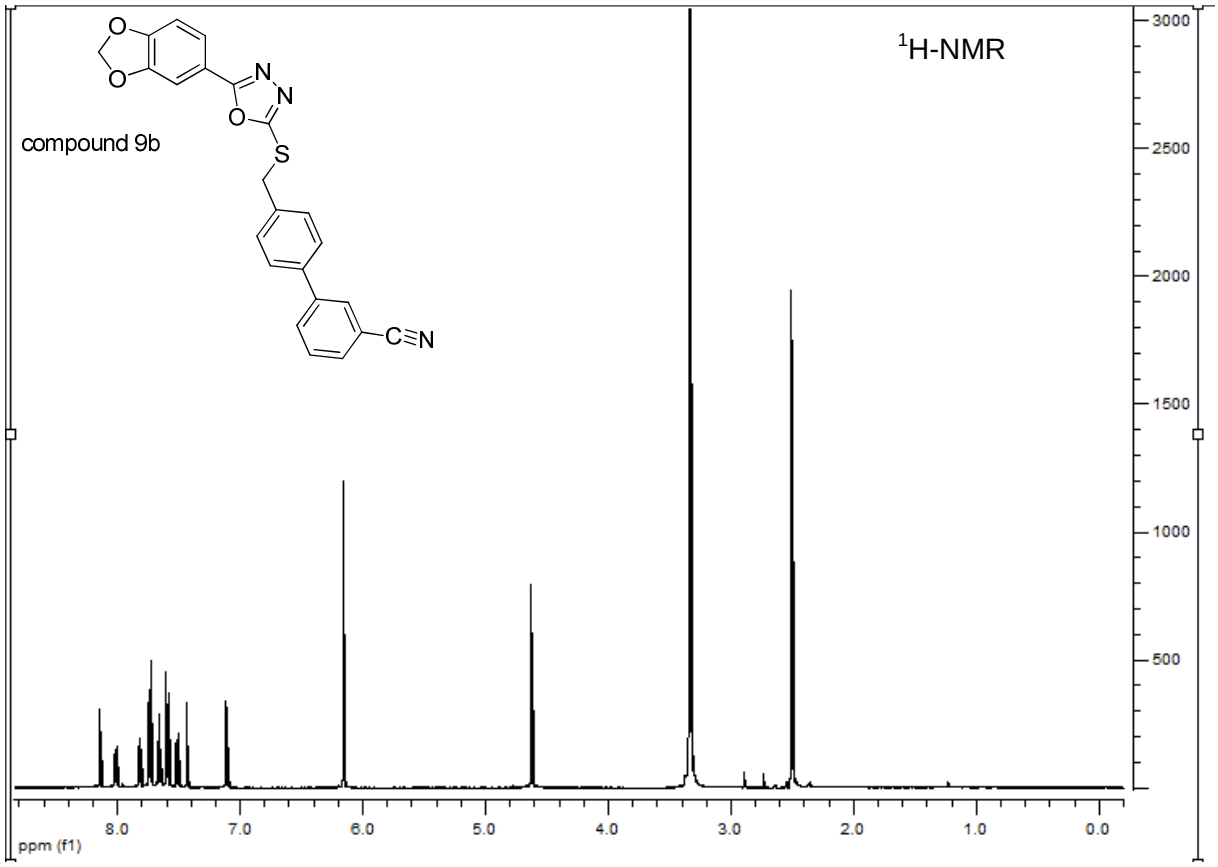
compound 9b
^{1}H-NMR
3000
2500
2000
1500
1000
500
8.0
7.0
6.0
5.0
4.0
3.0
2.0
1.0
0.0
ppm (f1)

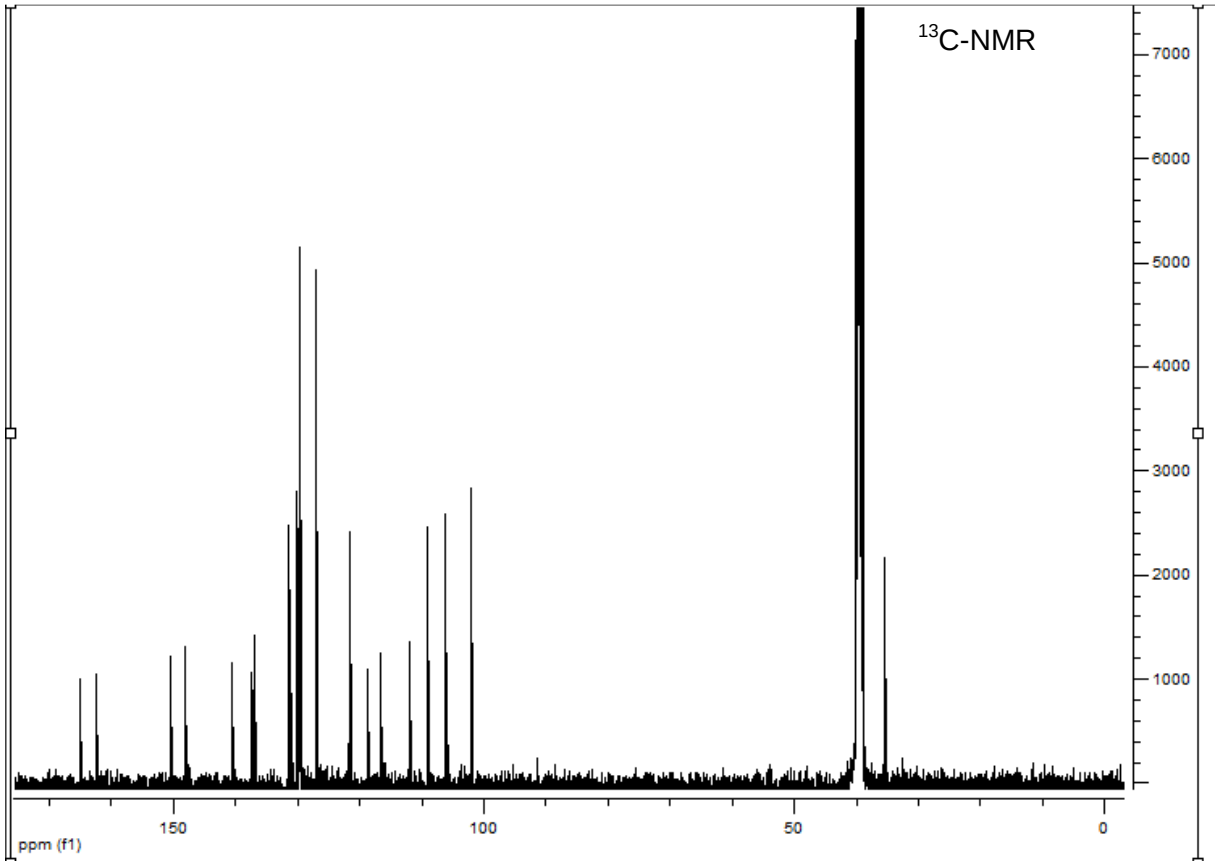
^{13}C-NMR
7000
6000
5000
4000
3000
2000
1000
150
100
50
0
ppm (f1)

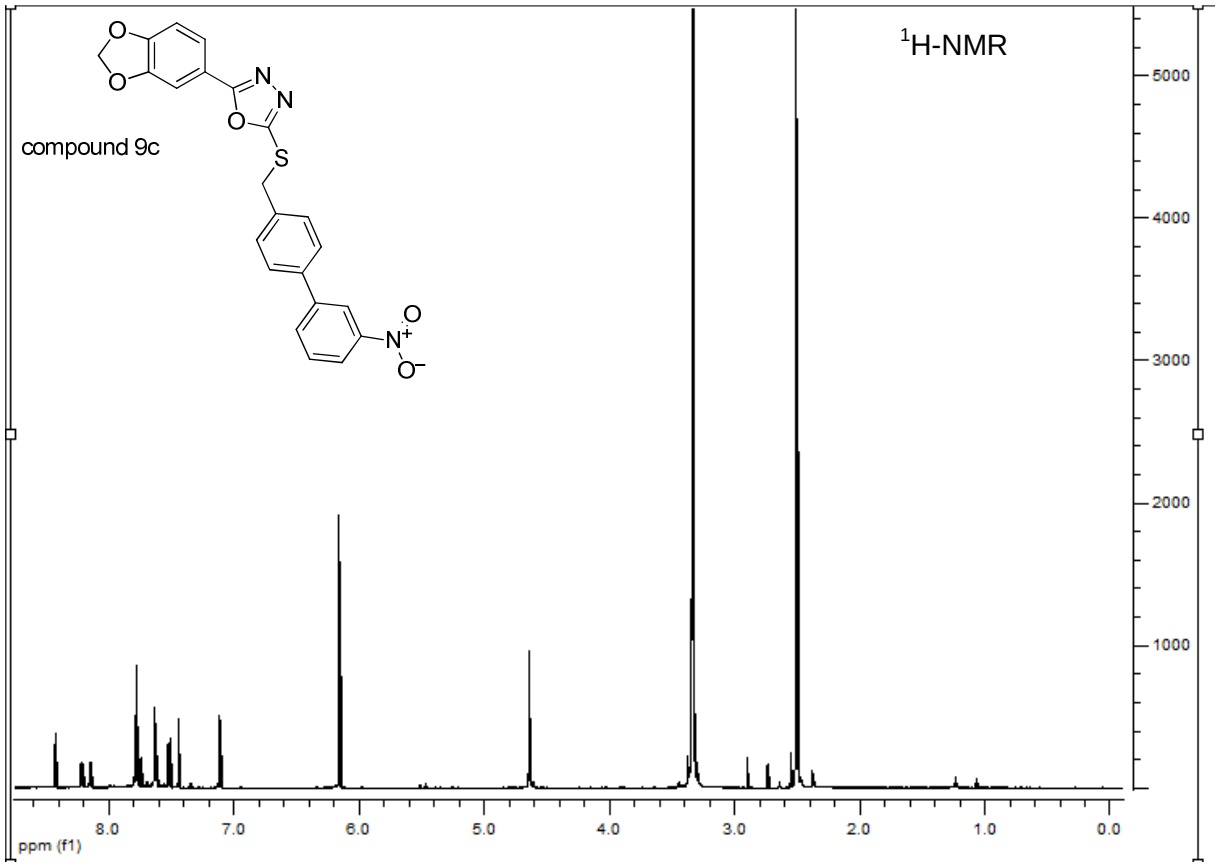
compound 9c
^{1}H-NMR
5000
4000
3000
2000
1000
8.0
7.0
6.0
5.0
4.0
3.0
2.0
1.0
0.0
ppm (f1)

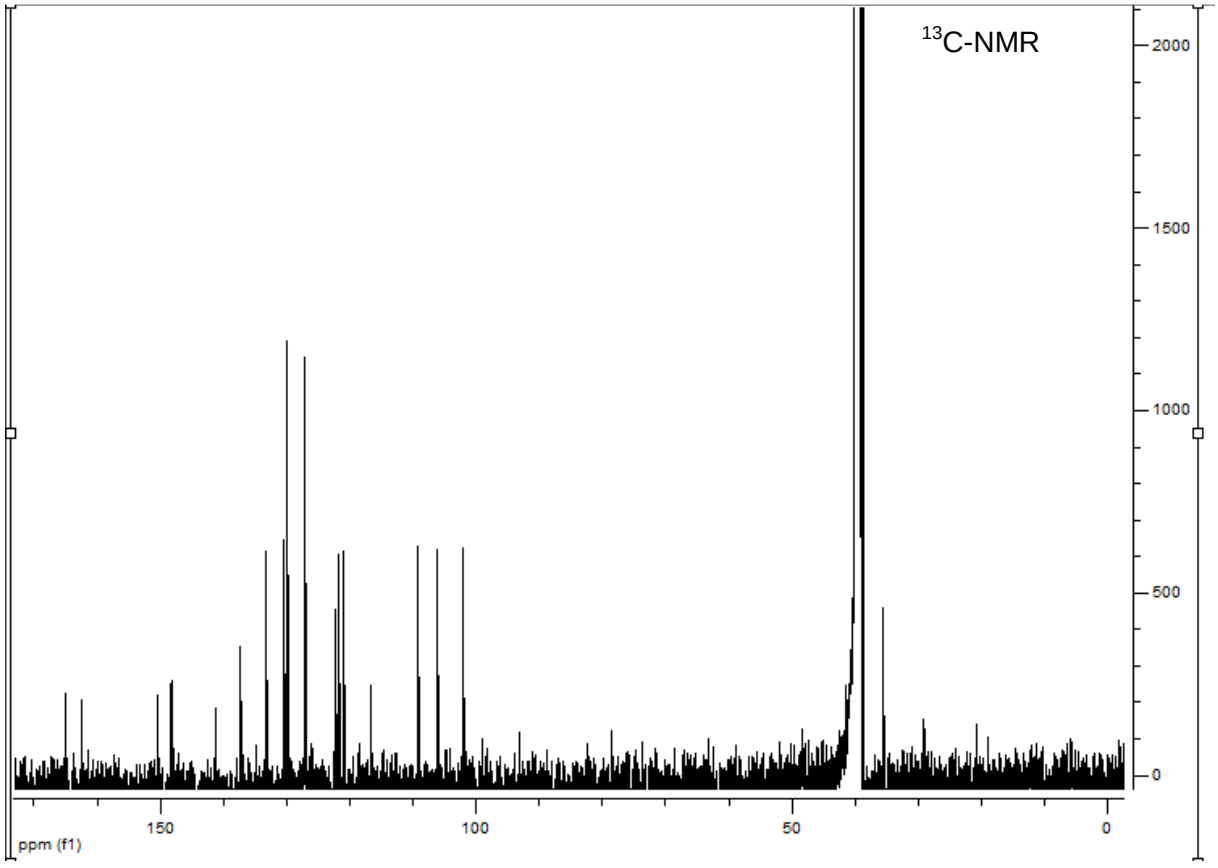
^{13}C-NMR
2000
1500
1000
500
0
150
100
50
0
ppm (f1)

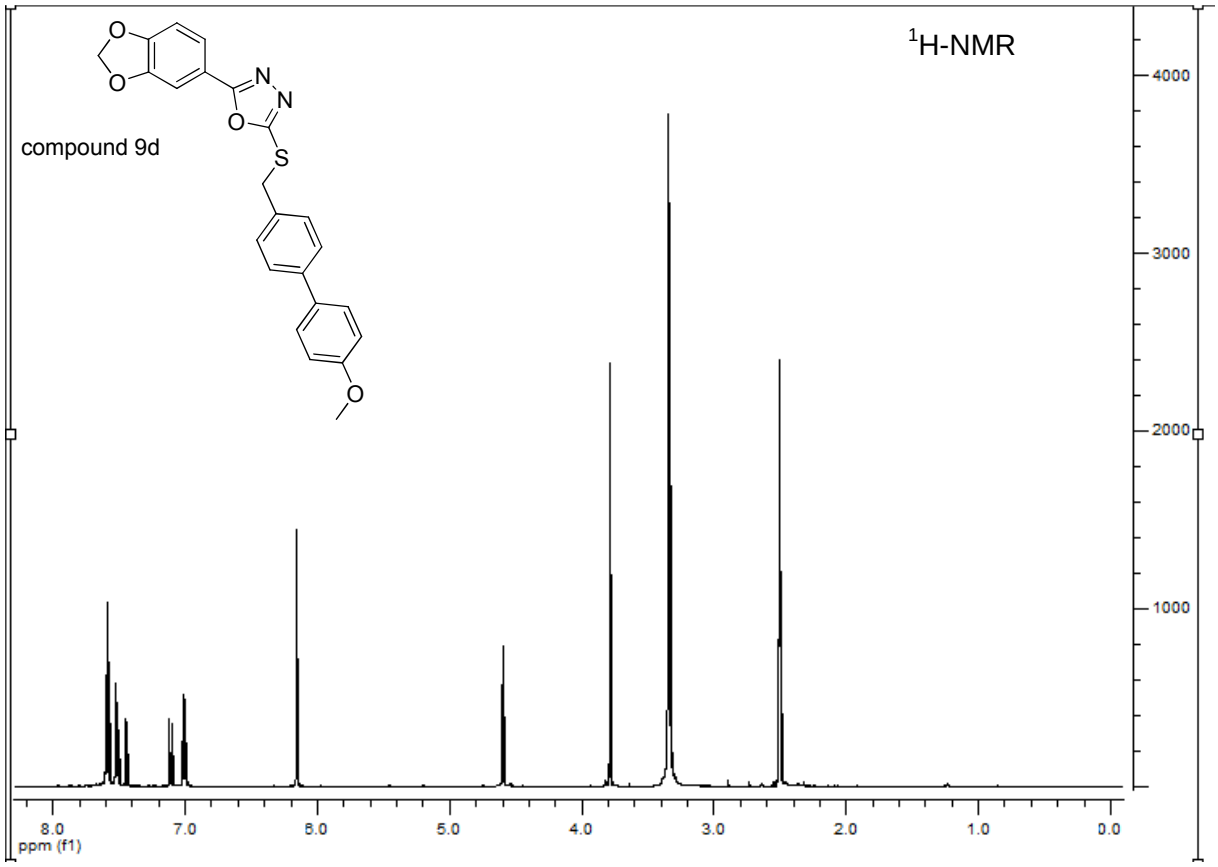
compound 9d
^{1}H-NMR
4000
3000
2000
1000
8.0
7.0
6.0
5.0
4.0
3.0
2.0
1.0
0.0
ppm (f1)

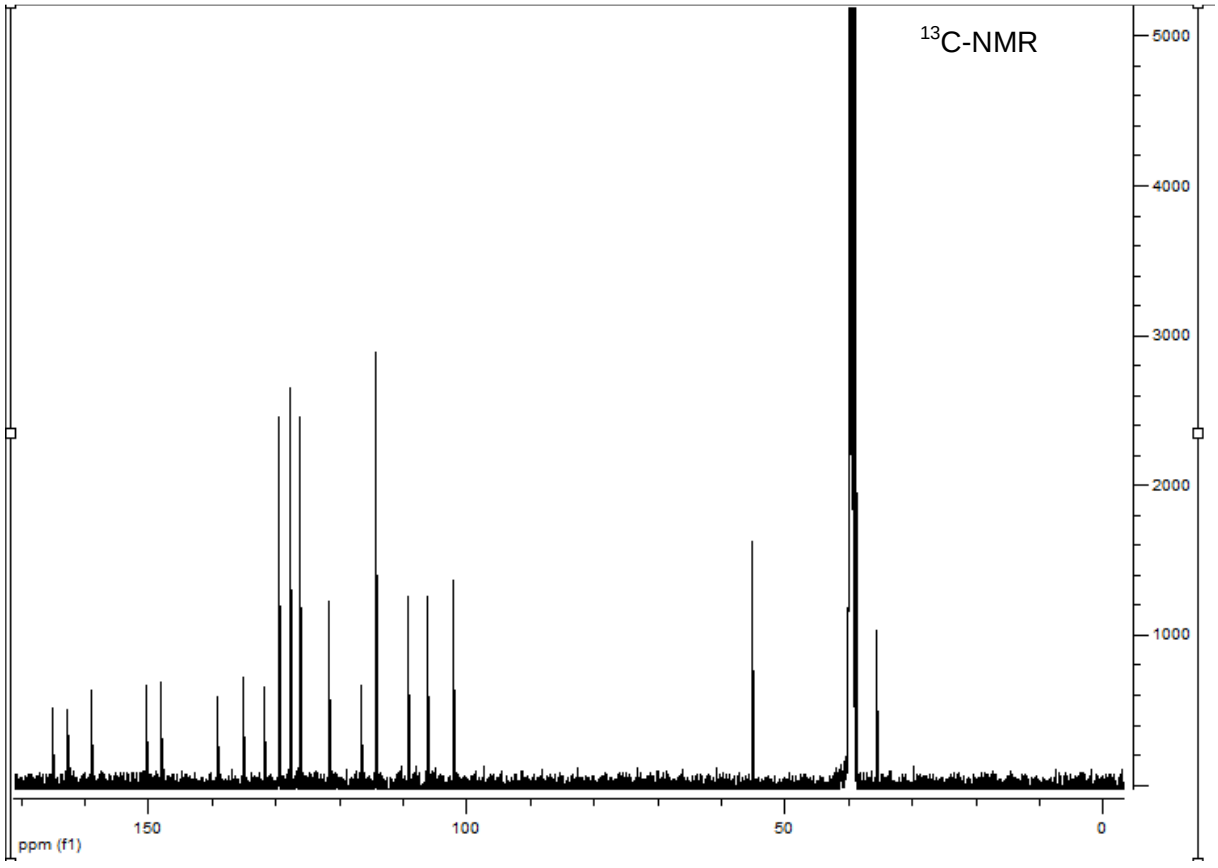
^{13}C-NMR
5000
4000
3000
2000
1000
150
100
50
0
ppm (f1)

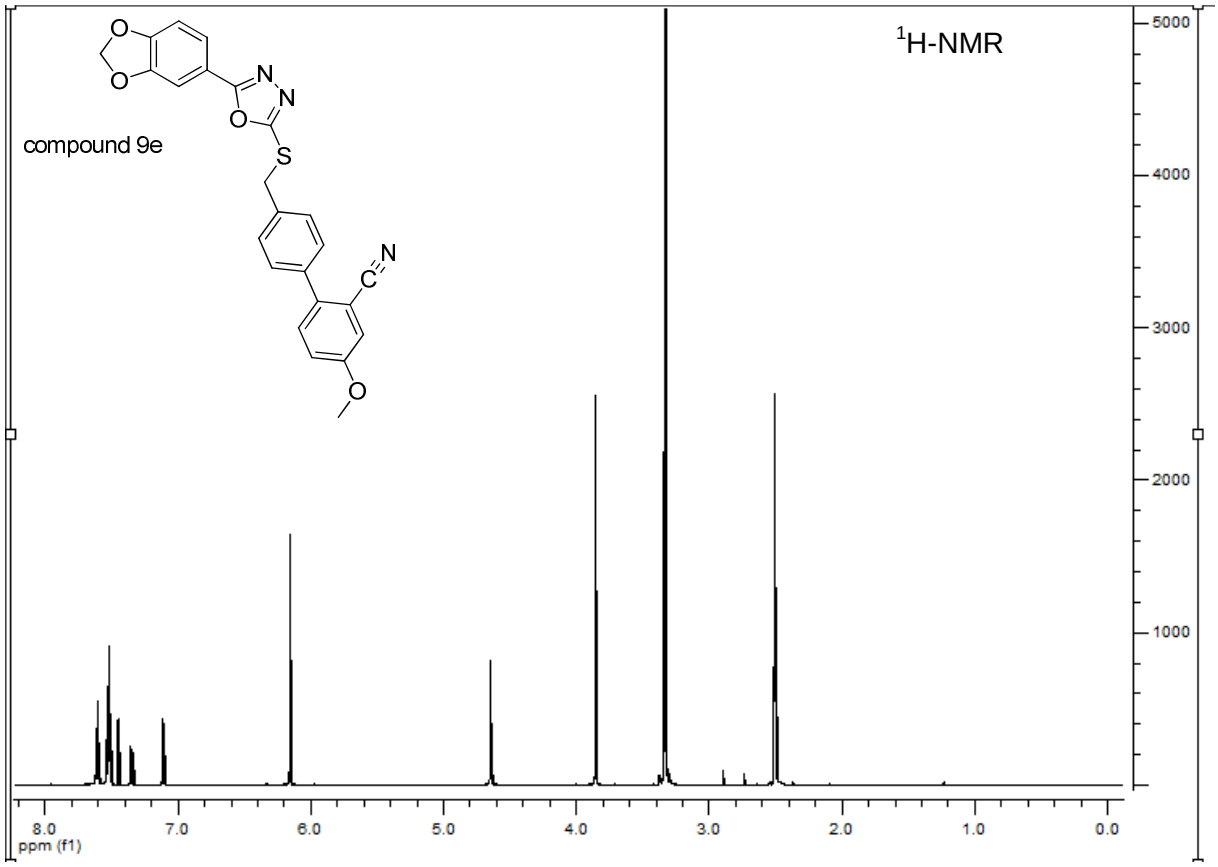
compound 9e
^{1}H-NMR
5000
4000
3000
2000
1000
8.0
7.0
6.0
5.0
4.0
3.0
2.0
1.0
0.0
ppm (f1)

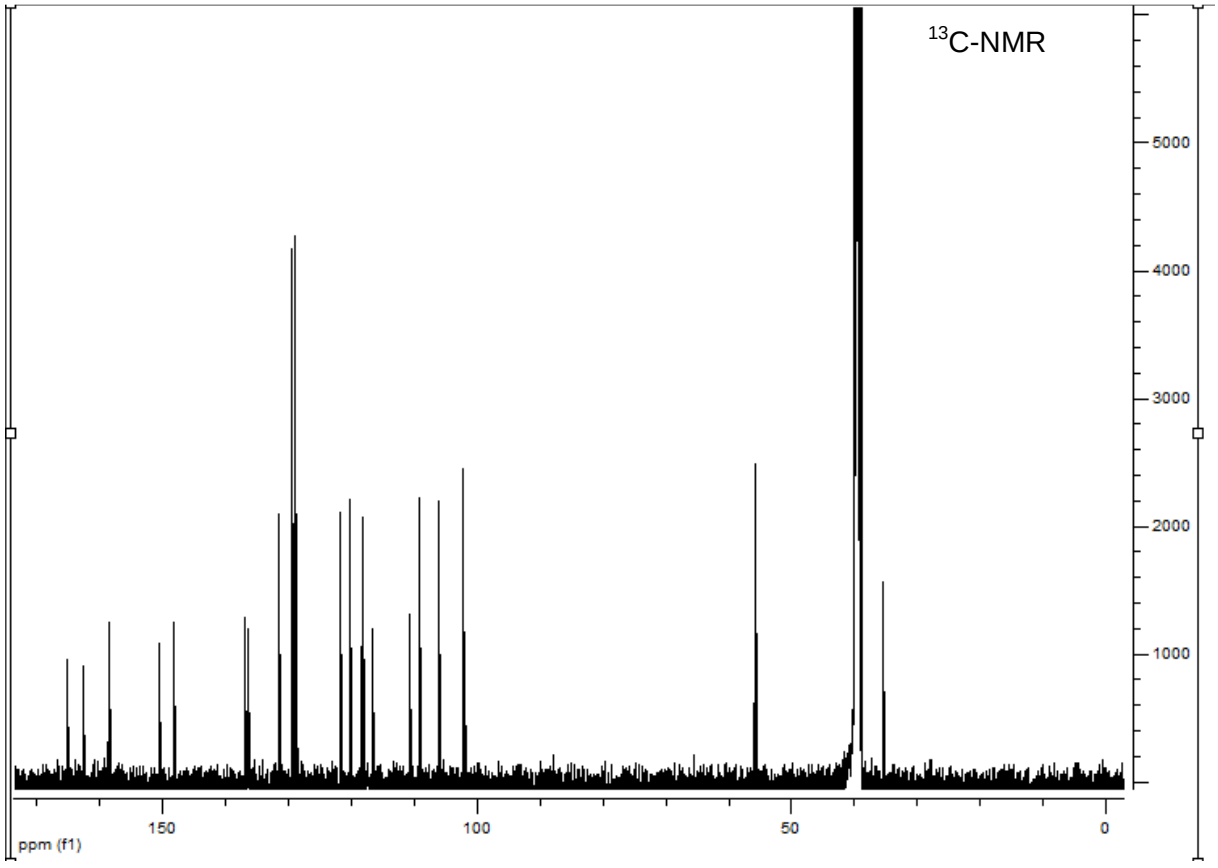
^{13}C-NMR
5000
4000
3000
2000
1000
150
100
50
0
ppm (f1)

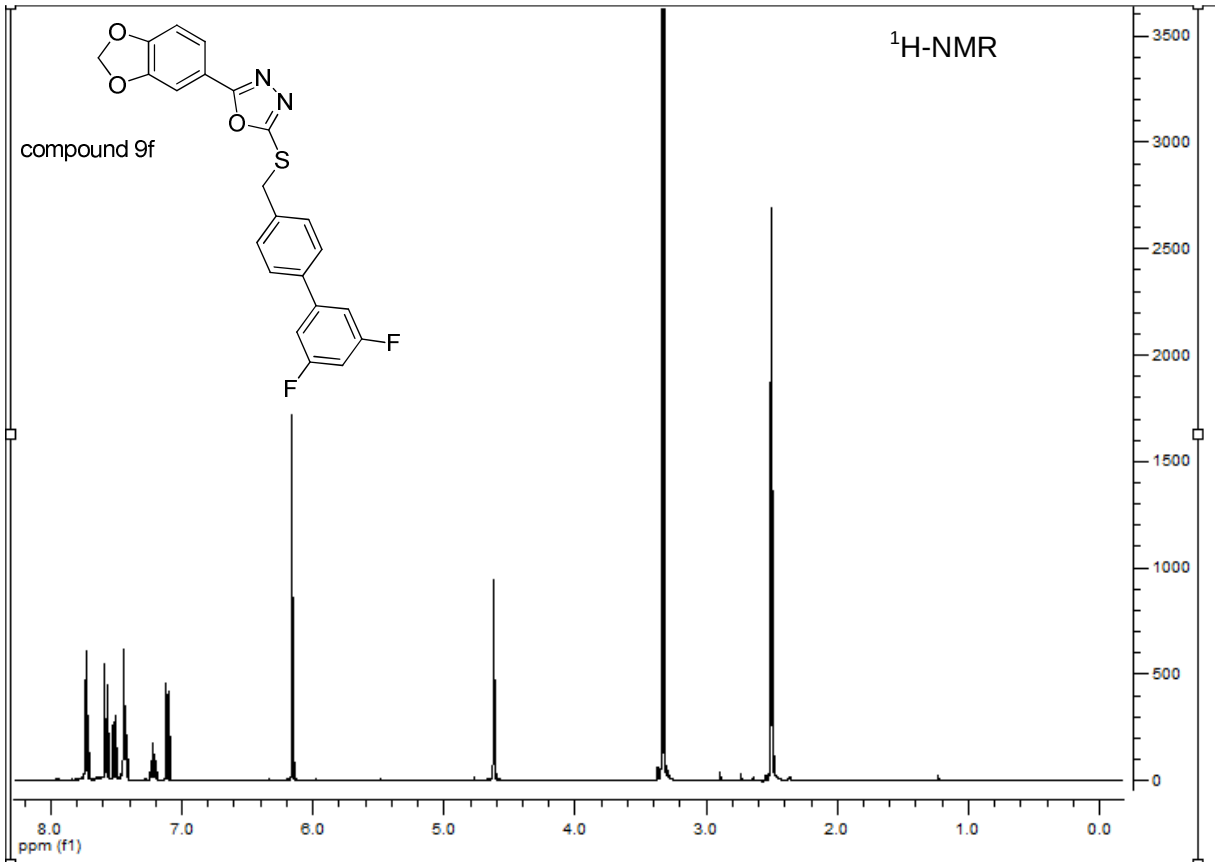
compound 9f
^{1}H-NMR
3500
3000
2500
2000
1500
1000
500
0
8.0
7.0
6.0
5.0
4.0
3.0
2.0
1.0
0.0
ppm (f1)

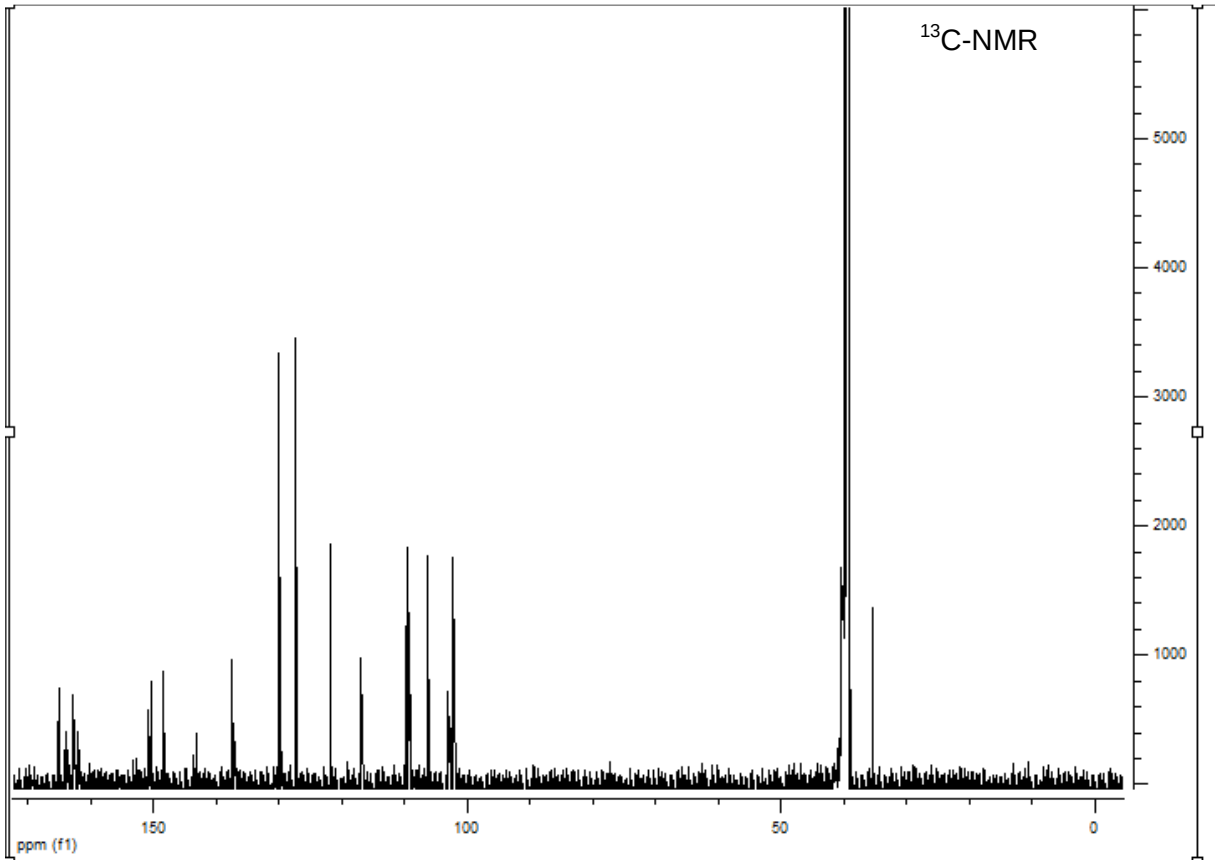
^{13}C-NMR
5000
4000
3000
2000
1000
150
100
50
0
ppm (f1)

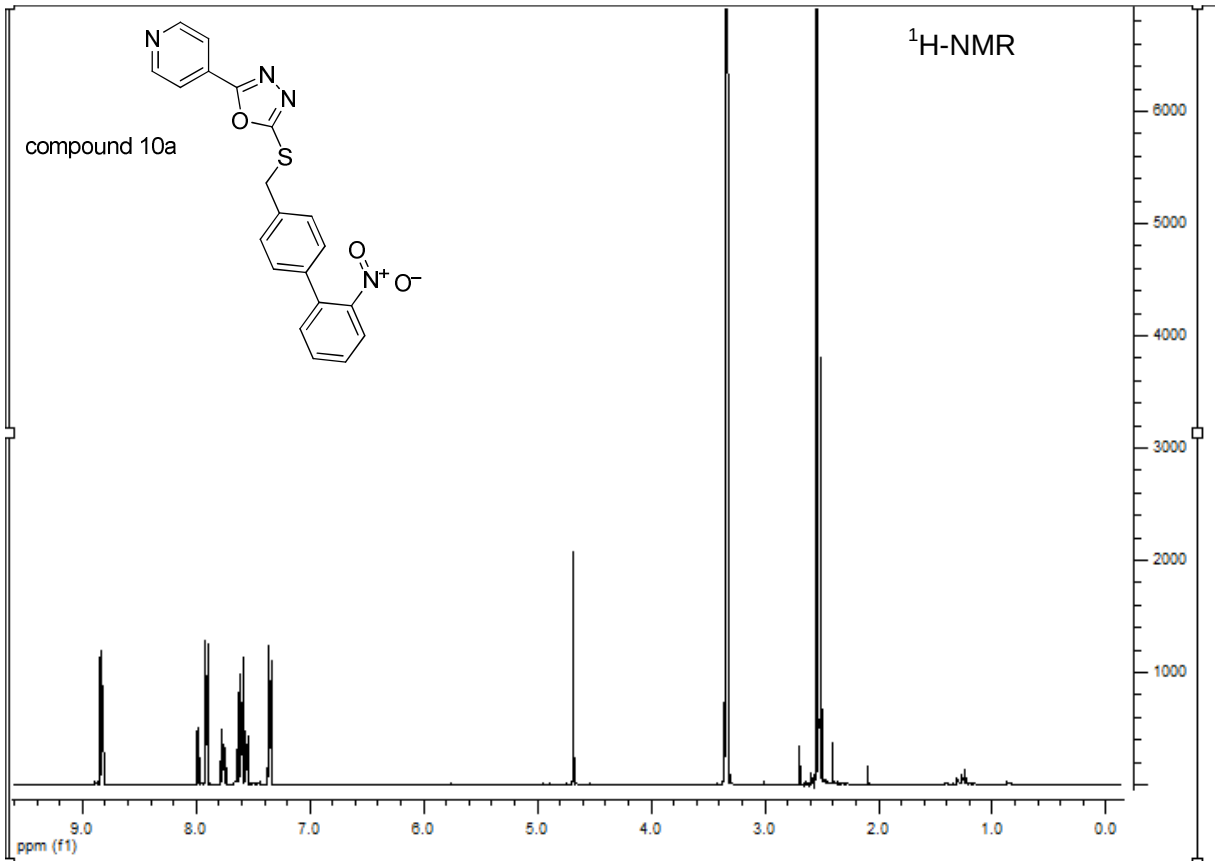
compound 10a
^{1}H-NMR
6000
5000
4000
3000
2000
1000
9.0
8.0
7.0
6.0
5.0
4.0
3.0
2.0
1.0
0.0
ppm (f1)

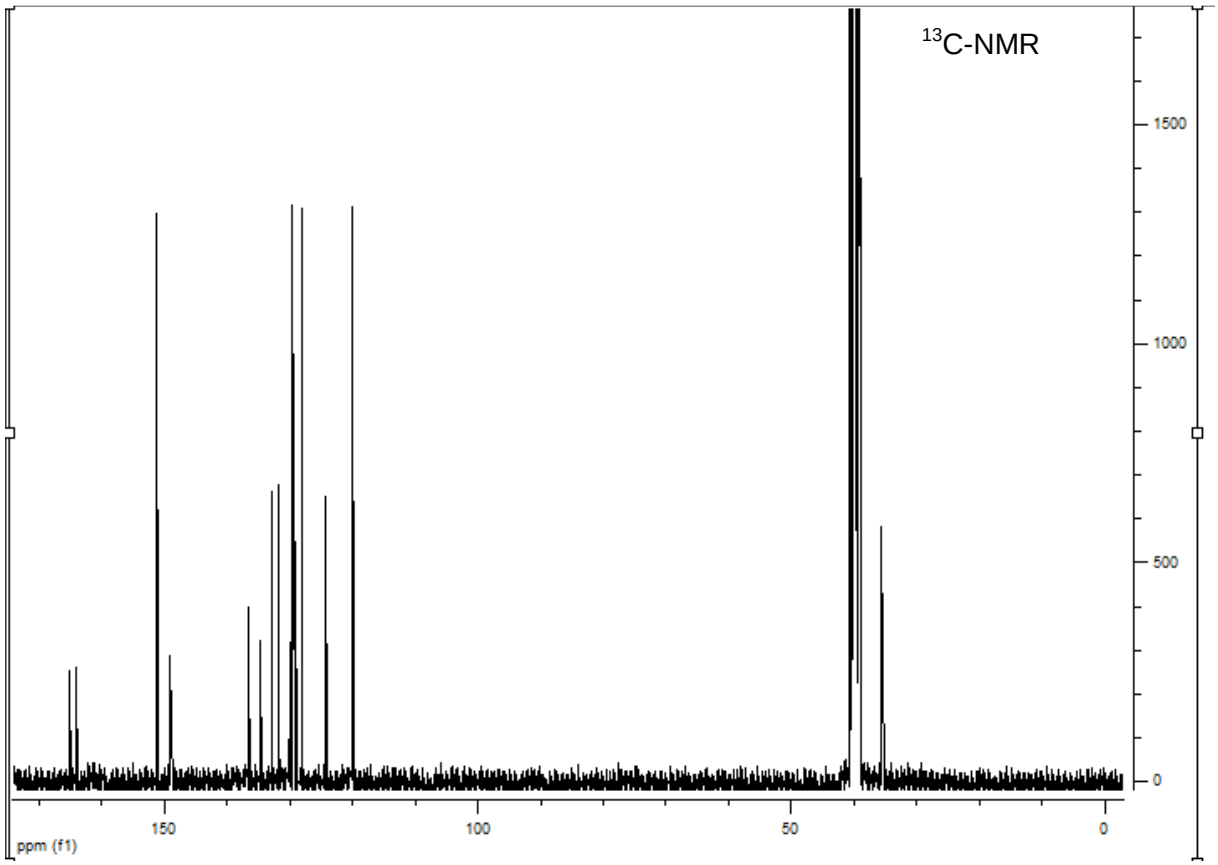
^{13}C-NMR
1500
1000
500
0
150
100
50
0
ppm (f1)

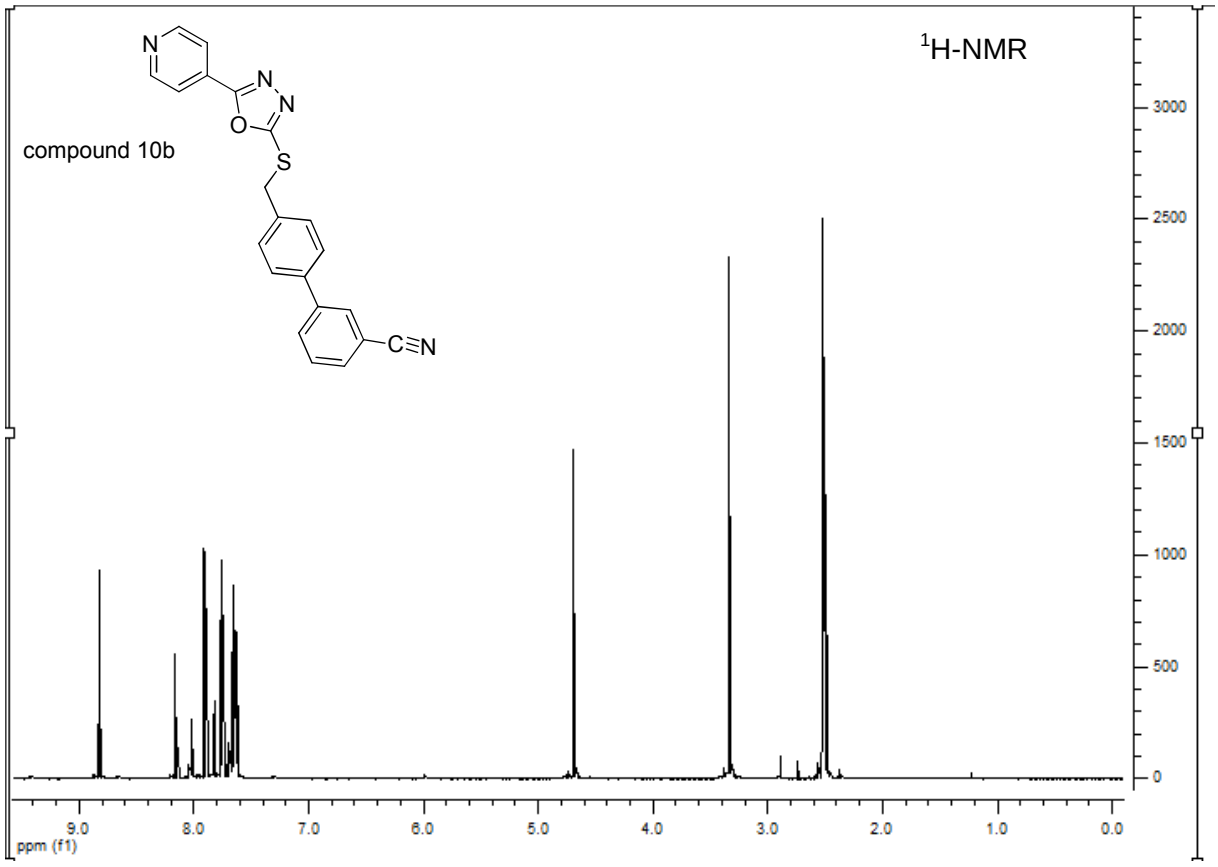
compound 10b
^{1}H-NMR
ppm (f1)

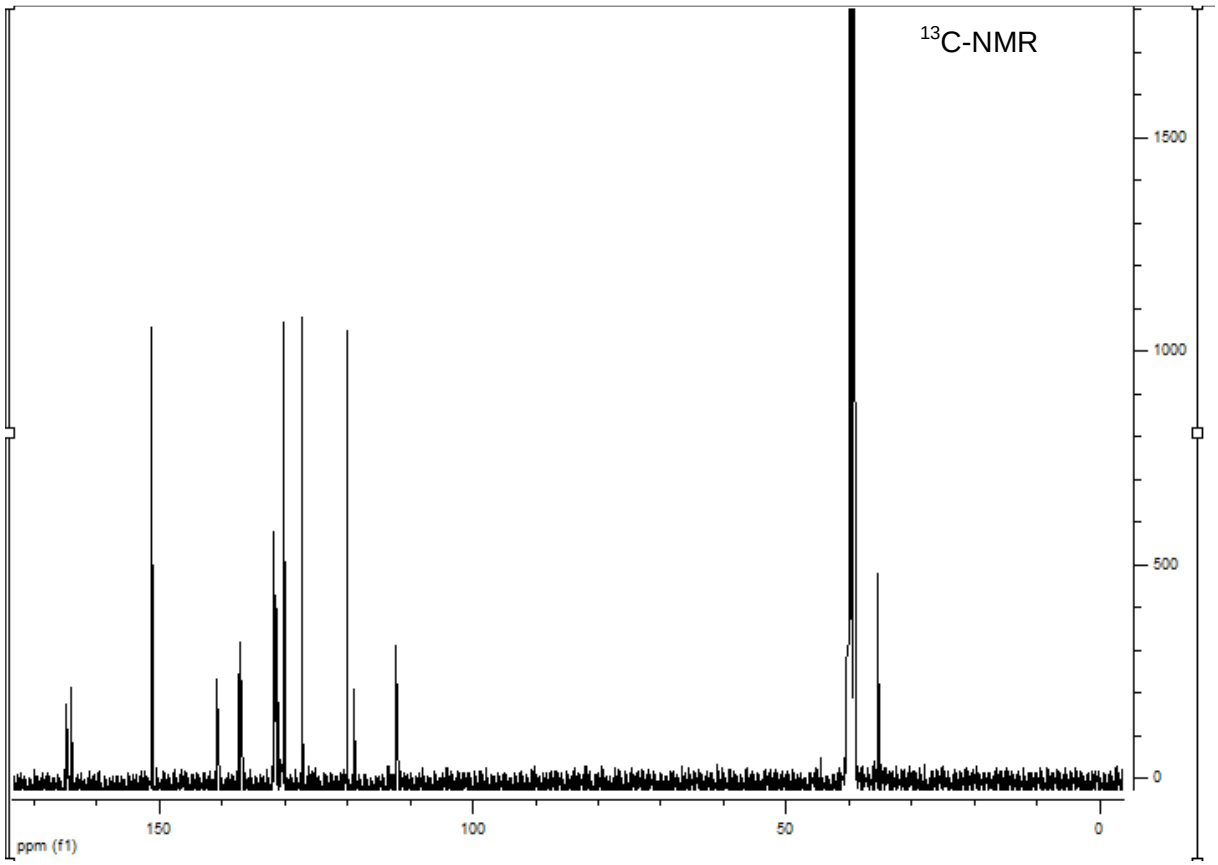
^{13}C-NMR
ppm (f1)

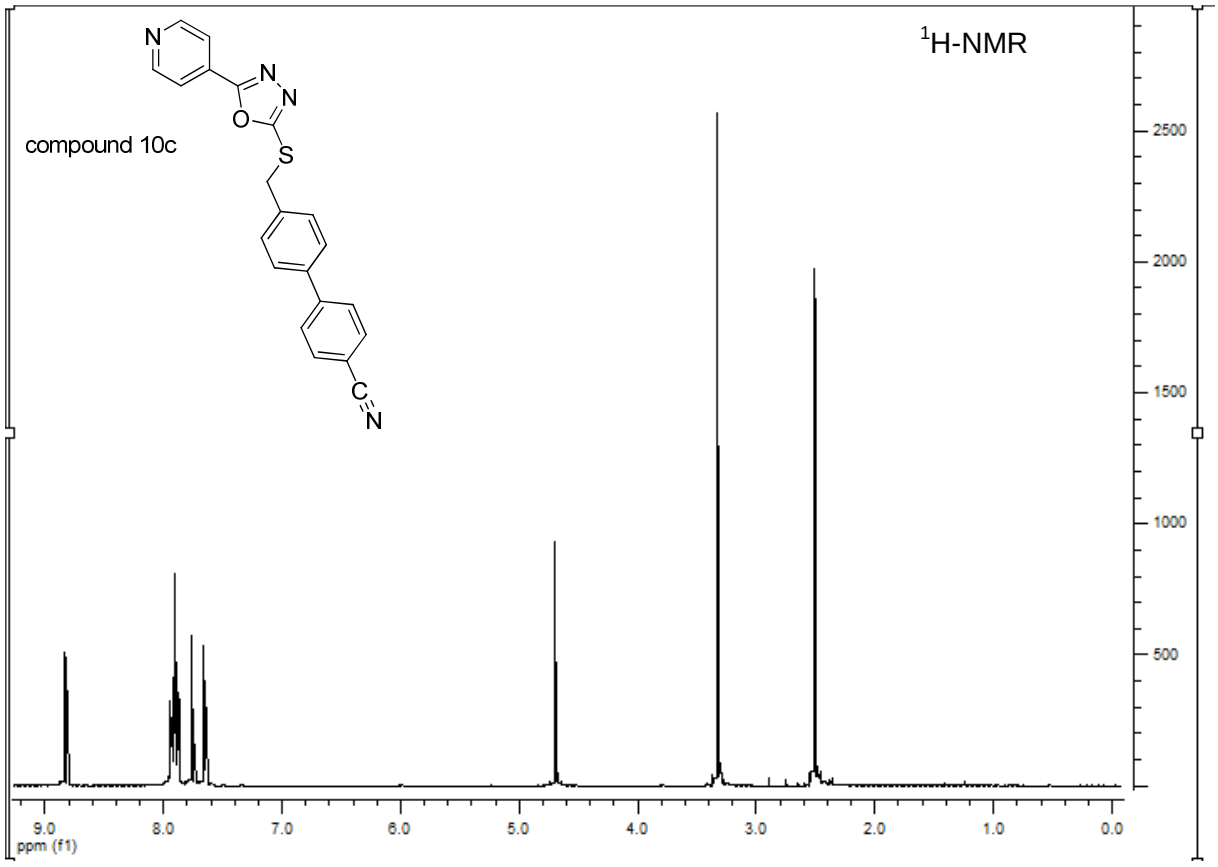
compound 10c
^{1}H-NMR
2500
2000
1500
1000
500
9.0
8.0
7.0
6.0
5.0
4.0
3.0
2.0
1.0
0.0
ppm (f1)

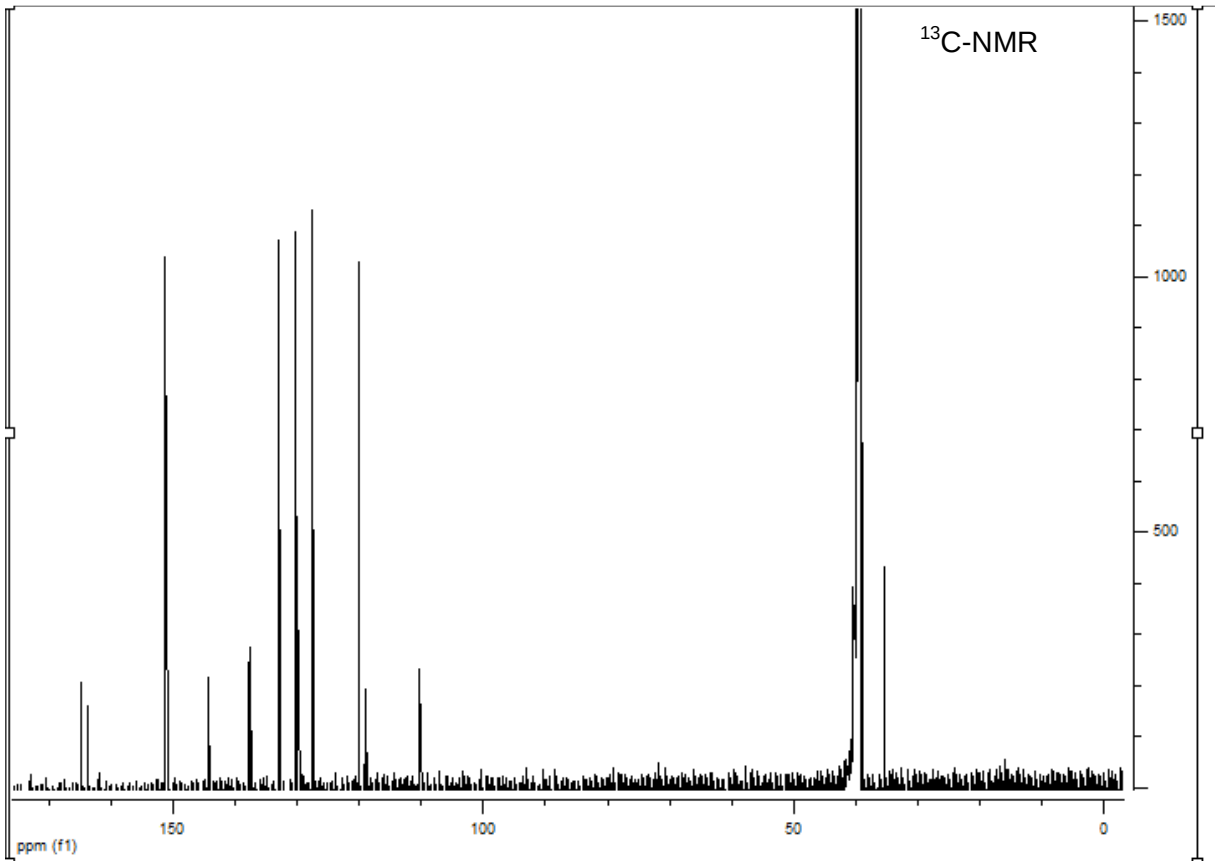
^{13}C-NMR
1500
1000
500
150
100
50
0
ppm (f1)

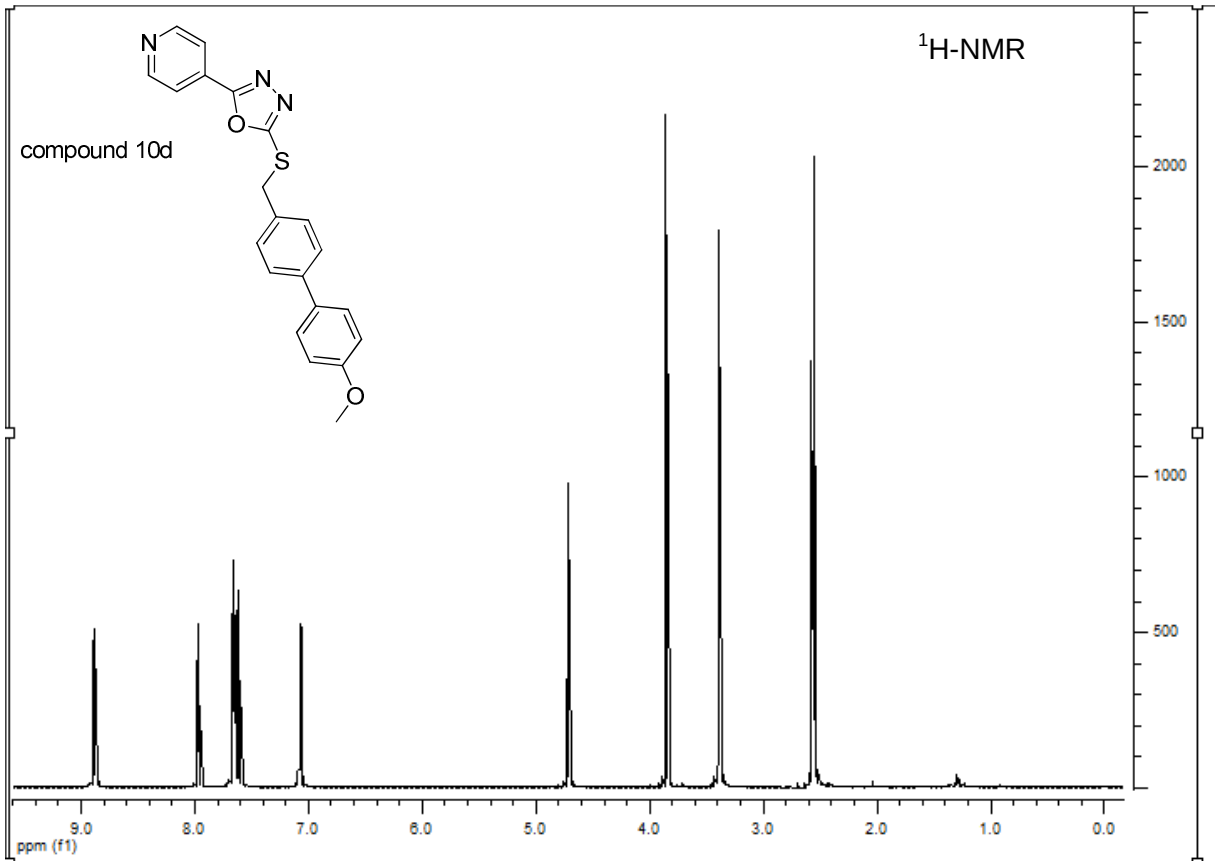
compound 10d
^{1}H-NMR
2000
1500
1000
500
9.0
8.0
7.0
6.0
5.0
4.0
3.0
2.0
1.0
0.0
ppm (f1)

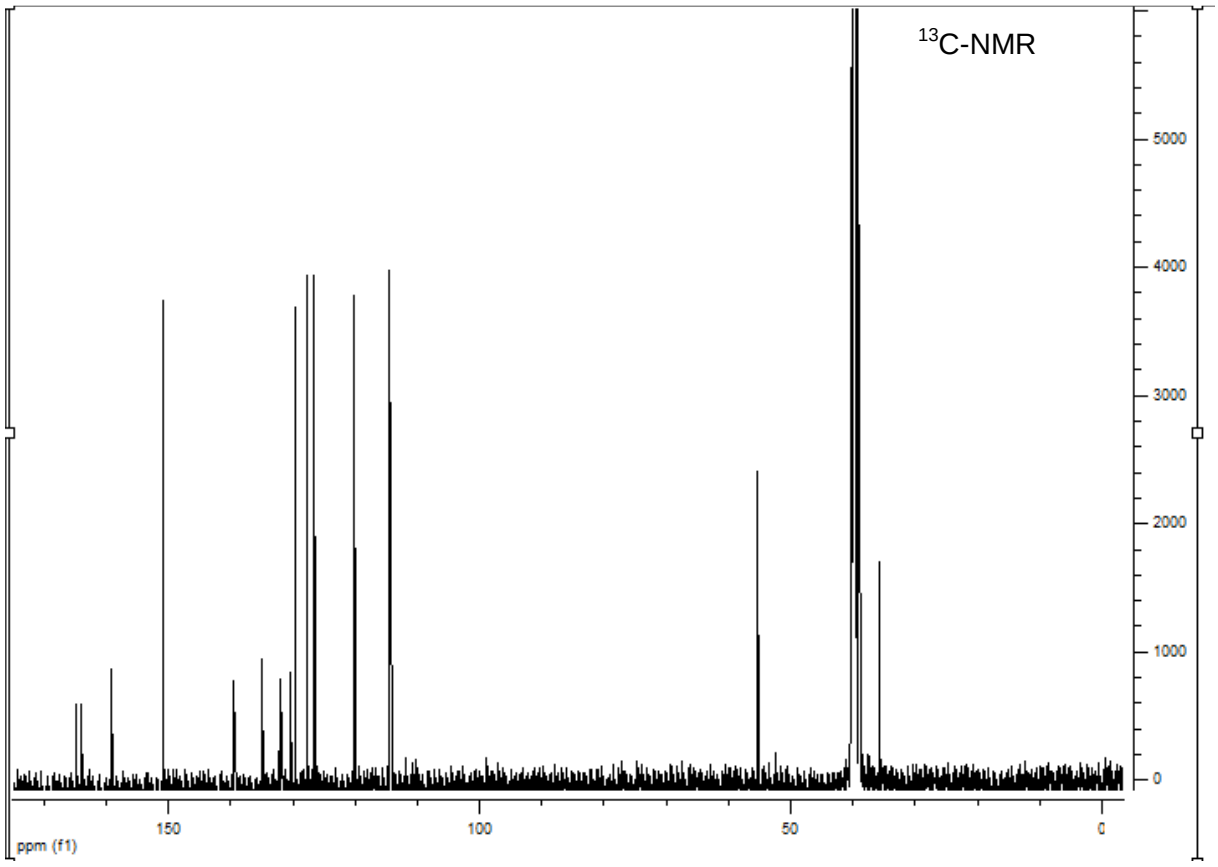
^{13}C-NMR
5000
4000
3000
2000
1000
0
150
100
50
0
ppm (f1)

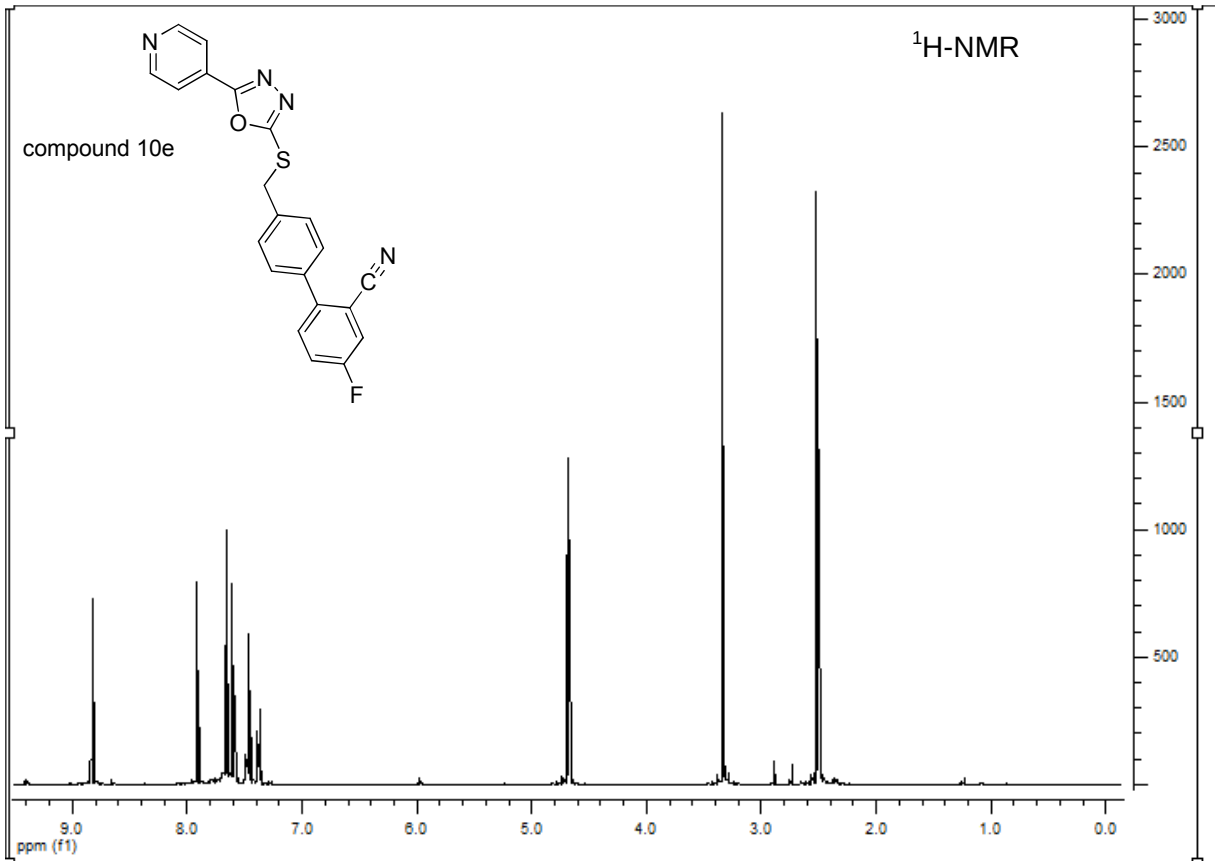
compound 10e
^{1}H-NMR
N
N
N
O
S
C≡N
F
3000
2500
2000
1500
1000
500
9.0
8.0
7.0
6.0
5.0
4.0
3.0
2.0
1.0
0.0
ppm (f1)

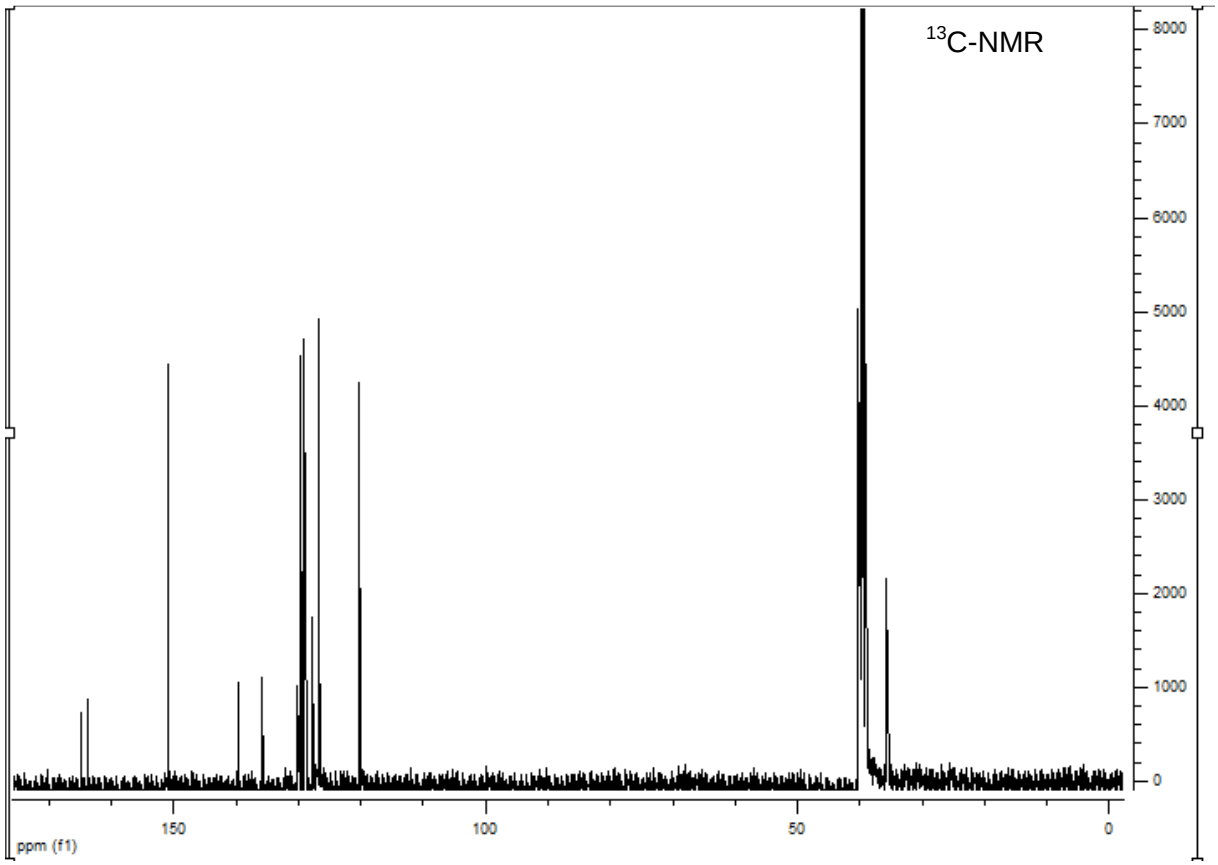
^{13}C-NMR
8000
7000
6000
5000
4000
3000
2000
1000
0
150
100
50
0
ppm (f1)

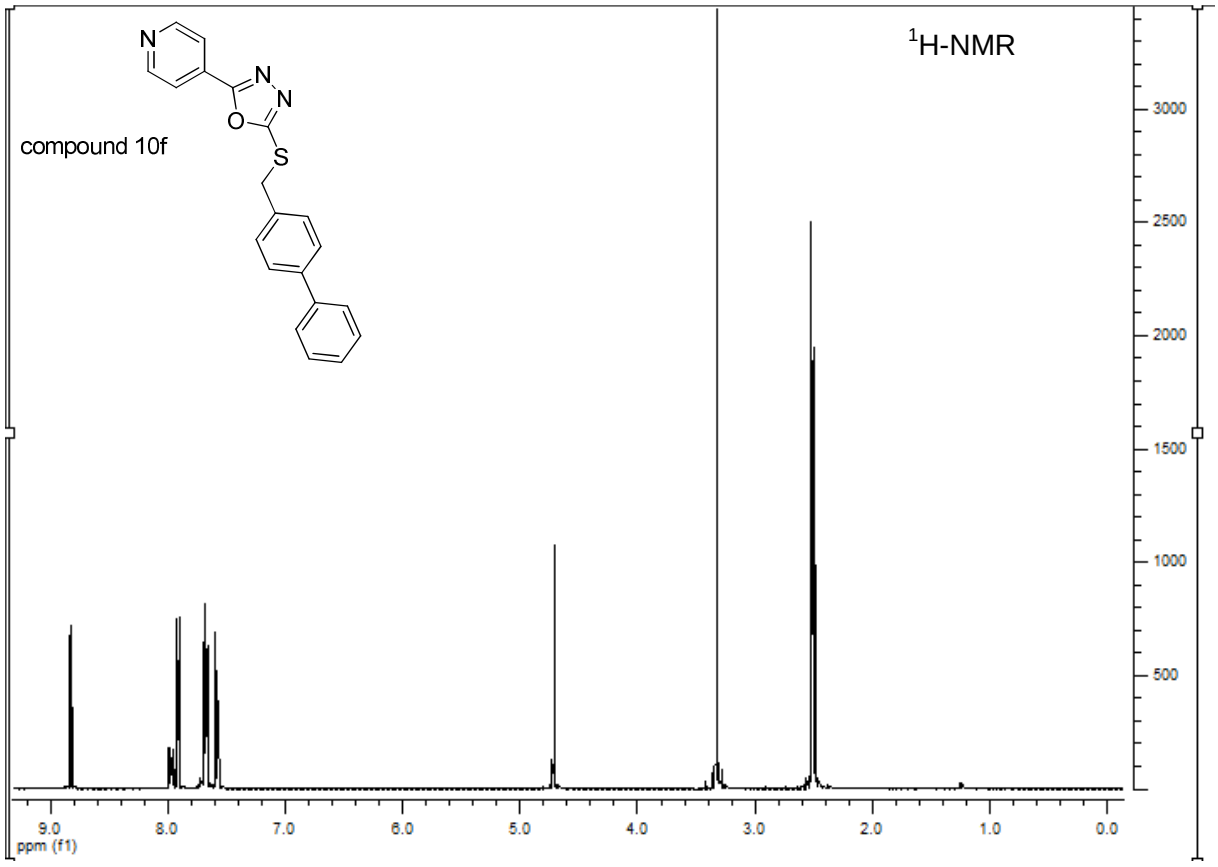
compound 10f
^{1}H-NMR
3000
2500
2000
1500
1000
500
9.0
8.0
7.0
6.0
5.0
4.0
3.0
2.0
1.0
0.0
ppm (f1)

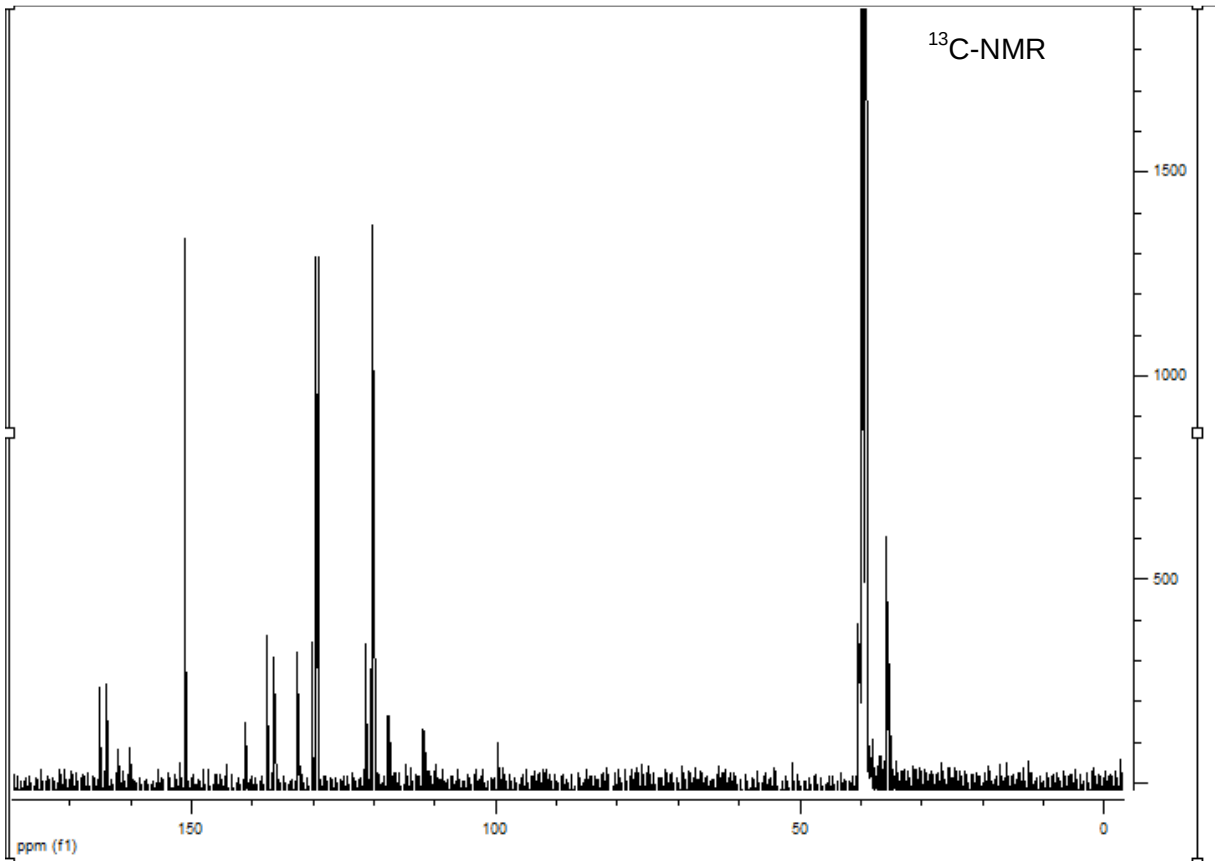
^{13}C-NMR
1500
1000
500
150
100
50
0
ppm (f1)

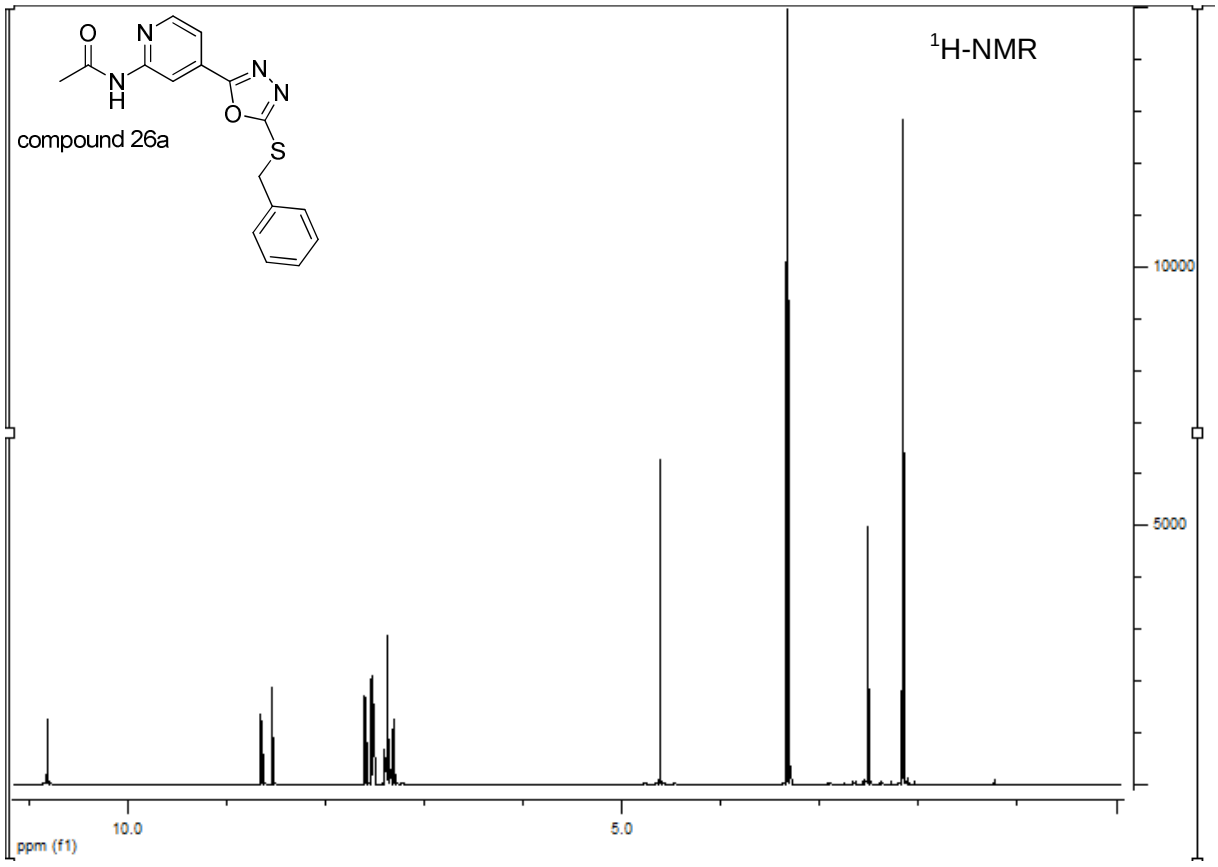
compound 26a
^{1}H-NMR
10000
5000
10.0
5.0
ppm (f1)

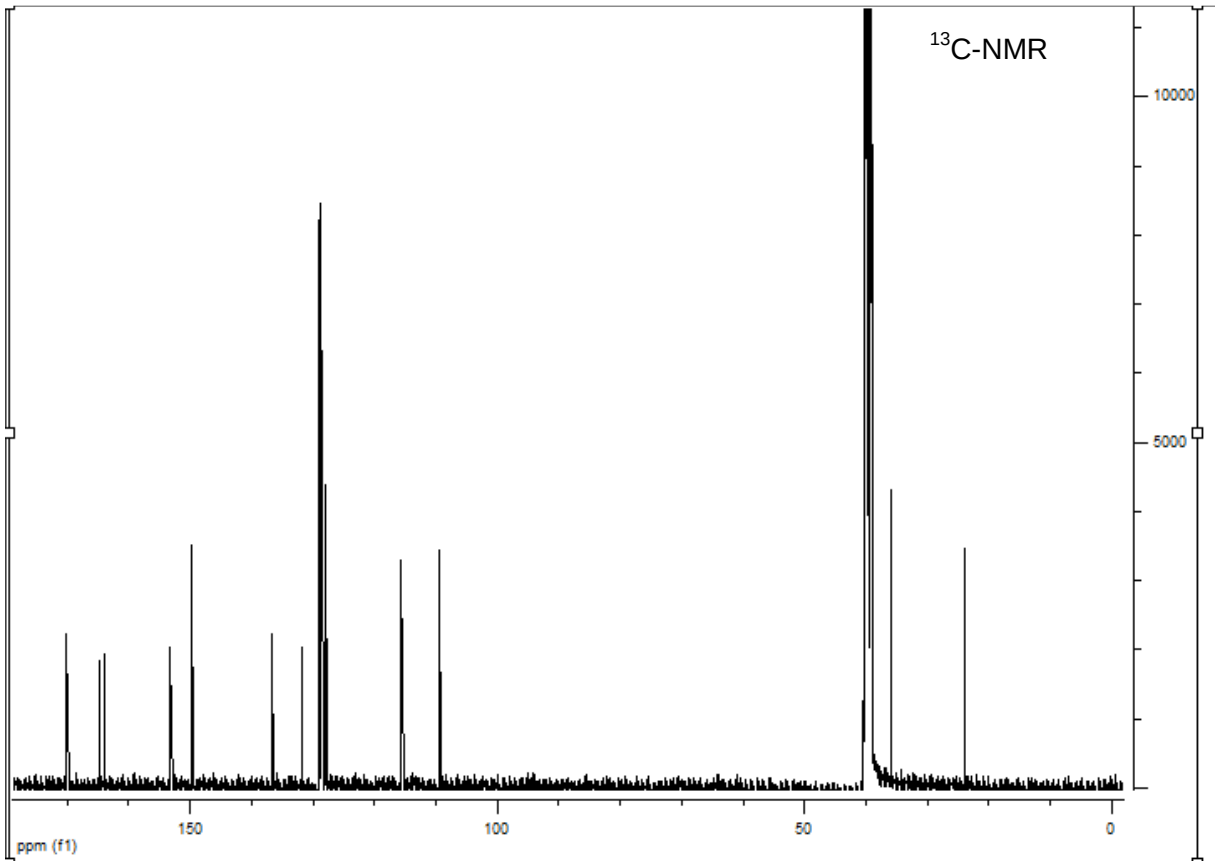
^{13}C-NMR
10000
5000
150
100
50
0
ppm (f1)

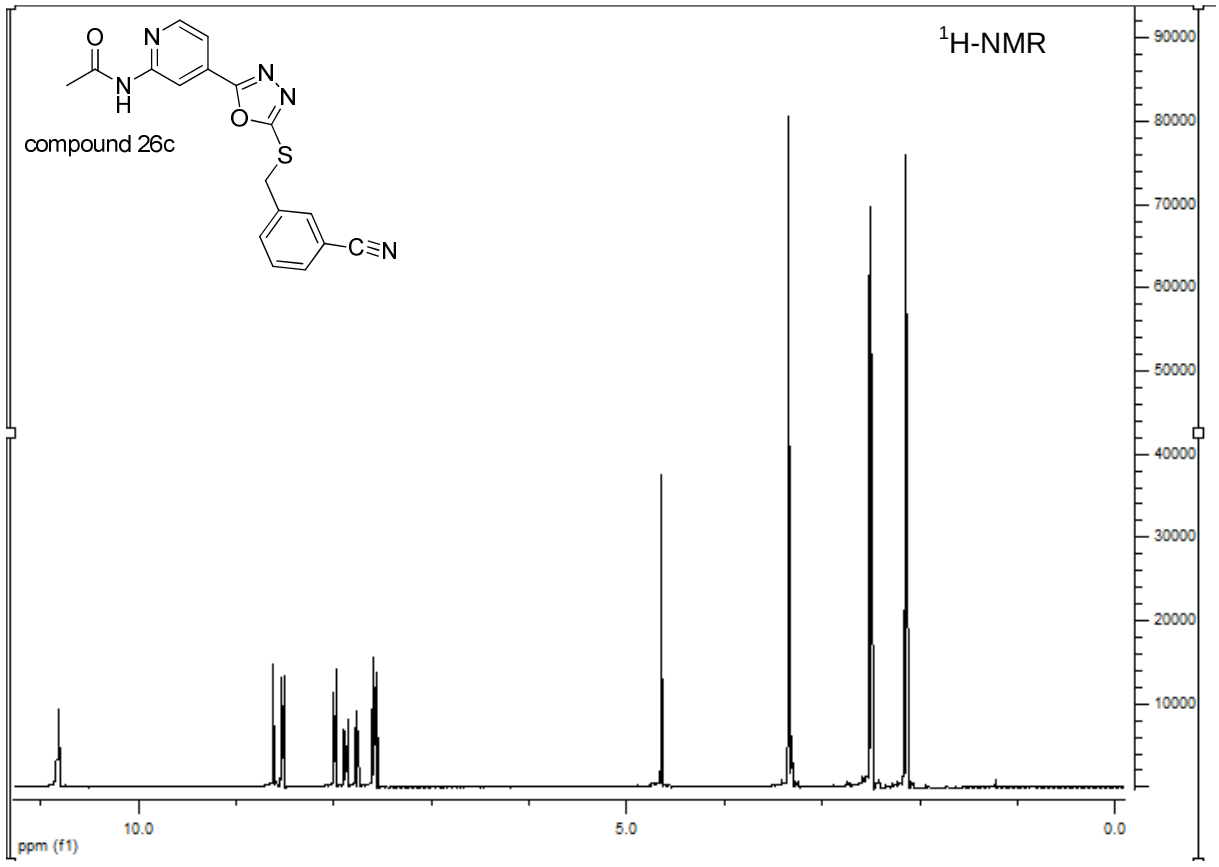

^{13}C-NMR

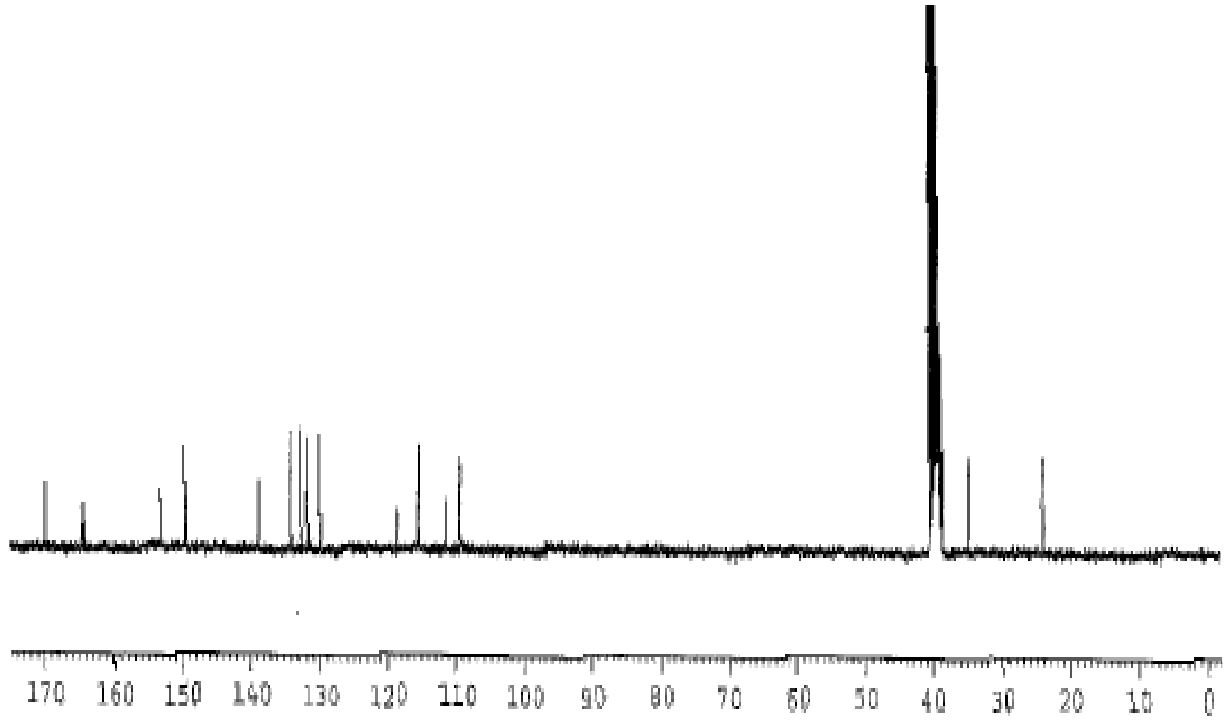

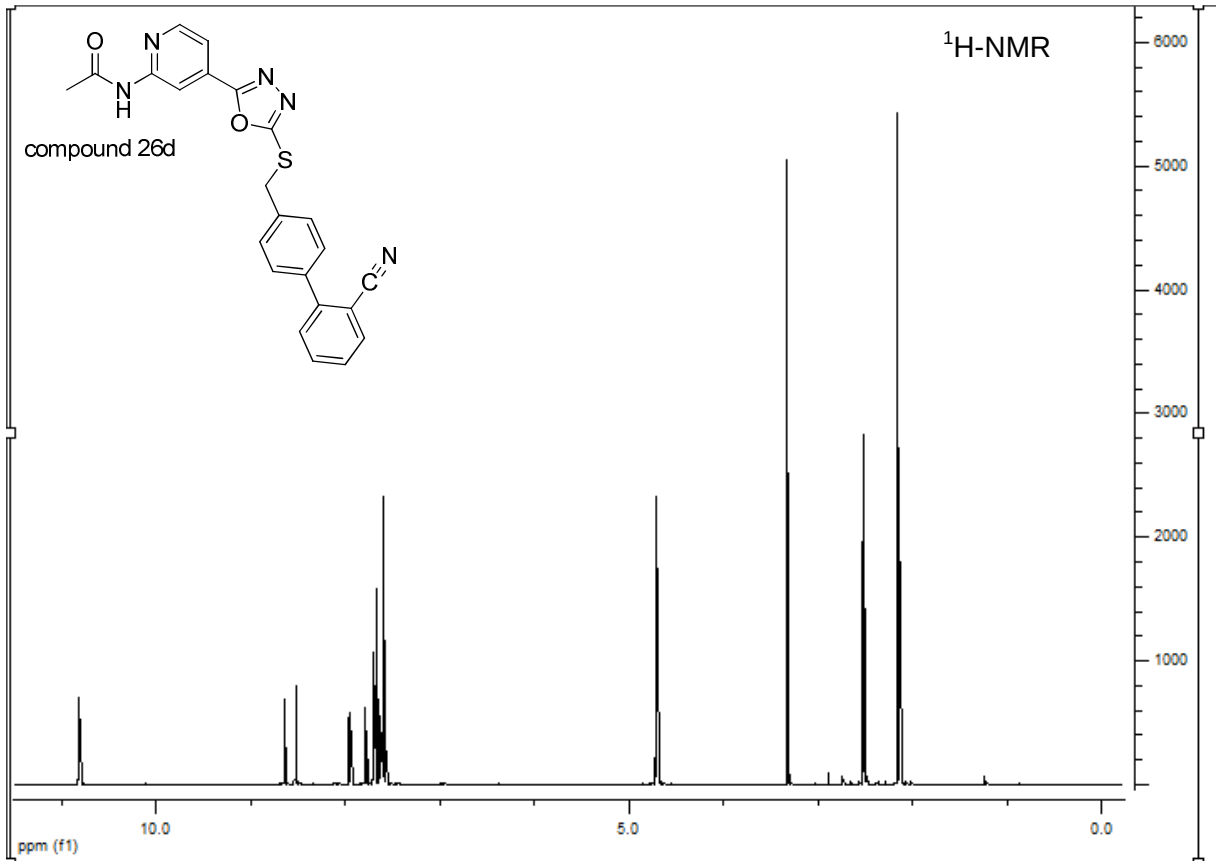
compound 26d
^{1}H-NMR
6000
5000
4000
3000
2000
1000
10.0
5.0
0.0
ppm (f1)

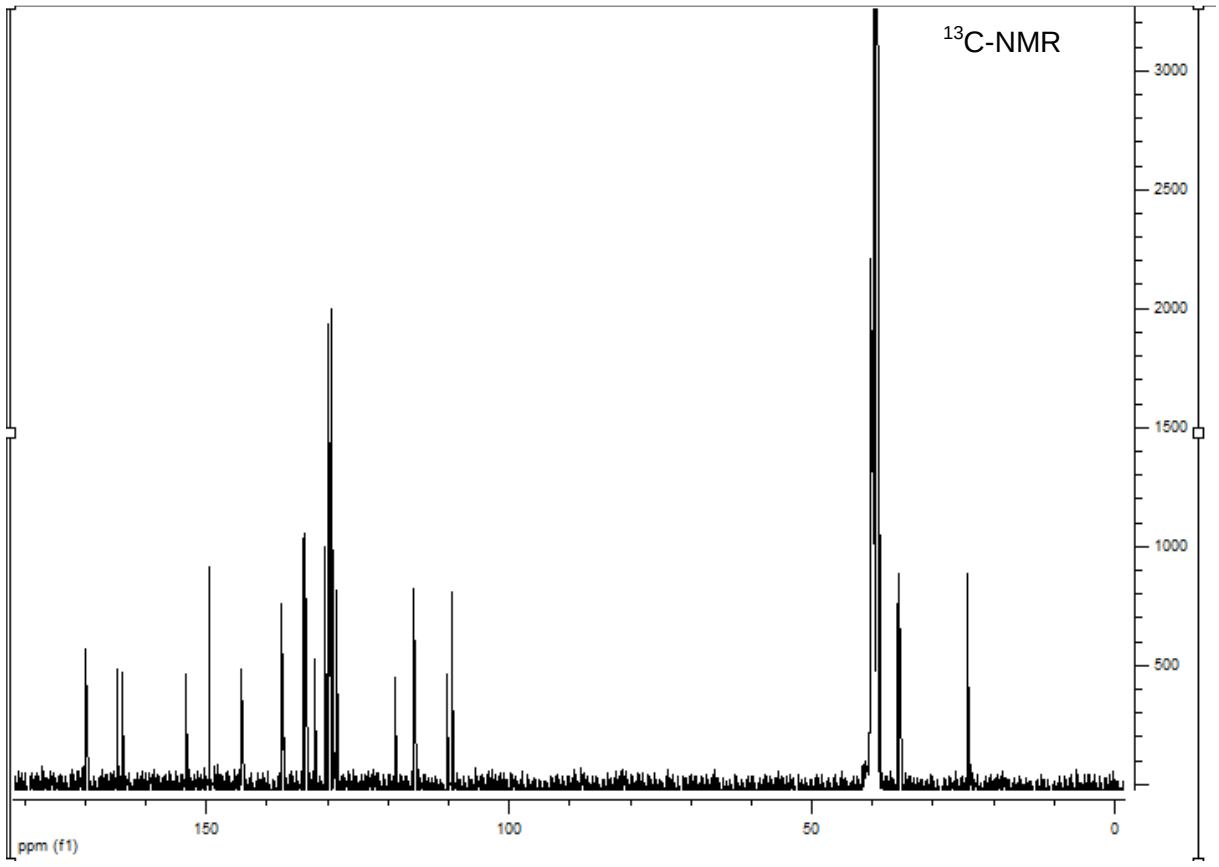
^{13}C-NMR
3000
2500
2000
1500
1000
500
150
100
50
0
ppm (f1)

4.1.5 Oxadiazolderivate und deren Verwendung als GSK-3-Inhibitoren

Der Inhalt dieses Kapitels enthält Auszüge aus der Patentanmeldung:

Boris Schmidt, Fabio Lo Monte, Thomas Kramer, Hagit Eldar-Finkelman, Fred Van Leuven
Verbindungen als Glykogen Synthase Kinase 3 (GSK-3) Inhibitoren für die Behandlung von GSK-3-vermittelten Erkrankungen *Deutsche Patentanmeldung* **2011**, Nr. 10 2011 106 990.2.

Die Untersuchungen zum Oxadiazol-Grundgerüst führten zur Synthese potenter und selektiver GSK-3-Inhibitoren. Die aktivsten Verbindungen haben ein biphenylisches System und zeigten ihre *in vivo* Effektivität bereits im Zebrafisch-Embryo. Viele der Biphenylderivate inhibieren beide Isoformen von GSK-3 bereits im nanomolaren Bereich (Abb. 20). Darüber hinaus konnten durch eine Variation der Substituenten am biphenylischen System selektive GSK-3α-Inhibitoren synthetisiert werden.

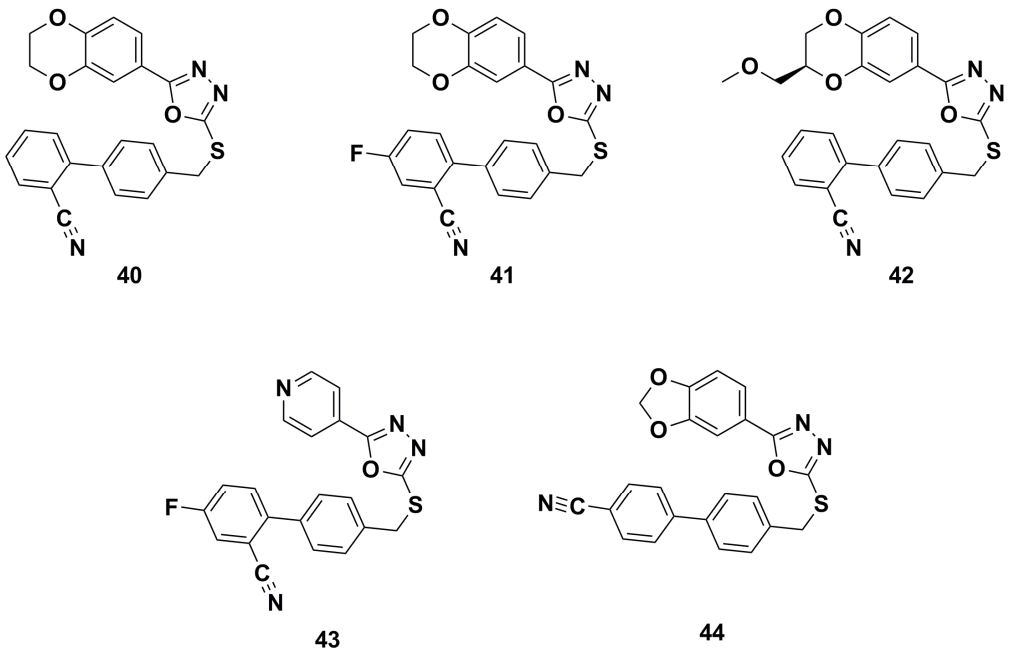

Abb. 20: Beispiele einiger zur Patentanmeldung eingereichten GSK-3-Inhibitoren.

Durch diese α-Selektivität eröffnen sich neue Möglichkeiten für *in vivo* Untersuchungen dieser Isoform. Ferner konnte belegt werden, dass die Diskriminierung einer GSK-3-Isoform möglich ist. Diese Tatsache lässt vermuten, dass auch die Synthese selektiver GSK-3β-Inhibitoren durchführbar ist.
Neben der Verwendung dieser GSK-3-Inhibitoren im Bereich der Alzheimer-Demenz wurden auch andere GSK-3-vermittelte Erkrankungen in die Patentanmeldung mit aufgenommen.

Die im Rahmen dieser Arbeit von Fabio Lo Monte synthetisierten Verbindungen:

BSc4260, BSc4261, BSc4262, BSc4263, BSc4293, BSc4306, BSc4392, BSc4393, BSc4394, BSc4395, BSc4396, BSc4397, BSc4398, BSc4399, BSc4401, BSc4402, BSc4403, BSc4404, BSc4405, BSc4406, BSc4407, BSc4408, BSc4409, BSc4410, BSc4411, BSc4412, BSc4413, BSc4414, BSc4415, BSc4416, BSc4603, BSc4604, BSc4605, BSc4606, BSc4607, BSc4608, BSc4609, BSc4610, BSc4611, BSc4612, BSc4613, BSc4614, BSc4615, BSc4616, BSc4617, BSc4618, BSc4619, BSc4620, BSc4621, BSc4622, BSc4623, BSc4624, BSc4625, BSc4626, BSc4634, BSc4670, BSc4672, BSc4674, BSc4676, BSc4678, BSc4680, BSc4681, BSc4682, BSc4683, BSc4684, BSc4686, BSc4687, BSc4688, BSc4689, BSc4734, BSc4788, BSc4789 BSc4790, BSc4791, BSc4792, BSc4793, BSc4794

Verbindungen als Glykogen Synthase Kinase 3 (GSK-3) Inhibitoren für die Behandlung von GSK-3-vermittelten Erkrankungen

1. Beschreibung

Die vorliegende Erfindung betrifft Verbindungen, die als selektive Liganden der Glykogen Synthase Kinase 3 (GSK-3) wirken und für die Behandlung von GSK-3-vermittelten Erkrankungen verwendet werden können. Die erfindungsgemäßen Verbindungen wirken als Inhibitoren der Glykogen Synthase Kinase 3 (GSK-3).

GSK-3 ist eine hoch konservierte Familie von Serin/Threoninproteinkinasen. Beim Menschen kodieren zwei Gene zwei unterschiedliche, aber eng miteinander verbundenen GSK-3 Formen, die so genannte GSK-3α und GSK-3β. Sie zeigen insgesamt 84% Identität und 98% Identität innerhalb ihrer katalytischen Domäne, der Hauptunterschied zwischen den beiden Proteinkinasen besteht in einem Glycin-reichen Abschnitt in der N-terminalen Domäne von GSK-3α. Dennoch hat sich in embryonal letalen Phänotypen der GSK-3β gezeigt, dass beide Formen der GSK-3 nicht funktionell austauschbar sind.

GSK-3 spielt eine wichtige Funktion im Wnt-Signalweg. Durch die Stimulation des Wnt-Signalweges wird GSK-3 inaktiviert, wodurch sich β-Catenin im Zellkern ansammelt, um dort mit TCF / LEF einen Transkriptionsfaktor zu formen, der eine Vielzahl von Genen reguliert. GSK-3 phosphoryliert unter anderem den Zellzyklusregulator β-Catenin, Cyclin D1, Cyclin E, p21CIP1 und c-Myc, wodurch diese Ubiquitin-abhängig abgebaut werden. In Abwesenheit von Insulin phosphoryliert aktive GSK-3 die Glykogen-Synthase und eIF2B, wodurch diese inaktiviert werden. Die Bindung von Insulin an seinen Plasmamembran Rezeptor führt zur Aktivierung von PKB / Akt, was wiederum zur Phosphorylierung und Inaktivierung von GSK-3 führt. Folglich sind dadurch die Glykogen-Synthase und eIF2B aktiviert, wodurch die Glykogen und Protein-Synthese stimuliert werden. GSK-3 hat weiterhin pro-apoptotische Funktion in neuronalen Zellen. Im Gegensatz dazu ist GSK-3 auch für das Überleben von Zellen beschrieben worden. In GSK-3β-Knockout-Mäusen führte die TNFα-induzierte Apoptose von Hepatozyten zu einem

frühen Tod während der Embryonalentwicklung der Mäuse. Zudem wird der GSK-3 und CK1 eine Funktion bei der Regelung der zirkadianen Uhr bei Drosophila und in Säugetieren nachgesagt. Schließlich spielt sowohl die GSK-3 Aktivität/Inaktivität als auch die räumliche Verteilung eine wesentliche Rolle während der Entwicklung, insbesondere im Rahmen der Polaritätsbestimmung.

Kaum ein anderes Enzym besitzt einen so großen Einfluss auf eine Vielzahl zellulärer Vorgänge wie GSK-3. Unter anderem wurde ein Einfluss von GSK-3 auf folgende physiologischen Funktionen beschrieben: den Wnt und Hedgehog Signalweg, in der Transkription, der Regulation des Zellteilungszyklus, der Antwort auf DNA-Schäden, der Regulation des Zelltods und dem Überleben der Zelle, kardiovaskuläre und neuronale Funktionen, dem Insulin-Transduktionsweg, der Differenzierung, Regulation des zirkadianen Rhythmus und der Entwicklung/Erhaltung von Stammzellen. Bis heute wurden rund 40 Substrate identifiziert, die von GSK-3 phosphoryliert werden.

Fünf Studien haben die Suche nach pharmakologischen Inhibitoren der GSK-3 besonders angeregt: Erstens, die Stimmungsstabilisierenden Eigenschaften von Lithium, dem ersten GSK-3-Inhibitor überhaupt. Zweitens die Insulin-mimetischen Eigenschaften von GSK-3-Inhibitoren. Drittens die Wechselwirkung von GSK-3 mit Presenilin-1, die GSK-3-abhängigen Amyloid-β Produktion und abnorme tau-Phosphorylierung in der Alzheimer-Krankheit. Viertens, die Beteiligung der GSK-3 im neuronalen Zelltod und der Neuroprotektion durch GSK-3-Inhibitoren und fünftens die Aufrechterhaltung der Pluripotenz von embryonalen Stammzellen in der Abwesenheit von Feeder-Zellen durch GSK-3-Inhibitoren. Über 30 GSK-3-Inhibitoren wurden bisher identifiziert. An der Identifizierung neuer GSK-3-Inhibitoren besteht daher nach wie vor ein fortlaufend großes Interesse.

Zu den Krankheiten, die mit GSK-3 Inhibitoren behandelt werden können, gehören insbesondere die Alzheimer-Krankheit und andere Tauopathien, Asthma, bipolare affektive Störungen, Depression, Nervenzelltod und Schlaganfall, Parkinson, Huntington, Skelettmuskelatrophie, Kardioprotektion, Haarverlust, verringerte Spermienmotilität, Diabetes und damit in Zusammenhang stehende Folgeerkrankungen, z.B. Syndrom X und Adipositas, Erkrankungen, die durch

einzellige Parasiten verursacht werden, transmissible spongiforme Enzephalopathie, Schizophrenie, Krankheiten des zirkadianen Rhythmus und Krebs.

Im Stand der Technik sind bereits einige GSK-3 Inhibitoren und ihr therapeutisches Potential beschrieben worden. In einem Review von Cohen and Goedert, *Nat. Rev. Drug. Discov.*, 2004, 3: 480-87, wurden einige potentielle GSK-3 Inhibitoren, wie z.B. SB 216763, SB 415286, CHIR 98014, CHIR 99021, AR A014418, 1-Azakenpaullone und Bis-7-indolylmaleimide für eine Vielzahl von therapeutischen Anwendungen beschrieben.

Im Stand der Technik sind (R)-Roscovitin, Aloisin A, Indirubin-3´-oxim, Pyrazolpyridin, Aminothiazol, Alsterpaullon und 1-Aza-9-oxafluoren als GSK-3 Inhibitoren identifiziert worden.

Obwohl bereits einige GSK-3 Inhibitoren im Stand der Technik bekannt sind, spielt die GSK-3 bei klassischen Krankheiten wie Alzheimer und Krebs eine so entscheidende Rolle, dass weiterhin und auch zukünftig ein großes Interesse daran besteht, weitere GSK-3 Inhibitoren zu identifizieren.

Aufgabe der vorliegenden Erfindung ist es daher, weitere Verbindungen bereitzustellen, die in der Lage sind, die GSK-3 zu inhibieren.

Diese Aufgabe wird erfindungsgemäß durch die technische Lehre der unabhängigen Ansprüche gelöst. Weitere vorteilhafte Ausgestaltungen der Erfindung ergeben sich aus den abhängigen Ansprüchen, der Beschreibung, den Figuren sowie den Beispielen.

Überraschend wurde gefunden, dass die Verbindungen gemäß allgemeiner Formel (I) Inhibitoren der Glykogen Synthase Kinase 3 (GSK-3) sind und damit auch für die Prophylaxe und Behandlung von GSK-3-vermittelten Erkrankungen geeignet sind.

Somit betrifft die vorliegende Erfindung Verbindungen der allgemeinen Formel (I)

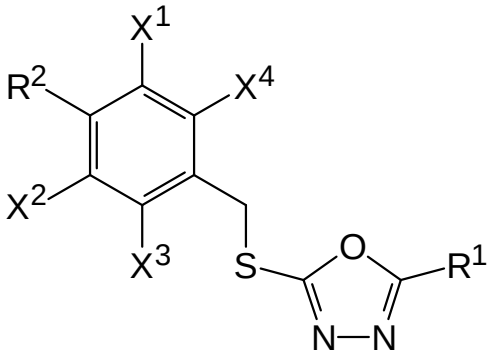

worin

R^1 für einen der folgenden Reste steht:

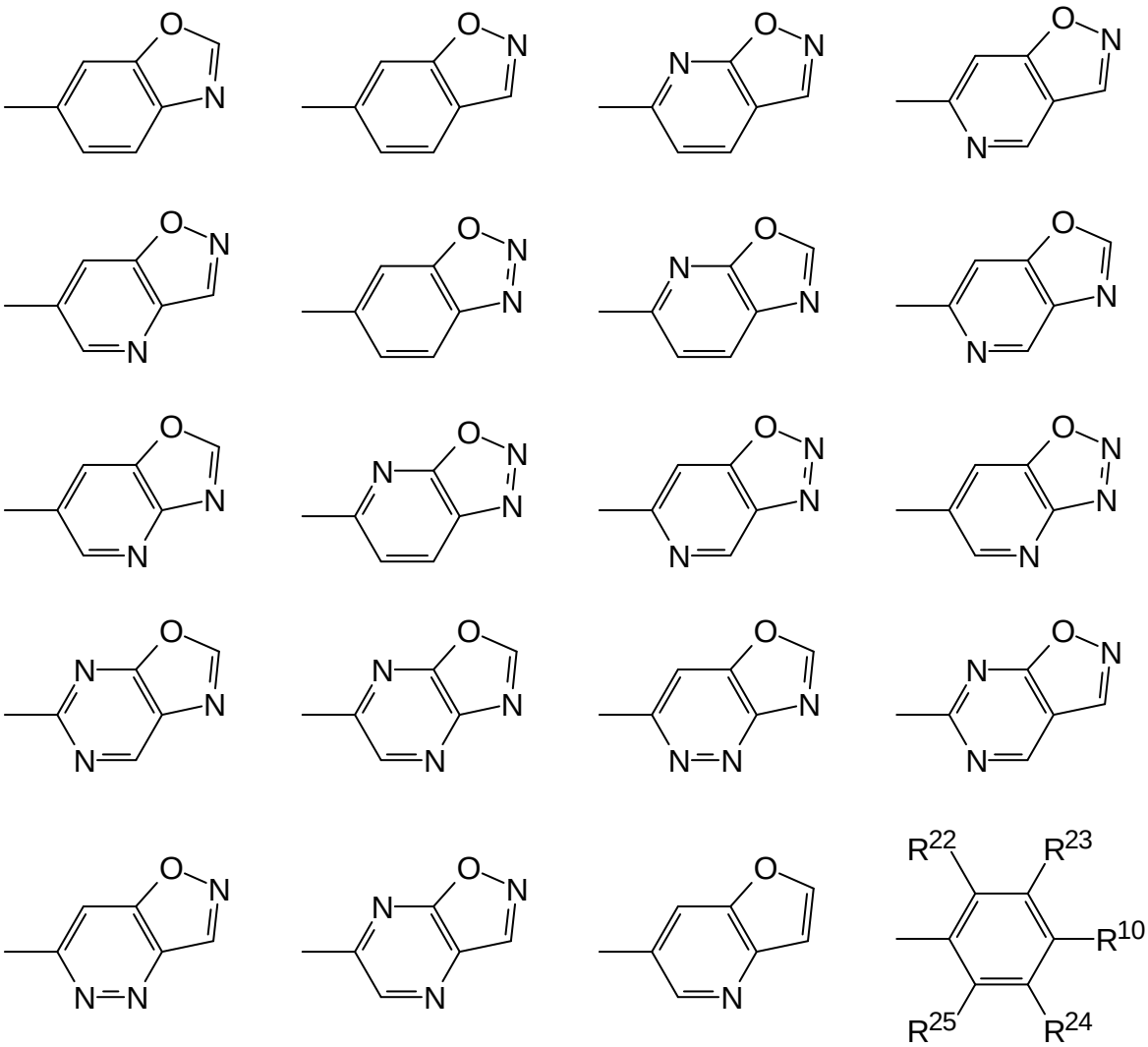

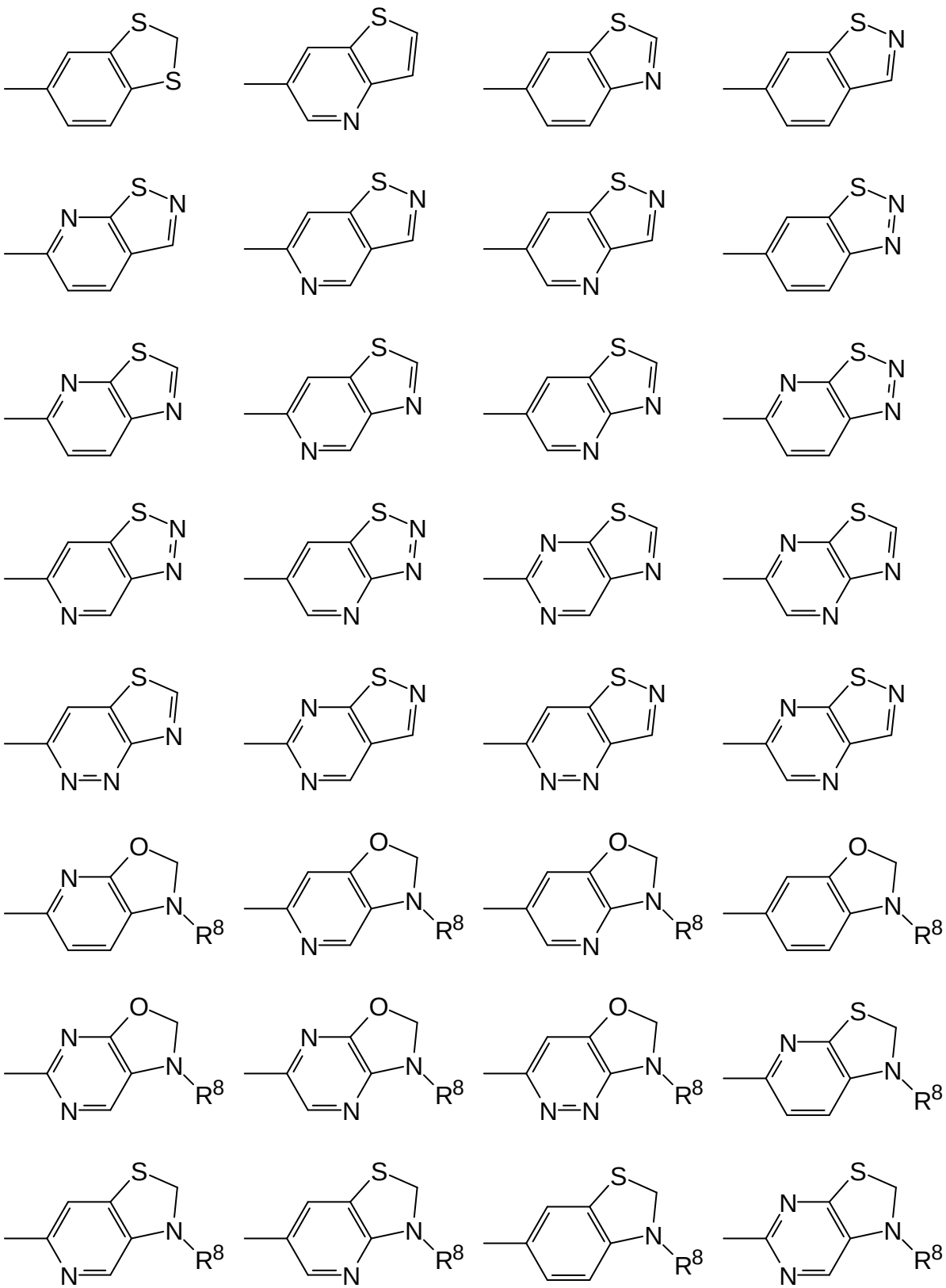

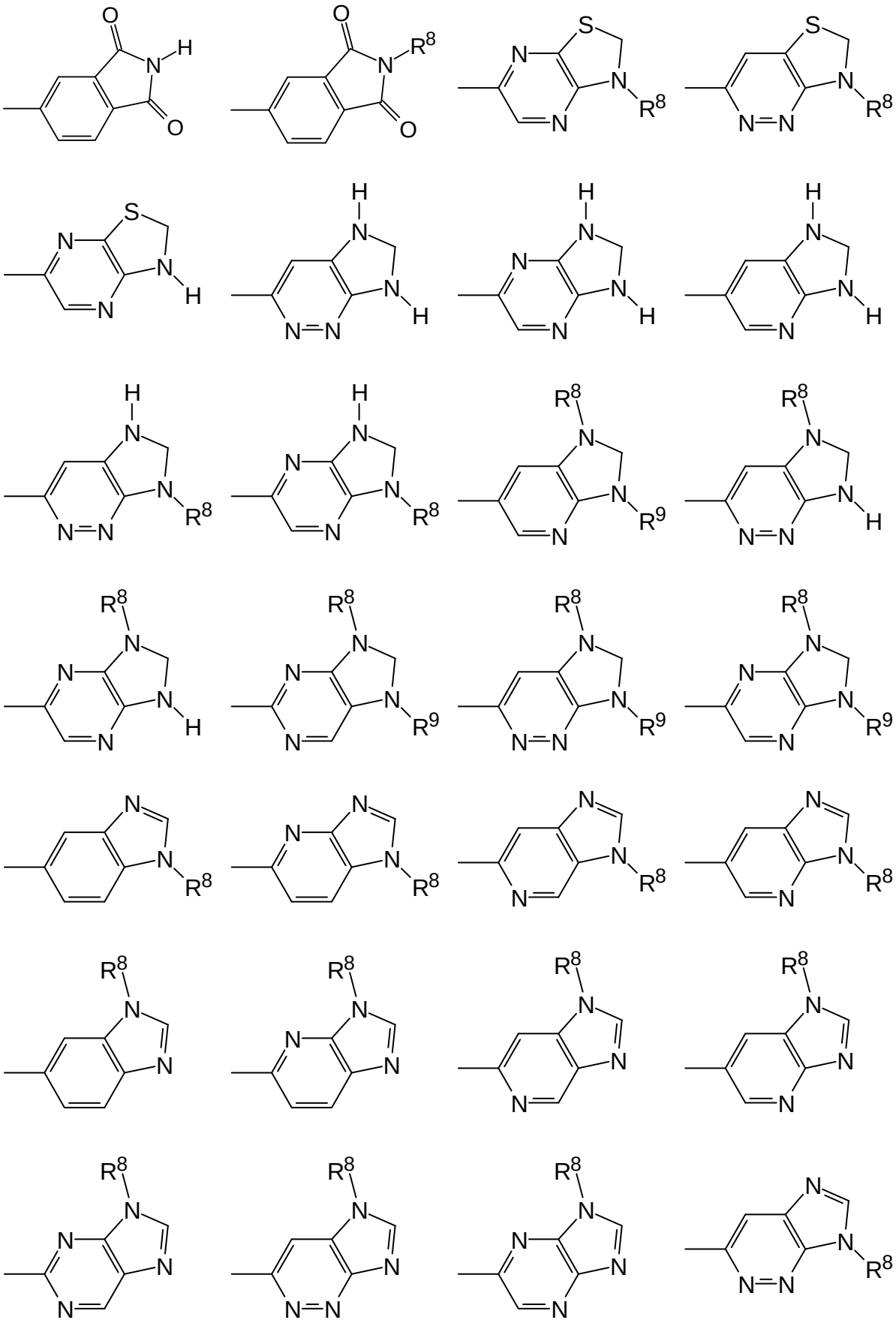

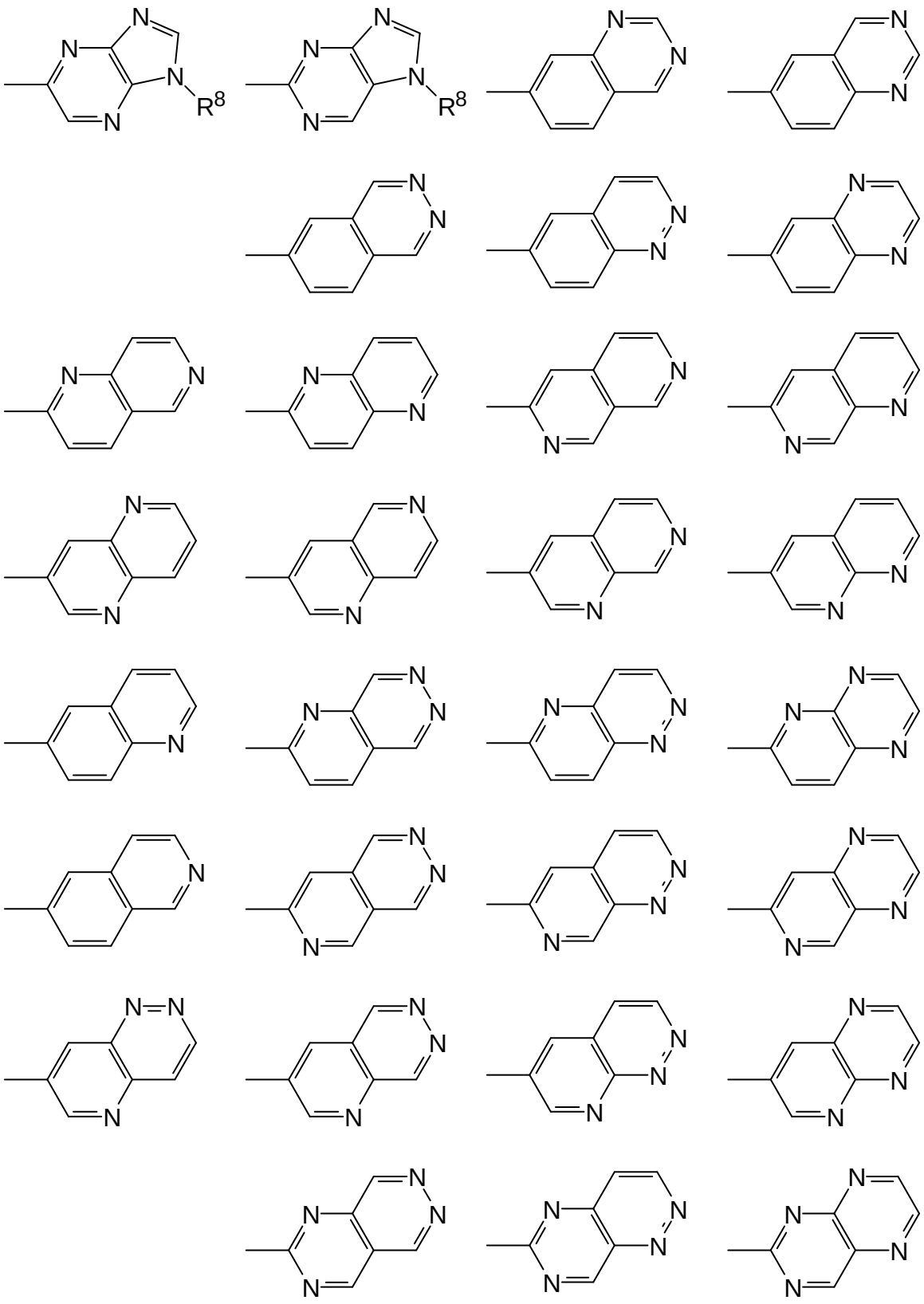

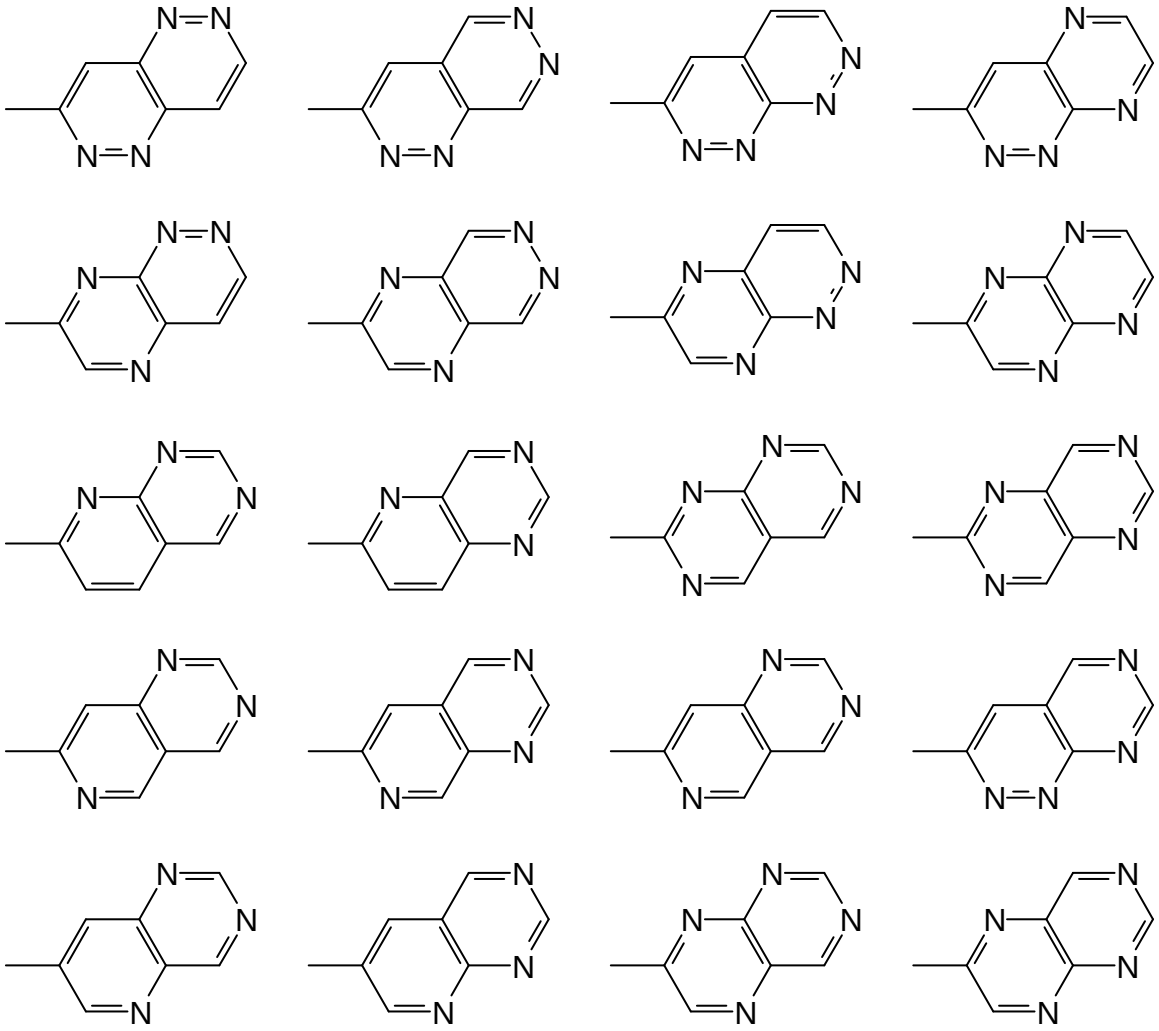

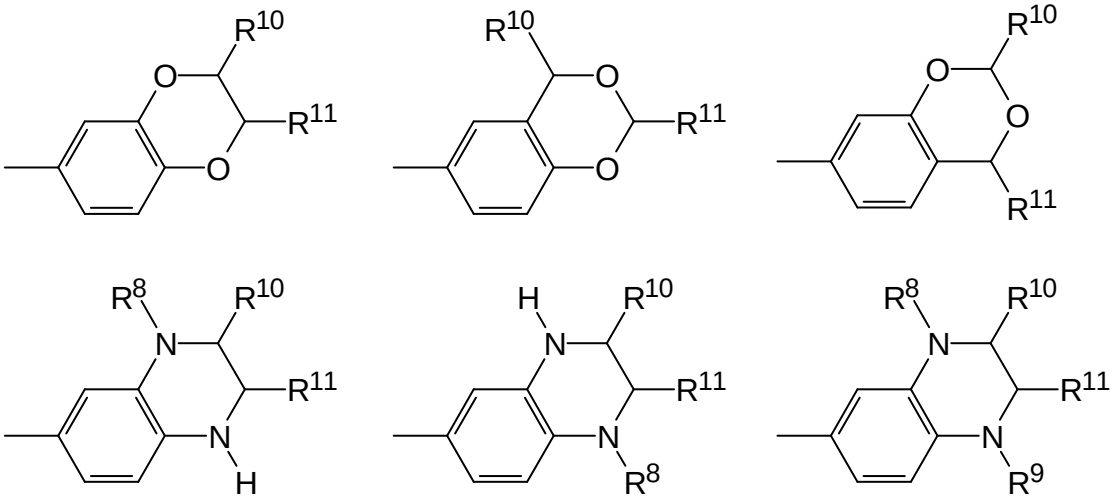

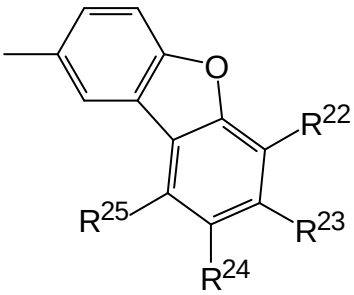
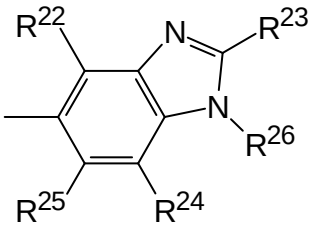
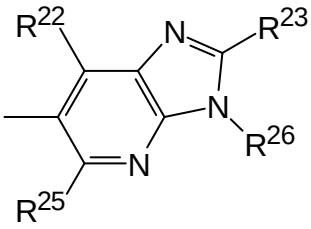
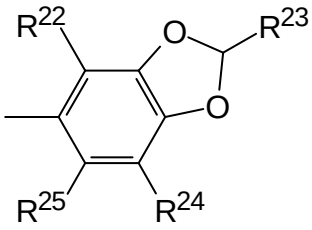
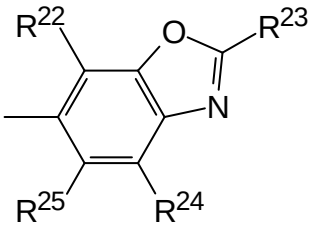
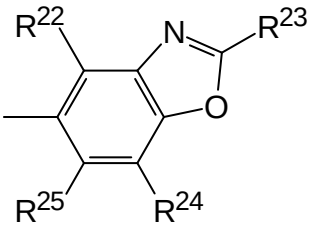
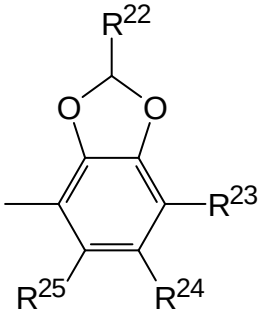
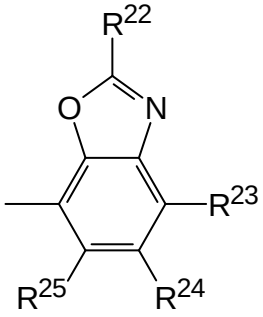
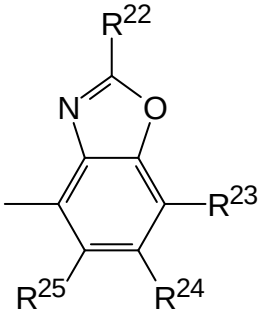
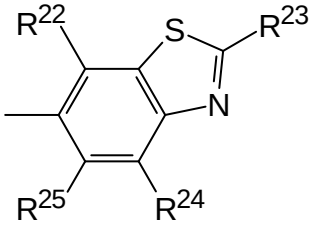
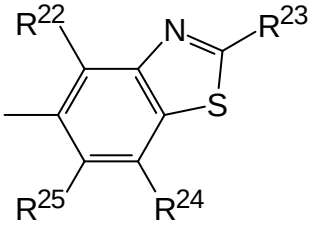
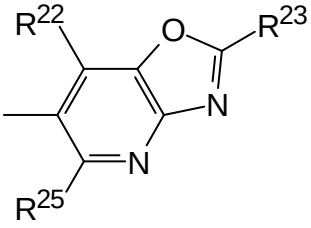
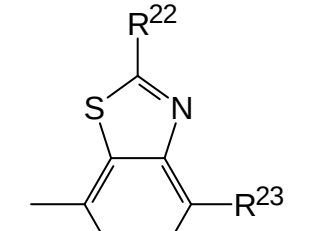
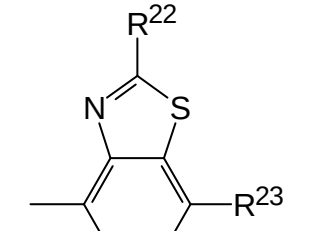
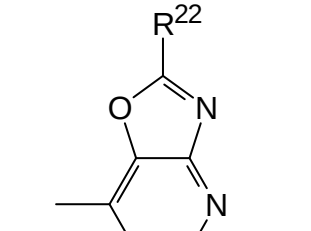

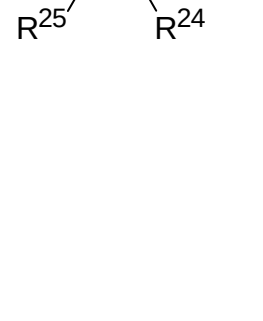


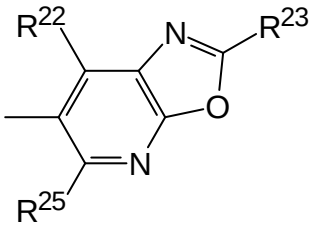
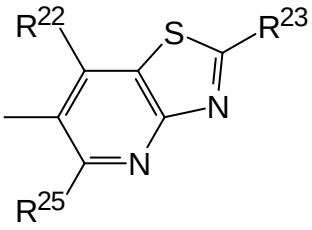
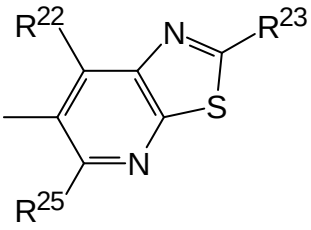
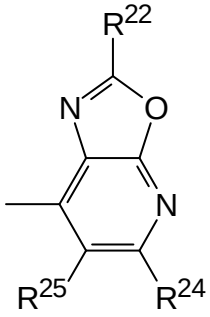
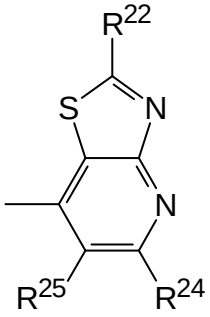
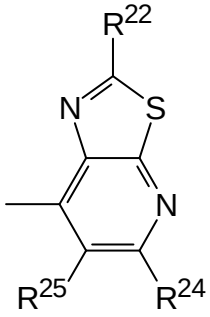
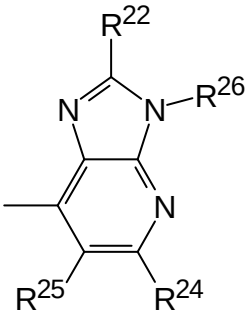
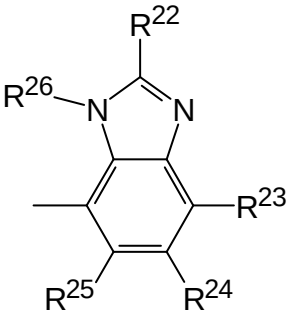
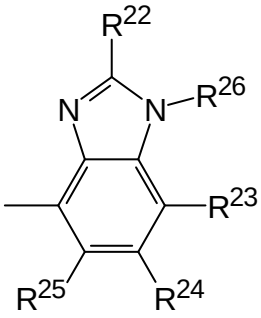
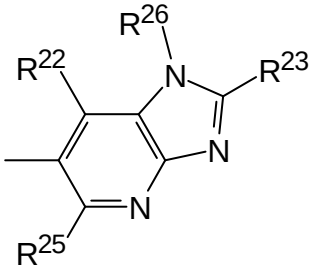
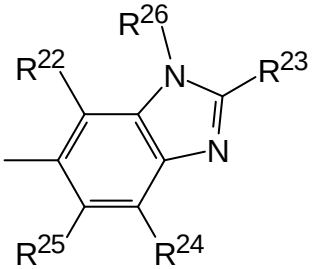
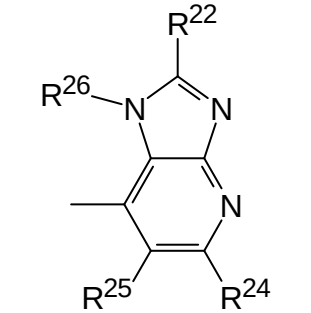
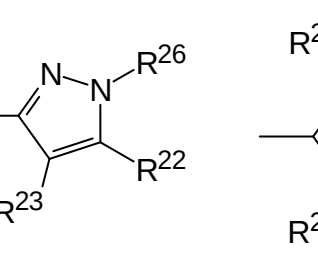
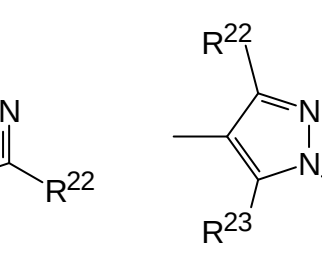

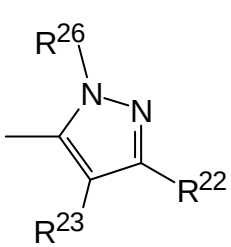

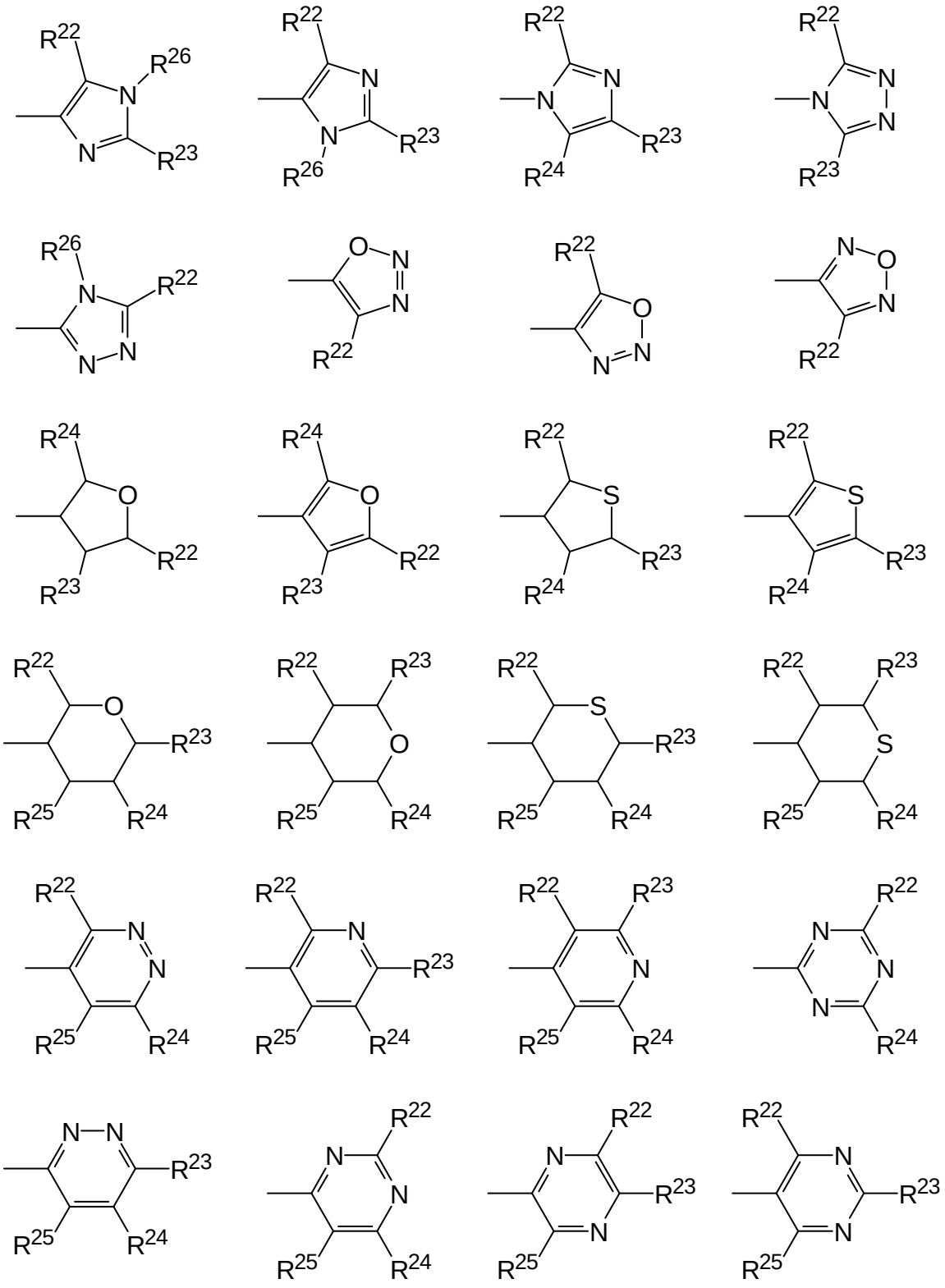

R^2 für einen der folgenden Reste steht $-X^{15}$,

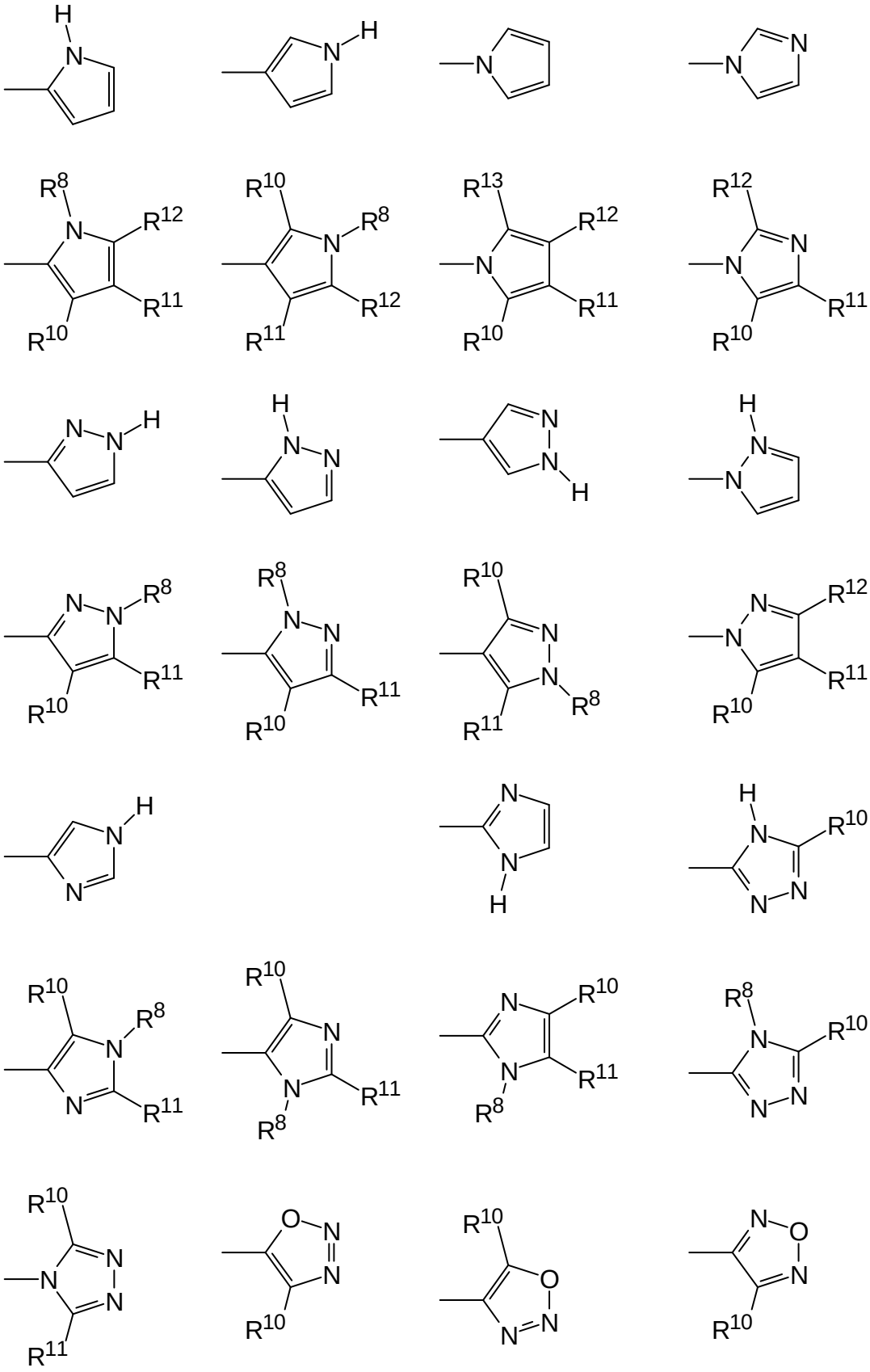

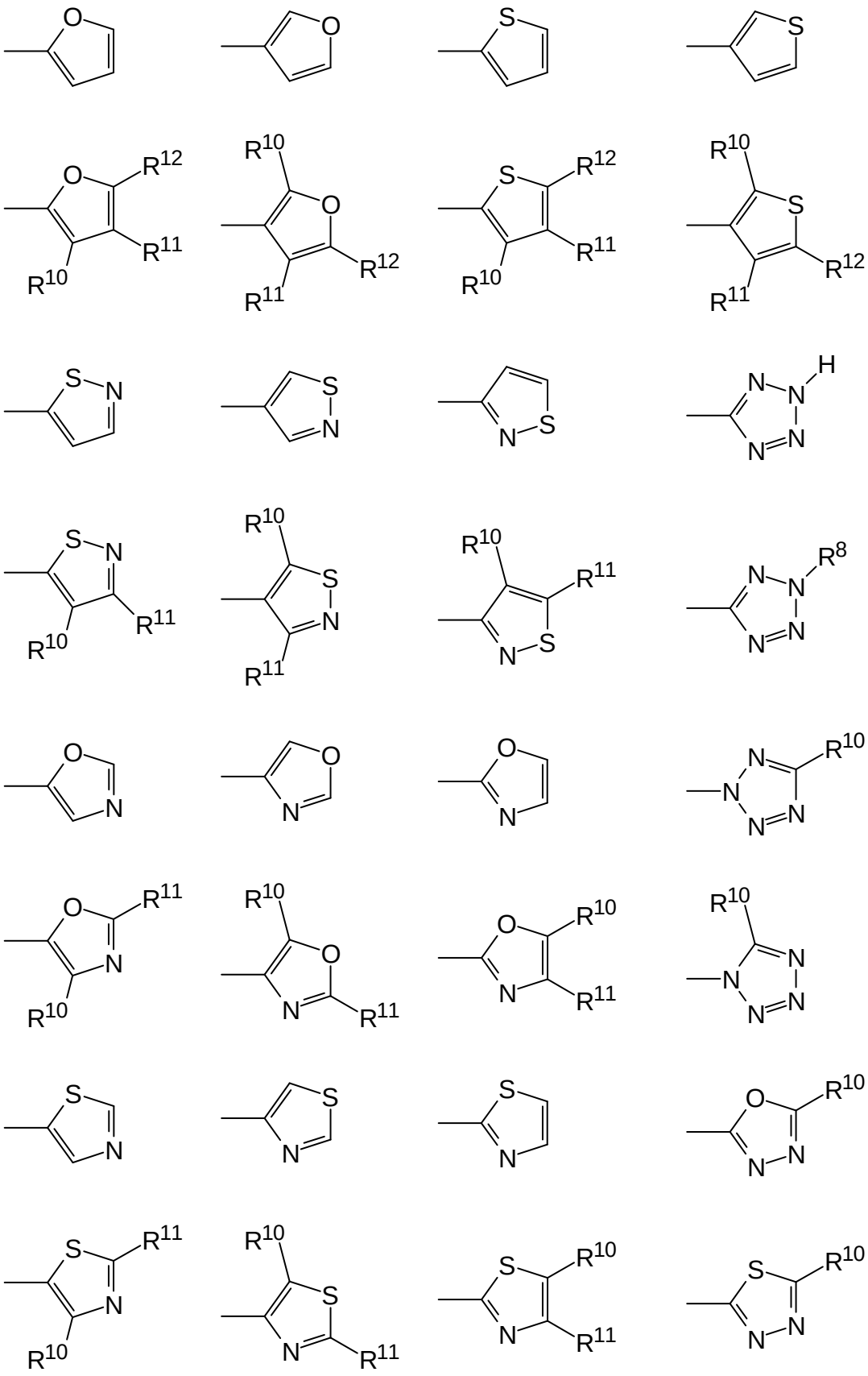

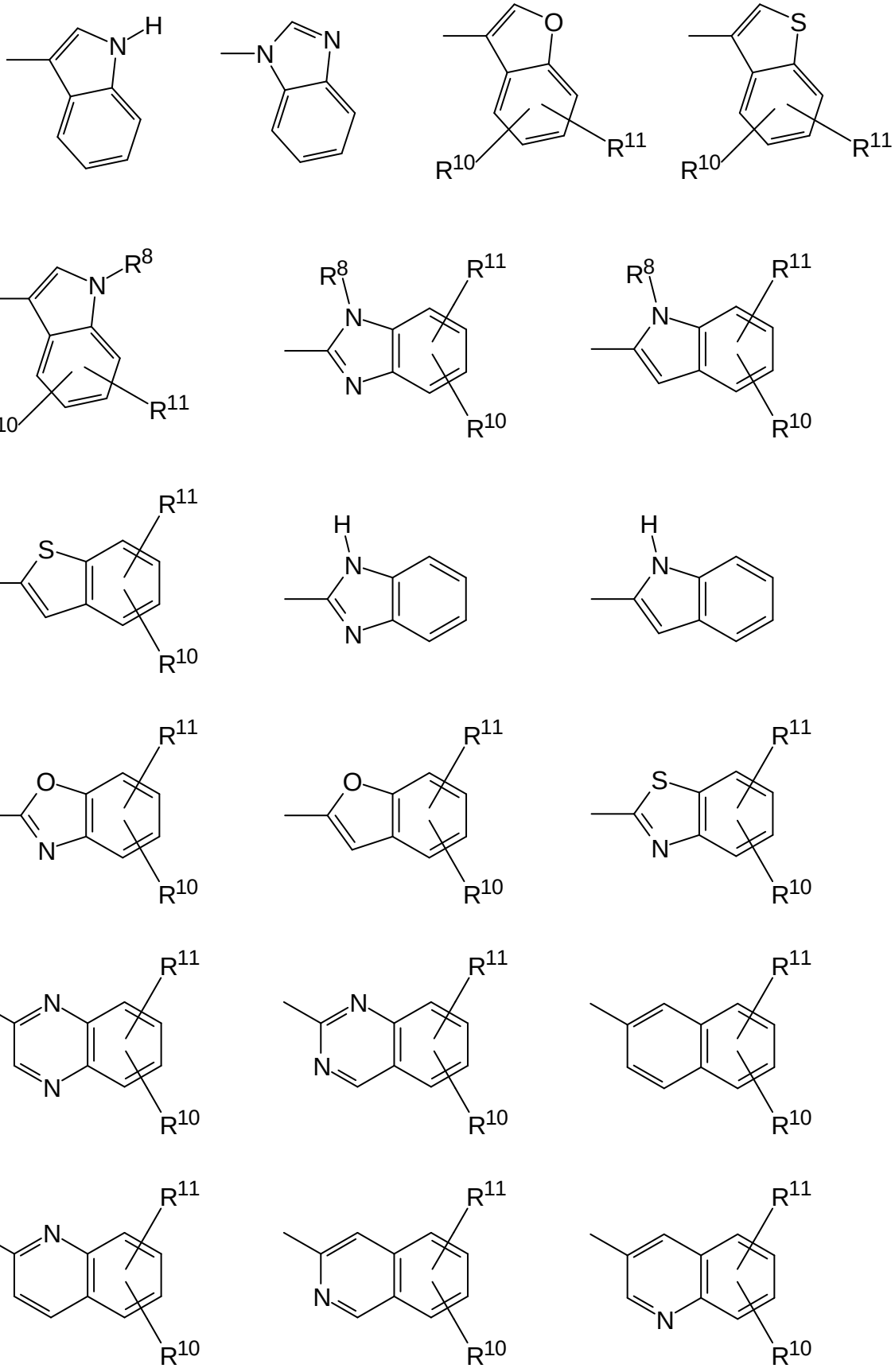
H
N
N
N
O
R10
R11
S
R10
R11
R8
N
R10
R11
R8
N
N
R11
R10
R8
N
R11
R10
S
R10
R11
H
N
N
H
N
O
N
R10
R11
O
R10
R11
S
N
R10
R11
N
N
R10
R11
N
N
R10
R11
N
R10
R11
N
R10
R11
N
R10
R11

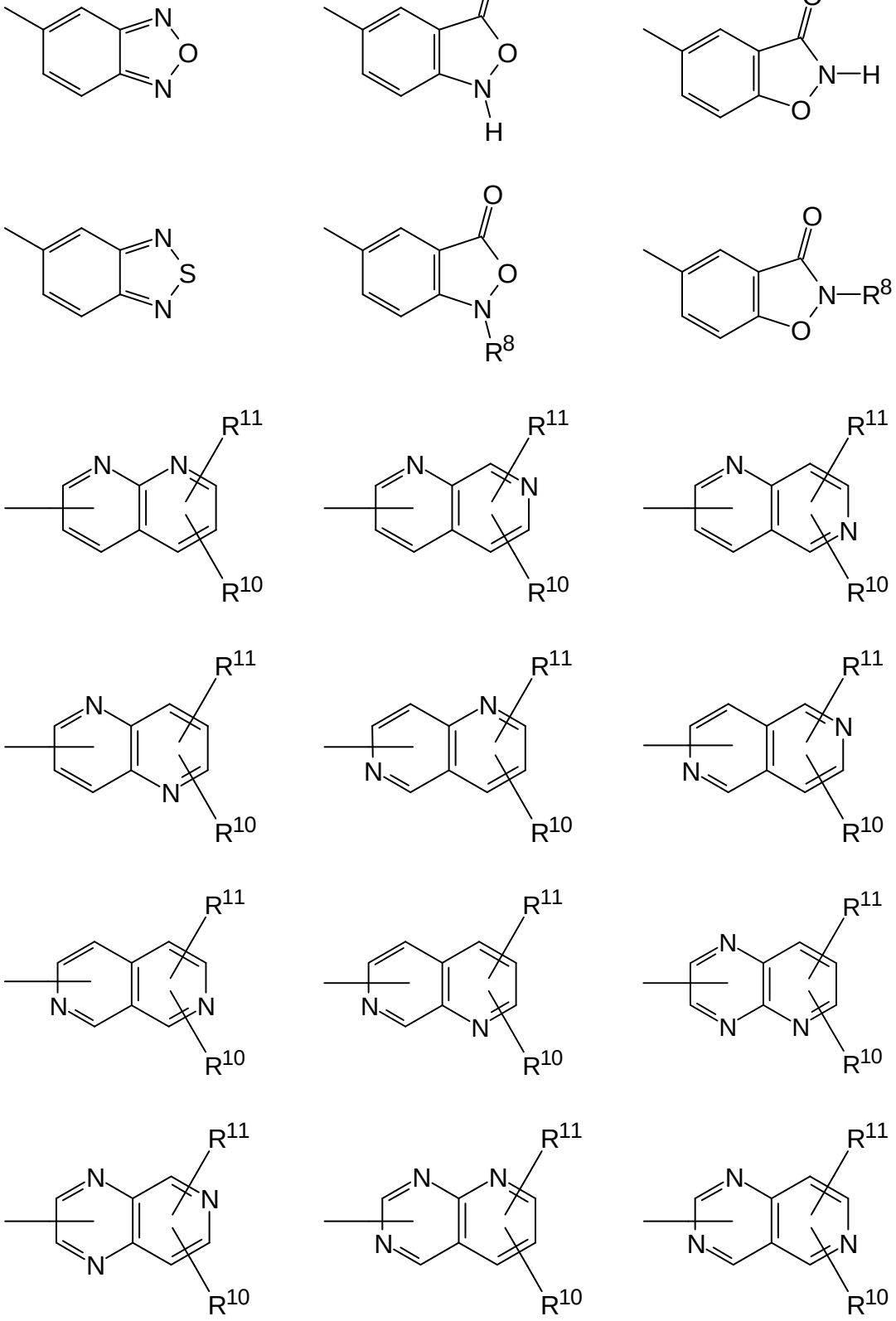

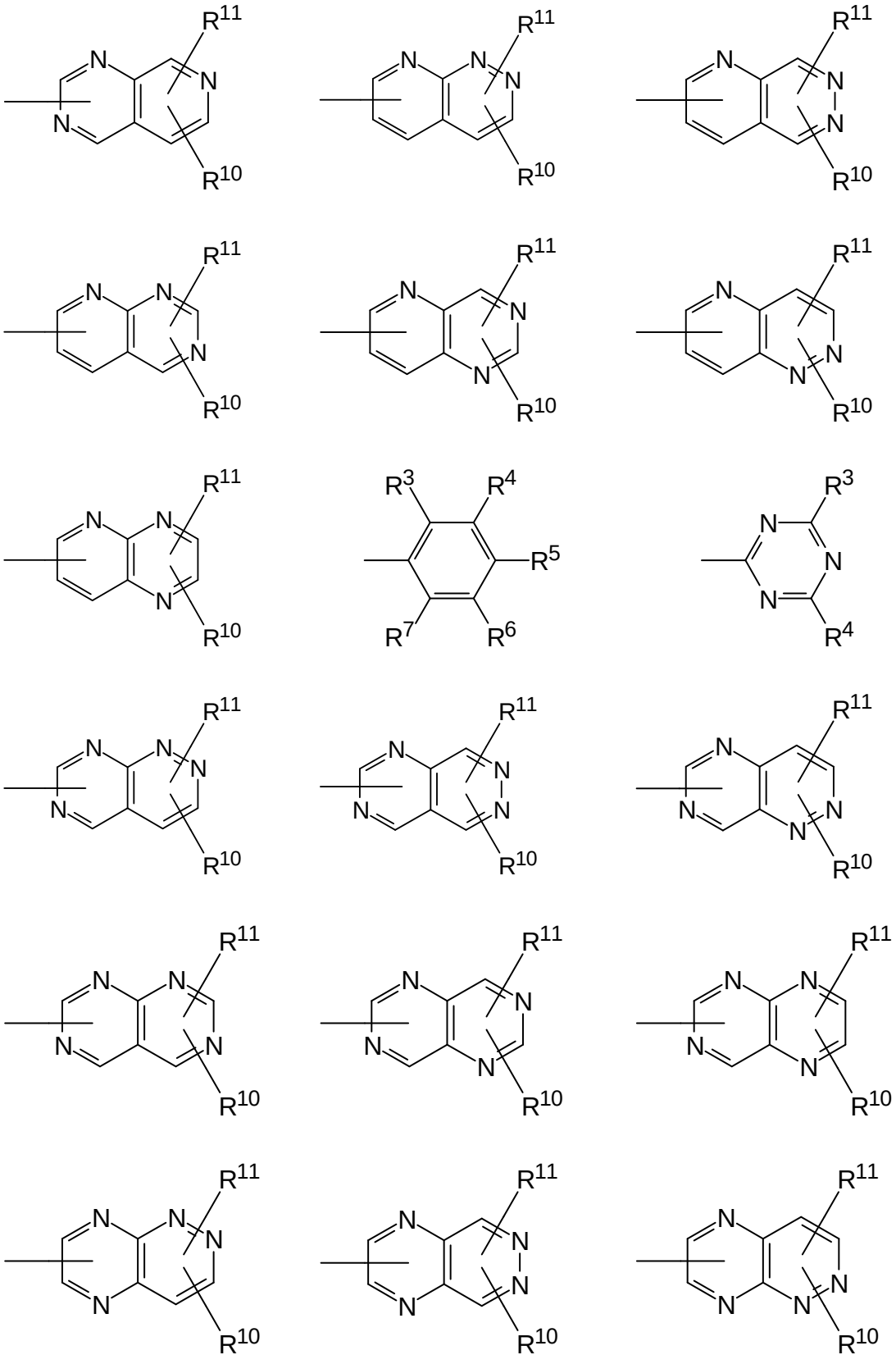

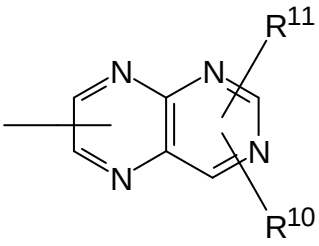
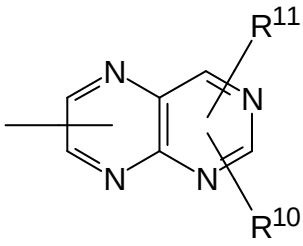
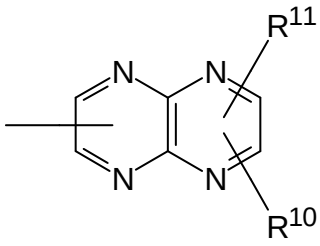
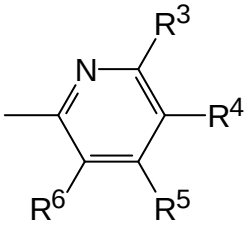
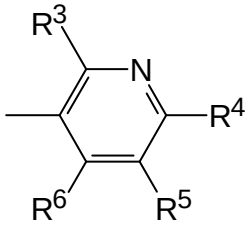
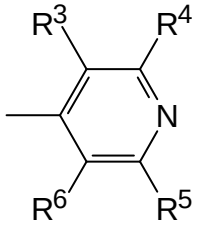
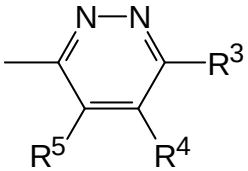
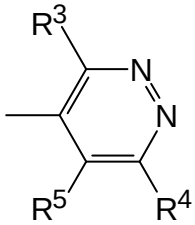
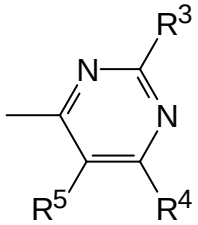
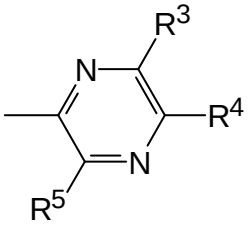
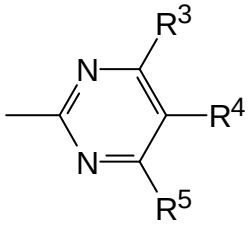
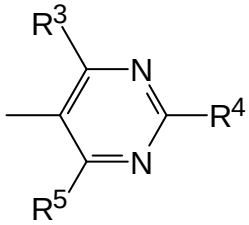

R^3, R^4, R^5, R^6, R^7, R^{10}, R^{11}, R^{12}, R^{13} unabhängig voneinander folgende Reste bedeuten:

$-R^{14}$, $-R^{15}$, $-R^{16}$, $-R^{17}$, $-R^{18}$, $-R^{19}$, $-R^{20}$, $-(CH_2)_n-R^{14}$, $-(CH_2)_n-R^{15}$, $-(CH_2)_n-R^{16}$, $-(CH_2)_n-R^{17}$, $-(CH_2)_n-R^{18}$, $-(CH_2)_n-R^{19}$, $-(CH_2)_n-R^{20}$;

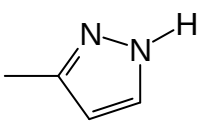
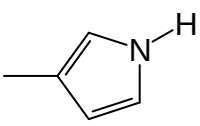
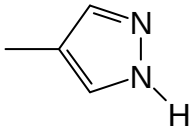

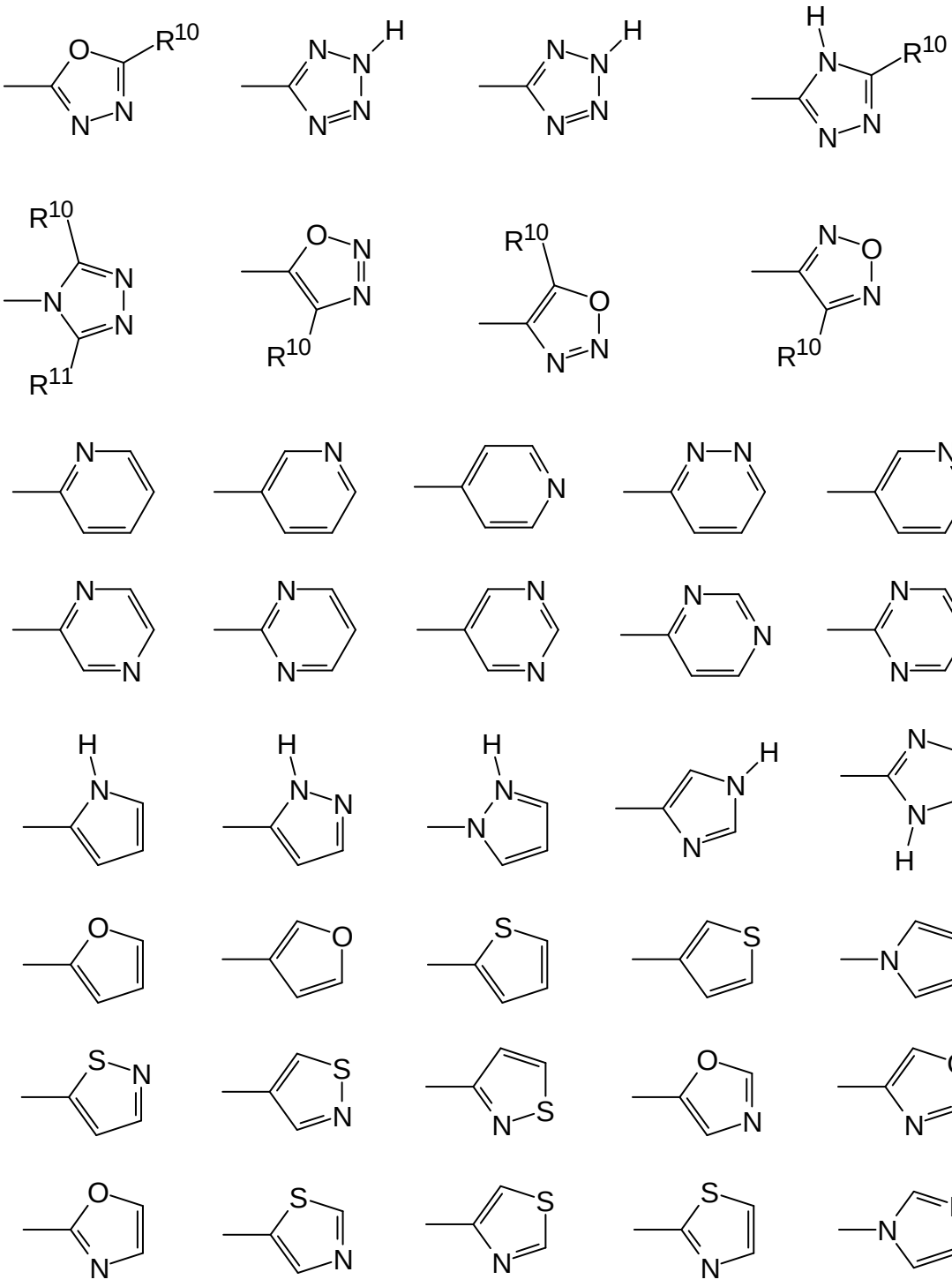

R^8, R^9 und R^{26} unabhängig voneinander folgende Reste bedeuten:

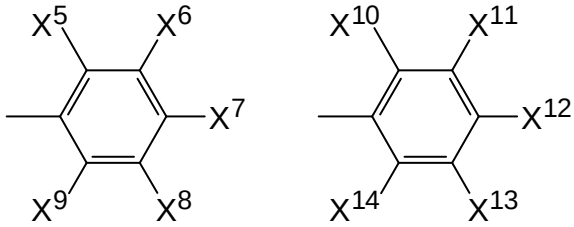

–H, –CH_2F, –CHF_2, –CF_3, –CH_2Cl, –CH_2Br, –CH_2I, –CH_2–CH_2F, –CH_2–CHF_2, –CH_2–CF_3, –CH_2–CH_2Cl, –CH_2–CH_2Br, –CH_2–CH_2I, cyclo-C_3H_5, cyclo-C_4H_7, cyclo-C_5H_9, cyclo-C_6H_{11}, cyclo-C_7H_{13}, cyclo-C_8H_{15}, –Ph, –CH_2–Ph, –CH_2–CH_2–Ph, –CH_2–CH_2–CH_2–Ph, –CH=CH–Ph, –C≡C–Ph, –CPh_3, –CH_3, –C_2H_5, –C_3H_7, –$CH(CH_3)_2$, –C_4H_9, –CH_2–$CH(CH_3)_2$, –$CH(CH_3)$–C_2H_5, –$C(CH_3)_3$, –C_5H_{11}, –$CH(CH_3)$–C_3H_7, –CH_2–$CH(CH_3)$–C_2H_5, –$CH(CH_3)$–$CH(CH_3)_2$, –$C(CH_3)_2$–C_2H_5, –CH_2–$C(CH_3)_3$, –$CH(C_2H_5)_2$, –C_2H_4–$CH(CH_3)_2$, –C_6H_{13}, –C_7H_{15}, –C_8H_{17}, –C_3H_6–$CH(CH_3)_2$, –C_2H_4–$CH(CH_3)$–C_2H_5, –$CH(CH_3)$–C_4H_9, –CH_2–$CH(CH_3)$–C_3H_7, –$CH(CH_3)$–CH_2–$CH(CH_3)_2$, –$CH(CH_3)$–$CH(CH_3)$–C_2H_5, –CH_2–$CH(CH_3)$–$CH(CH_3)_2$, –CH_2–$C(CH_3)_2$–C_2H_5, –$C(CH_3)_2$–C_3H_7, –$C(CH_3)_2$–$CH(CH_3)_2$, –C_2H_4–$C(CH_3)_3$, –$CH(CH_3)$–$C(CH_3)_3$, –$CH=CH_2$, –CH_2–$CH=CH_2$, –$C(CH_3)=CH_2$, –CH=CH–CH_3, –C_2H_4–$CH=CH_2$, –CH_2–CH=CH–CH_3, –CH=CH–C_2H_5, –CH_2–$C(CH_3)=CH_2$, –$CH(CH_3)$–CH=CH, –$CH=C(CH_3)_2$, –$C(CH_3)$=CH–CH_3, –CH=CH–CH=CH_2, –C_3H_6–$CH=CH_2$, –C_2H_4–CH=CH–CH_3, –CH_2–CH=CH–C_2H_5, –CH=CH–C_3H_7, –CH_2–CH=CH–CH=CH_2, –CH=CH–CH=CH–CH_3, –CH=CH–CH_2–CH=CH_2, –$C(CH_3)$=CH–CH=CH_2, –CH=$C(CH_3)$–CH=CH_2, –CH=CH–$C(CH_3)=CH_2$, –C_2H_4–$C(CH_3)=CH_2$, –CH_2–$CH(CH_3)$–CH=CH_2, –$CH(CH_3)$–CH_2–CH=CH_2, –CH_2–CH=$C(CH_3)_2$, –CH_2–$C(CH_3)$=CH–CH_3, –$CH(CH_3)$–CH=CH–CH_3, –CH=CH–$CH(CH_3)_2$, –CH=$C(CH_3)$–C_2H_5, –$C(CH_3)$=CH–C_2H_5, –$C(CH_3)=C(CH_3)_2$, –$C(CH_3)_2$–CH=CH_2, –$CH(CH_3)$–$C(CH_3)=CH_2$, –$C(CH_3)$=CH–CH=CH_2, –CH=$C(CH_3)$–CH=CH_2, –CH=CH–$C(CH_3)=CH_2$, –C_4H_8–$CH=CH_2$, –C_3H_6–CH=CH–CH_3, –C_2H_4–CH=CH–C_2H_5, –CH_2–CH=CH–C_3H_7, –CH=CH–C_4H_9, –C_3H_6–$C(CH_3)=CH_2$, –C_2H_4–$CH(CH_3)$–CH=CH_2, –CH_2–$CH(CH_3)$–CH_2–CH=CH_2, –$CH(CH_3)$–C_2H_4–CH=CH_2, –C_2H_4–CH=$C(CH_3)_2$, –C_2H_4–$C(CH_3)$=CH–CH_3, –CH_2–$CH(CH_3)$–CH=CH–CH_3, –$CH(CH_3)$–CH_2–CH=CH–CH_3, –CH_2–CH=CH–$CH(CH_3)_2$, –CH_2–CH=$C(CH_3)$–C_2H_5, –CH_2–$C(CH_3)$=CH–C_2H_5, –$CH(CH_3)$–CH=CH–C_2H_5, –CH=CH–CH_2–$CH(CH_3)_2$, –CH=CH–$CH(CH_3)$–C_2H_5, –CH=$C(CH_3)$–C_3H_7, –$C(CH_3)$=CH–C_3H_7, –CH_2–$CH(CH_3)$–$C(CH_3)=CH_2$, –$CH(CH_3)$–CH_2–$C(CH_3)=CH_2$, –$CH(CH_3)$–$CH(CH_3)$–CH=CH_2, –CH_2–$C(CH_3)_2$–CH=CH_2, –$C(CH_3)_2$–CH_2–CH=CH_2, –CH_2–$C(CH_3)=C(CH_3)_2$, –$CH(CH_3)$–CH=$C(CH_3)_2$, –$C(CH_3)_2$–CH=CH–CH_3, –$CH(CH_3)$–$C(CH_3)$=CH–CH_3, –CH=$C(CH_3)$–$CH(CH_3)_2$, –$C(CH_3)$=CH–$CH(CH_3)_2$,

–$C(CH_3)=C(CH_3)$–C_2H_5, –CH=CH–$C(CH_3)_3$, –$C(CH_3)_2$–$C(CH_3)=CH_2$, –$CH(C_2H_5)$–$C(CH_3)=CH_2$, –$C(CH_3)(C_2H_5)$–CH=CH_2, –$CH(CH_3)$–$C(C_2H_5)=CH_2$, –CH_2–$C(C_3H_7)=CH_2$, –CH_2–$C(C_2H_5)$=CH–CH_3, –$CH(C_2H_5)$–CH=CH–CH_3, –$C(C_4H_9)=CH_2$, –$C(C_3H_7)$=CH–CH_3, –$C(C_2H_5)$=CH–C_2H_5, –$C(C_2H_5)=C(CH_3)_2$, –$C[C(CH_3)_3]=CH_2$, –$C[CH(CH_3)(C_2H_5)]=CH_2$, –$C[CH_2$–$CH(CH_3)_2]=CH_2$,

–C_2H_4–CH=CH–CH=CH_2, –CH_2–CH=CH–CH_2–CH=CH_2, –CH=CH–C_2H_4–CH=CH_2, –CH_2–CH=CH–CH=CH–CH_3, –CH=CH–CH_2–CH=CH–CH_3, –CH=CH–CH=CH–C_2H_5, –CH_2–CH=CH–C(CH_3)=CH_2, –CH_2–CH=C(CH_3)–CH=CH_2, –CH_2–C(CH_3)=CH–CH=CH_2, –CH(CH_3)–CH=CH–CH=CH_2, –CH=CH–CH_2–C(CH_3)=CH_2, –CH=CH–CH(CH_3)–CH=CH_2, –CH=C(CH_3)–CH_2–CH=CH_2, –C(CH_3)=CH–CH_2–CH=CH_2, –CH=CH–CH=C(CH_3)$_2$, –CH=CH–C(CH_3)=CH–CH_3, –CH=C(CH_3)–CH=CH–CH_3, –C(CH_3)=CH–CH=CH–CH_3, –CH=C(CH_3)–C(CH_3)=CH_2, –C(CH_3)=CH–C(CH_3)=CH_2, –C(CH_3)=C(CH_3)–CH=CH_2, –CH=CH–CH=CH–CH=CH_2, –C≡CH, –C≡C–CH_3, –CH_2-C≡CH, –C_2H_4–C≡CH, –CH_2–C≡C–CH_3, –C≡C–C_2H_5, –C_3H_6–C≡CH, –C_2H_4–C≡C–CH_3, –CH_2–C≡C–C_2H_5, –C≡C–C_3H_7, –CH(CH_3)–C≡CH, –CH_2–CH(CH_3)–C≡CH, –CH(CH_3)–CH_2–C≡CH, –CH(CH_3)–C≡C–CH_3, –C_4H_8–C≡CH, –C_3H_6–C≡C–CH_3, –C_2H_4–C≡C–C_2H_5, –CH_2–C≡C–C_3H_7, –C≡C–C_4H_9, –C_2H_4–CH(CH_3)–C≡CH, –CH_2–CH(CH_3)–CH_2–C≡CH, –CH(CH_3)–C_2H_4–C≡CH, –CH_2–CH(CH_3)–C≡C–CH_3, –CH(CH_3)–CH_2–C≡C–CH_3, –CH(CH_3)–C≡C–C_2H_5, –CH_2–C≡C–CH(CH_3)$_2$, –C≡C–CH(CH_3)–C_2H_5, –C≡C–CH_2–CH(CH_3)$_2$, –C≡C–C(CH_3)$_3$, –CH(C_2H_5)–C≡C–CH_3, –C(CH_3)$_2$–C≡C–CH_3, –CH(C_2H_5)–CH_2–C≡CH, –CH_2–CH(C_2H_5)–C≡CH, –C(CH_3)$_2$–CH_2–C≡CH, –CH_2–C(CH_3)$_2$–C≡CH, –CH(CH_3)–CH(CH_3)–C≡CH, –CH(C_3H_7)–C≡CH, –C(CH_3)(C_2H_5)–C≡CH, –C≡C–C≡CH, –CH_2–C≡C–C≡CH, –C≡C–C≡C–CH_3, –CH(C≡CH)$_2$, –C_2H_4–C≡C–C≡CH, –CH_2–C≡C–CH_2–C≡CH, –C≡C–C_2H_4–C≡CH, –CH_2–C≡C–C≡C–CH_3, –C≡C–CH_2–C≡C–CH_3, –C≡C–C≡C–C_2H_5, –C≡C–CH(CH_3)–C≡CH, –CH(CH_3)–C≡C–C≡CH, –CH(C≡CH)–CH_2–C≡CH, –C(C≡CH)$_2$–CH_3, –CH_2–CH(C≡CH)$_2$, –CH(C≡CH)–C≡C–CH_3, –O–CH_2–CH(OCH_3)$_2$, –O–CH_2–CH(OC_2H_5)$_2$, –O–C_2H_4–CH(OCH_3)$_2$, –O–C_2H_4–CH(OC_2H_5)$_2$, –NH–CH_2–CH(OCH_3)$_2$, –NH–CH_2–CH(OC_2H_5)$_2$, –NH–C_2H_4–CH(OCH_3)$_2$, –NH–C_2H_4–CH(OC_2H_5)$_2$, –CH_2–CH(OCH_3)$_2$ oder –CH_2–CH(OC_2H_5)$_2$;

R^{23} ist –R^{27} oder 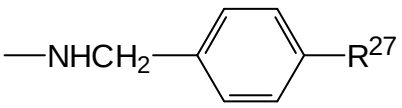 oder 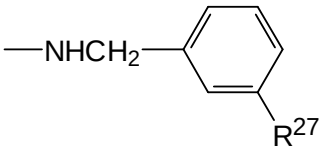

R^{14}, R^{15}, R^{16}, R^{17}, R^{18}, R^{19}, R^{20}, R^{21}, R^{22}, R^{24}, R^{25}, R^{27} unabhängig voneinander folgende Reste bedeuten:

–H, –CH_2F, –CHF_2, –CF_3, –CH_2Cl, –CH_2Br, –CH_2I, –CH_2–CH_2F, –CH_2–CHF_2, –CH_2–CF_3, –CH_2–CH_2Cl, –CH_2–CH_2Br, –CH_2–CH_2I, cyclo-C_3H_5, cyclo-C_4H_7, cyclo-C_5H_9, cyclo-C_6H_{11}, cyclo-C_7H_{13}, cyclo-C_8H_{15}, –Ph, –CH_2–Ph, –CH_2–CH_2–Ph, –CH_2–CH_2–CH_2–Ph, –CH=CH–Ph,

–C≡C–Ph, –CPh$_3$, –CH$_3$, –C$_2$H$_5$, –C$_3$H$_7$, –CH(CH$_3$)$_2$, –C$_4$H$_9$, –CH$_2$–CH(CH$_3$)$_2$, –CH(CH$_3$)–C$_2$H$_5$, –C(CH$_3$)$_3$, –C$_5$H$_{11}$, –CH(CH$_3$)–C$_3$H$_7$, –CH$_2$–CH(CH$_3$)–C$_2$H$_5$, –CH(CH$_3$)–CH(CH$_3$)$_2$, –C(CH$_3$)$_2$–C$_2$H$_5$, –CH$_2$–C(CH$_3$)$_3$, –CH(C$_2$H$_5$)$_2$, –C$_2$H$_4$–CH(CH$_3$)$_2$, –C$_6$H$_{13}$, –C$_7$H$_{15}$, –C$_8$H$_{17}$, –C$_3$H$_6$–CH(CH$_3$)$_2$, –C$_2$H$_4$–CH(CH$_3$)–C$_2$H$_5$, –CH(CH$_3$)–C$_4$H$_9$, –CH$_2$–CH(CH$_3$)–C$_3$H$_7$, –CH(CH$_3$)–CH$_2$–CH(CH$_3$)$_2$, –CH(CH$_3$)–CH(CH$_3$)–C$_2$H$_5$, –CH$_2$–CH(CH$_3$)–CH(CH$_3$)$_2$, –CH$_2$–C(CH$_3$)$_2$–C$_2$H$_5$, –C(CH$_3$)$_2$–C$_3$H$_7$, –C(CH$_3$)$_2$–CH(CH$_3$)$_2$, –C$_2$H$_4$–C(CH$_3$)$_3$, –CH(CH$_3$)–C(CH$_3$)$_3$, –CH=CH$_2$, –CH$_2$–CH=CH$_2$, –C(CH$_3$)=CH$_2$, –CH=CH–CH$_3$, –C$_2$H$_4$–CH=CH$_2$, –CH$_2$–CH=CH–CH$_3$, –CH=CH–C$_2$H$_5$, –CH$_2$–C(CH$_3$)=CH$_2$, –CH(CH$_3$)–CH=CH, –CH=C(CH$_3$)$_2$, –C(CH$_3$)=CH–CH$_3$, –CH=CH–CH=CH$_2$, –C$_3$H$_6$–CH=CH$_2$, –C$_2$H$_4$–CH=CH–CH$_3$, –CH$_2$–CH=CH–C$_2$H$_5$, –CH=CH–C$_3$H$_7$, –CH$_2$–CH=CH–CH=CH$_2$, –CH=CH–CH=CH–CH$_3$, –CH=CH–CH$_2$–CH=CH$_2$, –C(CH$_3$)=CH–CH=CH$_2$, –CH=C(CH$_3$)–CH=CH$_2$, –CH=CH–C(CH$_3$)=CH$_2$, –C$_2$H$_4$–C(CH$_3$)=CH$_2$, –CH$_2$–CH(CH$_3$)–CH=CH$_2$, –CH(CH$_3$)–CH$_2$–CH=CH$_2$, –CH$_2$–CH=C(CH$_3$)$_2$, –CH$_2$–C(CH$_3$)=CH–CH$_3$, –CH(CH$_3$)–CH=CH–CH$_3$, –CH=CH–CH(CH$_3$)$_2$, –CH=C(CH$_3$)–C$_2$H$_5$, –C(CH$_3$)=CH–C$_2$H$_5$, –C(CH$_3$)=C(CH$_3$)$_2$, –C(CH$_3$)$_2$–CH=CH$_2$, –CH(CH$_3$)–C(CH$_3$)=CH$_2$, –C(CH$_3$)=CH–CH=CH$_2$, –CH=C(CH$_3$)–CH=CH$_2$, –CH=CH–C(CH$_3$)=CH$_2$, –C$_4$H$_8$–CH=CH$_2$, –C$_3$H$_6$–CH=CH–CH$_3$, –C$_2$H$_4$–CH=CH–C$_2$H$_5$, –CH$_2$–CH=CH–C$_3$H$_7$, –CH=CH–C$_4$H$_9$, –C$_3$H$_6$–C(CH$_3$)=CH$_2$, –C$_2$H$_4$–CH(CH$_3$)–CH=CH$_2$, –CH$_2$–CH(CH$_3$)–CH$_2$–CH=CH$_2$, –CH(CH$_3$)–C$_2$H$_4$–CH=CH$_2$, –C$_2$H$_4$–CH=C(CH$_3$)$_2$, –C$_2$H$_4$–C(CH$_3$)=CH–CH$_3$, –CH$_2$–CH(CH$_3$)–CH=CH–CH$_3$, –CH(CH$_3$)–CH$_2$–CH=CH–CH$_3$, –CH$_2$–CH=CH–CH(CH$_3$)$_2$, –CH$_2$–CH=C(CH$_3$)–C$_2$H$_5$, –CH$_2$–C(CH$_3$)=CH–C$_2$H$_5$, –CH(CH$_3$)–CH=CH–C$_2$H$_5$, –CH=CH–CH$_2$–CH(CH$_3$)$_2$, –CH=CH–CH(CH$_3$)–C$_2$H$_5$, –CH=C(CH$_3$)–C$_3$H$_7$, –C(CH$_3$)=CH–C$_3$H$_7$, –CH$_2$–CH(CH$_3$)–C(CH$_3$)=CH$_2$, –CH(CH$_3$)–CH$_2$–C(CH$_3$)=CH$_2$, –CH(CH$_3$)–CH(CH$_3$)–CH=CH$_2$, –CH$_2$–C(CH$_3$)$_2$–CH=CH$_2$, –C(CH$_3$)$_2$–CH$_2$–CH=CH$_2$, –CH$_2$–C(CH$_3$)=C(CH$_3$)$_2$, –CH(CH$_3$)–CH=C(CH$_3$)$_2$, –C(CH$_3$)$_2$–CH=CH–CH$_3$, –CH(CH$_3$)–C(CH$_3$)=CH–CH$_3$, –CH=C(CH$_3$)–CH(CH$_3$)$_2$, –C(CH$_3$)=CH–CH(CH$_3$)$_2$, –C(CH$_3$)=C(CH$_3$)–C$_2$H$_5$, –CH=CH–C(CH$_3$)$_3$, –C(CH$_3$)$_2$–C(CH$_3$)=CH$_2$, –CH(C$_2$H$_5$)–C(CH$_3$)=CH$_2$, –C(CH$_3$)(C$_2$H$_5$)–CH=CH$_2$, –CH(CH$_3$)–C(C$_2$H$_5$)=CH$_2$, –CH$_2$–C(C$_3$H$_7$)=CH$_2$, –CH$_2$–C(C$_2$H$_5$)=CH–CH$_3$, –CH(C$_2$H$_5$)–CH=CH–CH$_3$, –C(C$_4$H$_9$)=CH$_2$, –C(C$_3$H$_7$)=CH–CH$_3$, –C(C$_2$H$_5$)=CH–C$_2$H$_5$, –C(C$_2$H$_5$)=C(CH$_3$)$_2$, –C[C(CH$_3$)$_3$]=CH$_2$, –C[CH(CH$_3$)(C$_2$H$_5$)]=CH$_2$, –C[CH$_2$–CH(CH$_3$)$_2$]=CH$_2$, –C$_2$H$_4$–CH=CH–CH=CH$_2$, –CH$_2$–CH=CH–CH$_2$–CH=CH$_2$, –CH=CH–C$_2$H$_4$–CH=CH$_2$, –CH$_2$–CH=CH–CH=CH–CH$_3$, –CH=CH–CH$_2$–CH=CH–CH$_3$, –

CH=CH–CH=CH–C_2H_5, –CH_2–CH=CH–C(CH_3)=CH_2, –CH_2–CH=C(CH_3)–CH=CH_2, –CH_2–C(CH_3)=CH–CH=CH_2, –CH(CH_3)–CH=CH–CH=CH_2, –CH=CH–CH_2–C(CH_3)=CH_2, –CH=CH–CH(CH_3)–CH=CH_2, –CH=C(CH_3)–CH_2–CH=CH_2, –C(CH_3)=CH–CH_2–CH=CH_2, –CH=CH–CH=C(CH_3)$_2$, –CH=CH–C(CH_3)=CH–CH_3, –CH=C(CH_3)–CH=CH–CH_3, –C(CH_3)=CH–CH=CH–CH_3, –CH=C(CH_3)–C(CH_3)=CH_2, –C(CH_3)=CH–C(CH_3)=CH_2, –C(CH_3)=C(CH_3)–CH=CH_2, –CH=CH–CH=CH–CH=CH_2, –C≡CH, –C≡C–CH_3, –CH_2-C≡CH, –C_2H_4–C≡CH, –CH_2–C≡C–CH_3, –C≡C–C_2H_5, –C_3H_6–C≡CH, –C_2H_4–C≡C–CH_3, –CH_2–C≡C–C_2H_5, –C≡C–C_3H_7, –CH(CH_3)–C≡CH, –CH_2–CH(CH_3)–C≡CH, –CH(CH_3)–CH_2–C≡CH, –CH(CH_3)–C≡C–CH_3, –C_4H_8–C≡CH, –C_3H_6–C≡C–CH_3, –C_2H_4–C≡C–C_2H_5, –CH_2–C≡C–C_3H_7, –C≡C–C_4H_9, –C_2H_4–CH(CH_3)–C≡CH, –CH_2–CH(CH_3)–CH_2–C≡CH, –CH(CH_3)–C_2H_4–C≡CH, –CH_2–CH(CH_3)–C≡C–CH_3, –CH(CH_3)–CH_2–C≡C–CH_3, –CH(CH_3)–C≡C–C_2H_5, –CH_2–C≡C–CH(CH_3)$_2$, –C≡C–CH(CH_3)–C_2H_5, –C≡C–CH_2–CH(CH_3)$_2$, –C≡C–C(CH_3)$_3$, –CH(C_2H_5)–C≡C–CH_3, –C(CH_3)$_2$–C≡C–CH_3, –CH(C_2H_5)–CH_2–C≡CH, –CH_2–CH(C_2H_5)–C≡CH, –C(CH_3)$_2$–CH_2–C≡CH, –CH_2–C(CH_3)$_2$–C≡CH, –CH(CH_3)–CH(CH_3)–C≡CH, –CH(C_3H_7)–C≡CH, –C(CH_3)(C_2H_5)–C≡CH, –C≡C–C≡CH, –CH_2–C≡C–C≡CH, –C≡C–C≡C–CH_3, –CH(C≡CH)$_2$, –C_2H_4–C≡C–C≡CH, –CH_2–C≡C–CH_2–C≡CH, –C≡C–C_2H_4–C≡CH, –CH_2–C≡C–C≡C–CH_3, –C≡C–CH_2–C≡C–CH_3, –C≡C–C≡C–C_2H_5, –C≡C–CH(CH_3)–C≡CH, –CH(CH_3)–C≡C–C≡CH, –CH(C≡CH)–CH_2–C≡CH, –C(C≡CH)$_2$–CH_3, –CH_2–CH(C≡CH)$_2$, –CH(C≡CH)–C≡C–CH_3, –OH, –OCH_3, –OC_2H_5, –OC_3H_7, –O–cyclo-C_3H_5, –OCH(CH_3)$_2$, –OC(CH_3)$_3$, –OC_4H_9, –OPh, –OCH_2–Ph, –$OCPh_3$, –SH, –NO_2, –SCH_3, –SC_2H_5, –SC_3H_7, –S–cyclo-C_3H_5, –SCH(CH_3)$_2$, –SC(CH_3)$_3$, –F, –Cl, –Br, –I, –P(O)(OH)$_2$, –P(O)(OCH_3)$_2$, –P(O)(OC_2H_5)$_2$, –P(O)(OCH(CH_3)$_2$)$_2$, –C(OH)[P(O)(OH)$_2$]$_2$, –Si(CH_3)$_2$(C(CH_3)$_3$), –Si(C_2H_5)$_3$, –Si(CH_3)$_3$, –N_3, –CN, –OCN, –NCO, –SCN, –NCS, –CHO, –$COCH_3$, –COC_2H_5, –COC_3H_7, –CO–cyclo-C_3H_5, –COCH(CH_3)$_2$, –COC(CH_3)$_3$, –COOH, –COCN, –$COOCH_3$, –$COOC_2H_5$, –$COOC_3H_7$, –COO–cyclo-C_3H_5, –COOCH(CH_3)$_2$, –COOC(CH_3)$_3$, –OOC–CH_3, –OOC–C_2H_5, –OOC–C_3H_7, –OOC–cyclo-C_3H_5, –OOC–CH(CH_3)$_2$, –OOC–C(CH_3)$_3$, –$CONH_2$, –$CONHCH_3$, –$CONHC_2H_5$, –$CONHC_3H_7$, –CONH–cyclo-C_3H_5, –CONH[CH(CH_3)$_2$], –CONH[C(CH_3)$_3$], –CON(CH_3)$_2$, –CON(C_2H_5)$_2$, –CON(C_3H_7)$_2$, –CON(cyclo-C_3H_5)$_2$, –CON[CH(CH_3)$_2$]$_2$, –CON[C(CH_3)$_3$]$_2$, –$NHCOCH_3$, –$NHCOC_2H_5$, –$NHCOC_3H_7$, –NHCO–cyclo-C_3H_5, –NHCO–CH(CH_3)$_2$, –NHCO–C(CH_3)$_3$, –NHCO–OCH_3, –NHCO–OC_2H_5, –NHCO–OC_3H_7, –NHCO–O–cyclo-C_3H_5, –NHCO–OCH(CH_3)$_2$, –NHCO–OC(CH_3)$_3$,

–NH_2, –$NHCH_3$, –NHC_2H_5, –NHC_3H_7, –NH–cyclo-C_3H_5, –$NHCH(CH_3)_2$, –$NHC(CH_3)_3$, –$N(CH_3)_2$, –$N(C_2H_5)_2$, –$N(C_3H_7)_2$, –N(cyclo-$C_3H_5)_2$, –$N[CH(CH_3)_2]_2$, –$N[C(CH_3)_3]_2$, –$SOCH_3$, –SOC_2H_5, –SOC_3H_7, –SO–cyclo-C_3H_5, –$SOCH(CH_3)_2$, –$SOC(CH_3)_3$, –SO_2CH_3, –$SO_2C_2H_5$, –$SO_2C_3H_7$, –SO_2–cyclo-C_3H_5, –$SO_2CH(CH_3)_2$, –$SO_2C(CH_3)_3$, –SO_3H, –SO_3CH_3, –$SO_3C_2H_5$, –$SO_3C_3H_7$, –SO_3–cyclo-C_3H_5, –$SO_3CH(CH_3)_2$, –$SO_3C(CH_3)_3$, –O–SO_2CH_3, –O–$SO_2C_2H_5$, –O–$SO_2C_3H_7$, –O–SO_2–cyclo-C_3H_5, –O–$SO_2CH(CH_3)_2$, –O–$SO_2C(CH_3)_3$, –SO_2NH_2, –OCF_3, –OC_2F_5, –O–$COOCH_3$, –O–$COOC_2H_5$, –O–$COOC_3H_7$, –O–COO–cyclo-C_3H_5, –O–$COOCH(CH_3)_2$, –O–$COOC(CH_3)_3$, –NH–CO–NH_2, –NH–CO–$NHCH_3$, –NH–CO–NHC_2H_5, –NH–CO–NHC_3H_7, –NH–CO–NH–cyclo-C_3H_5, –NH–CO–$NH[CH(CH_3)_2]$, –NH–CO–$NH[C(CH_3)_3]$, –NH–CO–$N(CH_3)_2$, –NH–CO–$N(C_2H_5)_2$, –NH–CO–$N(C_3H_7)_2$, –NH–CO–N(cyclo-$C_3H_5)_2$, –NH–CO–$N[CH(CH_3)_2]_2$, –NH–CO–$N[C(CH_3)_3]_2$, –NH–CS–NH_2, –NH–CS–$NHCH_3$, –NH–CS–NHC_2H_5, –NH–CS–NHC_3H_7, –NH–CS–NH–cyclo-C_3H_5, –NH–CS–$NH[CH(CH_3)_2]$, –NH–CS–$NH[C(CH_3)_3]$, –NH–CS–$N(CH_3)_2$, –NH–CS–$N(C_2H_5)_2$, –NH–CS–$N(C_3H_7)_2$, –NH–CS–N(cyclo-$C_3H_5)_2$, –NH–CS–$N[CH(CH_3)_2]_2$, –NH–CS–$N[C(CH_3)_3]_2$, –NH–C(=NH)–NH_2, –NH–C(=NH)–$NHCH_3$, –NH–C(=NH)–NHC_2H_5, –NH–C(=NH)–NHC_3H_7, –NH–C(=NH)–NH–cyclo-C_3H_5, –NH–C(=NH)–$NH[CH(CH_3)_2]$, –NH–C(=NH)–$NH[C(CH_3)_3]$, –NH–C(=NH)–$N(CH_3)_2$, –NH–C(=NH)–$N(C_2H_5)_2$, –NH–C(=NH)–$N(C_3H_7)_2$, –NH–C(=NH)–N(cyclo-$C_3H_5)_2$, –O–CO–NH_2, –NH–C(=NH)–$N[CH(CH_3)_2]_2$, –NH–C(=NH)–$N[C(CH_3)_3]_2$, –O–CO–$NHCH_3$, –O–CO–NHC_2H_5, –O–CO–NHC_3H_7, –O–CO–NH–cyclo-C_3H_5, –O–CO–$NH[CH(CH_3)_2]$, –O–CO–$NH[C(CH_3)_3]$, –O–CO–$N(CH_3)_2$, –O–CO–$N(C_2H_5)_2$, –O–CO–$N(C_3H_7)_2$, –O–CO–N(cyclo-$C_3H_5)_2$, –O–CO–$N[CH(CH_3)_2]_2$, –O–CO–$N[C(CH_3)_3]_2$, –O–CO–OCH_3, –O–CO–OC_2H_5, –O–CO–OC_3H_7, –O–CO–O–cyclo-C_3H_5, –O–CO–$OCH(CH_3)_2$, –O–CO–$OC(CH_3)_3$, –O–CH_2–$CH(OCH_3)_2$, –O–CH_2–$CH(OC_2H_5)_2$, –O–C_2H_4–$CH(OCH_3)_2$, –O–C_2H_4–$CH(OC_2H_5)_2$, –NH–CH_2–$CH(OCH_3)_2$, –NH–CH_2–$CH(OC_2H_5)_2$, –NH–C_2H_4–$CH(OCH_3)_2$, –NH–C_2H_4–$CH(OC_2H_5)_2$, –CH_2–OPh, –CH_2–O–CH_2Ph, –NH–CH_2–OH, –NH–C_2H_4–OH, –NH–C_3H_6–OH, –NH–C_4H_8–OH, –NH–C_5H_{10}–OH, –NH–CH_2–OCH_3, –NH–C_2H_4–OCH_3, –NH–C_3H_6–OCH_3, –NH–C_4H_8–OCH_3, –NH–C_5H_{10}–OCH_3, –NH–CH_2–OC_2H_5, –NH–C_2H_4–OC_2H_5, –NH–C_3H_6–OC_2H_5, –NH–C_4H_8–OC_2H_5, –NH–C_5H_{10}–OC_2H_5, –CH_2–OH, –C_2H_4–OH, –C_3H_6–OH, –C_4H_8–OH, –C_5H_{10}–OH, –CH_2–$CH(OCH_3)_2$ oder –CH_2–$CH(OC_2H_5)_2$;

X^1, X^2, X^3, X^4, X^5, X^6, X^7, X^8, X^9, X^{10}, X^{11}, X^{12}, X^{13} und X^{14} unabhängig voneinander folgende Reste bedeuten:

–H, $-CF_3$, $-CH_3$, $-C_2H_5$, $-C_3H_7$, $-CH(CH_3)_2$, –OH, $-OCH_3$, $-OC_2H_5$, $-OC_3H_7$, –OPh, $-NO_2$, –F, –Cl, –Br, –I, –CN, $-COCH_3$, $-COC_2H_5$, $-COC_3H_7$, –COOH, $-COOCH_3$, $-COOC_2H_5$, $-COOC_3H_7$, $-OCF_3$, –Ph, oder $-CH_2-Ph$, Tetrazol;

X^{15} für einen der folgenden Reste steht:

–H, $-CF_3$, $-CH_3$, $-C_2H_5$, $-C_3H_7$, $-CH(CH_3)_2$, –OH, $-OCH_3$, $-OC_2H_5$, $-OC_3H_7$, –OPh, $-NO_2$, –F, –Cl, –Br, –I, –CN, $-COCH_3$, $-COC_2H_5$, $-COC_3H_7$, –COOH, $-COOCH_3$, $-COOC_2H_5$, $-COOC_3H_7$, $-OCF_3$, $-CO-NH-R^{21}$, $-CH_3$, $-C_2H_5$, $-C_3H_7$, $-CH(CH_3)_2$, $-C_4H_9$, $-CH_2-CH(CH_3)_2$, $-CH(CH_3)-C_2H_5$, $-C(CH_3)_3$, $-C_5H_{11}$, $-CH=CH_2$, $-CH_2-CH=CH_2$, –Ph, $-CH_2-Ph$, $-CH_2-CH_2-Ph$, $-CH_2-CH_2-CH_2-Ph$, –CH=CH–Ph oder $-NH-CO-R^{21}$;

n ist eine ganze Zahl ausgewählt aus 1, 2, 3, 4 oder 5;

sowie deren Metallkomplexe, Salze, Enantiomere, Enantiomerengemische, Diastereomere, Diastereomerengemische, Tautomere, Hydrate, Solvate, und Racemate der vorgenannten Verbindungen.

Die vorliegende Erfindung betrifft ferner Verbindungen gemäß der allgemeinen Formel (I) zur Verwendung als Inhibitoren oder Antagonisten, insbesondere bevorzugt als kompetitive Antagonisten oder inverse Agonisten von GSK-3.

Antagonisten sind hierbei Verbindungen, welche durch vorrangige Interaktion mit der Kinase deren Aktivierung durch einen Agonisten verhindern oder hemmen können. Ein kompetitiver Antagonist konkurriert mit einem Agonisten um die Bindung an die Kinase und kann durch höhere Agonistenkonzentrationen entsprechend dem Massenwirkungsgesetz wieder verdrängt werden. Es kommt durch einen kompetitiven Antagonisten zu einer Parallelverschiebung der Dosis-Wirkungskurve eines Agonisten.

Inverse Agonisten sind hierin Verbindungen, die an die Kinase mit konstitutiver Aktivität binden und deren Aktivität herabsetzen. Ein inverser Agonist führt im Gegensatz zu einem vollen Agonisten somit zu einem negativen Effekt, bzw. einem

pharmakologischen Effekt, welcher dem des Agonisten entgegengesetzt ist. Dies kann stattfinden, indem solche Verbindungen die Bindung eines Korepressors bewirken bzw. fördern. Die Verbindungen gemäß allgemeiner Formel (I) werden hierin allgemein als Inhibitoren von GSK-3 bezeichnet.

GSK-3 Inhibitoren sind für die Verwendung in der Medizin relevant, da GSK-3 in den letzten Jahren zunehmend mit schwer wiegenden Erkrankungen, wie Alzheimer-Krankheit und andere Tauopathien, Asthma, bipolare affektive Störungen, Depression, Nervenzelltod und Schlaganfall, Parkinson, Huntington, Skelettmuskelatrophie, Kardioprotektion, Haarverlust, verringerte Spermienmotilität, Diabetes und damit in Zusammenhang stehende Folgeerkrankungen, wie Syndrom X und Adipositas, Erkrankungen, die durch einzellige Parasiten verursacht werden, transmissible spongiforme Enzephalopathie, Schizophrenie, Krankheiten des zirkadianen Rhythmus und Krebs in Verbindung gebracht wurde.

Des weiteren sind die folgenden subgenerischen Formeln der allgemeinen Formel (I) bevorzugt:

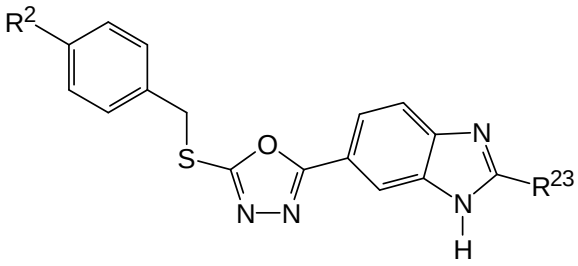

Formel B

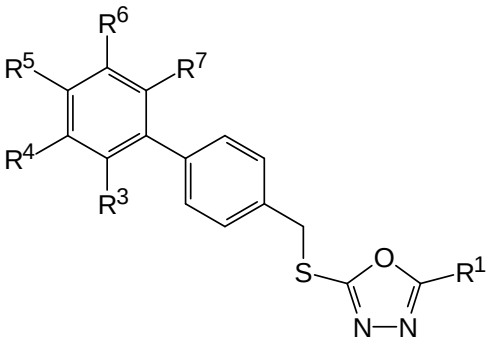

Formel A

Formel C

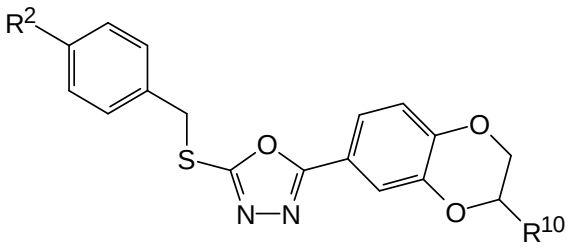

Formel D

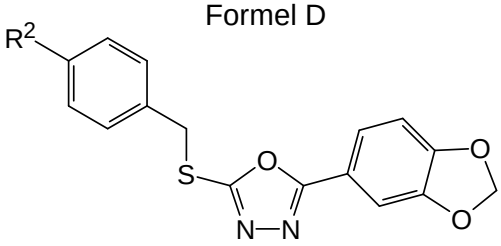

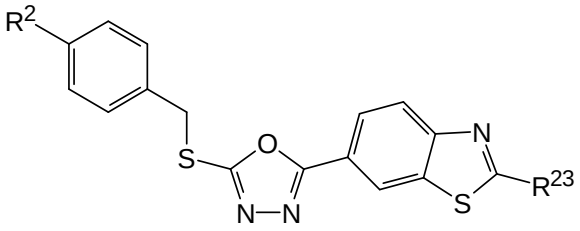

Formel E

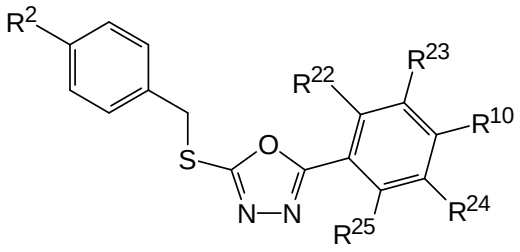

Formel F

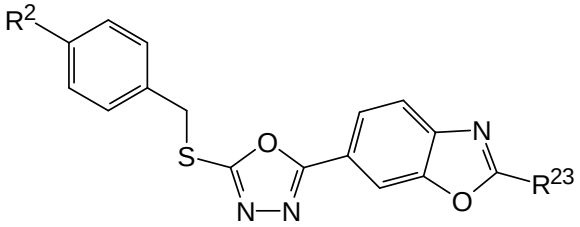

Formel G

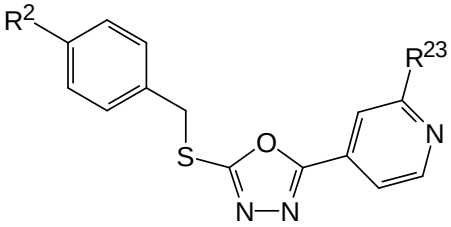

Formel H

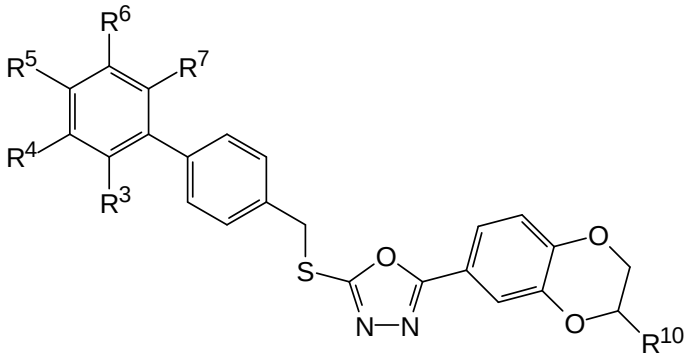

Formel J

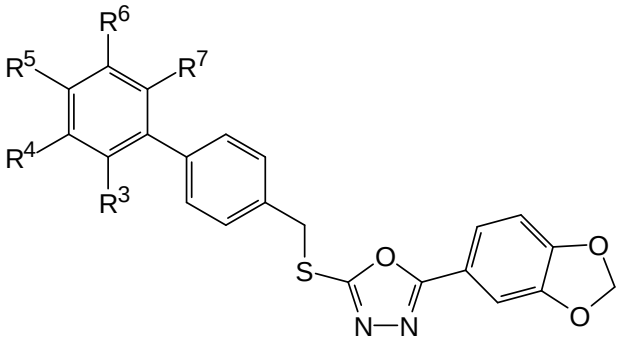

Formel K

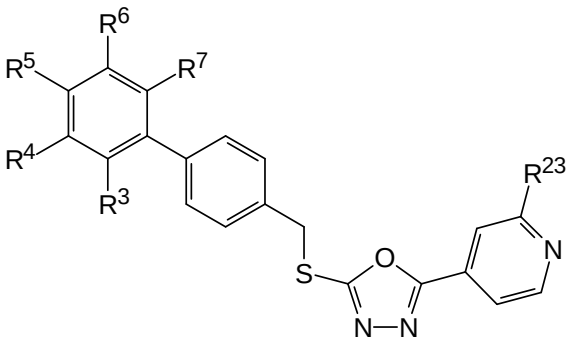

Formel L

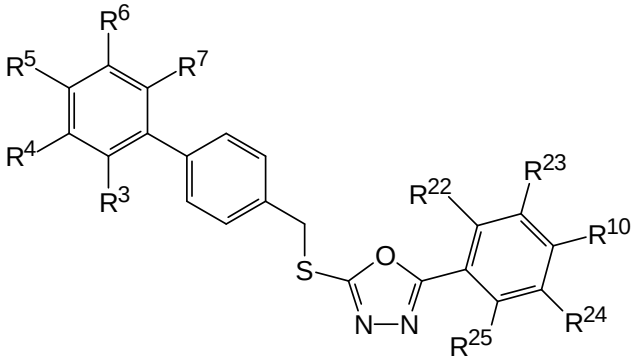

Formel M

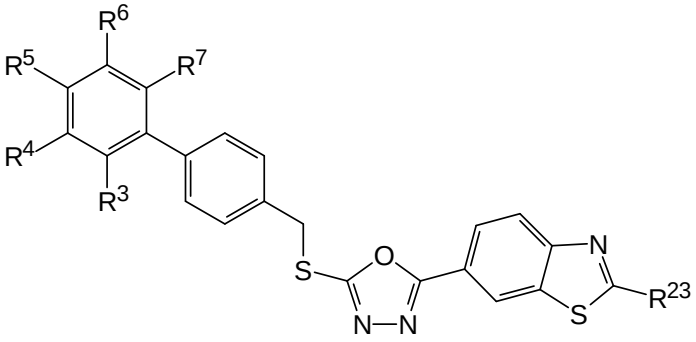

Formel N

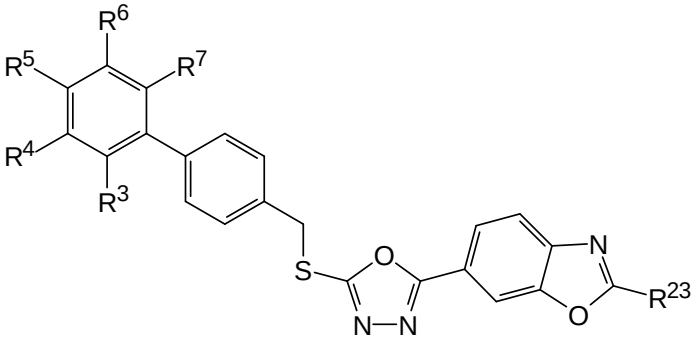

Formel O

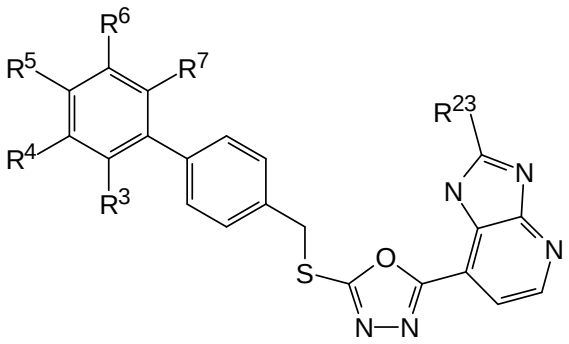

Formel P

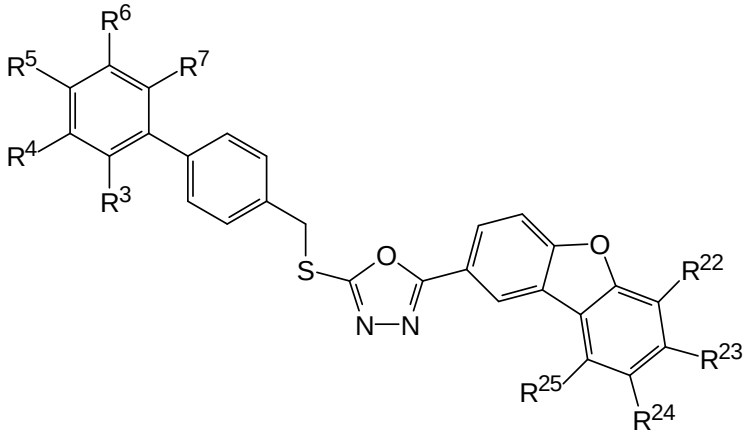

Formel Q

4.2 Untersuchungen zu anderen Kinasen

4.2.1 Die Parkinson-Krankheit und das Potential von LRRK2

Der Inhalt dieses Kapitels wurde bereits veröffentlicht:

Thomas Kramer*, Fabio Lo Monte*, Stefan Göring, Ghislaine Marlyse Okala Amombo, Boris Schmidt[‡]
Small molecule kinase inhibitors for LRRK2 and their application to Parkinson´s disease models, *ACS Chemical Neuroscience* **2012**, 3, 151-160. DOI: 10.1021/cn200117j

Die Parkinson-Krankheit ist die zweithäufigste neurodegenerative Erkrankung und zirka 4% der Menschen über 80 Jahre sind davon betroffen.[129-130] Diese Krankheit ist durch mehrere motorische und nicht-motorische Symptome charakterisiert. Vier dieser Symptome, Tremor, Rigor, Bradykinesie und posturale Instabilität werden als Kardinalsyndrome bezeichnet.[131] Die typischen Kennzeichen dieser Erkrankung in *post mortem* Gehirngewebe sind der Verlust der dopaminergen Neuronen und der *substantia nigra*. Darüber hinaus wurden verschiedene Proteinablagerungen wie *α-synuclein* mit dieser Krankheit assoziiert.[132-133] Gegenwärtig gibt es keine Heilmittel für die Parkinson-Krankheit, sondern nur Therapiemöglichkeiten zur Linderung der Symptome.[129,134]

Viele Mutationen wurden bereits mit der Parkinson-Krankheit in Verbindung gebracht, jedoch scheinen die Mutationen in dem für das LRRK2-Protein (*leucine-rich repeat kinase 2*) kodierenden Gen die aussichtsreichsten Kandidaten für eine *Target*-gerichtete Therapie zu sein.[135-137] LRRK2 ist ein großes und komplexes Protein, welches aus der *ankyrin-like*-Domäne (ANK), der *leucin-rich repeat*-Domäne (LRR), der *Ras of complex*-Domäne (Roc), der *C-terminal of Roc*-Domäne (COR), der Kinase-Domäne und der *C-terminal WD40*-Domäne (WD40) besteht (Abb. 21). Bisher wurden nur sehr wenige *in vitro* und *in vivo* Daten zu diesem Protein veröffentlicht, da es erst seit einiger Zeit im Fokus der Parkinson-Forschung steht.

Abb. 21: Schematische Darstellung der LRRK2-Domänen.

Das Review befasst sich mit den bisher publizierten Inhibitoren zu LRRK2 und den wichtigsten Mutationen dieser Kinase. Bestehende Tiermodelle werden vorgestellt und das Potential dieser Kinase als *Target* für die Parkinson-Krankheit kritisch diskutiert. Diese Themen wurden im Rahmen eines neu gestarteten Projekts untersucht und zusammengefasst, um eine Grundlage für die Synthese neuer LRRK2-Inhibitoren zu schaffen.

ACS Chemical Neuroscience

Review

pubs.acs.org/acschemicalneuroscience

Small Molecule Kinase Inhibitors for LRRK2 and Their Application to Parkinson's Disease Models

Thomas Kramer,[†] Fabio Lo Monte,[†] Stefan Göring, Ghislaine Marlyse Okala Amombo, and Boris Schmidt*

Clemens Schöpf - Institute of Organic Chemistry and Biochemistry, Technische Universität Darmstadt, 64287 Darmstadt, Germany

ABSTRACT: Parkinson's disease (PD) is the second most common neurodegenerative disorder. Several single gene mutations have been linked to this disease. Mutations in the gene encoding leucine-rich repeat kinase 2 (LRRK2) indicate LRRK2 as promising therapeutic target for the treatment of PD. LRRK2 mutations were observed in sporadic as well as familial PD patients and have been investigated intensively. LRRK2 is a large and complex protein, with multiple enzymatic and protein-interaction domains, each of which is effected by mutations. The most common mutation in PD patients is G2019S. Several LRRK2 inhibitors have been reported already, although the crystal structure of LRRK2 has not yet been determined. This review provides a summary of known LRRK2 inhibitors and will discuss recent in vitro and in vivo results of these inhibitors.

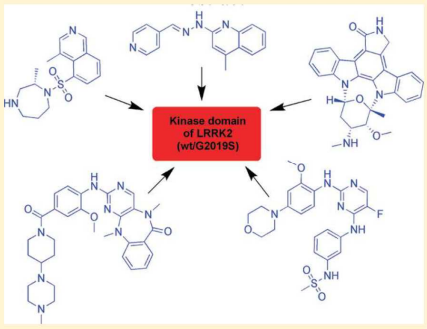

KEYWORDS: *Parkinson's disease, leucine-rich repeat kinase 2 (LRRK2), LRRK2 inhibitors, mutations, animal models*

Parkinson's disease (PD) is the second most prevalent neurodegenerative disorder after Alzheimer's disease, effecting up to ~4% of the population over 80.[1,2] PD is characterized by a large number of motoric and non-motoric symptoms. Four of them are designated as cardinal features: tremor at rest, rigidity, akinesia, and postural instability.[3] PD patients usually develop dementia during the course of the disease and gradually develop depression. The National Institute for Health and Clinical Excellence (NICE, U.K.) published guidelines for the diagnosis and management of patients with PD, which is used by most experts.[2,4] The typical hallmarks of PD in post-mortem brain tissue are loss of dopaminergic neurons of the substantia nigra, associated with the formation of fibrillar aggregates composed of α-synuclein and other proteins (e.g. Lewy bodies).[5,6] Presently, there is no cure for PD and the mainstay therapy is still the drug levodopa (L-Dopa).[2,7] L-Dopa is highly effective in reducing motor symptoms; nevertheless, there are two major problems, the side-effects and that patients become therapy resistant.[7,8] Adenosine A2a receptor antagonists have been shown to reduce PD-like features in animal studies through interaction with the specific dopamine receptor subtype D2 in the basal ganglia, making it more sensitive to dopamine. The adenosine A2a receptor antagonists SYN-115 from Synosia Therapeutics is currently in a phase IIb trial.[7] Other approaches are the metabotropic glutamate receptors (mGluRs), which are members of the G-protein-coupled receptor (GPCR) superfamily. They participate in the modulation of synaptic transmission and neuronal excitability throughout the central nervous system. Several studies indicate the therapeutic utility of mGluR ligands in neurological and psychiatric disorders and make mGluRs promising targets for non-dopaminergic drug discovery in PD. $mGluR_5$ is the target of drug development programmes at major pharmaceutical companies, e.g. Roche and Novartis.[7,9,10]

Several single gene mutations have been identified and linked to PD, for example, DJ-1, UCH-L1, SNCA, PRKN, and LRRK2.[1,2,5,11−14] However, mutations in the LRRK2 gene are the most common cause of familial and sporadic late-onset PD.[15] Since the LRRK2 gene mutations have been linked to PD, several inhibitors were reported to inhibit this kinase. We reviewed the literature and summarized the relevant data.

■ LRRK2: STRUCTURE AND MUTATIONS

The leucine-rich repeat kinase 2 (LRRK2) encodes a large multidomain protein with 2527 amino acids. Several independent domains have been established or predicted for the LRRK2 protein, including an ankyrin-like (ANK) domain, a leucine-rich repeat (LRR) domain, a Ras (renin-angiotensin system) of complex (Roc) domain, which belongs to the Ras GTPase family, followed by a C-terminal of ROC (COR) domain, a kinase (Kinase) domain, and a C-terminal WD40 domain (Figure 1).[16−18]

Beside the structural homology to the MAP kinase kinase kinases (MAPKKK) LRRK2 shares other biochemical features with MAPKKK, like autophosphorylation and interaction with kinase-specific chaperones.[19] LRRK2 is expressed in various brain regions and in several other organs, for example, in the lung, kidney, and heart.[20−22] LRRK2 efficiently phosphorylates

Received: November 25, 2011
Accepted: January 18, 2012
Published: January 18, 2012

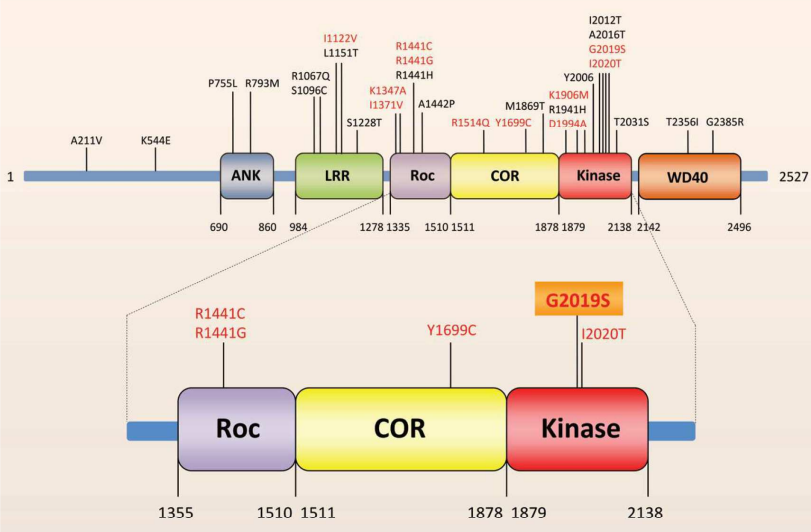

Figure 1. Schematic illustration of domains and most common PD-linked point mutations of LRRK2. Red marked mutations have been linked to altered kinase activity. ANK, ankyrin-like domain; LRR, leucin-rich repeat domain; Roc, Ras of complex domain, which belongs to the Ras GTPase family; COR, C-terminal of Roc domain; Kinase, kinase domain; WD40, C-terminal WD40 domain. The five putatively pathogenic mutations are enlarged.

moesin at Thr[558] in vitro, raising the idea that moesin may be a physiological substrate of LRRK2. Moreover, ezrin and radixin are phosphorylated by LRRK2, which are involved in moesin binding actin.[23,24] LRRK2 predominantly exists as a dimer under native conditions. The wild-type (wt) LRRK2 dimer displays increased kinase activity versus its monomeric counterpart.[25,26] More than 20 LRRK2 mutations have been linked to autosomal-dominant parkinsonism, and five of them are considered definitely pathogenic (R1441C, R1441G, Y1699C, G2019S, I2020T).[17,18,27] The most common mutation, which is present in more than 85% of PD patients carrying LRRK2 mutations, is G2019S.[28] In some ethnic groups the frequency of the LRRK2-G2019S mutation has been found to be even higher. For example, 13−40% of all PD patients in the Ashkenazi Jewish and northern African Arab population have this mutation, whereas in the Asian population this mutation is much less common.[17,28] The G2019S, R1441C, and R1441G mutations increase the LRRK2 kinase activity and both the kinase as well as the GTPase activities of LRRK2 are required to induce cell death.[6,29−32] The GTPase domain-associated R1441C mutation in combination with the G2019S kinase domain mutation increased the kinase activity up to 7-fold relative to wild-type protein.[33] It was reported that expression of G2019S mutant in Drosophila dendritic arborization neurons causes several dendrite defects, including tau mislocalization in dendrites, tau hyperphosphorylation at the T^{212}/S^{214} sites, dendrite degeneration, and microtubule fragmentation.[34] Furthermore, the LRRK2-G2019S mutant caused a progressive degeneration of nigral dopaminergic neurons in rats.[35] In addition, the autokinase activity of the LRRK2 mutant I2020T was found to be increased in comparison to wild-type.[19] Mutations within or near the GTPase domain including R1514Q, Y1699C, and I1371V increase kinase activity, while the alteration of the lysine residue K1347A leads to an ablation of this. The I1122V mutation in the LRR domain nominally increases kinase activity, whereas the D1994A and K1906M mutations in the kinase domain are able to diminish respectively to inhibit kinase activity.[31] Replacing the kinase domain with a "kinase-dead" version blocks inclusion body formation and delays cell death.[36] In addition, LRRK2 is able to phosphorylate MAPKKK 3, 4, 6, and 7 in vitro. This indicates that MAPKKK are molecular targets of LRRK2 mutants, whereby LRRK2 could be linked to neurotoxicity, cellular stress, and apoptosis.[37,38] LRRK2 provides a potential therapeutic target utilizing the knowledge gained in neuroprotective kinase inhibition.

■ IN VIVO MODELS AND STUDIES

Several studies using in vivo models of LRRK2 fostered the understanding of neurobiology, pathogenesis, and utility of potential therapeutics. The Drosophila model revealed that a LRRK2 loss-of-function mutant leads to significantly impaired locomotive activity and that LRRK2 is critical for the integrity of dopaminergic neurons (DA).[39] Another study showed that transgenic Drosophila harboring G2019S, Y1699C, or G2385 LRRK2 variants exhibit late-onset loss of DA and reduced lifespan.[40] Liu et al. used the GAL4/UAS system to generate transgenic Drosophila expressing either wild-type human LRRK2 or LRRK2-G2019S. They reported that expression of either wild-type human LRRK2 or LRRK2-G2019S in the photoreceptor cells caused retinal degeneration. Furthermore, they observed that expression of LRRK2 or LRRK2-G2019S in neurons produced adult-onset selective loss of dopaminergic neurons and locomotor dysfunction.[41,42] Overexpression of human LRRK2 wild-type, R1441C, and G2019S in DA of transgenic *C. elegans* models was sufficient to induce neurodegeneration and behavioral deficits, whereas knockout of the *C. elegans* LRRK2 homologue, LRK-1, prevents the LRRK2-induced neurodegeneration.[43] The blockage of zebrafish LRRK2 protein by morpholinos caused embryonic lethality and severe development defects such as growth retardation and loss of neurons. In addition, the deletion of the WD40 domain of zebrafish LRRK2 by morpholinos revealed Parkinsonism-like

Table 1. Staurosporine and Derivatives as LRRK2 Inhibitors

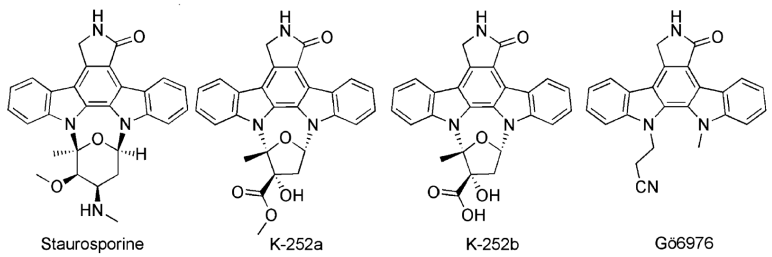

no.	name	IC_{50} wild-type LRRK2	IC_{50} LRRK2-G2019S	substrate	selectivity[a]	in vivo	lit.
1	Staurosporine	~1 nM;[b] 2 nM;[b] 8.2 nM;[d] 40 nM[e]	0.2 nM;[f] 1.8 nM;[c] 40 nM[e]	GST-moesin; LRRKtide; MBP[g]	2		58, 60−62
2	K-252a	~25 nM;[b] 3.6 nM[c]	2.8 nM[c]	LRRKtide			60, 61
3	K-252b	~50 nM[b]		LRRKtide			61
4	Gö6976	~250 nM[b]		LRRKtide			61

[a]Number of all kinases, including LRRK2. [b]Goat GST-LRRK2. [c]GST-LRRK2 (970−2527; wt/G2019S). [d]full-length LRRK2. [e]GST-LRRK2 (wt/G2019S). [f]Full-length Strep-tag LRRK2 (G2019S). [g]Myelin basic protein (MBP).

phenotypes, including loss of dopaminergic neurons in the diencephalon and locomotion defects.[44] Remarkably, another research group failed to reproduce the phenotypic loss of dopaminergic neurons in zebrafish.[45] Nevertheless, the zebrafish model may be a useful vertebrate model. The presence of a LRRK2 protein excess in LRRK2 wild-type and G2019S mice showed exacerbated α-synuclein A53T-mediated cytotoxicity. This result raised the idea that inhibition of LRRK2 expression may provide an applicable strategy to ameliorate α-synuclein-induced neurodegeneration in PD.[46] Expression of full-length LRRK2 wild-type did not induce any significant neuronal loss in the nigrostriatal system of adult rats, whereas expression of human LRRK2-G2019S mutant causes progressive degeneration of nigral dopaminergic neurons.[35] Bacterial artificial chromosome (BAC) transgenic mice expressing LRRK2 wild-type, LRRK2-R1441G, and LRRK2-G2019S have shown evidence of neurodegeneration.[24,47,48] Furthermore, the LRRK2-R1441G BAC transgenic mice revealed tau to be hyperphosphorylated in brain tissues.[48] However, LRRK2 knockout mice lacking the kinase domain of LRRK2 are viable and live a normal life span. Thus, LRRK2 is not essential for mouse development and maintenance of DA.[49] However, expression of the human LRRK2-G2019S mutation in transgenic mice is sufficient to recreate the slowly progressive degeneration of dopaminergic neurons that forms the hallmark pathology of familial and sporadic PD.[50] Several mice studies investigated the potential of LRRK2 as therapeutic strategy for the treatment of PD.[51−57] Two independent lines of LRRK2 germ-line deletion mice indicated that LRRK2 plays an essential role in the regulation of protein homeostasis during aging. Therefore, the authors concluded that LRRK2 inhibition may not represent a suitable therapeutic strategy for the treatment of PD.[54] Another research group created inducible transgenic rats expressing LRRK2 with G2019S substitution and recapitulated the initiation process of dopaminergic dysfunction. However, the mutation was not sufficient to develop dopaminergic neurodegeneration or to induce neuron death in transgenic rats.[57] Data obtained from a R1441C knockin mouse suggested that this mutation impairs stimulated dopamine neurotransmission and D2 receptor function. The R1441C mutation could represent pathogenic precursors preceding dopaminergic degeneration in PD brains.[53] A novel herpes simplex virus (HSV) amplicon-based mouse model of LRRK2 dopaminergic neurotoxicity was developed to determine the efficacy of several LRRK2 kinase inhibitors. Nonetheless, a significant loss of tyrosine hydroxylase-positive neurons was induced due to HSV amplicon-mediated delivery of LRRK2-G2019S, whereas the HSV amplicon-mediated delivery of LRRK2-D1994A caused no neuronal loss. The injection of the LRRK2 kinase inhibitors can attenuate the loss of tyrosine hydroxylase-positive neurons induced by HSV-G2019S. Thus, the inhibition of LRRK2 kinase activity may hold potential to protect against LRRK2 toxicity and consequently for the treatment of neurodegeneration in PD.[58] Hence, LRRK2 kinase inhibition holds potential for the treatment of PD. In the following, we will give a summary of small molecule LRRK2 kinase inhibitors. The inhibition effect of $ROCO^{LRRK2}$ fragments will not be discussed.[59]

SMALL MOLECULE KINASE INHIBITORS FOR LRRK2

LRRK2 is a large protein with several discrete domains. It surfaced as a therapeutic target when the kinase activity and the most common LRRK2 mutation, G2019S, were associated with neurotoxicity and PD. The first LRRK2 inhibitors derived from library screening efforts were mostly ATP-competitive. There are only few inhibitors, which were specifically developed to inhibit LRRK2. Thus, the majority of the compounds inhibits more than one kinase at the concentration indicated in the tables. The data in Table 1 derived from a limited number of in vitro assays using wild-type LRRK2 and G2019S-LRRK2. These assays vary in the concentration of LRRK2-constructs, substrate, and ATP; thus, the mere comparison of IC_{50} is misleading. The high sensitive assays utilize radioisotopes, which allow detection of both autophosphorylation and substrate phosphorylation, but are less suitable for high-throughput screening (HTS). High-throughput capability was achieved by time-resolved fluorescence resonance energy transfer (TF-FRET) and the amplified luminescent proximity homogeneous (AlphaScreen) assays.[62] Although truncated LRRK2 and its full-length analog display similar phosphorylation activity, differences have been noticed. This may be a

Table 2. Maleimide Derivatives as LRRK2 Inhibitors

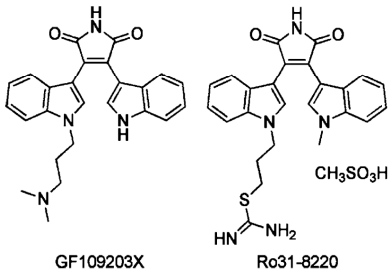

		IC50					
no.	name	wild-type LRRK2	LRRK2-G2019S	substrate	selectivity[a]	in vivo	lit.
5	GF109203X	2190 nM[b]	2620 nM[b]	MBP[c]	2		58
6	Ro31-8220	2671 nM;[d] 50 nM[b]	1922 nM;[d] 5160 nM[b]	LRRKtide; MBP[c]	2		58, 60

[a]Number of all kinases, including LRRK2. [b]GST-LRRK2 (wt/G2019S). [c]Myelin basic protein (MBP). [d]GST-LRRK2 (970-2527; wt/G2019S).

Table 3. 5-Iodotubericidin as LRRK2 Inhibitor

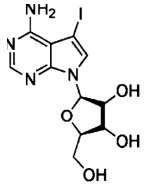

		IC50					
no.	name	wild-type LRRK2	LRRK2-G2019S	substrate	selectivity[a]	in vivo	lit.
7	5-iodo-tubericidin	14780 nM[b]	3410 nM[b]	MBP[c]	2		58

[a]Number of all kinases, including LRRK2. [b]GST-LRRK2 (wt/G2019S). [c]Myelin basic protein (MBP).

Table 4. Sorafenib as LRRK2 Inhibitor

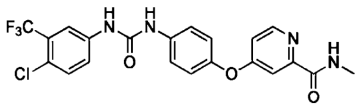

		IC50					
no.	name	wild-type LRRK2	LRRK2-G2019S	substrate	selectivity[a]	in vivo	lit.
8	sorafenib	5580 nM[b]	1230 nM[b]	MBP[c]	2	*C. elegans*; Drosophila	58

[a]Number of all kinases, including LRRK2. [b]GST-LRRK2 (wt/G2019S). [c]Myelin basic protein (MBP).

result from the utilization of different substrates, for example, LRRKtide and myelin basic protein (MBP).[60,63]

Staurosporine (**1**) is one of the widely used kinase inhibitors. This unselective compound equipotently inhibited both wild-type LRRK2 and LRRK2-G2019S (truncated and full-length) with an IC_{50} ranging from 0.2 to 40 nM (Table 1).[58,60−62] Its inhibitory effect concerning LRRK2 was determined in different in vitro assays, for example, radioactive, TF-FRET, and AlphaScreen assay. These assays utilized different substrates such as synthetic peptides, for example, LRRKtide and potential physiological substrates: GST-Moesin. Staurosporine (**1**) had a similar inhibitory profile against LRRK1/LRRK2 autophosphorylation and MBP phosphorylation.[58] Its isoindolinone derivatives K-252a/b (**2**/**3**) and Gö6976 (**4**) also inhibited wild-type LRRK2 and LRRK2-G2019S in the nanomolar range, whereas the maleimide analoga GF109203X (**5**) and Ro31-8220 (**6**) inhibited wild-type and LRRK2-G2019S in the low micromolar range only (Table 2).[58,60,61] Ro31-8220 (**6**) is remarkable for the potent inhibition of MBP phosphorylation with an IC_{50} of 50 nM in the TF-FRET assay.

The inhibitory potency of 5-Iodotubericidin (**7**) (Table 3) and Sorafenib (**8**) (Table 4) was more than 4-fold higher for LRRK2-G2019S compared to wild-type LRRK2.[58] Sorafenib (**8**) was up to 50% more selective for wild-type LRRK2 than for wild-type LRRK1. LRRK2-G2019S induced toxicity in rat primary cortical neuronal cultures (TUNEL assay) was completely protected by 5 μM of Sorafenib (**8**). Furthermore, it protected against LRRK2-G2019S-induced neurodegeneration in *C. elegans* and in Drosophila.[64]

The indolinones GW5074 (**9**) and Indirubin-3'-monoxime (**10**) were ~3-fold more active concerning LRRK2-G2019S than its corresponding wild-type. GW5074 (**9**) and Indirubin-3'-monoxime (**10**) inhibited LRRK2-G2019S with IC_{50}'s of 880 nM and ~1.3 μM, respectively.[58,61] They inhibited the closely related LRRK1 and LRRK2 in a similar manner. GW5074 (**9**) and Indirubin-3'-monoxime (**10**) inhibited LRRK2-mediated

Table 5. Indolinone Dervivatives as LRRK2 Inhibitors

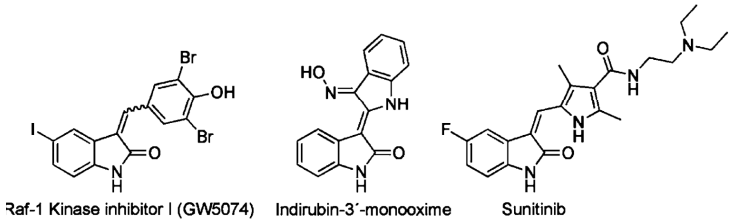

		IC$_{50}$					
no.	name	wild-type LRRK2	LRRK2-G2019S	substrate	selectivity[a]	in vivo	lit.
9	Raf-1 kinase inhibitor I (GW5074)	~500 nM;[b] 3150 nM[c]	880 nM[c]	LRRKtide; MBP[d]	2	HSV[g] amplicon-based mouse model	58, 61
10	Indirubin-3′-monooxime	4830 nM[c]	1310 nM[c]	MBP[d]	2	HSV[g] amplicon-based mouse model	58
11	Sunitinib	79 nM;[e] 15 nM[f]	19 nM;[e] 26 nM[f]	Nictide; LRRKtide	85		60, 63, 65

[a]Number of all kinases, including LRRK2. [b]Goat GST-LRRK2. [c]GST-LRRK2 (wt/G2019S). [d]Myelin basic protein (MBP). [e]GST-LRRK2 (1326–2527; wt/G2019S). [f]GST-LRRK2 (970–2527; wt/G2019S). [g]Herpes simplex virus.

Table 6. Quinoline Derivatives as LRRK2 Inhibitors

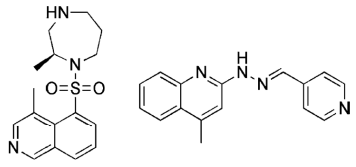

		IC$_{50}$					
no.	name	wild-type LRRK2	LRRK2-G2019S	substrate	selectivity[a]	in vivo	lit.
12	H-1152	244 nM[b]	600 nM;[c] 150 nM[b]	GST-Moesin; Nictide	85		62, 63, 65
13	Compound 4		4100 nM[d]		13		67

[a]Number of all kinases, including LRRK2. [b]GST-LRRK2 (1326-2527; wt/G2019S). [c]full-length Strep-tag LRRK2 (G2019S). [d]GST-LRRK2 (G2019S).

phosphorylation of LRRKtide and MBP, and additionally the phosphorylation of the eukaryotic translation initiation factor 4E-binding protein (4E-BPI), a putative physiological LRRK2 substrate. Furthermore, they attenuated LRRK2-G2019S induced cell injury and cell death. GW5074 (**9**) rescued the reduction of the density of tyrosine hydroxylase-positive fibers in a herpes simplex virus (HSV) amplicon-based mouse model of LRRK2 dopaminergic neurotoxicity. In addition, GW5074 (**9**) prevented LRRK2-G2019S induced inflammation, increase in isolectin B_4 (ILB4)-positive cells in the striatum and substantia nigra pairs compacta.[58] Both Sorafenib (**8**) and GW5074 (**9**) were found to protect against LRRK2-G2019S-induced neurodegeneration in *C. elegans* and in Drosophila.[64] The well-known kinase inhibitor Sunitinib (**11**) was also investigated concerning its ability to inhibit LRRK2 (Table 5). It inhibited the LRRK2-mediated phosphorylation of Nictide and LRRKtide with an IC$_{50}$ of 15–79 nM (truncated wild-type and LRRK2-G2019S).[60,63,65] The selectivity of Sunitinib (**11**) was profiled in a panel of 85 kinases. Sunitinib (**11**) inhibits LRRK2-G2019S, its wild-type, and 12 further kinases at 1 μM by more than 80%.[60,63,65] However, the less selective Sunitinib (**11**) is capable to suppress the activity of full-length LRRK2 expressed from Swiss-3T3 fibroblast cells.[63] The apparent potency of Sunitinib (**11**) to inhibit wild-type LRRK2 drops to an IC$_{50}$ of 370 nM at cellular ATP concentration (1 mM).[66] In addition, studies of endogenous LRRK2 activity and phosphorylation in EBV-transformed lymphoblastoid cells, derived from a PD patient harboring a homozygous LRRK2-G2019S mutation, revealed that Sunitinib (**11**) inhibited the phosphorylation of Ser^{910} and Ser^{935} more potently than in wild-type cells.[65] A comparable result was observed for the inhibitor H-1152 (**12**) (Table 6). H-1152 (**12**) is a known ROCK2 inhibitor. This compound was profiled in a panel of 85 kinases and found to inhibit Aurora B kinase, BRSK2, wild-type LRRK2, and LRRK2-G2019S at the relevant concentration. H-1152 (**12**) displayed IC$_{50}$'s ranging from 150 to 600 nM in radioisotope or AlphaScreen phosphorylation assays of wild-type LRRK2 and LRRK2-G2019S. Unfortunately, the structure determination of the LRRK2 kinase domain by X-ray crystallography was not reported yet. A docking analysis of H-1152 (**12**) utilized homology modeling of LRRK2, by superimposing the protein C_α atoms of the LRRK2 model with the reported ROCK1-H-1152 complex. This analysis indicated a backbone interaction with the NH atom of Ala^{1950} (PDB code of ROCK1-H-1152 not published). Furthermore, the two methyl groups of H-1152 (**12**) were observed to make lipophilic contacts with the ATP binding site. The amino acid Ala^{2016} was found to be close to H-1152 (**12**). This can

Table 7. Y-27632 as LRRK2 Inhibitor

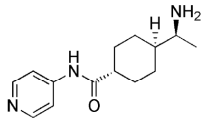

no.	name	IC_{50} wild-type LRRK2	IC_{50} LRRK2-G2019S	substrate	selectivity[a]	in vivo	lit.
14	Y-27632	2300 nM[b]	1800 nM;[c] 1000 nM[b]	GST-Moesin; Nictide	85		62, 63

[a]Number of all kinases, including LRRK2. [b]GST-LRRK2 (1326-2527; wt/G2019S). [c]Full-length Strep-tag LRRK2 (G2019S).

Table 8. Anthracene and Phenanthrene Derivatives as LRRK2 Inhibitors

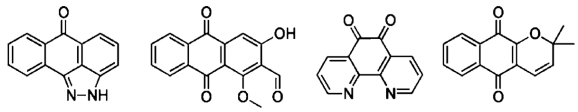

no.	name	IC_{50} wild-type LRRK2	IC_{50} LRRK2-G2019S	substrate	substrate selectivity[a]	in vivo	lit.
15	SP600125	3100 nM[b]	5000 nM[b]	MBP[c]	2		58
16	Damnacanthal	7810 nM[b]	9450 nM[b]	MBP[c]	2		58
17	LDN-73794	3500 nM[d]		PLK-peptide	2		68
18	LDN-22684[e]	6900 nM[f]	6100 nM[f]	PLK-peptide			69

[a]Number of all kinases, including LRRK2. [b]GST-LRRK2 (wt/G2019S). [c]Myelin basic protein (MBP). [d]Purified from BAC-transgenic mouse brain. [e]Non-ATP competitive. [f]Human LRRK2 (970-2527; wt/G2019S).

Table 9. Pyrimidine Derivatives as LRRK2 Inhibitors

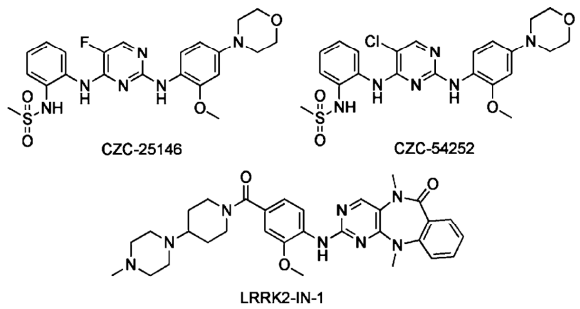

no.	name	IC_{50} wild-type LRRK2	IC_{50} LRRK2-G2019S	substrate	selectivity[a]	in vivo	lit.
19	CZC-25146	4.76 nM[b]	6.87 nM[b]	LRRKtide	LRRKtide	male CD-1 mice	71
20	CZC-54252	1.28 nM[b]	1.85 nM[b]	LRRKtide	LRRKtide	male CD-1 mice	71
21	LRRK2-IN-1	13 nM[c]	6 nM[c]	Nictide	Nictide	Male C57BL/6 mice	70

[a]Number of all kinases, including LRRK2. [b]Human LRRK2 (wt/G2019S). [c]GST-LRRK2 (1326−2527; wt/G2019S).

contribute to crucial drug resistance, because the IC_{50} of H-1152 (**12**) for the LRRK2 mutant A2016T increased up to ~30-fold.[63] Another commercially available quinoline derivative, Compound 4 (**13**), inhibited the autophosphorylation of LRRK2-G2019S with an IC_{50} of 4.1 μM (Table 6). It was screened in a small kinase panel of 13 kinases at 10 μM concentration. There was no other inhibitory effect, except for MLK1.[67] This observation can be rationalized by the similarity of the kinase domains of MLK and LRRK2. Compound 4 (**13**) was analyzed in a homology model of LRRK2 using the structure of the transforming growth factor-beta (TGF-β) activated kinase 1 (TAK1; PDB code: 2EVA). This homology model of the LRRK2 kinase domain with inhibitor Compound 4 (**13**) indicated hydrogen bond interactions between Compound 4 (**13**) and Ala^{1950}. It was found that the 4-pyridine ring was located in the solvent exposed region of LRRK2. Moreover, a comparison of ATP and Compound 4 (**13**) docking revealed that the 4-methyl quinoline moiety overlapped with the adenine rings of ATP. The treatment of murine dopaminergic SN4741 cells with 10 μM of Compound 4 (**13**) restored their cell survival rates in an oxidative stress-induced test to the level of the control cells. The neurotoxicity test with primary rat cortical neuronal cells revealed cell survival rates of 85% at 10 μM and a significantly increased toxicity at 100 μM.[67] In a kinase panel of 85 kinases the known ROCK inhibitor Y-27632 (**14**) was found to additionally inhibit PRK2,

Table 10. Pharmocokinetic Profile of the Currently Best Published LRRK2 inhibitors CZC-25146 and LRRK2-IN-1[a]

name	route	dose (mg/kg)	T_{max} (h)	C_{max} (ng/mL)	$AUC_{0-\infty}$ (h·ng/mL)	$T_{1/2}$ (h)	CL (mL/min/kg)	V_{ss} (L/kg)	F (%)	BBB penetration (%)	lit.
CZC-25146 (male CD-1 mice)	IV	1	0	154	419–434	1.6	2.3	5.4		4	71
	PO	5	0.25	1357	2878–2894	1			133		
LRRK2-IN-1 (male C57BL/6 mice)	IV	1			2974	4.47	5.6	1.71		not efficiently	70
	PO	10	1.0	1618	14758				49.3		

[a]IV = intravenous injection; PO = oral delivery; T_{max} = time of maximum plasma concentration; C_{max} = maximum plasma concentration; $AUC_{0-\infty}$ = area under the curve (measure of exposure); $T_{1/2}$ = half life; CL = plasma clearance; V_{ss} = volume of distribution; F = oral bioavailability; BBB = blood-brain barrier.

MNK1, wild-type LRRK2 and LRRK2-G2019S at 10 μM (Table 7). Y-27632 (**14**) inhibited truncated LRRK2-G2019S with an IC_{50} of 1 μM in a radioisotope assay. Furthermore, the full-length Strep-tag LRRK2-G2019S was inhibited with an IC_{50} of 1.8 μM in an AlphaScreen assay.[62,63] The anthracene and phenanthrene derivatives SP60012 (**15**), Damnacanthal (**16**), LDN-73794 (**17**), and LDN-22684 (**18**) inhibited LRRK2-G2019S and wild-type LRRK2 in the low micromolar range (Table 8).[58,68,69] LDN-73794 (**17**) was confirmed to be ATP competitive, whereas LDN-22684 (**18**) was found to be a non-ATP competitive inhibitor. Further studies revealed LDN-22684 (**18**) to be neither GTP competitive nor substrate competitive. Hence, it was deduced that LDN-22684 (**18**) is an allosteric LRRK2 inhibitor.[68,69] Three compounds were especially developed to inhibit LRRK2, namely, CZC-25146 (**19**), CZC-54252 (**20**), and LRRK2-IN-1 (**21**) (Table 9).[70,71] CZC-25146 (**19**) and CZC-54252 (**20**) inhibited the activity of recombinant human wild-type LRRK2 with an IC_{50} ranging from ~1 to ~5 nM. The G2019S mutant was inhibited with an IC_{50} ranging from ~2 to ~7 nM in a TF-FRET assay. In addition, they were screened against a kinase panel of 185 kinases and exhibited good selectivity. CZC-25146 (**19**) inhibited five other kinases, PLK4, GAK, TNK1, CAMKK2, and PIP4K2C, with high potency only, but none of them have been classified as predictors of genotoxicity or hematopoietic toxicity.[72,73] Furthermore, it prevents mutant LRRK2-induced injury of cultured rodent and human neurons with mid-nanomolar potency. In vivo pharmacology established a volume of distribution of 5.4 L/kg and a clearance of 2.3 L/h/kg for CZC-25146 (**19**). Unfortunately, it exhibited a poor brain penetration of just 4% (Table 10).[71]

A HTS and subsequent lead optimization provided the LRRK2 inhibitor LRRK2-IN-1 (**21**). It inhibited both truncated wild-type LRRK2 and LRRK2-G2019S with IC_{50} values of 13 and 6 nM, but LRRK2-A2016T and LRRK2-A2016T+G2019S mutants were found to be ~400-fold more resistant to LRRK2-IN-1 (**21**) (Table 9).[70] This was explained by a molecular docking study of LRRK2-IN-1 (**21**) bound to a homology model of LRRK2 (A2016T), which revealed an unfavorable steric interaction as observed for H-1152 (**12**). The confirmed reversible ATP competitive inhibitor LRRK2-IN-1 (**21**) was selective in kinase panels containing more than 470 kinases. Surprisingly, under the same conditions as employed for LRRK2, LRRK2-IN-1 lacked inhibition of LRRK1. The kinase panels revealed additional inhibition of DCLK1, DCLK2, as well as MAPK7 and supported IC_{50}'s of greater than 1 μM for AURKB, CHEK2, MKNK2, MYLK (smMLCK), NUAK1, PLK1, and RPS6KA2. LRRK2-IN-1 (**21**) induced a similar dose-dependent Ser^{910} and Ser^{935} dephosphorylation and loss of 14–3–3 binding to endogenous LRRK2 in human-derived neuroblastoma SHSY5Y cells and mouse Swiss3T3 cells. Pharmacokinetic studies of LRRK2-IN-1 (**21**) revealed a half-life of 4.5 h and a bioavailability of 49.3% in mice (Table 10). An insufficient blood-brain barrier (BBB) permeation was concluded from the LRRK2 phosphorylation status in the kidney versus brain, which imposes limits on this "useful first-generation 'tool'".[70]

So far, just a small number of LRRK2 inhibitors have been synthesized and profiled in kinase panels. The best of the reported compounds display both high activity and selectivity. However, these reported best-in-class compounds do not pass the BBB efficiently, which limits their potential in animal models of PD. Maybe the patent literature holds additional treasures, waiting to be released.[74–79]

■ CONCLUSION AND PERSPECTIVES

The importance of the G2019S mutation in the kinase domain of LRRK2 derives from the association with the second most common neurodegenerative disease: Parkinson's disease. The late-onset sporadic classical PD affects almost 2% of the world population over 65 years of age.[80] The availability of suitable HTS assay formats such as TF-FRET or AlphaScreen provided first inhibitors of LRRK2 activity with moderate selectivity. Lead optimization resulted in first generation tools and second-generation inhibitors, which displayed promising pharmacokinetic properties, but are limited by insufficient brain uptake or brain activity. The increase in patent applications (e.g., Glaxo Group Limited and Cellzome Limited) indicates a target on the rise. TTT-3002, a drug candidate of TauTaTis, exhibited good results in LRRK2 inhibition. A phase I clinical trial of TTT-3002 is expected to start in 2011.[74–79,81]

The clinical development of LRRK2 inhibitors is impaired by the lack of public data of relevant pharmacology, biology, and even biomarkers. Moreover, the gain of function in LRRK2 mutations may require fundamentally different dosing regimes for mutation carriers versus other PD patients resulting in personalized medicine. This dosage may very up to 100-fold, implying genomic profiling, patient stratification and a wide therapeutic window. Several in vivo invertebrate models indicate neurotoxic hyperactivity of LRRK2 kinase, but the number of LRRK2 kinase activity studies in mouse models is rather limited. New LRRK2 animal models may provide essential information for target validation and suitable biomarkers for end point identification in drug development. Passage of the blood-brain barrier remains a challenge, yet LRRK2 function may be important outside the CNS. Moreover, the consequences of LRRK2 inhibition are not sufficiently established in animal models or humans to conclude a safe inhibition rate in mutation carriers or normal PD patients nor to rule out therapy resistance in gain of function mutations.

Furthermore, just a small number of substrates has been reported to date and this may increase. Hence, an effective and safe inhibition of LRRK2 kinase activity has yet to be confirmed in vivo, in vitro. Any novel therapy must be evaluated against established PD therapies, which results in either extended or large clinical trials. A robust and approved biomarker may enable shorter or smaller trials; however, this may take years to develop and to gain approval.[82−84] Recently, the LRRK-2 phosphorylation sites Ser^{910}, Ser^{935}, Ser^{955}, and Ser^{973} were suggested as biomarkers for LRRK2 because the treatment of LRRK2 expressing cells with LRRK2-IN-1 (**21**) revealed these phosphorylations to be disrupted. However, the kinases and phosphatases responsible for the regulation of these phosphorylation sites have yet to be identified.[85]

Type-I-kinase inhibitors are notorious for their selectivity problems, which frequently cause adverse events in humans. In addition, drug resistance or diminished activity has been observed, which may be caused by kinase domain mutations. LRRK2 features many mutations, which imposes problems to find a useful drug candidate.[63,70] A new generation of kinase inhibitors, called type-II-inhibitors, may reduce some of these problems.[86,87] They bind to the ATP site and extend into an adjacent allosteric site. This allosteric site is not as highly conserved as the ATP binding site and may provide a strategy to obtain improved selectivity. LRRK2 is a particularly challenging target: the G2019S gain of function mutation requires very efficient inhibition to reduce the activity to the wild-type level. The lack of brain permeable inhibitors leaves an open fundamental question: how much G2019S LRRK2 inhibition is required in vivo? In summary, it can be stated that LRRK2 inhibition provides potential to treat PD, albeit further research and clarification is inevitable.

■ AUTHOR INFORMATION

Corresponding Author

*Fax: +496151-163278. Telephone: +496151-164531. E-mail: schmidt_boris@t-online.de.

Author Contributions

†These authors contributed equally to this work.

Funding

This work was supported by the Technische Universität Darmstadt.

Notes

The authors declare no competing financial interest.

■ REFERENCES

(1) Ross, O. A., and Farrer, M. J. (2005) Pathophysiology, pleiotrophy and paradigm shifts: genetic lessons from Parkinson's disease. *Biochem. Soc. Trans. 33*, 586−590.

(2) Davie, C. A. (2008) A review of Parkinson's disease. *Br. Med. Bull. 86*, 109−127.

(3) Jankovic, J. (2008) Parkinson's disease: clinical features and diagnosis. *J. Neurol. Neurosurg. Psychiatry 79*, 368−376.

(4) Clarke, C. E. (2007) Parkinson's disease. *BMJ - Clin. Rev. 335*, 441−445.

(5) Zimprich, A., Biskup, S., Leitner, P., Lichtner, P., Farrer, M., Lincoln, S., Kachergus, J., Hulihan, M., Uitti, R. J., Calne, D. B., Stoessl, A. J., Pfeiffer, R. F., Patenge, N., Carbajal, I. C., Vieregge, P., Asmus, F., Müller-Myhsok, B., Dickson, D. W., Meitinger, T., Strom, T. M., Wszolek, Z. K., and Gasser, T. (2004) Mutations in LRRK2 cause autosomal-dominant parkinsonism with pleomorphic pathology. *Neuron 44*, 601−607.

(6) Berwick, D. C., and Harvey, K. (2011) LRRK2 signaling pathways: the key to unlocking neurodegeneration? *Trends Cell Biol. 21*, 257−265.

(7) Smith, K. (2010) Treatment frontiers. *Nature - Parkinson's Disease Outlook 466*, 15−18.

(8) Poewe, W. (2006) The natural history of Parkinson's disease. *J. Neurol. 253*, VII/2−VII/6.

(9) Duty, S. (2010) Therapeutic potential of targeting group III metabotropic glutamate receptors in the treatment of Parkinson's disease. *Br. J. Pharmacol. 161*, 271−287.

(10) Niswender, C. M., and Conn, P. J. (2010) Metabotropic glutamate receptors: physiology, pharmacology, and disease. *Annu. Rev. Pharmacol. Toxicol. 50*, 295−322.

(11) Paisán-Ruíz, C., Jain, S., Evans, E. W., Gilks, W. P., Simón, J., van der Brug, M., López de Munain, A., Aparicio, S., Martínez Gil, A., Khan, N., Johnson, J., Martinez, J. R., Nicholl, D., Carrera, I. M., Pena, A. S., de Silva, R., Lees, A., Martí-Massó, J. F., Pérez-Tur, J., Wood, N. W., and Singleton, A. B. (2004) Cloning of the gene containing mutations that cause PARK8-linked Parkinson's disease. *Neuron 44*, 595−600.

(12) Valente, E. M., Abou-Sleiman, P. M., Caputo, V., Muqit, M. M. K., Harvey, K., Gispert, S., Ali, Z., Del Turco, D., Bentivoglio, A. R., Healy, D. G., Albanese, A., Nussbaum, R., González-Maldonado, R., Deller, T., Salvi, S., Cortelli, P., Gilks, W. P., Latchman, D. S., Harvey, R. J., Dallapiccola, B., Auburger, G., and Wood, N. W. (2004) Hereditary early-onset Parkinson's disease caused by mutations in PINK1. *Science 304*, 1158−1160.

(13) Bonifati, V., Rizzu, P., van Baren, M. J., Schaap, O., Breedveld, G. J., Krieger, E., Dekker, M. C. J., Squitieri, F., Ibanez, P., Joosse, M., van Dongen, J. W., Vanacore, N., van Swieten, J. C., Brice, A., Meco, G., van Duijn, C. M., Oostra, B. A., and Heutink, P. (2003) Mutations in the DJ-1 gene associated with autosomal recessive early-onset parkinsonism. *Science 299*, 256−259.

(14) Kitada, T., Asakawa, S., Hattori, N., Matsumine, H., Yamamura, Y., Minoshima, S., Yokochi, M., Mizuno, Y., and Shimizu, N. (1998) Mutations in the parkin gene cause autosomal recessive juvenile parkinsonism. *Nature 392*, 605−608.

(15) Tan, E. K., and Schapire, A. H. (2011) LRRK2 as a therapeutic target in Parkinson's disease. *Eur. J. Neurol. 18*, 545−546.

(16) Deng, J., Lewis, P. A., Greggio, E., Sluch, E., Beilina, A., and Cookson, M. R. (2008) Structure of the ROC domain from the Parkinson's disease-associated leucine-rich repeat kinase 2 reveals a dimeric GTPase. *Proc. Natl. Acad. Sci. U.S.A. 105*, 1499−1504.

(17) Giasson, B. I., and Van Deerlin, V. M. (2008) Mutations in LRRK2 as a cause of Parkinson's disease. *Neurosignals 16*, 99−105.

(18) Mata, I. F., Wedemeyer, W. J., Farrer, M. J., Taylor, J. P., and Gallo, K. A. (2006) LRRK2 in Parkinson's disease: protein domains and functional insights. *Trends Neurosci. 29*, 286−293.

(19) Gloeckner, C. J., Kinkl, N., Schumacher, A., Braun, R. J., ÓNeill, E., Meitinger, T., Kolch, W., Prokisch, H., and Ueffing, M. (2006) The Parkinson disease causing LRRK2 mutation I2020T is associated with increased kinase activity. *Hum. Mol. Genet. 15*, 223−232.

(20) Li, X., Tan, Y., Poulose, S., Olanow, C. W., Huang, X., and Yue, Z. (2007) Leucine-rich repeat kinase 2 (LRRK2)/PARK8 possesses GTPase activity that is altered in familial Parkinson's disease R1441C/G mutants. *J. Neurochem. 103*, 238−247.

(21) Biskup, S., Moore, D. J., Celsi, F., Higashi, S., West, A. B., Andrabi, S. A., Kurkinen, K., Yu, S., Savitt, J. M., Waldvogel, H. J., Faull, R. L. M., Emson, P. C., Torp, R., Ottersen, O. P., Dawson, T. M., and Dawson, V. L. (2006) Localization of LRRK2 to membranous and vesicular structures in mammalian brain. *Ann. Neurol. 60*, 557−569.

(22) Giasson, B. I., Covy, J. P., Bonini, N. M., Hurtig, H. I., Farrer, M. J., Trojanowski, J. Q., and Van Deerlin, V. M. (2006) Biochemical and pathological characterization of Lrrk2. *Ann. Neurol. 59*, 315−322.

(23) Jaleel, M., Nichols, R. J., Deak, M., Campbell, D. G., Gillardon, F., Knebel, A., and Alessi, D. R. (2007) LRRK2 phosphorylates moesin at threonine-558: characterization of how Parkinson's disease mutants affect kinase activity. *Biochem. J. 405*, 307−317.

(24) Li, T., Yang, D., Sushchky, S., Liu, Z., and Smith, W. (2011) Models for LRRK2-Linked Parkinsonism. *Parkinson's Dis. 2011*, 1−16.
(25) Berger, Z., Smith, K. A., and La Voie, M. J. (2010) Membrane localization of LRRK2 is associated with increased formation of the highly active LRRK2 dimer and changes in its phosphorylation. *Biochemistry 49*, 5511−5523.
(26) Greggio, E., Zambrano, I., Kaganovich, A., Beilina, A., Taymans, J., Daniels, V., Lewis, P., Jain, S., Ding, J., Syed, A., Thomas, K. J., Baekelandt, V., and Cookson, M. R. (2008) The Parkinson disease-associated leucine-rich repeat kinase 2 (LRRK2) is a dimer that undergoes intramolecular autophosphorylation. *J. Biol. Chem. 283*, 16906−16914.
(27) Taylor, J. P., Mata, I. F., and Farrer, M., J. (2006) LRRK2: a common pathway for parkinsonism, pathogenesis and prevention? *Trends Mol. Med. 12*, 76−82.
(28) Seol, W. (2010) Biochemical and molecular features of LRRK2 and its pathophysiological roles in Parkinson's disease. *BMB Rep. 43*, 233−244.
(29) Cookson, M. R. (2010) The role of leucine-rich repeat kinase 2 (LRRK2) in Parkinson's disease. *Nat. Rev. Neurosci. 11*, 791−797.
(30) West, A. B., Moore, D. J., Biskup, S., Bugayenko, A., Smith, W. W., Ross, C. A., Dawson, V. L., and Dawson, T. M. (2005) Parkinson's disease-associated mutations in leucine-rich repeat kinase 2 augment kinase activity. *Proc. Natl. Acad. Sci. U.S.A. 102*, 16842−16847.
(31) West, A. B., Moore, D. J., Choi, C., Andrabi, S. A., Li, X., Dikeman, D., Biskup, S., Zhang, Z., Lim, K., Dawson, V. L., and Dawson, T. M. (2007) Parkinson's disease-associated mutations in LRRK2 link enhanced GTP-binding and kinase activities to neuronal toxicity. *Hum. Mol. Genet. 16*, 223−232.
(32) Xiong, Y., Coombes, C. E., Kilaru, A., Li, X., Gitler, A. D., Bowers, W. J., Dawson, V. L., Dawson, T. M., and Moore, D. J. (2010) GTPase activity plays a key role in the pathobiology of LRRK2. *PLoS Genet. 6*, e1000902.
(33) Webber, P. J., Smith, A. D., Sen, S., Renfrow, M. B., Mobley, J. A., and West, A. B. (2011) Autophosphorylation in the Leucine-Rich Repeat Kinase 2 (LRRK2) GTPase Domain Modifies Kinase and GTP-Binding Activities. *J. Mol. Biol. 412*, 94−100.
(34) Lin, C., Tsai, P., Wu, R., and Chien, C. (2010) LRRK2 G2019S mutation induces dendrite degeneration through mislocalization and phosphorylation of tau by recruiting autoactivated GSK3ß. *J. Neurosci. 30*, 13138−13149.
(35) Dusonchet, J., Kochubey, O., Stafa, K., Yound, S. M. Jr, Zufferey, R., Moore, D. J., Schneider, B. L., and Aebischer, P. (2011) A rat model of progressive nigral neurodegeneration induced by the Parkinson's disease-associated G2019S mutation in LRRK2. *J. Neurosci. 31*, 907−912.
(36) Greggio, E., Jain, S., Kingsbury, A., Bandopadhyay, R., Lewis, P., Kaganovich, A., van der Brug, M. P., Belina, A., Blackinton, J., Thomas, K. J., Ahmad, R., Miller, D. W., Kesavapany, S., Singleton, A., Lees, A., Harvey, R. J., Harvey, K., and Cookson, M. R. (2006) Kinase activity is required for the toxic effects of mutant LRRK2/dardarin. *Neurobiol. Dis. 23*, 329−341.
(37) Hsu, C. H., Chan, D., Greggio, E., Saha, S., Guillily, M. D., Ferree, A., Raghavan, K., Shen, G. C., Segal, L., Ryu, H., Cookson, M. R., and Wolozin, B. (2010) MKK6 binds and regulates expression of Parkinson's disease-related protein LRRK2. *J. Neurochem. 112*, 1593−1604.
(38) Gloeckner, C. J., Schumacher, A., Boldt, K., and Uefffing, M. (2009) The Parkinson disease-associated protein kinase LRRK2 exhibits MAPKKK activity and phosphorylates MKK3/6 and MKK4/7, in vitro. *J. Neurochem. 109*, 959−968.
(39) Lee, S. B., Kim, W., Lee, S., and Chung, J. (2007) Loss of LRRK2/PARK8 induces degeneration of dopaminergic neurons in Drosophila. *Biochem. Biophys. Res. Commun. 358*, 534−539.
(40) Ng, C., Mok, S. Z. S., Koh, C., Ouyang, X., Fivaz, M. L., Tan, E., Dawson, V. L., Dawson, T. M., Yu, F., and Lim, K. (2009) Parkin protects against LRRK2 G2019S mutant-induced dopaminergic neurodegeneration in Drosophila. *J. Neurosci. 29*, 11257−11262.
(41) Liu, Z., Wang, X., Yu, Y., Li, X., Wang, T., Jiang, H., Ren, Q., Jiao, Y., Sawa, A., Moran, T., Ross, C. A., Montell, C., and Smith, W. W. (2008) A Drosophila model for LRRK2-linked parkinsonism. *Proc. Natl. Acad. Sci. U.S.A. 105*, 2693−2698.
(42) Smith, W. W. (2010) Leucine-rich kinase 2 (LRRK2) Drosophila Model For Parkinsońs Disease: Wildtype1 (WT1) and G2019S Mutant Flies. U.S. 2010/0175140 A1.
(43) Yao, C., El Khoury, R., Wang, W., Byrd, T. A., Pehek, E. A., Thacker, C., Zhu, X., Smith, M. A., Wilson-Delfosse, A. L., and Chen, S. G. (2010) LRRK2-mediated neurodegeneration and dysfunction of dopaminergic neurons in a Caenorhabditis elegans model of Parkinson's disease. *Neurobiol. Dis. 40*, 73−81.
(44) Sheng, D., Qu, D., Kwok, K. H. H., Ng, S. S., Lim, A. Y. M., Aw, S. S., Lee, C. W. H., Sung, W. K., Lufkin, T., Jesuthasan, S., Sinnakaruppan, M., and Liu, J. (2010) Deletion of the WD40 domain of LRRK2 in Zebrafish causes Parkinsonism-like loss of neurons and locomotive defect. *PLoS Genet. 6*, e1000914.
(45) Ren, G., Xin, S., Zhong, H., and Lin, S (2011) Disruption of LRRK2 does not cause specific loss of dopaminergic neurons in zebrafish. *PLoS Genet. 6*, e20630.
(46) Lin, X., Parisiadou, L., Gu, X., Wang, L., Shim, H., Sun, L., Xie, C., Long, C., Yang, W., Ding, J., Chen, Z. Z., Gallant, P. E., Tao-Cheng, J., Rudow, G., Troncoso, J. C., Liu, Z., Li, Z., and Cai, H. (2009) Leucine-rich repeat kinase 2 regulates the progression of neuropathology induced by Parkinson's-disease-related mutant alpha-synuclein. *Neuron 64*, 807−827.
(47) Li, X., Patel, J. C., Wang, J., Avshalumov, M. V., Nicholson, C., Buxbaum, J. D., Elder, G. A., Rice, M. E., and Yue, Z. (2010) Enhanced striatal dopamine transmission and motor performance with LRRK2 overexpression in mice is eliminated by familial Parkinson's disease mutation G2019S. *J. Neurosci. 30*, 1788−1797.
(48) Li, Y., Liu, W., Oo, T. F., Wang, L., Tang, Y., Jackson-Lewis, V., Zhou, C., Geghman, K., Bogdanov, M., Przedborski, S., Beal, M. F., Burke, R. E., and Li, C. (2009) Mutant LRRK2(R1441G) BAC transgenic mice recapitulate cardinal features of Parkinson's disease. *Nat. Neurosci. 12*, 826−828.
(49) Andreas-Mateos, E., Mejias, R., Sasaki, M., Li, X., Lin, B. M., Biskup, S., Zhang, L., Banerjee, R., Thomas, B., Yang, L., Liu, G., Beal, M. F., Huso, D. L., Dawson, T. M., and Dawson, V. L. (2009) Unexpected lack of hypersensitivity in LRRK2 knock-out mice to MPTP (1-methyl-4-phenyl-1,2,3,6-tetrahydropyridine). *J. Neurosci. 29*, 15846−15850.
(50) Ramonet, D., Daher, J. P. L, Lin, B. M., Stafa, K., Kim, J., Banerjee, R., Westerlund, M., Pletnikova, O., Glauser, L., Yang, L., Liu, Y., Swing, D. A., Beal, M. F., Troncoso, J. C., McCaffery, J. M., Jenkins, N. A., Copeland, N. G., Galter, D., Thomas, B., Lee, M. K., Dawson, T. M., Dawson, V. L., and Moore, D. J. (2011) Dopaminergic neuronal loss, reduced neurite complexity and autophagic abnormalities in transgenic mice expressing G2019S mutant LRRK2. *PloS ONE 6*, e18568.
(51) Melrose, H. L., Dächsel, J. C., Behrouz, B., Lincoln, S. J., Yue, M., Hinkle, K. M., Kent, C. B., Korvatska, E., Taylor, J. P., Witten, L., Liang, Y. Q., Beevers, J. E., Boules, M., Dugger, B. N., Serna, V. A., Gaukhman, A., Yu, X., Castanedes-Casey, M., Braithwaite, A. T., Ogholikhan, S., Yu, N., Bass, D., Tyndall, G., Schellenberg, G. D., Dickson, D. W., Janus, C., and Farrer, M. J. (2010) Impaired dopaminergic neurotransmission and microtubule-associated protein tau alterations in human LRRK2 transgenic mice. *Neurobiol. Dis. 40*, 503−517.
(52) Melrose, H. L., Kent, C. B., Taylor, J. P., Dachsel, J. C., Hinkle, K. M., Lincoln, S. J., Mok, S. S., Culvenor, J. G., Masters, C. L., Tyndall, G. M., Bass, D. I., Ahmed, Z., Andorfer, C. A., Ross, O. A., Wszolek, Z. K., Delldonne, A., Dickson, D. W., and Farrer, M. J. (2007) A comparative analysis of leucine-rich repeat kinase 2 (Lrrk2) expression in mouse brain and Lewy body disease. *Neuroscience 147*, 1047−1058.
(53) Tong, Y., Pisani, A., Martella, G., Karouani, M., Yamaguchi, H., Pothos, E. N., and Shen, J. (2009) R1441C mutation in LRRK2

impairs dopaminergic neurotransmission in mice. *Proc. Natl. Acad. Sci. U.S.A. 106*, 14622−14627.
(54) Tong, Y., Yamaguchi, H., Giaime, E., Boyle, S., Kopan, R., Kelleher, R. J. III, and Shen, J. (2010) Loss of leucine-rich repeat kinase 2 causes impairment of protein degradation pathways, accumulation of alpha-synuclein, and apoptotic cell death in aged mice. *Proc. Natl. Acad. Sci. U.S.A. 107*, 9879−9884.
(55) Wang, L., Xie, C., Greggio, E., Parisiadou, L., Shim, H., Sun, L., Chandran, J., Lin, X., Lai, C., Yang, W., Moore, D. J., Dawson, T. M., Dawson, V. L., Chiosis, G., Cookson, M. R., and Cai, H. (2008) The chaperone activity of heat shock protein 90 is critical for maintaining the stability of leucine-rich repeat kinase 2. *J. Neurosci. 28*, 3384−3391.
(56) Winner, B., Melrose, H. L., Zhao, C., Hinkle, K. M., Yue, M., Kent, C., Braithwaite, A. T., Ogholikhan, S., Aigner, R., Winkler, J., Farrer, M. J., and Gage, F. H. (2011) Adult neurogenesis and neurite outgrowth are impaired in LRRK2 G2019S mice. *Neurobiol. Dis. 41*, 706−716.
(57) Zhou, H., Huang, C., Tong, J., Hong, W. C., Liu, Y., and Xia, X. (2011) Temporal expression of mutant LRRK2 in adult rats impairs dopamine reuptake. *Int. J. Biol. Sci. 7*, 753−761.
(58) Lee, B. D., Shin, J., VanKampen, J., Petrucelli, L., West, A. B., Ko, H. S., Lee, Y., Maguire-Zeiss, K. A., Bowers, W. J., Federoff, H. J., Dawson, V. L., and Dawson, T. M. (2010) Inhibitors of leucine-rich repeat kinase-2 protect against models of Parkinson's disease. *Nat. Med. 16*, 998−1000.
(59) Klein, C. L., Rovelli, G., Springer, W., Schall, C., Gasser, T., and Kahle, P. J. (2009) Homo- and heterodimerization of ROCO kinases: LRRK2 kinase inhibition by the LRRK2 ROCO fragment. *J. Neurochem. 111*, 703−715.
(60) Anand, V. S., Reichling, L. J., Lipinski, K., Stochaj, W., Duan, W., Kelleher, K., Pungaliya, P., Brown, E. L., Reinhart, P. H., Somber, R., Hirst, W., Riddle, S. M., and Braithwaite, S. P. (2009) Investigation of leucine-rich repeat kinase 2: enzymological properties and novel assays. *FEBS J. 276*, 466−478.
(61) Covy, J. P., and Giasson, B. I. (2009) Identification of compounds that inhibit the kinase activity of leucine-rich repeat kinase 2. *Biochem. Biophys. Res. Commun. 378*, 473−477.
(62) Pedro, L., Padrós, J., Beaudet, L., Schubert, H.-D., Gillardon, F., and Dahan, S. (2010) Development of a high-throughput AlphaScreen assay measuring full-length LRRK2(G2019S) kinase activity using moesin protein substrate. *Anal. Biochem. 404*, 45−51.
(63) Nichols, R. J., Dzamko, N., Hutti, J. E., Cantley, L. C., Deak, M., Moran, J., Bamborough, P., Reith, A. D., and Alessi, D. R. (2009) Substrate specificity and inhibitors of LRRK2, a protein kinase mutated in Parkinson's disease. *Biochem. J. 424*, 47−60.
(64) Liu, Z., Hamamichi, S., Lee, B. D., Yang, D., Ray, A., Caldwell, G. A., Caldwell, K. A., Dawson, T. M., Smith, W. W., and Dawson, V. L. (2011) Inhibitors of LRRK2 kinase attenuate neurodegeneration and Parkinson-like phenotypes in Caenorhabditis elegans and Drosophila Parkinson's disease models. *Hum. Mol. Genet. 20*, 3933−3942.
(65) Dzamko, N., Deak, M., Hentati, F., Reith, A. D., Prescott, A. R., Alessi, D. R., and Nichols, R. J. (2010) Inhibition of LRRK2 kinase activity leads to dephosphorylation of Ser(910)/Ser(935), disruption of 14−3-3 binding and altered cytoplasmic localization. *Biochem. J. 430*, 405−413.
(66) Reichling, L. J., and Riddle, S. M. (2009) Leucine-rich repeat kinase 2 mutants I2020T and G2019S exhibit altered kinase inhibitor sensitivity. *Biochem. Biophys. Res. Commun. 384*, 255−258.
(67) Yun, H., Heo, H. Y., Kim, H. H., DooKim, N., and Seol, W. (2011) Identification of chemicals to inhibit the kinase activity of leucine-rich repeat kinase 2 (LRRK2), a Parkinson's disease-associated protein. *Bioorg. Med. Chem. Lett. 21*, 2953−2957.
(68) Liu, M., Dobson, B., Glicksman, M. A., Yue, Z., and Stein, R. L. (2010) Kinetic mechanistic studies of wild-type leucine-rich repeat kinase 2: characterization of the kinase and GTPase activities. *Biochemistry 49*, 2008−2017.
(69) Liu, M., Poulose, S., Schuman, E., Zaitsev, A. D., Dobson, B., Auerbach, K., Seyb, K., Cuny, G. D., Glicksman, M. A., Stein, R. L., and Yue, Z. (2010) Development of a mechanism-based high-throughput screen assay for leucine-rich repeat kinase 2--discovery of LRRK2 inhibitors. *Anal. Biochem. 404*, 186−192.
(70) Deng, X., Dzamko, N., Prescott, A., Davies, P., Liu, Q., Yang, Q., Lee, J.-D., Patricelli, M. P., Nomanbhoy, T. N., Alessi, D. R., and Gray, N. S. (2011) Characterization of a selective inhibitor of the Parkinson's disease kinase LRRK2. *Nat. Chem. Biol. 7*, 203−205.
(71) Ramsden, N., Perrin, J., Ren, Z., Lee, B. D., Zinn, N., Dawson, V. L., Tam, D., Bova, M., Lang, M., Drewes, G., Bantscheff, M., Bard, F., Dawson, T. M., and Hopf, C. (2011) Chemoproteomics-Based Design of Potent LRRK2-Selective Lead Compounds That Attenuate Parkinson's Disease-Related Toxicity in Human Neurons. *ACS Chem. Biol. 6*, 1021−1028.
(72) Olaharski, A. J., Bitter, H., Gonzaludo, N., Kondru, R., Goldstein, D. M., Zabka, T. S., Lin, H., Singer, T., and Kolaja, K. (2010) Modeling bone marrow toxicity using kinase structural motifs and the inhibition profiles of small molecular kinase inhibitors. *Toxicol. Sci. 118*, 266−275.
(73) Olaharski, A. J., Gonzaludo, N., Bitter, H., Goldstein, D., Kirchner, S., Uppal, H., and Kolaja, K. (2009) Identification of a kinase profile that predicts chromosome damage induced by small molecule kinase inhibitors. *PLoS Comput. Biol. 5*, e1000446.
(74) Chan, B., Estrada, A., Sweeney, Z., and Mciver, E. G. (2011) Pyrazolopyridines as inhibitors of the kinase LRRK2. WO 2011/141756 A1.
(75) Kim, J. W., Lee, J., Song, H.-J., Kim, Y., Lee, H. K., Choi, J.-S., Lim, S.-H., and Chang, S. (2011) Kinase Inhibitors. WO 2011/053861 A1.
(76) Lee, J., Song, H.-J., Koh, J. S., Lee, L. K., Kim, Y., Chang, S., Kim, H. W., Chang, S., Lim, S.-H., Choi, J.-S., Kim, J.-H., and Kim, S.-W. (2011) Kinase Inhibitors. WO 2011/060295 A1.
(77) Mciver, E. G., Smiljanic, E., Harding, D. J., and Hough, J. (2010) Compounds (I). WO 2010/106333 A1.
(78) Nichols, P. L., Eatherton, A. J., Bamborough, P., Jandu, K. S., Philips, O. J., and Andreotti, D. (2011) WO 2011/038872 A1.
(79) Ramsden, N. (2009) Use Of LRRK2 Inhibitors For Neuro-degenerative Disease. WO 2009/127642 A2.
(80) Correia Guedes, L., Ferreira, J. J., Rosa, M. M., Coelho, M., Bonifati, V., and Sampaio, C. (2010) Worldwide frequency of G2019S LRRK2 mutation in Parkinson's disease: A systematic review. *J. Prak. Rel. Dis. 16*, 237−242.
(81) http://www.tautatis.com/home.html (2011).
(82) Yue, Z. (2012) Genetic mouse models for understanding LRRK2 biology, pathology and pre-clinical application. *Parkinsonism Relat. Disord. 18* (Suppl 1), S180−182.
(83) Yue, Z., and Lachenmayer, M. L. (2011) Genetic LRRK2Models of Parkinson's Disease: Dissecting the Pathogenic Pathway and Exploring Clinical Applications. *Movement Disord. 26*, 1386−1397.
(84) http://www.pdonlineresearch.org/ (2012).
(85) Doggett, E. A., Zhao, J., Mork, C. N., Hu, D., and Nichols, R. J. (2012) Phosphorylation of LRRK2 serines 955 and 973 is disrupted by Parkinsoń disease mutations and LRRK2 pharmacological inhibition. *J. Neurochem. 120*, 37−45.
(86) Davis, M. I., Hunt, J. P., Herrgard, S., Ciceri, P., Wodicka, L. M., Pallares, G., Hocker, M., Treiber, D. K., and Zarrinkar, P. P. (2011) Comprehensive analysis of kinase inhibitor selectivity. *Nat. Biotechnol. 29*, 1046−1051.
(87) Rauh, D. (2010) Inaktive Kinasekonformationen stabilisieren. *Nachr. Chem. 58*, 118−121.

4.2.2 Die Behandlung der akuten myeloischen Leukämie durch FLT-3

Der Inhalt dieses Kapitels wird voraussichtlich im Juli 2012 eingereicht und befindet sich derzeit in der Rohfassung:

Ghislaine Marlyse Okala Amombo*, Thomas Kramer*, Fabio Lo Monte*, Stefan Göring, Steven Smith, Stephanie Kolb, Robert Schubenel, Karlheinz Baumann, Boris Schmidt‡

Inhibitor modification - An inhibition shift from γ-secretase to FLT-3, *Bioorganic & Medicinal Chemistry Letters*, wird voraussichtlich im Juli eingereicht.

Die akute myeloische Leukämie (AML) ist eine aggressive und bösartige Erkrankung des blutbildenden Systems mit einer Langzeitüberlebensdauer von 25-70% bei Patienten unter 60 Jahren.[138-139] Aktivierende Mutationen von FLT-3 (*FMS-like tyrosine kinase-3*) sind häufige molekulare Anomalien, die bei AML-Patienten gefunden werden können.[140] Infolgedessen stellt diese Kinase ein interessantes *Target* zur Behandlung der AML dar. FLT-3-Inhibitoren aus verschiedenen Strukturklassen erzielten bereits erste Erfolge in den präklinischen und klinischen Studien.[141]

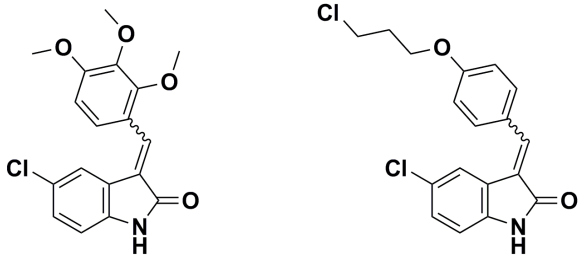

Abb. 22: Strukturen durch die das FLT-3-Projekt initiiert wurde.

Durch vorherige Untersuchungen des Indolinon-Grundgerüsts im Bereich der Alzheimer-Demenz wurde durch ein *Kinase-Panel* festgestellt, dass Derivate dieser Strukturklasse das Potential für selektive FLT-3-Inhibitoren besitzen (Abb. 22).

Mit Hilfe einer Struktur-Aktivitäts-Beziehung konnten durch dieses Grundgerüst mehrere ATP-kompetitive FLT-3-Inhibitoren synthetisiert werden. Es wurden Aktivitäten im nanomolaren Bereich erhalten und die *in vivo* Evaluation einiger Verbindungen im Wildtyp-Zebrafisch-Embryo belegte, dass diese Inhibitoren im getesteten Konzentrationsbereich keine Toxizität aufweisen.

Die im Rahmen dieser Arbeit von Fabio Lo Monte synthetisierten Verbindungen:

BSc4533 (16m), BSc4535 (16o), BSc4537 (16g), BSc4539 (16h), BSc4541 (16b)

In Klammern die Verbindungsnummer in der Publikation.

Inhibitor modification – An inhibition shift from γ-secretase to FLT-3

Ghislaine Marlyse Okala Amombo[a,*], Thomas Kramer[a,*], Fabio Lo Monte[a,*], Stefan Göring[a], Steven Smith[a], Stephanie Kolb[a], Robert Schubenel[b], Karlheinz Baumann[b] and Boris Schmidt[a,†]

[a] Clemens Schöpf-Institute of Organic Chemistry and Biochemistry, Technische Universität Darmstadt, Petersenstr. 22, D-64287 Darmstadt, Germany

[b] F. Hoffmann-La Roche Ltd., Pharmaceutical Division, Preclinical Research CNS, Bldg. 70/345, CH-4070 Basel, Switzerland

* These authors contributed equally to this work.

[†] Corresponding author. Tel.: +49 6151 163075; fax: +49 6151 163278

E-mail address: Schmidt_boris@t-online.de (B. Schmidt).

+ Electronic supplementary information (ESI) available: Experimental section and assay conditions.

Keywords: Acute myeloid leukaemia, FLT-3, kinase inhibitor, γ-secretase

Abstract

FLT-3 is an interesting target for the treatment of acute myeloid leukaemia (AML). Due to previous findings concerning the γ-secretase we use the indolinone scaffold as pattern to synthesize several FLT-3 inhibitors. We analyzed the SAR of these inhibitors and decreased their impact on γ-secretase activity. Simultaneously, we increased the inhibitory activity versus FLT-3.

Acute myeloid leukaemia (AML) is an aggressive haematological malignancy with long-term survival rates of 25%-70% in patients younger than 60 years and only 5%-15% in older patients.[1,2] Activating mutations of FLT-3 (FMS-like tyrosine kinase-3) are abundant molecular abnormalities found in AML.[3] FLT-3 is essential for the normal function of stem cells and the immune system and is primarily expressed in immature hematopoietic cells.[4] It contains an extracellular ligand binding domain, a transmembrane domain, and,

intracellularly, a juxtamembrane domain followed by the tyrosine kinase domain, which is interrupted by a kinase insert region.[5,6] Internal-tandem duplications (ITDs) and tyrosine kinase domain (TKD) point mutations are the two major classes of activating FLT-3 mutations identified in AML patients.[7] FLT-3/ITD mutations can be estimated to occur in ~23% of *de novo* AML.[8] Several ATP-competitive FLT-3 inhibitors were developed from a number of research groups to afford a molecularly targeted therapy for this disease.[9] Compounds of several structural families are potent inhibitors of the FLT-3 kinase and some of them have been promising in preclinical as well as clinical trials, Scheme 1.[5-10]

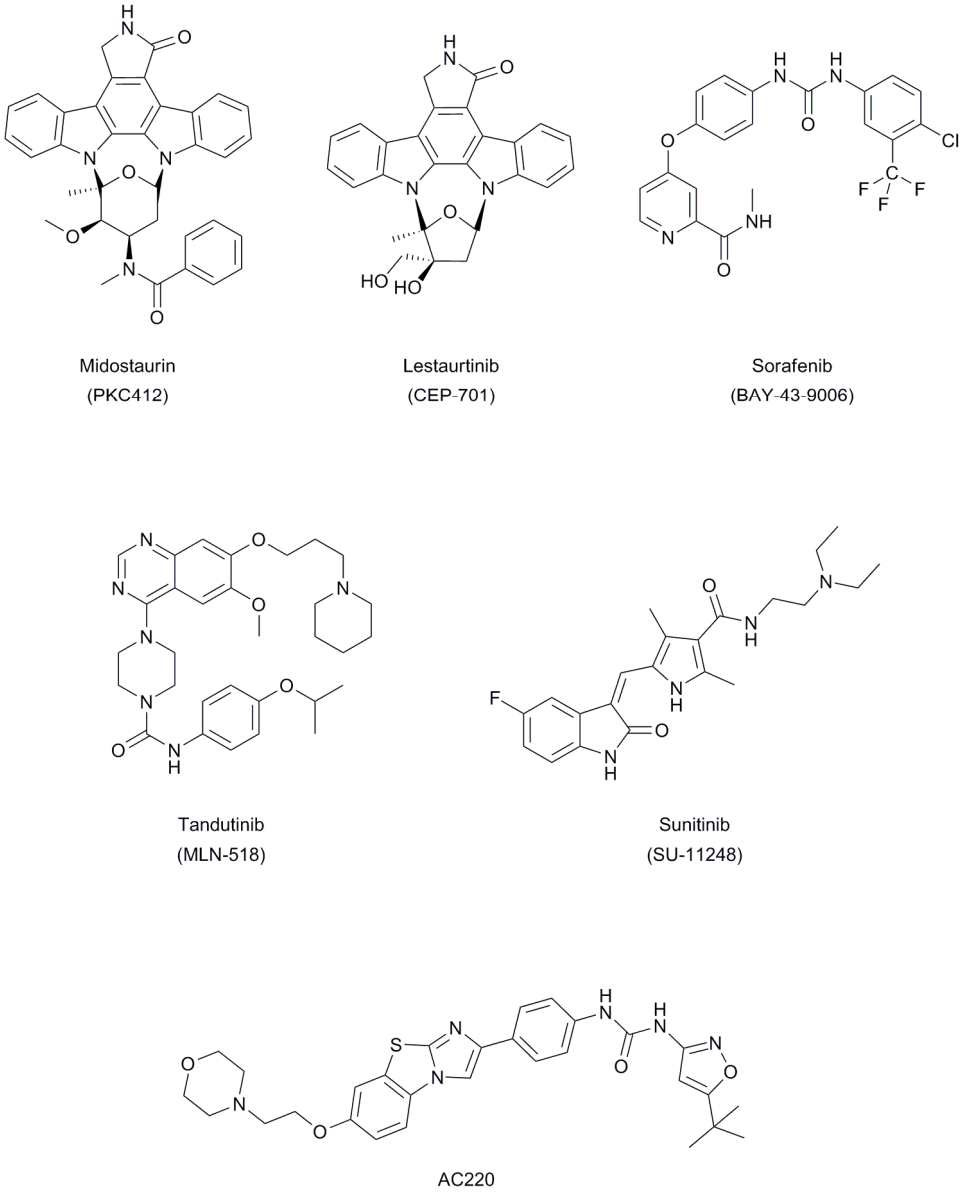

Scheme 1: FLT-3 inhibitors evaluated in preclinical or clinical trials.[5-7,9,10]

Altogether the published data suggest that FLT-3 is an attractive therapeutic target for the development of kinase inhibitors for AML and other associated diseases.[11]

Working on γ-secretase inhibitors in the research field of Alzheimer´s disease we synthesized several compounds based on an indolinone scaffold. During the evaluation of different inhibitors on a kinase panel two substances displayed significant inhibition (98% and 89% at 10 µM) of the tyrosine kinase FLT-3, Scheme 2.[11]

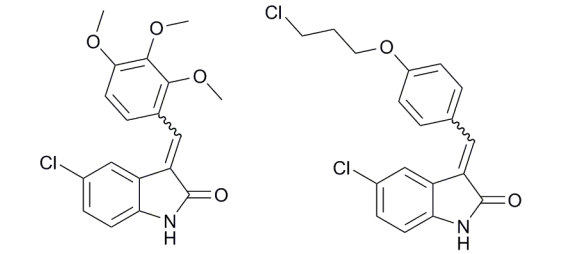

1 (89% FLT-3 inhibition at 10 µM) **2** (98% FLT-3 inhibition at 10 µM)

Scheme 2: Screening hits of potential FLT-3 inhibitors in a kinase panel of 43 kinases.[11]

Regarding this and the fact that FLT-3 is not known to exert effects on the amyloid precursor protein metabolism we exploit these structures to synthesize various FLT-3 inhibitors. One objective of our research was to decrease the effect on γ-secretase and to improve meanwhile the inhibitory activity against FLT-3. The inhibitor structure of **2** guided the variation of the structure-activity relationship (SAR) study.

Several synthesis conditions were utilized to generate various aldehydes as starting materials for the Knoevenagel condensation. Initially, alkyl or benzyl halides were coupled with 4-hydroxybenzaldehydes (**3**) under basic conditions to obtain a series of elongated benzaldehydes (**4a-l**), Scheme 3.[11] The ether (**6**) was formed in a microwave reactor by substitution of an aromatic fluoride (**5**) with a 4-(4-methyl-1H-imidazol-1-yl)phenole.[12] A fluoride benzaldehyde (**7**) was substituted to its corresponding sulfonyl (**8**) and imidazol benzaldehyde (**9**), Scheme 3. A two step synthesis resulted in the azobenzene derivative **11**. The 4-aminobenzaldehyde **10** was converted to its diazonium derivative via diazotation and the final azobenzene (**11**) was formed by an azo coupling reaction.[13] Finally, 9-methyl-9H-carbazole (**12**) was converted to the bulky aldehyde **13** in a two step procedure under Vilsmeier-Haack conditions, Scheme 3.[14]

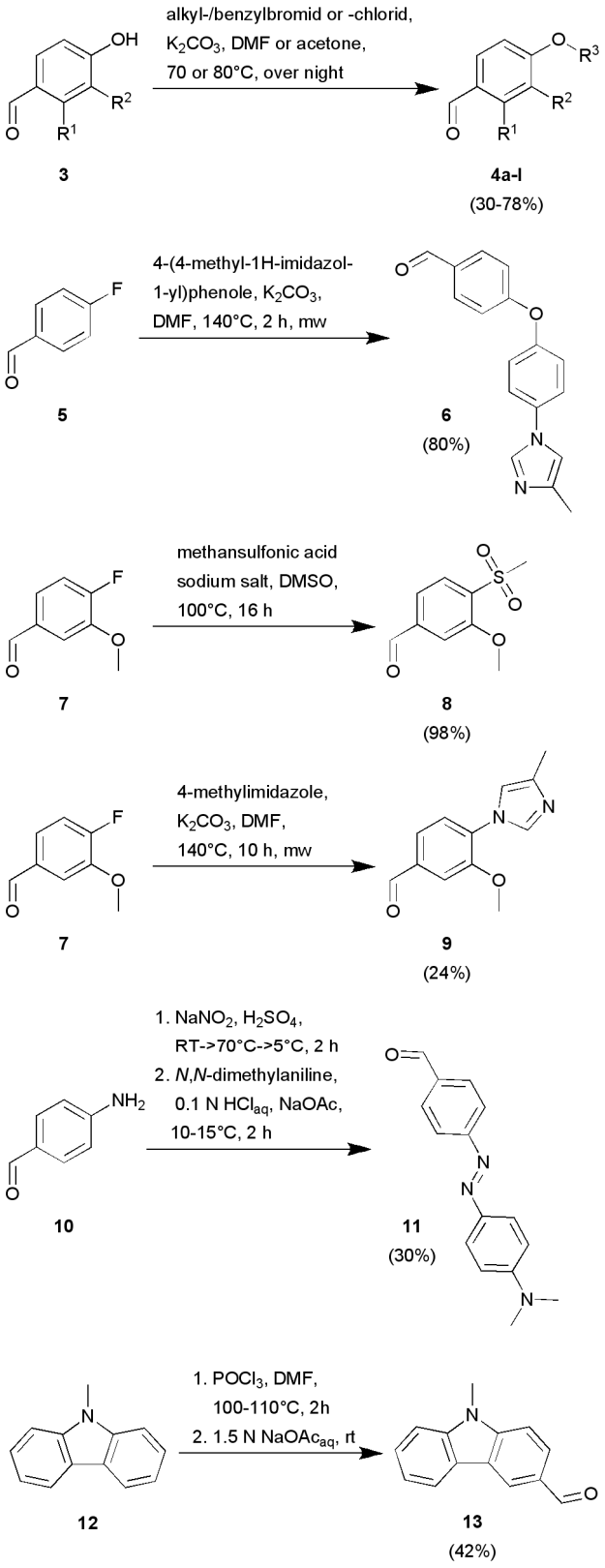

Scheme 3: Aldehyde syntheses (R^1 = H, OMe; R^2 = H, OMe; R^3 = alkyl/benzyl moieties).[11-14]

Commercially available and previously synthesized benzaldehydes were coupled with the indolinones **15** under microwave supported Knoevenagel conditions, Scheme 4.[11] Afterwards, the product **16f** was further derivatized and we obtained the tetrazole **16v**. The resulting products (**16a-u**) were obtained in yields up to 97%, Table 1.

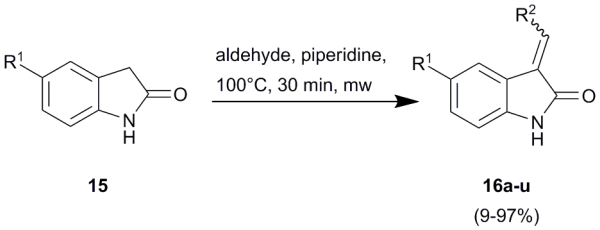

15 **16a-u** (9-97%)

Scheme 4: Synthesis of indolinone derivatives under microwave conditions (R^1 = H, Cl; R^2 = Phenyl moieties).[11]

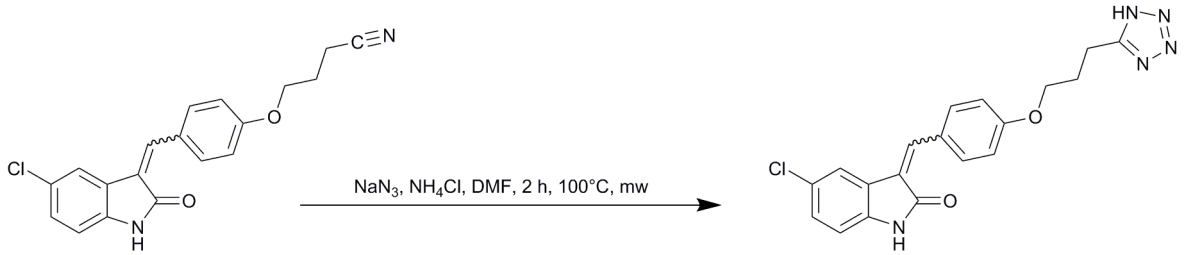

16f **16v** (62%)

Scheme 5: Tetrazole synthesis under microwave conditions.[15]

Human recombinant FLT-3 was used in the FLT-3 *in vitro* kinase assay to ascertain the inhibitor activity. After 90 min incubation time at room temperature the phosphorylated substrate peptides phospho-Ulight-CAGAGAIETDKEYYTVKD (Starting unphosphorylated peptide concentration: 100 nM) were determined with the LANCE detection method.[16] The results are expressed as a percent of control (Staurosporine) specific activity ((measured specific activity/control specific activity) x 100) obtained in the presence of the test compounds (10 µM), Table 1.

Table 1: Synthesized indolinones, their chemical properties and *in vitro* assay results.[11,16]

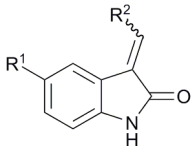

Compound	R^1	R^2	FLT-3 Inhibition -ratio[a]	IC_{50} (µM) $A\beta_{42}$ LPECL Assay[b]	Toxicity (µM)[c]	Yield (%)	ClogP[d]
Staurosporine[e]	-	-	100	n.t.[f]	n.t.[f]	-	4.19
Sunitinib[e]	-	-	100	n.t.[f]	n.t.[f]	-	3.00
2[11]	Cl	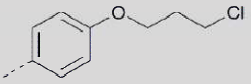	96	-	-	-	5.04
16a	Cl	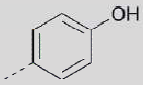	94	47.6	N (40)	28	3.53
16b	Cl	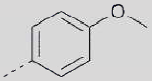	85	>40	N (40)	88	4.12
16c	Cl	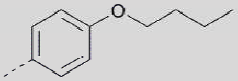	79	>40	N (40)	83	5.71
16d	Cl	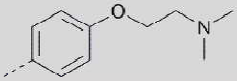	99	7.6	N (40)	65	4.22
16e	Cl	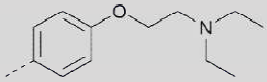	100	17.7	Y (40)	55	5.28
16f	Cl	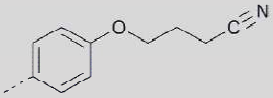	96	>40	Y (40)	90	3.94
16g	Cl	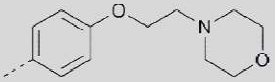	96	11.3	N (40)	84	4.24
16h	Cl	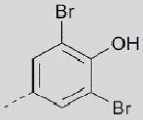	97	15.0	N (40)	97	5.10
16i	Cl	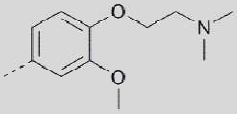	98	11.5	Y (40)	31	3.96
16j	Cl	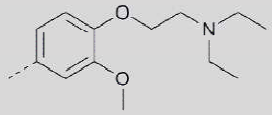	99	11.5	Y (40)	42	5.02
16k	Cl	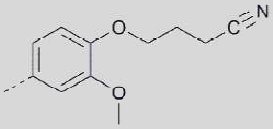	87	>160	N (160)	67	3.68
16l	Cl	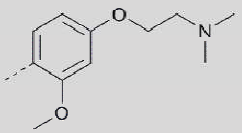	100	10.0	N (40)	71	4.31

[a] Percent of control (Stauroporine) specific activity ((measured specific activity/control specific activity) x 100); activity at a concentration of 10 µM; [b] Aβ liquid phase electrochemiluminescence (LPECL) assay, H4 APP#9 cells; [c] Determined in H4-cells, Y = Yes, N = No; [d] Calculated by ChemDraw Ultra (9.0.1); [e] Control; [f] n.t. = not tested.

Table 1: continued.[11,16]

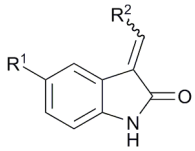

Compound	R^1	R^2	FLT-3 Inhibition -ratio[a]	IC_{50} (µM) $A\beta_{42}$ LPECL Assay[b]	Toxicity (µM)[c]	Yield (%)	ClogP[d]
16m	Cl	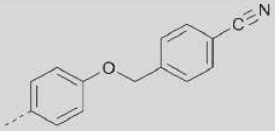	75	27.3	N (40)	93	5.32
16n	Cl	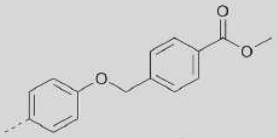	58	38.8	N (40)	70	5.86
16o	Cl	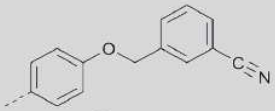	77	>40	N (40)	48	5.32
16p	Cl	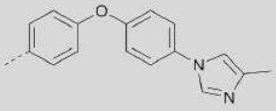	83	5.4	Y (10)	41	5.88
16q	H	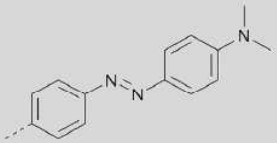	77	>80	N (80)	9	5.55
16r	Cl	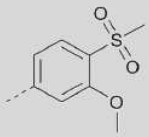	48	7.3	Y (20)	85	2.49
16s	Cl	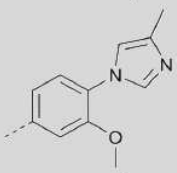	74	6.7	Y (80)	55	4.25
16t	Cl	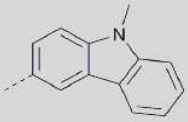	69	19.8	N (80)	17	6.04
16u	H	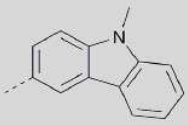	78	27.6	Y (80)	15	5.07
16v	Cl	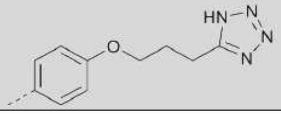	83	17.7	Y (40)	62	3.76

[a] Percent of control (Stauroporine) specific activity ((measured specific activity/control specific activity) x 100); activity at a concentration of 10 µM; [b] Aβ liquid phase electrochemiluminescence (LPECL) assay, H4 APP#9 cells; [c] Determined in H4-cells, Y = Yes, N = No; [d] Calculated by ChemDraw Ultra (9.0.1); [e] Control; [f] n.t. = not tested.

To approve the observed FLT-3 inhibition-ratio we determined the IC_{50} values of compounds **16e** and **16k**. Both compounds showed good IC_{50} values, 4.1 nM for **16e** and 17.0 nM for **16k**. These activities indicated that we have synthesized a series of potent FLT-3 inhibitors. Indolinones are well known kinase inhibitors with diverse application.[17] To determine the broader selectivity of our most active FLT-3 inhibitor **16e** we screened at a concentration of 1 µM against 50 human protein kinases, Figure 1. Most of the 50 kinases in this panel showed an activity higher than 80%, whereas FLT-3 displayed a residual activity of only 14.7%. The only kinases, which were also significantly inhibited by this compound, were the Ser/Thr kinase HGK (MAP4K4) and the Tyr kinase JAK3.

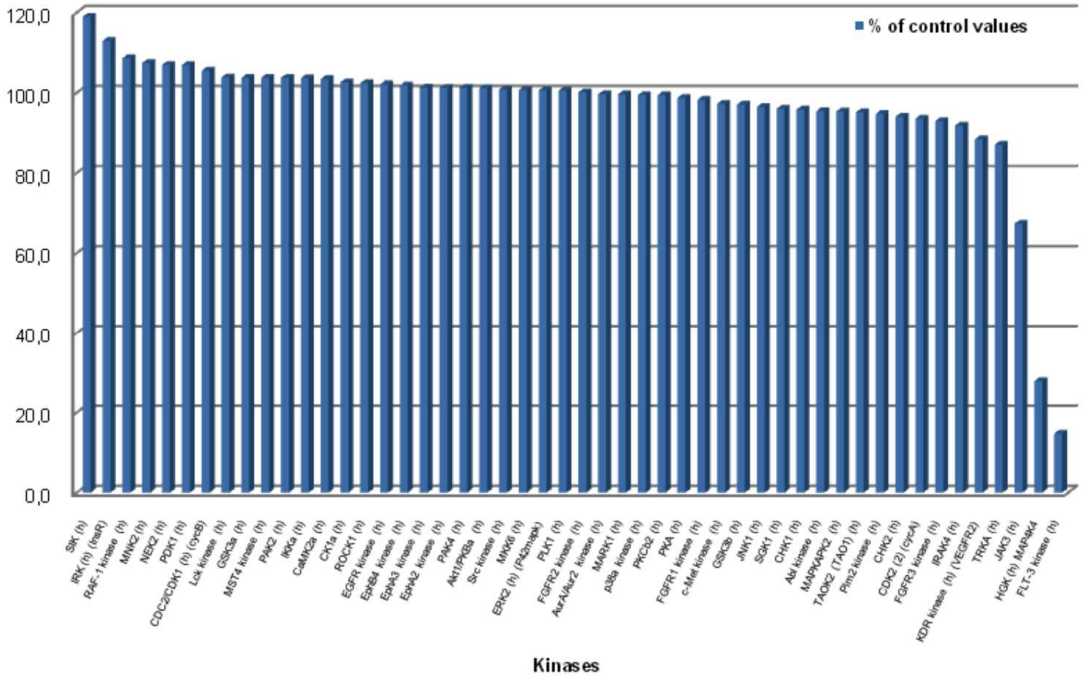

Figure 1: Screening of compound **16e** against a panel of human protein kinases. Each bar represents the activity of one individual protein kinase (Determination method: Percent of control (Staurosporine) specific activity [(measured specific activity/control specific activity) x 100]). Compound **16e** was tested against 50 protein kinases at a concentration of 1 µM. See the Supporting Information for more details.[16]

In addition to the H4 APP#9 cell-based toxicity assay, we established a zebrafish embryo phenotype assay, which enabled the toxicity determination in whole organisms.[11] The embryos were collected and maintained in E2 medium at 28℃. Compound **16e** was added 4-5 hpf (hours post fertilization) and the phenotypes were compared after 48 hpf. Compound **16e** causes a development delay at 20 µM, Figure 2. Compared to the control, zebrafish embryos treated with **16e** were still covered by the chorion. Nevertheless, they did not reveal other abnormalities. The zebrafish embryos exhibit no lethality and peculiarities at a concentration below 20 µM of **16e**.

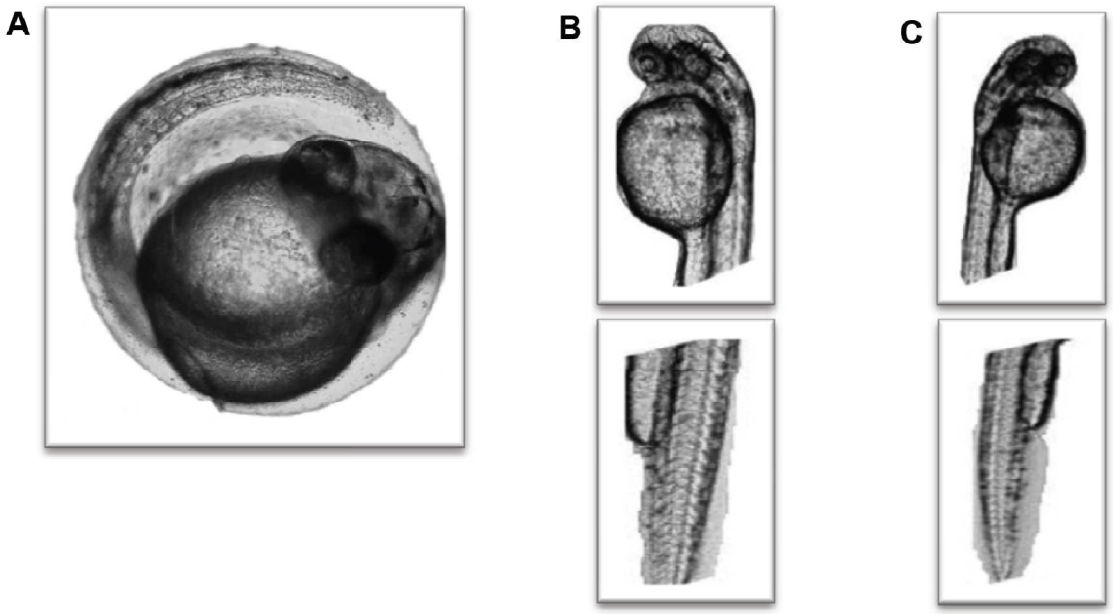

Figure 2: Exposure of zebrafish embryos to A) 20 µM of **16e**, B) 5 µM of **16e**, C) control. The embryos were collected and maintained in E2 medium at 28℃. Compound **16e** was added 4-5 hpf (hours post fertilization) and the phenotypes were compared after 48 hpf.

The docking studies of the FLT-3 crystal structure (PDB: 1RJB) and compounds **16e** and **16k** revealed the possibility to determine potential inhibitor-enzyme interactions, Figure 3.[8]

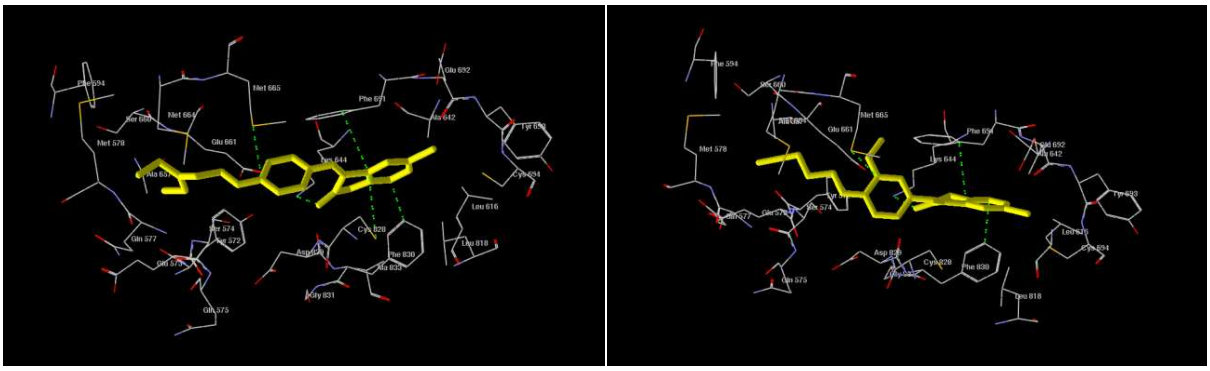

Figure 3: Docking of compound **16e** (left) and **16k** (right) into the PDB crystal structure 1RJB of FLT-3; important interactions are highlighted; Software: Molegro Virtual Docker 5.

In both cases the docking result offers four possible interactions. The indolinone motif interacts edge-to-face with the Phe830 of the DFG motif. In addition, the indolinone fits to the FLT-3 hinge region by face-to-face interplay with Phe691 and hydrogen bonding with Lys644.[8] The phenyl group of the inhibitors interacts with Met665.[18] The FLT-3 *in vitro* assay results revealed that an electron donor motif is needed at the end. For example compound **16c**, which lacks this motif, showed a decrease inhibition activity compared to **16d,f**. This could be explained by a polar area formed by Glu573 and Gln577, which is in close vicinity.

A comparison of the FLT-3 inhibition results and the docking studies offers the possible suggestion that the benzylidene indolinone moiety could cover the entrance of the ATP-binding site (compound **16a,b,h**) and the elongated alkyl chain could act as an "anchor" in the inner side of the ATP-binding pocket, e.g. **16d-g**. Furthermore, a comparison of the FLT-3 inhibition results of Table 1 revealed that bulky residues at the phenyl moiety lead to a decreased inhibition activity.

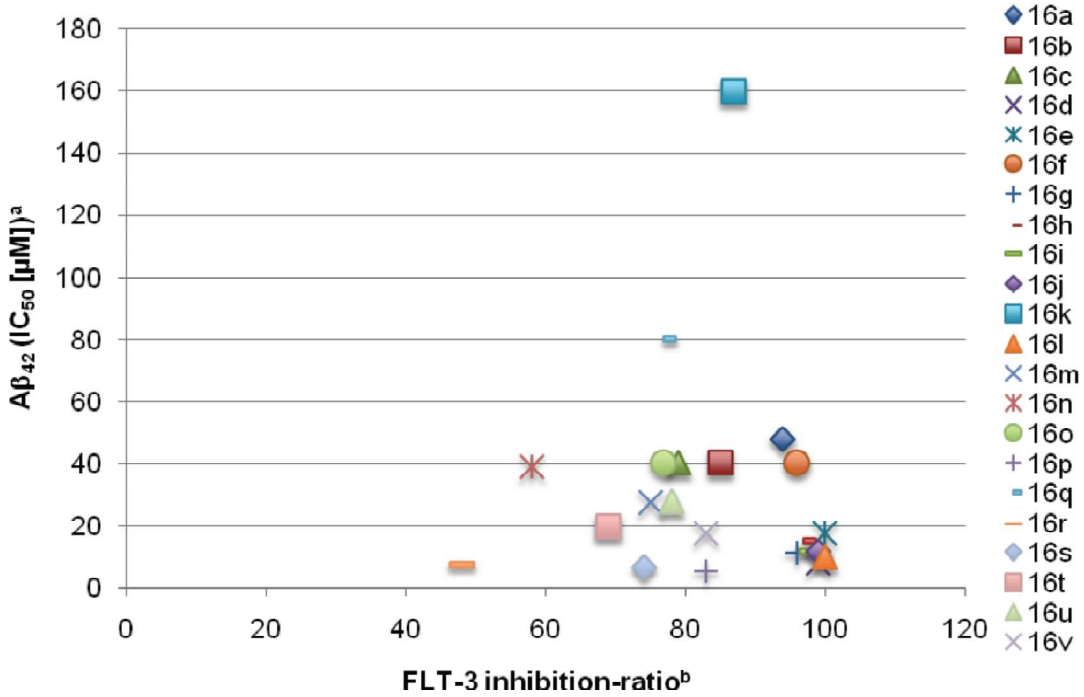

Figure 4: Correlation plot of FLT-3 activity inhibition and $A\beta_{42}$ inhibition (IC_{50}); [a] Values at 40 are >40, see Table 1; [b] Determination method: Percent of control (Staurosporine) specific activity [(measuredspecific activity/control specific activity) x 100]).

The inhibitory activity of the synthesized compounds in the secretase assay cannot be correlated to the FLT-3 inhibition-ratio, Figure 4. In the case of compounds **16f** and **16k** we expected the same result, but surprisingly, they were not active against the γ-secretase, Table 1 and Figure 4. In comparison with other compounds, e.g. **16d,i** and **16m,o**, the nitrile and alkyl chain combination is important for this selectivity and good FLT-3 inhibition activity.

In conclusion, starting from the screening hit **2** we have synthesized in a short time manner several potent FLT-3 inhibitors. We could limit the toxicity level of **16e** using a H4 APP#9 cell-based and a zebrafish embryo phenotype assay. The combination of FLT-3 *in vitro* results and docking studies revealed some possible enzyme-inhibitor interactions with the amino acids Lys644, Met665, Phe691 and Phe830. Furthermore, we could realize our aim to be selective towards the γ-secretase. Future work could be the further derivatisation/substitution of the chloride at the indolinone motif.

References and notes

1. Kindler, T.; Lipka, D. B.; Fischer, T. *Blood* **2010**, *116*, 5089.
2. Levis, M.; Small, D. *Expert Opin Investig Drugs* **2003**, *12*, 1951.
3. Pratz, K. W.; Levis, M. J. *Curr. Drug Targets* **2010**, *11*, 781.
4. Griffith, J.; Black, J.; Faerman, C.; Swenson, L.; Wynn, M.; Lu, F.; Lippke, J.; Saxena, K. *Mol. Cell* **2004**, *13*, 169.
5. Advani, A. S. *Curr. Pharm. Des.* **2005**, *11*, 3449.
6. Paz, K.; Zhu, Z. *Expert Opin. Ther. Targets* **2005**, *9*, 1147.
7. Zarrinkar, P. P.; Gunawardane, R. N.; Cramer, M. D.; Gardner, M. F.; Brigham, D.; Belli, B.; Karaman, M. W.; Pratz, K. W.; Pallares, G.; Chao, Q.; Sprankle, K. G.; Patel, H. K.; Levis, M.; Armstrong, R. C.; James, J.; Bhagwat, S. S. *Blood* **2009**, *114*, 2984.
8. Mahboobi, S.; Uecker, A.; Sellmer, A.; Cenac, C.; Hocher, H.; Pongratz, H.; Eichhorn, E.; Hufsky, H.; Trumpler, A.; Sicker, M.; Heidel, F.; Fischer, T.; Stocking, C.; Elz, S.; Bohmer, F. D.; Dove, S. *J Med Chem* **2006**, *49*, 3101.
9. Zhang, W.; Konopleva, M.; Shi, Y. X.; McQueen, T.; Harris, D.; Ling, X.; Estrov, Z.; Quintas-Cardama, A.; Small, D.; Cortes, J.; Andreeff, M. *J Natl Cancer Inst* **2008**, *100*, 184.
10. www.clinicaltrail.gov **Nov. 2011**.
11. Hottecke, N.; Liebeck, M.; Baumann, K.; Schubenel, R.; Winkler, E.; Steiner, H.; Schmidt, B. *Bioorg Med Chem Lett* **2010**, *20*, 2958.
12. Fischer, C.; Munoz, B.; Zultansky, S.; Methot, J.; Zhou, H.; Brown, W. C. *WO 2008/156580 A1* **2008**.
13. Perez-Moreno, J.; Zhao, Y.; Clays, K.; Kuzyk, M. G.; Shen, Y.; Qiu, L.; Hao, J.; Guo, K. *J Am Chem Soc* **2009**, *131*, 5084.
14. Langendoen, A.; Plug, J. P. M.; Koomen, G.-J.; Pandit, U. K. *Tetra* **1989**, *45*, 1759.
15. Monte, F. L.; Kramer, T.; Bolander, A.; Plotkin, B.; Eldar-Finkelman, H.; Fuertes, A.; Dominguez, J.; Schmidt, B. *Bioorg Med Chem Lett* **2011**, *21*, 5610.
16. www.cerep.fr.
17. Prakash, C. R.; Raja, S. *Mini Rev Med Chem* **2012**, *12*, 98.
18. Salonen, L. M.; Ellermann, M.; Diederich, F. *Angew. Chem.* **2011**, *123*, 4908.

Supporting Information

Inhibitor modification – An inhibition shift from γ-secretase to FLT-3

Ghislaine Marlyse Okala Amombo*[a], Thomas Kramer*[a], Fabio Lo Monte*[a], Stefan Göring[a], Steven Smith[a], Stephanie Kolb[a], Robert Schubenel[b], Karlheinz Baumann[b] and Boris Schmidt†[a]

[a] *Clemens Schöpf - Institute of Organic Chemistry and Biochemistry, Technische Universität Darmstadt, 64287 Darmstadt, Hessen, Germany, Fax: +496151-163278; Tel: +496151 164531*

[b] *F. Hoffmann-La Roche Ltd, Pharmaceutical Division, Preclinical Research CNS, Bldg. 70/345, CH- 4070 Basel, Switzerland,*

† E-mail: schmidt_boris@t-online.de

*These authors contributed equally to this work.

Table of Content:

I. General comments

The ^{1}H-NMR spectra were recorded on a Bruker AC 300 spectrometer at 300 MHz and Bruker AC 500 spectrometer at 500 MHz. The ^{13}C-NMR spectra were recorded on a Bruker AC 300 spectrometer at 75 MHz and Bruker AC 500 spectrometer at 125 MHz. Chemical shifts are reported as ppm downfield from Me_4Si. Mass spectrometry was performed on a Bruker-Franzen Esquire LC mass spectrometer and a MAT 95 double focussing sector field MS. Microwave experiments were carried out using a Biotage® Initiator™ microwave apparatus. All microwave experiments were carried out in sealed microwave process vials utilizing the standard absorbance level (300 W maximum power). High performance liquid chromatographies were carried out in an Agilent 1100 (column: reversed phase, Zorbax Eclipse XDB-C8, 4.6 x 150 mm; 254 nm). The eluent is composed of: a) H_2O (1% TFA) (A) and acetonitrile (B) with a gradient: 30 to 90% B within 12 min. All reagents and solvents were purchased at ABCR, Acros, Sigma Aldrich and VWR.

II. Experimental methods and chemical data

1. General Procedure for synthesis of benzaldehyds 4a-l

K_2CO_3 (2.40 eq.) and the aldehyde **3** (1.00 eq.) were suspended in acetone or dimethylformamide. Then an alkyl/benzyl bromide/chloride (1.00 eq.) was added. This reaction suspension was stirred at 70°C over night. After complete turnover water was added and the aqueous solution was extracted with chloroform. The combined organic layers were dried with $MgSO_4$ and the solvent was removed in vacuo. The resulting residue was purified by column chromatography on silica gel or recrystallized in an appropriate solvent to provide the desired product.

4-butoxybenzaldehyde 4a

The resulting product is a bright yellow oil (51%). **HPLC**: R_t = 6.85 min. **^{1}H-NMR** ($CDCl_3$, 300 MHz): δ [ppm] = 9.88 (s, 1H), 7.82 (d, 2H, *J* = 8.8 Hz), 6.98 (d, 2H, *J* = 8.8 Hz), 4.05 (t, 2H, *J* = 6.4 Hz), 1.85-1.75 (m, 2H), 1.57-1.44 (m, 2H), 0.99 (t, 3H). **^{13}C-NMR** ($CDCl_3$, 75 MHz): δ [ppm] = 191.0, 164.4, 132.1, 129.9, 114.9, 68.3, 31.2, 19.3, 13.9. **MS** (EI, 70 eV): *m/z* = 178 [M^+].

4-(2-(diethylamino)ethoxy)benzaldehyde 4b

The resulting brown oil (78%) was used in the next step without further analysis.

4-(3-chloropropoxy)benzaldehyde 4c

The resulting bright yellow oil (57%) was used in the next step without further analysis.

4-(4-formylphenoxy)butannitrile 4d

The resulting product is a bright yellow oil (65%). **HPLC**: R_t = 4.71 min. **^{1}H-NMR** ($CDCl_3$, 300 MHz): δ [ppm] = 9.89 (s, 1H), 7.84 (d, 2H, *J* = 8.8 Hz), 7.01 (d, 2H, *J* = 8.8 Hz), 4.17 (t, 2H, *J* = 5.7 Hz), 2.61 (t, 2H, *J* = 7.1 Hz), 2.23-2.14 (m, 2H). **^{13}C-NMR** ($CDCl_3$, 75 MHz): δ [ppm] = 190.8, 163.4, 132.2, 130.5, 119.0, 114.9, 65.7, 25.4, 14.3. **MS** (EI, 70 eV): *m/z* = 189 [M^+].

4-(2-morpholinoethoxy)benzaldehyde 4f

The resulting bright yellow oil (52%) was used in the next step without further analysis.

4-((4-formylphenoxy)methyl)benzonitrile 4g

The resulting product is a colorless solid (51%). **HPLC**: R_t = 6.76 min. **^{1}H-NMR** ($CDCl_3$, 500 MHz): δ [ppm] = 9.90 (s, 1H), 7.86 (d, 2H, *J* = 8.8 Hz), 7.70 (d, 2H, *J* = 8.4 Hz), 7.55 (d, 2H, *J* = 8.4 Hz), 7.07 (d, 2H, *J* = 8.8 Hz), 5.21 (s, 2H). **^{13}C-NMR** ($CDCl_3$, 125 MHz): δ [ppm] = 190.8, 163.2, 141.5, 132.7, 132.2, 130.8, 127.7, 118.6, 115.2, 112.3, 69.2, 52.3. **MS** (EI, 70 eV): *m/z* = 237 [M^+].

Methyl 4-((4-formylphenoxy)methyl)benzoate 4h

The resulting product is a colorless solid (43%). **HPLC**: R_t = 6.90 min. **^{1}H-NMR** ($CDCl_3$, 500 MHz): δ [ppm] = 9.89 (s, 1H), 8.07 (d, 2H, *J* = 8.4 Hz), 7.84 (d, 2H, *J* = 8.8 Hz), 7.50 (d, 2H, *J* = 8.4 Hz), 7.07 (d, 2H, *J* = 8.8 Hz), 5.21 (s, 2H), 3.93 (s, 3H). **^{13}C-NMR** ($CDCl_3$, 125 MHz): δ [ppm] = 190.8, 166.8, 163.4, 141.2, 132.2, 130.5, 130.2, 130.2, 127.1, 115.3, 69.7, 52.3. **MS** (EI, 70 eV): *m/z* = 270 [M^+].

3-((4-formylphenoxy)methyl)benzonitrile 4i

The resulting product is a colorless solid (30%). **HPLC**: R_t = 6.76 min. **^{1}H-NMR** ($CDCl_3$, 500 MHz): δ [ppm] = 9.91 (s, 1H), 7.86 (d, 2H, *J* = 8.8 Hz), 7.75 (s, 1H), 7.69-7.64 (m, 2H), 7.54-7.51 (m, 1H), 7.50 (d, 2H, *J* = 8.4 Hz), 7.08 (d, 2H, *J* = 8.8 Hz), 5.18 (s, 2H). **^{13}C-NMR** ($CDCl_3$, 125 MHz): δ [ppm] = 190.8, 163.1, 137.8, 132.2, 132.0, 131.6, 130.9, 130.7, 129.7, 118.6, 115.2, 113.1, 69.0. **MS** (EI, 70 eV): *m/z* = 237 [M^+].

4-(2-(dimethylamino)ethoxy)-3-methoxybenzaldehyde 4j

The resulting bright brown oil (47%) was used in the next step without further analysis.

4-(2-(diethylamino)ethoxy)-3-methoxybenzaldehyde 4k

The resulting bright brown oil (45%) was used in the next step without further analysis.

4-(4-formyl-2-methoxyphenoxy)butannitrile 4l

The resulting product is a bright yellow oil (69%). **HPLC**: R_t = 4.34 min. **^{1}H-NMR** ($CDCl_3$, 500 MHz): δ [ppm] = 9.86 (s, 1H), 7.44 (dd, 1H, *J* = 1.8 Hz, *J* = 8.1 Hz), 7.42 (d, 1H, *J* = 1.8 Hz), 6.98 (d, 1H, *J* = 8.1 Hz), 4.21 (t, 2H, *J* = 5.8 Hz), 3.92 (s, 3H), 2.65 (t, 2H, *J* = 7.1 Hz), 2.25-2.20 (m, 2H). **^{13}C-NMR** ($CDCl_3$, 125 MHz): δ [ppm] = 191.0, 153.4, 150.2, 130.8, 126.7, 119.1, 112.2, 109.6, 66.6, 56.1, 25.5, 14.3.

2. Synthesis of 4-(2-(dimethylamino)ethoxy)benzaldehyde 4m and 4-(2-(dimethyl amino)- ethoxy)-2-methoxybenzaldehyde 4n

For the synthesis of 4-(2-(dimethylamino)ethoxy)benzaldehyde **4m** see the mentioned reference. The resulting brown oil (63%) was used in the next step without further analysis. For the synthesis of 4-(2-(dimethylamino)ethoxy)-2-methoxybenzaldehyde **4n** see the mentioned reference. The resulting product is a bright brown oil (66%). **HPLC**: R_t = 0.75 min, 1.11 min. **^{1}H-NMR** ($CDCl_3$, 300 MHz): δ [ppm] = 10.28 (s, 1H), 7.79 (d, 1H, *J* = 8.7 Hz), 6.54 (dd, 1H, *J* = 2.2 Hz, *J* = 8.7 Hz), 6.49 (d, 1H, *J* = 2.2 Hz), 4.13 (t, 2H, *J* = 5.7 Hz), 3.88 (s, 3H), 2.75 (t, 2H, *J* = 5.7 Hz), 2.35 (s, 6H). **^{13}C-NMR** ($CDCl_3$, 75 MHz): δ [ppm] = 188.4, 165.5, 163.7, 130.9, 119.3, 106.2, 98.9, 66.4, 58.2, 55.8, 46.0.

3. Synthesis of 4-(4-(4-methyl-1*H*-imidazol-1-yl)phenoxy)benzaldehyde 6

A mixture of 4-(4-methyl-1H-imidazol-1-yl)phenole (1.74 g, 10 mmol), 4-fluorobenzaldehyde (1.24 g, 10 mmol) and anhydrous K_2CO_3 (1.38 g, 10 mmol) in abs. dimethylformamide (5 mL) was heated at 140°C under microwave irradiat ion for 2 h. The cooled reaction mixture was diluted with ethyl acetate (5 mL), filtered through a plug of silica gel, and washed with ethyl acetate (10-20 mL). The combined organic extracts were concentrated, and the resulting residue was purified by column chromatography on silica gel to provide the desired product in 80% as a brown oil. **HPLC**: R_t = 2.64 min. **^{1}H-NMR** (DMSO-d_6, 500 MHz): δ [ppm] = 9.94 (s, 1H), 8.26 (m, 1H), 7.95 (m, 2H), 7.75 (m, 3H), 7.31 (m, 2H), 7.18 (m, 2H), 2.14 (s, 3H). **^{13}C-NMR** (DMSO-d_6, 125 MHz): δ [ppm] = 191.5, 162.1, 153.2, 135.6, 133.8, 132.0, 131.4, 129.9, 129.3, 122.4, 122.2, 121.5, 118.1, 117.6, 116.0, 13.6. **MS** (EI, 70 eV): *m/z* = 278 [M^+].

4. Synthesis of 3-methoxy-4-(methylsulfonyl)benzaldehyde 8

Methanesulfinic acid sodium salt (125 mg, 0.81 mmol) and 4-fluoro-3-methoxybenzaldehyde **7** (91.06 mg, 0.89 mmol) were dissolved in dry DMSO (3 mL), under nitrogen. The mixture was stirred at 100°C for 16h and then poured into ice. The formed precipitate was collected by filtration, washed with water and dried to afford 258 mg (98%) of white solid. The crude solid was used in next step without any further purification. **HPLC**: R_t = 2.66 min. **^{1}H-NMR** (DMSO-d_6, 500 MHz): δ [ppm] = 10.00 (s, 1H), 8.11 (d, 1H, *J* = 7.9 Hz), 7.53 (dd, 1H, *J* = 1.3 Hz, *J* = 7.9 Hz), 7.49 (d, 1H, *J* = 1.2 Hz), 4.02 (s, 3H), 3.18 (s, 3H). **^{13}C-NMR** (DMSO-d_6, 125 MHz): δ [ppm] = 190.8, 184.4, 157.7, 141.5, 133.5, 130.7, 123.3, 110.9, 56.7, 42.9.

5. Synthesis of 2-methoxy-4-(4-methyl-1H-imidazol-1-yl)benzaldehyde 9

A mixture of 4-fluoro-3-methoxybenzaldehyde **7** (1.22 g, 7.92 mmol) and 4-methylimidazole (1.24 g, 15.07 mmol) in dry dimethylformamide was degassed and flushed with argon for 20 min. Afterwards K_2CO_3 (1.66 g, 11.98 mmol) was added and the reaction suspension was heated at 140°C under microwave irradiation for 10 h. Then water was added and the aqueous solution was extracted with ethyl acetate. The combined organic layers were washed with brine, dried with Na_2SO_4 and the solvent was removed in vacuo. The resulting residue was purified by column chromatography on silica gel (solvent: ethyl acetate) and provide 411 mg (24%) of the orange product. The product was used in the next step without detailed analysis. **HPLC**: R_t = 1.37 min. **MS** (EI, 70 eV): *m/z* = 216 [M^+].

6. Synthesis of (E)-4-((4-(dimethylamino)phenyl)diazenyl)benzaldehyde 11

For the synthesis of compound **11** see the mentioned reference in the publication. Used in the next step without further analysis.

7. Synthesis of 9-methyl-9H-carbazole-3-carbaldehyde 13

For the synthesis of compound **13** see the mentioned reference in the publication. Used in the next step without further analysis.

8. General Procedure for synthesis of 3-substituted indol-2-ones

Equimolar amounts (0.3 mmol) of 5-chlorooxindole/oxindole and aldehyde were dissolved in methanol (1 ml), a drop of piperidine (30 µl) was added and the mixture heated at 100°C under microwave irradiation for 30 min. The reaction mixture was cooled to room temperature and the resulting precipitate was removed by filtration, carefully washed with methanol and recrystallized at least once from methanol to give the desired product in good yield.

5-chloro-3-(4-(3-chloropropoxy)benzyliden)indolin-2-one 2

The resulting product is a yellow solid (30%). **HPLC**: R_t = 8.06 min, 8.44 min. **^{1}H-NMR** (DMSO-d_6, 500 MHz): δ [ppm] = 10.69 (s, 2H), 8.49 (d, 2H, *J* = 8.9 Hz), 7.89 (s, 1H), 7.80 (d, 1H, *J* = 2.0 Hz), 7.70 (d, 2H, *J* = 8.9 Hz), 7.66 (s, 1H), 7.56 (d, 1H, *J* = 2.0 Hz), 7.27 (dd, 1H, *J* = 2.0 Hz, *J* = 8.3 Hz), 7.20 (dd, 1H, *J* = 2.0 Hz, *J* = 8.3 Hz), 7.13 (d, 2H, *J* = 8.9 Hz), 7.07 (d, 2H, *J* = 8.9 Hz), 6.89 (d, 1H, *J* = 8.3 Hz), 6.81 (d, 1H, *J* = 8.3 Hz), 4.20 (t, 4H, *J* = 5.9 Hz), 3.81 (m, 4H), 2.20 (m, 4H). **^{13}C-NMR** (DMSO-d_6, 125 MHz): δ [ppm] = 168.5, 167.1, 160.6, 160.0, 141.4, 138.8, 138.7, 137.9, 134.8, 131.6, 129.2, 127.5, 127.3, 127.0, 126.3, 125.3, 124.9, 124.8, 123.0, 122.8, 121.4, 119.3, 114.8, 114.3, 111.4, 110.5, 64.6, 64.5, 41.9, 31.6. **MS** (EI, 70 eV): *m/z* = 347 [M^+].

5-chloro-3-(4-hydroxybenzylidene)indolin-2-one 16a

The resulting product is an orange solid (28%). **HPLC**: R_t = 5.39 min, 6.15 min. **^{1}H-NMR** (DMSO-d_6, 500 MHz): δ [ppm] = 10.69 (s, 2H), 8.41 (d, 2H, *J* = 8.9 Hz), 7.80 (s, 1H), 7.76 (d, 1H, *J* = 2.0 Hz), 7.60 (m, 4H), 7.25 (dd, 1H, *J* = 2.0 Hz, *J* = 8.3 Hz), 7.15 (dd, 1H, *J* = 2.0 Hz, *J* = 8.3 Hz), 6.88 (m, 3H), 6.80 (m, 3H). **^{13}C-NMR** (DMSO-d_6, 125 MHz): δ [ppm] = 168.8, 167.3, 162.1, 160.7, 141.1, 139.6, 138.7, 138.4, 135.4, 132.1, 128.7, 127.8, 126.9, 125.1, 124.8, 124.8, 124.1, 123.3, 123.1, 121.3, 120.9, 118.8, 116.0, 115.7, 111.2, 110.3. **MS** (EI, 70 eV): *m/z* = 271 [M^+].

5-chloro-3-(4-methoxybenzyliden)indolin-2-one 16b

The resulting product is a yellow solid (88%). **HPLC**: R_t = 7.06 min, 7.50 min. **^{1}H-NMR** (DMSO-d_6, 500 MHz): δ [ppm] = 10.69 (s, 2H, $NH_{E/Z}$), 8.49 (d, 2H, *J* = 8.9 Hz), 7.88 (s, 1H), 7.80 (d, 1H, *J* = 2.0 Hz), 7.70 (d, 2H, *J* = 8.9 Hz), 7.66 (s, 1H), 7.56 (d, 1H, *J* = 2.0 Hz), 7.27 (dd, 1H, *J* = 2.0 Hz, *J* = 8.3 Hz), 7.19 (dd, 1H, *J* = 2.0 Hz, *J* = 8.3 Hz), 7.12 (d, 2H, *J* = 8.9 Hz), 7.05 (d, 2H, *J* = 8.9 Hz), 6.89 (d, 1H, *J* = 8.3 Hz), 6.81 (d, 1H, *J* = 8.3 Hz), 3.85 (d, 6H). **^{13}C-NMR** (DMSO-d_6, 125 MHz): δ [ppm] = 168.6, 167.1, 161.6, 160.9, 141.4, 138.3, 137.9, 134.8, 131.6, 129.2, 127.5, 127.3, 126.8, 126.2, 125.3, 124.9, 124.7, 122.9, 122.8, 121.4, 119.3, 114.4, 113.7, 111.4, 110.5, 55.4, 55.4. **MS** (EI, 70 eV): *m/z* = 285 [M^+].

3-(4-butoxybenzyliden)-5-chloroindolin-2-one 16c

The resulting product is a yellow solid (83%). **HPLC**: R_t = 8.42 min, 8.71 min. **^{1}H-NMR** (DMSO-d_6, 500 MHz): δ [ppm] = 10.60 (s, 2H), 8.46 (d, 2H, *J* = 8.9 Hz), 7.79 (s, 1H), 7.71 (d, 2H, *J* = 8.9 Hz), 7.65 (s, 1H), 7.63 (d, 1H, *J* = 2.0 Hz), 7.56 (d, 1H, *J* = 2.0 Hz), 7.20 (dd, 1H, *J* = 2.0 Hz, *J* = 8.3 Hz), 7.13 (dd, 1H, *J* = 2.0 Hz, *J* = 8.3 Hz), 7.05 (d, 2H, *J* = 8.9 Hz), 6.98 (d, 2H, *J* = 8.9 Hz), 6.85 (d, 1H, *J* = 8.3 Hz), 6.78 (d, 1H, *J* = 8.3 Hz), 4.05 (t, 4H, *J* = 6.5 Hz),

1.75-1.71 (m, 4H), 1.50-1.43 (m, 4H), 0.96-0.94 (m, 6H). **^{13}C-NMR** (DMSO-d_6, 125 MHz): δ [ppm] = 168.5, 167.1, 161.0, 160.3, 141.3, 138.7, 138.6, 137.6, 134.7, 131.3, 128.8, 127.2, 127.0, 126.6, 126.0, 125.2, 124.9, 124.7, 122.8, 121.4, 119.0, 114.6, 114.0, 111.1, 110.3, 67.4, 67.3, 41.9, 41.9, 30.6, 18.6, 13.6. **MS** (EI, 70 eV): *m/z* = 327 [M^+].

5-chloro-3-(4-(2-(dimethylamino)ethoxy)benzyliden)indolin-2-one 16d

The resulting product is a yellow solid (65%). **HPLC**: R_t = 3.28 min, 4.38 min. **^{1}H-NMR** (DMSO-d_6, 500 MHz): δ [ppm] = 10.69 (s, 2H), 8.48 (d, 2H, *J* = 8.9 Hz), 7.89 (s, 1H), 7.80 (d, 1H, *J* = 2.0 Hz), 7.69 (d, 2H, *J* = 8.9 Hz), 7.66 (s, 1H), 7.56 (d, 1H, *J* = 2.0 Hz), 7.27 (dd, 1H, *J* = 2.0 Hz, *J* = 8.3 Hz), 7.20 (dd, 1H, *J* = 2.0 Hz, *J* = 8.3 Hz), 7.12 (d, 2H, *J* = 8.9 Hz), 7.05 (d, 2H, *J* = 8.9 Hz), 6.89 (d, 1H, *J* = 8.3 Hz), 6.81 (d, 1H, *J* = 8.3 Hz), 4.16-4.13 (m, 4H), 2.66-2.63 (m, 4H), 2.22 (d, 12H). **^{13}C-NMR** (DMSO-d_6, 125 MHz): δ [ppm] = 168.6, 167.1, 160.9, 160.2, 141.4, 138.8, 137.9, 134.8, 131.6, 129.2, 127.5, 127.3, 126.8, 126.1, 125.3, 125.2 124.9, 124.7, 122.9, 122.8, 121.4, 119.3, 114.8, 114.3, 111.4, 110.5, 66.1, 66.0, 57.6, 57.6, 45.5. **MS** (EI, 70 eV): *m/z* = 342 [M^+].

5-chloro-3-(4-(2-(diethylamino)ethoxy)benzyliden)indolin-2-one 16e

The resulting product is an orange solid (55%). **HPLC**: R_t = 4.28 min, 4.92 min. **^{1}H-NMR** (DMSO-d_6, 500 MHz): δ [ppm] = 10.69 (s, NH), 8.48 (d, 2H, *J* = 8.9 Hz,), 7.87 (s, 1H), 7.80 (d, 1H, *J* = 2.0 Hz), 7.68 (d, 2H, *J* = 8.9 Hz), 7.66 (s, 1H), 7.56 (d, 1H, *J* = 2.0 Hz), 7.27 (dd, 1H, *J* = 2.0 Hz, *J* = 8.3 Hz), 7.20 (dd, 1H, *J* = 2.0 Hz, *J* = 8.3 Hz), 7.11 (d, 2H, *J* = 8.9 Hz), 7.04 (d, 2H, *J* = 8.9 Hz), 6.88 (d, 1H, *J* = 8.3 Hz), 6.81 (d, 1H, *J* = 8.3 Hz), 4.13-4.10 (m, 4H), 2.80-2.78 (m, 4H), 2.57-2.53 (m, 8H), 0.99-0.96 (m, 12H). **^{13}C-NMR** (DMSO-d_6, 125 MHz): δ [ppm] = 168.5, 167.1, 160.9, 160.2, 141.4, 138.8, 137.9, 134.8, 131.6, 129.1, 127.5, 127.3, 126.7, 126.1, 125.2, 124.8, 124.7, 122.8, 122.8, 121.4, 119.2, 114.8, 114.3, 111.3, 110.5, 66.7, 66.6, 51.2, 47.0, 46.9, 11.9, 11.9. **MS** (EI, 70 eV): *m/z* = 370 [M^+].

4-(4-((5-chloro-2-oxoindolin-3-yliden)methyl)phenoxy)butannitrile 16f

The resulting product is a yellow solid (90%). **HPLC**: R_t = 6.99 min, 7.48 min. **^{1}H-NMR** (DMSO-d_6, 500 MHz): δ [ppm] = 10.69 (s, 2H), 8.49 (d, 2H, *J* = 8.9 Hz), 7.89 (s, 1H), 7.80 (d, 1H, *J* = 2.0 Hz), 7.70 (d, 2H, *J* = 8.9 Hz), 7.66 (s, 1H), 7.56 (d, 1H, *J* = 2.0 Hz), 7.26 (dd, 1H, *J* = 2.0 Hz, *J* = 8.3 Hz), 7.20 (dd, 1H, *J* = 2.0 Hz, *J* = 8.3 Hz), 7.13 (d, 2H, *J* = 8.9 Hz), 7.06 (d, 2H, *J* = 8.9 Hz), 6.89 (d, 1H, *J* = 8.3 Hz), 6.81 (d, 1H, *J* = 8.3 Hz), 4.14 (t, 4H, *J* = 5.9 Hz), 2.73 (m, 4H), 2.50 (m, 4H). **^{13}C-NMR** (DMSO-d_6, 125 MHz): δ [ppm] = 168.6, 167.1, 160.6, 159.9, 141.4, 138.9, 138.7, 137.8, 134.8, 131.6, 129.2, 127.6, 127.3, 127.0, 126.4, 125.3,

124.9, 123.0, 122.8, 121.4, 120.2, 119.3, 114.8, 114.3, 111.4, 110.5, 66.1, 24.6, 13.4. **MS** (EI, 70 eV): *m/z* = 338 [M^+].

5-chloro-3-(4-(2-morpholinoethoxy)benzyliden)indolin-2-one 16g

The resulting product is a yellow solid (84%). **HPLC**: R_t = 3.35 min, 4.65 min. **^{1}H-NMR** (DMSO-d_6, 500 MHz): δ [ppm] = 10.69 (s, 2H), 8.48 (d, 2H, *J* = 8.9 Hz), 7.88 (s, 1H), 7.80 (d, 1H, *J* = 2.0 Hz), 7.69 (d, 2H, *J* = 8.9 Hz), 7.66 (s, 1H), 7.56 (d, 1H, *J* = 2.0 Hz), 7.27 (dd, 1H, *J* = 2.0 Hz, *J* = 8.3 Hz), 7.20 (dd, 1H, *J* = 2.0 Hz, *J* = 8.3 Hz), 7.13 (d, 2H, *J* = 8.9 Hz), 7.06 (d, 2H, *J* = 8.9 Hz), 6.89 (d, 1H, *J* = 8.3 Hz), 6.81 (d, 1H, *J* = 8.3 Hz), 4.21-4.18 (m, 4H), 3.59 (m, 8H), 2.72 (m, 4H), 2.50 (m, 8H). **^{13}C-NMR** (DMSO-d_6, 125 MHz): δ [ppm] = 168.6, 167.1, 160.8, 160.0, 141.4, 138.8, 137.9, 134.8, 131.6, 129.2, 127.5, 127.3, 126.8, 125.3, 124.9, 122.9, 122.8, 121.4, 119.3, 114.9, 114.4, 111.3, 110.5, 66.2, 65.5, 56.9, 53.9. **MS** (EI, 70 eV): *m/z* = 384 [M^+].

5-chloro-3-(3,5-dibromo-4-hydroxybenzylidene)indolin-2-one 16h

The resulting product is an orange solid (97%). **HPLC**: R_t = 6.98 min, 7.65 min. **^{1}H-NMR** (DMSO-d_6, 500 MHz): δ [ppm] = 10.50 (d, 2H), 8.75 (s, 2H), 8.49 (s, 2H), 7.84 (s, 1H), 7.59 (s, 1H), 7.60 (m, 2H), 7.20 (dd, 1H, *J* = 2.0 Hz, *J* = 8.3 Hz), 7.05 (dd, 1H, *J* = 2.0 Hz, *J* = 8.3 Hz), 6.85 (d, 1H, *J* = 8.3 Hz), 6.76 (d, 1H, *J* = 8.3 Hz). **^{13}C-NMR** (DMSO-d_6, 125 MHz): δ [ppm] = 168.9, 167.4, 159.1, 155.3, 138.2, 137.4, 134.2, 128.6 125.1, 124.7, 120.6, 117.6, 114.1, 110.9, 109.9. **MS** (EI, 70 eV): *m/z* = 429 [M^+].

5-chloro-3-(4-(2-(dimethylamino)ethoxy)-3-methoxybenzyliden)indolin-2-one 16i

The resulting product is a dark yellow solid (31%). **HPLC**: R_t = 3.40 min, 4.53 min. **^{1}H-NMR** (DMSO-d_6, 500 MHz): δ [ppm] = 10.67 (s, NH), 8.66 (d, 1H, *J* = 2.1 Hz), 7.87-7.85 (m, 2H), 7.80 (d, 1H, *J* = 2.1 Hz), 7.69 (d, 1H, *J* = 2.1 Hz), 7.65 (s, 1H), 7.35 (d,1H, *J* = 1.9 Hz), 7.32-7.31 (m, 1H), 7.28 (dd, 1H, *J* = 2.1 Hz, *J* = 8.3 Hz), 7.20 (dd, 1H, *J* = 2.1 Hz, *J* = 8.3 Hz), 7.16 (d, 1H, *J* = 8.5 Hz), 7.10 (d, 1H, *J* = 8.5 Hz), 6.89 (d, 1H, *J* = 8.3 Hz), 6.83 (d, 1H, *J* = 8.3 Hz), 4.14 (t, 4H, *J* = 5.9 Hz), 3.83 (s, 3H), 3.81 (s, 3H), 2.65 (m, 4H), 2.23 (s, 6H), 2.22 (s, 6H). **^{13}C-NMR** (DMSO-d_6, 125 MHz): δ [ppm] = 168.6, 167.2, 150.8, 150.0, 148.7, 148.1, 141.4, 139.4, 138.8, 138.2, 129.0, 127.9, 127.4, 127.1, 126.3, 125.3, 124.8, 124.6, 123.6, 122.9, 122.7, 121.7, 119.2, 115.4, 113.1, 112.8, 112.1, 111.4, 110.5, 66.7, 66.6, 67.6, 55.6, 55.4, 45.6. **MS** (EI, 70 eV): *m/z* = 271 [M^+].

5-chloro-3-(4-(2-(diethylamino)ethoxy)-3-methoxybenzyliden)indolin-2-one 16j

The resulting product is a dark yellow solid (42%). **HPLC**: R_t = 4.32 min, 5.07 min. **^{1}H-NMR** (DMSO-d_6, 500 MHz): δ [ppm] = 10.67 (s, NH), 8.66 (d, 1H, *J* = 2.0 Hz), 7.87-7.85 (m, 2H), 7.80 (d, 1H, *J* = 2.0 Hz), 7.69 (d, 1H, *J* = 2.0 Hz), 7.65 (s, 1H), 7.35 (d, 1H, *J* = 1.9 Hz), 7.32-7.31 (m, 1H), 7.28 (dd, 1H, *J* = 2.0 Hz, *J* = 8.3 Hz), 7.20 (dd, 1H, *J* = 2.0 Hz, *J* = 8.3 Hz), 7.16 (d, 1H, *J* = 8.5 Hz), 7.10 (d, 1H, *J* = 8.5 Hz), 6.89 (d, 1H, *J* = 8.3 Hz), 6.83 (d, 1H, *J* = 8.3 Hz), 4.11 (m, 4H), 3.83 (s, 3H), 3.81 (s, 3H), 2.80 (m, 4H), 2.56 (m, 8H), 0.98 (m, 12H). **^{13}C-NMR** (DMSO-d_6, 125 MHz): δ [ppm] = 168.6, 167.2, 150.9, 150.0, 148.7, 148.1, 141.4, 139.4, 138.8, 138.2, 129.0, 128.0, 127.4, 127.0, 126.3, 125.3, 124.8, 124.6, 123.6, 122.9, 122.7, 121.7, 119.2, 115.4, 113.2, 112.8, 112.1, 111.4, 110.5, 67.2, 67.1, 55.6, 55.5, 51.2, 47.1, 11.9. **MS** (EI, 70 eV): *m/z* = 400 [M^+].

4-(4-((5-chloro-2-oxoindolin-3-yliden)methyl)-2-methoxyphenoxy) butannitrile 16k

The resulting product is a bright orange solid (67%). **HPLC**: R_t = 6.78 min, 7.24 min. **^{1}H-NMR** (DMSO-d_6, 500 MHz): δ [ppm] = 10.67 (s, NH), 8.67 (d, 1H, *J* = 2.0 Hz), 7.88 (s, 1H), 7.86 (dd, 1H, *J* = 2.0 Hz, *J* = 8.5 Hz), 7.80 (d, 1H, *J* = 2.1 Hz), 7.69 (d, 1H, *J* = 2.1 Hz), 7.66 (s, 1H), 7.37 (d, 1H, *J* = 1.9 Hz), 7.35-7.33 (m, 1H), 7.28 (dd, 1H, *J* = 2.1 Hz, *J* = 8.3 Hz), 7.20 (dd, 1H, *J* = 2.1 Hz, *J* = 8.3 Hz), 7.17 (d, 1H, *J* = 8.5 Hz), 7.12 (d, 1H, *J* = 8.5 Hz), 6.89 (d, 1H, *J* = 8.3 Hz), 6.83 (d, 1H, *J* = 8.3 Hz), 4.13 (t, 4H, *J* = 6.1 Hz), 3.85 (s, 3H), 3.82 (s, 3H), 2.66 (m, 4H), 2.06 (m, 4H). **^{13}C-NMR** (DMSO-d_6, 125 MHz): δ [ppm] = 168.6, 167.2, 150.4, 149.6, 148.8, 148.2, 141.5, 139.3, 138.8, 138.0, 129.1, 127.8, 127.5, 127.4, 126.8, 125.3, 124.8, 123.5, 123.0, 122.8, 121.7, 120.1, 119.2, 115.5, 113.2, 112.5, 111.4, 110.5, 66.7, 66.5, 55.6, 55.5, 24.7, 24.7. **MS** (EI, 70 eV): *m/z* = 368 [M^+].

5-chloro-3-(4-(2-(dimethylamino)ethoxy)-2-methoxybenzyliden)indolin-2-one 16l

The resulting product is a yellow solid (71%). **HPLC**: R_t = 3.58 min, 4.80 min. **^{1}H-NMR** (DMSO-d_6, 500 MHz): δ [ppm] = 10.65 (d, NH), 8.82 (d, 1H, *J* = 8.7 Hz), 7.96 (s, 1H), 7.69 (s, 1H), 7.64-7.62 (m, 2H), 7.43 (d, 1H, *J* = 2.1 Hz), 7.24 (dd, 1H, *J* = 2.1 Hz, *J* = 8.3 Hz), 7.18 (dd, 1H, *J* = 2.1 Hz, *J* = 8.3 Hz), 6.87 (d, 1H, *J* = 8.3 H), 6.80 (d, 1H, *J* = 8.3 H), 6.72 (m, 2H), 6.62 (m, 2H), 4.15 (m, 4H), 3.91 (s, 3H), 3.87 (s, 3H), 2.65 (t, 4H), 2.23 (s, 6H), 2.22 (s, 6H). **^{13}C-NMR** (DMSO-d_6, 125 MHz): δ [ppm] = 168.6, 167.1, 162.9, 162.4, 160.3, 159.6, 141.2, 138.8, 133.7, 133.6, 132.3, 130.8, 128.8, 127.4, 127.3, 125.3, 124.8, 124.3, 123.1, 122.2, 121.4, 118.9, 115.0, 114.9, 111.2, 110.5, 106.0, 105.6, 99.0, 98.1, 66.2, 66.1, 57.7, 56.0, 55.8, 45.6. **MS** (EI, 70 eV): *m/z* = 372 [M^+].

4-((4-((5-chloro-2-oxoindolin-3-yliden)methyl)phenoxy)methyl)benzonitrile 16m

The resulting product is a yellow solid (93%). **HPLC**: R_t = 8.17 min, 8.54 min. **^{1}H-NMR** (DMSO-d_6, 500 MHz): δ [ppm] = 10.70 (s, 2H), 8.49 (d, 2H, *J* = 8.9 Hz), 7.88 (m, 5H), 7.80 (d, 1H, *J* = 2.0 Hz), 7.71 (d, 2H, *J* = 8.9 Hz), 7.69 (s, 1H), 7.67 (d, 4H), 7.53 (d, 1H, *J* = 2.0 Hz), 7.27 (dd, 1H, *J* = 2.0 Hz, *J* = 8.3 Hz), 7.20 (m, 3H), 7.14 (d, 2H, *J* = 8.9 Hz), 6.89 (d, 1H, *J* = 8.3 Hz), 6.81 (d, 1H, *J* = 8.3 Hz), 5.33 (d, 4H, *J* = 2.9 Hz). **^{13}C-NMR** (DMSO-d_6, 125 MHz): δ [ppm] = 168.5, 167.1, 160.2, 159.5, 142.4, 141.4, 138.9, 138.6, 137.7, 134.7, 132.4, 131.6, 129.2, 128.2, 127.6, 127.3, 126.7, 125.3, 125.1, 124.9, 123.2, 122.8, 121.4, 119.3, 118.7, 115.2, 114.7, 111.4, 110.6, 110.5, 68.5, 68.4, 52.1. **MS** (EI, 70 eV): *m/z* = 386 [M^+].

Methyl 4-((4-((5-chloro-2-oxoindolin-3-yliden)methyl)phenoxy)methyl)-benzoate 16n

The resulting product is a yellow solid (70%). **HPLC**: R_t = 8.31 min, 8.66 min. **^{1}H-NMR** (DMSO-d_6, 500 MHz): δ [ppm] = 10.70 (s, 2H), 8.49 (d, 2H, *J* = 8.9 Hz), 8.00 (m, 4H), 7.89 (s, 1H), 7.80 (d, 1H, *J* = 2.0 Hz), 7.70 (d, 2H, *J* = 8.9 Hz), 7.66 (s, 1H), 7.62 (m, 4H), 7.53 (d, 1H, *J* = 2.0 Hz), 7.27 (dd, 1H, *J* = 2.0 Hz, *J* = 8.3 Hz), 7.20 (m, 3H), 7.14 (d, 2H, *J* = 8.9 Hz), 6.89 (d, 1H, *J* = 8.3 Hz), 6.81 (d, 1H, *J* = 8.3 Hz), 5.13 (d, 4H, *J* = 3.0 Hz), 3.86 (s, 6H). **^{13}C-NMR** (DMSO-d_6, 125 MHz): δ [ppm] = 168.5, 167.1, 166.0, 160.4, 159.7, 142.2, 141.4, 138.9, 138.6, 137.8, 134.7, 131.9, 131.6, 129.3, 129.2, 129.1, 127.6, 127.3, 127.2, 126.6, 125.3, 125.0, 124.9, 123.1, 122.8, 121.4, 119.3, 115.2, 114.7, 111.4, 110.5, 68.8, 68.7, 52.1. **MS** (EI, 70 eV): *m/z* = 419 [M^+].

3-((4-((5-chloro-2-oxoindolin-3-yliden)methyl)phenoxy)methyl)benzonitrile 16o

The resulting product is a yellow solid (90%). **HPLC**: R_t = 8.12 min, 8.53 min. **^{1}H-NMR** (DMSO-d_6, 500 MHz): δ [ppm] = 10.70 (s, 2H), 8.50 (d, 2H, *J* = 8.9 Hz), 7.96 (d, 2H), 7.89 (s, 1H), 7.85-7.81 (m, 5H), 7.72 (d, 2H, *J* = 8.9 Hz), 7.67 (s, 1H), 7.63 (m, 2H), 7.54 (d, 1H, *J* = 2.0 Hz), 7.27 (dd, 1H, *J* = 2.0 Hz, *J* = 8.3 Hz), 7.21 (m, 3H), 7.15 (d, 2H, *J* = 8.9 Hz), 6.89 (d, 1H, *J* = 8.3 Hz), 6.81 (d, 1H, *J* = 8.3 Hz), 5.28 (d, 4H, *J* = 3.0 Hz). **^{13}C-NMR** (DMSO-d_6, 125 MHz): δ [ppm] = 168.5, 167.1, 160.2, 159.6, 141.4, 138.9, 138.6, 138.4, 137.8, 134.7, 132.6, 132.5, 131.8, 131.6, 131.2, 129.8, 129.2, 127.6, 127.2, 126.7, 125.3, 125.0, 124.9, 123.2, 122.8, 121.4, 119.3, 118.6, 115.2, 114.7, 111.5, 111.4, 110.5, 68.3, 68.2. **MS** (EI, 70 eV): *m/z* = 386 [M^+].

5-chloro-3-(4-(4-methyl-1H-imidazol-1-yl)phenoxy)benzylidene)indolin-2-one 16p

The resulting product is a yellow solid (41%). **HPLC**: R_t = 5.53 min, 6.15 min. **^{1}H-NMR** (DMSO-d_6, 500 MHz): δ [ppm] = 10.76 (s, 2H), 8.11 (dd, 2H, *J* = 1.3 Hz, *J* = 6.8 Hz), 7.92 (m, 1H), 7.84 (m, 1H), 7.75 (m, 1H), 7.66 (m, 4H), 7.50 (m, 2H), 7.41 (m, 2H), 7.24 (m, 10H), 7.16 (m, 2H), 7.08 (m, 2H), 6.89 (m, 2H), 6.81 (m, 1H), 2.16 (s, 6H). **^{13}C-NMR** (DMSO-d_6, 125 MHz): δ [ppm] = 172.4, 168.87, 167.47, 159.55, 158.97, 154.17, 154.10, 142.0, 139.6, 138.8, 138.5, 137.6, 135.2, 133.9, 132.2, 129.9, 129.6, 129.3, 127.9, 127.7, 127.5, 126.4, 125.9, 125.4, 124.8, 123.0, 122.4, 122.4, 121.9, 121.9, 120.6, 118.4, 117.8, 114.8, 111.9, 111.09, 14.52, 14.04. **MS** (EI, 70 eV): *m/z* = 427 [M^+].

3-(4-(4-(dimethylamino)phenyl)diazenyl)benzylidene)indolin-2-one 16q

The resulting product is a red solid (9%). **^{1}H-NMR** (DMSO-d_6, 500 MHz): δ [ppm] = 10.65 (s, 1H), 7.86 (m, 6H), 7.66 (m, 2H), 7.22 (m, 2H), 6.87 (m, 5H), 3.09 (s, 6H). **^{13}C-NMR** (DMSO-d_6, 125 MHz): δ [ppm] = 168.6, 152.8, 143.0, 142.7, 135.4, 134.9, 130.6, 130.3, 127.9, 125.0, 122.56, 122.0, 121.2, 120.9, 120.8, 111.6, 110.2, 29.8. **MS** (EI, 70 eV): *m/z* = 368 [M^+].

5-chloro-3-(3-methoxy-4-(methylsulfonyl)benzylidene)indolin-2-one 16r

The resulting product is an orange solid (85%). **HPLC**: R_t = 4.75 min, 6.48 min. **^{1}H-NMR** (DMSO-d_6, 500 MHz): δ [ppm] = 10.81 (s, 2H), 8.59 (s, 1H), 8.01 (s, 1H), 7.94 (d, 1H, *J* = 8.0 Hz), 7.88 (m, 3H), 7.72 (s, 1H), 7.63 (s, 1H), 7.50 (d, 1H, *J* = 8.0 Hz), 7.46 (d, 1H, *J* = 2.1 Hz), 7.33 (dd, 1H, *J* = 2.1 Hz, *J* = 8.3 Hz), 7.29 (dd, 1H, *J* = 2.1, *J* = 8.3 Hz), 6.91 (d, 1H, *J* = 8.3 Hz), 6.86 (d, 1H, *J* = 8.3 Hz), 4.02 (s, 3H), 3.32 (s, 3H), 3.31 (s, 3H). **^{13}C-NMR** (DMSO-d_6, 125 MHz): δ [ppm] = 168.4, 167.0, 157.3, 156.7, 142.6, 141.7, 140.7, 140.4, 136.9, 135.9, 130.8, 129.7, 129.6, 129.5, 129.12, 129.1, 128.6, 126.7, 126.1, 125.5, 124.6, 122.9, 122.4, 121.5, 120.9, 116.0, 114.4, 112.1, 111.5, 56.6, 56.3. **MS** (EI, 70 eV): *m/z* = 363 [M^+].

5-chlor-3-(3-methoxy-4-(4-methyl-1H-imidazol-1-yl)benzylidene)indoline 16s

The resulting product is an orange solid (55%). **HPLC**: R_t = 4.10 min, 4.89 min. **^{1}H-NMR** (DMSO-d_6, 500 MHz): δ [ppm] = 10.78 (s, 2H), 8.70 (d, 1H, *J* = 1.7 Hz), 7.99 (s, 1H), 7.96 (d, 1H, *J* = 8.5 Hz), 7.92 (d, 1H, *J* = 1.3 Hz), 7.91 (d, 1H, *J* = 1.3 Hz), 7.86 (d, 1H, *J* = 2.1 Hz), 7.73 (s, 1H), 7.63 (d, 1H, *J* = 2.1 Hz), 7.61 (d, 1H, *J* = 1.5 Hz), 7.57 (d, 1H, *J* = 8.1 Hz), 7.51 (d, 1H, *J* = 8.2 Hz), 7.43 (d, 1H, *J* = 10.4 Hz), 7.32 (dd, 1H, *J* = 2.1 Hz, *J* = 8.3 Hz), 7.26 (m, 3H), 6.92 (d, 1H, *J* = 8.3 Hz), 6.86 (d, 1H, *J* = 8.3 Hz), 3.92 (s, 3H), 3.90 (s, 3H), 2.17 (s, 6H). **^{13}C-NMR** (DMSO-d_6, 125 MHz): δ [ppm] = 170.0, 168.7, 152.6, 154.4, 141.1, 143.6, 139.5, 138.7, 138.6, 138.5, 138.4, 135.6, 135.4, 131.5, 130.2, 129.2, 129.0, 128.7, 128.5, 127.8,

127.7, 127.3, 126.8, 126.7, 125.8, 123.9, 124.1, 121.6, 118.2, 118.0, 117.9, 115.7, 113.3, 112.6, 57.9, 57.7, 50.3, 15.3. **MS** (ESI, 70 eV): *m/z* = 366 [M^+].

5-chloro-3-((9-methyl-9H-carbazol-3-yl)methylene)indolin-2-one 16t

The resulting product is a yellow solid (17%). **HPLC**: R_t = 8.61 min, 8.90 min. **^{1}H-NMR** (DMSO-d_6, 500 MHz): δ [ppm] = 10.70 (s, 1H), 8.12 (d, 1H, *J* = 7.8 Hz), 7.79 (m, 5H), 7.54 (m, 1H), 7.25 (m, 2H), 6.88 (m, 1H), 3.95 (s, 3H). **^{13}C-NMR** (DMSO-d_6, 125 MHz): δ [ppm] = 138.7, 167.3, 142.2, 141.6, 141.3, 140.6, 139.7, 138.6, 131.1, 128.8, 127.7, 127.4, 127.1, 127.5, 126.3, 125.7, 125.2, 124.8, 124.3, 124.0, 123.1, 122.8, 122.2, 121.9, 121.8, 121.0, 120.4, 119.9, 119.7, 118.9, 111.2, 110.4, 109.9, 109.8, 109.5, 29.2. **MS** (EI, 70 eV): *m/z* = 358 [M^+].

3-((9-methyl-9H-carbazol-3-yl)methylene)indolin-2-one 16u

The resulting product is a yellow solid (15%). **HPLC**: R_t = 8.13 min, 8.32 min. **^{1}H-NMR** (DMSO-d_6, 500 MHz): δ [ppm] = 10.51 (s, 1H), 8.51 (m, 1H), 8.16 (d, 1H, *J* = 7.7 Hz), 7.80 (s, 1H), 7.67 (m, 4H), 7.48 (m, 1H), 7.18 (m, 3H), 6.82 (m, 2H), 3.88 (s, 3H). **^{13}C-NMR** (DMSO-d_6, 125 MHz): δ [ppm] = 169.4, 142.9, 141.7, 141.6, 138.1, 131.2, 129.8, 127.7, 126.7, 125.4, 122.9, 122.6, 122.2, 121.9, 121.8, 121.4, 120.9, 119.9, 110.4, 109.9, 29.5. **MS** (EI, 70 eV): *m/z* = 324 [M^+].

9. Synthesis of 3-(4-(3-(1*H*-tetrazol-5-yl)propoxy)benzyliden)-5-chloroindolin-2-one 16v

4-(4-((5-chloro-2-oxoindolin-3-ylidene)methyl)phenoxy)butannitrile **16f** (20 mg, 0.06 mmol), sodium azide (46 mg, 0.71 mmol) und ammonium chloride (38 mg, 0.71 mmol) were added to dimethylformamide (0.7 mL) and stirred for 2 h at 100℃ under microwave irradiation. After cooling to room temperature the reaction solution was added to water, acidified with 2 N HCl and extracted three times with ethyl acetate. The combined organic layers were dried over sodium sulphate, filtered and the solvent was removed in vacuo. The resulting residue was purified by column chromatography on silica gel to provide the desired product in 62% as brown solid. **HPLC**: R_t = 6.61 min. **^{1}H-NMR** (DMSO-d_6, 500 MHz): δ [ppm] = 12.10 (s, NH), 10.13 (s, NH), 7.95 (s, 1H), 7.28 (d, 1H, *J* = 8.6 Hz), 7.24 (d, 2H, *J* = 8.8 Hz), 7.20 (dd, 1H, *J* = 2.3 Hz, *J* = 8.6 Hz), 7.15 (d, 2H, *J* = 8.8 Hz), 6.77 (d, 1H, *J* = 2.3 Hz) 4.13 (t, 2H, *J* = 6.0 Hz), 2.70 (t, 2H, *J* = 7.1 Hz), 2.08 (m, 2H). **^{13}C-NMR** (DMSO-d_6, 125 MHz): δ [ppm] = 162.3, 157.9, 157.5, 135.4, 131.0, 130.6, 126.4, 126.0, 124.1, 123.6, 121.5, 120.3, 116.7, 115.5, 65.8, 30.8, 24.8. **MS** (EI, 70 eV): *m/z* = 353 (M^+).

III. FTL3 *in vitro* assay conducted by Cerep

1. Reference compound Data

Assay: FLT-3 Kinase *(h)*

Reference compound: Staurosporine

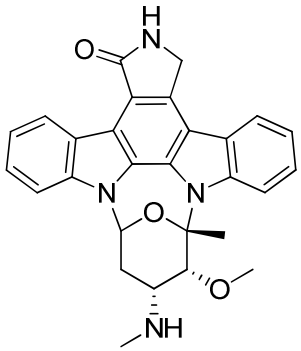

IC_{50} (M) = 9.1E-10

nH = 1.7

2. Experimental conditions

Assay: FLT-3 Kinase *(h)*

Source: human recombinant (insect cells)

Substrate: ATP + Ulight-CAGAGAIETDKEYYTVKD (100 nM)

Incubation: 90 min, RT

Measured Component: Phospho-Ulight- CAGAGAIETDKEYYTVKD

Detection Method: LANCE

3. Analysis and expression of results

The results are expressed as a percent of control specific activity ((measured specific activity/control specific activity) x 100) obtained in the presence of the compounds.

The IC_{50} value (concentration causing a half-maximal inhibition of control specific activity) and Hill coefficient(s) (nH) were determined by non-linear regression analysis of the inhibition curve generated with mean replicate values using Hill equation curve fitting (Y D + [(A-D)/ $(1-(IC_{50})^{nH})$], where Y = specific activity, D = minimum specific, A = maximum specific activity, C = compound concentration, $C_{50} = IC_{50}$, and nH = slope factor).

This analysis was performed using software developed at Cerep (Hill software) and validated by comparison with data generated by the commercial software SigmaPlot® 4.0 for Windows® (1997 by SPSS inc.).

IV. Selectivity screening of compound 16e conducted by Cerep

The ExpresS Diversity kinase profile is a fast turnaround profile conducted by Cerep. Percentage kinase activities of compound **16e** at 1 µM in panels of human protein kinases determined by Cerep. Measurements were performed in duplicate and the average was taken.

Kinase	% of Control Values[1]	Kinase	% of Control Values[1]
Abl kinase *(h)*	95.4	JAK3 *(h)*	67.3
Akt1/PKBα *(h)*	101.1	JNK1 *(h)*	96.4
AurA/Aur2 kinase *(h)*	99.6	KDR kinase *(h)* (VEGFR2)	88.4
CaMK2α *(h)*	103.4	Lck kinase *(h)*	103.8
CDC2/CDK1 *(h)* (cycB)	105.5	MAPKAPK2 *(h)*	95.3
CDK2 *(h)* (cycA)	93.5	MARK1 *(h)*	99.6
CHK1 *(h)*	95.8	MKK6 *(h)*	100.7
CHK2 *(h)*	94.0	MNK2 *(h)*	107.4
CK1α *(h)*	102.6	MST4 kinase *(h)*	103.7
c-Met kinase *(h)*	97.2	NEK2 *(h)*	106.9
EGFR kinase *(h)*	102.1	p38α kinase *(h)*	99.4
EphA2 kinase *(h)*	101.2	PAK2 *(h)*	103.7
EphA3 kinase *(h)*	101.3	PAK4 *(h)*	101.2
EphB4 kinase *(h)*	101.8	PDK1 *(h)*	106.9
ERK_2 *(h)* ($P42^{mapk}$)	100.6	Pim2 kinase *(h)*	94.7
FGFR1 kinase *(h)*	98.2	PKA *(h)*	98.7
FGFR2 kinase *(h)*	100.1	PKCβ2 *(h)*	99.4
FGFR3 kinase *(h)*	92.9	PLK1 *(h)*	100.5
FLT-3 kinase *(h)*	14.7	RAF-1 kinase *(h)*	108.6
GSK3α *(h)*	103.7	ROCK1 (h)	102.4
GSK3β *(h)*	97.0	SGK1 *(h)*	96.0
HGK *(h)* MAP4K4	27.8	SIK *(h)*	118.9
IKKα *(h)*	103.6	Src kinase *(h)*	100.8
IRAK4 *(h)*	91.8	TAOK2 (TAO1) *(h)*	95.1
IRK *(h)* (InsR)	112.9	TRKA *(h)*	87.0

[1] The results are expressed as a percent of control specific activity ((measured specific activity/control specific activity) x 100) obtained in the presence of the compounds (control = staurosporine).

Assay Kinase	Source	Substrate/Stimulus/Tracer	Incubation	Measured Component
Abl kinase *(h)*	human recombinant (insect cells)	ATP + Ulight-TK peptide (100 nM)	60 min RT	phospho-Ulight-TK- peptide
Akt1/ PKBα *(h)*	human recombinant (insect cells)	ATP + CREBtide (CKRREILSRRPSYRK) (25 nM)	60 min RT	phospho-CREBtide (CKRREILSRRPSYRK)
AurA/Aur 2 kinase *(h)*	human recombinant (Sf21 cells)	ATP + Ulight-RRRSLLE (100 nM)	15 min RT	phospho-Ulight-RRRSLLE
CaMK2α *(h)*	human recombinant	ATP + Ulight-CGSGSGRPRTSSFAEG (50 nM)	30 min RT	phospho-Ulight-CGSGSGRPRTSSFAEG
CDC2/CDK1 (h) (cycB)	human recombinant (insect cells)	ATP + Ulight-CFFKNIVTPRTPPPSQGK-amide (100 nM)	15 min RT	phospho-Ulight-CFFKNIVTPRTPPPSQGK-amide
CDK2 *(h)* (cycA)	human recombinant	ATP + Ulight-CFFKNIVTPRTPPPSQGK-amide (50 nM)	30 min RT	phospho-Ulight-CFFKNIVTPRTPPPSQGK-amide
CHK1 *(h)*	human recombinant (insect cells)	ATP + CREBtide (CKRREILSRRPSYRK) (25 nM)	30 min RT	phospho-CREBtide (CKRREILSRRPSYRK)
CHK2 *(h)*	human recombinant (insect cells)	ATP + CREBtide (CKRREILSRRPSYRK) (25 nM)	15 min RT	phospho-CREBtide (CKRREILSRRPSYRK)
CK1α *(h)*	human recombinant	ATP + Ulight-ARTKQTARKSTGGKAPRKQLAGCG (25 nM)	60 min RT	phospho-Ulight-ARTKQTARKSTGGKAPRKQLAGCG
c-Met kinase *(h)*	human recombinant (insect cells)	ATP + Ulight-CAGAGAIETDKEYYTVKD (25 nM)	60 min RT	phospho-Ulight-CAGAGAIETDKEYYTVKD
EGFR kinase *(h)*	human recombinant (insect cells)	ATP + Ulight-CAGAGAIETDKEYYTVKD (100 nM)	15 min RT	phospho-Ulight-CAGAGAIETDKEYYTVKD
EphA2 kinase *(h)*	human recombinant	ATP + Ulight-TK peptide (50 nM)	30 min RT	phospho-Ulight-TK- peptide
EphA3 kinase	human recombinant	ATP + Ulight-TK peptide (50 nM)	60 min RT	phospho-Ulight-TK- peptide

(h)				
EphB4 kinase *(h)*	human recombinant (insect cells)	ATP + Ulight-TK peptide (100 nM)	90 min RT	phospho-Ulight-TK- peptide
ERK2 *(h)* ($P42^{mapk}$)	human recombinant (*E. coli*)	ATP + Ulight-CFFKNIVTPRTPPPSQGK-amide (100 nM)	15 min RT	phospho-Ulight-CFFKNIVTPRTPPPSQGK-amide
FGFR1 kinase *(h)*	human recombinant (insect cells)	ATP + Ulight-CAGAGAIETDKEYYTVKD (100 nM)	60 min RT	phospho-Ulight-CAGAGAIETDKEYYTVKD
FGFR2 kinase *(h)*	human recombinant	ATP + Ulight-CAGAGAIETDKEYYTVKD (25 nM)	15 min RT	phospho-Ulight-CAGAGAIETDKEYYTVKD
FGFR3 kinase *(h)*	human recombinant	ATP + Ulight-CAGAGAIETDKEYYTVKD (100 nM)	90 min RT	phospho-Ulight-CAGAGAIETDKEYYTVKD
FLT-3 kinase *(h)*	human recombinant (insect cells)	ATP + Ulight-CAGAGAIETDKEYYTVKD (100 nM)	90 min RT	phospho-Ulight-CAGAGAIETDKEYYTVKD
GSK3α *(h)*	human recombinant	ATP + Ulight-CFFKNIVTPRTPPPSQGK-amide (100 nM)	60 min RT	phospho-Ulight-CFFKNIVTPRTPPPSQGK-amide
GSK3β *(h)*	human recombinant	ATP + Ulight-CFFKNIVTPRTPPPSQGK-amide (100 nM)	90 min RT	phospho-Ulight-CFFKNIVTPRTPPPSQGK-amide
HGK *(h)* (MAP 4K4)	human recombinant	ATP + Ulight-FLGFTYVAP (50 nM)	90 min RT	phospho-Ulight-FLGFTYVAP
IKKα *(h)*	human recombinant (Sf21 cells)	ATP + Ulight-IkappaB-alpha (100 nM)	30 min RT	phospho-Ulight-IkappaB-alpha
IRAK4 *(h)*	human recombinant (insect cells)	ATP + Ulight-FLGFTYVAP (50 nM)	90 min RT	phospho-Ulight-FLGFTYVAP
IRK *(h)* (InsR)	human recombinant	ATP + Ulight-Poly GAT[EAY(1:1:1)]n (50 nM)	10 min RT	phospho-Ulight-Poly GAT[EAY(1:1:1)]n
JAK3 *(h)*	human recombinant	ATP + Ulight-CAGAGAIETDKEYYTVKD (100 nM)	60 min RT	phospho-Ulight-CAGAGAIETDKEYYTVKD
JNK1 *(h)*	human recombinant (*E. coli*)	ATP + Ulight-CFFKNIVTPRTPPPSQGK-amide	60 min RT	phospho-Ulight-CFFKNIVTPRTPPPSQGK-amide

		(100 nM)		
KDR kinase *(h)* (VEGFR 2)	human recombinant (Sf9 cells)	ATP + Ulight-CAGAGAIETDKEYYTVKD (100 nM)	60 min RT	phospho-Ulight-CAGAGAIETDKEYYTVKD
Lck kinase *(h)*	human recombinant (insect cells)	ATP + Ulight-Poly GAT[EAY(1:1:1)]n (25 nM)	30 min RT	phospho-Ulight-Poly GAT[EAY(1:1:1)]n
MAPKAPK2 *(h)*	human recombinant (*E. coli*)	ATP + CREBtide (CKRREILSRRPSYRK) (25 nM)	15 min RT	phospho-CREBtide (CKRREILSRRPSYRK)
MARK1 *(h)*	human recombinant	ATP + Ulight-RRRSLLE (50 nM)	30 min RT	phospho-Ulight-RRRSLLE
MKK6 *(h)*	human recombinant	ATP + inactive p38a (50 nM)	10 min RT	phospho-p38a
MNK2 *(h)*	human recombinant (Sf21 cells)	ATP + CREBtide (CKRREILSRRPSYRK) (25 nM)	90 min RT	phospho-CREBtide (CKRREILSRRPSYRK)
MST4 kinase *(h)*	human recombinant	ATP + Ulight TM- PKC (50 nM)	30 min RT	Phospho-Ulight-TM-PKC
NEK2 *(h)*	human recombinant (insect cells)	ATP + Ulight-FLGFTYVAP (50 nM)	60 min RT	phospho-Ulight-FLGFTYVAP
p38α kinase *(h)*	human recombinant (*E. coli*)	ATP + Ulight-CFFKNIVTPRTPPPSQGK-amide (100 nM)	60 min RT	phospho-Ulight-CFFKNIVTPRTPPPSQGKamide
PAK2 *(h)*	human recombinant (Sf9 cells)	ATP + Ulight-RRRSLLE (50 nM)	60 min RT	phospho-Ulight-RRRSLLE
PAK4 *(h)*	human recombinant (insect cells)	ATP + Ulight-RRRSLLE (50 nM)	30 min RT	phospho-Ulight-RRRSLLE
PDK1 *(h)*	human recombinant (insect cells)	ATP + Ulight-FLGFTYVAP (400 nM)	90 min RT	phospho-Ulight-FLGFTYVAP
Pim2 kinase *(h)*	human recombinant (insect cells)	ATP + CREBtide (CKRREILSRRPSYRK) (25 nM)	60 min RT	phospho-CREBtide (CKRREILSRRPSYRK)
PKA *(h)*	human recombinant	ATP + Ulight-RRRSLLE (50 nM)	10 min RT	phospho-Ulight-RRRSLLE

	(*E. coli*)			
PKCβ2 *(h)*	human recombinant	ATP + CREBtide (CKRREILSRRPSYRK) (25 nM)	15 min RT	phospho-CREBtide (CKRREILSRRPSYRK)
PLK1 *(h)*	human recombinant	ATP + Ulight-FLGFTYVAP (40 nM)	60 min RT	phospho-Ulight-FLGFTYVAP
RAF-1 kinase *(h)*	human recombinant	ATP + Ulight-ARTKQTARKSTGGKAPRKQLAGCG (50 nM)	180 min RT	phospho-Ulight-ARTKQTARKSTGGKAPRKQLAGCG
ROCK1 *(h)*	human recombinant	ATP + Ulight-RRRSLLE (50 nM)	30 min RT	phospho-Ulight-RRRSLLE
SGK1 *(h)*	human recombinant	ATP + Ulight-RRRSLLE (50 nM)	30 min RT	phospho-Ulight-RRRSLLE
SIK *(h)*	human recombinant (Sf21 cells)	ATP + CREBtide (CKRREILSRRPSYRK) (25 nM)	90 min RT	phospho-CREBtide (CKRREILSRRPSYRK)
Src kinase *(h)*	human recombinant (insect cells)	ATP + Ulight-Poly GAT[EAY(1:1:1)]n (5 nM)	10 min RT	phospho-Ulight-Poly GAT[EAY(1:1:1)]n
TAOK2 (TAO1) *(h)*	human recombinant	ATP + Ulight-FLGFTYVAP (40 nM)	60 min RT	phospho-Ulight-FLGFTYVAP
TRKA *(h)*	human recombinant (insect cells)	ATP + Ulight-Poly GAT[EAY(1:1:1)]n (5 nM)	10 min RT	phospho-Ulight-Poly GAT[EAY(1:1:1)]n

V. γ-Secretase assay and cell-based toxicity assay conducted by Roche

See Ref. 11 in the publication.

VI. Toxicity assay: Determination of the *in vivo* activity on wt zebrafish embryos

The wt zebrafish embryos were collected and placed into 24-well plates, ten embryos per well and maintained in E2 medium at 28℃. Compounds were added 5 hpf (50% epiboly) and the embryos allowed to grow in chemical compound solution up to 2 days. The phenotypes were compared using the Axio Scope.A1 microscope system from Carl Zeiss at 48 hpf. **Animal husbandry.** All animal experiments were conducted and documented according to the federal and local regulation.

5. Zusammenfassung

Die vorliegende Arbeit beschreibt die erfolgreiche Entwicklung von hochaktiven und selektiven GSK-3-Inhibitoren, die im Jahre 2011 zu einer Patentanmeldung führte.

Durch eine neu etablierte Synthese konnten, ausgehend von Verbindung **27**, schnell und effizient viele Harnstoffderivate synthetisiert und optimiert werden. Der Hauptteil dieser Verbindungen zeigte eine analoge bzw. höhere Aktivität für GSK-3β (Abb. 23). Darüber hinaus konnte im Vergleich zu Verbindung **27**, bei ähnlicher Selektivität, eine verringerte Toxizität im Wildtyp-Zebrafisch-Embryo nachgewiesen werden.

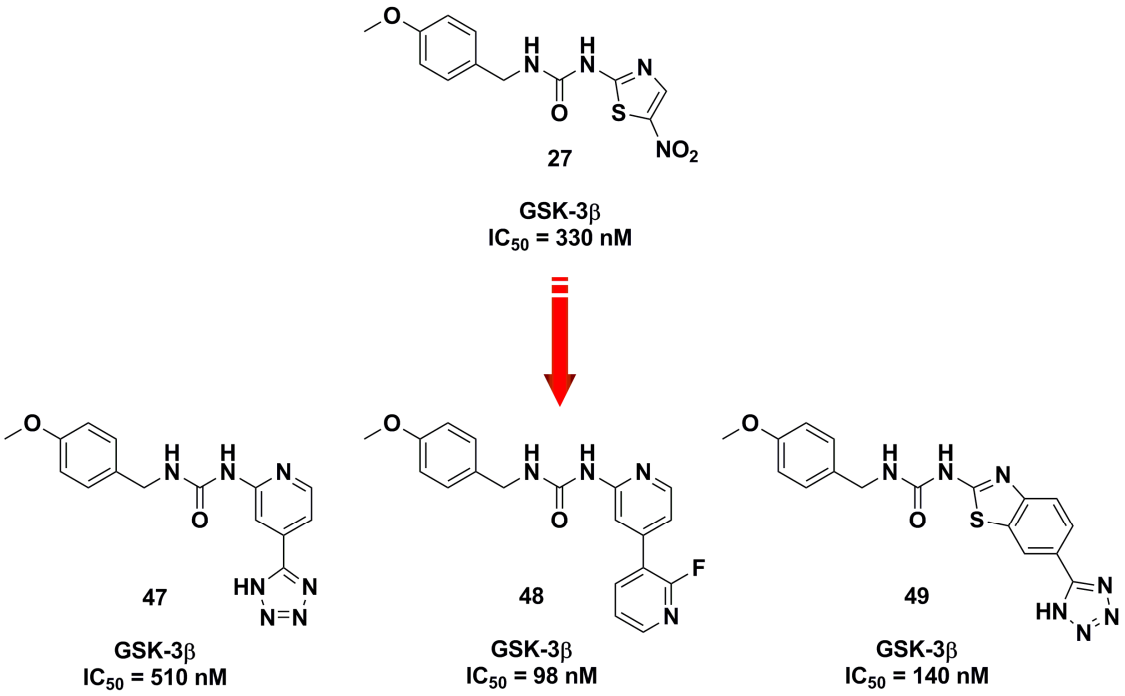

Abb. 23: Ausgangspunkt und Ergebnis der Harnstoffderivatisierung.

Die durch die Harnstoffderivatisierung gewonnenen Kenntnisse über die ATP-Bindungstasche und die Anfertigung des GSK-3-Reviews stellten sehr gute Ansatzpunkte für die Folgeprojekte dar. Mit Hilfe dieser Daten konnte ein vereinfachtes Schema der ATP-Bindungstasche angefertigt werden, in dem relevante Bindungsbereiche für GSK-3-Inhibitoren markiert wurden. Diese Strategie diente der Synthese neuer Verbindungen, die das Oxadiazol-Grundgerüst als Ausgangspunkt hatten. Auf diese Weise gelang die Herstellung zahlreicher

biphenylischer Systeme, die nanomolare Aktivitäten gegenüber GSK3-α und GSK-3β aufweisen konnten (Abb. 24).

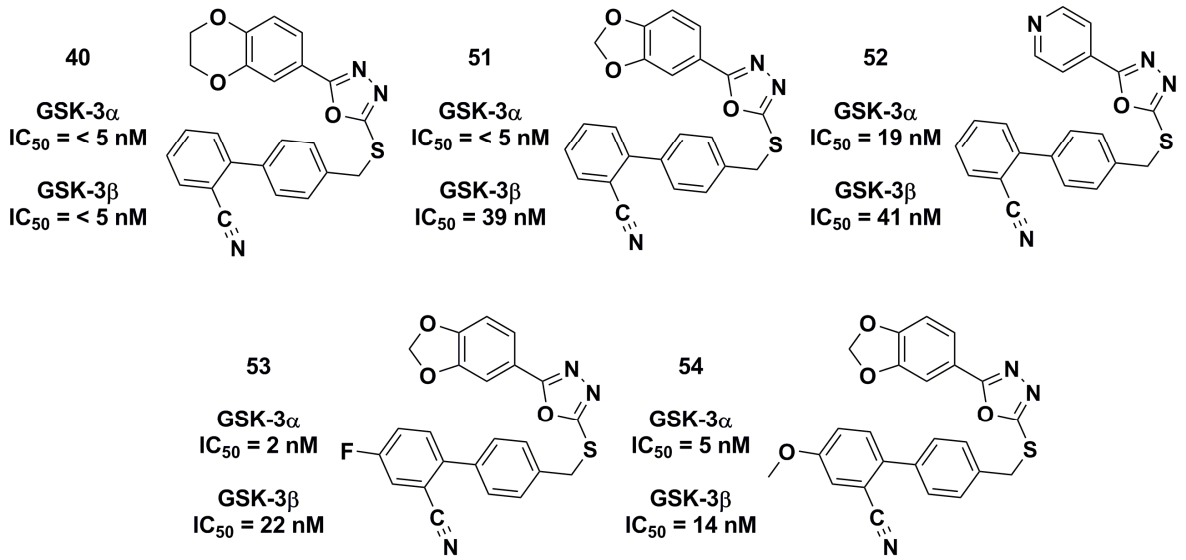

Abb. 24: Übersicht einiger der aktivsten Biphenylderivate.

Diese GSK-3-Inhibitoren zeigten gegenüber vier anderen Kinasen keine bzw. geringe Aktivität und konnten auch im Wildtyp-Zebrafisch-Embryo sehr gute Ergebnisse erzielen. Um die Interaktion dieser Inhibitoren mit der Gelenk-Region zu steigern und deren Löslichkeit zu erhöhen, wurden unterschiedliche Linkersysteme in die Inhibitoren eingefügt. Für Verbindung **39** konnte hierdurch die Aktivität im Vergleich zu Verbindung **52** gesteigert werden. Dieser Inhibitor zeigte zudem eine mehr als 5000-fache Selektivität für GSK-3. Das eingefügte Linkersystem in Verbindung **42** erhöhte, im Vergleich zu Struktur **40**, die Löslichkeit um das 10-fache, senkte jedoch geringfügig die Aktivität (Abb. 25).

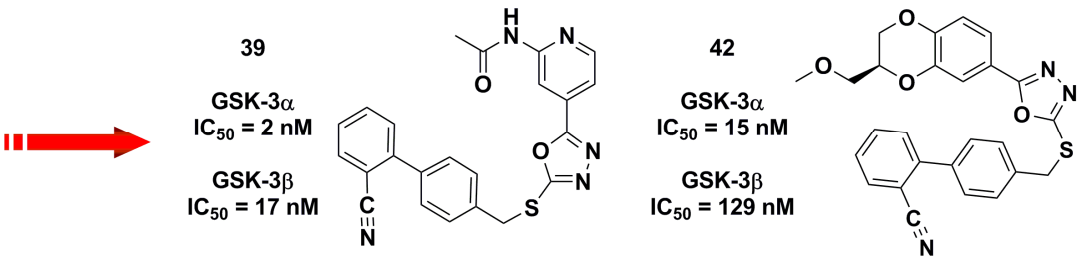

Abb. 25: Erzieltes Ergebnis der Linkersysteme.

Durch die Variation des Substitutionsmusters am biphenylischen System konnte die bisher höchste Selektivität für eine GSK-3-Isoform erzielt werden. Die beste Verbindung dieser Serie, GSK-3-Inhibitor **41**, war 92-fach selektiver für GSK-3α gegenüber GSK-3β (Abb. 26).

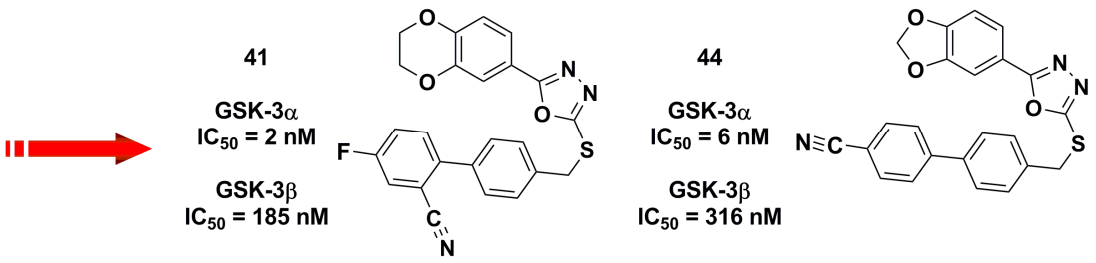

Abb. 26: Diskriminierung einer GSK-3-Isoform.

Verbindung **44** zeigte zwar eine geringere Selektivität für GSK-3α, wies jedoch gegenüber 48 von 50 Kinasen keine oder eine sehr geringe inhibitorische Aktivität auf (Abb. 27). Eine Inhibition unter 25% wird von Cerep (Dienstleistungsunternehmen für klinische Entwicklung) als nicht signifikant betrachtet und erhärtet somit die Aussage, dass der GSK-3-Inhibitor **44** ein außerordentlich selektiver Inhibitor ist.

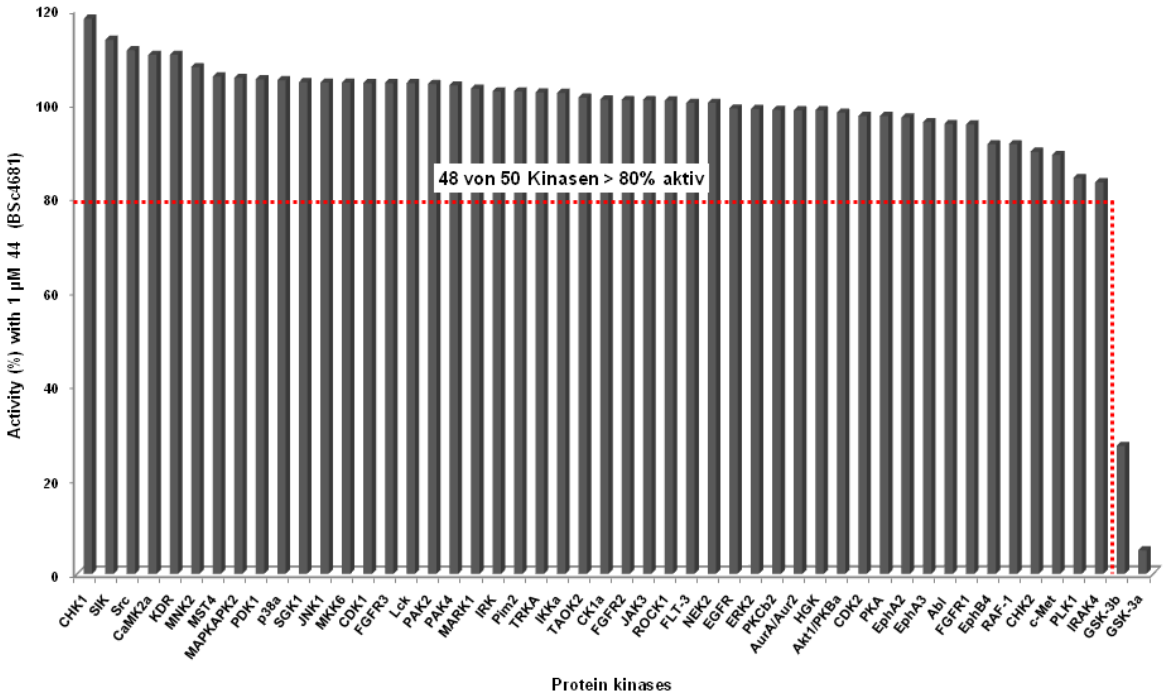

Abb. 27: Aktivität von Verbindung **44** gegenüber 50 Kinasen.

Die GSK-3-Inhibitoren **39**, **41**, **42** und **44** wurden ebenfalls im Wildtyp-Zebrafisch-Embryo evaluiert und waren im Messbereich (< 30 µM) nicht toxisch. Einige der biphenylischen Derivate wurden bereits in transgenen AD-Mäusen getestet. Zu diesem Zweck wurden *scale-up*-Synthesen von einigen Verbindungen durchgeführt, um eine für die *in vivo* Versuche entsprechende Menge zur Verfügung zu stellen. Die Untersuchungen ergaben jedoch, dass keine Penetration der Blut-Hirn-Schranke stattgefunden hat. Drei weitere Verbindungen werden derzeit in transgenen Mäusen evaluiert.

Im Rahmen eines neuen Projekts wurde ein LRRK2-Review angefertigt, in dem die bisher publizierten Inhibitoren dieser Kinase zusammengefasst sind. Alle relevanten Daten zu diesen Verbindungen, Tiermodelle für LRRK2 und Mutationen im LRRK2-Gen werden diskutiert. Hierbei wurde das Potential von LRRK2-Inhibitoren im Bereich der Parkinson-Krankheit kritisch diskutiert und eine Grundlage für neue Projekte geschaffen.

Durch die Verwendung des Indolinon-Grundgerüsts konnten sehr aktive FLT-3-Inhibitoren synthetisiert werden (Abb. 28). Die Evaluierung einer dieser Inhibitoren im *Kinase-Panel* bestätigte zudem eine gute Selektivität gegenüber FLT-3. Die *in vivo* Evaluation im Wildtyp-Zebrafisch-Embryo belegte, dass diese Inhibitoren im getesteten Konzentrationsbereich (< 30 µM) nicht toxisch sind.

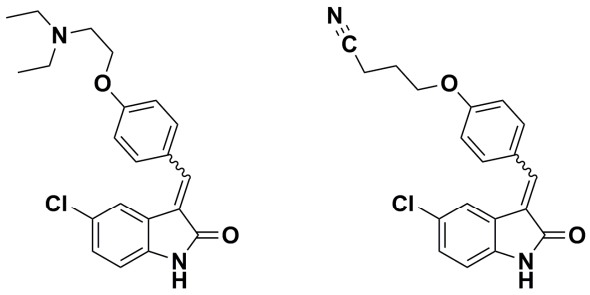

55

FLT-3
IC_{50} = 4.1 nM

56

FLT-3
IC_{50} = 17.0 nM

Abb. 28: Beispiele für die Aktivität der synthetisierten FLT-3-Inhibitoren.

6. Ausblick

Die in dieser Arbeit hergestellten Verbindungen zählen zu den aktivsten und selektivsten GSK-3-Inhibitoren, die bisher veröffentlicht und patentiert worden sind. GSK-3 wird mit einer Vielzahl von Krankheiten assoziiert, wodurch die Anwendung dieser Inhibitoren für viele Indikationsgebiete denkbar wäre. Somit liegt es nahe, weitere Arbeiten an diesen Strukturen voranzutreiben.

Im Bereich der Wirkstoffforschung ist vor allem die Penetration der Blut-Hirn-Schranke eine Herausforderung für viele Verbindungen. Obwohl die *in-vivo* Effektivität dieser Verbindungen bereits im Wildtyp-Zebrafisch-Embryo gezeigt werden konnte, wurde in transgenen AD-Mäusen noch kein Effekt beobachtet. Aufgrund dessen sollte der Fokus auf die Löslichkeit dieser Verbindungen gelegt werden. Hierbei könnte die Insertion von Stickstoffatomen in das biphenylische System schon zu einer Erhöhung der Löslichkeit führen. Auch ein Austausch der ersten Phenylgruppe durch Piperazin wäre eine denkbare Option (Abb. 29).

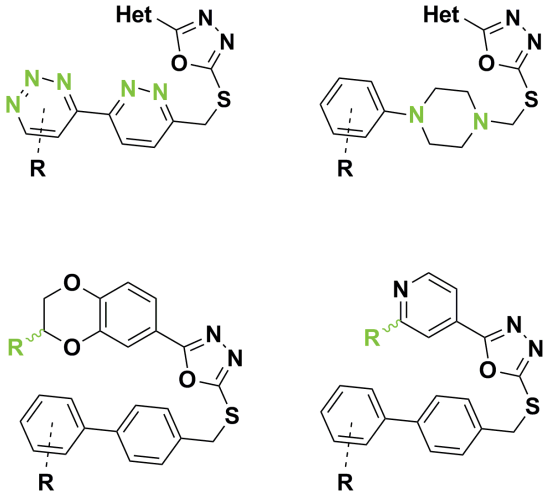

Abb. 29: Optionen zum Erhöhen der Löslichkeit bestehender Verbindungen.

Durch die Einführung verschiedener Linkersysteme konnte in dieser Arbeit bereits gezeigt werden, dass die Löslichkeit und Interaktion mit der Gelenk-Region gesteigert werden kann. Aus diesem Grunde wäre eine Untersuchung verschiedener Linker eine weitere Möglichkeit zur Löslichkeitssteigerung.

Aus der Literatur ist bekannt, dass bislang noch keine effektive Diskriminierung einer GSK-3-Isoform durch einen Inhibitor erzielt wurde. Desweiteren ist momentan nicht vollständig geklärt, ob beide Isoformen in der Pathologie der AD involviert sind. Sollte jedoch eine Diskriminierung für eine Therapie notwendig sein, um eventuelle Nebenwirkungen zu vermeiden, ist eine Selektivität unerlässlich. Durch die im Rahmen dieser Arbeit synthetisierten selektiven GSK-3α-Inhibitoren eröffnet sich somit die Möglichkeit der direkten Inhibition. Zu diesem Zweck sollte die Variation der Substituenten am biphenylischen System weiter verfolgt werden (Abb. 30). Bislang konnte die Kristallstruktur von GSK-3α noch nicht gelöst werden. Diese könnte aber in Zukunft eine Erklärung für die Selektivität bieten.

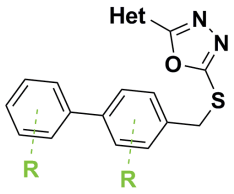

Abb. 30: Variation der Substituenten am biphenylischen System.

Erste Hinweise einiger hergestellter Verbindungen weisen bereits darauf hin, dass auch eine selektive GSK-3β Inhibition möglich sein könnte. Eine Kristallstruktur des Inhibitors im Komplex mit GSK-3β könnte Hinweise für weitere selektivitätssteigernde Interaktionen geben. Die Steigerung der Selektivität für eine GSK-3-Isoform ist jedoch nicht nur auf das biphenylische System zu beschränken. Es könnten auch Überlegungen angestrebt werden den Heterozyklus bzw. das Oxadiazol auszutauschen (Abb. 31).

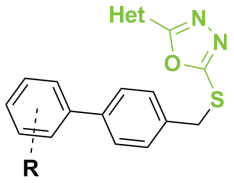

Abb. 31: Variation des Heterozyklus und Oxadiazols.

Bestehende Verbindungen sollten zudem in Tiermodellen anderer Krankheiten evaluiert werden, um das Potential dieser GSK-3-Inhibitoren auszuschöpfen.

7. Literaturverzeichnis

1. Stelzmann, R. A.; Schnitzlein, H. N.; Murtagh, F. R. An English Translation of Alzheimer´s 1907 Paper, "Über eine eigenartige Erkrankung der Hirnrinde". *Clinical Anatomy* **1995,** 8, 429-431.
2. Alzheimer, A. . Über eine eigenartige Erkrankung der Hirnrinde. *Allgemeine Zeitschrift für Psychiatrie und psychisch-gerichtliche Medizin* **1907,** 64, 146-148.
3. Zur Verfügung gestellt von M. Sc. Jiamin Gu und M. Sc. Upendra Rao Anumala in Kooperation mit dem Klinikum Darmstadt.
4. Ittner, L. M.; Götz, J. Amyloid-β and tau - a toxic pas de deux in Alzheimer´s disease. *Nature Reviews Neuroscience* **2011,** 12, 67-72.
5. LaFerla, F. M.; Green, K. N.; Oddo, S. Intracellular amyloid-β in Alzheimer´s disease *Nature Reviews Neuroscience* **2007,** 8, 499-509.
6. Perrin, R. J.; Fagan, A. M.; Holtzman, D. M. Multimodal techniques for diagnosis and prognosis of Alzheimer´s disease. *Nature* **2009,** 461, 916-922.
7. Jakob-Roetne, R.; Jacobsen, H. Die Alzheimer-Demenz: von der Pathologie zu therapeutischen Ansätzen. *Angew. Chem.* **2009,** 121, 3074-3105.
8. Citron, M. Alzheimer´s disease: strategies for disease modification. *Nature Reviews Drug Discovery* **2010,** 9, 387-398.
9. Mangialasche, F.; Solomon, A.; Winblad, B.; Mecocci, P.; Kivipelta, M. Alzheimer´s disease: clinical trials and drug development. *Lancet Neurol.* **2010,** 9, 702-716.
10. Qizilbash, N.; Whitehead, A.; Higgins, J.; Wilcock, G.; Schneider, L.; Farlow, M. Cholinesterase Inhibition for Alzheimer Disease. *JAMA* **1998,** 280, 1777-1782.
11. Candelario-Jalil, E. A role for cyclooxygenase-1 in β-amyloid-induced neuroinflammation. *Aging* **2009,** 1, 350-353.
12. Frautschy, S. A. Thinking outside the box about COX-1 in Alzheimer's disease. *Neurobiology of Disease* **2010,** 38, 492-494.
13. Müller, T.; Meyer, H. E.; Egensperger, R.; Marcus, K. . The amyloid precursor protein intracellular domain (AICD) as modulator of gene expression, apoptosis, and cytoskeletal dynamics—Relevance for Alzheimer's disease. *Progress in Neurobiology* **2008,** 85, 393-406.
14. De Strooper, B.; Vassar, R.; Golde, T. The secretases: enzymes with therapeutic potential in Alzheimer disease. *Nature Reviews Neurology* **2010,** 6, 99-107.
15. Li, H.; Wolfe, M. S.; Selkoe, D. J. Toward Structural Elucidation of the γ-Secretase Complex. *Structure* **2009,** 17, 326-334.
16. Small, D. H.; Klaver, D. W.; Foa, L. Presenilins and the γ-secretase: still a complex problem. *Molecular Brain* **2010,** 3, 1-6.
17. Shah, S.; Lee, S.; Tabuchi, K.; Hao, Y.; Yu, C.; LaPlant, Q.; Ball, H.; Dann III, C. E.; Südhof, T.; Yu, G. Nicastrin Functions as a γ-Secretase-Substrate Receptor. *Cell* **2005,** 122, 435-447.
18. Herreman, A.; Van Gassen, G.; Bentahir, M.; Nyabi, O.; Craessaerts, K.; Mueller, U.; Annaert, W.; De Strooper, B. γ-Secretase activity requires the presenilin-dependent trafficking of nicastrin through the Golgi apparatus but not its complex glycosylation. *Journal of Cell Science* **2002,** 116, 1127-1136.
19. Brammens, L.; Chávez-Gutiérrez, L.; Tolia, A.; Zwijsen, A.; De Strooper, B. Functional and Topological Analysis of Pen-2, the Fourth Subunit of the γ-Secretase Complex. *JBC* **2011,** 286, 12271-12282.
20. Martocchia, A.; Falaschi, P. Current Strategies of Therapy in Alzheimer's Disease *The Open Neuropsychopharmacology Journal* **2008,** 1, 19-23.
21. Melnikova, I. Therapies for Alzheimer´s disease. *Nature Reviews Drug Discovery* **2007,** 6, 341-342.
22. Dovey, H. F.; John, V.; Anderson, J. P.; Chen, L. Z.; De Saint Andrieu, P.; Fang, L. Y.; Freedman, S. B.; Folmer, B.; Goldbach, E.; Holsztynska, E. J.; Hu, K. L.; Johnson-

Wood, K. L.; Kennedy, S. L.; Kholodenko, D.; Knops, J. E.; Latimer, L. H.; Lee, M.; Liao, Z.; Lieberburg, I. M.; Motter, R. N.; Mutter, L. C.; Nietz, J.; Quinn, K. P.; Sacchi, K. L.; Seubert, P. A.; Shopp, G. M.; Thorsett, E. D.; Tung, J. S.; Wu, J.; Yang, S.; Yin, C. T.; Schenk, D. B.; May, P. C.; Altstiel, L. D.; Bender, M. H.; Boggs, L. N.; Britton, T. C.; Clemens, J. C.; Czilli, D. L.; Dieckman-McGinty, D. K.; Droste, J. J.; Fuson, K. S.; Gitter, B. D.; Hyslop, P. A.; Johnstone, E. M.; Li, W.-Y.; Little, S. P.; Mabry, T. E.; Miller, F. D.; Ni, B.; Nissen, J. S.; Porter, W. J.; Potts, B. D.; Reel, J. K.; Stephenson, D.; Su, Y.; Shipley, L. A.; Whitesitt, C. A.; Yin, T.; Audia, J. E. Functional gamma-secretase inhibitors reduce beta-amyloid peptide levels in brain. *Journal of Neurochemistry* **2001,** 76, 173-181.

23. Best, J. D.; Jay, M. T.; Otu, F.; Ma, J.; Nadin, A.; Ellis, S.; Lewis, H. D.; Pattison, C.; Reilly, M.; Harrison, T.; Shearman, M. S.; Williamson, T. L.; Atack, J. R. Quantitative Measurement of Changes in Amyloid-β(40) in the Rat Brain and Cerebrospinal Fluid following Treatment with the γ-Secretase Inhibitor LY-411575 [N^2-[(2S)-2-(3,5-Difluorophenyl)-2-hydroxyethanoyl]-N^1-[(7S)-5-methyl-6-oxo-6,7-dihydro-5H-dibenzo[b,d]azepin-7-yl]-L-alaninamide]. *JPET* **2005,** 313, 902-908.
24. Artavanis-Tsakonas, S.; Rand, M. D.; Lake, R. J. Notch Signaling: Cell Fate Control and Signal Integration in Development. *Science* **1999,** 284, 770-776.
25. Best, J. D.; Jay, M. T.; Otu, F.; Churcher, I.; Reilly, M.; Morentin-Gutierrez, P.; Pattison, C.; Harrison, T.; Shearman, M. S.; Atack, J. R. In Vivo Characterization of Aβ(40) Changes in Brain and Cerebrospinal Fluid Using the Novel γ-Secretase Inhibitor N-[cis-4-[(4-Chlorophenyl)sulfonyl]-4-(2,5-difluorophenyl)cyclohexyl]-1,1,1-trifluoromethanesulfonamide (MRK-560) in the Rat. *JPET* **2006,** 317, 786-790.
26. Venugopal, C.; Demos, C. M.; Jagannatha Rao, K. S.; Papolla, M. A. Beta-secretase: Structure, Function, and Evolution. *CNS Neurol Disord Drug Targets* **2008,** 7, 278-294.
27. Cole, S. L.; Vassar, R. The Alzheimer's disease β-secretase enzyme, BACE1. *Molecular Neurodegeneration* **2007,** 2, 1-25.
28. Hemming, M. L.; Elias, J. E.; Gygi, S. P.; Selkoe, D. J. Identification of β-Secretase (BACE1) Substrates Using Quantitative Proteomics. *PLoS ONE* **2009,** 4, e8477.
29. Stanton, R. A.; Gernert, K. M.; Nettles, J. H.; Aneja, R. Drugs That Target Dynamic Microtubules: A New Molecular Perspective. *Medicinal Research Reviews* **2011,** 31, 443-481.
30. Mazanetz, M. P.; Fischer, P. Untangling tau hyperphosphorylation in drug design for neurodegenerative diseases. *Nature Reviews Drug Discovery* **2007,** 6, 464-479.
31. Schneider, A.; Mandelkow, E. Tau-Based Treatment Strategies in Neurodegenerative Diseases. *Neurotherapeutics* **2008,** 5, 443-457.
32. Drechsel, D. N.; Hyman, A. A.; Cobb, M. H.; Kirschner, M. W. Modulation of the Dynamic Instability of Tubulin Assembly by the Microtubule-Associated Protein Tau. *Molecular Biology of the Cell* **1992,** 3, 1141-1154.
33. Brunden, K. R.; Trojanowski, J. Q.; Lee, V. M. Y. Advances in tau-focused drug discovery for Alzheimer´s and related disease. *Nature Reviews Drug Discovery* **2009,** 8, 783-793.
34. Schneider, A.; Biernat, J.; von Bergen, M.; Mandelkow, E. M. Phosphorylation that Detaches Tau Protein from Microtubules (Ser262, Ser214) Also Protects It against Aggregation into Alzheimer Paired Helical Filaments. *Biochemistry* **1999,** 38, 3549-3558.
35. Schneider, A.; Falkai, P.; Papassotiropoulos, A. Molekulare Grundlagen Tau-Protein-vermittelter Toxizität. *Nervenarzt* **2010,** 81, 1289-1297.
36. Manning, G.; Whyte, D. B.; Martinez, R.; Hunter, T.; Sudarsanam, S. The Protein Kinase Complement of the Human Genome. *Science* **2002,** 298, 1912-1934.
37. Bossemeyer, D. Protein kinases - structure and function. *FEBS Letters* **1995,** 369, 57-61.
38. Cohen, P. Protein kinases - the major drug targets of the twenty-first century. *Nature Reviews Drug Discovery* **2002,** 1, 309-315.

39. Ubersax, J. A.; Ferrell Jr, J. E. Mechanism of specificity in protein phosphorylation. *Nature Reviews Molecular Cell Biology* **2007,** 8, 530-541.
40. Ghose, A. K.; Herbertz, T.; Pippin, D. A.; Salvino, J. M.; Mallamo, J. P. Knowledge Based Prediction of Ligand Binding Modes and Rational Inhibitor Design for Kinase Drug Discovery. *J. Med. Chem* **2008,** 51, 5149-5171.
41. ter Haar, E.; Coll, J. T.; Austen, D. A.; Hsiao, H.; Jain, J. Structure of GSK3β reveals a primed phoshorylation mechanism. *Nature Structural Biology* **2001,** 8, 593-596.
42. Grant, S. K. Therapeutic Protein Kinase Inhibitors. *Cell. Mol. Life Sci.* **2009,** 66, 1163-1177.
43. Rauh, D. Inaktive Kinasekonformationen stabilisieren. *Nachrichten aus der Chemie* **2010,** 58, 118-121.
44. Liu, Y.; Gray, N. S. Rational design of inhibitors that bind to inactive kinase conformations. *Nature Chemical Biology* **2006,** 2, 358-364.
45. Morphy, R. Selectively Nonselective Kinase Inhibition: Striking the Right Balance. *J. Med. Chem* **2010,** 53, 1413-1437.
46. Zuccotto, F.; Ardini, E.; Casale, E.; Angiolini, M. Through the "Gatekeeper Door": Exploiting the Active Kinase Conformation. *J. Med. Chem* **2010,** 53, 2681-2694.
47. Zhang, J.; Yang, P. L.; Gray, N. S. Targeting cancer with small molecule kinase inhibitors. *Nature Reviews Cancer* **2009,** 9, 28-39.
48. Singh, J.; Petter, R. C.; Baillie, T. A.; Whitty, A. The resurgence of covalent drugs. *Nature Reviews Drug Discovery* **2011,** 10, 307-317.
49. Frame, S.; Cohen, P. GSK3 takes centre stage more than 20 years after its discovery. *Biochem. J.* **2001,** 359, 1-16.
50. Doble, B. W.; Woodgett, J. R. GSK-3: tricks of the trade fo a multi-tasking kinase. *Journal of Cell Science* **2003,** 116, 1175-1186.
51. Cohen, P.; Frame, S. The renaissance of GSK3. *Nature Reviews Molecular Cell Biology* **2001,** 2, 769-776.
52. Ali, A.; Hoeflich, K. P.; Woodgett, J. R. Glycogen Synthase Kinase-3: Properties, Functions, and Regulation. *Chem. Rev.* **2001,** 101, 2527-2540.
53. Mukai, F.; Ishiguro, K.; Sano, Y.; Fujita, S. C. Alternative splicing isoform of tau protein kinase I/glycogen synthase kinase 3β. *Journal of Neurochemistry* **2002,** 81, 1073-1083.
54. Dajani, R.; Fraser, E.; Roe, S. M.; Young, N.; Good, V.; Dale, T. C.; Pearl, L. H. Crystal Structure of Glycogen Synthase Kinase 3β: Structural Basis for Phosphate-Primed Substrate Specificity and Autoinhibition. *Cell* **2001,** 105, 721-732.
55. Bax, B.; Carter, P. S.; Lewis, C.; Guy, A. R.; Bridges, A.; Tanner, R.; Pettman, G.; Mannix, C.; Culbert, A. A.; Brown, M. J. B.; Smith, D. G.; Reith, A. D. . The Structure of Phosphorylated GSK-3β Complexed with a Peptide, FRATtide, that Inhibits β-Catenin Phosphorylation. *Structure* **2001,** 9, 1143-1152.
56. Jope, R. S.; Johnson, G. V. W. The glamour and gloom of glycogen synthase kinase-3. *Trends in Biochemical Sciences* **2004,** 29, 95-102.
57. Martinez, A. Preclinical Efficacy on GSK-3 Inhibitors: Towards a Future Generation of Powerful Drugs. *Medicinal Research Reviews* **2008,** 28, 773-796.
58. Jope, R. S.; Yuskaitis, C. J.; Beurel, E. Glycogen Synthase Kinase-3 (GSK3): Inflammation, Diseases, and Therapeutics. *Neurochem Res.* **2007,** 32, 577-595.
59. Hur, E.; Zhou, F. GSK3 signalling in neural development. *Nature Reviews Neuroscience* **2010,** 11, 539-551.
60. Klein, P. S.; Melton, D. A. A molecular mechanism for the effect of lithium on development. *Proc. Natl. Acad. Sci.* **1996,** 93, 8455-8459.
61. Mora, A.; Sabio, G.; González-Polo, R. A.; Cuenda, A.; Alessi, D. R.; Alonso, J. C.; Fuentes, J. M.; Soler, G.; Centeno, F. Lithium inhibits caspase 3 activation and dephosphorylation of PKB and GSK3 induced by K^+ deprivation in cerebellar granule cells. *Journal of Neurochemistry* **2001,** 78, 199-206.

62. Ryves, W. J.; Harwood, A. J. Lithium Inhibits Glycogen Synthase Kinase-3 by Competition for Magnesium. *Biochemical and Biophysical Research Communications* **2001,** 280, 720-725.
63. Ryves, W. J.; Dajani, R.; Pearl, L.; Harwood, A. J. Glycogen Synthase Kinase-3 Inhibition by Lithium and Beryllium Suggests the Presence of Two Magnesium Binding Sites. *Biochemical and Biophysical Research Communications* **2002,** 290, 967-972.
64. Bhat, R. V.; Budd, S. L. GSK3β Signalling: Casting a Wide Net in Alzheimer´s Disease. *Neurosignals* **2002,** 11, 251-261.
65. Kremer, A.; Louis, J. V.; Jaworski, T.; Van Leuven, F. GSK3 and Alzheimer´s disease: facts and fiction... *Frontiers in Molecular Neuroscience* **2011,** 4, 1-10.
66. Bhat, R.V.; Budd Haeberlein, S. L.; Avila, J. Glycogen synthase kinase 3: a drug target for CNS therapies. *Journal of Neurochemistry* **2004,** 89, 1313-1317.
67. Lucas, J. J.; Hernández, F.; Gómez-Ramos, P.; Morán, M. A.; Hen, R.; Avila, J. Decreased nuclear β-catenin, tau hyperphosphorylation and neurodegeneration in GSK-3β conditional transgenic mice. *The EMBO Journal* **2001,** 20, 27-39.
68. Engel, T.; Goni-Oliver, P.; Lucas, J. J.; Avila, J.; Hernández, F. Chronic lithium administration to FTDP-17 tau and GSK-3beta overexpressing mice prevents tau hyperphosphorylation and neurofibrillary tangle formation, but pre-formed neurofibrillary tangles do not revert. *Journal of Neurochemistry* **2006,** 99, 1445-1455.
69. Hooper, C.; Killick, R.; Lovestone, S. The GSK3 hypothesis of Alzheimer´s disease. *Journal of Neurochemistry* **2008,** 104, 1433-1439.
70. Jackson, G. R.; Wiedau-Pazos, M.; Sang, T.; Wagle, N.; Brown, C. A.; Massachi, S.; Geschwind, D. H. Human Wild-Type Tau Interacts with wingless Pathway Components and Produces Neurofibrillary Pathology in Drosophila. *Neuron* **2002,** 34, 509-519.
71. Wang, Y.; Zhang, J.; Du, X.; Zhao, L.; Tian, Q.; Zhu, L.; Wang, S.; Wang, J. Temporal correlation of the memory deficit with Alzheimer-like lesions induced by activation of glycogen synthase kinase-3. *Journal of Neurochemistry* **2008,** 106, 2364-2374.
72. Cohen, P.; Goedert, M. GSK3 Inhibitors: Development and Therapeutic Potential. *Nature Reviews Drug Discovery* **2004,** 3, 479-487.
73. Bhat, R. V.; Berg, S.; Burrows, J.; Lindquist, J. GSK-3 Inhibitors for the treatment of Alheimer´s Disease. *Top Med Chem* **2008,** 2, 137-174.
74. Cross, D. A. E.; Culbert, A. A.; Chalmers, K. A.; Facci, L.; Skaper, S. D.; Reith, A. D. Selective small-molecule inhibitors of glycogen synthase kinase-3 activity protect primary neurones from death. *Journal of Neurochemistry* **2001,** 77, 94-102.
75. Meijer, L.; Flajolet, M.; greengard, P. Pharmacological inhibitors of glycogen synthase kinase 3. *Trends in Pharmacological Sciences* **2004,** 25, 471-480.
76. Grimes, C. A.; Jope, R. S. The multifaceted roles of glycogen synthase kinase 3β in cellular signaling. *Progress in Neurobiology* **2001,** 65, 391-426.
77. Koh, S.; Noh, M. Y.; Kim, S. H. Amyloid-beta-induced neurotoxicity is reduced by inhibition of glycogen synthase kinase-3. *Brain Research* **2008,** 1188, 254-262.
78. Bhat, R.; Xue, Y.; Berg, S.; Hellberg, S.; Ormö, M.; Nilson, Y.; Radesäter, A.; Jerning, E.; Markgren, P.; Borgegard, T.; Nylöf, M.; Giménez-Cassina, A.; Hernández, F.; Lucas, J. J.; Díaz-Nido, J.; Avila, J. Structural Insights and Biological Effects of Glycogen Synthase Kinase 3-specific Inhibitor AR-A014418. *JBC* **2003,** 278, 45937-45945.
79. Phiel, C. J.; Wilson, C. A.; Lee, V. M.-Y.; Klein, P. S. GSK-3α regulates production of Alzheimer's disease amyloid-β peptides. *Nature* **2003,** 423, 435-439.
80. Jaworski, T.; Dewachter, I.; Lechat, B.; Gees, M.; Kremer, A.; Demedts, D.; Borghgraef, P.; Devijver, H.; Kügler, S.; Patel, S.; Woodgett, J. R.; Van Leuven, F. GSK-3α/β kinases and amyloid production in vivo. *Nature* **2011,** 480, E4-E5.
81. Phiel, C. J.; Wilson, C. A.; Lee, V. M.-Y.; Klein, P. S. Phiel et al. reply *Nature* **2011,** 480, E6.

82. Saitoh, M.; Kunitomo, J.; Kimura, E.; Hayase, Y.; Kobayashi, H.; Uchiyama, N.; Kawamoto, T.; Tanaka, T.; Mol, C. D.; Dougan, D. R.; Textor, G. S.; Snell, G. P.; Itoh, F. Design, synthesis and structure-activity relationship of 1,3,4-oxadiazole derivatives as novel inhibitors of glycogen synthase kinase-3β. *Bioorg. Med. Chem.* **2009,** 17, 2017-2029.
83. Saitoh, M.; Kunitomo, J.; Kimura, E.; Iwashita, H.; Uno, Y.; Onishi, T.; Uchiyama, N.; Kawamoto, T.; Tanaka, T.; Mol, C. D.; Dougan, D. R.; Textor, G. S.; Snell, G. P.; Takizawa, M.; Itoh, F.; Kori, M. 2-{3-[4-(Alkylsulfinyl)phenyl]-1-benzofuran-5-yl}-5-methyl-1,3,4-oxadiazole Derivatives as novel Inhibitors of glycogen Synthase Kinase-3β with Good Brain Permeability. *J. Med. Chem* **2009,** 52, 6270-6286.
84. Onishi, T.; Iwashita, H.; Uno, Y.; Kunitomo, J.; Saitoh, M.; Kimura, E.; Fujita, H.; Uchiyama, N.; Kori, M.; Takizawa, M. A novel glycogen synthase kinase-3 inhibitor 2-methyl-5-(3-{4-[(S)-methylsulfinyl]phenyl}-1-benzofuran-5-yl)-1,3,4-oxadiazole decreases tau phosphorylation and ameliorates cognitive deficits in a transgenic model of Alzheimer's disease. *Journal of Neurochemistry* **2011,** 119, 1330-1340.
85. Khanfar, M. A.; Hill, R. A.; Kaddoumi, A.; El Sayed, K. A. Discovery of novel GSK-3β inhibitors with potent in vitro and in vivo activities and excellent brain permeability using combined ligand- and structure-based virtual screening. *J. Med. Chem* **2010,** 53, 8534-8545.
86. Naerum, L.; Norskov-Lauritsen, L.; Olesen, P. H. Scaffold Hopping and Optimization towards Libraries of Glycogen Synthase Kinase-3 Inhibitors. *Bioorg. Med. Chem. Lett.* **2002,** 12, 1525-1528.
87. Bregman, H.; Williams, D. S.; Ekin Atilla, G.; Carroll, P. J.; Meggers, E. An Organometallic Inhibitor for Glycogen Synthase Kinase 3. *J. Am. Chem. Soc.* **2004,** 126, 13594-13595.
88. Ekin, Atilla-Gokcumen, G.; Williams, D. S.; Bregman, H.; Pagano, N.; Meggers, E. Organometallic Compounds with Biological Activity: A Very Selective and Hoghly Potent Cellular Inhibitor for Glycogen Synthase Kinase 3. *ChemBioChem* **2006,** 7, 1443-1450.
89. Martinez, A.; Gil, C.; Perez, D. I. Glycogen Synthase Kinase 3 Inhibitors in the Next Horizon for Alzheimer's Disease Treatment. *International Journal of Alzheimer´s Disease* **2011,** 2011, 1-7.
90. Eldar-Finkelman, H.; Licht-Murava, A.; Pietrokovski, S.; Eisenstein, M. Substrate competitive GSK-3 inhibitors - strategy and implications. *Biochim. Biophys. Acta* **2010,** 1804, 598-603.
91. Feng, L.; Geisselbrecht, Y.; Blanck, S.; Wilbuer, A.; Atilla-Gokcumen, G. E.; Filippakopoulos, P.; Kräling, K.; Celik, M. A.; Maksimoska, J.; Marmorstein, R.; Frenking, G.; Knapp, S.; Essen, L.; Meggers, E. Structurally Sophisticated Octahedral Metal Complexes as Highly Selective Protein Kinase Inhibitors. *J. Am. Chem. Soc.* **2011,** 133, 5976-5986.
92. Eldar-Finkelman, H. Glycogen synthase kinase 3: an emerging therapeutic target. *Trends in Molecular Medicine* **2002,** 8, 126-132.
93. Cao, Q.; Lu, X.; Feng, Y. Glycogen synthase kinase-3β positively regulates the proliferation of human ovarian cancer cells. *Cell Research* **2006,** 16, 671-677.
94. Garcea, G.; Manson, M. M.; Neal, C. P.; Pattenden, C. J.; Sutton, C. D.; Dennison, A. R.; Berry, D. P. Glycogen Synthase Kinase-3 Beta; A New Target in Pancreatic Cancer? *Current Cancer Drug Targets* **2007,** 7, 209-215.
95. Martinez, A.; Castro, A.; Dorronsoro, I.; Alonso, M. Glycogen Synthase Kinase 3 (GSK-3) Inhibitors as New Promising Drugs for Diabetes, Neurodegeneration, Cancer, and Inflammation. *Medicinal Research Reviews* **2002,** 22, 373-384.
96. Force, T.; Woodgett, J. R. Unique and Overlapping Functions of GSK-3 Isoforms in Cell Differentiation and Proliferation and Cardiovascular Development. *JBC* **2009,** 284, 9643-9647.
97. Sato, N.; Meijer, L.; Skaltsounis, L.; Greengard, P.; Brivanlou, A. H. Maintenance of pluripotency in human and mouse embryonic stem cells through activation of Wnt

signaling by a pharmacological GSK-3 specific inhibitor. *Nature Medicine* **2004,** 10, 55-63.
98. Ribé, E. M.; Pérez, M.; Puig, B.; Gich, I.; Lim, F.; Cuadrado, M.; Sesma, T.; Catena, S.; Sánchez, B.; Nieto, M.; Gómez-Ramos, P.; Morán, M. A.; Cabodevilla, F.; Samaranch, L.; Ortiz, L.; Pérez, A.; Ferrer, I.; Avila, J.; Gómez-Isla, T. . Accelerated amyloid deposition, neurofibrillary degeneration and neuronal loss in double mutant APP/tau transgenic mice. *Neurobiology of Disease* **2005,** 20, 814-822.
99. Pérez, M.; Ribe, E.; Rubio, A.; Lim, F.; Morán, M. A.; Gómez-Ramos, P.; Ferrer, I.; Isla, M. T. G.; Avila, J. . Characterization of a Double (Amyloid Precursor Protein-Tau) Transgenic: Tau Phosphorylation and Aggregation. *Neuroscience* **2005,** 130, 339-347.
100. Terwel, D.; Muyllaert, D.; Dewachter, I.; Borghgraef, P.; Croes, S.; Devijver, H.; Van Leuven, F. Amyloid Activates GSK-3β to Aggravate Neuronal Tauopathy in Bigenic Mice. *The American Journal of Pathology* **2008,** 172, 786-798.
101. Oddo, S.; Caccamo, A.; Shepherd, J. D.; Murphy, M. P.; Golde, T. E.; Kayed, R.; Metherate, R.; Mattson, M. P.; Akbari, Y.; LaFerla, F. M. Triple-Transgenic Model of Alzheimer's Disease with Plaques and Tangles: Intracellular Aβ and Synaptic Dysfunction. *Neuron* **2003,** 39, 409-421.
102. Lewis, J.; Dickson, D. W.; Lin, W.; Chisholm, L.; Corral, A.; Jones, G.; Yen, S.; Sahara, N.; Skipper, L.; Yager, D.; Eckman, C.; Hardy, J.; Hutton, M.; McGowan, E. Enhanced Neurofibrillary Degeneration in Transgenic Mice Expressing Mutant Tau and APP. *Science* **2001,** 293, 1487-1491.
103. Lewis, J.; McGowan, E.; Rockwood, J.; Melrose, H.; Nacharaju, P.; Van Slegtenhorst, M.; Gwinn-Hardy, K.; Murphy, M. P.; Baker, M.; Yu, X.; Duff, K.; Hardy, J.; Corral, A.; Lin, W.; Yen, S.; Dickson, D. W.; Davies, P.; Hutton, M. Neurofibrillary tangles, amyotrophy and progressive motor disturbance in mice expressing mutant (P301L) tau protein. *Nature Genetics* **2000,** 25, 402-405.
104. Noble, W.; Planel, E.; Zehr, C.; Olm, V.; Meyerson, J.; Suleman, F.; Gaynor, K.; Wang, L.; LaFrancois, J.; Feinstein, B.; Burns, M.; Krishnamurthy, P.; Wen, Y.; Bhat, R.; Lewis, J.; Dickson, D.; Duff, K. Inhibition of glycogen synthase kinase-3 by lithium correlates with reduced tauopathy and degeneration in vivo. *Proc. Natl. Acad. Sci.* **2005,** 102, 6990-6995.
105. Paquet, D.; Schmid, B.; Haass, C. Transgenic Zebrafish as a Novel Animal Model to Study Tauopathies and Other Neurodegenerative Disorders in vivo. *Neurodegenerative Disease* **2010,** 7, 99-102.
106. Paquet, D.; Bhat, R.; Sydow, A.; Mandelkow, E.; Berg, S.; Hellberg, S.; Fälting, J.; Distel, M.; Köster, R. W.; Schmid, B.; Haass, C. A zebrafish model of tauopathy allows in vivo imaging of neuronal cell death and drug evaluation. *J. Clin. Invest.* **2009,** 119, 1382-1395.
107. Lee, H.; Tsai, J.; Liao, P.; Tsai, W.; Lin, K.; Chuang, C.; Sun, C.; Chang, W.; Tsai, H. Glycogen synthase kinase 3α and 3β have distinct functions during cardiogenesis of zebrafish embryo. *BMC Development Biology* **2007,** 7, 1-15.
108. Götz, J.; Ittner, L. M. Animal models of Alzheimer´s disease and frontotemporal dementia. *Nature Reviews Neuroscience* **2008,** 9, 532-544.
109. Bissantz, C.; Kuhn, B.; Stahl, M. A Medicinal Chemist´s Guide to Molecular Interactions. *J. Med. Chem* **2010,** 53, 5061-5084.
110. Salonen, L. M.; Ellermann, M.; Diederich, F. Aromatische Ringe in chemischer und biologischer Erkennung: Energien und Strukturen. *Angew. Chem.* **2011,** 123, 4908-4944.
111. Kuhn, B.; Mohr, P.; Stahl, M. Intramolecular Hydrogen Bonding in Medicinal Chemistry. *J. Med. Chem* **2010,** 53, 2601-2611.
112. Hardegger, L. A.; Kuhn, B.; Spinnler, B.; Anselm, L.; Ecabert, R.; Stihle, M.; Gsell, B.; Thoma, R.; Diez, J.; Benz, J.; Plancher, J.; Hartmann, G.; Banner, D. W.; Haap, W.; Diederich, F. Systematische Untersuchung von Halogenbrücken in Protein-Ligand-Wechselwirkungen. *Angew. Chem.* **2011,** 123, 329-334.

113. Meyer, E. A.; Castellano, R. K.; Diederich, F. Wechselwirkungen mit aromatischen Ringen in chemischen und biologischen Erkennungsprozessen. *Angew. Chem.* **2003,** 115, 1244-1287.
114. Paulini, R.; Müller, K.; Diederich, F. Orthogonal Multipolar Interactions in Structural Chemistry and Biology. *Angew. Chem. Int. Ed.* **2005,** 44, 1788-1805.
115. Hof, F.; Scofield, D. M.; Schweizer, B.; Diederich, F. A Weak Attractive Interaction between Organic Fluorine and an Amide Group. *Angew. Chem.* **2004,** 116, 5166-5169.
116. Fischer, F. R.; Schweizer, W. B.; Diederich, F. Molecular Torsion Balances: Evidence for Favorable Orthogonal Dipolar Interactions Between Organic Fluorine and Amide Groups. *Angew. Chem. Int. Ed.* **2007,** 46, 8270-8273.
117. Weinmann, H.; Metternich, R. Drug Discovery Process for Kinase Inhibition. *ChemBioChem* **2005,** 6, 455-459.
118. Perola, E. An Analysis of the Binding Efficiencies of Drugs and Their Leads in Successful Drug Discovery Programs. *J. Med. Chem* **2010,** 53, 2986-2997.
119. Bleicher, K. H.; Böhm, H.; Müller, K.; Alanine, A. I. Hit and Lead Generation: Beyond High-Throughput Screening. *Nature Reviews Drug Discovery* **2003,** 2, 369-378.
120. Bhal, S. K.; Kassam, K.; Peirson, I. G.; Pearl, G. M. The Rule of five Revisited: Applying Log D in Place of Log P in Drug-Likeness Filters. *Molecular Pharmaceutics* **2007,** 4, 556-560.
121. Lipinski, C. A.; Lombardo, F.; Dominy, B. W.; Feeney, P. J. Experimental and computational approaches to estimate solubility and permeability in drug discovery and development settings. *Advanced Drug Delivery Reviews* **2001,** 46, 3-26.
122. Edwards, R. H. Drug delivery via the blood-brain barrier. *Nature Neuroscience* **2001,** 4, 221-222.
123. Fernandes, J.; Gattass, C. R. Topological Polar Surface Area Defines Substrate Transport by Multidrug Resistance Associated Protein 1 (MRP1/ABCC1). *J. Med. Chem* **2009,** 52, 1214-1218.
124. Ertl, P.; Rohde, B.; Selzer, P. Fast Calculation of Molecular Polar Surface Area as a Sum of Fragment-Based Contributions and Its Application to the Prediction of Drug Transport Properties. *J. Med. Chem* **2000,** 43, 3714-3717.
125. Müller, K.; Faeh, C.; Diederich, F. Fluorine in Pharmaceuticals: Looking Beyond Intuition. *Science* **2007,** 317, 1881-1886.
126. Hagmann, W. K. The Many Roles for Fluorine in Medicinal Chemistry. *J. Med. Chem* **2008,** 51, 4359-4369.
127. Morgenthaler, M.; Schweizer, E.; Hoffmann-Röder, A.; Benini, F.; Martin, R. E.; Jaeschke, G.; Wagner, B.; Fischer, H.; Bendels, S.; Zimmerli, D.; Schneider, J.; Diederich, F.; Kansy, M.; Müller, K. Predicting and tuning Physicochemical Properties in Lead Optimization: Amine Basicities. *ChemMedChem* **2007,** 2, 1100-1115.
128. Alavijeh, M. S.; Chishty, M.; Qaiser, M. Z.; Palmer, A. M. Drug Metabolism and Pharmacokinetics, the Blood-Brain-Barrier, and Central Nervous System Drug Discovery. *NeuroRx* **2005,** 2, 554-571.
129. Ross, O. A.; Farrer, M. J. Pathophysiology, pleiotrophy and paradigm shifts: genetic lessons from Parkinson´s disease. *Biochem. Soc. Trans.* **2005,** 33, 586-590.
130. Davie, C. A. A review of Parkinson´s disease. *Br. Med. Bull.* **2008,** 86, 109-127.
131. Jankovic, J. Parkinson´s disease: clinical features and diagnosis. *J. Neurol. Neurosurg. Psychiatry* **2008,** 79, 368-376.
132. Zimprich, A.; Biskup, S.; Leitner, P.; Lichtner, P.; Farrer, M.; Lincoln, S.; Kachergus, J.; Hulihan, M.; Uitti, R. J.; Calne, D. B.; Stoessl, A. J.; Pfeiffer, R. F.; Patenge, N.; Carbajal, I. C.; Vieregge, P.; Asmus, F.; Müller-Myhsok, B.; Dickson, D. W.; Meitinger, T.; Strom, T. M.; Wszolek, Z. K.; Gasser, T. Mutations in LRRK2 cause autosomal-dominant parkinsonism with pleomorphic pathology. *Neuron* **2004,** 44, 601-607.
133. Berwick, D. C.; Harvey, K. LRRK2 signalling pathways: the key to unlocking neurodegeneration? *Trends Cell Biol.* **2011,** 21, 257-265.

134. Smith, K. Treatment frontiers - Parkinson´s Disease Outlook. *Nature* **2010,** 466, 15-18.
135. Giasson, B. I.; Van Deerlin, V. M. Mutations in LRRK2 as a cause of Parkinson´s disease. *Neurosignals* **2008,** 16, 99-105.
136. Mata, I. F.; Wedemeyer, W. J.; Farrer, M. J.; Taylor, J. P.; Gallo, K. A. LRRK2 in Parkinson´s disease: protein domains and functional insights. *Trends Neurosci.* **2006,** 29, 286-293.
137. Taylor, J. P.; Mata, I. F.; Farrer, M. J. LRRK2: a common pathway for parkinsonism, pathogenesis and prevention? *Trends Mol. Med.* **2006,** 12, 76-82.
138. Levis, M.; Small, D. Novel FLT3 tyrosine kinase inhibitors. *Expert Opin. Investig. Drugs* **2003,** 12, 1951-1962.
139. Kindler, T.; Lipka, D. B.; Fischer, T. FLT3 as a therapeutic target in AML: still challenging after all these years. *Blood* **2010,** 116, 5089-5102.
140. Pratz, K. W.; Levis, M. J. Bench to bedside targeting of FLT3 in acute leukemia. *Curr Drug Targets* **2010,** 11, 781-789.
141. Mahboobi, S.; Uecker, A.; Sellmer, A.; Cénac, C.; Höcher, H.; Pongratz, H.; Eichhorn, E.; Hufsky, H.; Trümpler, A.; Sicker, M.; Heidel, F.; Fischer, T. Stocking, C.; Elz, S.; Böhmer, F. D.; Dove, S. Novel Bis(1H-indol-2-yl)methanones as Potent Inhibitors of FLT3 and Platelet-Derived Growth Factor Receptor Tyrosine Kinase. *J. Med. Chem* **2006,** 49, 3101-3115.

Fabio Lo Monte
Eschersheimer Landstraße 511
60431 Frankfurt am Main

Frankfurt am Main, den 26.03.2012

Eidesstattliche Erklärung

Ich erkläre hiermit an Eides statt, dass ich meine Dissertation selbstständig und nur mit den angegebenen Hilfsmitteln angefertigt habe.

Fabio Lo Monte

Fabio Lo Monte
Eschersheimer Landstraße 511
60431 Frankfurt am Main

Frankfurt am Main, den 26.03.2012

Erklärung

Ich erkläre hiermit, noch keinen Promotionsversuch unternommen zu haben.

Fabio Lo Monte

Fabio Lo Monte
Eschersheimer Landstraße 511
60431 Frankfurt am Main

Geburtsdatum/-ort	16. September 1980, Hilden
Nationalität	Italienisch
Familienstand	ledig
Promotion	3/2009-3/2012 Durchführung der Doktorarbeit am Clemens Schöpf-Institut der organischen Chemie und Biochemie an der TU Darmstadt unter Anleitung von Prof. Dr. Boris Schmidt; Schwerpunkt meiner Arbeit medizinische/organische Chemie
Aufbaustudium	9/2007-2/2009 Master of Science (Angewandte Chemie) an der Hochschule Niederrhein in 3. Semestern abgeschlossen; Anfertigung der Masterarbeit in Chemical and Analytical Sciences (CAS) der Sanofi-Aventis Deutschland GmbH
Ende Erststudium	9/2006-4/2007 Praktikum und Erstellung der Diplomarbeit in der medizinischen Chemie der Merck KGaA Darmstadt; Abschluss zum Dipl. Chemie-Ingenieur zu Beginn des 8. Semesters; Aufnahme in das Student Excellence Program von Merck (STEP)
Studium	10/2003-2/2005 Beginn des Bachelorstudiums Biochemie an der Heinrich-Heine-Universität Düsseldorf 3/2005 Wechsel an die Hochschule Niederrhein in Krefeld zum Studiengang Chemieingenieurwesen; Anrechnung aller erbrachten Leistungen und Einstufung in das 4. Semester
Berufsausbildung	9/2000-6/2003 Ausbildung zum Chemielaboranten beim Landesumweltamt NRW

Schulausbildung	9/1997-7/2000 Abitur am Dietrich-Bonhoeffer-Gymnasium
Berufserfahrung	7/2003-9/2003 Chemielaborant - Landesumweltamt NRW 9/2007-9/2008 Wissenschaftlicher Mitarbeiter am Institut für Hochpolymere und Hygieneprodukte (IHHP) 3/2008-8/2008 Tutor in der organischen Chemie
Sprachkenntnisse	Italienisch (Muttersprache) Deutsch (Muttersprache) Englisch (Fließend) Spanisch (Fließend) Portugiesisch (Verständnis) Französisch (Verständnis)
Referenzen	Professor Boris Schmidt; Technische Universität Darmstadt; *schmidt_boris@mac.com* Dr. Wolfgang Stähle; Merck KGaA; *staehle@merck.de* Professor Michael Lindemann; Hochschule Niederrhein; *michael.lindemann@hs-niederrhein.de* Professor Andrea Wanninger; Hochschule Niederrhein; *andrea.wanninger@hs-niederrhein.de*

Frankfurt am Main, den 26.03.2012